

Polarization and Electronic State Configuration of III-N Surfaces and
Plasma-Enhanced Atomic Layer Deposited Dielectric Interfaces

by

Brianna Eller

A Dissertation Presented in Partial Fulfillment
of the Requirements for the Degree
Doctor of Philosophy

Approved April 2015 by the
Graduate Supervisory Committee:

Robert Nemanich, Chair
Srabanti Chowdhury
Martha McCartney
Fernando Ponce
David Smith

ARIZONA STATE UNIVERSITY

May 2015

ABSTRACT

GaN and AlGaN have shown great potential in next-generation power and RF electronics. However, these devices are limited by reliability issues such as leakage current and current collapse that result from surface and interface states on GaN and AlGaN. This dissertation, therefore, examined these electronic states, focusing on the following two points:

First, the surface electronic state configuration was examined with regards to the polarization bound 10^{13} charges/cm² that increases with aluminum content. This large bound charge requires compensation either externally by surface states or internally by the space charge regions as relates to band bending. In this work, band bending was measured after different surface treatments of GaN and AlGaN to determine the effects of specific surface states on the electronic state configuration. Results showed oxygen-terminated N-face GaN, Ga-face GaN, and Ga-face Al_{0.25}Ga_{0.75}N surface were characterized by similar band bending regardless of the polarization bound charge, suggesting a Fermi level pinning state $\sim 0.4\text{-}0.8$ eV below the conduction band minimum. On oxygen-free Ga-face GaN, Al_{0.15}Ga_{0.85}N, Al_{0.25}Ga_{0.75}N, and Al_{0.35}Ga_{0.65}N, band bending increased slightly with aluminum content and thus did not exhibit the same pinning behavior; however, there was still significant compensating charge on these surfaces ($\sim 10^{13}$ charges/cm²). This charge is likely related to nitrogen vacancies and/or gallium dangling bonds.

In addition, this work investigated the interface electronic state configuration of dielectric/GaN and AlGaN interfaces with regards to deposition conditions and aluminum

content. Specifically, oxygen plasma-enhanced atomic layer deposited (PEALD) was used to deposit SiO₂. Growth temperature was shown to influence the film quality, where room temperature deposition produced the highest quality films in terms of electrical breakdown. In addition, the valence band offsets (VBOs) appeared to decrease with the deposition temperature, which likely related to an electric field across the Ga₂O₃ interfacial layer. VBOs were also determined with respect to aluminum content at the PEALD-SiO₂/Al_xGa_{1-x}N interface, giving 3.0, 2.9, 2.9, and 2.8 eV for 0%, 15%, 25%, and 35% aluminum content, respectively—with corresponding conduction band offsets of 2.5, 2.2, 1.9, and 1.8 eV. This suggests the largest difference manifests in the conduction band, which is in agreement with the charge neutrality level model.

ACKNOWLEDGEMENTS

Dr. Nemanich, please accept my sincerest gratitude for the assistance and inspiration you have provided me throughout my Ph.D. experience. No doubt, I will continue to benefit from your advice and inspiration in the years to come. Your mentoring has been tremendously motivational; the truth is, without your constant support and enthusiasm, my Ph.D. experience would not have been nearly as successful. You are truly a remarkable advisor, who is invested in motivating and providing opportunities for each student to meet her individual goals. Thank you for supporting me in these goals.

I would also like to thank my committee members—Dr. Srabanti Chowdhury, Dr. Martha McCartney, Dr. Fernando Ponce, and Dr. David Smith—for serving on my committee and contributing to the development of this work, especially considering the additional hardship imposed; your time as well as your thoughtful comments and suggestions—which no doubt will contribute to the strength of this work—are greatly appreciated.

To the other group members at the Nanoscience Laboratory, I would like to extend particularly special appreciation. Dr. Jialing Yang, thank you for your collaboration and cooperation with this work. While you have been influential to the quality and direction of this work, your dedication and work ethic has served as inspiration throughout this process. I am also grateful to my peers who have contributed to this work—particularly Xingye Wang, Manpuneet Kaur, Sarah Rupprecht, Joe Shamma, and Chris England. Dr. Franz Koeck, your skill with equipment is unparalleled. We are so fortunate to have your expertise in the lab. I certainly could not have completed this work as efficiently without your help. In addition, I greatly appreciate the effort of the graduate students before me—

Dr. Fu Tang, Dr. Yang Sun, Dr. Chiyu Zhu, Dr. Xin Liu, and Dr. Tianyin Sun—who built the equipment and established laboratory protocols. Your success in the laboratory provided the foundation for this work. In addition, your advice and mentorship offered me daily relief, support, and inspiration. To Mei Hao and Aaron Papagalos, I would like to thank you for letting me act as a mentor; while I can only hope I provided some inspiration and guidance, I have greatly appreciated and benefitted from the opportunity to assist, teach, and advise you.

Araceli Vizcarra, Ebony Shalley, Rose Murrietta, Ixchell Paape, Jane Laux, Deborah Denson and the rest of the staff working in the Department of Physics, your support has not been unnoticed or unappreciated. Navigating the bureaucracy of ASU is not always an easy task, and your knowledge and aid has made all the difference. Thank you for your excellent assistance.

In addition, I appreciate the technical expertise at the LeRoy Eyring Center for Solid State Science. In particular, I would like to thank Dr. Barry Wilkens for Rutherford backscattering spectroscopy measurement, Dr. Emmanuel Soignard for x-ray reflectivity measurement, and Dr. Diana Convey for spectroscopic ellipsometry measurement. Moreover, thank you to the staff at the Center for Solid State Electronics Research in the cleanroom for your maintenance and operation, particularly Arthur Handugan, Jerry Eller, and Stefan Myhajlenko.

The Office of Naval Research through the DEFINE MURI program, N00014-10-1-0937, has supported this research. This program has provided opportunities for not only sound and influential research but also for personal learning and development. Thank you to all

those who have contributed to this project over the last five years. In particular, thank you to Dr. Baishakhi Mazumder and Dr. Umesh Mishra from University of California, Santa Barbara, Dr. Rathnait Long and Dr. Paul McIntyre from Stanford University, and Christine Jackson, Dr. Aaron Arehart Dr. Steven Ringel, and Dr. Siddharth Rajan from Ohio State University, who helped problem solve, supply samples, and characterization. Also, I appreciate the efforts of all those who have worked to organize this program and reviews, particularly Dr. Paul Maki, Dr. Umesh Mishra, Dr. Dan Green, Dr. Srabanti Chowdhury, and Erika Klukovich. In addition, I would like to thank the National Science Foundation of Arizona and Arizona State University for their financial support and backing throughout this process.

Finally, to my friends and family, there are not the enough words to express my gratitude. For all the sacrifices you have made so I could achieve this goal, I thank you. To my supportive parents, your love and acceptance have always helped sustain and guide me. To my siblings, your friendship and support—as well as the dedication you show to your own goals—has always inspired me. I am truly fortunate and blessed to have you all in my life.

Lastly, to my beloved fiancé, thank you for fighting it out with me. Thank you for the sleepless nights, supporting me in my stressed-out moments, and the endless supply of popcorn. Thank you for always being there. Your unwavering support throughout times of excitement and hardship has been a blessing, and I cannot wait to start the next chapter of our lives together.

TABLE OF CONTENTS

	Page
LIST OF TABLES	x
LIST OF FIGURES	xviii
LIST OF PUBLICATIONS	xxxv
CHAPTER	
1. INTERFACE ELECTRONIC STATE CONFIGURATION OF GAN AND	
ALGAN.....	1
I. Device Reliability	5
A. Gate Leakage.....	5
B. Current Collapse.....	12
II. Electronic State Theory	18
A. Surface State Configurations	18
B. Interface State Configurations.....	26
III. Processing Related Effects.....	44
A. Cleaning and Surface Processing.....	44
B. Dielectric Passivation and Interface Processing.....	56
C. Post-Deposition and Post-Metallization Processing	72
IV. Summary and Conclusions	73
References.....	75
2. PLASMA-ENHANCED ATOMIC LAYER DEPOSITION	92
A. History and Development	94
II. Principles of ALD	96

CHAPTER	Page
A. Adsorption Mechanisms	96
B. Growth Models.....	99
C. Reactant Chemistry	111
III. Plasma-Enhanced Reactions	119
A. Plasma Basics.....	120
B. PEALD Reactor Configurations.....	122
C. Advantages and Disadvantages	124
IV. Specific PEALD Reactions.....	128
A. Reactor Configuration.....	128
B. Dimethylaluminum Isopropoxide (DMAI)	129
C. Tetrakis(ethylmethylamino)hafnium (TEMAHf)	136
D. Tri(dimethylamino)silane (TDMAS).....	138
V. Conclusion	138
References.....	138
3. PHOTOELECTRON SPECTROSCOPY	147
I. X-ray Photoelectron Spectroscopy	148
A. X-ray Sources.....	148
B. Analyzers.....	149
C. Core Level Spectra	150
D. Characteristics and Limitations.....	154
II. Ultraviolet Photoelectron Spectroscopy.....	157

CHAPTER	Page
A. UV source	158
B. Precision and Limitations.....	158
C. Example Spectra.....	160
III. Characterization with Photoelectron Spectroscopy	160
A. Electron Affinity	160
B. Band Bending.....	161
C. Band Alignment	163
D. Film Composition	164
E. Film Thickness	165
F. Band Gap	166
References.....	167
4. KELVIN PROBE METHOD.....	169
I. Principals of Operation.....	170
II. Surface Potentials`	173
A. Surface Work Function	173
B. Surface Band Bending.....	174
C. Surface Dipole.....	174
D. Surface Photovoltage	175
References.....	176

CHAPTER	Page
5. POLARIZATION EFFECTS OF GAN AND ALGAN: POLARIZATION BOUND CHARGE, BAND BENDING, AND ELECTRONIC SURFACE STATES.....	178
I. Experiment.....	183
II. Results	185
III. Discussion.....	190
IV. Conclusions.....	193
References.....	194
6. CHARACTERIZATION OF PLASMA-ENHANCED ATOMIC LAYER DEPOSITION OF SiO ₂ USING TRIS(DIMETHYLAMINO)SILANE ON GAN.....	198
I. Experiment.....	202
II. Results	204
III. Discussion.....	210
A. Chemisorption.....	210
B. Growth Characteristics.....	211
D. Electrical Characteristics.....	213
C. Interface Characteristics.....	214
IV. Conclusions.....	216
References.....	217
7. SURFACE BAND BENDING AND INTERFACE ALIGNMENT OF PLASMA-ENHANCED ATOMIC LAYER DEPOSITED SiO ₂ ON AL _x GA _{1-x} N	222

CHAPTER	Page
I. Experiment.....	224
II. Results	227
III. Discussion.....	232
A. Ga 3d to VBM Energy Difference	232
B. Band Bending and Surface States	234
C. Interface Alignment and Band Offsets.....	235
IV. Conclusions.....	238
References.....	238
 8. PRECISION CONTROL OF DIELECTRIC/GAN AND ALGAN INTERFACES	 242
I. Summary of Previous Work	242
II. Future Potential and Development.....	244
A. Ga ₂ O ₃ as an Interface Passivation Layer.....	244
B. Tuning Dielectric Properties	245
C. Dielectric/AlGaN/GaN Heterostructures	251
References.....	252
 REFERENCES	 254
 APPENDIX	
A. NOTATION USED FOR PRECURSOR LIGANDS	317
B. ADDITIONAL PEALD RESEARCH	318

LIST OF TABLES

Table	Page
<p>1.1 Material Properties of Si, GaAs, SiC, and GaN, where M is the Mobility, E is the Relative Permittivity, E_g is the Band Gap Energy, the BFOM Ratio is the Baliga Figure of Merit (Related to the Conduction Loss at Low Frequency), and T_{max} is the Maximum Temperature Before Degradation of the Material. Reprinted from U.K. Mishra, <i>et al.</i>, <i>Proc. IEEE</i> 90, 1022 (2002) [1]. Copyright 2002, Institute of Electrical and Electronics Engineers.....</p>	2
<p>1.2 Competitive Advantages of GaN-Based Devices. Reprinted from U.K. Mishra, <i>et al.</i>, <i>Proc. IEEE</i> 90, 1022 (2002) [1]. Copyright 2002, Institute of Electrical and Electronics Engineers.....</p>	3
<p>1.3 Lattice Constants (a and c), Piezoelectric Constants (e_{31} and e_{33}), Elastic Constants (C_{13} and C_{cc}), Spontaneous Polarization (P_{SP}), and Polarization Bound Charge (P) of GaN and AlN. The Lattice and Piezoelectric Constants (e_{31} and e_{33}) as well as the Spontaneous Polarization are Determined by the Generalized Gradient Calculation as Described in Reference [106]. The Elastic Constants are Determined by an Average of the Values Presented in References [96-104]. Values for $Al_xGa_{(1-x)}N$ may be Determined by Linear Interpolation.....</p>	20
<p>1.4 Summary of Band Gap, Electron Affinity, and Charge Neutrality Levels for GaN and AlN, where the CNL is Included for Several Different Methods of Calculation Including the Tight Binding (ETB) [143], Local Density Approximation (LDA) [141], and Two</p>	

Table	Page
Different First Principle (FP) Calculations [146,148] as well as the Experimental Values [149-152], which are Deduced from Schottky Barrier Measurements.....	35
1.5 Valence Band and Conduction Band Offsets Calculated for Dielectrics on GaN as Calculated by the Local Density Approximation and Charge Neutrality Level Model [141,189]. All Band Offsets are Given in eV.....	40
1.6 Valence Band and Conduction Band Offsets Measured for Dielectrics on GaN. If One of the Offsets is Deduced from the Measured Band Offset and the Band Gap, it is Denoted with “*”. the Deposition Method is Noted where ALD = Atomic Layer Deposition, Dry Term. Ox. = Dry Thermal Oxidation, E-Beam = Electron Beam, ECR = Electron Cyclotron Resonance, MBD = Molecular Beam Deposition, PEALD = Plasma-Enhanced Atomic Layer Deposition, PECVD = Plasma-Enhanced Chemical Vapor Deposition, PEMBD = Plasma-Enhanced Molecular Beam Deposition, and Pulsed Laser = Pulsed Laser Deposition. In Addition, the Characterization Method is Noted where CV = Capacitance-Voltage Measurements, EELS = Electron Energy Loss Spectroscopy, PL = Photoluminescence, UPS = Ultraviolet Photoelectron Spectroscopy, UV = UV Adsorption, UV-Vis = UV-Visible Adsorption, and XPS = X-Ray Photoelectron Spectroscopy. All Offsets are Given in eV.....	41
1.7 Comparison Between the Theoretical Band Offset Calculations [141] and Experimental Measurements [160-181]. Materials that are Characterized by a Discrepancy >0.4 eV are Shown in Bold. All Band Offsets are Given in eV.....	42

Table	Page
1.8 Theoretical and Experimental Band Offsets on AlGaN. the Deposition Method is Noted where ECR-CVD = Electron Cyclotron Resonance Chemical Vapor Deposition, MBD = Molecular Beam Deposition, and Vap. Cooling Cond. = Vapor Cooling Condensation. In Addition, the Characterization Method is Noted where EELS = Electron Energy Loss Spectroscopy, and XPS = X-Ray Photoelectron Spectroscopy. All Offsets are Given in eV.	43
1.9 Theoretical and Experimental Band Offsets on AlN. Note the Experimental Band Offsets for InN/AlN are Given for the Al-Face and the N-Face, Respectively. the Deposition Method is Noted where MOCVD = Metal Organic Chemical Vapor Deposition, and PEMBD = Plasma-Enhanced Molecular Beam Deposition. in Addition, the Characterization Method is Noted where XPS = X-Ray Photoelectron Spectroscopy. All Offsets are Given in eV.	43
2.1 Densities of Plasma Species in O ₂ Plasma, as Typically Used in ALD Processes. Data are Presented for Two Different Pressures and the Electron Temperature, T _e , and Energy, E _{ion} , of Ions Accelerated to the (Grounded) Substrate are Also Given. the Data Have Been Compiled from the Modeling Described in Ref 124 for an Inductively Coupled Plasma Operated at a Source Power of 500 W. the Excited Species O* and O ₂ * Correspond to the Lowest Metastable State Being O(¹ D) and O ₂ (a ¹ Δ _g), Respectively. Reprinted from H. B. Profijt <i>et al.</i> , <i>J. Vac. Sci. Technol. A</i> 29 , 050801 (2011) [11]. Copyright 2011, American Vacuum Society.	120

Table	Page
2.2 Al ₂ O ₃ Thin Film Properties on Si Wafers Grown by Remote PEALD and DMAI at 25°C and 200°C. Reprinted from Yang <i>et al. J. Vac. Sci. Technol. A</i> 32 , 021514 (2014) [131]. Copyright 2014, American Vacuum Society.....	135
2.3 Overview of the HfO ₂ Deposition Conditions and Film Analysis. Summarized from S. B. S. Heil <i>et al., J. Vac. Sci. Technol. A</i> 25 , 1357 (2007) [147]. Copyright 2007, American Vacuum Society.....	137
3.1 XPS Spectral Features of Al ₂ O ₃ from Mg K _α Radiation. Reprinted from Sygelloui <i>et al.</i> [4]. Copyright 2011, American Institute of Physics.....	153
3.2 XPS Spectral Features of HfO ₂ from Al K _α Monochromatic Radiation. Reprinted from Milanov <i>et al.</i> [5]. Copyright 2007, American Institute of Physics.....	153
3.3 XPS Spectral Features of SiO ₂ from Mg K _α Radiation. Reprinted from Chourasia <i>et al.</i> [6]. Copyright 2006, American Institute of Physics.....	154
3.4 Discharge Lines from Gas Commonly Used in UPS, i.e. He, Ne, and Ar. Modified from Ref [7]. Copyright 2004, Thermo Electron Corporation.....	158
5.1 Band Gap, Polarization, and Corresponding Polarization Bound Charge for GaN, AlN, and Al _x Ga _{1-x} N.....	181
5.2 Oxygen Coverage (in ML) on N-face GaN, Ga-face GaN, and Ga-face AlGa _n as Determined after the Various Cleaning Steps as Given by XPS.....	187

Table	Page
5.3 Atomic Ratio of N/Ga(Al) as Determined from Al 2p, Ga 3d, and N 1s Core Level Intensities, Respective Atomic Sensitivity Factors of 0.19, 0.31, and 0.42, and Effective Attenuation Lengths as Determined from the NIST Database [30].....	188
5.4 Band Bending (in eV) for N-face GaN, Ga-face GaN, and Ga-face AlGaN as Determined After the Various Cleaning Steps as Given by XPS.....	189
5.5 Concentration of External Compensation Charge (10^{13} Charges/cm ²) on N-Face GaN, Ga-Face GaN, and Ga-Face AlGaN as Determined After the Various Cleaning Steps as Given by XPS.....	189
6.1 Summary of ALD Research with a SiO ₂ Growth.....	201
6.2 SiO ₂ Content and Deposition Characteristics Determined as by RBS and XPS. (Thickness Measurements were Confirmed with XRR; However, the Sample Deposited at 550°C Did Not Provide Reliable Results, Most Likely Due to Contamination in the Film.....	206
6.3 Interface Characteristics of SiO ₂ as Deposited by PEALD, where an Increase in Temperature Results in a Decrease in the Valence Band Offset (VBO) and Increase in Ga-O Concentration, which Likely Relates to the Subcutaneous Growth of an Interfacial Ga ₂ O ₃ Layer. (In this Case, the % Concentration is Relative to the Total Oxygen Content in the Sample as Measured by XPS.).....	207
6.4 Summary of Electrical Characteristics as Relates to Deposition Temperature, Including Breakdown Voltage in MV/cm, Leakage Current in A/cm ² , and Hysteresis in	

Table	Page
V. the ALD SiO ₂ Dielectric Layers were Not the Same Thickness Due to Changes in the Growth Rate from the Plasma Pretreatment as Noted.....	210
7.1 Band Gap Characteristics of Al _x Ga _{1-x} N as Determined from Aluminum Content. These Values were Determined by Linear Interpolation of GaN and AlN Properties [11]. The Doping Density Determined the Position of the Fermi Level to be ~0.1 eV Below the Conduction Band.....	224
7.2 Energy Position of VBM and Ga 3d Core Level of Al _x Ga _{1-x} N as Dependent on Aluminum Content. These Values Determined $(E_{Ga3d}-E_{VBM})_{Al_xGa_{(1-x)N}}$ and the Surface Band Bending. All Energies are Given in eV.....	228
7.3 Core Level Results for Ga 3d, Al 2p, Ga 3s, Si 2s, and O 1s Spectra of ~3 nm PEALD-Deposited SiO ₂ on Al _x Ga _{1-x} N as Dependent on Aluminum Content, Including the Peak Position and Full-Width Half-Maximum (FWHM). All Energies are Given in eV.....	231
7.4 Summary of Expected and Measured Energy Differences Between the VBM and Ga 3d Core Level of Al _x Ga _{1-x} N as Dependent on Aluminum Content. the Measured Values were ~0.4 eV Below the Expected Values. All Energies are Given in eV.....	232
7.5 Surface Polarization Conditions of Al _x Ga _{1-x} N as Dependent on Aluminum Content. The Polarization and Polarization Bound Charge are Determined from the Concentration of Aluminum, and the Compensation Charge is Calculated from the Band Bending.....	234

Table	Page
7.6 VBOs as Determined from XPS Si 2s and Ga 3d Core Levels. The Conduction Band Offset is Determined from Known Band Gaps of the Materials, where the Band Gap of SiO ₂ is 8.9 eV. All Energies are Given in eV.	236

LIST OF FIGURES

Figure	Page
1.1 Possible Gate Leakage Mechanisms at Metal-Semiconductor (a, b, and c) and Metal-Insulator-Semiconductor (d) Interfaces.....	6
1.2 (a) Unified Model for Near-Surface Electronic States of AlGa _N , (b) a Combined Distribution of State Density, and (c) the TSB Model for Current Transport at the Schottky Interface. Reprinted from Hasegawa <i>et al.</i> , <i>J. Vac. Sci. Technol. B</i> 21 , 1844 (2003) [43]. Copyright 2003, American Vacuum Society.....	10
1.3 (a) Schematic Representation of Drain Current Collapse. Models Presented for Current Collapse (b) Under Drain Stress and (c) Under Gate Stress. Reprinted from Hasegawa <i>et al.</i> , <i>J. Vac. Sci. Technol. B</i> 21 , 1844 (2003) [43]. Copyright 2003, American Vacuum Society.....	13
1.4 Model of Device Showing the Location of the Virtual Gate and Schematic Representation of the Device Including the Virtual Gate. Reprinted from Vetry <i>et al.</i> , <i>IEEE Trans. Electron Devices</i> 48 , 560 (2001) [63]. Copyright 2002 Institute of Electrical and Electronics Engineers.....	14
1.5 Crystal Structure, Spontaneous Polarization Fields (P_{SP}), and Piezoelectric Polarization Fields (P_{PE}) for GaN (top) and Al _x Ga _(1-x) N (bottom). Reprinted from Yu, <i>et al.</i> , <i>J. Vac. Sci. Technol. B</i> 17 , 1742 (1999) [94]. Copyright 1999, American Vacuum Society.....	19

Figure	Page
1.6 Band Bending Schematic for Ga- and N-Face GaN. Both Surfaces are Screened by $\sim 10^{13}$ Charges/cm ² . (NOTE: the Position of the Ionized Donors and Electrons in the Material Corresponds to the Physical Position Rather than the Energy Level within the Band Gap.).....	22
1.7 Schematic Top View of the Vacancy and the Vacancy Complex. The Atomic Positions of the First Two Layers (Three Layer Vacancy Complex) are Displayed. Open and Closed Circles Represent First- and Second-Layer Atoms. For Anion Termination, the White and Black Circles Correspond to Nitrogen and Group-III Atoms, Respectively. For the Case of the Cation-Terminated Surface, the Open and Closed Circles Illustrate First-Layer Group-III Atoms and Second-Layer Nitrogen. the $p(2 \times 2)$ Unit Cell Used in All Calculations is Indicated. Reprinted from Fritsch <i>et al.</i> , <i>Phys. Rev. B</i> 57 , 15360 (1998) [121]. Copyright 1998, American Physical Society.....	24
1.8 Schematic of the Metal-Semiconductor Interface Models According to (a) Schottky-Mott, (b) Bardeen-Heine, and (c) Tersoff.....	27
1.9 Schematic Representation of the Interface Defect Densities According to (a) the MIGS Model, (b) the Unified Defect Model, and (c) the DIGS Model (or the Positional Surface Disorder Model).....	29
1.10 Schematic of Suggested Defect Mechanism Due to Deposition of Metal Atoms on Clean III-V Surfaces. This Process (i.e., a Defect Must be Formed) Needs to Occur Only About Once for Every Hundred Metal Atoms Striking the Surface to Account for Fermi	

Figure	Page
Level Pinning. Reprinted from Spicer <i>et al.</i> , <i>J. Vac. Sci. Technol.</i> 16 , 1422 (1979) [133]. Copyright 1980, American Vacuum Society.....	31
1.11 Unified Disorder Induced Gap States (DIGS) Model Explaining the Correlation Between I-S and M-S Interfaces. Surface Disorder Introduces DIGS Whose Density Depends on the Degree of Disorder (I: Good I-S Interface, II: Poor I-S Interface, and III M-S Interface). the Physical Meaning of E_{CNL} Can be Interpreted as the Fermi Energy of the DIGS Spectrum where Charge Neutrality is Achieved. E_{CNL} is the Branch Point Between the Bonding and Antibonding States in the Gap. Reprinted from H. Hasegawa and H. Ohno <i>J. Vac. Sci. Technol. B</i> 4 , 1130 (1986) [44]. Copyright 1986 American Vacuum Society.....	32
1.12 The CNL is a Weighted Average of the Density of States. It is Repelled by a Large Density of States in the Valence or Conduction Band. Reprinted from J. Robertson and B. Falabretti, <i>J. Appl. Phys.</i> 100 , 014111 (2006) [141]. Copyright 2006, American Institute of Physics.....	33
1.13 Trend of the CNL/Band Gap Ratio vs. (a) Harrison’s Bond Polarity and (b) Ionicity of Garcia and Cohen. As the Band Gap Becomes More Direct with Higher Ionicity, the CNL Moves Higher in the Gap. Reprinted from J. Robertson and B. Falabretti, <i>J. Appl. Phys.</i> 100 , 014111 (2006) [141]. Copyright 2006, American Institute of Physics.....	36

Figure	Page
1.14 Calculated Band Offsets of Dielectrics on GaN. Reprinted from J. Robertson and B. Falabretti, <i>J. Appl. Phys.</i> 100 , 014111 (2006) [141]. Copyright 2006, American Institute of Physics.....	37
2.1 Schematic Representation of the Layer-By-Layer Deposition Process of Thermal and Plasma-Enhanced ALD. During Reactant or Plasma Exposure, the Surface is Exposed to a Reactant Gas or Plasma.....	92
2.2 (a) Number of Publications Regarding ALD per Year Between 1991 and November 17, 2014 Found in Web of Science. (b) Number of Publications Regarding Plasma-Enhanced ALD per Year Between 1991 and November 17, 2014 Found in Web of Science.....	95
2.3 Chemisorption Mechanisms for ALD Growth by (a) Ligand Exchange, (b) Dissociation, or (c) Association.....	98
2.4 Ideal Close Packing Structure of Precursor Ligands. the Area of the Shade Unit Cell is Given by $2\sqrt{3}R_L^2$. Modified from R.L. Puurunen, <i>Chem. Vap. Dep.</i> 9 , 249 (2003) [89]. Copyright 2003, WILEY-VCH Verlag GmbH & Co.....	100
2.5 Effect of the Reactant Partial Pressure p on the Amount of Material Chemisorbed in a Gas-Solid Reaction: (a) the Equilibrium Chemisorption Coverage Q^{eq} in Reversible Adsorption (Equilibrium Constants $1 \leq K \leq 10^4$) and (b) the Chemisorption Coverage Q after Saturation in Irreversible Adsorption. Reprinted from R. L. Puurunen, <i>J. Appl. Phys.</i> 97 , 121301 (2005) [7]. Copyright 2005, American Institute of Physics.....	103

2.6 Schematic Representation of Five Reaction Cycles, Assuming Irreversible Adsorption: (a) Chemisorption Coverage Q as a Function of Time t (Solid Line: ML_z Species Adsorbed in the Reaction of the Reactant a Assumed to be of Type ML_n , Dashed Line: Species Adsorbed in the Reaction of Reactant B; the Beginning and End of a Reaction Cycle and Steps 1–4 are Indicated), (b) the Amount of Atoms M Adsorbed C_m as a Function of Time t , (c) the Deposition Rate of M Atoms dc_m/dt as a Function of Time t [Obtained as the Time Derivative of the Curve in Panel (b)], (d) Amount of Material Deposited c_m as a Function of the Number of Reaction Cycles n , and (e) the GPC Δc_m as a Function of the Number of Reaction Cycles n . Reprinted from R. L. Puurunen, *J. Appl. Phys.* **97**, 121301 (2005) [7]. Copyright 2005, American Institute of Physics. 107

2.7 Variation of the GPC with the ALD Processing Temperature in the *ALD Window*: (a) the GPC Decreases with Temperature, (b) the GPC is Constant with Temperature (Possible with Different Values at Different Temperature Ranges, as Shown by the Dashed Line), (c) the GPC Increases with Temperature, and (d) the GPC First Increases and then Decreases with Temperature. Reprinted from R. L. Puurunen, *J. Appl. Phys.* **97**, 121301 (2005) [7]. Copyright 2005, American Institute of Physics. 107

2.8 Common Relationship Between the GPC and Temperature, where the Region of Constant Growth is Called the “ALD Growth Window.” 108

2.9 Dependency of the GPC on the Number of Reaction Cycles in Different Types of ALD Processes (Ref. 247): (a) Linear Growth, (b) Substrate-Enhanced Growth, (c)

Figure	Page
Substrate-Inhibited Growth of Type 1, and (d) Substrate-Inhibited Growth of Type 2. Reprinted from R. L. Puurunen, <i>J. Appl. Phys.</i> 97 , 121301 (2005) [7]. Copyright 2005, American Institute of Physics.	109
2.10 Schematic Illustration with Increasing Number of Reaction Cycles <i>n</i> of Selected Growth Modes Possible in ALD: (a) Two-Dimensional Growth, (b) Island Growth, and (c) Random Deposition. Reprinted from R. L. Puurunen, <i>J. Appl. Phys.</i> 97 , 121301 (2005) [7]. Copyright 2005, American Institute of Physics.	111
2.11 Materials Deposited by Atomic Layer Deposition. This Includes Compound Materials, such as Oxides, Nitrides, Carbides, Sulfides, Fluorides, Phosphides, Selenides, and Pure Elements as Shown. Modified from Ref. 7, 120, and 121	112
2.12 Molecular Structure for Common Precursor Ligands. Reprinted from R.L. Puurunen, <i>J. Appl. Phys.</i> 97 , 121301 (2005) [7]. Copyright 2003, American Institute of Physics...	115
2.13 (a) Elemental Metal Reactants Used in ALD: No Ligands; (b) Metal Halide Reactants Used in ALD: F, B, Cl or I Ligands; (c) Metal Alkoxide Reactants Used in ALD: OMe, OEt, O ⁱ Pr, O ⁱ Bu, O ^t Bu, mmp, or dmae Ligands; (d) Metal B-Diketonate Reactants Used in ALD: acac, thd, hfac, od, and, or methd Ligands; (e) Metal Amide Reactants Used in ALD: NMe ₂ , NEtMe, NEt ₂ , or N(SiMe ₃) ₂ Ligands; (f) Metal Amidinate Reactants Used in ALD: ⁱ PrAMD and ^t BuAMD Ligands; (g) Metal Alkyl Reactants Used in ALD: Me, Et, ⁱ Pr, Ay, ⁿ Bu, ⁱ Bu, ^t Bu, or Np Ligands; and (h) Metal Cyclopentadienyl Reactants Used in ALD: Cp, Cp ^{Me} , Cp*, Cp ^{Et} , Cp ^{iPr} , or Cp(SiMe ₃)	

Figure	Page
Ligands. (See Appendices A and B for clarification of ligand chemistry.) Reprinted from R. L. Puurunen, <i>J. Appl. Phys.</i> 97 , 121301 (2005) [7]. Copyright 2005, American Institute of Physics.....	116
2.14 Schematic Reactor Configurations for (a) Radical-Enhanced, (b) Direct, and (c) Remote PEALD [1].....	122
2.15 Schematic of Remote Oxygen Plasma-Enhanced Atomic Layer Deposition Chamber at the Nanoscience Laboratory.....	129
2.16 Al ₂ O ₃ Growth Rate Vs. DMAI Dose Time, O ₂ Plasma Exposure Time, and N ₂ Purge Time. These Values are Set to be 0.6 s, 8 s and 20 s when They are Not Variable, and Substrate Temperature was Set at 190°C. Reprinted from Yang <i>et al. J. Vac. Sci. Technol. A</i> 32 , 021514 (2014) [131]. Copyright 2014, American Vacuum Society.....	131
2.17 Al ₂ O ₃ Growth Rate Vs. Substrate Temperature, Determining the ALD Window of 25 to 220 °C. The Square Represents the Increased Growth Rate Caused by the Longer Plasma Pulse Time. The Inset Shows the Film Thickness Vs. Number of PEALD Cycles for the Sample at 200°C. Reprinted from Yang <i>et al. J. Vac. Sci. Technol. A</i> 32 , 021514 (2014) [131]. Copyright 2014, American Vacuum Society.....	132
2.18 The Number of Al Atoms Deposited Per Cycle as Determined by RBS (a) and the Film Mass Density as Measured by XRR (b) for PEALD Al ₂ O ₃ Grown with DMAI at Different Temperatures. Reprinted from Yang <i>et al. J. Vac. Sci. Technol. A</i> 32 , 021514 (2014) [131]. Copyright 2014, American Vacuum Society.....	133

Figure	Page
2.19 XPS Spectra of Al 2p (a), O 1s (b), and C 1s (c) Peaks for 10 nm (i) as-Grown and (ii) Annealed Al ₂ O ₃ Thin Film Deposited at 200°C. Reprinted from Yang <i>et al. J. Vac. Sci. Technol. A</i> 32 , 021514 (2014) [131]. Copyright 2014, American Vacuum Society.	134
2.20 XPS Spectra of Al 2p (a), O 1s (b), and C 1s (c) Peaks for 10 nm Al ₂ O ₃ Thin Film Deposited at Room Temperature with (i) 8s and (ii) 40s O ₂ Plasma During Deposition. Reprinted from Yang <i>et al., J. Vac. Sci. Technol. A</i> 32 , 021514 (2014) [131]. Copyright 2014, American Vacuum Society.	134
2.21 Growth Rate as Related to the Precursor Pulse Time.	136
2.22 Temperature Dependence of the Growth Rate for the TEMAHF and O ₂ Plasma Process.	136
3.1 Energy Diagram of a Semiconductor with a Photo-Emitted Electron of Energy $h\nu$. Conservation of Energy Determines the Binding Energy, where $E_B = h\nu - \phi - E_K$.	147
3.2 (a) Schematic of a Twin Anode X-Ray Source and (b) Monochromated Al Anode.	149
3.3 Schematic of the Typical Hemispherical Analyzer Used in XPS. Modified from R. Smart <i>et al.</i> [2]. Copyright University of Hong Kong.	150
3.4 Example Backgrounds for Core Level Fittings for (a) Background and Core Level Peak Fittings for (b) a Step-Down Background Fitting, (c) a Linear Background Fitting, and (d) a Shirley Background Fitting. Modified from R. Smart <i>et al.</i> [2]. Copyright University of Hong Kong.	152

Figure	Page
3.5 Explanation of the Auger Process on the Basis of Atomic Level Schemes. A Primary Electron Produces an Initial Hole in the Core Level and the Escaping Electron is Indicated by a Broken Arrow; Another Electron is Deexcited from a Higher Shell, Core Level in (a,b,c) and the Valence Band of a Solid (d). The Deexcited Energy is then Transferred to a Third Electron, which Leaves the System as an Auger Electron. Reprinted from Lüth, <i>Solid Surfaces, Interfaces, and Thin Films</i> , 5 th Ed. (Springer, Heidelberg, Germany, 2010), pp. 50 [1]. Copyright 2010, Springer.....	155
3.6 Illustration of a Photoemission Spectra, where the Electrons that have Undergone Scattering Processes on Their Way Into Vacuum are Detected at Lower Energy and Form a Continuous Background of the So-Called Secondary Electrons. Modified from Lüth, <i>Solid Surfaces, Interfaces, and Thin Films</i> , 5 th Ed. (Springer, Heidelberg, Germany, 2010), pp. 312 [1]. Copyright 2010, Springer.....	156
3.7 UPS Spectra of (a) Oxygen-Terminated n-Type Ga-Face GaN, (b) 1 nm as-Deposited Al ₂ O ₃ on n-Type, Ga-Face GaN, (c) 1 nm as-Deposited HfO ₂ on n-Type, Ga-Face GaN, Giving the Electron Affinity and VBM. The Valence Band Maximum (VBM) is the Difference Between the Fermi Level and the Low-Binding Energy Cutoff, and the Width of the Spectrum, W, is Used to Calculate the Electron Affinity of the Oxide. Reprinted from Yang <i>et al.</i> [9]. Copyright 2012, American Institute of Physics.....	159
3.8 Energy Distribution of a Semiconductor Exposed to Ultraviolet Light, Generating a UPS Spectrum. Low Binding-Energy (Or High-Kinetic Energy) Cutoff of the Spectrum is	

Figure	Page
Used to Determine the VBM while the High-Binding Energy (Or Low-Kinetic Energy) Cutoff is Used to Determine the Electron Affinity or Ionization Energy.....	161
3.9 Surface Band Bending Measurements (bottom) were Determined from the Position the Ga 3d Core Level as Determined from XPS (top) by the Given Equation (middle). Reprinted from Eller <i>et al.</i> , <i>J. Electron. Mater.</i> 43 , 4560 (2014) [12]. Copyright 2014, Springer US.....	162
3.10 Band Offsets (bottom) are Determined from the Difference Between the Ga 3d and Corresponding Oxide Core Level as Determined from the XPS (top) by the Given Equation (middle).....	164
3.11 O 1s Energy Loss Spectra from 10 nm Annealed Al ₂ O ₃ on Si as Deposited at 200°C. the Zero Loss Energy Represents the O 1s Core Level. Ev is the Valence Band Maximum; Ec is the Conduction Band Minimum; and Eg is the Band Gap. Reprinted from Yang <i>et al.</i> [19]. Copyright 2014, American Vacuum Society.....	167
4.1 Schematic Band Diagram of Parallel Plate Capacitor Formed from Two Materials (a) in Isolation, (b) Short-Circuited, and (c) Connected by a DC Bias Equal and Opposite to the CPD. Reprinted from L. Kronik <i>et al.</i> , <i>Surf. Sci. Rep.</i> 37 , 1 (1999) [1]. Copyright 1999, Elsevier Science B.V.....	169
4.2 Schematic Diagram of the Tip-Sample Spacing During Tip Oscillation. Here D_0 Represents the Mean Spacing and d_1 the Amplitude of Tip Motion, Thus $2d_1$ Represents the Total Tip Displacement. Modified from UHVKP Technology Manual 7.3 [2].....	170

Figure	Page
4.3 (a) Circuit Diagram of the Tip Amplifier: the Specimen (bottom Plate of the Kelvin Capacitor C_K) is Connected to Earth via a Computer-Steered Backing Potential V_b . the Tip Signal i_{tot} is Input Directly to an I/V Converter, Having Feedback Resistance R_f ; S Denotes the first Stage Amplifier Summing Point and C_p the Tip Parasitic Capacity. R_1 and R_2 Set the Voltage Gain of the Preamplifier Stage, the Output Signal V_{out} Passes via a Low Pass Filter (LPF) to the Analog-To-Digital (AD) Converter of the Data Acquisition System. (b) Simplified Diagram of the First Stage Amplifier where the I/V Converter is Represented by its Input Resistance R_{in} . Analysis of this Circuit Shows that, for Low Frequencies (< 1000 Hz), the Signal Lost to the Parasitic Capacitance i_2 is Negligible thus $i_{tot} = i_1$. Modified from UHVKP Technology Manual 7.3 [2].	171
4.4 Example of a Kelvin Probe Signal Under Conditions of High Modulation Index. the Peak-To Peak Voltage, $V_{ptp} = -3.25$ V, where the Peak-To-Peak Height is Being Negative If the Trough Appears Before the Peak. Modified from UHVKP Technology Manual 7.3 [2].	172
4.5 Plot of V_{ptp} versus V_b Showing the Linear Behavior. Note that the Line Crosses the V_b Axis at the Point where the Sum of the Contact and Backing Potentials are Zero. Modified from UHVKP Technology Manual 7.3 [2].	173
4.6 Schematic Band Diagram of Parallel Plate Capacitor Formed from a Metal and Semiconductor (a) in Isolation, (b) Short-Circuited, and (c) Connected by a DC Bias	

Figure	Page
Equal and Opposite to the CPD. Reprinted from L. Kronik <i>et al.</i> , <i>Surf. Sci. Rep.</i> 37 , 1 (1999) [1]. Copyright 1999, Elsevier Science B.V.....	174
4.7 Schematic Diagram of the Electronic Band Structure at a Semiconductor Surface. Reprinted from L. Kronik <i>et al.</i> , <i>Surf. Sci. Rep.</i> 37 , 1 (1999) [1]. Copyright 1999, Elsevier Science B.V.....	175
4.8 Example of Surface Photovoltage Effects where the Band Bending is Flattened Under UV Illumination. (a) in n-Type Material, the SPV Corresponds to Accumulation of Photo-Generated Holes Near the Surface Region while Photo-Generated Electrons Accumulate on the Far Side of the Depletion Region. Conversely, (b) in p-Type Material, the SPV Corresponds to Accumulation of Photo-Generated Electrons Near the Surface Region while Photo-Generated Holes Accumulate on the Far Side of the Depletion Region.....	176
5.1 Crystal Structure, Spontaneous Polarization Fields (\mathbf{P}_{SP}), and Piezoelectric Polarization Fields (\mathbf{P}_{PE}) for GaN (top) and $Al_xGa_{(1-x)}N$ (bottom). Reprinted from Yu, <i>et al.</i> , <i>J. Vac. Sci. Technol. B</i> 17 , 1742 (1999) [4]. Copyright 1999, American Vacuum Society.....	180
5.2 Theoretical (a) and Experimental (b) Band Bending Schematic for Ga- and N-Face GaN. Both Surfaces are Screened by $\sim 10^{13}$ charges/cm ² . (NOTE: the Position of the Ionized Donors and Electrons in the Material Corresponds to their Physical Position	

Figure	Page
rather than their Energy Level within the Band Gap.) Reprinted from Eller <i>et al.</i> , <i>J. Vac. Sci. Technol. B</i> 31 , 050807 (2013) [2]. Copyright 2013, American Vacuum Society.....	182
5.3 O 1s Peak for N-Face GaN (a), Ga-Face GaN (b), and Ga-Face Al _{0.25} Ga _{0.75} N (c) as Received (i), After <i>Ex-Situ</i> Cleaning (ii), and After <i>In-Situ</i> Cleaning (iii). Note: Core Levels were Shifted to the Corresponding Flat Band Position, Allowing Direct Comparison of the Oxygen States.....	186
5.4 XPS Results for N-Face GaN (a), Ga-Face GaN (b), and Ga-Face Al _{0.25} Ga _{0.75} N (c) as Received (i), After <i>Ex-Situ</i> Cleaning (ii), and After <i>In-Situ</i> Cleaning (iii).....	187
5.5 Surface Bend Bending Measurements (bottom) were Determined from the Position the Ga 3d Core Level as Determined from XPS (top) by the Given Equation (middle).....	188
5.6 Correlation Between the Surface Band Bending and Film Content, i.e. Oxygen Coverage (a) and Relative Nitrogen Surface Concentration (b) for N-face GaN, Ga-face GaN, and Ga-face Al _{0.25} Ga _{0.75} N.....	190
5.7 Suggested Charge Transfer Model for Pinning State on N- and Ga-face GaN and AlGaN.....	191
6.1 Schematic of Remote Oxygen-PEALD Chamber.....	202
6.2 Growth Per Cycle (GPC) of ALD SiO ₂ as a Function of TDMAS (a), Oxygen Plasma (b), and Nitrogen Pulse (c) Times with a Constant Substrate Temperature of 30°C. the Timing for Each Respective Gas Phase was 1.6 s, 16 s, and 30 s When Not Otherwise Specified.....	205

Figure	Page
6.3 The Growth Per Cycle (GPC) of ALD SiO ₂ at Substrate Temperatures Varying from 30 to 550°C, where the Precursor Dosing Time was 1.6 s, Oxygen Plasma Time was 16 s, and Nitrogen Purge Time was 30 s. Results Show No Apparent ALD Growth Window and Thermal Decomposition at 550°C.	205
6.4 O 1s, N 1s, C 1s, and Si 2s XPS Spectra of ~30 nm SiO ₂ Deposited at 30°C, 270°C, and 550°C	207
6.5 O 1s, C 1s, Si 2s, and Ga 3s Core Level Spectra for 40 Cycles of SiO ₂ on GaN for Various Deposition Temperatures. (NOTE: Given the Large Growth Rate at 550°C, Samples Grown at this Temperature were Grown with Only 20 Cycles Such that the Substrate was Still Detectable.)	208
6.6 5-μm ² AFM Images of (a) Wet-Chemical Cleaned GaN Surface as well as ~30 nm SiO ₂ Films as Deposited at (b) 30°C, (c) 270°C, and (d) 550°C. the RMS Heights were Averaged for Three Different Positions on the Sample. AFM Images Provided Courtesy of Sarah Rupprecht.	208
6.7 CV and IV Curves for (a) 31 nm SiO ₂ Films Deposited at 30°C, (b) 42 nm SiO ₂ Films Deposited at 270°C, and (c) 11 nm SiO ₂ Films Deposited at 550°C on GaN. Electrical Measurements Provided Courtesy of Wenwen Li.	209
6.8 Chemisorption Mechanism for TDMAS on an OH-Terminated Surface.	211
6.9 Schematic of the Effective Band Offset Measurements of SiO ₂ /GaN, with a Subcutaneous Oxide Layer. The Thickness of the Ga ₂ O ₃ Layer Increases with	

Figure	Page
Temperature; However, the Potential Drop Decreases Across this Layer with Temperature as well. This Decrease is Related to the Removal of Acceptor-Like Defects that are Introduced by the O ₂ Plasma and Affected High-Temperature Annealing.....	213
7.1 The Inverse of the Energy Band Gap with Respect to the Electronic Component of the Dielectric Constant for a Range of Dielectrics.....	223
7.2 Band Offsets (bottom) as Determined by the Difference Between the XPS Ga 3d and Si 2s Core Levels (top) by the Given Equation (middle).....	226
7.3 XPS Spectra of Residual Carbon (Left) and Oxygen (Right) Contamination After 680°C N ₂ /H ₂ Plasma Surface Treatment. For Both Elements, the Contamination Levels were Below the Detection Limit of the XPS.....	227
7.4 XPS Spectra of Ga 3s, Al 2p, and Ga 3d Core Levels After 680°C N ₂ /H ₂ Plasma Surface Treatment. The N 1s Peak is Not Included as it is Obscured by a Ga Auger Peak. the Dotted Lines Indicate Core Level Positions of the GaN Surface.....	228
7.5 XPS Spectra of Ga 3d Core Level to the VBM of GaN (top), Al _{0.15} Ga _{0.85} N (top-middle), Al _{0.25} Ga _{0.75} N (bottom-middle), and Al _{0.35} Ga _{0.65} N (bottom). The Position of the VBM is Determined by Linear Extrapolation of the Low-Binding Energy Cut-Off. (NOTE: the Positions of the Ga 3d Core Level were Aligned for Comparison in this Plot and Do Not, Therefore, Represent that Experimentally Determined Values Described for the VBM and Core Level Positions.) In Addition, the Peak at ~17 eV is the N 2s Core Level.....	229

Figure	Page
7.6 XPS Spectra of Ga 3d Core Level to the VBM Difference of GaN After Different Plasma Treatments, Resulting in Different Surface States. One Clean Results in an Oxygen-Free Surface while the Other Gives ~1 ML of Oxygen Coverage as Shown by the O 1s Core Level in the Inset. (NOTE: the Positions of the Ga 3d Core Level were Aligned to Account for Differences in Band Bending.) In Addition, the Peak at ~17 eV is the N 2s Core Level.....	229
7.7. 10 nm PEALD SiO ₂ as Deposited on GaN and Annealed at 400°C in N ₂ Ambient. the Binding Energy Difference Between the Si 2s Core Level and Valence Band Maximum of SiO ₂ was Calculated as Shown.....	230
7.8 XPS Spectra for the Ga 3s, Si 2s, and Ga 3d Core Levels of ~3 nm PEALD SiO ₂ on GaN (top), Al _{0.15} Ga _{0.85} N (top-middle), Al _{0.25} Ga _{0.75} N (bottom-middle), and Al _{0.35} Ga _{0.65} N (bottom) After Deposition. the Peak-To-Peak Differences Used to Calculate the Valence Band Offsets, i.e. $E_{Ga3s}-E_{Si2s}$ and $E_{Si2s}-E_{Ga3d}$, are Indicated.....	231
7.9 XPS Spectra for the Ga 3s, Si 2s, and Ga 3d Core Levels of ~3 nm PEALD SiO ₂ on GaN, Al _{0.15} Ga _{0.85} N (top-middle), Al _{0.25} Ga _{0.75} N (bottom-middle), and Al _{0.35} Ga _{0.65} N (bottom) After 400°C in N ₂ Ambient. the Peak-To-Peak Differences Used to Calculate the Valence Band Offsets, i.e. $E_{Ga3s}-E_{Si2s}$ and $E_{Si2s}-E_{Ga3d}$, are Indicated.....	231
7.10 (a) N 1s Core Levels After 680°C N ₂ /H ₂ Plasma Surface Treatment as Dependent on Aluminum Content, and (b) N 1s Core Levels of GaN as Dependent on Plasma	

Figure	Page
Treatment. (NOTE: These Peaks were Shifted to Account for Any Differences in Band Bending.).....	233
7.11 Band Alignment as Determined by the Charge Neutrality Level Model. the Heavy Lines Correspond to the Conduction and Valence Bands of $\text{Al}_x\text{Ga}_{1-x}\text{N}$, while the Thinner Lines Correspond the Conduction and Valence Bands of SiO_2 . Experimental Offset Measurements are Given for 0%, 15%, 25%, and 35% Al-Content in Blue Followed with the Theoretical Results in Parentheses for Comparison. The Theory is Linearly Interpolated from the CNLs Given by Robertson and Falabretti [24].	237
8.1 Schematic of EE-ALD Chamber as Modified to Include Plasma Processing, UV Illumination, and Sample Biasing.....	248
8.2 Interface Charge Distribution at the AlGaN/GaN Heterostructure, where the Changes in Surface States on the AlGaN Layer or Dielectric/AlGaN Interface Will Affect the Charge Distribution and may Have Possible Implication on the 2DEG Concentration. 252	

LIST OF PUBLICATIONS

Brianna S. Eller, Jialing Yang, and Robert J. Nemanich, *J. Vac. Sci. Technol. A* **31**, 050807 (2012). “Electronic surface and interface states on GaN and AlGaN”

Brianna S. Eller, Jialing Yang, and Robert J. Nemanich, *J. Electron. Mater.* **43**, 4560 (2014). “Polarization effects of GaN and AlGaN: polarization bound charge, band bending, and electronic surface states”

Brianna S. Eller, Wenwen Li, Sarah Rupprecht, Srabanti Chowdhury, and Robert J. Nemanich, to be submitted (2015). “Characterization of plasma-enhanced atomic layer deposition of SiO₂ using tris(dimethylamino)silane on GaN”

Brianna S. Eller and Robert J. Nemanich, to be submitted (2015). “Surface band bending and interface alignment of plasma-enhanced atomic layer deposited SiO₂ on Al_xGa_{1-x}N”

Jialing Yang, Brianna S. Eller, Chiyu Zhu, Chris England, and Robert J. Nemanich, *J. Appl. Phys.* **112**, 053710 (2012). “Comparative band alignment of plasma-enhanced atomic layer deposited high-k dielectrics on gallium nitride”

Jialing Yang, Brianna S. Eller, Manpuneet Kaur, and Robert J. Nemanich, *J. Vac. Sci. Technol. A* **32**, 021514 (2014). “Characterization of plasma-enhanced atomic layer deposition of Al₂O₃ by dimethylaluminum isopropoxide”

Jialing Yang, Brianna S. Eller, and Robert J. Nemanich, *J. Appl. Phys.* **116**, 123702 (2014). “Surface band bending and band alignment of plasma enhanced atomic layer deposited dielectrics on Ga- and N-face gallium nitride.”

N. A. Sanford, L. H. Robins, P. T. Blanchard, K. Soria, B. Klein, B. S. Eller, K. A. Bertness, J. B. Schlager, and A. W. Sanders, *J. Appl. Phys.* **113**, 174306 (2013). “Studies of photoconductivity and field effect transistor behavior in examining drift mobility, surface depletion, and transient effects in Si-doped GaN nanowires in vacuum and air”

Xin Liu, Chiyu Zhu, Brianna S. Eller, Tianyin Sun, Christophe J. Jezewsky, Sean W. King, and Robert J. Nemanich, *J. Vac. Sci. Technol. B* **30**, 052203 (2012). “Cu film thermal stability on plasma cleaned polycrystalline Ru”

Yang Sun, Brianna S. Eller, and Robert J. Nemanich, *J. Appl. Phys.* **110**, 084303 (2011). “Photo-induced Ag deposition on periodically poled lithium niobate: concentration and intensity dependence”

PART I: INTRODUCTION

CHAPTER 1. ELECTRONIC STATE CONFIGURATION OF GAN AND ALGAN

As published in Brianna S. Eller, Jialing Yang, and Robert J. Nemanich, J. Vac. Sci. Technol. A 31, 050807 (2012).

Mitigating multi-lateral ecological and environmental concerns will define next-generation technology. Power electronic technologies, in particular, promise to contribute significantly to this endeavor, where GaN remains one of, if not the, most promising candidates in these technologies. The potential of GaN-based power transistors is a result of its superior material properties in comparison to other materials associated with competing technologies such as Si, SiC, and GaAs as summarized in TABLE 1.1. Consequently, GaN-based technologies maintain a competitive advantage. (See TABLE 1.2, where the first column presents the next major milestones needed to be achieved to advance power technologies; the second column presents the enabling feature of GaN-based technologies in achieving these milestones; and the third presents the consequential technological advantages [1].) Specifically, the high power per unit width allows for smaller devices, which enable easier manufacturing and higher impedance; this further enables easier matching to the system, which can be complicated with other materials such as GaAs. The high breakdown voltage allows GaN-based devices to operate at higher voltages, reduces the need for voltage conversion, decreases power requirements, and simplifies cooling. Furthermore, GaN is a direct-gap semiconductor critical to light-emitting diode-technologies; utilizing this overlap in technologies will help drive down development costs.

TABLE 1.1 Material properties of Si, GaAs, SiC, and GaN, where μ is the mobility, ϵ is the relative permittivity, E_g is the band gap energy, the BFOM ratio is the Baliga figure of merit (related to the conduction loss at low frequency), and T_{\max} is the maximum temperature before degradation of the material. Reprinted from U.K. Mishra, *et al.*, *Proc. IEEE* **90**, 1022 (2002) [1]. Copyright 2002, Institute of Electrical and Electronics Engineers.

	μ ($\text{cm}^2/\text{V}\cdot\text{s}$)	ϵ (ratio)	E_g (eV)	BFOM (ratio)	T_{\max} ($^{\circ}\text{C}$)
Si	1300	11.4	1.1	1.0	300
GaAs	5000	13.1	1.4	9.6	300
SiC	260	9.7	2.9	3.1	600
GaN	1500	9.5	3.4	24.6	700

Accordingly, a wide range of superior devices has been reported in the past several years, including heterostructure field-effect transistors (HFETs), heterojunction bipolar transistors (HBTs), bipolar junction transistors (BJTs), Schottky and p-i-n rectifiers, and metal-oxide-semiconductor field-effect transistors (and metal-insulator-semiconductor field-effect transistors, MISFETs). To date, power transistors are typically Si based, which are more limited in their performance. For example, the on-resistance of Si-power MOSFETs has already been surpassed by that of GaN-power MOSFETs [2]. Furthermore, Si devices degrade at temperatures above 150°C [3]. GaN MOSFETs (and metal-insulator-semiconductor field-effect transistors, MISFETs) can operate at much higher temperatures, provide lower leakage currents, and reduce power consumption. GaN Schottky rectifiers have the potential for higher switching speeds and larger standoff voltages than SiC or Si, and GaN p-i-n rectifiers demonstrate high switching speeds due to the absence of minority carriers. There is also evidence that simple GaN BJTs would perform well at low current densities [4]. Moreover, AlGaN/GaN heterostructures are promising, because the disparate polarization of the materials engenders a 2D electron gas (2DEG) at the interface, which effectively reduces on-resistance and thus power loss.

The consequential high electron mobility makes AlGaN/GaN heterostructures ideal for high-frequency requirements associated with HFETs and high electron mobility transistors (HEMTs), which have demonstrated one order higher power density and higher efficiency than Si-based RF and microwave transistors. In other words, a wide range of power electronics will significantly benefit from the development of GaN and AlGaN. However, despite the promise of GaN-based electronics, there are still some issues that need to be addressed before this technology will replace existing Si-technologies: namely, developing methods of epitaxial growth of high-quality single GaN crystals, selective formation of n-type regions, and minimization of interface states between the gate dielectric and GaN or AlGaN substrate.

TABLE 1.2 Competitive advantages of GaN-based devices. Reprinted from U.K. Mishra, *et al.*, *Proc. IEEE* **90**, 1022 (2002) [1]. Copyright 2002, Institute of Electrical and Electronics Engineers.

Need	Enabling Feature	Performance Advantage
High Power/Unit Width	wide band gap, high field	compact, ease of matching
High Voltage Operation	high breakdown field	eliminate/reduce step down
High Linearity	HEMT technology	optimum band allocation
High Frequency	high electron velocity	bandwidth μ -wave/mm-wave
High Efficiency	high operating voltage	power saving, reduced cooling
Low Noise	high gain, high velocity	high dynamic range receivers
High Temperature Operation	wide band gap	rugged, reliable, reduced cooling needs
Thermal Management	SiC substrate	high power devices with reduced cooling needs
Technology Leverage	direct band gap, enabler for lighting	driving force for technology low cost

In this review, we address the latter. The large concentration of defects on GaN and AlGaN surfaces as well as dielectric/GaN or AlGaN interfaces results in a large leakage current and current collapse, degrading device performance and reliability; however, the mechanisms responsible for these reliability issues have not yet been fully established given the complexity of interface states. More explicitly, GaN and AlGaN are polar materials, with a large bound polarization charge at the interface that requires

compensation. If the polarization charge is compensated internally, it leads to unrealistically large band bending in n-type, Ga-face GaN or AlGaN and thus, in conjunction with experimental results, suggests heavy external compensation with a large distribution of electronic surface states. Yet, the nature of these states has remained ambiguous. In the following pages, we will, therefore, summarize the current understanding of the role of electronic states in GaN and AlGaN-based devices. We look at energy band diagrams; this includes polarization charge compensation and band bending at the surface as well as band alignment modeling at the interface. Theoretical band alignment modeling includes those given by the metal-induced gap states model, the unified defect model, the disorder-induced gap states model, and the chemical reaction model. These generate band-offset values, which we will analyze in comparison to experimental measurements, highlighting the effectiveness and shortcomings of the models. In particular, we find that such models do not consistently provide reliable results. It is likely that a more comprehensive and intricate understanding of the electronic state configuration is needed to improve these models. Generally, these calculations assume a perfectly ordered interface, which is not physically achievable. This discrepancy is likely related to variations in crystal structure, differences in stoichiometry, unobserved band bending, or the presence of an interfacial oxide layer. These factors can be influenced by various processing such as wet chemical cleaning, ion sputtering, vacuum annealing, gaseous annealing, plasma annealing, dielectric passivation material and deposition method, as well as post-deposition and post-metallization treatments, which may affect oxygen coverage, organic and inorganic contamination, structural defects, bonding configurations, defect states, adsorbates,

pinning states, etc. In other words, understanding the role of electronic states at GaN and AlGaN is a difficult task, which is affected by many factors.

I. Device Reliability

As mentioned, the high concentration of electronic defect states in GaN-based electronics causes deleterious reliability issues. The most notable are the large gate leakage current in HEMTs, HFETs, and MOSFETs (or MISFETs) as well as current collapse in HEMTs and HFETs. The failure mechanisms associated with these issues have been extensively studied, but a complete understanding has yet to be described. Most studies suggest that the issues are related to hot-electron-based mechanisms, where hot electrons are trapped in defect states, and partially stress dependent, as stressing beyond a critical voltage induces additional damage likely related to the inverse piezoelectric effect [5,6]. However, the specific states that drive these mechanisms remain unclear. Furthermore, it has been suggested that the two failure modes may not be associated with one another. In other words, there are two possible distinct failure mechanisms, which may be related to different electronic states [7]. Thus, the electronic state configuration is a complex issue, and while there has been significant effort to engineer these issues out of the devices using epitaxial layer design, chip metallization, passivation schemes, and general device topology and layout [8], it is unlikely that the devices will be fully optimized without a better understanding of their role.

A. Gate Leakage

Gate leakage refers to current lost through the gate by electron tunneling, degrading power efficiency and noise performance. In general, there are several gate leakage

mechanisms typically discussed as summarized in FIG 1.1, including Schottky or thermionic emission (TE) [9-15], thermionic field emission (TFE) [10-12,15-21], trap-assisted tunneling (TAT) [10,16-18,21-24], dislocation-assisted tunneling (DAT) [17,20,25-28], defect hopping [16-18,29,30], Fowler-Nordheim tunneling (FNT) [23], Frenkel-Poole emission (FPE) [14,20,26], and space charged limited current (SCLC) [31-33]. The dominant mechanism in any given device may be temperature dependent, bias dependent, and device specific.

In forward bias, the gate leakage at Schottky interfaces is often attributed to thermionic (or Schottky) emission and thermionic field emission [9-21]; however, most researchers agree that this mechanism must be coupled with another defect-related mechanism. For

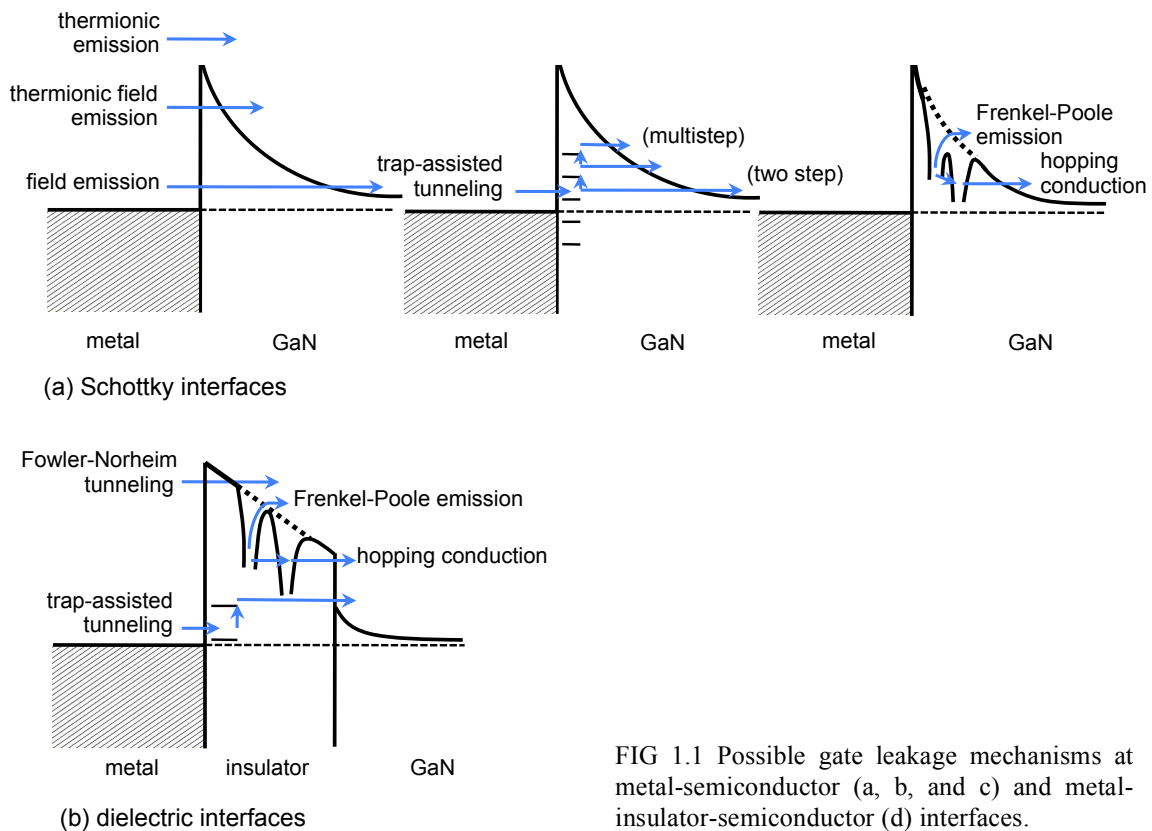


FIG 1.1 Possible gate leakage mechanisms at metal-semiconductor (a, b, and c) and metal-insulator-semiconductor (d) interfaces.

example, Carrano *et al.* [10] suggested that TE and TFE theories aptly describe experimental gate-leakage data only in addition to proposed deep-level bulk states that act as trapping states within tunneling distance of the interface. These defect states have been described as a continuum possibly related to the contamination layer on clean GaN, threading dislocations that reach the surface, and defects created by the Ti adhesion layer. Yu *et al.* [13] investigated the application of TE and TFE models assuming a triangular Schottky potential and also suggest that there is an enhanced tunneling component, which is demonstrated by the discrepancy of the Schottky barrier heights as measured by I-V-T and C-V measurements; the researchers, therefore, conclude that there are defects near the surface region. Shen *et al.* [31] used space charge limited current investigations to determine that deep traps ~ 0.2 eV below the conduction band minimum are likely trapping centers. In other words, most research agrees that TE and TFE account for only a fraction of the gate leakage in forward bias; while the small theoretical emission current may be related to an uncertain evaluation of the Schottky barrier, it is clear that the gate leakage mechanism must be augmented by some trap-induced mechanism.

Reverse-bias Schottky interfaces are more influential to the gate leakage phenomenon and thus have been more extensively studied. Miller *et al.* [16,17] adapted an analytical model from the forward bias case, assuming that the current is small in reverse bias such that electrons may tunnel from the gate into the semiconductor as well as from the semiconductor into the gate. Comparisons between extensive empirical gate leakage measurements in HFETs and two-dimensional simulations suggest that vertical tunneling (or TE/TFE) is the dominant mechanism, though lateral tunneling from the edge of the

gate to the drain (hopping) or trap-assisted tunneling (TAT) also contributed to the total leakage current. The leakage current is thus assumed to consist of two mechanisms that are temperature dependent. Temperature dependent modeling by Karmalkar *et al.* [18] on the off-state gate current in AlGaIn/GaN HEMTs shows that TAT dominates at temperatures <500K and direct TFE dominates at temperatures >500K. Similarly, Zhang *et al.* [20] conducted temperature-dependent studies, suggesting the dominant mechanism at temperatures >150K is Frenkel-Poole emission (FPE) and at temperatures <150K is TAT. Based on inferred Schottky barrier heights and room-temperature gate leakage results, they further conclude that highly conductive dislocations are likely responsible for TAT. These results are consistent with those of Kaun *et al.* [34], who showed that decreasing the threading dislocation density from $\sim 2 \times 10^{10}$ to $\sim 5 \times 10^7$ cm⁻² yielded up to a 45-fold decrease in the average reverse Schottky diode current.

The polarization may also have an integral role in the reverse-bias gate leakage mechanism. The polarization, therefore, becomes an important factor in determining device behavior as pointed out by Ganguly *et al.* [35] in InAlN/AlN/GaN devices. Similar work as been applied to AlGaIn/GaN HEMTs by Yan *et al.* [26]. Using the near-surface electric field beneath the Schottky barrier, they interpret the experimental results in terms of FPE between ~ 300 and 450K, concurrent with a forward TAT current. Studies by Sudharsanan *et al.* [24] show that increases in the polarization and internal electric field at the Schottky barrier occur with a simultaneous increase of gate leakage. This suggests that the leakage current mechanism must be related to defect states that also increase with the polarization. Given the lattice mismatch between AlGaIn and GaN, one possibility is

that an increase in aluminum concentration results in strain-induced defects, such as dislocation loops and threading segments at the interface and in AlGa_N, or perhaps the increased internal electric field has induced additional defects near the surface and in AlGa_N. Other studies have highlighted the importance of the electric field profile in devices, where stress-tested devices are characterized by higher leakage currents and defect densities via the inverse piezoelectric effect [5,6]. It has been argued that stress-induced defects are related to pits and grain boundaries near the gate edge where the electric field would be highest [31,33,36-41]. However, as Johnson *et al.* [42] pointed out, other defects may also be associated with the increase in post-electrical stressed devices, where the gate edge defects provide only a partial explanation for device failure. Other mechanisms such as drain-edge pits, metal diffusion, or oxide-related states as well as other native defects also influence device performance. On the other hand, externally stressing devices likely result in different behavior than increasing the polarization. It is, therefore, worth considering that an increase in polarization causes an increase in the bound charge and consequentially an increase in the compensation charge or surface states.

Such an argument would be more consistent with an alternative model proposed by Hasegawa *et al.* [43], where the electronic states act as pinning states rather than tunnel-assisting traps. In this research, the disorder induced gap state (DIGS) model—which will be discussed later—and additional empirical results are assumed to explain the mechanism of gate leakage in AlGa_N/Ga_N as summarized in FIG 1.2a. This work suggests that the near-surface electronic states are aptly described by a U-shaped

continuum common to III-V semiconductors [44] with an additional discrete peak at E_c -0.37 eV. (See FIG 1.2b.) This discrete peak likely corresponds to a N-vacancy and thus depends on the individual sample processing treatments. In other words, the continuum is

$$N_{SS} = N_{SSO} \exp \left(\frac{|E - E_{CNL}|}{E_{CNL}} \right), \quad (1)$$

where N_{SSO} is the minimum surface state density, and E_{CNL} is the energy position of the charge neutrality level with respect to the valence band maximum. E_{Oj} and n_j determine the distribution shape of the continuum; $j = a$ for acceptor-like states above E_{CNL} , and $j = d$ for donor-like states below E_{CNL} . The result is that the Fermi level is pinned near E_{CNL} , generating a thin Schottky barrier (TSB) as shown in FIG 1.2c. The thin Schottky barrier (TSB) more easily allows for electron tunneling, generating the TFE path responsible for the large leakage current in both forward and reverse directions. Hashizume *et al.* [45] later applied this model to experimental work, showing that the simulation reproduces experimental I-V-T measurements and gives excellent fitting for I-V curves in both forward and reverse bias.

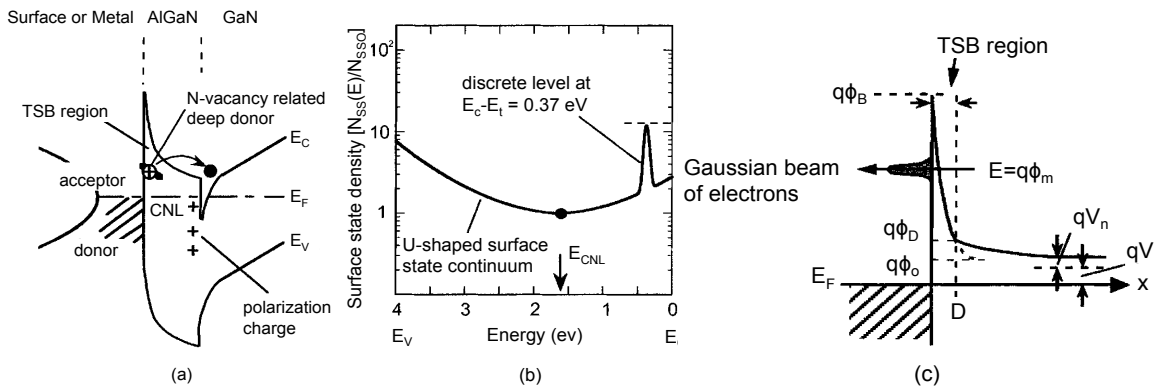


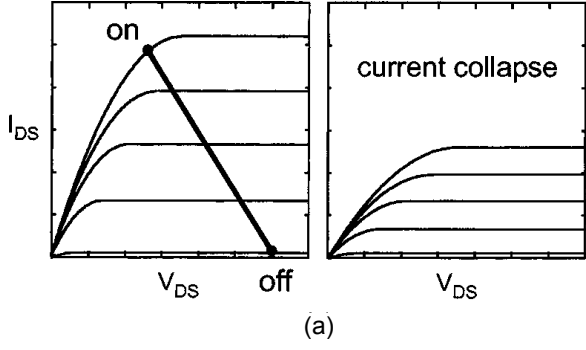
FIG 1.2 (a) Unified model for near-surface electronic states of AlGaIn, (b) a combined distribution of state density, and (c) the TSB model for current transport at the Schottky interface. Reprinted from Hasegawa *et al.*, *J. Vac. Sci. Technol. B* **21**, 1844 (2003) [43]. Copyright 2003, American Vacuum Society.

In other words, defect states play an integral role in gate leakage either through a trap-based tunneling/emission mechanism or Schottky barrier pinning. Consequently, research has sought to mitigate their effects using gate dielectrics, which generate an additional barrier for tunneling and emission processes. The most recent studies have included investigations into prevalent gate dielectrics such as SiO₂ [46-50], SiN_x [50,51], HfO₂ [52-55], Al₂O₃ [51,53-58], and AlN [23,59]. In general, these studies demonstrate an effective means of reducing the gate leakage in comparison to direct metal Schottky contacts. For example, SiO₂ and Al₂O₃ can reduce the gate leakage by three-four orders of magnitude [47,48,51]. Other studies have focused on the comparative behavior of the dielectrics. In one such study, Miyazaki *et al.* [53] compared the effectiveness of HfO₂ to Al₂O₃ on GaN metal-oxide-semiconductor heterostructure field-effect transistors (MOSHFETs). They found that Al₂O₃/GaN has a superior quality interface relative to HfO₂/GaN as demonstrated by the lower hysteresis and interface state density. Additionally, the gate leakage current of the Al₂O₃ MOSHFET is decreased by five to eight orders of magnitude in comparison to that of the HfO₂ MOSHFET. Al₂O₃/AlGaN/GaN MOSHFETs have, also, been characterized by a higher 2DEG concentration than SiN_x-passivated devices [51]. Other investigations have examined surface oxides as potential gate dielectrics and passivation schemes [60,61], which appear to improve gate leakage currents; however, Ľapajna *et al.* [62] pointed out that although HEMTs with native surface oxide appear to effectively reduce leakage current prior to stress, such devices often see a dramatic increase in gate leakage after stress measurements. The specifics of the gate leakage mechanism in these metal-insulator-semiconductor (MIS) structures may therefore depend on the specific material and deposition method as these factors will play a role in

determining the defects in the insulator and at the insulator-semiconductor interface. Liu *et al.* [23] show that in contrast with predominant thermionic field emission models for forward-bias Schottky contacts, forward bias $\text{Al}_2\text{O}_3/\text{AlGaIn}/\text{GaN}$ HEMTs are characterized by trap-assisted tunneling and Frenkel-Poole emission at temperatures $>0^\circ\text{C}$ and Fowler-Nordheim emission at temperatures $<0^\circ\text{C}$. Similar studies with HfO_2 [14] also conclude that Frenkel-Poole emission is the most dominant mechanism at high temperatures. Bi *et al.* [55] have suggested that the defect states in atomic layer deposited (ALD) HfO_2 associated with this mechanism are related to oxygen vacancies, which can be passivated with a post-deposition N_2 plasma in forward biased devices—though not reverse bias where another leakage mechanism likely dominates.

B. Current Collapse

Drain current collapse is the other major limiting factor in AlGaIn/GaN power electronics, which describes a significant reduction in the I-V curves when measured under large-amplitude high-frequency gate swings [63]. Subsequent measurements show that there is a reduction in drain current under drain stress, when the saturation region is in the on-state, and gate stress, when the channel region is pinched off in the off-state condition [64] as shown in FIG 1.3a. These results are inconsistent with other III-V MISFETs. In these devices, it is expected that on-state drain stress causes the capture of electrons from the 2DEG by deep level traps ultimately decreasing the drain current; therefore, the off-state gate stress should inject electrons back into the channel and result in an increase in drain current rather than the experimentally observed decrease.



● neutralized deep donors by electron capture

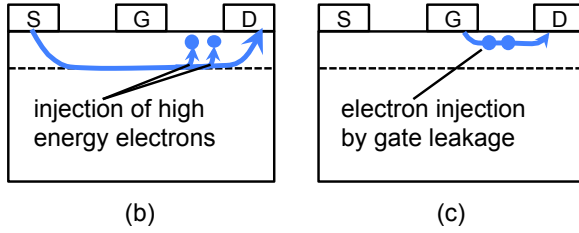


FIG 1.3 (a) Schematic representation of drain current collapse. Models presented for current collapse (b) under drain stress and (c) under gate stress. Reprinted from Hasegawa *et al.*, *J. Vac. Sci. Technol. B* **21**, 1844 (2003) [43]. Copyright 2003, American Vacuum Society.

Hasegawa *et al.* [43] have proposed a model to explain this behavior under drain and gate stress as summarized in FIG 1.3b and c, respectively. Using the density of states distribution in FIG 1.2a, this model assumes that electrons are injected from the 2DEG to the surface states of AlGa_N near the drain under drain stress, reducing the drain current and expanding the depletion width. When the voltage is switched to the off-state, the electrons are emitted from these states leading to recovery transients, according to the following equation:

$$N_{emit}(t) = \int N_{SS}(E) \left[1 - \exp\left(-\frac{1}{\tau(E)}\right) \right], \quad (2)$$

where

$$\tau(E) = \frac{1}{N_c \sigma_n v_{thn}} \exp\left(\frac{E_c - E}{kT}\right). \quad (3)$$

Hasegawa *et al.* has determined that this model fits the experimental data, where the total density of the discrete peak at 0.37 eV is 5×10^{11} defects/cm². Once the voltage is

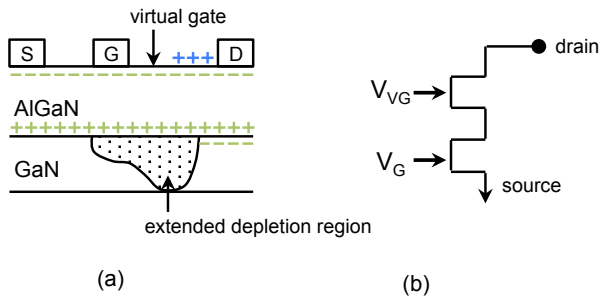


FIG 1.4 Model of device showing the location of the virtual gate and schematic representation of the device including the virtual gate. Reprinted from Vetury *et al.*, *IEEE Trans. Electron Devices* **48**, 560 (2001) [63]. Copyright 2002 Institute of Electrical and Electronics Engineers.

switched back to the off-state condition, the electrons from the discrete peak are quickly emitted, giving rise to a fast transient. There is also another slower transient, which is associated with the emission of electrons from the continuum of surface states, which have a wider range of time constants and cause the formation of a virtual gate.

The concept of a “virtual gate” was proposed by Vetury *et al.* [63] in 2001. In this model, a negative surface potential behaves like a negatively biased metal gate as depicted in FIG 1.4. The voltage across the gate, V_{VG} , is thus determined by the total amount of trapped charge in the gate-drain region. In other words, this model argues that the surface of an as-grown wafer has a net positive surface charge, which arises from screening of a negative polarization bound charge. The formation of a virtual gate, therefore, arises from a reduction in this net positive charge either by removal of the positively charged defects or the trapping of electrons in donor-like defects. As trapping occurs and the states fill, the formation of the virtual gate causes an increase in the depletion region and consequent decrease in the electric field at the gate edge. The current collapse is thus related to how quickly the surface state charge is neutralized, where the trapping is strongly dependent on the electric field between the gate and the drain. To restore the current, the net positive surface charge must be replaced. This can occur with the removal of electrons from the trapping states with forward bias or the accumulation of holes at the

surface. This model has since been further developed by Koudymov *et al.* [65] and Morardi *et al.* [66], where the modeling strategy is based on a reasonable set of assumptions and a smaller number of fitting parameters. Subsequent simulations closely agree with experimental measurements in AlGaIn/GaN HFETs.

Currently, the formation of a virtual gate is widely accepted as the cause of the current collapse phenomenon [67,68] and has been confirmed by several microscopy measurements [69,70]; however, it remains unclear which electronic states play a role in the creation of the virtual gate. Experimental results vary greatly—even with regards to the location of the defects in AlGaIn/GaN heterostructures, which have been measured at the surface close to the gate edge [71,72], in the AlGaIn layer [71,73] at the AlGaIn/GaN interface [72,74], and in the GaN buffer [71]. Additional research has focused exclusively on traps in the GaN buffer layer in AlGaIn/GaN HFETs, measuring non-localized trapping defects at 0.6-1.6 eV [41] with respect to the GaN valence band maximum and in AlGaIn/GaN HEMTs, measuring defects at 0.5 and 2.8 eV [75] and 0.45 and 0.78 eV [76]. There are several likely reasons for these discrepancies. As mentioned, Marcon *et al.* [7] have suggested that reliability issues are not necessarily linked, which suggests that there are several different traps involved. Furthermore, the discrepancies suggest that the defects may be situationally specific and depend on processing conditions or device design. For example, Klein *et al.* [77,78] measured the photoionization energies of the traps at 1.8 and 2.85 eV in GaN FETs, which may have corresponded to grain boundaries or dislocations and carbon-related defects, respectively. These results are consistent with the work of Bardwell *et al.* [64] and Uren *et al.* [79], which showed that current collapse

is proportional to carbon contamination and thus dependent on the cleaning process used during device fabrication. Similarly, the presence of grain boundaries or dislocations may depend on the deposition conditions. Fehlberg *et al.* [80] suggested that the passivant deposition conditions may be more influential than the specific dielectric material after investigating the complex relationship between the stress in the SiN_x layer, the molar fraction of aluminum in AlGaN, and the transport properties of the 2DEG in HFETs. While this particular study does not specifically focus on the current collapse phenomenon, the effects of these conditions on the 2DEG concentration suggest that the strain and molar fraction may influence the condition of the trapping states. Additionally, device design also plays a role in the concentration and distribution of defects. Douglas *et al.* [81] demonstrated that there is a linear relationship between the critical degradation voltage and the gate length, suggesting that the electric field is the main cause of degradation. Similarly, Liu *et al.* [82] have shown that trap densities are dependent on the drain bias voltage. While it is possible that these defects are related to structural defects such as grain boundaries and pits, it is worth considering other alternatives as well such as oxidation or gate diffusion, which may be affected by the strong electric field. The gate material should also be considered. Esposto *et al.* [83] presented results that the diffusion may introduce traps as shown with copper gates. In other words, there seems to be very little consensus as to which defects play a role in current collapse.

Passivation schemes and gate dielectrics have also been applied to mitigate current collapse. SiN_x remains the most extensively studied dielectric, utilized in passivated HFETs [84] and HEMTs [85,86] as well as MOS-HEMTs [87]. Comparative studies

between HfO_2 , Al_2O_3 , and SiN_x MOSHEMTs [87] show that SiN_x is the most effective gate dielectric at reducing current collapse. However, it remains unclear whether SiN_x eliminates the trapping states responsible for the virtual gate or presents a barrier, either preventing electron trapping within these states and formation of additional negative surface charge [88,89]. In light of the current collapse mechanism presented by Hasegawa *et al.*, it would seem likely that SiN_x passivates the N-vacancy and thus reduces current collapse. This is further supported by the work of Hashizume *et al.* [68,90,91], which finds that Al_2O_3 on N_2 plasma pretreated AlGaIn is an effective passivation method in HEMTs. In this case, the passivation of the N-vacancy could be satisfied by the N_2 plasma. On the other hand, these models do not explain the surface states with slower transients, which contribute to the formation of the virtual gate. Therefore, it seems unlikely that passivation of the N-vacancy alone is enough to reduce the current collapse phenomenon. Alternatively, Kim *et al.* [92] and Gao *et al.* [67,93] have suggested that the formation of the virtual gate is a result of charging from ionized water molecules on the device surface in a process Gao *et al.* dubbed as “electric-field-driven” oxidation. This process would be prevented by a hydrophobic passivation layer like SiN_x .

These reliability issues emphasize the importance of understanding the role of defect states in GaN-based materials, focusing on the electronic states inherent in these materials and induced by device stressing. In the rest of the review, we will focus on the former. This is not to negate the importance of the stress-dependent work, which will certainly prove crucial for device development. However, understanding the role of the

electronic states inherent to these materials is a complex issue even without the extra component of additional states.

II. Electronic State Theory

The electronic configurations associated with III-N technologies are fundamentally different from those of traditional silicon and other zinc-blende III-V technologies. This discrepancy is a direct result of the large polarization in III-N materials, resulting bound polarization charge, and compensating electron states. These charge states generate built-in electric fields, which play a crucial role in the electric and optical properties of these materials. In other words, there is an inherent distribution of charge in these materials, which cannot be eliminated. The goal is then to engineer the electronic state configuration to alleviate the failure mechanisms. Therefore, awareness of how electronic states may influence these properties is essential to understanding basic device behavior and future device development. The basics are thus described in the following section.

A. Surface State Configurations

1. Polarization

As mentioned, GaN and other III-V nitrides are characterized by a macroscopic polarization, \vec{P} , where \vec{P} is the sum of the spontaneous polarization inherent to the equilibrium lattice, \vec{P}_{SP} , and the piezoelectric polarization induced by strain, \vec{P}_{PE} , as illustrated in FIG 1.5 [94]. Since the polarization is inherent to the material, each component can be determined from *ab initio* calculations using material constants; i.e. the elastic constants (C_{13} and C_{33}), the piezoelectric coefficients (e_{13} and e_{33}), and the lattice

constants (a_0 and a). Considering the strain component of the polarization along the c -axis,

$$\vec{P}_{PE} = 2 \frac{a-a_0}{a_0} \left(e_{31} - \frac{c_{13}}{c_{33}} 3_{33} \right) \hat{c}. \quad (4)$$

It is found that the piezoelectric polarization is negligible for relaxed GaN and AlN [95] using the constant values summarized in TABLE 1.3. The spontaneous polarization, on the other hand, is large for GaN and AlN and has been calculated using the Berry-phase approach and local density [105-107] or generalized gradient approximations [106,108]. These calculations show the spontaneous polarization is negative for the Ga- and Al-face (0001) wurtzite GaN (-0.029 C/m^2) and AlN (-0.081 C/m^2), and thus implies that the spontaneous polarization points toward the bulk. This produces a negative bound

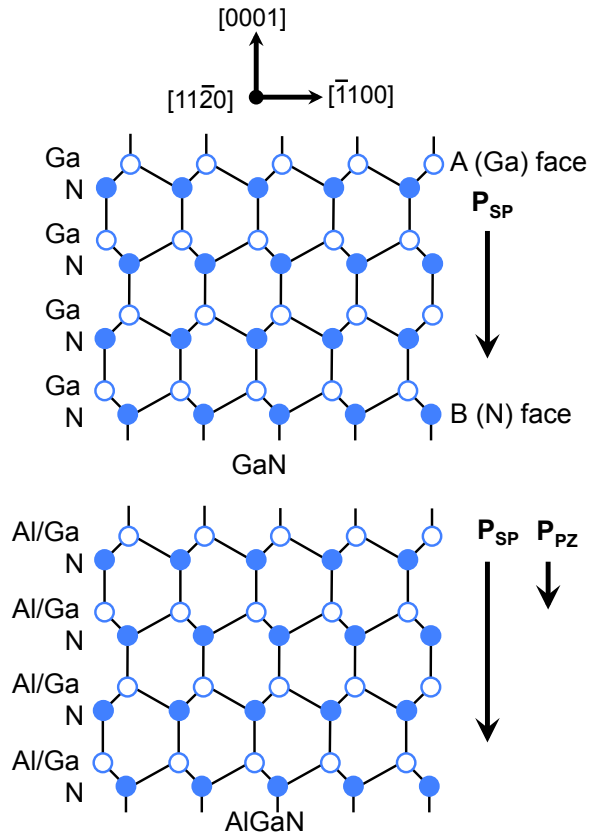


FIG 1.5 Crystal structure, spontaneous polarization fields (P_{SP}), and piezoelectric polarization fields (P_{PE}) for GaN (top) and $Al_xGa_{(1-x)}N$ (bottom). Reprinted from Yu, *et al.*, *J. Vac. Sci. Technol. B* **17**, 1742 (1999) [94]. Copyright 1999, American Vacuum Society.

polarization charge of $\sim 1.81 \times 10^{13}$ and $\sim 5.06 \times 10^{13}$ charges/cm² for GaN and AlN crystals, respectively. Similarly, there will be an equivalent positive bound polarization charge on the N-face of GaN and AlN. (Note the concentration of the polarization bound charge increases with aluminum content. This is because the magnitude of the spontaneous polarization is sensitive to structural parameters, where the increase in the anion-cation bond length along the (0001) axis from GaN to AlN corresponds to an increase in the spontaneous polarization along the c-axis of the wurtzite structure [94].)

TABLE 1.3 Lattice constants (a and c), piezoelectric constants (e_{31} and e_{33}), elastic constants (C_{13} and C_{33}), spontaneous polarization (P_{SP}), and polarization bound charge (ρ) of GaN and AlN. The lattice and piezoelectric constants (e_{31} and e_{33}) as well as the spontaneous polarization are determined by the generalized gradient calculation as described in reference [106]. The elastic constants are determined by an average of the values presented in references [96-104]. Values for $Al_xGa_{(1-x)}N$ may be determined by linear interpolation.

	GaN	AlN
a (Å)	3.189	3.112
c (Å)	5.185	3.982
e_{31} (C/m ²)	-0.37	-0.62
e_{33} (C/m ²)	0.67	1.50
C_{13} (GPa)	94.1	111
C_{33} (GPa)	348	356
P_{SP} (C/m ²)	-0.029	-0.081
ρ (cm ⁻²)	2.12×10^{13}	5.62×10^{13}

Experimentally determining the spontaneous polarization has traditionally proven difficult in III-V nitrides; however, there has been some success more recently. Yan *et al.* [109] measured the thermodynamic coefficients of expansion to determine a spontaneous polarization of -0.0219 ± 0.0005 C/m² ($\sim 1.37 \times 10^{13}$ charges/cm²). Alternatively, Lähnemann *et al.* [110] used microphotoluminescence and cathodoluminescence spectroscopy to measure the energies of excitons in various stacking faults and self-consistent Poisson-Schrödinger equations to determine a spontaneous polarization of -

$0.0220 \pm 0.0007 \text{ C/m}^2$ ($\sim 1.37 \times 10^{13}$ charges/cm²). These values are $\sim 0.01 \text{ C/m}^2$ less than the theoretical values. There have been no such experimental measurements of the spontaneous polarization in AlN.

2. Band Bending and Tilting

Charge neutrality and Gauss's Law lead to a system where the overall charge of the system must be neutral; therefore, the large bound polarization charge of these materials must be compensated. The nature and distribution of the compensation affects the internal electric field of the materials and ultimately device performance. It is, therefore, important to understand the implications of the compensation charge distribution, which is presented in this section in terms of energy band diagram features such as band bending and bend tilting.

Band bending is an important device characteristic to consider, because it describes the energy profile of electrons at the interface: downward band bending favors the accumulation of electrons and upward band bending results in the depletion of electrons. Determination of the band bending is thus closely related to the distribution of electronic states at the interface. Consider, for example, Ga-face, n-type GaN with a doping density of 10^{17} cm^{-3} , and assume the negative bound polarization charge of $\sim 2.1 \times 10^{13}$ charges/cm² is entirely compensated internally by positive ionized donors. This type of compensation is characterized by the formation of a space-charge layer near the surface and determines surface band bending:

$$\Phi_S = \frac{qN_{SS}^2}{2\varepsilon\varepsilon_0N_d}, \quad (5)$$

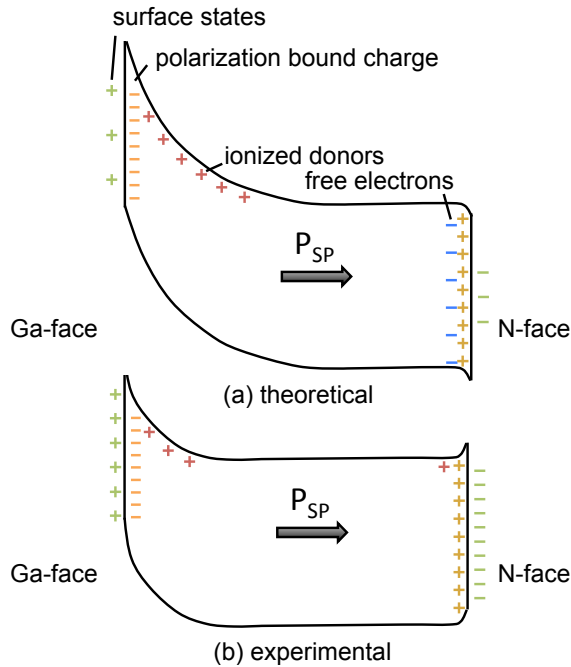


FIG 1.6 Band bending schematic for Ga- and N-face GaN. Both surfaces are screened by $\sim 10^{13}$ charges/cm². (NOTE: the position of the ionized donors and electrons in the material corresponds to their physical position rather than their energy level within the band gap.)

where q is the charge of an electron, ϵ is the relative permittivity of GaN, ϵ_0 is the permittivity of free space, N_d is the doping density, and N_{ss} is the net charge of the surface states in C/cm². This calculation would give a surface potential of -420 V, which corresponds to 420 eV upwards band bending at the GaN surface and an average electric field of 200 MV/m. In equilibrium, the large field leads to inversion or accumulation, which would limit the band bending to approximately the band gap of the material, 3.4 eV [111,112]. (See FIG 1.6a). The polarization bound charge cannot, therefore, be completely compensated internally by positive ionized donors. Experimental band bending measurements for Ga-face GaN are typically reported to be between 0.3 and 1.5 eV [113-115], well below the band gap value. In order to achieve the experimental band bending, the depletion region is reduced to ~ 56 -126 nm for the doping density mentioned, which corresponds to $\sim 5.6 \times 10^{11}$ - 1.3×10^{12} ionized donors/cm². Since the polarization charge will be fully compensated, the surface must be compensated by an

additional $\sim 2.0 \times 10^{13}$ charges/cm². This compensation must therefore take place externally by charged electronic surface states. (See FIG 1.6b). A similar argument can be made for N-face, n-type GaN with the same doping density, where assuming the bound polarization charge is maximally screened by electron accumulation results in downward band bending of 0.1 eV [116]. However, experimental measurements show upward band bending of ~ 0.1 -1.0 eV [112,117,118], which corresponds to 2.0×10^{13} to 2.4×10^{13} surface charges/cm². In other words, both faces are characterized by $\sim 10^{13}$ charges/cm².

In other cases, the configuration of the electronic states may lead to band tilting rather than band bending, which describes the existence of a constant electric field across a material. Band tilting models are applicable to materials with no internal charge such that all charge is localized at the interfaces or surfaces. For example, in some cases, dielectrics may be characterized by a charge distribution at the surface and dielectric/substrate interface. In other cases, this model is applicable to the AlGa_N layer in AlGa_N/Ga_N-based devices, where the polarization charge at the surface and/or interface leads to a field in the dielectric. In such cases, the electric field in the dielectric or semiconductor can be determined as if it were a parallel plate capacitor.

3. Surface and Defect States

As mentioned, the concentration of electronic surface states is on the order of 10^{13} charges/cm², which is large compared to other materials used in devices. However, despite their importance, the nature of these states has remained elusive and intimately depends on specific deposition and processing conditions. In this subsection, we briefly

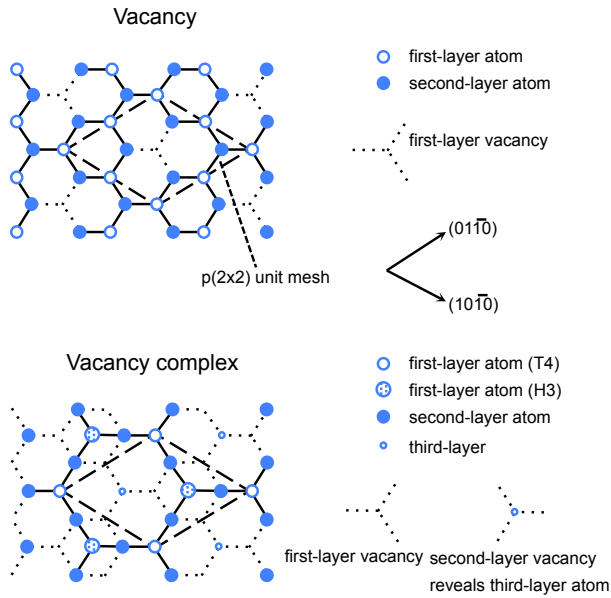


FIG 1.7 Schematic top view of the vacancy and the vacancy complex. The atomic positions of the first two layers (three layer vacancy complex) are displayed. Open and closed circles represent first- and second-layer atoms. For anion termination, the white and black circles correspond to nitrogen and group-III atoms, respectively. For the case of the cation-terminated surface, the open and closed circles illustrate first-layer group-III atoms and second-layer nitrogen. The $p(2 \times 2)$ unit cell used in all calculations is indicated. Reprinted from Fritsch *et al.*, *Phys. Rev. B* **57**, 15360 (1998) [121]. Copyright 1998, American Physical Society.

discuss possible surface states, which, for simplicity, are distinguished into two types: intrinsic and extrinsic.

Intrinsic surface states are associated with an ordered reconstruction that occurs at the termination of the crystal structure. These were first presented by Tamm [119] in 1932 and Shockley [120] in 1939 in accordance with the wavefunction solutions to the Schrödinger equation at the boundary of a periodic crystalline potential, where the electron wavefunctions decay exponentially into vacuum. The distinction between the Shockley and Tamm states is associated with the method of calculation; Shockley considered the electrons with the nearly free electron approximation and thus better describes metallic surfaces, while Tamm considered the tight-binding model as expressed by linear combinations of atomic orbitals and thus better describes semiconductor materials. In 1998, Fritsch *et al.* [121] applied a similar calculation method to GaN, using the local density approximation (LDA) and the pseudopotential model to the anion- and

cation-terminated (0001) surfaces of wurtzite GaN and AlN. These calculations show that the stable surface configurations differ from the bulk, where vacancy structures are thought to be the most stable configurations as shown in FIG 1.7. These results agree with additional studies by Northrup *et al.* [122] and Smith *et al.* [123]. However, the structure of the surface vacancy complex may also vary with the growth conditions, where metal-rich conditions favor the adsorption of a metal adlayer on the cation-terminated surface. This reconstructed surface determines the electronic surface states on AlN and GaN, where the hexagonal reconstruction is the most likely for both materials [121], which leads to extensive dangling bonds and vacancies.

Any deviation from this perfectly reconstructed surface is associated with extrinsic surface states. In GaN and AlN, these defects are likely to be extensive and include variations in surface reconstructions, grain boundaries, dislocation defects, structural defects, and native oxides as well as adsorbates such as oxygen, carbon, and hydrogen, each with their own corresponding energy and charge states. which states are influential depends on the deposition, cleaning, and processing methods and conditions. Experimental research shows that the band bending on GaN is upwards regardless of the crystal orientation, which indicates positively charged states on the Ga face and negatively charged states on the N face. It has been posited by French [124] that the most likely states are structural defects, Ga termination, surface contamination (such as absorbed oxygen atoms), surface states, adsorbates, or additional charge compensation.

B. Interface State Configurations

Interface electronic states are further complicated as the interface formation process may generate additional defect states. Over the past century, several models have been developed and refined to describe a semiconductor interface. However, the subtlety and complexity of interface electronic states have frustrated attempts to create a unified predictive theory. The original concept of interface modeling was presented independently by Schottky [125] and Mott [126]. This model can be derived for metal-semiconductor interfaces such that the Schottky barrier height (SBH, Φ_B) is described by the difference between the work function of the metal, ϕ_M , and the electron affinity of the semiconductor, X_S , as shown in FIG 1.8a:

$$\Phi_B = \phi_M - X_S. \quad (6)$$

The Schottky-Mott model assumes that the metal and semiconductor are at equilibrium, such that there is no charge transfer or direct interaction and therefore no dipole across the interface. The simplicity of this model proves ineffective at determining experimental results, which often demonstrate little dependence on the metal work function. This led Bardeen [127] to adapt the model in 1947 to include interface states. Bardeen recognized that a low density of interface states energetically located in the semiconductor gap could sufficiently “pin” the Fermi level. Therefore, as the metal and semiconductor are brought into contact, charge can flow across the interface to fill or deplete the surface states in the semiconductor. This charge transfer results in an interfacial dipole, Δ , which can then freely compensate the difference between the metal and semiconductor work functions as shown in FIG 1.8b and summarized in the following equation:

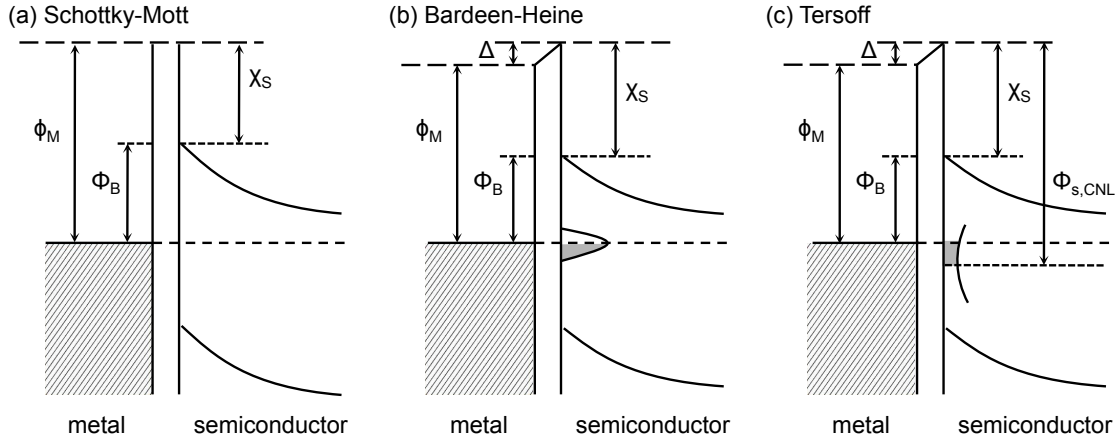


FIG 1.8 Schematic of the metal-semiconductor interface models according to (a) Schottky-Mott, (b) Bardeen-Heine, and (c) Tersoff.

$$\Phi_B = \phi_M - X_S - \Delta . \quad (7)$$

In 1965, Heine [128] further advanced this model by elaborating on the nature of the surface defects in the Bardeen model. The Bardeen-Heine model points out that localized states cannot exist at the interface when coupled to a continuum of free electrons present in the metal, but rather the tails of the electron wavefunctions will decay into the semiconductor and induce states within the band gap. These states have come to be known as metal-induced gap states (MIGS). In 1977, Flores and Tejedor [129] argued that the metal-like behavior responsible for the MIGS in the metal/semiconductor heterostructure is also applicable to semiconductor/semiconductor heterostructures. The interface dipole is thus induced when the charge neutrality points of the two semiconductors are not aligned at the interface [130]. Tersoff [131] further refined this concept, arguing that the single most important property at a semiconductor heterostructure is the ‘line up,’ which occurs to minimize the interface dipole as shown in

FIG 1.8c. In other words, the semiconductors will align at the charge neutrality point rather than at the electron affinity. The resulting SBH gives

$$\Phi_B = S(\phi_M - \Phi_{S,CNL}) + (\Phi_{S,CNL} - X_S), \quad (8)$$

where $\Phi_{S,CNL}$ is the charge neutrality point with respect to the vacuum level, and S is the Schottky pinning factor. This factor determines the strength of the Fermi pinning; in the absence of pinning, $S=1$, reducing Equation 8 to the Schottky-Mott model, while in the limit of strong pinning, $S=0$, pinning the barrier height at the charge neutrality level (CNL) of the semiconductor. However, even decades after Tersoff first proposed this theory, the scientific community has continued to explore for a unified theory, where the major point of contention is the nature of the charge transfer at the interface. Some models, as with the electron affinity model, maintain that there is no charge transfer at the interface. Others detail the nature of the charge transfer, and a subset of these models account for the nature of the transfer differently with regards to the various states responsible for Fermi pinning and the position of the charge neutrality level.

1. Schottky Pinning

As mentioned, the Schottky pinning factor (S) is intricately linked to the interface defect density; however, this requires a fundamental understanding of the interface defects, which has remained elusive. Consequently, several models exist to explain this phenomenon. These include the MIGS model, the unified defect model, the DIGS model, and the chemical reaction model.

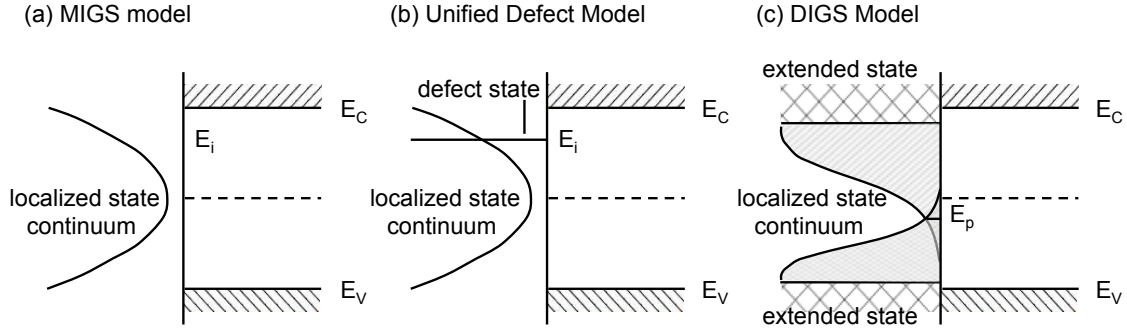


FIG 1.9 Schematic representation of the interface defect densities according to (a) the MIGS model, (b) the unified defect model, and (c) the DIGS model (or the positional surface disorder model).

As previously mentioned, the MIGS model assumes that there are intrinsic states within the energy gap of the semiconductor, which can be related to the exponential decay of the electron wave functions from a metal when in intimate contact with a semiconductor as shown in FIG 1.9a. Mönch [132] compiled results of barrier heights at M-S interfaces with respect to their dielectric constants, giving a semiempirical theoretical expression for the Schottky pinning factor:

$$S = \frac{1}{1 + e^2 N_{MIGS} \delta / (\epsilon \epsilon_0)} \quad (9)$$

$$= \frac{1}{1 + 0.1(\epsilon_\infty - 1)^2} \quad (10)$$

where N_{MIGS} is the density of interface states per unit area, δ is their extent into the semiconductor, and ϵ_∞ is electronic permittivity of the semiconductor. This model has also been used to describe insulator/semiconductor interfaces with some success, though it is unclear where MIGS would originate in such a system.

Spicer *et al.* [133,134] noticed that for III-V compounds the pinning phenomenon occurs not only at metal/semiconductor heterojunctions but also at oxide/bulk semiconductor interfaces. Furthermore, the Fermi level stabilizes after a fraction of a monolayer of oxide

or metal is added to the surface before MIGS could be fully established. They, therefore, suggest that the pinning is a result of the interaction between the adatoms and the semiconductor surface regardless of the electronic configuration of the adatom. This results in a new model for pinning based on interface defect states, where defect formation is caused by the energy released when the atom is adsorbed. The thermal energy produced by chemisorption of an adatom can excite a constituent atom from the semiconductor, generating a vacancy as shown in FIG 1.10, and the vacancy states characterize Fermi level pinning. These localized defect states coexist with the usual U-shaped continuum as shown in FIG 1.9a. However, this model can be problematic, as it requires explicit identification of defect states on an atomic level and fails to explain many experimental results. Furthermore, it has yet to be explicitly applied to GaN-based studies.

Hasegawa *et al.* [135] have proposed a similar model where the disorder induced at the surface region of the semiconductor is responsible for pinning as shown in FIG 1.9c, where departure from the crystalline structure generates “Anderson localized states.” It is assumed that these defect states are several monolayers thick and energetically distributed within the energy band gap. These assumptions were based on experimental C-V and photocapacitance transient spectroscopy measurements that showed: (1) all N_{ss} distributions are U-shaped, which are characterized by a minimum density, $N_{ss,min}$, at $E(min)$ and the radius of curvature; (2) the magnitude of $N_{ss,min}$ and the radius of curvature are sensitive to sample species and processing. (For example, high-temperature annealing resulted in higher $N_{ss,min}$ and sharper curvature.); (3) $E(min)$ corresponds to the

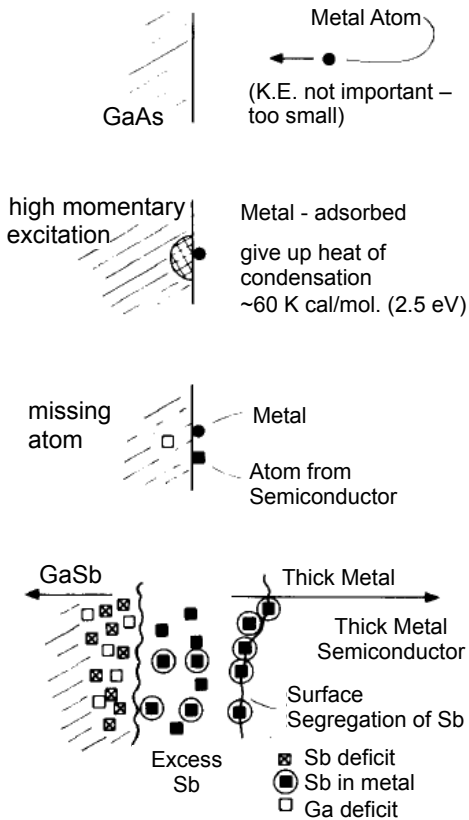


FIG 1.10 Schematic of suggested defect mechanism due to deposition of metal atoms on clean III-V surfaces. This process (i.e., a defect must be formed) needs to occur only about once for every hundred metal atoms striking the surface to account for Fermi level pinning. Reprinted from Spicer *et al.*, *J. Vac. Sci. Technol.* **16**, 1422 (1979) [133]. Copyright 1980, American Vacuum Society.

CNL and fluctuates very little with processing steps, typically $\leq \pm 0.05$ eV; and (4) the Fermi level is pinned at this level [44]. In FIG 1.11, Hasegawa explicitly summarizes how various bonding configurations affect the distribution of states. This gives rise to the following Schottky pinning factor [136]:

$$S = \operatorname{sech}(\delta/\lambda), \quad (11)$$

where

$$\lambda = \sqrt{\epsilon\epsilon_0/[e^2N_{DIGS}(E_0)]}, \quad (12)$$

δ is the thickness of the disorder layer and $N_{DIGS}(E_0)$ is the volume density of DIGS at E_0 .

On the other hand, most of the models overlook the chemical reactivity, which has been challenged by Andrews and Phillips [137]. In particular, they noticed a strong linear

correlation between the heat of formation, ΔH_f , and the SBH, which is consistent with what the researchers called “moderately strong” bonding on Si. Brillson [138] conducted a similar study on compound semiconductors. The curves show a strong correlation between reactive ($\Delta H_f < 0$) and non-reactive ($\Delta H_f > 0$) interfaces. While this model does not give rise to an explicit microscopic explanation of the Fermi level pinning, it does suggest that the chemical reactivity may affect the interface states and SBH. To date, such studies have not been reported on GaN or AlGaN.

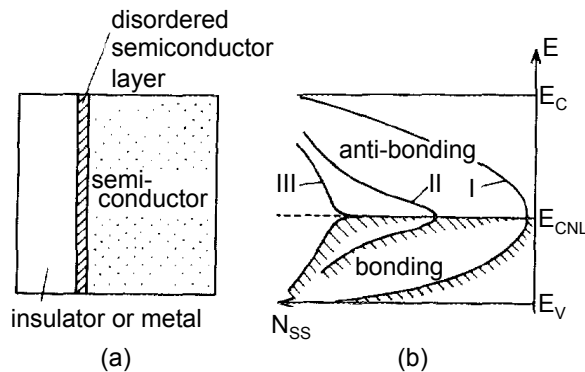


FIG 1.11 Unified disorder induced gap states (DIGS) model explaining the correlation between I-S and M-S interfaces. Surface disorder introduces DIGS whose density depends on the degree of disorder (I: good I-S interface, II: poor I-S interface, and III M-S interface). The physical meaning of E_{CNL} can be interpreted as the Fermi energy of the DIGS spectrum where charge neutrality is achieved. E_{CNL} is the branch point between the bonding and antibonding states in the gap. Reprinted from H. Hasegawa and H. Ohno *J. Vac. Sci. Technol. B* 4, 1130 (1986) [44]. Copyright 1986 American Vacuum Society.

2. Band Line-up

In addition to the nature of Schottky pinning, there is also debate as to the point of alignment at a heterojunction, and again, the electron affinity and the charge neutrality level models have been considered. The electron affinity is the classical point of alignment as proposed by the Schottky-Mott model, which was later adapted by Anderson [139] for semiconductor/semiconductor heterojunctions. However, this model represents an idealized case and assumes no charge transfer at the interface.

The charge neutrality level is an alternative point of alignment at a heterostructure, where the concept is central to Fermi-level pinning and charge transfer. As previously mentioned, the charge neutrality level is essentially the energy where the gap states cross from donor-like to acceptor-like. (In one dimension, this energy corresponds to the branch point energy, E_B). In other words, the CNL is the weighted average of the density of states as shown in FIG 1.12. This value can be calculated from the band structure as the energy at which the simple Green's function is zero [140,141]:

$$G(E) = \int_{BZ} \int_{-\infty}^{\infty} \frac{N(E')dE'}{E-E'} = 0, \quad (13)$$

where the density of states, $N(E')$, can be determined by the local density approximation [131,140,141] or the empirical tight bonding model (ETB) [143]. In the LDA, the approximate electron density at each point is applied to the exchange energy in density functional theory (DFT) to determine the electronic band alignment. A consequence of this approximation is that the band gaps are typically too small and must be adjusted to the experimental values. In the ETB, the Bloch functions are derived assuming the

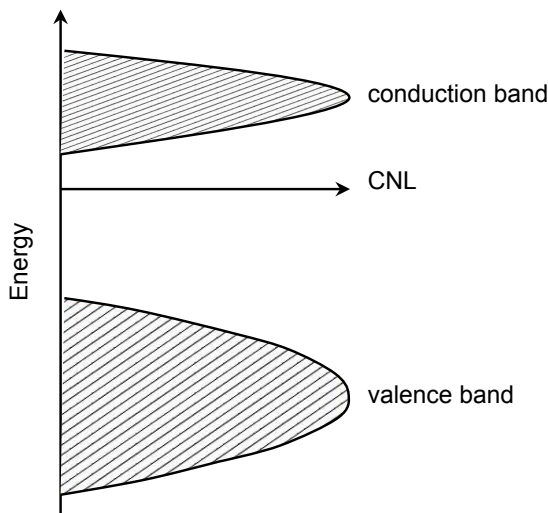


FIG 1.12 The CNL is a weighted average of the density of states. It is repelled by a large density of states in the valence or conduction band. Reprinted from J. Robertson and B. Falabretti, *J. Appl. Phys.* **100**, 014111 (2006) [141].

electrons are tightly bound to the ionic cores of the constituent atoms. A simplified version of this calculation has been presented by Cardona and Christensen [142,143] to provide quicker calculations. To accomplish this, they used Baldereschi's concept of mean-value points in the Brillouin zone [144]. The power of these methods is that they find the band offsets in terms of the semiconductor bulk properties for a wide range of bonding types without the need to characterize each bond explicitly. This is particularly useful for amorphous structures, where specific bonding structures may be difficult to characterize.

There have been other attempts to develop a model using explicit interface bonding as shown by Van de Walle [145,146], which rely on a complete description of the interfacial electronic distribution. This is accomplished by self-consistent calculations based on local DFT, applied momentum space formalism, and nonlocal norm-conserving pseudopotentials. In these calculations, the band gaps more accurately reflect the experimental values [147]. In another model as presented by Wei and Zunger [148], the natural band offsets are determined using a first-principles band structure method, using the LDA in DFT as implemented by the general potential, relativistic, all electron, linearized augmented plane wave method, and the Ceperly Alder exchange correlation potential. While this method does not calculate the CNL explicitly, Robertson [141] later revised the calculations to deduce the CNL for comparison. These results were later corrected to account for the changes in the valence band maximum because of hydrostatic volume deformation [149]. The calculated results from these models for GaN and AlN are summarized in TABLE 1.4.

TABLE 1.4 Summary of band gap, electron affinity, and charge neutrality levels for GaN and AlN, where the CNL is included for several different methods of calculation including the tight binding (ETB) [143], local density approximation (LDA) [141], and two different first principle (FP) calculations [146,148] as well as the experimental values [149-152], which are deduced from Schottky barrier measurements.

	Band Gap	EA	ETB	LDA	CNL		Expt.	
					FP ₁	FP ₂		
GaN	3.4	3.3	2.37	2.88	2.17	2.14	2.45-2.50	
AlN	6.2	0.6	2.97	3.97	2.87	2.94		
Al _x Ga _(1-x) N			$xX_{\text{AlN}} + (1-x)X_{\text{GaN}}$					

It is worth pointing out that the CNLs of III-V semiconductors have shown some interesting trends as calculated by Mönch [143,153]. In general, the CNL lies at the average bonding-antibonding gap, rather than at the minimum of the direct or indirect gap. With increasing polarity or ionicity, the valence bands becomes flatter as associated with a higher effective mass, and the conduction bands becomes increasingly direct with respect to the valence band maximum and a smaller density of states at the band edge. The CNL of higher polarity materials, i.e., GaN and AlN, is repelled by the higher density of states in the valence band and thus occurs higher in the band gap as shown in FIG 1.13. This is noteworthy in connection with the chemical reactivity model, where an increase in reactivity or ionicity is mirrored by an increase in the Schottky barrier at a Schottky interface. For the two models to be consistent, it would imply charge transfer at the interface, which is manifested in the minimization of the interface dipole or strong Fermi pinning. The nature of the interface dipole is thus the distinguishing factor in these models. Therefore, in cases where there is little or no charge transfer, the models should be in close agreement as there is no pinning factor. Furthermore, the reduction of the interface dipole results in a similar alignment, and the charge neutrality level and electron affinity models will provide similar results.

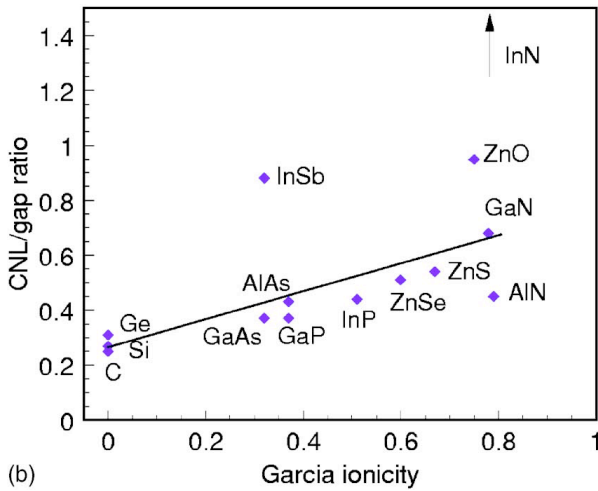
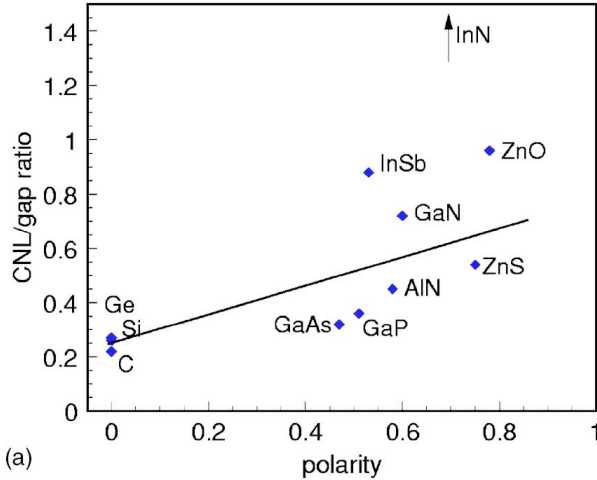


FIG 1.13 Trend of the CNL/band gap ratio vs. (a) Harrison's bond polarity and (b) ionicity of Garcia and Cohen. As the band gap becomes more direct with higher ionicity, the CNL moves higher in the gap. Reprinted from J. Robertson and B. Falabretti, *J. Appl. Phys.* **100**, 014111 (2006) [141]. Copyright 2006, American Institute of Physics.

3. Band Offsets

These band alignment models ultimately describe the band offsets, which are relevant to the confinement properties of carriers in the semiconductor. To date, the most extensive theoretical studies of the band offsets for various dielectric/GaN interfaces have been conducted by Robertson and Falabretti [141], using the MIGS pinning factor and CNL alignment as determined by the LDA. According to this model, the valence band offset (VBO) can be determined as

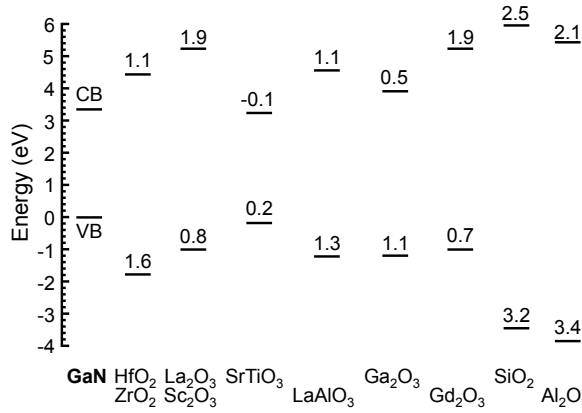


FIG 1.14 Calculated band offsets of dielectrics on GaN. Reprinted from J. Robertson and B. Falabretti, *J. Appl. Phys.* **100**, 014111 (2006) [141]. Copyright 2006, American Institute of Physics.

$$\Delta E_V = E_{CNL_{oxide}} - E_{CNL_{GaN}} - S[I_{GaN} - I_{oxide} - (E_{CNL_{oxide}} - E_{CNL_{GaN}})], \quad (14)$$

where I is the photo threshold energies, and ECNL is the charge neutrality level with respect to the valence band maximum for GaN and the respective oxide. The results as calculated by this model are summarized in FIG 1.14 and TABLE 1.5. Additionally, there have been a few publications on band offsets using first-principle and ab-initio calculations that analyze specific bonding configurations; studies by Zhang et al. [154] determined the conduction band offset (CBO) for PbTiO₃/GaN as 0.4 eV, and research by Nakayama and Murayama [155] approximately determined the conduction band offset for ZnO/GaN as 1.6 eV. However, they also cite a large range of values from 1.0 to 2.2 eV, depending on the surface processing, which suggests that the processing steps may be crucial when analyzing the band alignment models if such processing alters the interfacial bonding. Experimental band alignments for dielectrics on GaN are summarized in TABLE 1.6. Comparisons between the theoretical and empirical values—see TABLE 1.7—show that the model affords a good approximation for some heterostructures such as those with Sc₂O₃ [160-162], SrTiO₃ [163], and ZnO [164-167]. However, the model is not as reliable for other interfaces such as those with AlN [168,169], Al₂O₃ [111,170-172],

Ga₂O₃ [173], HfO₂ [111,170,171,174,175], La₂O₃ [160], MgO [176,177], Si₃N₄ [178-180], and SiO₂ [171,181].

These discrepancies are likely related to variations in crystal structure, differences in stoichiometry, unobserved band bending, or the presence of an interfacial oxide layer. In some cases, the discrepancy can be understood in terms of the band gap. This is the case for Al₂O₃, where the band gap ranges from 8.8 to 6.2 eV for α -crystalline to amorphous structures and is, therefore, dependent on the method of oxide film growth. The decrease in the band gap has been associated with defect-induced states located in the band gap [182], where the valence band maximum states are associated with the O 2p states, and the conduction band minimum states are associated with the Al 3s, 3p states [124]. Rehybridization between Al 3s, 3p, and O 2p, modifies the charge transfer between Al and O, and consequently decreases the band gap, increasing the valence band maximum. This explains why the results described in TABLE 1.6 show similar values for the conduction band offset (CBO) but a wide range of values for the VBO—though it does not explain the VBO of 0.1 eV, which is much lower than the other presented values deposited by a similar method. MgO has also shown band gap narrowing, where the band gap difference from crystalline MgO (7.8 eV) to amorphous MgO (6.1 eV) [183] is manifested in the valence band. This may account for the discrepancy in the MgO results as well. In other cases, such as HfO₂, there is a large range of experimentally measured offsets. It is possible that these fluctuations occur because of inconsistent processing methods, such as cleaning and deposition technique, which may result in varied oxygen coverage, dielectric stoichiometry, and interfacial bonding. Since the bonding

configuration greatly affects band offsets, this would result in a large range of offset values. Other, more probable, options are the measurements do not account for band bending, which may dramatically alter the band-offset values as discussed by Xu *et al.* [184], or the potential drop across the interfacial oxide layer, which may develop at the interface.

The band offsets of dielectrics on AlGa_xN and AlN are summarized in TABLE 1.8 and TABLE 1.9 [185-188], respectively. For AlGa_xN, Robertson [141] and Heidelberg [189] determined the theoretical band offsets, using the MIGS Schottky pinning factor and the CNL alignment; however, there are very few experimental results [90,190,191] and none of which that can be compared to the theoretical calculations. Furthermore, it is likely that such investigations on AlGa_xN will depend heavily on the aluminum content. Therefore, conclusions with regards to the band offsets of dielectrics on AlGa_xN are less evident at this time.

TABLE 1.5 Valence band and conduction band offsets calculated for dielectrics on GaN as calculated by the local density approximation and charge neutrality level model [141,189]. All band offsets are given in eV.

Material	Band Offset	
	VBO	CBO
AlN	0.4	2.4
Al ₂ O ₃	3.0	2.4
Ga ₂ O ₃	0.7	0.5
Gd ₂ O ₃	0.7	1.9
GdScO ₃	0.1	2.6
HfO ₂	1.6	1.1
HfSiO ₄	1.7	1.6
LaAlO ₃	1.3	1.1
La ₂ O ₃	0.7	2.0
MgO	2.0	2.6
PbTiO ₃	-0.2	0.4
Sc ₂ O ₃	0.7	2.0
Si ₃ N ₄	0.8	1.3
SiO ₂	3.1	2.6
SrTiO ₃	0.2	-0.1
Ta ₂ O ₅	1.1	0.1
Y ₂ O ₃	0.8	1.9
ZnO	0.9	-0.7
ZrO ₂	1.6	1.1

TABLE 1.6 Valence band and conduction band offsets measured for dielectrics on GaN. If one of the offsets is deduced from the measured band offset and the band gap, it is denoted with “*”. The deposition method is noted where ALD = atomic layer deposition, dry therm. ox. = dry thermal oxidation, E-beam = electron beam, ECR = electron cyclotron resonance, MBD = molecular beam deposition, PEALD = plasma-enhanced atomic layer deposition, PECVD = plasma-enhanced chemical vapor deposition, PEMBD = plasma-enhanced molecular beam deposition, and pulsed laser = pulsed laser deposition. In addition, the characterization method is noted where CV = capacitance-voltage measurements, EELS = electron energy loss spectroscopy, PL = photoluminescence, UPS = ultraviolet photoelectron spectroscopy, UV = UV adsorption, UV-vis = UV-visible adsorption, and XPS = x-ray photoelectron spectroscopy. All offsets are given in eV.

Material	Deposition	Specifics	Characterization	Band Offset		Reference
				VBO	CBO	
AlN	ECR MBD		<i>in-situ</i> XPS	0.8	2.0*	[168]
	reactive MBD	Al+NH ₃	<i>in-situ</i> XPS	1.4	1.4*	[169]
Al ₂ O ₃	PEALD	DMAI+O ₂ plasma	<i>in-situ</i> XPS and UPS	1.8	1.3*	[111]
	ALD	TMA+H ₂ O	<i>ex-situ</i> XPS and UPS	0.1	3.0*	[170]
	ALD	TMA+H ₂ O	XPS	1.2	2.0	[171]
	ALD	TMA+H ₂ O	CV		2.1	[172]
CaO	MBD	H ₂ -less	XPS	1.0	2.5*	[156]
Ga ₂ O ₃	dry therm. ox.		XPS	1.4	0.1*	[173]
(Gd,Ga) ₂ O ₃	E-beam	Ga ₅ Gd ₃ O ₁₂	<i>ex-situ</i> XPS	1.1	0.9	[157]
GdScO ₃ /SrTiO ₃	MBD		XPS	0.4	2.0*	[163]
HfO ₂	PEALD	TEMAH+O ₂ plasma	<i>in-situ</i> XPS and UPS	1.4	1.0*	[111]
	ALD	TEMAH+H ₂ O	<i>ex-situ</i> XPS and UPS	-1.9	4.3*	[170]
	ALD	TDMAH+H ₂ O	XPS	0.5	1.5	[171]
	MBD	Hf MBD+O ₂ plasma	<i>in-situ</i> XPS and UPS	0.3	2.1*	[174]
	Sputtering	Sputtering Hf +O ₂	XPS, UV	0.6	1.7	[175]
HfAlO	ALD	TMA/TDMAH+H ₂ O	XPS	0.8	1.6	[171]
LaAlO ₃ /SrTiO ₃	MBD		XPS	-0.3	2.5*	[163]
La ₂ O ₃	MBD		XPS	1.9	0.9*	[160]
(La ₂ O ₃) _{0.5} (SiO ₂) _{0.5}	Pulsed Laser	Laser+La ₂ O ₃ ,SiO ₂	XPS, EELS	0.9	1.4	[158]
Mg _{0.5} Ca _{0.5} O	PEMBD	Ca Mg MBD+O ₂ plasma	XPS, PL	0.7	3.4*	[159]
MgO	MBD	Mg MBD+O ₂	XPS	1.2	3.2*	[176]
	PEMBD	Mg MBD+O ₂ plasma	XPS	1.1	3.3*	[177]
Sc ₂ O ₃	MBD		XPS	0.8	2.1*	[160]
	PEMBD	Sc MBD+O ₂ plasma	XPS	0.4	2.1*	[161]
	Pulsed Laser		XPS	0.8	2.0*	[162]
Si ₃ N ₄	MBD	Si MBD+N ₂ plasma	<i>in-situ</i> XPS	-0.6	2.5*	[178]
	PEMBD		XPS	-0.4	2.4*	[179]
	ECR-PECVD	N ₂ +SiH ₄	XPS	1.0-1.2		[180]
SiO ₂	ALD	APTES+O ₃ +H ₂ O	XPS	2.4	3.0	[171]
	MBD	Si MBD+O ₂ plasma	<i>in-situ</i> XPS and UPS	2.0	3.6*	[181]
SrTiO ₃	MBD	SrO+(Ti+O ₂)	XPS	0.1	-0.2*	[163]
ZnO	PEMBD	Zn MBD+O ₂ plasma	<i>ex-situ</i> XPS and UPS	0.8	-0.8*	[164]
	Sputtering		XPS, PL UV-vis	0.5	-0.6	[165]
	Sputtering		temp-dependent IV	0.5*	-0.6	[166]
	Sputtering		XPS	0.7	-0.7	[167]

* Estimated value

TABLE 1.7 Comparison between the theoretical band offset calculations [141] and experimental measurements [160-181]. Materials that are characterized by a discrepancy >0.4 eV are shown in bold. All band offsets are given in eV.

Material	Deposition	Band Offset	
		VBO	CBO
AlN	CNL	0.4	2.4
	ECR MBD	0.8	
	reactive MBD	1.4	
Al ₂ O ₃	CNL	3.0	2.4
	PEALD	1.8	
	ALD	0.1	
	ALD		2.1
	ALD	1.2	2.0
Ga ₂ O ₃	CNL	0.7	0.5
	dry therm. ox.	1.4	
HfO ₂	CNL	1.6	1.1
	PEALD	1.4	
	MBD	0.3	
	ALD	-1.9	
	ALD	0.5	1.5
	Sputtering	0.6	1.7
La ₂ O ₃	CNL	0.7	2.0
	MBD	1.9	
MgO	CNL	2.0	2.6
	PEMBD	1.1	
	MBD	1.2	
Sc ₂ O ₃	CNL	0.7	2.0
	PEMBD	0.4	
	Pulsed Laser	0.8	
	MBD	0.8	
Si ₃ N ₄	CNL	0.8	1.3
	MBD	-0.6	
	PEMBD	-0.4	
	ECR-PCVD	1.0-1.2	
SiO ₂	CNL	3.1	2.6
	MBD	2.0	
	ALD	2.4	3.0
SrTiO ₃	CNL	0.2	-0.1
	MBD	0.1	
ZnO	CNL	0.9	-0.7
	MBD	0.8	
	Sputtering	0.5	-0.6
	Sputtering		-0.6
	Sputtering	0.7	-0.7

TABLE 1.8 Theoretical and experimental band offsets on AlGa_N. The deposition method is noted where ECR-CVD = electron cyclotron resonance chemical vapor deposition, MBD = molecular beam deposition, and vap. cooling cond. = vapor cooling condensation. In addition, the characterization method is noted where EELS = electron energy loss spectroscopy, and XPS = x-ray photoelectron spectroscopy. All offsets are given in eV.

Material	Deposition	Specifics	Characterization	Band Offset		Reference
				VBO	CBO	
Ga ₂ O ₃		LDA	CNL	0.6 ⁺	1.4 ⁺	[141,189]
GdScO ₃		LDA	CNL	-0.2 ⁺	2.3 ⁺	[141,189]
HfO ₂		LDA	CNL	1.6 ⁺	0.6 ⁺	[141,189]
Sc ₂ O ₃		LDA	CNL	0.8 ⁺	1.4 ⁺	[141,189]
Si ₃ N ₄		LDA	CNL	0.6 ⁺	0.9 ⁺	[189]
Si ₂ O ₃		LDA	CNL	3.4 ⁺	1.9 ⁺	[141,189]
Al ₂ O ₃	MBD	Al MBD+ECR plasma	<i>in-situ</i> XPS, EELS	0.8	2.1	[90]
SiN _x	ECR-CVD	SiH ₄ +N ₂	<i>in-situ</i> XPS, EELS	0.1	0.7	[90]
ZnO	vap. cooling cond.	TMA+H ₂ O	XPS	-1.5	0.8*	[190,191]

+ Theoretical value

* Estimated value

TABLE 1.9 Theoretical and experimental band offsets on AlN. Note the experimental band offsets for InN/AlN are given for the Al-face and the N-face, respectively. The deposition method is noted where MOCVD = metal organic chemical vapor deposition, and PEMBD = plasma-enhanced molecular beam deposition. In addition, the characterization method is noted where XPS = x-ray photoelectron spectroscopy. All offsets are given in eV.

Material	Deposition	Specifics	Characterization	Band Offset		Reference
				VBO	CBO	
Al ₂ O ₃		LDA	CNL	3.1 ⁺	-0.5 ⁺	[141]
Ga ₂ O ₃		LDA	CNL	0.7 ⁺	-2.1 ⁺	[141]
Gd ₂ O ₃		LDA	CNL	0.3 ⁺	-0.7 ⁺	[141]
HfO ₂		LDA	CNL	1.3 ⁺	-1.5 ⁺	[141]
HfSiO ₄		LDA	CNL	1.4 ⁺	-1.1 ⁺	[141]
LaAlO ₃		LDA	CNL	0.9 ⁺	-1.5 ⁺	[141]
La ₂ O ₃		LDA	CNL	0.4 ⁺	-0.6 ⁺	[141]
Sc ₂ O ₃		LDA	CNL	0.3 ⁺	-0.6	[141]
Si ₃ N ₄		LDA	CNL	0.4 ⁺	-1.3 ⁺	[141]
SiO ₂		LDA	CNL	2.9 ⁺	-0.1 ⁺	[141]
SrTiO ₃		LDA	CNL	-0.2 ⁺	-2.7 ⁺	[141]
Ta ₂ O ₅		LDA	CNL	0.7 ⁺	-2.5 ⁺	[141]
ZrO ₂		LDA	CNL	1.1 ⁺	-1.5 ⁺	[141]
InN	PE-MBD	In flux+N ₂ plasma	XPS	-1.5	-4.0*	[185,186]
				-3.1	-2.4*	[185,186]
MgO	MOCVD	(Cp ₂ Mg)+O ₂	XPS	0.2	1.5*	[187]
ZnO	PE-MBD	Zn+O ₂ plasma	XPS	-0.4	-3.3*	[188]

+ Theoretical value

* Estimated value

III. Processing Related Effects

The electronic states may depend on the various processing treatments, such as cleaning, dielectric passivation, post-deposition, and post-metallization treatments. These processing steps may affect states related to oxygen coverage, oxide layers, carbon contamination, structural defects, bonding configurations, vacancy defects, interstitials, adsorbates, pinning states, etc. Consequently, understanding how these treatments affect the surface and interface states will aid in the advancement of device technologies.

A. Cleaning and Surface Processing

Cleaning and processing of GaN and AlGaIn surfaces prior to dielectric deposition have proven a critical step in the optimization of device performance. Surface contamination on these materials is commonly related to carbon and oxygen as part of native oxides, adsorbates, and residual species. Spectroscopic ellipsometry by Edwards *et al.* [192] has determined that there is ~2-5 nm of contamination on air-exposed GaN; about half of this contamination consists of transparent inorganic and organic contamination, and the rest is presumed to be native oxide. On AlN and AlGaIn surfaces, it is expected that this ratio will vary slightly such that there is more native oxide, since aluminum is more easily oxidized than gallium [193,194]. The goal of cleaning GaN and AlGaIn is therefore to remove these contaminants without damaging the crystal order or introducing additional defect states. To accomplish this goal, research has focused on the cleaning of GaN prior to the fabrication of metal/GaN Schottky contacts, using both *ex-situ* and *in-situ* cleaning. *Ex-situ* cleaning has included solvents such as trichloroethylene, acetone, methanol, isopropanol, various acids and bases as well as UV/O₃. *In-situ* cleaning has included

room temperature or high temperature plasma, sputtering (Ar, Xe, Ne, N₂, H₂, and O₂), and vacuum, or gas (H₂, N₂, NH₃, and Ga flux) annealing as will be discussed below. In most cases, these studies focus on the cleaning of n-type, Ga-face GaN; deviations from this standard will be noted.

1. Wet Chemical Cleaning

Wet chemical cleans have been used to remove native oxides as well as organic and inorganic contamination ever since Hedman and Mårtensson published a study in 1980 [195], showing that submersion in 100°C H₃PO₄ and *in-situ* annealing at 300°C reduces oxygen and carbon contamination. More recent research has focused on the effectiveness of several wet chemical cleans; these include hydrochloric acid (HCl), hydrofluoric acid (HF), nitric acid (HNO₃), sulfuric acid (H₂SO₄), phosphoric acid (H₃PO₄), hydrogen peroxide (H₂O₂), sodium hydroxide (NaOH), potassium hydroxide (KOH), ammonium hydroxide (NH₄OH), ammonium fluoride (NH₄F), ammonium sulfide ((NH₄)₂S), RCA SC1 and SC2, buffered HF (BHF), and BHF vapor as well as UV/O₃—though not explicitly a wet chemical.

Since contaminants and native oxide consist mostly of carbon and oxygen, most research uses spectroscopy after exposure to various wet chemical cleans to determine their effectiveness. This was the approach taken by Smith *et al.* [196] and King *et al.* [197], who used Auger electron spectroscopy (AES) and x-ray photoelectron spectroscopy (XPS) to examine the effectiveness of several acids at removing oxygen and carbon from the surface, including HCl, HF, HNO₃, H₂SO₄, H₃PO₄, H₂O₂, NaOH, KOH, NH₄F, RCA SC1 and SC2, buffered HF (BHF), and BHF vapor as well as UV/O₃. Comparative

results show that HCl reduces oxygen coverage most effectively, while HF reduces carbon coverage most effectively. (UV/O₃ is shown to be an effective method to remove carbon contamination but only at the expense of further oxidizing the surface). Furthermore, these acidic cleanings result in very different surface chemistry. For example, HCl-treated samples are characterized by significant chlorine coverage on the surface. The strong bonding between chlorine and gallium or nitrogen and the inverse correlation between chlorine and oxygen on the surface suggest chlorine atoms occupy dangling bonds left by oxygen removal, preventing reoxidation during air exposure [197,198]. XPS also detects two chemical states associated with oxygen, where the core level at higher energy is typically associated with Ga-OH⁻ bonding, and that at lower energy is associated with Ga-O²⁻ bonding [197,199-201]. However, it has also been suggested that oxygen bonds to nitrogen and forms an oxynitride [197,200,202]. The HF-cleaned samples, on the other hand, show the binding energy of the C 1s core level after HF treatment shifts ~0.4 eV to higher binding energy in comparison with samples after HCl treatment. This shift suggests HF-treated samples are characterized by more C-O bonds, while HCl-treated samples are characterized by more C-H bonds.

Other studies have focused on preventing oxidation and reoxidation. Sulfur-based processes have been successfully used to this end on other semiconductors such as GaAs, because sulfur passivation is hydrophobic and easily removed with low-temperature annealing. Plucinski *et al.* [203] have demonstrated that atomically thin layers of sulfur deposited *in-situ* on a clean Ga adlayer on N-face GaN effectively inhibits oxidation on GaN. Furthermore, similarly sulfur-treated GaN surfaces have been shown to improve

ohmic contacts and photoluminescence [204-206]. Sulfur-based wet chemical cleans may induce similar results as shown by Diale *et al.* [207]. Their research suggests that, similar to the Cl termination that results from a HCl cleaning, $(\text{NH}_4)_2\text{S}$ cleaning results in S termination on the surface, which inhibits reoxidation. Consequently, $(\text{NH}_4)_2\text{S}$ -cleaned GaN is characterized by less carbon contamination, reduced oxygen coverage, a smaller RMS roughness, and a better stoichiometric ratio than HCl- or KOH-cleaned GaN. Solutions of sulfuric acid and hydrogen peroxide have also been used with some success on GaN. Nepal *et al.* [208] concluded that $\text{H}_2\text{O}_2:\text{H}_2\text{SO}_4$ (1:5, piranha, 80°C) cleaning is also more effective than HCl or HF cleaning, giving the best-quality ALD- $\text{Al}_2\text{O}_3/\text{GaN}$ interface in terms of roughness. However, it is unlikely that such a clean would completely remove all oxygen or carbon. This is supported by the work of Machuca and Liu *et al.* [209,210], who demonstrated that cleaning GaN with a 1:4 $\text{H}_2\text{O}_2:\text{H}_2\text{SO}_4$ at 90°C reduces oxygen and carbon coverage to ~ 0.9 ML and 0.7 ML, respectively.

Ammonium hydroxide is another wet chemical clean of interest, which is effective at reducing oxygen but not carbon on GaN and AlGaN surfaces. It is thus suggested that Ga_2O_3 dissolves in NH_4OH [90,193,211], which likely results in improved device performance. For example, in a study by Koyama *et al.* [212], results show that pretreatment of GaN in NH_4OH (50°C) results in better thermionic emission I-V characteristics of Au, Ag, and Pt/GaN Schottky contacts than those treated with HCl or HF. On one hand, these results may be surprising since NH_4OH -cleaned substrates should contain more carbon, which has also been shown to degrade device performance. On the other hand, the acids are not as effective at reducing the native oxide without

generating a Ga-rich surface, which ultimately leads to more defects at the interface that are influential to device degradation.

It is also worth mentioning that alkali cleaning on N-face GaN is different from that on Ga-face GaN, where hydroxide solutions such as KOH [213] and NaOH [214] as well as hot H₃PO₄ [215] can selectively etch the N-face GaN, causing morphology degradation. Li *et al.* [213] concluded that selective etching on N-face but not Ga-face GaN is a consequence of different nitrogen surface bonding states. On the N-face, hydroxide attacks the tetrahedrally bonded Ga atoms underneath the terminating N layer, forming Ga₂O₃ and NH₃. The Ga₂O₃ is then dissolved from the surface, leaving a new N-face that can be continuously etched. The Ga-face, on the other hand, is more stable. After Ga₂O₃ is removed from these surfaces, a nitrogen atom on the N-terminated surface is characterized by three occupied dangling bonds, which repel OH⁻. There are similar dangling bonds on N-face GaN, which will repel OH⁻; however, there is only one dangling bond per nitrogen rather than three. Consequently, OH⁻ will reach the Ga layer below and cause the etching process. (See FIG 1.5 for reference).

2. Vacuum Annealing

Given that wet chemical treatments cannot completely remove both oxygen and carbon contamination, researchers have looked elsewhere for effective cleaning processes, including *in-situ* annealing. Often these experiments are paired with *ex-situ* chemical cleans, which influence the effectiveness of the annealing. For example, Machuca and Liu *et al.* [209,210] combined the H₂O₂:H₂SO₄ wet chemical clean with an *in-situ* 700°C vacuum anneal ($\leq 10^{-10}$ Torr), reducing the respective oxygen and carbon coverage from

~0.9 ML and 0.7 ML to 0.08 ML and 0.01 ML. This would suggest that annealing at this temperature may effectively remove carbon but not oxygen. Diale *et al.* [207] also found that additional high temperature vacuum annealing of GaN after chemical treatment results in nearly complete removal of carbon contamination as measured by AES; however, these results also show nearly complete oxygen removal. The more effective cleaning is likely the result of the $(\text{NH}_4)_2\text{S}$ -clean used prior to annealing.

Smith and King *et al.* [197,196] have systematically evaluated the effectiveness of vacuum annealing at various temperatures. Their XPS results show the C 1s core level of wet-chemical-treated GaN shifts to lower binding energy after annealing at 500-600°C. This shift suggests that C-O bonding desorbs at this temperature range while C-H bonding requires a higher desorption temperature. This is confirmed by temperature programmed desorption and may explain why thermal desorption of carbon is more effective for HF-treated GaN than HCl-treated—where HF-treated GaN has more C-O bonded carbon remaining as mentioned earlier. Similarly, thermal desorption of Cl occurs at ~60°C, while thermal desorption of carbon likely occurs at temperatures above 900°C. Thermal desorption of surface oxide, however, also becomes significant at temperatures >900°C. Consequently, vacuum annealing is not an effective method of oxide removal, since sublimation of Ga also occurs at this temperature, which introduces additional defect states.

3. Gas Annealing

Similar research has focused on the effects of annealing in gaseous environments, particularly NH_3 . King *et al.* [197] have annealed GaN in NH_3 at 800°C, reducing carbon

contamination below the XPS detection limit and leaving only ~ 0.1 ML oxygen. A comparable study by Tracy *et al.* [216] has reduced both oxygen and carbon below the detection limit of XPS and ultraviolet photoemission spectroscopy (UPS). Moreover, the Ga/N ratio decreases from 1.3 to 1.0 after annealing, indicating a more favorable stoichiometry. However, other studies were not as successful such as those by Machuca *et al.* [209] and Grabow *et al.* [217], showing ~ 0.48 ML and 0.92 ML oxygen coverage, respectively. It is likely that this discrepancy is related to the substrate growth or annealing conditions; at high temperatures, the purity of the ultra high vacuum chamber and annealing gas plays a crucial role in the effectiveness of NH_3 annealing. High-temperature NH_3 annealing has also been combined with N_2^+ ion bombardment and deposition of Ga metal by Bermudez *et al.* [223]. This study found that annealing $\leq 900^\circ\text{C}$ in NH_3 is only effective at removing carbon not oxygen. They proposed that oxygen at subsurface sites or in the form of Ga_2O_3 is inaccessible to NH_3 and thus requires annealing in NH_3 at temperatures $> 900^\circ\text{C}$ for removal.

4. Ion Sputtering and Annealing in Flux

In some cases, ion sputtering has proven a useful method in optimizing stoichiometry during cleaning. To date, several ions have been considered, including Ar^+ [218-220], Xe^+ [218], N_2^+ [218-221], and Ne^+ [219]. In some of these cases, namely Ar^+ , Xe^+ , and Ne^+ , sputtering causes defect formation with the preferential removal of nitrogen, forming metallic Ga clusters with subsequent annealing above 350°C [218]. In contrast, N_2^+ sputtering barely decreases the N/Ga ratio, and post annealing further increases that

ratio to near unity. It is also suggested that N_2^+ sputtering helps generate not only a stoichiometric but also an ordered GaN (1x1) surface [218,219,221].

Annealing in a flux of Ga is another suitable method of contamination removal that maintains stoichiometry and may be more effective at reducing defect formation. Work by Asif Kahn *et al.* [222] demonstrated that this method can achieve atomically clean GaN after exposure to $\sim 5 \times 10^{15} \text{ cm}^{-2} \text{ min}^{-1}$ Ga flux at 900°C, while effectively removing carbon contamination; *in-situ* AES results show the intensity ratio of C KLL to N KLL is below 0.02, while oxygen contamination is close to the AES sensitivity limit. In a similar study, Bermudez *et al.* [223,224] cleaned GaN by depositing Ga metal on the sample surface followed by annealing in UHV at 900-950°C. The carbon and oxygen contamination is reduced below the AES sensitivity limit (>0.01 and 0.005 ML, respectively). As an alternative method, Bermudez [201] applied N_2^+ sputtering on GaN followed by 900°C UHV annealing to achieve similar contaminant reduction below the sensitivity limit of AES, suggesting that N_2^+ sputtering prior to annealing may help prevent the formation of N vacancies that occur during UHV annealing [225]. Both Ga and N_2^+ sputtering yield (1x1) ordered surfaces.

5. Plasma Annealing

In many cases, annealing in plasma, particularly H_2 and N_2 plasma, is more effective at removing contaminants than other methods at lower temperatures because of the reactivity of the plasma species. This has been shown by King *et al.* [197]; they found H_2 plasma can remove carbon and halogens at 450°C, which is much lower than the temperature needed to remove these contaminants in the vacuum, NH_3 , or Ga flux.

Combination with N₂ plasma makes the cleaning even more effective as shown by Yang *et al.* [111], who compared cleaning processes of H₂, N₂, and H₂/N₂ (1:4) plasma at 650°C. Moreover, N₂ plasma annealing at 700-750°C is a more effective method at removing carbon contamination than Ga deposition/readsorption as demonstrated by Schulz *et al.* [226]; though deposition/readsorption is a more efficient method of oxygen removal. Both methods result in clear (1x1) LEED patterns. These results suggest that plasma annealing is a comparatively effective means of reducing carbon.

Many studies have also investigated the effectiveness of plasma annealing at removing oxygen. For example, after removing carbon contamination *ex-situ* with HCl and UV/O₃, Lee *et al.* [227] investigated the effects of N₂ and N₂/H₂ plasma at removing oxygen from GaN at 750°C or 900°C. At both temperatures, both carbon and oxygen are below the limit of AES sensitivity; however, a large amount of surface oxygen ($2 \times 10^{22} \text{ cm}^{-3}$) and carbon ($3 \times 10^{20} \text{ cm}^{-3}$) is still measured on GaN by secondary ion mass spectroscopy (SIMS). Hashizume and Inagaki *et al.* [90,228,229] reported that ECR H₂ and N₂ plasma at 280°C is effective at significantly reducing but not eliminating oxygen and carbon from AlGaN. Furthermore, the samples cleaned with H₂ plasma are characterized by a decrease in the N signal as measure by XPS, suggesting that H₂ plasma reacts with the surface to form volatile NH_x groups. This may cause N-vacancy related defects, or metallic Ga and/or Al on the surface, degrading device performance. The N₂ plasma is thus believed to suppress the formation of N vacancies. Jin and Hashizume *et al.* [228,230], using dry etching with ECR CH₄/H₂/Ar plasma, have also suggested this hypothesis.

Similar studies have shown that plasma cleaning can improve reliability issues and device performance. Meyer *et al.* [231] demonstrated that SF₆- and/or O₂- plasma cleaned SiN_x/AlGaIn/GaN HEMTs achieve better current collapse characteristics than untreated or wet chemical treated devices, which is likely connected to their relative effectiveness at removing carbon from AlGaIn. Similarly, Guhel *et al.* [232] used O₂ plasma to remove carbon and/or CF₄ plasma to remove oxygen, where the largest drain current and smallest knee voltages were obtained using the combined (O₂+CF₄) pretreatment. It is thus observed that this pretreatment may decrease the influence of electrical traps located at the AlGaIn surface. Hoshi *et al.* [233] reported that an optimized NH₃ plasma can remove carbon contamination and suppress current collapse in SiN_x/AlGaIn/GaN HEMTs; however, an extended NH₃ plasma process may degrade the stoichiometric composition of the AlGaIn surface and impact current collapse suppression. Kim *et al.* [234] have suggested that NH₃ plasma may introduce interstitial H⁺, which passivates bulk defects and explains the lower current collapse in NH₃-plasma treated AlGaIn/GaN HEMTs compared to N₂-plasma treated. This is supported by the work of Hierro *et al.* [235], who maintain that hydrogen can passivate bulk defects in n-type GaN through plasma processing. They propose that although the formation energy of H⁺ is higher than that of H⁻ in n-type GaN [236], H⁺ can diffuse deeper into GaN to passivate the deep level defects due to a lower migration barrier [236]. It may also be worth mentioning that the effects in p-type GaN may be different, where the incorporation of hydrogen can form a Mg-H complex. Therefore, as Nakamura *et al.* [237] reported the resistivity of p-type GaN annealed in NH₃ above 400°C significantly increases. This ultimately leads to

degradation of the carrier concentration in p-type GaN and reduced device performance [237-239].

6. ALD Precursor Cleaning

Atomic layer deposition (ALD) is a chemical vapor deposition (CVD) technique, which uses a self-limiting gas-phase chemical process and consequently generates uniform and conformal thin films [240]. One cycle of ALD growth consists of four steps: first, a self-limiting reaction between the substrate and the first reactant or precursor; second, a purge step to remove non-reacted precursor and gaseous by-products of the reaction; third, a self-limiting reaction between the second reactant and the first reactant absorbed on the surface; and lastly, another purge step [241]. This gives a growth rate in terms of growth per cycle (GPC), typically 0.5-1 Å. Consequently, the thickness of the film can be precisely controlled, giving uniform and conformal films.

This series of chemistry driven half-cycles can be employed in cleaning as well as deposition. In the ALD deposition of Al₂O₃, the reactants used are most commonly trimethylaluminum (TMA) and H₂O. Experiments on GaAs [242] and InGaAs [243] show that the first TMA pulse removes the trivalent oxides of gallium and arsenic. It has been suggested that the removal is associated with a ligand exchange mechanism between TMA and the native oxide, where the Al³⁺ ion in Al(CH₃)₃ preferentially replaces As³⁺ and Ga³⁺ in the related oxide, forming AlO_x and volatile As(CH₃)₃ and Ga(CH₃)₃ [244,245]. Similar studies have been applied to GaN with less success. One study by Sivasubramani *et al.* [202] shows no significant reduction of Ga-oxide after the first TMA half cycle. In

another study by Liu *et al.* [246], results show that a H₂O pretreatment results in fewer interface traps as will be discussed later.

7. Summary

In summary, there has been much progress on cleaning GaN and AlGaN with *ex- and in-situ* processes. In terms of *ex-situ* processes, cleaning with UV/O₃ and HF are most effective at removing carbon contamination for both GaN and AlGaN, while HCl, HF, NH₄OH, and (NH₄)₂S are most effective at removing oxygen. In some of these cases, the wet chemical leaves Cl- or S-termination, which inhibits surface reoxidation. The *pH* and oxide-reduction potential of the selected etchant are also crucial to obtaining an oxide-free and balanced-stoichiometry surface [247]. However, complete contamination removal has not been achieved by *ex-situ* cleaning methods alone. Further *in-situ* treatments, such as Ga deposition/readsorption or N₂⁺ sputtering along with high temperature annealing, are more likely to be effective at removing carbon and oxygen. Additionally, H₂/N₂ and NH₃ gas and/or plasma may be more efficient at passivating the surface and bulk defects. The polarization of the substrate may be a factor as well because of the stability of various bonding; namely, the Ga-face is more stable than N-face in hydroxide solutions and hot H₃PO₄. It is also likely that the magnitude of the polarization will affect the cleaning, where increasing the polarization is achieved by increasing the aluminum content and altering the surface chemistry.

Ultimately, these cleans will have a profound effect on device performance, where the cleaning requirements vary with the specifics of the desired device. For example, cleaning requirements for metal/GaN interfaces may be different from that for gate

dielectric/GaN. For example, residual Cl and S on the GaN surface may enhance the adhesion of metals and improve device performance. Similarly, plasma or ion sputtering can improve the ohmic contact properties of metal/GaN by causing point defects such as donor-like nitrogen vacancies, which may create a thin n-type layer between the metal and GaN. However, for dielectric/GaN interfaces, these vacancies may induce electrically active defects at the interface or in the dielectric, degrading the device. In other words, understanding interface electronic states is even more complicated as it must integrate the results of various surface treatments, dielectric properties and growth methods, metal contacts, and device behavior.

B. Dielectric Passivation and Interface Processing

Device behavior can also be modified with the incorporation of dielectrics, which are typically used to mitigate reliability issues in one of two ways: as a gate dielectric and as a passivation layer. The distinction between these two functions is not typically emphasized since the dielectric often functions as both. However, there are some cases where different dielectrics are employed for each component. Thus, for clarity, the two are distinguished by their position in the device, where the gate dielectric is the material underneath the gate, which mitigates gate leakage, and the channel passivation layer is the material between the gate and the drain, which mitigates current collapse. The device characteristics will therefore depend critically on the dielectric properties; the two most important being the band gap and the dielectric constant, where one determines the confinements characteristics of the carriers and the other relates to the electric field across the dielectric. Ideally, a gate insulator would have a large band gap and a large

dielectric constant, resulting in large band offsets that permit carrier confinement and large capacitance that permits device scaling; however, the two properties are often inversely related. There are other factors to consider as well, such as the crystal structure of the dielectric. In many cases, amorphous materials are preferred to crystalline, since crystalline materials may be characterized by grain boundaries. These defects serve as tunneling paths or trapping states and thus mitigate the effectiveness of the dielectric. Single crystal structures, on the other hand, may be promising but often require high temperature deposition as well as consideration of the lattice mismatch between the semiconductor and insulator. If this parameter is not optimized, it may result in a high concentration of structural defects at the interface. Furthermore, the deposition method and material type may alter the defect concentration at the interface or in the insulator, which affect trap-assisted tunneling processes. Additionally, the thermal and chemical properties must be considered when evaluating an insulator. In other words, there are several parameters to be considered when evaluating the effectiveness of a dielectric.

To date, a number of dielectrics have been considered for passivation layers and gate dielectrics on GaN and AlGaN devices. The following section will give a detailed discussion of recent research, which considers various dielectrics, including silicon oxide (SiO_2), silicon nitride (SiN_x), aluminum nitride (AlN), low-temperature gallium nitride (GaN), gallium oxide (Ga_2O_3), aluminum oxide (Al_2O_3), hafnium oxide (HfO_2), zirconium oxide (ZrO_2), titanium oxide (TiO_2), scandium oxide (Sc_2O_3), magnesium oxide (MgO), calcium oxide (CaO), lanthanum oxide (La_2O_3), lutetium oxide (Lu_2O_3), gadolinium oxide (Gd_2O_3), tantalum oxide (Ta_2O_3), zinc oxide (ZnO), and praseodymium

oxide (Pr_2O_3). There are other dielectrics that have been considered as well, but these represent the most prominently used in GaN-based studies.

For clarity, it should be noted that comparing the performance of these dielectrics can be potentially problematic since surface pretreatments, dielectric deposition, device fabrication, and post-deposition treatments are not consistent between different studies. Additionally, studies that report the interface trap density (D_{it}) conventionally describe the minimum measured value, which is not necessarily representative of the distribution of states across the band gap and may not even represent the actual minimum value, depending on the range of the probing technique. For simplicity, this convention is continued in the following section, but it should be kept in mind that these values may be misleading.

1. SiO_2 and SiN_x

On GaN and AlGaN, the most extensively researched dielectrics are SiO_2 and SiN_x [47,50,85,90,248-253], which have been considered both as gate insulators and channel passivation layers. Their appeal is largely related to their current widespread use in Si-based technologies, and thus they are well-understood materials. Furthermore, they have been proven effective at reducing leakage current by ~ 4 orders of magnitude and increasing the gate voltage that results in current collapse in MOSHFETs and MISFETs (metal-insulator-semiconductor heterostructure field-effect transistors). [47,48,51].

Comparatively, SiN_x is a better dielectric in terms of the dielectric constant (~ 7.5) at the expense of the band gap (~ 5.0 eV). Additionally, SiN_x may be advantageous because it is unlikely to oxidize the substrate during dielectric deposition like SiO_2 and may passivate

nitrogen-vacancy related defects on the surface during dielectric growth. Ultimately, this should result in a lower D_{it} . For example, using ECR-PECVD SiN_x , Nakasaki *et al.* [180] measured the D_{it} of SiN_x/GaN to be $5 \times 10^{10} \text{ cm}^{-2} \text{ eV}^{-1}$, after NH_4OH wet-chemical and N_2 -plasma pretreatments. Alternatively, using RF-PECVD SiO_2 , they measured the D_{it} of SiO_2/GaN to be $3 \times 10^{11} \text{ cm}^{-2} \text{ eV}^{-1}$, after the same wet chemical pretreatment. In other words, the D_{it} of SiN_x/GaN is ~ 6 times lower than the D_{it} of SiO_2/GaN . On the other hand, the D_{it} is sensitive to the processing and deposition conditions, and therefore, there are cases where SiO_2/GaN interfaces will have a lower D_{it} than SiN_x/GaN . In a study by Arulkumaran *et al.* [254], the D_{it} is compared for e-beam SiO_2 , PECVD SiO_2 , and PECVD SiN_x in GaN MIS devices; their respective D_{it} were 5.3×10^{11} , 2.5×10^{11} , and $6.5 \times 10^{11} \text{ cm}^{-2} \text{ eV}^{-1}$. In this case, PECVD-deposited SiO_2 has a smaller concentration of interface traps than similarly grown SiN_x . Similarly, Bae *et al.* [250] reported not only a lower D_{it} and electron trapping but also a lower leakage current and improved reproducibility properties for $\text{SiO}_2/\text{nitrided-thin-Ga}_2\text{O}_3/\text{GaN}$ ($D_{it}=4 \times 10^{11} \text{ cm}^{-2} \text{ eV}^{-1}$) relative to SiN_x/GaN ($D_{it}=9 \times 10^{11} \text{ cm}^{-2} \text{ eV}^{-1}$). Moreover, in terms of current collapse, ALD-deposited SiO_2 [47,248,251] is comparable to PECVD SiN_x [252] passivation on AlGaIn/GaN HFETs.

Combinations of SiO_2 or SiN_x have also been tried as passivation layers and/or gate insulators because of the reciprocal nature of the dielectric constants and band gaps of these materials; as mentioned, SiO_2 has a smaller dielectric constant (3.9) but a larger band gap (8.9 eV) than SiN_x . Therefore, an alloy such as SiON should have an intermediate dielectric constant (3.9-7.5 eV) and band gap (5.0-9.0), which depend on the

stoichiometry of the film. One such alloy has been studied on HEMTs by Arulkumaran *et al.* [255] and Balachander *et al.* [256]. Their results show that SiON not only reduces the gate leakage current by four orders of magnitude in comparison to unpassivated devices but also reduces current collapse and hysteresis width in comparison to SiN_x-passivated HEMTs. Similarly, stacked SiN_x/SiO₂ structures have been employed. In these studies, Balachander *et al.* [257] have illustrated that SiN_x/SiO₂-passivated AlGaIn/GaN HEMTs have a slightly lower current collapse and a higher leakage current compared to SiO₂-passivated devices as well as a lower leakage current and a slightly higher current collapse compared with SiN_x-passivated devices. In another study by Lachab *et al.* [50], the gate dielectric and channel passivation dielectric are differentiated; 4.2 nm SiO₂ is used as the gate insulator, and 30 nm SiN_x is used as the channel passivation layer. Results show that separating the two successfully suppresses the leakage current and current collapse.

2. Other Nitrides

In addition to SiN_x, other nitrides, namely AlN, have been studied as a gate dielectric and/or passivation layer. AlN has a small mismatch with respect to GaN (~0.3%) [258], which may minimize strain-induced defects at the interface depending on the deposition method. For example, sputtered AlN on AlGaIn/GaN heterostructures has been compared to e-beam SiO₂ and PECVD SiN_x by Chen *et al.* [259]. Of these three heterostructures, the AlN-passivated has the highest 2DEG mobility and a higher 2DEG density than SiO₂-passivated and unpassivated structures—though not SiN_x-passivated. Furthermore, high-temperature strain-relaxation is also best optimized for AlN [260]. On the other hand,

high energy sputtering may cause surface damage and ultimately limit the performance and reliability of the device. Consequently, other deposition methods have been considered as well. In MOCVD-grown AlN/GaN MIS structures, Hashizume *et al.* [261] measured a low D_{it} ($<1 \times 10^{11} \text{ cm}^{-2} \text{ eV}^{-1}$), and in ALD-AlN/AlGaN/GaN HEMTs, Huang *et al.* [262] have shown an atomically sharp interface between AlN and AlGaN as well as significant reduction in current collapse and dynamic on-resistance.

Low-temperature GaN has also been investigated as a potential gate insulator. On one hand, it may be counterintuitive to consider GaN a gate dielectric; however, the distinction is that dielectric GaN is grown at low temperature. Low-temperature-grown GaN has very different qualities than high-temperature-grown GaN, namely a poor crystalline quality and very high resistivity [263]. It may therefore be advantageous as a dielectric given the small lattice mismatch. Furthermore, deposition can be done *in-situ* after growth, which limits contamination. For these reasons, Kao *et al.* [264] have considered low-temperature, GaN-passivated AlGaN/GaN HFETs in comparison with SiO₂ and SiN_x-passivated devices. Their results show that GaN may be a better gate dielectric than SiO₂ or SiN_x, giving the highest sheet carrier concentration (~50% higher than that of unpassivated HFET) and reduction in current collapse because of the superior lattice match. On the other hand, the band gap of GaN is small with insignificant band offsets, and therefore, GaN may not be as effective at limiting the leakage current.

3. Gallium Oxide

Ga₂O₃ is also of interest as a gate dielectric and passivation layer for GaN and AlGaN MOS devices, with a band gap of 4.8 eV and dielectric constant of 10.2-14.2. One of the

benefits of Ga₂O₃ is that it can be natively grown on GaN via thermal and chemical process, which can limit contamination at the interface [265,266]. Unfortunately, thermal oxidization is extremely slow for temperatures <800°C [199], and higher temperatures may cause surface damage as previously mentioned. Lee *et al.* [266] circumvented this issue by oxidizing GaN in a H₃PO₄ solution with a pH value of 3.5 and laser illumination. This oxidation process achieves a D_{it} of 2.5x10¹¹ cm⁻²eV⁻¹ with a reasonable leakage current (6x10⁻⁷A/cm² at -20 V) and reasonable forward and reverse breakdown field (2.80 MV/cm and 5.70 MV/cm respectively). However, the relatively small band gap of 4.8eV of Ga₂O₃ cannot effectively suppress the leakage current. Moreover, Ga₂O₃ is also difficult to grow on AlGaN, where aluminum is more easily oxidized than gallium.

4. Aluminum Oxide

Amorphous Al₂O₃ [88,267-269] has been favored by many studies because of the large band gap (~7 eV), sufficient dielectric constant (~10), high breakdown field (10 MV/cm), high thermal (<850°C) and chemical stability on AlGaN. Hashizume *et al.* [90] demonstrated MBE-grown, Al₂O₃-passivated AlGaN/GaN is characterized by good control of drain current up to V_{GS}=+3 V, no current collapse under the quiescent gate voltage stress, and lower leakage current at forward bias compared to SiN_x-passivation. This is likely a result of the larger conduction band offset of Al₂O₃. ALD-grown Al₂O₃ has also shown some favorable results by Park *et al.* [267] and Chang *et al.* [269], the latter calculating a D_{it} of (4-9)x10¹¹ cm⁻²eV⁻¹. As mentioned, ALD results may vary depending on the deposition conditions; Liu *et al.* [246] found that pretreatment with H₂O prior to ALD growth yields an extremely low D_{it} (~2 x10¹⁰ cm⁻²eV⁻¹). In other words,

Al_2O_3 exhibits excellent performance in suppressing gate leakage and current collapse in GaN-based devices; this dielectric has a lower D_{it} by an order of magnitude, a higher dielectric constant, and similar gate leakage suppression compared to reports of Si-based dielectrics. However, the dielectric constant of Al_2O_3 is still relatively low in comparison with other materials, and thus, Al_2O_3 -passivated devices may also be characterized by a less than optimal threshold voltage shift and decrease in transconductance. It may therefore be advantageous to use Al_2O_3 as an interfacial passivation layer with a higher dielectric constant film, such as HfO_2 [270].

5. Hafnium and Related Oxides

Amorphous hafnium and related oxides have shown significant promise because of their high dielectric constants (~20-25) [271] and sufficient band gaps (5.8 eV). For this reason, HfO_2 is currently used to replace SiO_2 as the gate insulator in Si-based MOSFET fabrication, which allows for device scaling. HfO_2 is, therefore, likely to effectively diminish the gate leakage in GaN-based MOSFETs as well. Liu *et al.* [175] demonstrated that this is indeed the case, where sputtered HfO_2 reduces the leakage current by five orders of magnitude from unpassivated HEMTs. This work also shows that HfO_2 reduces current collapse, increases gate voltage swing, and augments cut off frequencies. Furthermore, HfO_2 -based devices exhibit only a small reduction in transconductance because of the relatively high-k dielectric constant. Another study of ALD- HfO_2/GaN by Chang *et al.* [271] reveals a D_{it} of $2 \times 10^{11} \text{ cm}^{-2} \text{ eV}^{-1}$ in addition to negligible current collapse and a low leakage current density (10^{-7} - 10^{-8} A/cm^2 at 1 MV/cm).

On the other hand, HfO₂ is less thermally and chemically stable than Al₂O₃, where amorphous HfO₂ crystallizes into predominantly monoclinic polycrystalline films on Si at only 300–500°C [272,273]. This is disadvantageous as crystalline structures are more likely to contain grain boundaries, which enhance leakage. Consequently, in an attempt to combine the stability and larger band gap of Al₂O₃ with the large dielectric constant of HfO₂, there have been several investigations into stacked HfO₂/Al₂O₃ as well as HfAlO alloys. For example, Yue *et al.* [270] fabricated a HfO₂/Al₂O₃-passivated AlGaN/GaN MOSHEMTs using ALD. Their device had no measureable C-V hysteresis, a small threshold voltage shift, a maximum drain current of 0.8A/mm, a peak g_s of 150 mS/mm, and leakage current at least six orders of magnitude smaller than an unpassivated HEMT. Furthermore, as long as the device surface was properly passivated, the device did not show current collapse; a single layer of Al₂O₃ could adequately suppresses current collapse, and additional HfO₂ layers more effectively reduced the leakage current. In addition to the stacked structure, Liu *et al.* [246] have also investigated MOCVD HfAlO (10% Al) to achieve a higher stability and crystallization temperature with respect to HfO₂ and higher dielectric constant with respect to Al₂O₃. Results give a D_{it} between 7.8x10¹⁰ and 2.38x10¹⁰ cm⁻²eV⁻¹, depending on the pre-deposition surface processing.

Other related high-k materials comparable to HfO₂ have also been considered, such as ZrO₂ with a band gap of ~5.8 eV and dielectric constant of ~20 as well as TiO₂ with a band gap of 3.2 eV and a dielectric constant of ~24-96, depending on the TiO₂ film phase [274]. ZrO₂/GaN HEMTs have been studied by Balachander *et al.* [275]. In these devices, the maximum current density (1.17A/mm) is twice that of unpassivated devices, and the

leakage current is four orders of magnitude lower. It appears thus that ZrO₂ may still be less effective than HfO₂ in this regard, though it is difficult to ascertain without a more direct comparison. Other studies by Hu *et al.* [276] on GaN MOSHEMTs with TiO₂ as a gate insulator and passivation layer show the device is characterized by twice the maximum drain current (0.84A/mm), a higher breakdown field (13 MV/cm), a decreased D_{it} (6.4x10¹¹ cm⁻²eV⁻¹), and a significantly suppressed current collapse. Furthermore, the leakage current in reverse bias (~5.1x10⁻⁹A/cm² at 1 MV/cm) is comparable to other high-k materials; however, given the small band gap of TiO₂, it may further benefit from an additional higher band-gap dielectric capping layer. Similar to the combination of HfO₂ and Al₂O₃ or SiO₂ and SiN_x, the stacked structure would augment the overall band gap of the combined dielectric, though slightly compromising the high-k benefits.

6. Scandium and Magnesium Oxides

Sc₂O₃ has a sufficient band gap of 6.3 eV, high dielectric constant of ~14, and a lattice mismatch of ~9% for cubic bixbyite crystalline films, such that the (111) orientation is parallel to (0001) GaN. This orientation has been obtained via MBE deposition in several reports [277-279], which consider heteroepitaxy as beneficial to the electrical properties. In particular, these studies argue that epitaxial dielectrics may minimize the density of surface states, by occupying surface dangling bonds on the substrate. On the other hand, MBE may not yet be readily scalable for high-yield manufacturing. Therefore, Wang *et al.* [280] have also investigated the performance of ALD Sc₂O₃ thin films on AlGaN/GaN devices, which result in a polycrystalline dielectric film with some misoriented grains. This group suggested that these devices have excellent electrical properties such as high

I_{on}/I_{off} ratio and low subthreshold slope. Mehandru *et al.* [281] also determined that Sc_2O_3 is efficient at reducing current collapse, where Sc_2O_3 -passivated devices were characterized by ~40% less current collapse than unpassivated devices. Furthermore, the effectiveness of Sc_2O_3 passivation is not strongly affected by high-energy (40 MeV) proton irradiation and thus may be of interest in environments with high fluxes of ionizing radiation [282].

MgO has also been considered as a gate passivation layer and gate insulator with a large band gap (8.0 eV), sufficient dielectric constant (~10), and small lattice mismatch (-6.5%), where Sc_2O_3 and MgO both effectively suppress the current collapse in AlGaIn/GaN HEMTs and have a respective D_{it} of 5×10^{11} and $2 \times 10^{11} \text{ cm}^{-2} \text{ eV}^{-1}$, as shown by Luo *et al.* [283]. Furthermore, they suggest that these dielectrics may be advantageous over SiN_x with regards to long-term device stability because of the smaller hydrogen content in the films, though comparative studies have not yet confirmed this. In other words, Sc_2O_3 and MgO are effective passivation layers with slightly different advantages; MgO may be more effective as a gate dielectric given its larger band gap while Sc_2O_3 is more chemically stable and less likely to oxidize. Polyakov *et al.* [284] have therefore investigated MgScO/GaN relative to Sc_2O_3 and MgO/GaN in an attempt to take better advantage of these properties. The result is a lower D_{it} at the MgScO/GaN interface ($\sim 1 \times 10^{11} \text{ cm}^{-2} \text{ eV}^{-1}$) than either Sc_2O_3 /GaN or MgO/GaN.

The lattice mismatch of MgO can be further decreased with a magnesium calcium alloy, forming crystalline Mg_xCa_yO as shown by Gila *et al.* [285]. Depending on the composition, the lattice mismatch varies from -6.5 to 6.9 eV, where $Mg_{0.5}Ca_{0.5}O$ is the

lowest (-0.23%) of the compositions studied. It may be possible to further decrease the lattice mismatch with a slightly different composition. However, while MgCaO is more stable than MgO, it does not exhibit the stability required for optimal device performance. The research, therefore, suggests the addition of a Sc₂O₃ capping layer.

7. Rare Earth Oxides

In addition to Sc₂O₃, rare earth oxides have also been considered as a device dielectric because of their high dielectric values and thermal stability. La₂O₃ is one such material, with a large dielectric constant (18–27) and sufficient band gap (4.3–6.4 eV), depending on the crystal structure; for cubic, the dielectric constant is 18, and for hexagonal, the dielectric constant is 27. The high dielectric constant suggests it would improve device transconductance; however, La₂O₃/GaN is also characterized by a large lattice mismatch (~20%), and therefore has a larger D_{it} and leakage current than Sc₂O₃/GaN devices [279]. Work by Chiu *et al.* [286] has also suggested that La₂O₃ is not effective at mitigating gate leakage, where La₂O₃-passivated AlGaIn/GaN HEMTs reduce the leakage current by only one order of magnitude relative to unpassivated devices. Furthermore, this material is also hygroscopic, which is unfavorable to device performance. La₂O₃ may, therefore, be a favorable constituent in an alloyed dielectric. In one such study, Yang *et al.* [287] alloyed La₂O₃ with Lu₂O₃, fabricating LaLuO-passivated MOSHEMTs. Lu₂O₃ has a large band gap with better hygroscopic immunity but a lower dielectric constant and crystallization temperature. Therefore, the alloy should increase the hygroscopic immunity and band gap at the expense of the thermal stability and dielectric constant. Device characterization shows a leakage current lower than the unpassivated devices with

a reasonable maximum drain current (0.82A/mm at a gate bias of +3V) and a high transconductance (~192 mS/mm).

Gd₂O₃ is another rare earth oxide that has been considered, where the dielectric constant (11.4) and band gap (5.3 eV) are sufficient. Similar to Sc₂O₃, Gd₂O₃ is characterized by a bixbyite crystalline structure and grows with the (111) plane parallel to (0001) GaN; however, Gd₂O₃ has a much larger lattice mismatch (~20%), which results in a larger D_{it} and interface roughness in dielectric/GaN MOSFETs as shown by Gila *et al.* [288]. On the other hand, this dielectric has still been characterized by a sufficiently low D_{it} as shown by Das *et al.* [289], where single crystal Gd₂O₃ has been deposited on HCl-cleaned AlGaIn/GaN heterostructures and has a D_{it} of 1-3x10¹¹ cm⁻²eV⁻¹. However, the leakage current for single crystal Gd₂O₃/GaN MOS capacitors as measured by Chang *et al.* [290] was mediocre (4.6x10⁻⁶ mA/cm²) with small current collapse and hysteresis. Given the large lattice mismatch, mediocre dielectric constant, and adequate band gap, it seems unlikely that Gd₂O₃ could surpass other dielectrics on similar devices. It may, therefore, be beneficial to consider Gd₂O₃ in conjunction with another dielectric such as SiO₂. In another study, Johnson *et al.* [291,292] fabricated Gd₂O₃/GaN-based MOSFETs with an additional SiO₂ layer between the gate and Gd₂O₃ to further reduce the leakage current and increase the breakdown field. In other words, crystalline Gd₂O₃ is a mediocre dielectric in terms of mitigating reliability issues because of the large lattice mismatch but an advantageous dielectric in terms of the thermal stability on GaN (<1100°C) [290]. It may, therefore, be that this dielectric is more successful as an amorphous film, such as Ga₂O₃(Gd₂O₃), which has demonstrated high thermal stability <800-900°C on InGaAs.

[293,294]. In a study by Ren *et al.* [295], e-beam amorphous $\text{Ga}_2\text{O}_3(\text{Gd}_2\text{O}_3)/\text{GaN}$ MOSFETs are characterized by a significantly reduced gate leakage current at elevated temperature relative to unpassivated devices. In fact for these MOSFETs, device operation improved at increased temperatures $<400^\circ\text{C}$.

8. Zinc and Miscellaneous Oxides

Other dielectrics, such as ZnO [190,296,297] have been considered as gate insulators and/or passivation layers on GaN and AlGaN/GaN-based devices. In particular, ZnO is very similar to GaN, with the same crystal structure, a similar band gap, and small lattice mismatch. Chiou *et al.* [190,191] have shown that this dielectric can be used to improve the interface quality of AlGaN/GaN HEMTs. Additional surface processing such as $(\text{NH}_4)_2\text{S}$ or HCl treatments may further improve the quality of the interface by reducing the surface states with the formation of Ga-S and Ga-Cl bonds on the AlGaN surface. Consequently, these devices have a reduced current collapse relative to unpassivated AlGaN/GaN MOSHEMTs. However, given its small band gap (3.4 eV), it is unlikely that ZnO will be an effective gate dielectric and may benefit from a stacked or alloyed structure.

Ta_2O_5 is another transparent oxide with a large dielectric constant (~ 25) but a relatively small band gap (4.4 eV). In particular, this dielectric has shown some benefits over traditional dielectrics. Wang *et al.* [298] investigated variations in the 2DEG carrier concentration of AlGaN/GaN structures passivated with MOCVD Ta_2O_5 relative to SiO_2 , Al_2O_3 , and Si_3N_4 . Their results show that for thin Ta_2O_5 films (2-4 nm) the 2DEG increases but decreases for thicker films (>4 nm). This behavior suggests that there is

positive charge at the Ta₂O₅/AlGa_N interface but the majority of charge in the bulk is fixed and negative. Therefore as the oxide thickness increases, the number of negative charges increases, reducing the 2DEG. The 2DEG concentration of SiN_x-passivated structures, on the other hand, increases with thickness. The authors suggest that this may be related to an increase in the piezoelectric polarization charge due to strain. In another comparative study of ALD dielectrics on AlN/GaN HEMTs, Deen *et al.* [299] compared the effectiveness of Ta₂O₅ relative to HfO₂, showing that Ta₂O₅ may give better device performance. Ta₂O₅-passivated devices have a smaller surface roughness and D_{it} ($2.4 \times 10^{13} \text{ cm}^{-2} \text{ eV}^{-1}$) than HfO₂-passivated ($10^{13} \text{ cm}^{-2} \text{ eV}^{-1}$) as well as a greatly improved transconductance, which is likely related to a higher dielectric constant. Furthermore, despite the lower band gap, the Ta₂O₅ structures are characterized by a comparable gate leakage current. This research would suggest that thin Ta₂O₅ might prove advantageous.

Other oxides, such as Pr₂O₃ [300], may also prove influential in the development of GaN-based devices; this review has provided an overview of some of the most promising to date, though is by no means comprehensive.

9. Summary

In summary, there have been some significant strides in mitigating reliability issues with dielectric passivation schemes and gate dielectrics, but there is still no perfect solution. The complexity of this issue is intricately linked to the reciprocal nature of the dielectric constant and band gap and may also be related to the different mechanisms responsible for gate leakage and current collapse. For examples, since current collapse is associated with defects at the AlGa_N or Ga_N surfaces, the most likely cause may be either nitrogen

vacancies or electric field driven oxidation from atmospheric moisture. Therefore, the most effective dielectrics at mitigating this mechanism are nitrides, such as SiN₂, AlN, and even GaN, as most experimental studies demonstrate. In addition, nitride passivation increases the 2DEG concentration in AlGaN/GaN structures. On the other hand, the band gap of the nitrides is smaller than many of the oxides, making them less effective at reducing the leakage current. Therefore, N₂ plasma treated oxides could come to play an integral role in future devices; N₂ plasma influences the passivation of nitrogen vacancies or the nitridation of the dielectric. Either mechanism might explain the success of Al₂O₃ with N₂ plasma processing.

Al₂O₃ remains one of the more competitive dielectrics given the large band gap, thermal and chemical stability. On the other hand, Al₂O₃ has a lower dielectric constant and thus a lower transconductance. Consequently, Al₂O₃ may be better as an interfacial passivation layer with a higher dielectric material, such as HfO₂, ZrO₂, or even Ta₂O₅. However, these oxides also have a concentration of negative bulk charge, which may correspond to oxygen-related defects. This charge could decrease the 2DEG carrier concentration and aid in leakage current. It is also worth noting that native oxides are not yet an effective means of passivation, and given the large number of defects that are created after electrical stressing, it may prove crucial to remove the native oxides prior to deposition.

There has also been some success with epitaxial dielectric passivation schemes and gate oxides. It is suggested that these dielectrics will decrease the D_{it} given the small lattice mismatch with Sc₂O₃, MgO, and CaO. However, while there is no direct comparison,

experiments have obtained similar D_{it} and interface qualities with amorphous films as well. It, therefore, seems unlikely that epitaxial films will be advantageous to the advancement of GaN-based devices. Amorphous films can be deposited at lower temperatures and are not as likely to crystallize, which may help to prevent the formation of defects with associated gate leakage mechanisms such as trap-assisted tunneling or Frenkel-Poole emission.

C. Post-Deposition and Post-Metallization Processing

Given the success of N_2 plasma treatments, other attempts to passivate surface states have focused on post-deposition and post-metallization techniques, which have been shown to reduce the deep-level traps and interface states [14,114,301-304]. For example, Edwards *et al.* [305] report that after dielectric deposition, NH_3 plasma can reduce current collapse and increase reliability for microwave operation of $SiN_x/AlGaN/GaN$ HEMTs. The improved performance is possibly associated with incorporated H^+ , which may passivate bulk defects in GaN.

There has also been success with post-metallization treatments. For example, Peng *et al.* [301] demonstrated that post-metallization annealing (PMA) at $350^\circ C$ in N_2 on $SiN_x/AlGaN/GaN$ HEMTs improves the direct-current, radio-frequency small signal, and power performance. It is suggested that PMA improves the quality of the passivation layer by N diffusion through the SiN_x into N vacancies in the AlGaN, suppressing current collapse; the plasma process may also recover the dry-etch damage at the Schottky metal/AlGaN interface, reducing leakage current. Similarly, Zhou *et al.* [303] found improved DC performance of ALD $Al_2O_3/AlGaN/GaN$ HEMTs after 10 min $600^\circ C$ PDA

in N₂ atmosphere. This treatment reduces deep-level traps, ultimately increasing the maximum transconductance and gate-drain breakdown voltage. Other studies by Wu *et al.* [114] reported the D_{it} of ALD-Al₂O₃/GaN MOS structures is reduced from ~1.5x10¹² cm⁻²eV⁻¹ to 7x10¹⁰ cm⁻²eV⁻¹ after 800°C PMA in N₂, and Lin *et al.* [306] reported on the reduction in the leakage current in AlGaIn/GaN HEMTs by three orders of magnitude by PMA in N₂/H₂.

In other words, it is clear that post-deposition or post-metallization treatment plays a role in improving passivation effects and reducing current collapse and gate leakage. Most studies agree that PDA in some form of N₂ plasma or PMA in some form of N₂ gas ambient are effective ways at increasing device performance; however, it is not clear how the treatment passivates culpable electronic states.

IV. Summary and Conclusions

In summary, while research has addressed the properties and impact of electronic states, there is still a need for concentrated efforts to provide a more comprehensive understanding of interface and surface electronic states. It is clear from gate leakage and current collapse measurements that improving surface state passivation will play an integral part in mitigating failure mechanisms and augmenting device reliability. From polarization and band bending, we can determine that there is a significant density of states (10¹³ states/cm²) at the surface of GaN and AlN. *Ab initio* calculations seemingly imply that these surface states are associated with vacancies and vacancy complexes; however, such a pristine surface is rarely achieved on GaN or AlN, which are typically contaminated with high concentrations of structural defects, point defects, surface

contamination, and native oxide. Cleaning and surface processing is therefore an important step in device fabrication, where several cleans have been proven to increase device performance. For example, NH_4OH relative to acid etches was shown to improve device performance because of decreased Ga_2O_3 coverage. These results would suggest that the native oxide may be more influential than carbon, since the carbon contamination is often larger on NH_4OH cleaned samples. On the other hand, other research has shown that carbon is detrimental to device performance. Given the intricacy of the states, it is difficult to compare the impact of specific cleaning processes. Other cleaning processes were more successful at removing both oxygen and carbon contaminations, but they may have been at the expense of increasing other defects such as Ga or N vacancies. In some other cases, cleaning even produced stoichiometric GaN with contamination levels below the sensitivity of surface analysis techniques. However, such samples have not been connected with any specific surface reconstruction or device behavior. It thus remains unclear whether these samples have effectively mitigated the effects of the surface states. Furthermore, device structure requires the deposition of a passivation scheme, gate dielectric, and/or ohmic contact on the surface, which induces interface gap states as well as additional defect damage depending on the deposition process. There have been studies to evaluate the induced interface defects. While it is difficult to compare these studies given the multitudes of variables, research suggests Al_2O_3 and N_2 plasma currently show the most promise, producing surfaces with an interface trap density on the order of 10^{-10} charges/ cm^2 . In other words, of the $\sim 10^{13}$ states/ cm^2 required to screen the polarization bound charge, approximately one in every 1000 serves as an electron trap. This is a significant improvement. However, given the complexity and subtlety of the

electronic state configuration, a more systematic and comprehensive approach may be needed to fully optimize device performance.

V. Acknowledgements

This research was supported by the Office of Naval Research through the DEFINE MURI program, N00014-10-1-0937.

References

- [1] U. K. Mishra, P. Parikh, and Y. F. Wu, *Proc. IEEE* 90, 1022 (2002).
- [2] W. Saito, Y. Takada, M. Kuraguchi, K. Tsuda, I. Omura, T. Ogura, and H. Ohashi, *IEEE Trans. Electron Devices* 50, 2528 (2003).
- [3] Y. Niiyama, S. Ootomo, J. Li, T. Nomura, S. Kato, and T. P. Chow, *Semicond. Sci. Technol.* 25, 125006 (2010).
- [4] S. J. Pearton, and F. Ren, *Adv. Mater.* 12, 1571 (2000).
- [5] G. Meneghesso, G. Verzellesi, F. Danesin, F. Rampazzo, F. Zanon, A. Tazzoli, M. Meneghini, and E. Zanoni, *IEEE Trans. Device Mater. Rel.* 8, 332 (2008).
- [6] J. A. del Alamo, and J. Joh, *Microelectron. Reliab.* 49, 1200 (2010).
- [7] D. Marcon, J. Viaene, P. Favia, H. Bender, X. Kang, S. Lenci, S. Stoffels, and S. Decoutere, *Microelectron. Reliab.* 52, 2188 (2012).
- [8] J. Wuerfl, E. Bahat-Treidel, F. Brunner, E. Cho, O. Hilt, P. Ivo, A. Knauer, P. Kurpas, R. Lossy, M. Schulz, S. Singwald, M. Weyers, and R. Zhytnytska, *Microelectron. Reliab.* 51, 1710 (2011).
- [9] S. Mizuno, Y. Ohno, S. Kishimoto, K. Maezawa, and T. Mizutani, *Jpn. J. Appl. Phys. Part I* 41, 5125 (2002).
- [10] J. C. Carrano, T. Li, P. A. Grudowski, C. J. Eiting, R. D. Dupuis, and J. C. Campbell, *Appl. Phys. Lett.* 72, 542 (1998).
- [11] S. Oyama, T. Hashizume, and H. Hasegawa, *Appl. Surf. Sci.* 190, 322 (2002).
- [12] H. Hasegawa, and S. Oyama, *J. Vac. Sci. Technol. B* 20, 1647 (2002).
- [13] L. S. Yu, Q. Z. Liu, Q. J. Xing, D. J. Qiao, S. S. Lau, and J. Redwing, *J. Appl. Phys.* 84, 2099 (1998).
- [14] C. F. Shih, K. T. Hung, C. Y. Hsiao, S. C. Shu, and W. M. Li, *J. Alloys Compd.* 480, 541 (2009).
- [15] X. A. Cao, S. J. Pearton, G. Dang, A. P. Zhang, F. Ren, and J. M. Van Hove, *Appl. Phys. Lett.* 75, 4130 (1999).

- [16] E. J. Miller, X. Z. Dang, and E. T. Yu, *J. Appl. Phys.* 88, 5951 (2000).
- [17] E. J. Miller, E. T. Yu, P. Waltereit, and J. S. Speck, *Appl. Phys. Lett.* 84, 535 (2004).
- [18] S. Karmalkar D. M. Sathaiya, and M. S. Shur, *Appl. Phys. Lett.* 82, 3976 (2003).
- [19] B. Lambert, N. Labat, D. Carisetti, S. Karboyan, J. G. Tartarin, J. Thorpe, L. Brunel, A. Curutchet, N. Malbert, E. Latu-Romain, and M. Mermoux, *Microelectron. Reliab.* 52, 2184 (2012).
- [20] H. Zhang, E. J. Miller, and E. T. Yu, *J. Appl. Phys.* 99, 023703 (2006).
- [21] A. Fonserè, A. Pérez-Tomás, M. Placidi, J. Llobet, N. Baron, S. Chenot, Y. Cordier, J. C. Moreno, V. Iglesias, M. Porti, A. Bayerl, M. Lanza, and M. Nafia, *Appl. Phys. Lett.* 101, 093505 (2012).
- [22] L.-Y. Yang, Y. Hao, X.-H. Ma, J.-C. Zhang, C.-Y. Pan, J.-G. Ma, K. Zhang, and P. Ma, *Chin. Phys. B* 20, 117302 (2011).
- [23] Z. H. Liu, G. I. Ng, S. Arulkumaran, Y. K. T. Maung, and H. Zhou, *Appl. Phys. Lett.* 98, 163501 (2011).
- [24] S. Sudharsanan, and S. Karmalkar, *J. Appl. Phys.* 107, 064501 (2010).
- [25] X. A. Cao, E. B. Stokes, P. M. Sandvik, S. F. LeBoeuf, J. Kretchmer, and D. Walker, *IEEE Electron Device Lett.* 23, 535 (2002).
- [26] E. Arslan, S. Altindal, S. Özçelik, and E. Ozbay, *J. Appl. Phys.* 105, 023705 (2009).
- [27] D.-W. Yan, Z.-M. Zhu, J.-M. Cheng, X.-F. Gu, and H. Lu, *Chinese Phys. Lett.* 29 087204 (2012).
- [28] D. Yan, H. Lu, D. Cao, D. Chen, R. Zhang, and Y. Zheng, *Appl. Phys. Lett.* 97, 153503 (2010).
- [29] W. S. Tan, P. A. Houston, P. J. Parbrook, D. A. Wood, G. Hill, and C. R. Whitehouse, *Appl. Phys. Lett.* 80, 3207 (2002).
- [30] A. Mimouni, T. Fernández, J. Rodriguez-Tellez, A. Tazon, H. Baudrand, and M. Boussuis, *Electr. Electron. Eng.* 2, 397 (2012).
- [31] X. M. Shen, D. G. Zhao, Z. S. Liu, Z. F. Hu, H. Yang, and J. W. Liang, *Solid-State Electron.* 49, 847 (2005).
- [32] V. Lebedev, G. Cherkashinin, G. Ecke, I. Cimalla, and O. Ambacher, *J. Appl. Phys.* 101, 033705 (2007).
- [33] W. Xu, H. Rao, and G. Bosman, *Appl. Phys. Lett.* 100, 223504 (2012).
- [34] S. W. Kaun, M. H. Wong, S. DasGupta, S. Choi, R. Chung, U. K. Mishra, and J. S. Speck, *Appl. Phys. Express* 4, 024101 (2011).
- [35] S. Ganguly, A. Konar, Z. Hu, H. Xing, and D. Jena, *Appl. Phys. Lett.* 101, 253519 (2012).
- [36] G. Xie, E. Xu, B. Zhang, and W. T. Ng, *Microelectron. Reliab.* 52, 964 (2012).

- [37] M. M. Bajo, C. Hodges, M. J. Uren, and M. Kubali, *Appl. Phys. Lett.* 101, 033508 (2012).
- [38] M. Baemler, F. Gütle, V. Polyakov, M. Cäsar, M. Dammann, H. Konstanzer, W. Pletschen, W. Bronner, R. Quay, P. Waltereit, M. Mikulla, O. Ambacher, F. Bourgeois, R. Behtash, K. J. Riepe, P. J. Van de Wel, J. Klappe, and T. Rödle, *J. Electron. Mater.* 39, 756 (2010).
- [39] M. Āapajna, S. W. Kaun, M. H. Wong, F. Gao, T. Palacios, U. K. Mishra, J. S. Speck, and M. Kuball, *Appl. Phys. Lett.* 99, 223501 (2011).
- [40] C.-Y. Hu, and T. Hashizume, *J. Appl. Phys.* 111, 084504 (2012).
- [41] P. Makaram, J. Joh, J. A. del Alamo, T. Palacios, and C. V. Thompson, *Appl. Phys. Lett.* 96, 233509 (2010).
- [42] M. R. Johnson, D. A. Cullen, L. Liu, T. S. Kang, F. Ren, C.-Y. Chang, S. J. Pearton, S. Jang, J. W. Johnson, and D. J. Smith, *J. Vac. Sci. Technol. B* 30, 062204 (2012).
- [43] H. Hasegawa, T. Inagaki, S. Ootomo, and T. Hashizume, *J. Vac. Sci. Technol. B* 21, 1844 (2003).
- [44] H. Hasegawa, and H. Ohno, *J. Vac. Sci. Technol. B* 4, 1130 (1986).
- [45] T. Hashizume, J. Kotani, and H. Hasegawa, *Appl. Phys. Lett.* 84, 4884 (2004).
- [46] K. H. Lee, P. C. Chang, S. J. Chang, and Y. K. Su, *Solid-State Electron.* 72, 38 (2012).
- [47] C. J. Kirkpatrick, B. Lee, R. Suri, X. Yang, and V. Misra, *IEEE Electron Device Lett.* 33, 1240 (2012).
- [48] L. Pang, Y. Lian, D.-S. Kim, J.-H. Lee, and K. Kim, *IEEE Trans. Electron Devices* 59, 2650 (2012).
- [49] F. Husna, M. Lachab, M. Sultana, V. Adivarahan, Q. Fareed, and M. Asif Khan, *IEEE Trans. Electron Devices* 59, 2424 (2012).
- [50] M. Lachab, M. Sultana, H. Fatima, V. Adivarahan, Q. Fareed, and M. A. Khan, *Semicond. Sci. Technol.* 27, 125001 (2012).
- [51] T. Huang, X. Zhu, K. M. Wong, and K. M. Lau, *IEEE Electron Device Lett.* 33, 212 (2012).
- [52] Y. C. Chang, W. H. Chang, Y. H. Chang, J. Kwo, Y. S. Lin, S. H. Hsu, J. M. Hong, C. C. Tsai, and M. Hong, *Microelectron. Eng.* 87, 2042 (2010).
- [53] E. Miyazaki, Y. Goda, S. Kishimoto, and T. Mizutani, *Solid-State Electron.* 62, 152 (2011).
- [54] Y. C. Chang, M. L. Huang, Y. H. Chang, Y. J. Lee, H. C. Chiu, J. Kwo, and M. Hong, *Microelectron. Eng.* 88, 1207 (2011).
- [55] Z. W. Bi, Y. Hao, Q. Feng, T. T. Jiang, Y. R. Cao, J. C. Zhang, W. Mao, L. Lu, and Y. Zhang, *Sci. Chin. Phys. Mech. Astron.* 54, 2170 (2011).
- [56] H. Hahn, A. Alam, M. Heuken, H. Kalisch, and A. Vescan, *Semicond. Sci. Technol.* 27, 062001 (2012).

- [57] T. Hashizume, S. Anantathanasarn, N. Negoro, E. Sano, H. Hasegawa, K. Kumakura, and T. Makimoto, *Jpn. J. Appl. Phys.* 43, L777 (2004).
- [58] J. J. Freedman, T. Kubo, S. L. Selvaraj, and T. Egawa, *Jpn. J. Appl. Phys.* 50, 04DF03 (2011).
- [59] H.-A. Shih, M. Kudo, M. Akabori, and T.-K. Suzuki, *Jpn. J. Appl. Phys.* 51, 02BF01 (2012).
- [60] H.-C. Chiu, C.-W. Yang, C.-H. Chen, J. S. Fu, and F.-T. Chien, *Appl. Phys. Lett.* 99, 153508 (2011).
- [61] K. D. Chabak, D. E. Walker, M. R. Johnson, A. Crespo, A. M. Dabiran, D. J. Smith, A. M. Wowchak, S. K. Tetlak, M. Kossler, J. K. Gillespie, R. C. Fitch, and M. Trejo, *IEEE Electron Device Lett.* 32, 1677 (2011).
- [62] M. Āapajna, N. Killat, U. Chowdhury, J. L. Jimenez, and M. Kuball, *Microelectron. Reliab.* 52, 29 (2012).
- [63] R. Vetry, N. Q. Zhang, S. Keller, and U. K. Mishra, *IEEE Trans. Electron Devices* 48, 560 (2001).
- [64] J. A. Bardwell, S. Haffouz, W. R. McKinnon, C. Storey, H. Tang, G. I. Sproule, D. Roth, and R. Wang, *Electrochem. Solid-State Lett.* 10, H46 (2007).
- [65] A. Koudymov, M. S. Shur, G. Simin, K. Chu, P. C. Chao, C. Lee, J. Jimenez, and A. Balistreri, *IEEE Trans. Electron Devices* 55, 712 (2008).
- [66] M. Morardi, and P. Valizadeh, *IEEE Trans. Device Mater. Rel.* 10, 287 (2010).
- [67] F. Gao, D. Chen, B. Lu, H. L. Tuller, C. V. Thompson, S. Keller, U. K. Mishra, and T. Palacios, *IEEE Electron Device Lett.* 33, 1378 (2012).
- [68] M. Tajima, and T. Hashizume, *Jpn. J. Appl. Phys.* 50, 061001 (2011).
- [69] G. Meneghesso, G. Verzellesi, R. Pierobon, F. Rampazzo, A. Chini, U. K. Mishra, C. Canali, and E. Zanoni, *IEEE Trans. Electron Devices* 51, 1554 (2004).
- [70] A. M. Wells, M. J. Uren, R. S. Balmer, K. P. Hilton, T. Martin, and M. Missous, *Solid-State Electron.* 49, 279 (2005).
- [71] J. Joh, and J. A. del Alamo, *IEEE Trans. Electron Devices* 58, 132 (2011).
- [72] F. Berthet, Y. Guhel, H. Gualous, B. Boudart, J.-L. Trolet, M. Piccione, V. Sbrugnera, B. Grimbert, and C. Gaquière, *Solid-State Electron.* 72, 15 (2012).
- [73] S. DasGupta L. B. Biedermann, M. Sun, R. Kaplar, M. Marinella, K. R. Zavadil, S. Atcitty, and T. Palacios, *Appl. Phys. Lett.* 101, 243506 (2012).
- [74] W. Zhang, Y. Zhang, W. Mao, X.-H. Ma, J.-C. Zhang, and Y. Hao, *IEEE Electron Device Lett.* 34, 45 (2013).
- [75] C. Zhou, Q. Jiang, S. Huang, and K. J. Chen, *IEEE Electron Device Lett.* 33, 1132 (2012).
- [76] M. Faqir, M. Bouya, N. Malbert, N. Labat, D. Carisetti, B. Lambert, G. Verzellesi, and F. Fantini, *Microelectron. Reliab.* 50, 1520 (2010).

- [77] P. B. Klein, J. A. Freitas, S. C. Binari, and A. E. Wickenden, *Appl. Phys. Lett.* 75, 4016 (1999).
- [78] P. B. Klein, S. C. Binari, K. Ikossi, A. E. Wickenden, D. D. Koleske, and R. L. Henry, *Appl. Phys. Lett.* 79, 3527 (2001).
- [79] M. J. Uren, J. Möreke, and M Kuball, *IEEE Trans. Electron Devices* 59, 3327 (2012).
- [80] T. B. Fehlberg, J. S. Milne, G. A. Umana-Membreno, S. Keller, U. K. Mishra, B. D. Nener, and G. Parish, *IEEE Trans. Electron Devices* 58, 2589 (2011).
- [81] E. A. Douglas, C. Y. Chang, D. J. Cheney, B. P. Gila, C. F. Lo, L. Lu, R. Holzworth, P. Whiting, K. Jones, G. D. Via, J. Kim, S. Jang, F. Ren, and S. J. Pearton, *Microelectron. Reliab.* 51, 207 (2011).
- [82] L. Liu, F. Ren, S. J. Pearton, R. C. Fitch, D. E. Walker, K. D. Chabak, J. K. Gillespie, M. Kossier, M. Trejo, D. Via, and A. Crespo, *J. Vac. Sci. Technol. B* 29, 060603 (2011).
- [83] M. Esposto, V. Di Lecce, M. Bonaiuti, and A. Chini, *J. Electron. Mater.* 42, 15 (2013).
- [84] M. Fagerlind, and N. Rorsman, *J. Appl. Phys.* 112, 014511 (2012).
- [85] B. M. Green, K. K. Chu, E. M. Chumbes, J. A. Smart, J. R. Shealy, and L. F. Eastman, *IEEE Electron Device Lett.* 21, 268 (2000).
- [86] M. F. Romero, M. M. Sanz, I. Tanarro, A. Jiménez, and E. Muñoz, *J. Phys. D: Appl. Phys.* 43, 495202 (2010).
- [87] R. C. Fitch, D. E. Walker, K. D. Chabak, J. K. Gillespie, M. Kossler, M. Trejo, A. Crespo, L. Liu, T. S. Kang, C.-F. Lo, F. Ren, D. J. Cheney, and S. J. Pearton, *J. Vac. Sci. Technol. B* 29, 061204 (2011).
- [88] T. Mizutani, Y. Ohno, M. Akita, S. Kishimoto, and K. Maezawa, *IEEE Trans. Electron Devices* 50, 2015 (2003).
- [89] M. Higashiwaki, Y. Pei, R. Chu, and U. K. Mishra, *IEEE Trans. Electron Devices* 58, 1681 (2011).
- [90] T. Hashizume, S. Ootomo, T. Inagaki, and H. Hasegawa, *J. Vac. Sci. Technol. B* 21, 1828 (2003).
- [91] T. Hashizume, S. Ootomo, and H. Hasegawa, *Appl. Phys. Lett.* 83, 2952 (2003).
- [92] J. J. Kim, G. M. Yang, K.-H. Shim, and J. W. Yang, *Jpn. J. Appl. Phys.* 50, 096501 (2011).
- [93] F. Gao, B. Lu, L. Li, S. Kuan, J. S. Speck, C. V. Thompson, and T. Palacios, *Appl. Phys. Lett.* 99, 223506 (2011).
- [94] E. T. Yu, X. Z. Dang, P. M. Asbeck, S. S. Lau, and G. J. Sullivan, *J. Vac. Sci. Technol. B* 17, 1742 (1999).
- [95] O. Ambacher, J. Smart, J. R. Shealy, N. G. Weimann, K. Chu, M. Murphy, W. J. Schaff, L. F. Eastman, R. Dimitrov, L. Wittmer, M. Stutzmann, W. Rieger, and J. Hilsenbeck, *J. Appl. Phys.* 85, 3222 (1999).
- [96] V. A. Savastenko, and A. U. Sheleg, *Phys. Status Solidi A* 48, K135 (1978).
- [97] Y. Takagi, M. Ahart, T. Azuhata, T. Sota, K. Suzuki, and S. Nakamura, *Physica B* 219/220, 547 (1996).

- [98] A. Polian, M. Grimsditch, and I. Grezegory, *J. Appl. Phys.* 79, 3343 (1996).
- [99] R. B. Schwartz, K. Khachatryan, and E. R. Webber, *Appl. Phys. Lett.* 70, 1122 (1997).
- [100] C. Deger, E. Born, H. Angerer, O. Ambacher, M. Stutzmann, J. Hornsteiner, E. Riha, and G. Fischerauer, *Appl. Phys. Lett.* 72, 2400 (1998).
- [101] K. Tsubouchi, and N. Mikoshiba, *IEEE Trans. Sonics Ultrason.* 32, 634 (1985).
- [102] L. E. McNeil, M. Grimsditch, and R. H. French, *J. Am. Ceram. Soc.* 76, 1132 (1993).
- [103] K. Kim, W. R. L. Lambrecht, and B. Segall, *Phys. Rev. B* 53, 16310 (1996).
- [104] A. F. Wright, *J. Appl. Phys.* 82, 2833 (1997).
- [105] F. Bernardini, V. Fiorentini, and D. Vanderbilt, *Phys. Rev. B* 56, R10024 (1997).
- [106] F. Bernardini, V. Fiorentini, and D. Vanderbilt, *Phys. Rev. B* 63, 193201 (2001).
- [107] Y. Duan, J. Li, S.-S. Li, and J.-B. Xia, *J. Appl. Phys.* 103, 023705 (2008).
- [108] K. Shimada, A. Zenpuku, K. Fukiwara, K. Hazu, S. F. Chichibu, M. Hata, H. Sazawa, T. Takada, and T. Sota, *J. Appl. Phys.* 110, 074114 (2011).
- [109] W. S. Yan, R. Zhang, Z. L. Xie, X. Q. Xiu, P. Han, H. Lu, P. Chen, S. L. Gu, Y. Shi, Y. D. Zheng, and Z. G. Liu, *Appl. Phys. Lett.* 94, 042106 (2009).
- [110] J. Lähnemann, O. Brandt, U. Jahn, C. Pfüller, C. Roder, P. Dogan, F. Grosse, A. Belabbes, F. Bechstedt, A. Trampert, and L. Geelhaar, *Phys. Rev. B* 86, 081302(R). (2012).
- [111] J. Yang, B. S. Eller, C. Zhu, C. England, and R. J. Nemanich, *J. Appl. Phys.* 112, 053710 (2012).
- [112] H. W. Jang, J.-H. Lee, and J.-L. Lee, *Appl. Phys. Lett.* 80, 3955 (2002).
- [113] M. Hong, K. A. Anselm, J. Kwo, H. M. Ng, J. N. Baillargeon, A. R. Kortan, J. P. Mannaerts, A. Y. Cho, C. M. Lee, J. I. Chyi, and T. S. Lay, *J. Vac. Sci. Technol. B* 18, 1453 (2000).
- [114] Y. Q. Wu, T. Shen, P. D. Ye, and G. D. Wilk, *Appl. Phys. Lett.* 90, 143504 (2007).
- [115] W. J. Mecouch, B. P. Wagner, Z. J. Reitmeier, R. F. Davis, C. Pandarinath, B. J. Rodriguez, and R. J. Nemanich, *J. Vac. Sci. Technol. A* 23, 72 (2005).
- [116] U. Karrer, O. Ambacher, and M. Stutzmann, *Appl. Phys. Lett.* 77, 2012 (2000).
- [117] P. Lorenz, T. Haensel, R. Gutt, R. J. Koch, J. A. Schaefer, and S. Krischok, *Physica Status Solidi B* 247, 1658 (2010).
- [118] V. M. Polyakov, F. S. Tautz, S. Sloboshanin, J. A. Schaefer, A. S. Usikoy, and B. Ja. Ber, *Semicond. Sci. Technol.* 13, 1396 (1998).

- [119] I. Tamm, *Physik. Zeits. Sowjetunion* 1, 733 (1932).
- [120] W. Shockley, *Phys. Rev.* 56, 317 (1939).
- [121] J. Fritsch, O. F. Sankey, K. E. Schmidt, and J. B. Page, *Phys. Rev. B* 57, 15360 (1998).
- [122] J. E. Northrop, R. Di Felice, and J. Neugebauer, *Phys. Rev. B* 55, 13878 (1997).
- [123] A. R. Smith, R. M. Feenstra, D. W. Greve, J. Neugebauer, and J. E. Northrup, *Phys. Rev. Lett.* 79, 3934 (1997).
- [124] R. H. French, *J. Am. Ceram. Soc.* 73, 477 (1990).
- [125] W. Schottky, *Phys. Z* 41, 570 (1940).
- [126] N. F. Mott, *Math. Proc. Cambridge* 34, 568 (1938).
- [127] J. Bardeen, *Phys. Rev.* 71, 717 (1947).
- [128] V. Heine, *Phys. Rev.* 138, A1689 (1965).
- [129] F. Flores, and C. Tejedor, *J. Phys. France* 38, 949 (1977).
- [130] C. Tejedor, and F. Flores, *J. Phys. C. Solid State Phys.* 11, L19 (1977).
- [131] J. Tersoff, *Phys. Rev. B* 30, 4874 (1984).
- [132] W. Mönch, *Appl. Surf. Sci.* 92, 367 (1996).
- [133] W. E. Spicer, P. W. Chye, P. R. Skeath, C. Y. Su, and I. Lindau, *J. Vac. Sci. Technol.* 16, 1422 (1979).
- [134] W. E. Spicer, I. Lindau, P. Skeath, and C. Y. Su, *J. Vac. Sci. Technol.* 17, 1019 (1980).
- [135] H. Hasegawa, and T. Sawada, *Thin Solid Films* 103, 119 (1983).
- [136] H. Hasegawa, Y. Koyama, and T. Hashizume, *Jpn. J. Appl. Phys.* 38, 2634 (1999).
- [137] J. M. Andrews, and J. C. Phillips, *Phys. Rev. Lett.* 35, 56 (1975).
- [138] L. J. Brillson, *Phys. Rev. Lett.* 40, 260 (1978).
- [139] R. L. Anderson, *Solid-State Electron.* 5, 341 (1962).
- [140] J. Tersoff, *Phys. Rev. Lett.* 52, 465 (1984).
- [141] J. Robertson, and B. Falabretti, *J. Appl. Phys.* 100, 014111 (2006).
- [142] M. Cardona, and N. E. Christensen, *Phys. Rev. B* 35, 6182 (1987).

- [143] W. Mönch, *J. Appl. Phys.* 80, 5076 (1996).
- [144] A. Baldereschi, *Phys. Rev. B* 7, 5212 (1973).
- [145] A. Franciosi, and C. G. Van de Walle, *Surf. Sci. Rep.* 25, 1 (1996).
- [146] C. G. Van de Walle, and J. Neugebauer, *Appl. Phys. Lett.* 70, 2577 (1997).
- [147] G. C. Van de Walle, and R. M. Martin, *Phys. Rev. B* 35, 8154 (1987).
- [148] S. H. Wei, and A. Zunger, *Appl. Phys. Lett.* 72, 2011 (1998).
- [149] Y.-H. Li, A. Walsh, S. Chen, W.-J. Yin, J.-H. Yang, J. Li, J. L. F. Da Silva, X. G. Gong, and S. H. Wei, *Appl. Phys. Lett.* 94, 212109 (2009).
- [150] T. Sawada, Y. Ito, N. Kimura, K. Imai, K. Suzuki, and S. Sakai, *Appl. Surf. Sci.* 190, 326 (2002).
- [151] K. Shiojima, T. Sugahara, and S. Sakai, *Appl. Phys. Lett.* 74, 1936 (1999).
- [152] K. A. Rickert, A. B. Ellis, J. K. Kim, J.-L. Lee, F. J. Himpsel, F. Dwikusuma, and T. F. Kuech, *J. Appl. Phys.* 92, 6671 (2002).
- [153] J. Robertson, *J. Vac. Sci. Technol. B* 18, 1785 (2000).
- [154] J. Zhang, C. Yang, S. Wu, Y. Liu, M. Zhang, H. Chen, W. Zhang, and Y. Li, *Semicond. Sci. Technol.* 25, 035011 (2010).
- [155] T. Nakayama, and M. Murayama, *J. Cryst. Growth* 214/215, 299 (2000).
- [156] H. S. Craft, R. Collazo, M. D. Losego, S. Mita, Z. Sitar, and J.-P. Maria, *Appl. Phys. Lett.* 92, 082907 (2008).
- [157] T. S. Lay, M. Hong, J. Kwo, J. P. Mannaerts, W. H. Hung, and D. J. Huang, *Solid-State Electron.* 45, 1679 (2001).
- [158] L. G. Gao, B. Xu, H. X. Guo, Y. D. Xia, J. Yin, and Z. G. Liu, *Appl. Phys. Lett.* 94, 252901 (2009).
- [159] J. J. Chen, M. Hlad, A. P. Gerger, B. P. Gila, F. Ren, C. R. Abernathy, and S. J. Pearton, *J. Electron. Mater.* 36, 368 (2007).
- [160] V. D. Wheeler, *Ph. D. Thesis* North Carolina State University, 2010.
- [161] J.-J. Chen, B. P. Gila, M. Hlad, A. Gerger, F. Ren, C. R. Abernathy, and S. J. Pearton, *Appl. Phys. Lett.* 88, 142115 (2006).
- [162] C. Liu, E. F. Chor, L. S. Tan, and Y. Dong, *Appl. Phys. Lett.* 88, 222113 (2006).
- [163] H. S. Craft, *Ph. D. Thesis* University of North Carolina, 2010.

- [164] S.-K. Hong, T. Hanada, H. Makino, Y. Chen, H.-J. Ko, T. Yao, A. Tanaka, H. Sasaki, and S. Sato, *Appl. Phys. Lett.* 78, 3349 (2001).
- [165] H. F. Liu, G. X. Hu, H. Gong, K. Y. Zang, and S. J. Chua, *J. Vac. Sci. Technol. A* 26, 1462 (2008).
- [166] Y. I. Alivov, B. Xiao, S. Akarca-Biyikli, Q. Fan, H. Morkoç, D. Johnstone, O. Lopatiuk-Tirpak, L. Chernyak, and W. Litton, *J. Phys. Condens. Matter* 20, 085201 (2008).
- [167] B. Kramm, A. Laufer, D. Reppin, A. Kronenberger, P. Hering, A. Polity, and B. K. Meyer, *Appl. Phys. Lett.* 100, 094102 (2012).
- [168] G. Martin, S. Strite, A. Botchkarev, A. Agarwal, A. Rockett, H. Morkoç, W. R. L. Lambrecht, and B. Segall, *Appl. Phys. Lett.* 65, 610 (1994).
- [169] J. R. Waldrop, and R. W. Grant, *Appl. Phys. Lett.* 68, 2879 (1996).
- [170] M. R. Coan, J. H. Woo, D. Johnson, I. R. Gatabi, and H. R. Harris, *J. Appl. Phys.* 112, 024508 (2012).
- [171] R. Suri, *Ph. D. Thesis* North Carolina State University, 2010.
- [172] M. Esposito, S. Krishnamoorthy, D. N. Nath, S. Bajaj, T. H. Hung, and S. Rajan, *Appl. Phys. Lett.* 99, 133503 (2011).
- [173] W. Wei, Z. Qin, S. Fan, Z. Li, K. Shi, Q. Zhu, and G. Zhang, *Nanoscale Res. Lett.* 7, 562 (2012).
- [174] T. E. Cook, C. C. Fulton, W. J. Mecouch, R. F. Davis, G. Lucovsky, and R. J. Nemanich, *J. Appl. Phys.* 94, 7155 (2003).
- [175] C. Liu, E. F. Chor, and L. S. Tan, *Appl. Phys. Lett.* 88, 173504 (2006).
- [176] H. S. Craft, R. Collazo, M. D. Losego, S. Mita, Z. Sitar, and J.-P. Maria, *J. Appl. Phys.* 102, 074104 (2007).
- [177] J. J. Chen, B. P. Gila, M. Hlad, A. Gerger, F. Ren, C. R. Abernathy, and S. J. Pearton, *Appl. Phys. Lett.* 88, 042113 (2006).
- [178] T. E. Cook, C. C. Fulton, W. J. Mecouch, R. F. Davis, G. Lucovsky, and R. J. Nemanich, *J. Appl. Phys.* 94, 3949 (2003).
- [179] M. Kumar, B. Roul, T. N. Bhat, M. K. Rajpalke, A. T. Kalghatgi, and S. B. Krupanidhi, *Thin Solid Films* 520, 4911 (2012).
- [180] R. Nakasaki, T. Hashizume, and H. Hasegawa, *Physica E* 7, 953 (2000).
- [181] T. E. Cook, C. C. Fulton, W. J. Mecouch, K. M. Tracy, R. F. Davis, E. H. Hurt, G. Lucovsky, and R. J. Nemanich, *J. Appl. Phys.* 93, 3995 (2003).
- [182] I. Costina, and R. Franchy, *Appl. Phys. Lett.* 78, 4139 (2001).
- [183] V. V. Afanas'ev, A. Stesmans, K. Cherkaoui, and P. K. Hurley, *Appl. Phys. Lett.* 96, 052103 (2010).

- [184] X. Xu, X. Liu, Y. Guo, J. Wang, H. Song, S. Yang, H. Wei, Q. Zhu, and Z. Wang, *J. Appl. Phys.* 107, 104510 (2010).
- [185] P. D. C. King, T. D. Veal, P. H. Jefferson, C. F. McConville, T. Wang, P. J. Parbrook, H. Lu, and W. J. Schaff, *Appl. Phys. Lett.* 90, 132105 (2007).
- [186] C.-L. Wu, C.-H. Shen, and S. Gwo, *Appl. Phys. Lett.* 88, 032105 (2006).
- [187] A. L. Yang, H. P. Song, X. L. Liu, H. Y. Wei, Y. Guo, G. L. Zheng, C. M. Jiao, S. Y. Yang, Q. S. Zhu, and Z. G. Wang, *Appl. Phys. Lett.* 94, 052101 (2009).
- [188] T. D. Veal, P. D. C. King, S. A. Hatfield, L. R. Bailey, C. F. McConville, B. Martel, J. C. Moreno, E. Frayssinet, F. Semond, and J. Zúñiga-Pérez, *Appl. Phys. Lett.* 93, 202108 (2008).
- [189] G. Heidelberger, *Ph. D. Thesis* Rheinisch–Westfälischen Technischen Hochschule Aachen, 2009.
- [190] Y. Chiou, and C. Lee, *IEEE Trans. Electron Devices* 58, 3869 (2011).
- [191] Y.-L. Chiou, C.-S. Lee, and C.-T. Lee, *Appl. Phys. Lett.* 97, 032107 (2010).
- [192] N. V. Edwards, M. D. Bremser, T. W. Weeks, R. S. Kern, R. F. Davis, and D. E. Aspnes, *Appl. Phys. Lett.* 69, 2065 (1996).
- [193] T. Hashizume, S. Ootomo, R. Nakasaki, S. Oyama, and M. Kihara, *Appl. Phys. Lett.* 76, 2880 (2000).
- [194] F. Gonzalez-Posada, J. A. Bardwell, S. Moisa, S. Haffouz, H. Tang, A. F. Brana, and E. Munoz, *Appl. Surf. Sci.* 253, 6185 (2007).
- [195] J. Hedman, and N. Mårtensson, *Phys. Scr.* 22, 176 (1980).
- [196] L. L. Smith, S. W. King, R. J. Nemanich, and R. F. Davis, *J. Electron. Mater.* 25, 805 (1996).
- [197] S. W. King, J. P. Barnak, M. D. Bremser, K. M. Tracy, C. Ronning, R. F. Davis, and R. J. Nemanich, *J. Appl. Phys.* 84, 5248 (1998).
- [198] J. J. Uhlrich, L. C. Grabow, M. Mavrikakis, and T. F. Kuech, *J. Electron. Mater.* 37, 439 (2008).
- [199] S. D. Wolter, B. P. üer, D. L. Waltmyer, C. Onneby, S. E. Mohny, and R. J. Molnar, *Appl. Phys. Lett.* 70, 2156 (1997).
- [200] K. Prabhakaran, T. G. Andersson, and K. Nozawa, *Appl. Phys. Lett.* 69, 3212 (1996).
- [201] V. M. Bermudez, *J. Appl. Phys.* 80, 1190 (1996).
- [202] P. Sivasubramani, T. J. Park, B. E. Coss, A. Lucero, J. Huang, B. Brennan, Y. Cao, D. Jena, H. Xing, R. M. Wallace, and J. Kim, *Phys. Status Solidi Rapid Res. Lett.* 6, 22 (2012).
- [203] L. Plucinski, L. Colakerol, S. Bernardis, Y. Zhang, S. Wang, C. O'Donnell, K. E. Smith, I. Friel, and T. D. Moustakas, *Surf. Sci.* 600, 116 (2006).

- [204] Y. J. Lin, C. S. Lee, and C. T. Lee, *J. Appl. Phys.* 93, 5321 (2003).
- [205] J. O. Song, S. J. Park, and T. Y. Seong, *Appl. Phys. Lett.* 80, 3129 (2002).
- [206] G. L. Martinez, M. R. Curiel, B. J. Skromme, and R. J. Molnar, *J. Electron. Mater.* 29, 325 (2000).
- [207] M. Diale, F. D. Auret, N. G. Van der Berg, R. Q. Odendaal, and W. D. Roos, *Appl. Surf. Sci.* 246, 279 (2005).
- [208] N. Nepal, N. Y. Garces, D. J. Meyer, J. K. Hite, M. A. Mastro, and C. R. Eddy, *Appl. Phys. Express* 4, 055802 (2011).
- [209] F. Machuca, Z. Liu, Y. Sun, P. Pianetta, W. E. Spicer, and R. F. W. Pease, *J. Vac. Sci. Technol. A* 20, 1784 (2002).
- [210] Z. Liu, Y. Sun, F. Machuca, P. Pianetta, W. E. Spicer, and R. F. W. Pease, *J. Vac. Sci. Technol. B* 21, 1953 (2003).
- [211] T. Hashizume, R. Nakasaki, S. Ootomo, S. Oyama, and H. Hasegawa, *Mater. Sci. Eng. B* 80, 309 (2001).
- [212] Y. Koyama, T. Hashizume, and H. Hasegawa, *Solid State Electron.* 43, 1483 (1999).
- [213] D. Li, M. Sumiya, S. Fuke, D. Yang, D. Que, Y. Suzuki, Y. Fukuda, *J. Appl. Phys.* 90 4219 (2001).
- [214] A. R. Smith, R. M. Feenstra, D. W. Greve, M.-S. Shin, M. Skowronski, J. Neugebauer, and J. E. Northrup, *Appl. Phys. Lett.* 72, 2114 (1998).
- [215] Y. Jung, J. Ahn, K. H. Baik, D. Kim, S. J. Pearton, F. Ren, and J. Kim, *J. Electrochem. Soc.* 159, H117 (2012).
- [216] K. M. Tracy, W. J. Mecouch, R. F. Davis, and R. J. Nemanich, *J. Appl. Phys.* 94, 3163 (2003).
- [217] L. C. Grabow, J. J. Uhlrich, T. F. Kuech, and M. Mavrikakis, *Surf. Sci.* 603, 387 (2009).
- [218] R. W. Hunt, L. Vanzetti, T. Castro, K. M. Chen, L. Sorba, P. I. Cohen, W. Gladfelter, J. M. Van Hove, J. N. Kuznia, M. Asif Khan, and A. Franciosi, *Physica B* 185, 415 (1993).
- [219] Y.-H. Lai, C.-T. Yeh, J.-M. Hwang, H.-L. Hwang, C.-T. Chen, and W.-H. Hung, *J. Phys. Chem. B* 105, 10029 (2001).
- [220] H. Ishikawa, S. Kobayashi, Y. Koide, S. Yamasaki, S. Nagai, J. Umezaki, M. Koike, and M. Murakami, *J. Appl. Phys.* 81, 1315 (1997).
- [221] C. I. Wu, and A. Kahn, *J. Vac. Sci. Technol. B* 16, 2218 (1998).
- [222] M. Asif Khan, J. N. Kuznia, D. T. Olson, and R. Kaplan, *J. Appl. Phys.* 73, 3108 (1993).
- [223] V. M. Bermudez, R. Kaplan, M. Asif Khan, and J. N. Kuznia, *Phys. Rev. B* 48, 2436 (1993).
- [224] V. M. Bermudez, T. M. Jung, K. Doverspike, and A. E. Wickenden, *J. Appl. Phys.* 79, 110 (1996).

- [225] V. M. Bermudez, D. D. Koleske, and A. E. Wickenden, *Appl. Surf. Sci.* 126, 69 (1998).
- [226] Ch. Schulz, S. Kuhr, H. Geffers, Th. Schmidt, J. I. Flege, T. Aschenbrenner, D. Hommel, and J. Falta, *J. Vac. Sci. Technol. A* 29, 011013 (2011).
- [227] K. N. Lee, S. M. Donovan, B. Gila, M. Overberg, J. D. Mackenzie, C. R. Abernathy, and R. G. Wilson, *J. Electrochem. Soc.* 147, 3087 (2000).
- [228] T. Hashizume, and H. Hasegawa, *Appl. Surf. Sci.* 234, 387 (2004).
- [229] T. Inagaki, T. Hashizume, and H. Hasegawa, *Appl. Surf. Sci.* 216, 519 (2003).
- [230] Z. Jin, T. Hashizume, and H. Hasegawa, *Appl. Surf. Sci.* 190, 361 (2002).
- [231] D. J. Meyer, J. R. Flemish, and J. M. Redwing, *Appl. Phys. Lett.* 89, 223523 (2006).
- [232] Y. Guhel, B. Boudart, N. Vellas, C. Gaquiere, E. Delos, D. Ducatteau, Z. Bougrioua, and M. Germain, *Solid-State Electron.* 49, 1589 (2005).
- [233] S. Hoshi, T. Marui, M. Itoh, Y. Sano, and S. Seki, *IEICE Trans Electron.* E89C, 1052 (2006).
- [234] J. Kim, H. Choi, M. Ha, H. Song, C. Roh, J. Lee, J. Park, and C. Hahn, *Jpn. J. Appl. Phys.* 49 04DF05 (2010).
- [235] A. Hierro, S. A. Ringel, M. Hansen, J. S. Speck, U. K. Mishra, and S. P. DenBaars, *Appl. Phys. Lett.* 77, 1499 (2000).
- [236] J. Neugebauer, and C. G. Van de Walle, *Phys. Rev. Lett.* 75, 4452 (1995).
- [237] S. Nakamura, N. Iwasa, M. Senoh, and T. Mukai, *Jpn. J. Appl. Phys.* 31, 1258 (1992).
- [238] M. S. Brandt, N. M. Johnson, R. J. Molnar, R. Singh, and T. D. Moustakas, *Appl. Phys. Lett.* 64, 2264 (1994).
- [239] W. Götz, N. M. Johnson, J. Walker, D. P. Bour, H. Amano, and I. Akasaki, *Appl. Phys. Lett.* 67, 2666 (1995).
- [240] S. M. George, *Chem. Rev.* 110, 111 (2010).
- [241] R. L. Puurunen, *J. Appl. Phys.* 97, 121301 (2005).
- [242] M. Milojevic, C. L. Hinkle, F. S. Aguirre-Tostado, H. C. Kim, E. M. Vogel, J. Kim, and R. M. Wallace, *Appl. Phys. Lett.* 93, 252905 (2008).
- [243] M. Milojevic, F. S. Aguirre-Tostado, C. L. Hinkle, H. C. Kim, E. M. Vogel, J. Kim, and R. M. Wallace, *Appl. Phys. Lett.* 93, 202902 (2008).
- [244] Y. Cao, X. Li, A. Li, H. Li, and D. Wu, *Appl. Surf. Sci.* 263, 497 (2012).
- [245] C. L. Hinkle, A. M. Sonnet, E. M. Vogel, S. McDonnell, G. J. Hughes, M. Milojevic, B. Lee, F. S. Aguirre-Tostado, K. J. Choi, H. C. Kim, J. Kim, and R. M. Wallace, *Appl. Phys. Lett.* 92, 071901 (2008).

- [246] X. Liu, R. Yeluri, J. Lu, and U. K. Mishra, *J. Electron. Mater.* 42, 33 (2013).
- [247] A. N. Hattori, F. Kawamura, M. Yoshimura, Y. Kitaoka, Y. Mori, K. Hattori, H. Daimon, and K. Endo, *Surf. Sci.* 604, 1247 (2010).
- [248] X. Hu, A. Koudymov, G. Simin, J. Yang, M. Asif Khan, A. Tarakji, M. S. Shur, and R. Gaska, *Appl. Phys. Lett.* 79, 2832 (2001).
- [249] T. Mizutani, Y. Ohno, M. Akita, S. Kishimoto, and K. Maezawa, *Phys. Status Solidi A* 194, 447 (2002).
- [250] C. Bae, C. Krug, G. Lucovsky, A. Chakraborty, and U. Mishra, *J. Appl. Phys.* 96, 2674 (2004).
- [251] W. S. Tan, P. A. Houston, P. J. Parbrook, G. Hill, and R. J. Airey, *J. Phys. D: Appl. Phys.* 35, 595 (2002).
- [252] H. Kim, R. M. Thompson, V. Tilak, T. R. Prunty, J. R. Shealy, and L. F. Eastman, *IEEE Electron Device Lett.* 24, 421 (2003).
- [253] M. Sawada, T. Sawada, Y. Yamagata, K. Imai, H. Kimura, M. Yoshino, K. Iizuka, and H. Tomozawa, *J. Cryst. Growth* 189/190, 706 (1998).
- [254] S. Arulkumaran, T. Egawa, H. Ishikawa, T. Jimbo, and M. Umeno, *Appl. Phys. Lett.* 73, 809 (1998).
- [255] S. Arulkumaran, T. Egawa, H. Ishikawa, T. Jimbo, and Y. Sano, *Appl. Phys. Lett.* 84, 613 (2004).
- [256] K. Balachander, S. Arulkumaran, T. Egawa, Y. Sano, and K. Baskar, *Mater. Sci. Eng. B* 119, 36 (2005).
- [257] K. Balachander, S. Arulkumaran, Y. Sano, T. Egawa, and K. Baskar, *Phys. Status. Solidi. A* 202, R32 (2005).
- [258] A. Zoroddu, F. Bernardini, P. Ruggerone, and V. Fiorentini, *Phys. Rev. B* 64, 045208 (2001).
- [259] D. J. Chen, Y. Q. Tao, C. Chen, R. Zhang, Y. D. Zheng, M. J. Wang, B. Shen, Z. H. Li, G. Jiao, and T. S. Chen, *Appl. Phys. Lett.* 89, 252104 (2006).
- [260] D. J. Chen, Y. Q. Tao, C. Chen, Z. L. Xie, Z. Y. Zhai, X. S. Wu, P. Han, R. Zhang, and Y. D. Zheng, *J. Vac. Sci. Technol. B* 25, 1896 (2007).
- [261] T. Hashizume, E. Alekseev, D. Pavlidis, K. S. Boutros, and J. Redwing, *J. Appl. Phys.* 88, 1983 (2000).
- [262] S. Huang, Q. Jiang, S. Yang, C. Zhou, and K. J. Chen, *IEEE Electron Device Lett.* 33, 516 (2012)
- [263] C. J. Kao, J. K. Sheu, W. C. Lai, M. L. Lee, M. C. Chen, and G. C. Chi, *Appl. Phys. Lett.* 85, 1430 (2004).
- [264] C. J. Kao, M. C. Chen, C. J. Tun, G. C. Chi, J. K. Sheu, W. C. Lai, M. L. Lee, F. Ren, and S. J. Pearton, *J. Appl. Phys.* 98, 064506 (2005).
- [265] D. J. Fu, Y. H. Kwon, T. W. Kang, C. J. Park, K. H. Baek, H. Y. Cho, D. H. Shin, C. H. Lee, and K. S. Chung, *Appl. Phys. Lett.* 80, 446 (2002).
- [266] C.-T. Lee, H.-W. Chen, and H.-Y. Lee, *Appl. Phys. Lett.* 82, 4304 (2003).

- [267] K. Y. Park, H. I. Cho, J. H. Lee, S. B. Bae, C. M. Jeon, J. L. Lee, D. Y. Kim, C. S. Lee, and J. H. Lee, *Phys. Status Solidi C* 0, 2351 (2003).
- [268] P. D. Ye, B. Yang, K. K. Ng, J. Bude, G. D. Wilk, S. Halder, and J. C. M. Hwang, *Appl. Phys. Lett.* 86, 063501 (2005).
- [269] Y. C. Chang, W. H. Chang, H. C. Chiu, L. T. Tung, C. H. Lee, K. H. Shiu, M. Hong, J. Kwo, J. M. Hong, and C. C. Tsai, *Appl. Phys. Lett.* 93, 053504 (2008).
- [270] Y. Yue, Y. Hao, J. Zhang, J. Ni, W. Mao, Q. Feng, and L. Liu, *IEEE Electron Device Lett.* 29, 838 (2008).
- [271] Y. C. Chang, H. C. Chiu, Y. J. Lee, M. L. Huang, K. Y. Lee, M. Hong, Y. N. Chiu, J. Kwo, and Y. H. Wang, *Appl. Phys. Lett.* 90, 232904 (2007).
- [272] W. J. Zhu, T. Tamagawa, M. Gibson, T. Furukawa, and T. P. Ma, *IEEE Electron Device Lett.* 23, 649 (2002).
- [273] E. P. Gusev, J. C. Cabral, M. Copel, C. D'Emic, and M. Gribelyuk, *Microelectron. Eng.* 69, 145 (2003).
- [274] X. H. Xu, M. Wang, Y. Hou, S. R. Zhao, H. Wang, D. Wang, and S. X. Shang, *Cryst. Res. Technol.* 37, 431 (2002).
- [275] K. Balachander, S. Arulkumaran, H. Ishikawa, K. Baskar, and T. Egawa, *Phys. Status Solidi A* 202, R16 (2005).
- [276] C.-C. Hu, M.-S. Lin, T.-Y. Wu, F. Adriyanto, P.-W. Sze, C.-L. Wu, and Y.-H. Wang, *IEEE Trans. Electron Devices* 59, 121 (2012).
- [277] A. M. Herrero, B. P. Gila, C. R. Abernathy, S. J. Pearton, V. Craciun, K. Siebein, and F. Ren, *Appl. Phys. Lett.* 89, 092117 (2006).
- [278] X. Weng, W. Tian, D. G. Schlom, and E. C. Dickey, *Appl. Phys. Lett.* 96, 241901 (2010).
- [279] J. S. Jur, V. D. Wheeler, D. J. Lichtenwalner, J. P. Maria, and M. A. L. Johnson, *Appl. Phys. Lett.* 98, 042902 (2011).
- [280] X. Wang, O. I. Saadat, B. Xi, X. Lou, R. J. Molnar, T. Palacios, and R. G. Gordon, *Appl. Phys. Lett.* 101, 232109 (2012).
- [281] R. Mehandru, B. Luo, J. Kim, F. Ren, B. P. Gila, A. H. Onstine, C. R. Abernathy, S. J. Pearton, D. Gotthold, R. Birkhahn, B. Peres, R. Fitch, J. Gillespie, T. Jenkins, J. Sewell, D. Via, and A. Crespo, *Appl. Phys. Lett.* 82, 2530 (2003).
- [282] B. Luo, J. Kim, F. Ren, J. K. Gillespie, R. C. Fitch, J. Sewell, R. Dettmer, G. D. Via, A. Crespo, T. J. Jenkins, B. P. Gila, A. H. Onstine, K. K. Allums, C. R. Abernathy, S. J. Pearton, R. Dwivedi, T. N. Fogarty, and R. Wilkins, *Appl. Phys. Lett.* 82, 1428 (2003).
- [283] B. Luo, J. W. Johnson, J. Kim, R. M. Mehandru, F. Ren, B. P. Gila, A. H. Onstine, C. R. Abernathy, S. J. Pearton, A. G. Baca, R. D. Briggs, R. J. Shul, C. Monier, and J. Han, *Appl. Phys. Lett.* 80, 1661 (2002).

- [284] A. Y. Polyakov, N. B. Smirnov, B. P. Gila, M. Hlad, A. P. Gergerb, C. R. Abernathy, and S. J. Pearton, *J. Electrochem. Soc.* 154, H115 (2007).
- [285] B. P. Gila, G. T. Thaler, A. H. Onstine, M. Hlad, A. Gerger, A. Herrero, K. K. Allums, D. Stodilka, S. Jang, B. Kang, T. Anderson, C. R. Abernathy, F. Ren, and S. J. Pearton, *Solid-State Electron.* 50, 1016 (2006).
- [286] H. C. Chiu, C. W. Lin, C. H. Chen, C. W. Yang, C. K. Lin, J. S. Fu, L. B. Chang, R. M. Lin, and K. P. Hsueh, *J. Electrochem. Soc.* 157, H160 (2010).
- [287] S. Yang, S. Huang, H. Chen, C. Zhou, Q. Zhou, M. Schnee, Q.-T. Zhao, J. Schubert, and K. J. Chen, *IEEE Electron Device Lett.* 33, 979 (2012).
- [288] B. P. Gila, J. W. Johnson, R. Mehandru, B. Luo, A. H. Onstine, K. K. Allums, V. Krishnamoorthy, S. Bates, C. R. Abernathy, F. Ren, and S. J. Pearton, *Phys. Status Solidi A* 188, 239 (2001).
- [289] A. Das, L. Chang, and R. Lin, *AIP Advances* 2, 032159 (2012).
- [290] W. H. Chang, C. H. Lee, P. Chang, Y. C. Chang, Y. J. Lee, J. Kwo, C. C. Tsai, J. M. Hong, C.-H. Hsu, and M. Hong, *J. Cryst. Growth* 311, 2183 (2009).
- [291] J. W. Johnson, B. Luo, F. Ren, B. P. Gila, W. Krishnamoorthy, C. R. Abernathy, S. J. Pearton, J. I. Chyi, T. E. Nee, C. M. Lee, and C. C. Chuo, *Appl. Phys. Lett.* 77, 3230 (2000).
- [292] J. W. Johnson, B. P. Gila, B. Luo, K. P. Lee, C. R. Abernathy, S. J. Pearton, J. I. Chyi, T. E. Nee, C. M. Lee, C. C. Chuo, and F. Ren, *J. Electrochem. Soc.* 148, G303 (2001).
- [293] M. Hong, J. Kwo, T. D. Lin, and M. L. Huang, *MRS Bull.* 34, 514 (2009).
- [294] Y. D. Wu, T. D. Lin, T. H. Chiang, Y. C. Chang, H. C. Chiu, Y. J. Lee, M. Hong, C. A. Lin, and J. Kwo, *J. Vac. Sci. Technol. B* 28, C3H10 (2010).
- [295] F. Ren, M. Hong, S. N. G. Chu, M. A. Marcus, M. J. Schurman, A. Baca, S. J. Pearton, and C. R. Abernathy, *Appl. Phys. Lett.* 73, 3893 (1998).
- [296] C.-T. Lee, Y.-L. Chiou, and C.-S. Lee, *IEEE Electron Device Lett.* 31, 1220 (2010).
- [297] G. Vanko, M. Vallo, J. Bruncko, and T. Lalinský, *Vac.* 86, 672 (2012).
- [298] W. Wang, J. Derluyn, M. Germain, M. Leys, S. Degroote, D. Schreurs, and G. Borghs, *Jpn. J. Appl. Phys.* 45, L224 (2006).
- [299] D. Deen, D. Storm, D. Meyer, D. Scott, R. Bass, S. Binari, and T. Gougousi, *Physica Status Solidi C* 8, 2420 (2011).
- [300] C. Lin, H. Chiu, C. Lin, and J. S. Fu, *Microelectron. Reliab.* 51, 381 (2011).
- [301] H. Kim, M. Schuette, H. Jung, J. H. Song, J. Lee, W. Lu, and J. C. Mabon, *Appl. Phys. Lett.* 89, 053516 (2006).
- [302] M. Z. Peng, Y. K. Zheng, K. Wei, and X. Y. Liu, *Microelectron Eng.* 87, 2638 (2010).

- [303] H. Zhou, G. I. Ng, Z. H. Liu, and S. Arulkumaran, *Appl. Phys. Express.* 4, 104102 (2011).
- [304] K.-W. Kim, S.-D. Jung, D.-S. Kim, K.-S. Im, H.-S. Kang, J.-H. Lee, Y. Bae, D.-H. Kwon, and S. Cristoloveanu, *Microelectron. Eng.* 88, 1225 (2011).
- [305] A. P. Edwards, J. A. Mittereder, S. C. Binari, D. S. Katzer, D. F. Storm, and J. A. Roussos, *IEEE Electron Device Lett.* 26, 225 (2005).
- [306] Y.-S. Lin, Y.-W. Lain, and S. S. H. Hsu, *IEEE Electron Device Lett.* 31, 102 (2010).

PART II: EQUIPMENT AND EXPERIMENT

CHAPTER 2. PLASMA-ENHANCED ATOMIC LAYER DEPOSITION

Atomic layer deposition (ALD) is a chemical vapor deposition (CVD) technique that utilizes gas-solid reactions to synthesize ultra-thin, uniform and conformal films [1-10]. The crux of this deposition method is the self-limiting behavior of the gas-phase reactions. Therefore, unlike traditional CVD and physical vapor deposition (PVD), ALD growth is not flux dependent. Thicker films must thus be deposited layer by layer with several cycles of ALD growth, where one cycle deposits $\sim 0.5\text{-}2.0$ Å of material. More specifically, an ALD cycle consists of four steps as shown in FIG 2.1: first, a self-limiting reaction between the reactive surface and precursor; second, a purge step to remove non-reacted precursor and gaseous by-products; third, a self-limiting reaction between a second reactant and the precursor absorbed on the surface, which typically replaces the ligands of the precursor; and lastly, a secondary purge step, resulting in a fresh starting surface for subsequent cycles. Consequently, the film thickness can be controlled on an atomic scale, giving extremely uniform and conformal films.

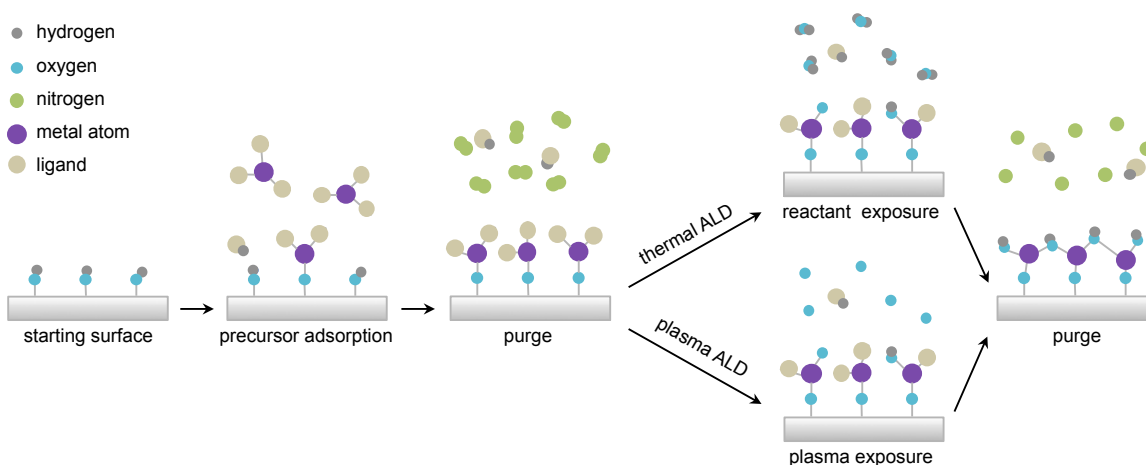


FIG 2.1 Schematic representation of the layer-by-layer deposition process of thermal and plasma-enhanced ALD. During reactant or plasma exposure, the surface is exposed to a reactant gas or plasma.

Plasma-enhanced ALD (PEALD) is an energy-enhanced method, where plasma is used during the cyclical deposition process. (See FIG 2.1.) The use of plasma reactants allows more freedom in processing conditions and a wider range of material properties than traditional thermal ALD. This is a consequence of the reactivity of the plasma, diminishing the demand for thermal energy and resulting in augmented material properties, lower substrate temperatures, larger choice of precursors, and increased growth rate [11].

There is tremendous potential for the future implementation of ALD as a result of its versatility. Thus, there have been extensive reviews published on this growing technology in the past few decades [1-74]. The depth and completeness of these reviews preclude the need for an additional. Consequently, this chapter is based heavily on the reviews already completed by Puurunen [7], Miikkulainen *et al.* [64], and Profijt *et al.* [11] with some additional research on more recent publications. In particular, this chapter focuses on basic ALD reactions and chemistry. More specifically, this chapter will first give an overview of the development of thermal and plasma ALD and then delve into specific reaction mechanics and chemistry. Hopefully, the reader will gain a strong understanding of the advantages of ALD—specifically PEALD—as well as why this deposition technique has played such a critical role in the research to follow. Additionally, the specifics of the PEALD processes used in this research to deposit metal oxides— HfO_2 , Al_2O_3 , and SiO_2 —on GaN substrates will be highlighted at the end of the chapter.

A. History and Development

The origins of ALD are somewhat disputed. Most commonly, Suntola *et al.* are recognized as the group that invented ALD-based processes. This group patented a process similar to ALD in the 1970s called “atomic layer epitaxy” [75]. However, Soviet Aleskovskii presented an earlier account of an ALD-like process at a conference in 1966 under the description of “molecular layering” [76]. Of the numerous review articles, only Russian articles cite the Soviet research group, and it seems the groups developed the technique without knowledge of the other. In the 1980s, the connection was finally made [77,78]; however, even after the connection, most researchers continue to cite the Finnish research group.

In the mid-1990s, the semiconductor industry recognized the potential of ALD and has since pushed for its development. In fact, Intel has adopted an ALD process to deposit Hf-based gate dielectrics, and it is expected that future technologies will rely on ALD for several key processing steps [79,87]. Consequently, research-based inquiries of ALD have increased over the past three decades [80]. (See FIG 2.2a) Thermal ALD remains the dominant ALD system, but PEALD has also begun to gain interest for the deposition of a variety of metal nitride, metal oxides, and metals. (See FIG 2.2b.)

PEALD was first conceptualized in 1991 by two Netherlander researchers, De Keisjer and van Opdorp, at the Philips Research Laboratories [81]. In this case, the Dutch group deposited GaAs at substrate temperatures between 430 and 500 °C using alternating pulses of AsH₃, GaMe₃ (trimethylgallium), and hydrogen plasma. Since these growth temperatures are close to the temperature of thermal decomposition of GaMe₃, the

reactivity of the plasma provides sufficiently fast surface kinetics for growth. In general, this showed that high reactivity PEALD allowed for more freedom in processing conditions and a wider range of material properties when compared to traditional thermal ALD [11]. Moreover, PEALD could significantly decrease the deposition temperature, reduce the impurities, and increase the growth rate and film density. Appendix B summarizes the PEALD-based research to date, and there are several companies developing commercial PEALD systems including ASM [82], Oxford Instruments [83], Beneq [84], Cambridge Nanotech [85], Applied Materials [86], Tokyo Electron Limited

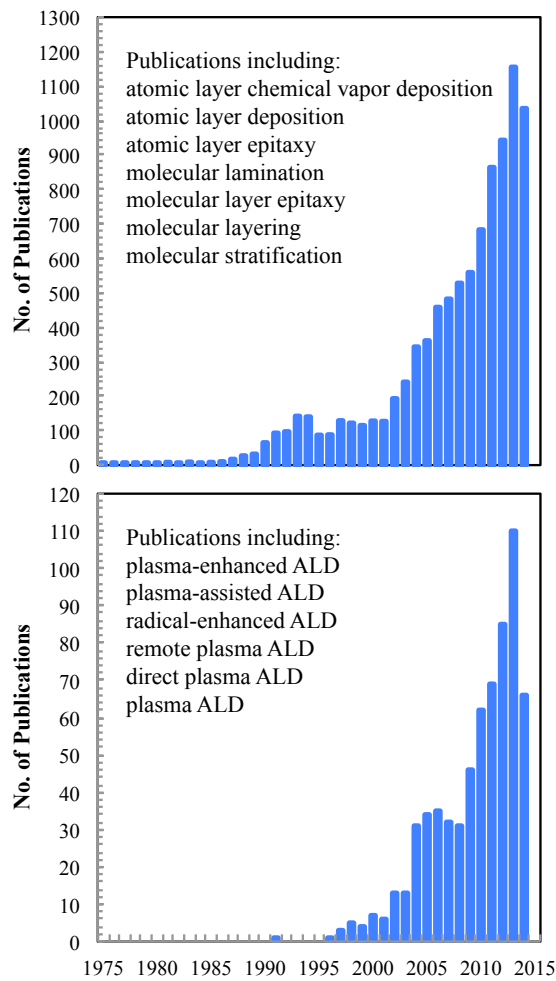


FIG 2.2 (a) Number of publications regarding ALD per year between 1991 and November 17, 2014 found in Web of Science. (b) Number of publications regarding plasma-enhanced ALD per year between 1991 and November 17, 2014 found in Web of Science.

[87], and Picosun [88].

II. Principles of ALD

As mentioned, ALD is a chemistry-driven process as dependent on the given reactants; this section will, thus, provide an overview of the adsorption mechanic and associated growth models required for successful ALD processes as well as discuss specific precursor chemistries.

A. Adsorption Mechanisms

A reactant of precursor may interact with the substrate surface by one of two mechanisms: physisorption and chemisorption. The division between these classifications is based on the strength of the interaction. Physisorption originates from weak interactions, which do not affect the structure of the precursor molecule. In this case, the interaction is not dependent on the type of molecules involved and may generate multilayers of physisorbed molecules. Chemisorption, on the other hand, involves reforming bonds, such that the precursor chemically bonds to the substrate surface. Consequently, only one layer of molecules may interact with the surface reactive sites.

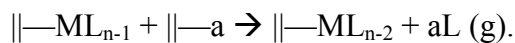
Understandably, the reaction mechanism plays a role in determining the reversibility of the reaction; as with most chemical processes, the reaction between the precursor and the substrate surface may be reversible or irreversible. For example, physisorption is always reversible, while chemisorption is only sometimes reversible. Under ALD conditions, the reaction must be self-terminating and saturating by nature. Such a reaction is not possible if the reaction is reversible; therefore successful ALD reaction mechanisms are limited to irreversible chemisorption.

The following scenario presents the most common of ALD reactions. Assume a precursor (ML_x), or reactant A, consists of a central metal atom (M), which is to be part of the deposited solid inorganic material (MZ_x), and ligands (L_x), which are removed by the second reactant, reactant B. Reactant B is often a non-metal hydride or reactant, which also provides the Z atoms for the inorganic material MZ_x . The mechanisms by which irreversible chemisorption can take place on a reactive site (a) are as follows [89]:

Ligand Exchange. In ligand exchange, the precursor is split at the surface; the metal is bonded to a surface site, while the ligand reacts with a surface group. This process produces a gaseous reaction by-product that is removed during the purge stage as shown in FIG 2.3a, and represented by the following:

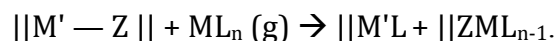


or

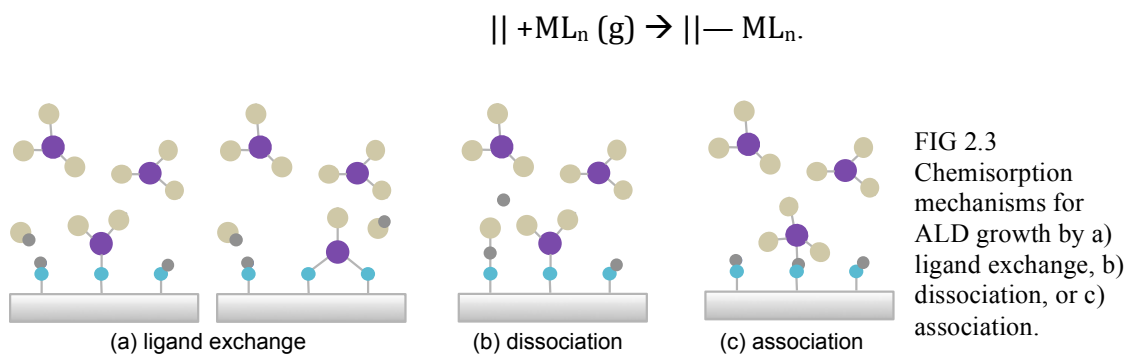


Note that ligand exchange may occur for more than one ligand, where the adsorbed atom may occupy more than one surface site.

Dissociation. Dissociation is the process where the precursor molecule is split into one or more reactive sites as shown in FIG 2.3b. Similar to ligand exchange, this process may proceed further on the surface, where the ligands occupy several reactive sites on the surface; however, this does not influence the number of metal atoms on the surface.



Association. Association describes the mechanism where the precursor forms a coordinative bond with the surface sites and bonds to the surface without the release of any ligands as shown in FIG 2.3c.



There may be additional reactions, which deviate from the three presented; however, these three represent the most common. Of these three, ligand exchange is often preferred. In this case, the removal of gaseous byproducts can help drive the reaction towards equilibrium. Furthermore, ligand exchange reduces steric hindrance and the number of reactive sites occupied by ligands. These factors determine the growth rate.

Steric hindrance. Steric hindrance refers to the space that is occupied by the unreacted ligands, where larger ligands may block the surface and additional reactive sites from adsorbing any other precursor molecules. In such cases, the surface is said to be covered.

Limited number of reactive sites. The number of reactive sites may also limit the growth rate if the number of surface sites is less than the number required for complete ligand coverage. In such case, there may still be exposed surface area without any sites to which the precursor can bond.

In other words, the growth rate of a material is limited by either steric hindrance or the concentration of reactive sites [7].

B. Growth Models

In light of this chemistry, it is important to draw a distinction. In ALD literature, a ‘monolayer’ represents the thickness of a self-terminated, fully saturated reaction; however, in almost all cases the ALD monolayer described is significantly smaller than the traditional monolayer of a crystal, which represents the thickness of a single layer of the MZ_x material.

Monolayer (capacity) for chemisorption is “the amount of adsorbate (adsorbed species), which is needed to occupy all adsorption sites as determined by the structure of the adsorbent (surface) and the chemical nature of the adsorptive (the reactant).”

Monolayer (capacity) for physisorption is “the amount needed to cover the surface with the complete monolayer of molecules in a close-packed array.”

Traditional monolayer of ALD-deposited materials is the thickness of a single layer of constituent atoms with the same stoichiometric ratio as the material.

In other words, while a traditional monolayer is an inherent material property dependent on the density and stoichiometry, an ALD monolayer is dependent on the parameters used during the ALD growth and defines the optimal growth per cycle or GPC.

1. Spatial

Several models have been developed to explain the expected ALD GPC. For example, Puurunen [45,89,90] has developed a simple mathematic model based on the mass

balance and chemisorption mechanisms to explain the growth rate per cycle. Specifically, this model relies on steric hindrance of ligands to determine the growth rate. In other words, the growth per cycle is related to the size and number of ligands absorbed on the surface after each cycle.

The total number of ligands is given by the following,

$$\Delta c_L = n\Delta c_M - \Delta c_a, \quad (1)$$

where Δc_M is the number of metal atoms per unit area absorbed, n is the number of ligands per reactant molecule, and Δc_a is the total number of ligands released per unit area after adsorption with the surface reactive sites. However, these variables are often difficult to determine given the varied interaction a precursor may have with the surface. The model must, therefore, use an approximation and assume the ligands are tightly packed as shown in FIG 2.4. Thus, the ligand coverage,

$$\theta = \frac{\Delta c_L}{\Delta c_L^{maxthr}}, \quad (2)$$

where Δc_L^{maxthr} is the theoretical upper limit for ligand packing density. From FIG 2.4, it can be determined that

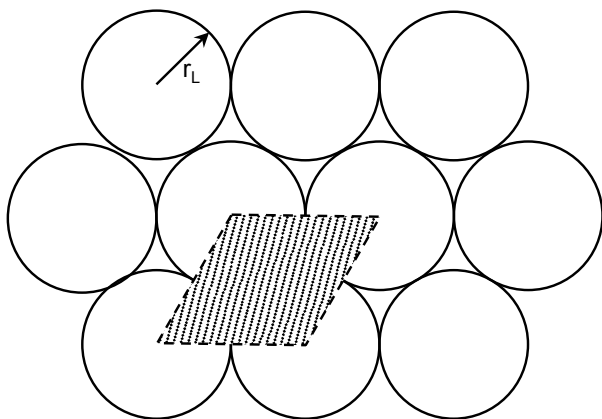


FIG 2.4 Ideal close packing structure of precursor ligands. The area of the shade unit cell is given by $2\sqrt{3}r_L^2$. Modified from R.L. Puurunen, *Chem. Vap. Dep.* 9, 249 (2003) [89]. Copyright 2003, WILEY-VCH Verlag GmbH & Co.

$$\Delta c_L^{maxthr} = \frac{1}{2\sqrt{3}r_L^2}. \quad (3)$$

In theory, the maximum of θ is unity; however, it is unlikely that such a value is achieved in experiment. Typically, the absorption of a ligand requires a hole larger than the ligand itself. Furthermore, the location of the surface sites may not permit full coverage. The model is thus also adapted to include the case where growth is limited by the number of reactive sites. The fraction of reactive sites that actually serve as adsorption sites,

$$f = \frac{\Delta c_a}{c_a}, \quad (4)$$

where c_a is the number of reactive sites per unit area available at the surface. Therefore,

$$\Delta c_M = \frac{1}{n} (\theta \Delta c_L^{maxthr} + f c_a), \quad (5)$$

and the growth per cycle,

$$\Delta h = \frac{M}{\rho N_A n} (\theta \Delta c_L^{maxthr} + f c_a), \quad (6)$$

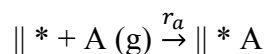
assuming the remaining ligands are removed by the secondary reactant. Here, M is the molar mass of the material, N_A is Avogadro's number, and ρ is the density of the material.

The reliability of this model relies on several limiting cases that are not included in the principle assumptions. The first is that the radii of the metal cations are larger than that of the ligands. If this is the case, growth per cycle is limited by the steric hindrance of the metal atoms rather than the ligands, and thus the above model is not applicable. However, this is an exceptional case. The second limiting case involves overlapping ligands, which

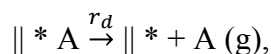
is much more likely in precursors with four or more ligands or where the ligands are not all of approximately equal size.

2. Adsorption Kinetics

In addition to adsorption mechanics, chemical kinetics also plays a critical role in adsorption processes associated with ALD. In this technique, the influence of parameters—such as temperature, reactant concentration, and pressure—on reaction rates are significant, as these parameters affect the adsorption process. In general, adsorption reactions are reversible consisting of both adsorption and desorption mechanisms as follows:



and



where r_a is the adsorption rate or number of molecules (A) adsorbed onto the surface per unit time, and r_d is the desorption rate or number of molecules (A) desorbed from the surface per unit time. The adsorption and desorption rates—and thus number of atoms on the surface—are affected by several parameters as follows [7]:

Partial Pressure. The first such parameter that will affect the amount of deposited material is the partial pressure of a reactant [91-93]. In general, the chemisorption coverage, Q , can be determined from the difference in the adsorption and desorption rates:

$$\frac{dQ}{dt} = r_a - r_d = k_a p(1 - Q) - k_d Q, \quad (7)$$

where k_a is the adsorption rate constant, k_d is the desorption rate constant, Q is the fraction of occupied surface sites, and p is the partial pressure of the molecule A . At saturation, chemisorption coverage is constant, i.e. $dQ/dt = 0$, and Eq. 7 becomes,

$$Q^{eq} = \frac{k_a p}{k_a p + k_d} = \frac{1}{1 + (Kp)^{-1}}, \quad (8)$$

where $K (=k_a/k_d)$ is the equilibrium constant of adsorption. When adsorption is reversible, $k_a \neq 0 \neq k_d$. Therefore, Q^{eq} increases with p , as shown in FIG 2.5a. However, to achieve ALD conditions with self-limiting reactions, adsorption must be irreversible, as mentioned, i.e. k_d to approaches zero. Thus,

$$\lim_{K \rightarrow \infty} Q^{eq} = 1 \quad (9)$$

In other words, Q will not increase with pressure but saturate at low reactant partial pressures, as shown in FIG 2.5b. On the other hand, operating at a low pressure may require adjustment of the other parameters: i.e., lower partial pressure operation may require longer exposure times to reach saturation.

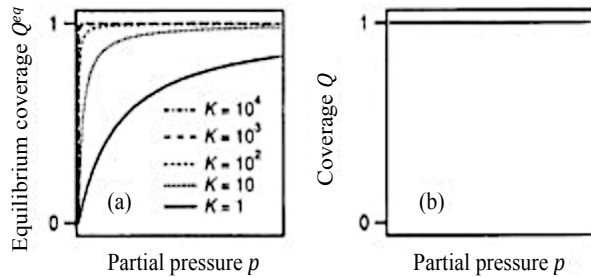


FIG 2.5 Effect of the reactant partial pressure p on the amount of material chemisorbed in a gas–solid reaction: (a) the equilibrium chemisorption coverage Q^{eq} in reversible adsorption (equilibrium constants $1 \leq K \leq 10^4$) and (b) the chemisorption coverage Q after saturation in irreversible adsorption. Reprinted from R. L. Puurunen, *J. Appl. Phys.* **97**, 121301 (2005) [7]. Copyright 2005, American Institute of Physics.

Time. The adsorption process is also influenced by time. Assuming other parameters are constant, i.e. pressure and temperature, integrating Eq. 7 gives the chemisorption coverage as a function of time, t :

$$Q = Q^{eq}(1 - e^{-(k_a p + k_d)t}). \quad (10)$$

Assuming chemisorption is irreversible, this equation can be reduced, giving $Q = 1 - e^{-k_a p t}$. The chemisorption coverage for this irreversible process is demonstrated in FIG 2.6a:

- *Step 1:* During exposure to a precursor ML_n , the chemisorption coverage increases to saturation. Assuming the process is irreversible, saturation corresponds with the surface reaction being fully terminated and limited by the reaction sites or steric hindrance of the ligands as previously discussed.
- *Step 2:* During purge, chemisorption coverage remains constant.
- *Step 3:* Exposure to the second reactant ideally reduces the number of adsorbed species introduced in Step 1 to zero by fully completing the reaction and introduces additional adsorbed surface species, such as -OH groups.
- *Step 4:* The final purge does not affect the chemisorption coverage of the second reactant either.

The total amount of material deposited, c_M , can be deduced from the behavior of the chemisorption coverage, Q , where c_M increases most significantly during Step 1 of the reaction cycles as shown in FIG 2.6b. The deposition rate with respect to time, dc_M/dt , is thus by FIG 2.6c, where the reaction rate is similarly most significant during Step 1.

(NOTE: these models assume the simplest growth conditions, where the amount of deposited material, c_M , increases linearly with the number of reaction cycles—see FIG 2.6d—and the GPC Δc_M is constant—see FIG 2.6e. Variations of these assumptions will be discussed in the following section.)

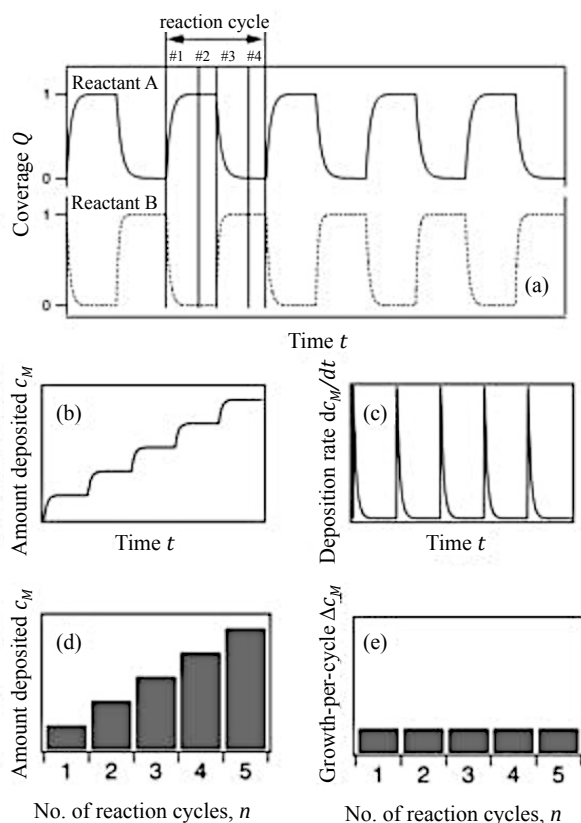


FIG 2.6 Schematic representation of five reaction cycles, assuming irreversible adsorption: (a) chemisorption coverage Q as a function of time t (solid line: ML_z species adsorbed in the reaction of the Reactant A assumed to be of type ML_n , dashed line: species adsorbed in the reaction of Reactant B; the beginning and end of a reaction cycle and Steps 1–4 are indicated), (b) the amount of atoms M adsorbed c_M as a function of time t , (c) the deposition rate of M atoms dc_M/dt as a function of time t [obtained as the time derivative of the curve in panel (b)], (d) amount of material deposited c_M as a function of the number of reaction cycles n , and (e) the GPC Δc_M as a function of the number of reaction cycles n . Reprinted from R. L. Puurunen, *J. Appl. Phys.* **97**, 121301 (2005) [7]. Copyright 2005, American Institute of Physics.

Temperature. The adsorption and desorption rate constants, k_i , dependence on temperature is generally described by the *Arrhenius equation*:

$$k_i = Ae^{-E_i/RT}, \quad (11)$$

where A is the pre-exponential factor, E_i is the activation energy, R is the gas constant, and T is the absolute temperature. This suggests temperature is exponentially related to reaction time; however, in practice, this is often an inaccurate representation, as the

amount of material adsorbed at saturation is affected by additional factors, as will be discussed.

3. *Variable GPC*

In some cases, the GPC is not consistent throughout the ALD process. In particular, the GPC is determined by the concentration of available reactive surface sites. However, the reactive sites may vary with temperature. In addition, the concentration of reactive sites on the substrate is often different from the concentration of reactive sites on the deposited material. As a result, the GPC may vary with the following parameters:

Temperature. The GPC is generally dependent on temperature, where temperature may affect the concentration of reactive surface sites or the preferred reaction mechanism before and after chemisorption. More specifically, there are four characteristic ways where the self-terminating ALD mechanism may vary with temperature as shown in FIG 2.7.

- *Decrease with temperature.* As shown in FIG 2.7a, the GPC may decrease with temperature. This behavior generally occurs when an increase in temperature decreases the concentration of reactive surface sites [94-96]. Alternatively, temperature may affect the relevant chemisorption mechanism, thus altering the L/M ratio in the chemisorbed species [97-100]. Moreover, if desorption is not negligible as preferred in ALD processes, an increase in temperature may also result in an increased desorption rate.
- *Constant with temperature.* In some cases, the GPC may be unaffected by temperature as shown in FIG 2.7b. This relationship is most commonly associated

with self-saturating growth. If the growth rate is limited by steric hindrance of the ligands, this constant relationship is expected. Additionally, an ALD process may exhibit this behavior if temperature does not affect the concentration of reactive sites [90,101,102]. The temperature at which the GPC becomes constant will vary with the deposition conditions and materials.

- *Increase with temperature.* The GPC may also increase with temperature as shown in FIG 2.7c; higher temperatures may enable additional reactions, which require additional thermal energy to overcome some energy barrier [103,104].

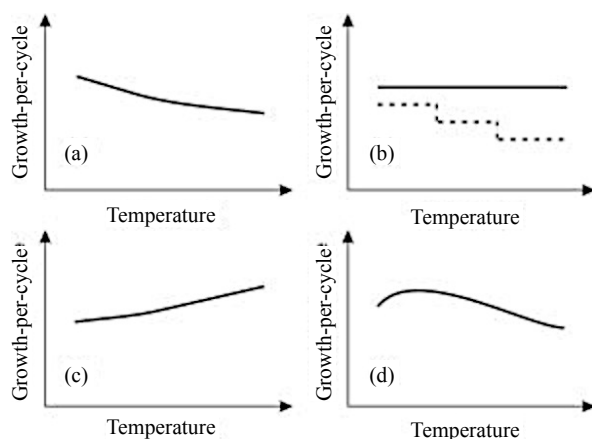


FIG 2.7 Variation of the GPC with the ALD processing temperature in the *ALD window*: (a) the GPC decreases with temperature, (b) the GPC is constant with temperature (possible with different values at different temperature ranges, as shown by the dashed line), (c) the GPC increases with temperature, and (d) the GPC first increases and then decreases with temperature. Reprinted from R. L. Puurunen, *J. Appl. Phys.* **97**, 121301 (2005) [7]. Copyright 2005, American Institute of Physics.

- *Increase and then decrease with temperature.* The GPC may also decrease after an initial increase. (See FIG 2.7d.) This GPC-temperature profile is generally related to the activation of some initial reactions, followed by a decreasing concentration of reactive sites [105,106].

In most cases, different relations between the GPC and temperature exist in different temperature regimes for the same ALD process as shown in FIG 2.8. This gives rise to the concept of the “ALD window,” which describes the temperature range in which the GPC is constant. Traditionally, a temperature within this range is favored during

processing; however, future work will continue to investigate whether deposition within the window is always desirable.

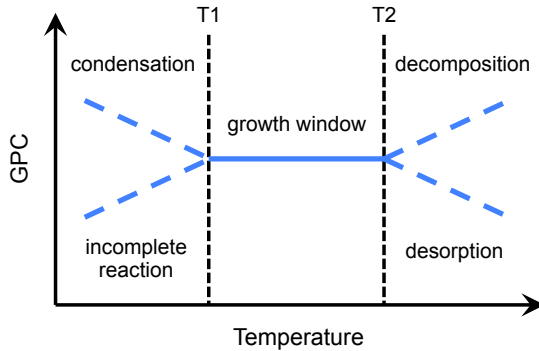


FIG 2.8 Common relationship between the GPC and temperature, where the region of constant growth is called the “ALD growth window.”

Number of Cycles. In some cases, the GPC associated with a given ALD process is dependent on the number of growth cycles completed. Since the ALD process modifies the chemical composition of the surface, the surface conditions of the first ALD cycle may vary from those of the n^{th} . More specifically, ALD growth characteristics can be classified into four groups depending on the relationship between the GPC and the number of ALD cycles, as follows [7]:

- *Linear growth:* In linear growth, the GPC remains constant, independent of the number of cycles. (See FIG 2.9a.) In other words, the growth rate is unaffected by the initial substrate surface. If the reaction is limited by reactive sites, then this type of growth occurs when the surface sites on the substrate surface are of the same concentration as that on a layer of deposited material. If the reaction is limited by steric hindrance, then this type of growth occurs when the ligand-to-metal ratio of the adsorbed species must remain constant [101,107,108].

- *Substrate-enhanced growth*: Substrate-enhanced growth is used to describe deposition processes where the GPC is higher within the first few cycles of deposition. (See FIG 2.9b.) The initial cycles where the growth rate decreases constitute the transient region, and the remaining cycles where the growth rate is constant constitute the steady region. Generally, substrate-enhanced growth occurs if the concentration of reactive sites on the substrate is higher than that on the ALD-grown material [109-111].
- *Substrate-inhibited growth*: Substrate-inhibited growth occurs when the GPC is lower in the transient region than in the steady region. Similar to substrate-enhanced growth, this growth mechanism occurs when the concentration of reactive sites on the substrate is lower than on the ALD-grown material [32,112-116]. (See FIG 2.9c.) Alternatively, there is a second type of substrate-inhibited growth, where the GPC demonstrates a local maximum before settling in the steady region. (See FIG 2.9d.) This growth behavior is associated with island formation [113,115].

Notice the GPC in each growth mode approaches a constant value after the first several cycles.

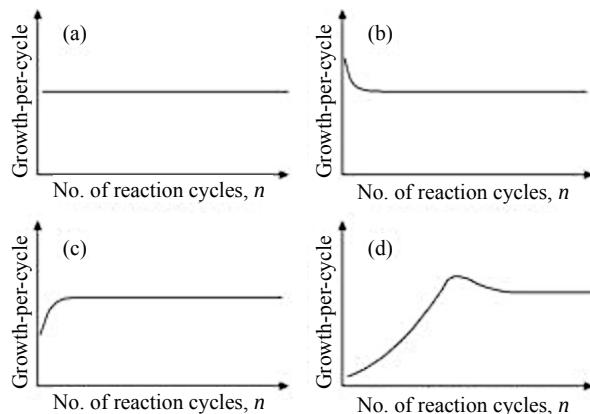


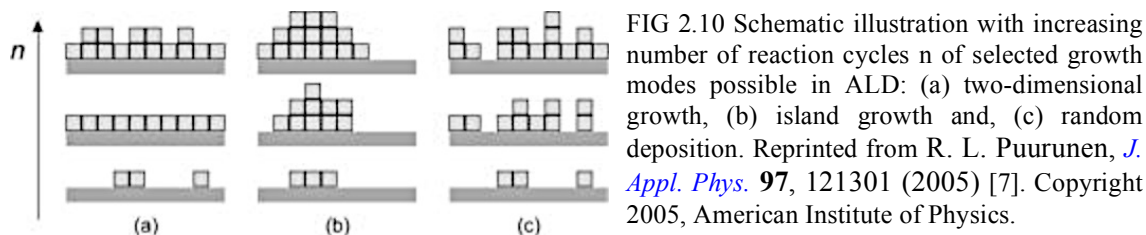
FIG 2.9 Dependency of the GPC on the number of reaction cycles in different types of ALD processes (Ref. 247): (a) linear growth, (b) substrate-enhanced growth, (c) substrate-inhibited growth of Type 1, and (d) substrate-inhibited growth of Type 2. Reprinted from R. L. Puurunen, *J. Appl. Phys.* **97**, 121301 (2005) [7]. Copyright 2005, American Institute of Physics.

Growth mode. The arrangement of absorbed material is determined by the growth mode. For the traditional layer-by-layer ALD processes, full monolayer growth is expected. However, there are a few exceptions to the traditional growth mode, where the growth is less than a monolayer per cycle. More specifically, there are three common growth modes possible with ALD [7]:

- *Two-dimensional growth:* Two-dimensional growth describes the expected layer-by-layer growth associated with ALD as shown in FIG 2.10a; in this case, the adsorbed material settles in the lowest unfilled material layer, giving conformal and uniform monolayer growth [117].
- *Island growth:* Island growth occurs when chemisorption is more likely to occur on the ALD-deposited material rather than the substrate [117,118]; consequently, if the first cycle does not fully satisfy monolayer growth, subsequent cycle will result in the accumulation of deposition on the areas with previous deposition, thus generating islands as shown in FIG 2.10b.
- *Random deposition:* In this growth mode, the deposition is statistically random, where every reactive site is equally likely [119]; since chemisorption reactions are still self-terminating, this growth mode still generally results in smooth ALD layers, where the growth per cycle is simply less than an ALD monolayer.

The growth mode may vary with the number of cycles as well, where the process may experience island growth within the first few cycles and then switch to two-dimensional growth or vice versa. This relationship is dependent on the specifics of the ALD

process. However, the relationship between the growth mode and variation of the GPC with the number of cycles are inconclusive.



C. Reactant Chemistry

As mentioned, variations in growth behavior generally relate to the chemistry and chemical properties of the initial reactant, which determine the relevant mechanism and characteristics of a given ALD process.

To date, ALD processes have been developed for oxides, nitrides, sulfides, carbides, fluorides, phosphides, selenides, and pure elements as summarized in FIG 2.11. Of these materials, oxides have been the most extensively studied and are generally grown from group 2-15 elements with an oxidizing reactant such as H_2O , O_3 , or O_2 plasma. In some cases, these reactions may use less prevalent oxidizers such as H_2O with a catalyst, hydrogen peroxide, alcohols, nitrous oxide, nitrogen dioxide, dinitrogen tetroxide, and metal alkoxide reactants. Nitrides have also been extensively studied and manufactured from metal compounds and ammonia NH_3 and N_2/NH_3 plasma or, in less common cases, N_2 , NH_3 + catalyst, amines, hydrazine, or an alkylamide reactant. Sulfides are not as developed as oxides or nitrides but have been produced from alkaline-earth metals and metal compounds with hydrogen sulfide, sulfide, or diethyl disulfide. Other compounds have been even less developed, but some processes still exist: carbides are possible with

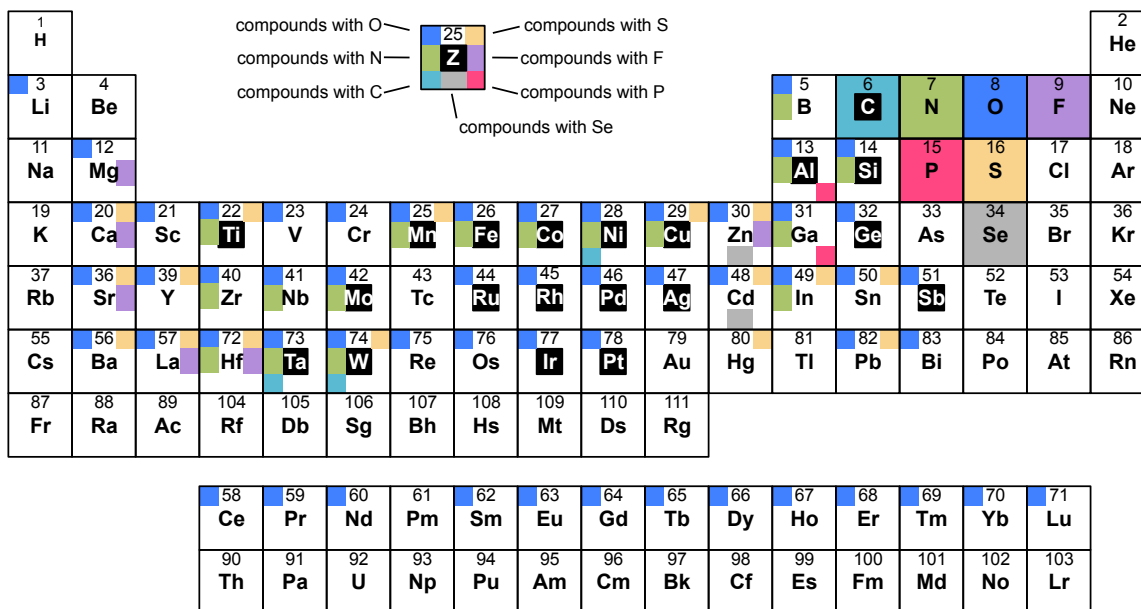


FIG 2.11 Materials deposited by atomic layer deposition. This includes compound materials, such as oxides, nitrides, carbides, sulfides, fluorides, phosphides, selenides, and pure elements as shown. Modified from Ref. 7, 120, and 121.

tantalum carbide, tungsten carbide, and nickel carbide using N_2 and H_2 plasma reactants; fluorides have been successful with some transition metals, e.g. lanthanum, hafnium, and zinc using HF; phosphides have been combined with aluminum and gallium using phosphine or phosphides; and selenides, i.e. copper and zinc selenide, have been deposited from hydrogen selenide, diethyl selenide, or diethyl diselenide. More recently, ALD has also been used to deposit pure metal and metalloid elements. In most cases, these elements are reduced by diatomic hydrogen, H_2 , plasma, or alcohols. Though for some metals, such as ruthenium, palladium, iridium, and platinum, the pure elements can be obtained even when an oxidizer is used for ligand removal [7,120,121].

In general, precursors may be gas, liquid, or solid compounds that are volatile at room temperature or elevated temperatures, thermally stable at ALD processing temperature (i.e. will not thermally decompose), and characterized by self-terminating reactions—or,

in other words, capable of achieving saturation in short processing times [4]. Other properties may vary with the reactant, which are divided into two categories: inorganics and metalorganics. Inorganic reactants are compounds that contain no carbon, such as elements or halides, while metalorganics reactants are compounds that contain carbon, such as alkoxides, β -diketonates, amides, and amidinates. There is also a subset of metalorganics that are characterized by direct metal-carbon bonding, known as organometallics. These include alkyls and cyclopentadienyls [7]. (See FIG 2.12 for a summary the molecular structure of the ligands.)

1. Elements

Elements are the simplest of ALD precursors and have been used to deposit a range of materials including oxides, nitrides, sulfides, phosphides, selenides, tellurides, and antimonides with the metals summarized in FIG 2.13a. Because these precursors are ligand free, the deposited films do not contain any contamination from unreacted ligands. Furthermore, the lack of ligands eliminates steric hindrance and theoretically results in full monolayer growth. Experimental results, on the other hand, often demonstrate growth rates less than a monolayer as a result of surface reconstruction, which may limit the growth rate. However, despite their benefits, elements have been decreasing in use. Since many elements do not have sufficiently high vapor pressure for ALD, the diversity of materials deposited by elements is limited. Moreover, elemental adsorption is often reversible, which limits self-saturation and subsequently mitigates many of the benefits of ALD. Consequently, elements are not often used in ALD processes.

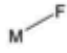
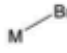
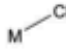
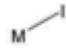
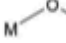
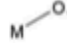
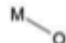
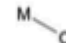
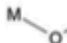

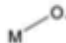
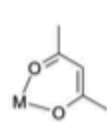
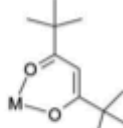
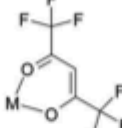
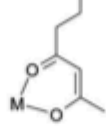
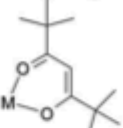
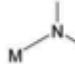
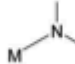
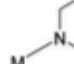
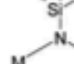
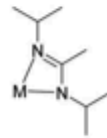
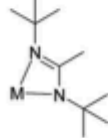







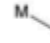




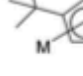

2. Halides

Halides were the original precursors used in ALD experiments. Since then, a variety of volatile halides compatible with ALD—shown in FIG 2.13b—have been extensively investigated. These compounds have excellent properties for ALD, including high reactivity and thermal stability, which allow for the deposition of a range of materials; though most commonly used to deposit oxides for microelectronic application, they can also be used to deposit nitrides, phosphides, selenides, arsenides, and pure metals. The high thermal stability results in a wide ALD growth window, while the small ligands reduce steric hindrance and result in almost monolayer growth. On the other hand, halides are often solids at room temperature, which can be difficult to vaporize. In addition, the gaseous by-products associated with these compounds—such as HF, HCl, HBr, and HI—are corrosive, etching the film, sample stage, or reactor, and may also absorb on surface reactive sites, resulting in non-conformal and impure films.

3. Alkoxides

Alkoxides were introduced as ALD reactants in the early 1990s. Since then, they have been developed for only a select few elements as shown in FIG 2.13c and can only be used to deposit oxides. This lack of versatility is likely a result of the difficulty cleaving the M-O bond. Furthermore, these compounds are characterized by low decomposition temperatures, and the reactions produce alcohols as a gaseous by-product. Alcohols are highly reactive and may readsorb onto the surface, interfering with growth. Furthermore, these compounds may have high carbon and hydrogen contents. Consequently, the popularity of alkoxides has been decreasing with the exception of ternary oxides in

FIG 2.12 Molecular structure for common precursor ligands. Reprinted from R.L. Puurunen, *J. Appl. Phys.* **97**, 121301 (2005) [7]. Copyright 2003, American Institute of Physics.

Inorganic	
Elements	M metal (no ligand)
Halides	<div style="display: flex; justify-content: space-around; align-items: center;"> <div style="text-align: center;">  F fluoride </div> <div style="text-align: center;">  Br bromide </div> <div style="text-align: center;">  Cl chloride </div> <div style="text-align: center;">  I iodide </div> </div>
Organic	
Alkoxides	<div style="display: flex; justify-content: space-around; align-items: center;"> <div style="text-align: center;">  OMe methoxy </div> <div style="text-align: center;">  OEt ethoxy </div> <div style="text-align: center;">  OⁱPr isopropoxy </div> <div style="text-align: center;">  OⁱBu isobutoxy </div> <div style="text-align: center;">  OTBu tert-butoxy </div> <div style="text-align: center;">  mmp 1-methoxy-2-methyl-2-propoxy </div> <div style="text-align: center;">  dmae dimethylamino ethoxy </div> </div>
β -diketonates	<div style="display: flex; justify-content: space-around; align-items: center;"> <div style="text-align: center;">  acac acetylacetonate </div> <div style="text-align: center;">  thd 2,2,6,6-tetramethyl-3,5-heptanedionate </div> <div style="text-align: center;">  hfac 1,1,1,5,5,5-hexafluoroacetylacetonate </div> <div style="text-align: center;">  od octane-2,4-dionate </div> <div style="text-align: center;">  methd 1-(2-methoxyethoxy)-2,2,6,6-tetramethyl-3,5-heptanedionate </div> </div>
Amides	<div style="display: flex; justify-content: space-around; align-items: center;"> <div style="text-align: center;">  NMe₂ dimethylamido </div> <div style="text-align: center;">  NEtMe ethylmethylamido </div> <div style="text-align: center;">  NEt₂ diethylamido </div> <div style="text-align: center;">  N(SiMe₃)₂ bis(trimethylsilyl)amido </div> </div>
Amidimates	<div style="display: flex; justify-content: space-around; align-items: center;"> <div style="text-align: center;">  ⁱPrAMD <i>N,N'</i>-diisopropylacetamidinate </div> <div style="text-align: center;">  ^tBuAMD <i>N,N'</i>-di-tert-butylacetamidinate </div> </div>
Organometallics	
Alkyls	<div style="display: flex; justify-content: space-around; align-items: center;"> <div style="text-align: center;">  Me methyl </div> <div style="text-align: center;">  Et ethyl </div> <div style="text-align: center;">  ⁱPr isopropyl </div> <div style="text-align: center;">  Ay allyl </div> <div style="text-align: center;">  ⁿBu n-butyl </div> <div style="text-align: center;">  ⁱBu isobutyl </div> <div style="text-align: center;">  ^tBu tert-butyl </div> <div style="text-align: center;">  Np neopentyl </div> </div>
Cyclopentadienyls	<div style="display: flex; justify-content: space-around; align-items: center;"> <div style="text-align: center;">  Cp cyclopentadienyl </div> <div style="text-align: center;">  Cp^{Me} methylcyclopentadienyl </div> <div style="text-align: center;">  Cp* pentamethylcyclopentadienyl </div> <div style="text-align: center;">  Cp^{Et} ethylcyclopentadienyl </div> <div style="text-align: center;">  Cp^{iPr} isopropylcyclopentadienyl </div> <div style="text-align: center;">  Cp(SiMe₃) trimethylsilylcyclopentadienyl </div> </div>

H																	He
Li	Be											B	C	N	O	F	Ne
Na	Mg											Al	Si	P	S	Cl	Ar
K	Ca	Sc	Ti	V	Cr	Mn	Fe	Co	Ni	Cu	Zn	Ga	Ge	As	Se	Br	Kr
Rb	Sr	Y	Zr	Nb	Mo	Tc	Ru	Rh	Pd	Ag	Cd	In	Sn	Sb	Te	I	Xe
Cs	Ba	La	Hf	Ta	W	Re	Os	Ir	Pt	Au	Hg	Tl	Pb	Bi	Po	At	Rn
Fr	Ra	Ac	Rf	Db	Sg	Bh	Hs	Mt	Ds	Rg							

Ce	Pr	Nd	Pm	Sm	Eu	Gd	Tb	Dy	Ho	Er	Tm	Yb	Lu
Th	Pa	U	Np	Pu	Am	Cm	Bk	Cf	Es	Fm	Md	No	Lr

(a) elements

H																	He
Li	Be											B	C	N	O	F	Ne
Na	Mg											Al	Si	P	S	Cl	Ar
K	Ca	Sc	Ti	V	Cr	Mn	Fe	Co	Ni	Cu	Zn	Ga	Ge	As	Se	Br	Kr
Rb	Sr	Y	Zr	Nb	Mo	Tc	Ru	Rh	Pd	Ag	Cd	In	Sn	Sb	Te	I	Xe
Cs	Ba	La	Hf	Ta	W	Re	Os	Ir	Pt	Au	Hg	Tl	Pb	Bi	Po	At	Rn
Fr	Ra	Ac	Rf	Db	Sg	Bh	Hs	Mt	Ds	Rg							

Ce	Pr	Nd	Pm	Sm	Eu	Gd	Tb	Dy	Ho	Er	Tm	Yb	Lu
Th	Pa	U	Np	Pu	Am	Cm	Bk	Cf	Es	Fm	Md	No	Lr

(b) halides

H																	He
Li	Be											B	C	N	O	F	Ne
Na	Mg											Al	Si	P	S	Cl	Ar
K	Ca	Sc	Ti	V	Cr	Mn	Fe	Co	Ni	Cu	Zn	Ga	Ge	As	Se	Br	Kr
Rb	Sr	Y	Zr	Nb	Mo	Tc	Ru	Rh	Pd	Ag	Cd	In	Sn	Sb	Te	I	Xe
Cs	Ba	La	Hf	Ta	W	Re	Os	Ir	Pt	Au	Hg	Tl	Pb	Bi	Po	At	Rn
Fr	Ra	Ac	Rf	Db	Sg	Bh	Hs	Mt	Ds	Rg							

Ce	Pr	Nd	Pm	Sm	Eu	Gd	Tb	Dy	Ho	Er	Tm	Yb	Lu
Th	Pa	U	Np	Pu	Am	Cm	Bk	Cf	Es	Fm	Md	No	Lr

(c) alkoxides

H																	He
Li	Be											B	C	N	O	F	Ne
Na	Mg											Al	Si	P	S	Cl	Ar
K	Ca	Sc	Ti	V	Cr	Mn	Fe	Co	Ni	Cu	Zn	Ga	Ge	As	Se	Br	Kr
Rb	Sr	Y	Zr	Nb	Mo	Tc	Ru	Rh	Pd	Ag	Cd	In	Sn	Sb	Te	I	Xe
Cs	Ba	La	Hf	Ta	W	Re	Os	Ir	Pt	Au	Hg	Tl	Pb	Bi	Po	At	Rn
Fr	Ra	Ac	Rf	Db	Sg	Bh	Hs	Mt	Ds	Rg							

Ce	Pr	Nd	Pm	Sm	Eu	Gd	Tb	Dy	Ho	Er	Tm	Yb	Lu
Th	Pa	U	Np	Pu	Am	Cm	Bk	Cf	Es	Fm	Md	No	Lr

(d) β -diketonates

H																	He
Li	Be											B	C	N	O	F	Ne
Na	Mg											Al	Si	P	S	Cl	Ar
K	Ca	Sc	Ti	V	Cr	Mn	Fe	Co	Ni	Cu	Zn	Ga	Ge	As	Se	Br	Kr
Rb	Sr	Y	Zr	Nb	Mo	Tc	Ru	Rh	Pd	Ag	Cd	In	Sn	Sb	Te	I	Xe
Cs	Ba	La	Hf	Ta	W	Re	Os	Ir	Pt	Au	Hg	Tl	Pb	Bi	Po	At	Rn
Fr	Ra	Ac	Rf	Db	Sg	Bh	Hs	Mt	Ds	Rg							

Ce	Pr	Nd	Pm	Sm	Eu	Gd	Tb	Dy	Ho	Er	Tm	Yb	Lu
Th	Pa	U	Np	Pu	Am	Cm	Bk	Cf	Es	Fm	Md	No	Lr

(e) amides

H																	He
Li	Be											B	C	N	O	F	Ne
Na	Mg											Al	Si	P	S	Cl	Ar
K	Ca	Sc	Ti	V	Cr	Mn	Fe	Co	Ni	Cu	Zn	Ga	Ge	As	Se	Br	Kr
Rb	Sr	Y	Zr	Nb	Mo	Tc	Ru	Rh	Pd	Ag	Cd	In	Sn	Sb	Te	I	Xe
Cs	Ba	La	Hf	Ta	W	Re	Os	Ir	Pt	Au	Hg	Tl	Pb	Bi	Po	At	Rn
Fr	Ra	Ac	Rf	Db	Sg	Bh	Hs	Mt	Ds	Rg							

Ce	Pr	Nd	Pm	Sm	Eu	Gd	Tb	Dy	Ho	Er	Tm	Yb	Lu
Th	Pa	U	Np	Pu	Am	Cm	Bk	Cf	Es	Fm	Md	No	Lr

(f) amidinates

H																	He
Li	Be											B	C	N	O	F	Ne
Na	Mg											Al	Si	P	S	Cl	Ar
K	Ca	Sc	Ti	V	Cr	Mn	Fe	Co	Ni	Cu	Zn	Ga	Ge	As	Se	Br	Kr
Rb	Sr	Y	Zr	Nb	Mo	Tc	Ru	Rh	Pd	Ag	Cd	In	Sn	Sb	Te	I	Xe
Cs	Ba	La	Hf	Ta	W	Re	Os	Ir	Pt	Au	Hg	Tl	Pb	Bi	Po	At	Rn
Fr	Ra	Ac	Rf	Db	Sg	Bh	Hs	Mt	Ds	Rg							

Ce	Pr	Nd	Pm	Sm	Eu	Gd	Tb	Dy	Ho	Er	Tm	Yb	Lu
Th	Pa	U	Np	Pu	Am	Cm	Bk	Cf	Es	Fm	Md	No	Lr

(g) alkyls

H																	He
Li	Be											B	C	N	O	F	Ne
Na	Mg											Al	Si	P	S	Cl	Ar
K	Ca	Sc	Ti	V	Cr	Mn	Fe	Co	Ni	Cu	Zn	Ga	Ge	As	Se	Br	Kr
Rb	Sr	Y	Zr	Nb	Mo	Tc	Ru	Rh	Pd	Ag	Cd	In	Sn	Sb	Te	I	Xe
Cs	Ba	La	Hf	Ta	W	Re	Os	Ir	Pt	Au	Hg	Tl	Pb	Bi	Po	At	Rn
Fr	Ra	Ac	Rf	Db	Sg	Bh	Hs	Mt	Ds	Rg							

Ce	Pr	Nd	Pm	Sm	Eu	Gd	Tb	Dy	Ho	Er	Tm	Yb	Lu
Th	Pa	U	Np	Pu	Am	Cm	Bk	Cf	Es	Fm	Md	No	Lr

(h) cyclopentadienyls

FIG 2.13 (a) Elemental metal reactants used in ALD: no ligands; (b) Metal halide reactants used in ALD: F, B, Cl or I ligands; (c) Metal alkoxide reactants used in ALD: OMe, OEt, OⁱPr, OⁱBu, O^tBu, mmp, or dmae ligands; (d) Metal β -diketonate reactants used in ALD: acac, thd, hfac, od, and, or methd ligands; (e) Metal amide reactants used in ALD: NMe₂, NEtMe, NEt₂, or N(SiMe₃)₂ ligands; (f) Metal amidinate reactants used in ALD: ¹PrAMD and ¹BuAMD ligands; (g) Metal alkyl reactants used in ALD: Me, Et, ¹Pr, Ay, ⁿBu, ¹Bu, ¹Bu, or Np ligands; and (h) Metal cyclopentadienyl reactants used in ALD: Cp, Cp^{Me}, Cp^{*}, Cp^{Et}, Cp^{iPr}, or Cp(SiMe₃) ligands. (See Appendices A and B for clarification of ligand chemistry.) Reprinted from R. L. Puurunen, *J. Appl. Phys.* **97**, 121301 (2005) [7]. Copyright 2005, American Institute of Physics.

combination—with metal halides.

4. β -diketonates

β -diketonates were introduced in the mid-1980s. As shown in FIG 2.13d, these compounds are the most versatile group of reactants as they are compatible with the greatest number of elements; however, despite their versatility, they have only been used to deposit a few materials, including oxides, sulfides, fluorides, and pure metals. (Nitrides are not possible with these compounds as a result of the difficulty of replacing the M-O bond.) β -diketonates are characterized by low deposition temperatures, $\sim 300^\circ\text{C}$, and have bulky ligands that result in significant steric hindrance and low GPCs. Moreover, these films may have considerable carbon and hydrogen contamination.

5. Amides

Amides consist of alkylamides and silylamides, which have been investigated since the 1990s. A few metals are available as amides reactants as shown in FIG 2.13e, which have been used to deposit oxides, nitrides, and selenides. However, the low decomposition temperature of these reactants can be problematic and may be as low as $\sim 150^\circ\text{C}$. Another common drawback of these precursors is the high concentration of carbon and hydrogen impurities.

6. Amidinates

Amidinates are the newest class of reactants. Given their novelty, only few elements have been investigated—see FIG 2.13f—and only oxides and pure metals have been investigated to date. However, amidinates will likely be compatible with most metals,

allowing for future development. These compounds result in self-terminating reactions, have low decomposition temperatures $\sim 300^{\circ}\text{C}$, and may also produce films with residual carbon, hydrogen, and nitrogen contamination.

7. Alkyls

Alkyls are highly reactive organometallic compounds that were introduced to ALD in the mid-1980s. They have been used to deposit oxides, nitrides, sulfides, phosphides, selenides, arsenides, and pure metals with the elements summarized in FIG 2.13g. Similar to elements and halides, alkyls are characterized by small ligands, resulting in low steric hindrance and a high GPC—typically 30% of a monolayer. The byproducts of the reaction are typically hydrocarbons (e.g. H_2O , H_2S , NH_3 ...etc.). In general, these byproducts are inert and do not readsorb or corrode the films but may leave residual carbon or hydrogen contamination. Unfortunately, alkyls can be used with very few elements and decompose at low deposition temperatures. For example, AlMe_2 decomposes $\sim 300^{\circ}\text{C}$ and contains $\sim 0.2\%$ carbon and $\sim 0.7\%$ hydrogen.

8. Cyclopentadienyls

Cyclopentadienyls have gained popularity as ALD reactants in the last decade. The attractiveness of these materials is related to the ease of synthesizing alkaline-earth metals. (See FIG 2.13h.) These compounds are also organometallic and highly reactive. However, despite their reactivity, these metals can only be used to deposit oxides, sulfides, and pure metals. The ligand sizes are moderate, resulting in moderate GPCs. Similar to alkyls, these compounds are characterized by a low decomposition

temperatures and some residual carbon and hydrogen content in the films depending on the deposition temperature.

9. Summary

Continued research with regards to ALD precursor chemistry will prove essential to the progress of ALD-based processes. In some cases, smart thermal-driven chemistry has provided unique solutions. For example, when SiO_2 is deposited by tris(*tert*-butoxy)silanol on Al_2O_3 , the growth is astronomical, ~ 12 nm/cycle. This large GPC is likely a result of the polymerization reaction in which the silanol inserts itself in the Al-O bonds [122]. Another example is the deposition of tungsten films with tungsten hexafluoride and disilane, which circumvents the traditional difficulties of depositing non-noble metals [123]. However, in many other cases, ALD is not yet a viable deposition option. For example, III-V materials, such as GaN, are still only in the initial stages of development as a consequence of the unfavorable reaction between group III alkyls and group V hybrids [40]. Therefore, continued research and innovative solutions with regards to precursor chemistry will help drive this technology forward.

III. Plasma-Enhanced Reactions

In most established ALD processes, thermal energy is used to provide the energy to drive the reaction between two reactants; however, plasma may also be used, where the reactivity of the radical species can provide the energy to drive the reaction. This technique is known as plasma-enhanced ALD (PEALD) and is—in many cases—advantageous over thermal ALD processes as will be discussed. Typically, PEALD utilizes O_2 , N_2 , or H_2 plasma or some combination thereof, as the second reactant to

remove the ligands of the initial reactant. Generally, this process results in the deposition of metal oxide, nitride, or pure metals.

A. Plasma Basics

Plasma is a collection of charged particles among a gas species, which is on average electrically neutral. The charge neutrality is commonly referred to as ‘quasi-neutral,’ since the plasma is electrically neutral on a macroscopic scale ($>1\text{mm}$) where the electron density of the plasma, n_e , is equal to the ion density, n_i . In general, plasmas are generated by ‘heating’ gasses, which accelerates constituent electrons. These electrons then collide with the gaseous species, commonly causing ionization depending on the energy of the incident species; the ionization generated by electron-induced collisions compensates for electron-loss collisions and sustains the plasma. If the incident electron is on the higher end of the energy distribution, the electron-induced collisions may excite or dissociate the gas species, leading to the formation of photons or reactive atomic and molecular neutrals known as ‘plasma radicals.’ Under typical ALD conditions, the ion and electron densities are several orders of magnitude lower than the plasma radicals.

TABLE 2.1 Densities of plasma species in O_2 plasma, as typically used in ALD processes. Data are presented for two different pressures and the electron temperature, T_e , and energy, E_{ion} , of ions accelerated to the (grounded) substrate are also given. The data have been compiled from the modeling described in ref 124 for an inductively coupled plasma operated at a source power of 500 W. The excited species O^* and O_2^* correspond to the lowest metastable state being $\text{O}(^1\text{D})$ and $\text{O}_2(^1\Delta_g)$, respectively. Reprinted from H. B. Profijt *et al.*, *J. Vac. Sci. Technol. A* **29**, 050801 (2011) [11]. Copyright 2011, American Vacuum Society.

Pressure (mTorr)	O_2 (cm^{-3})	O (cm^{-3})	O_2^* (cm^{-3})	O^* (cm^{-3})	O_2^+ (cm^{-3})	O^+ (cm^{-3})	O^- (cm^{-3})	n_e (cm^{-3})	T_e (eV)	E_{ion} (eV)
10	3×10^{14}	7×10^{13}	4×10^{13}	4×10^{12}	5×10^{10}	4×10^{10}	2×10^{10}	2×10^{10}	2.8	15.3
100	3×10^{15}	1×10^{14}	3×10^{14}	5×10^{10}	4×10^{10}	1×10^{10}	3×10^{10}	3×10^{10}	2.1	10.8

(See TABLE 2.1 for example of typical plasma constituent concentrations for O₂.) Consequently, the surface chemistry in PEALD is mainly determined by the interactions of the plasma radicals with the surface species.

In ALD, plasmas are typically generated using an electric field rather than thermal energy to accelerate the electrons, which results in a non-equilibrium system. Electrons in this system typically have an average temperature, T_e , of $\sim 3.5 \times 10^4$ K, while the gas temperature remains low, 300-500 K. Plasma under these conditions is thus dubbed a “cold plasma.”

There are three key properties of the plasma in ALD as follows [11]:

First, the reactive species is created in the gas phase, ensuring high reactivity at the substrate surface regardless (or almost regardless) of substrate conditions. This quality also suggests that the reactivity of the plasma can be adjusted with the plasma operating conditions, i.e. the gas type, flow, pressure, power, etc. This adaptability allows for greater processing diversity.

Second, despite the high reactivity of the plasma, the heat flux of the plasma on the substrate is relatively small. Since the plasma is under non-equilibrium conditions, only electrons have significant thermal energy, while ions and radical species supply very little heat to the surface. Moreover, since the plasma is only part of a cycle, which typically lasts for a few seconds, the plasma does not significantly heat the substrate.

Third, bombardment of the ions may provide additional energy to the substrate surface, which can enhance and enable surface reactions and diffusion rates. Similar to the reactivity of the plasma radicals, the presence and level of ion bombardment can also be

controlled by the reactor configuration and the plasma processing conditions, mainly pressure. On the other hand, ion bombardment may induce undesired surface damage, which can also be controlled by the reactor configuration and processing conditions.

In other words, the plasma can supply energy-enhanced reactivity independent of heat, which enables reactions not strictly accessible by the existing surface chemistry.

B. PEALD Reactor Configurations

The position of the plasma generation with respect to the substrate determines the prevalence of a relative species in the plasma at the surface, which can have significant effects on the substrate and depositions. In general, there are three standard PEALD designs, including radical-enhanced, direct, and remote. These reactants are summarized in FIG 2.14 and discussed in the following section.

1. Radical-Enhanced

In the first configuration, a thermal ALD reactor is generally adapted with a plasma generator, which allows for integrative processing of either thermal or plasma-enhanced

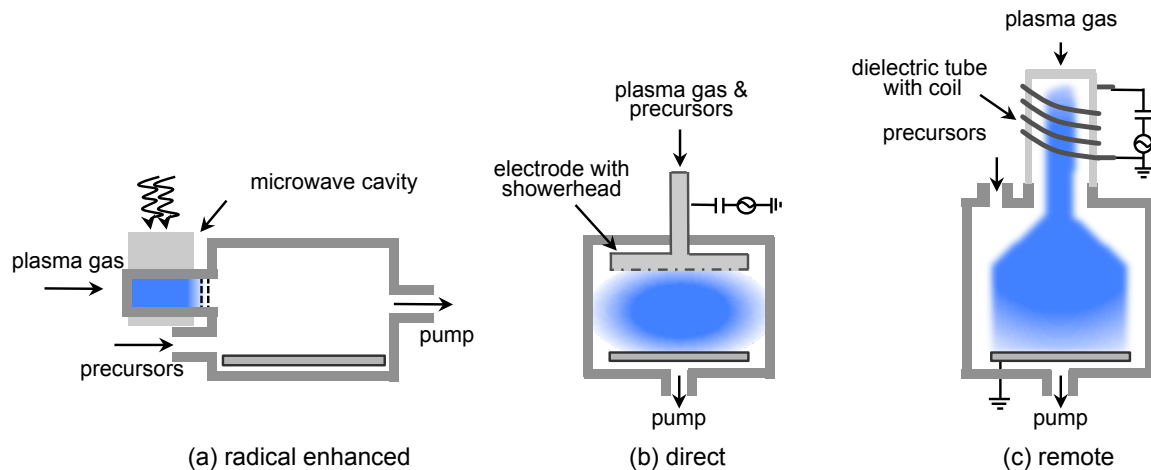


FIG 2.14 Schematic reactor configurations for a) radical-enhanced, b) direct, and c) remote PEALD [1].

ALD as seen in FIG 2.14a. (Note: these plasma sources are typically microwave- or radio-frequency driven and may be instrumental in sample cleaning and preparation as well as deposition.) Since this system is typically fitted to an existing system, the placement of the plasma source is constrained by the system design. Consequently, the plasma source is typically far from the ALD reaction zone. The plasma species must, therefore, travel through a length of tubing to reach the reaction zone, which increases the number of surface collisions between the plasma species and metal walls of the tubing. As a result, many of the ions and electrons in the plasma species are lost to recombination. The plasma is thus said to be 'radical-enhanced' since it has a larger concentration of radical species than the plasma at generation. However, the overall flux of the radicals at the sample surface may also decrease as a result of surface recombination and may, therefore, require long reactant exposure times to complete the surface reaction.

2. Direct

The second configuration is a derivation of traditional plasma-enhanced CVD. In this reactor design, the plasma is generated by two capacitively coupled parallel electrodes: i.e., one plate is powered at a radio frequency (typically 13.56 Hz), and the other is grounded. (See FIG 2.14b.) The substrate is then positioned on the grounded electrode, directly in the plasma generation. Consequently, this configuration is referred to as 'direct.' The gas may be delivered into the chamber in one of two ways: through a showerhead in the powered electrode, known as 'showerhead type' [124] or at the side of the electrodes, known as 'flow type' [125]. Since the plasma is generated very close to

the substrate, the ion flux and emission of high-energy photons may cause damage, and the extent of the damage is determined by the particular reactor design, processing conditions, and substrate materials. However, this design also ensures a significant radical flux and, subsequently, short reactant exposure times. As a result, this is the design most heavily used by industry, which prefers shorter cycle times despite the potential plasma damage.

3. Remote

The third configuration, the plasma generator is located farther from the sample stage, such that the substrate is not directly involved in the plasma generation as shown in FIG 2.14c. In this case, the plasma generator is located ‘remotely,’ and, therefore, ion and electron densities do not significantly decrease [126,127]. Subsequently, the remote configuration is characterized by a larger flux of radicals to the substrate than the radical-enhanced and less ion and photon damage than direct. Additionally, plasma conditions and substrate conditions can be varied independently of one another. In a direct plasma system, for example, altering the substrate temperature will also affect the temperature of the plasma as well as the density of the gas-phase species or generation of the plasma species [11]. A remote configuration, therefore, allows for more flexible processing, where the plasma properties can be optimized by the processing conditions.

C. Advantages and Disadvantages

In general, the major advantages associated with ALD in comparison to other deposition methods—such as MOCVD, MBE, PVD... etc.—are associated with the layer-by-layer deposition mechanism. In particular, these benefits include precise thickness control, high

uniformity, and high conformality, as previously mentioned. In addition, there are some benefits of PEALD in comparison with thermal ALD. The benefits are typically associated with the reactivity of the plasma as follows [11,128,129]:

Augmented Material Properties. For some applications, materials deposited by PEALD have been characterized by better material properties than those grown by thermal ALD. The material properties may include film density, impurity content, and electronic properties.

Reduced Deposition Temperature. Since the high reactivity of the radicals and kinetic energy of the ions supply energy to drive the reaction, significant thermal energy is not required. Consequently, PEALD can deposit high-quality films at much lower substrate temperatures. This feature accommodates a wider variety of substrates, which may be temperature sensitive.

Increased Growth Rate. In some cases, plasma-enhanced ALD has been shown to generate more reactive surface sites than thermal ALD. This enables a higher growth rate in cases where the GPC is reactive-site limited. Furthermore, since plasma-enhanced is more reactive than thermal ALD, the second reactant step is often shorter, decreasing cycle time. Consequently, PEALD can increase ALD throughput capabilities, a desirable trait for industrial applications.

Additional Precursor Availability. The higher reactivity of the plasma radicals also allows for the use of precursors with relatively high chemical and thermal stabilities; e.g. metal oxides from β -diketonates. These precursors exhibit little or no reactivity with H_2O but demonstrate high-quality oxides with O_2 plasma. Similarly, some

elemental metals, such as Ti and Ta, do not have any viable precursors compatible with the thermal ALD process.

Stoichiometric Control. The non-equilibrium aspects associated with ALD plasma can be tuned to control the surface reaction and ultimately the stoichiometry of the material. In particular, additional operating variables such as operating pressure, plasma power, exposure time, biasing voltage, and admixing additional gasses into the plasma can tune the surface reaction. For example, in some cases, N₂ gas may be introduced during the O₂ plasma reactant step, resulting in N-doped films. This is not possible with thermal ALD.

Processing Versatility. In addition, plasma may be used in other processing steps in addition to its applications in deposition, including substrate cleaning, pre-deposition treatments (e.g. oxidation or nitridation), post-deposition treatments (e.g. plasma post-deposition anneal or post-metallization anneal), or reactor cleaning.

Despite the many benefits of PEALD, there are still some drawbacks associated with plasma-enhanced ALD in comparison with thermal ALD [11,128,129].

Plasma-Induced Damage. During PEALD deposition, the surface is exposed to many reactive plasma species, which may cause other undesired reactions. In some cases, the plasma may cause oxidation or nitridation of the substrate material at a faster rate than the deposited film. The result may thus be a thick layer of oxidized or nitridized substrate under the deposited film, which is bound to have implications on device behavior. In addition, ion bombardment may cause undesired results during deposition or the formation of defects, such as bond breaking, atom displacement, and charge

accumulation across a dielectric. While many ions do not typically have the energies required to cause damage, the effects of ion bombardment can still significantly affect the electrical properties of the films, since the electrical properties are principally determined by the interface properties. These effects are mitigated by the remote PEALD configuration previously discussed, which decreases the flux of ions to the surface.

Decreased Conformality. Thermal ALD is sometimes more advantageous for depositing conformal films on substrates with structures with large aspect ratios. The reactive species associated with PEALD may undergo reactions with saturated surface sites in addition to the desired ALD reactions. When plasma radicals react with previously adsorbed radicals and species on the surface, they may form non-reactive molecules, which desorb from the surface. In structures with high-aspect ratios, the radicals will undergo an increased number of surface collisions in high-aspect-ratio structures, increasing the likelihood of an undesired reaction and reducing the flux of radicals to the extremities of the structure. The likelihood of recombination is, therefore, the most significant variable in assuring conformality in these structures, which may be improved by adjusting operating temperatures and plasma processing variables. Therefore, the key to achieving conformality in PEALD is to augment the radical density, thus overcoming the loss of radicals to recombination. As shown by Kariniemi *et al.* [130], this technique is applicable to oxide processes but is still problematic in H₂-plasma processes, due to the recombination of the hydrogen radicals.

Challenging Industrial Scale-up. Another class of challenges associated with PEALD is related to industrial scale up. In general, the equipment necessary for PEALD is more complex than that of thermal ALD. Consequently, it is unlikely that plasma systems will be adopted for industrial processing without substantial comparative advantages.

In addition, there are some limitations of ALD in comparison with other deposition methods as well. In particular, ALD is a slow process, which—while suitable for thin films (perhaps $< 1 \mu\text{m}$)—is not practical for thicker films on the order of several micron. In addition, the range of materials is limited by the chemistry design of the precursors as previously mentioned. Consequently, many technologically significant materials cannot be deposited with ALD, including Si, Ge, GaN, etc. On the other hand, ALD is still a relatively new technology, and thus many of the obstacles may be overcome by future development [40,105].

IV. Specific PEALD Reactions

In this research, a remote oxygen PEALD system is used to deposit Al_2O_3 , HfO_2 , and SiO_2 on GaN-based substrates; specifically, the relevant reactions include the application of dimethylaluminum isopropoxide (DMAI), tetrakis(ethylmethylamino)hafnium (TEMAHf), and tri(dimethylamino) silane (TDMAS) in this system, which will be discussed in detail in this sections.

A. Reactor Configuration

The PEALD at the Nanoscience Laboratory is a custom-built, remote oxygen plasma system as shown in FIG 2.15. This system is generally maintained at a background pressure of $\sim 6.0 \times 10^{-8}$ Torr. During deposition, oxygen plasma is ignited with 13.56 MHz

rf-excitation applied at 200 W to a helical copper coil wrapped around a 32 mm diameter quartz tube and maintained ~ 100 mTorr with a flow rate of 35 sccm; however, the plasma power, chamber pressure, and gas flow rate are all adjustable to achieve the desired deposition characteristics. The temperature of each precursor bubbler is adjusted to ensure the appropriate vapor pressure as shown, and the gas lines between the bubbler and the chamber are heated slightly higher than the corresponding bubbler temperature to prevent condensation. Labview software controls the pulse time sequencing of the gas phase chemicals, which varies depending on the ALD process as will be discussed further.

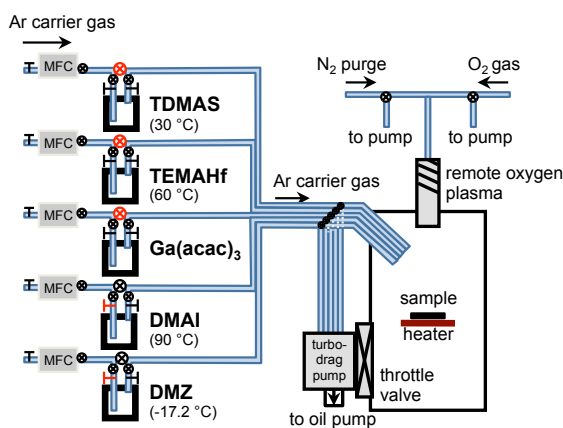


FIG 2.15 Schematic of remote oxygen plasma-enhanced atomic layer deposition chamber at the Nanoscience Laboratory.

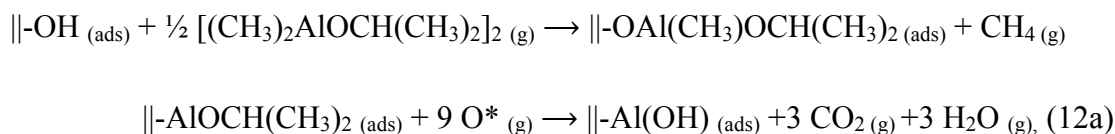
B. Dimethylaluminum Isopropoxide (DMAI)

Our results for PEALD Al_2O_3 using DMAI have recently been published by Jialing Yang, Brianna S. Eller, Manpuneet Kaur, and Robert J. Nemanich [131] in the Journal of Vacuum Science and Technology A; the following section briefly summarizes these results.

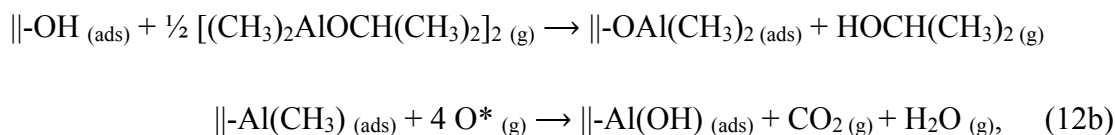
Traditionally, ALD of Al₂O₃ utilizes the extensively studied and established Al precursor, trimethyl-aluminum (TMA or Al(CH₃)₃) [7,132]. The research, however, utilizes a less common reactant as TMA presents concerns—TMA is not only pyrophoric but also highly reactive with H₂O. Dimethylaluminum isopropoxide (DMAI and [(CH₃)₂AlOCH(CH₃)₂]₂) is the alternative used here; this precursor has an appropriate vapor pressure for ALD processes, is not pyrophoric, and is more stable than TMA [133-137].

1. Chemisorption mechanism

The relevant binary reactions for DMAI in PEALD have been reported by Langereis and Potts *et al.* [134,136] as follows:



and



which occur simultaneously.

2. Self-limiting Growth

Sequence and timing of the gas phases were optimized to ensure self-saturating growth as shown in FIG 2.16. This optimization process was conducted at 190 °C, which is within the ALD growth window. Self-limiting growth is achieved for DMAI precursor pulse

times ≥ 0.2 s, O₂ plasma ≥ 6 s, and the N₂ purge ≥ 18 s. Therefore, a 0.6 s DMAI precursor pulse, 8 s O₂ plasma exposure, and 40 s N₂ purge pulse are employed for the standard Al₂O₃ process at 190°C.

The effects of O₂ plasma power were also investigated in this study as shown in the inset of FIG 2.16. The results indicate the growth rate increases with plasma power between 30 to 150 W and stabilizes for power >150 W. Consequently, a plasma power of 200 W is adopted for subsequent growth conditions.

Under these operating conditions, the GPC is ~ 1.5 Å/cycle. This growth rate is slightly higher than reported in thermal ALD studies, which report ~ 0.7 - 1.2 Å/cycle at temperatures ~ 150 - 200 °C [136,138]. As mentioned, an increased growth rate is expected for a PEALD process as a result of the reactivity of the oxygen plasma [135,136,139,140], where the mechanism responsible for the increased growth rate may be related to an increase in the density of surface reactive sites and/or a reduction of steric hindrance [131,136,139,140].

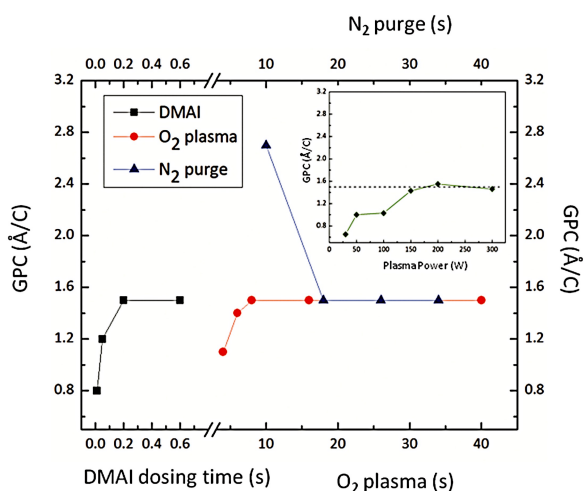


FIG 2.16 Al₂O₃ growth rate vs. DMAI dose time, O₂ plasma exposure time, and N₂ purge time. These values are set to be 0.6 s, 8 s and 20 s when they are not variable, and substrate temperature was set at 190 °C. Reprinted from Yang *et al. J. Vac. Sci. Technol. A* **32**, 021514 (2014) [131]. Copyright 2014, American Vacuum Society.

3. Temperature Window

Using the optimized parameters described above, the temperature dependence of DMAI was also investigated. As shown in FIG 2.17, there is a constant growth rate in the PEALD temperature window of ~25 to 220 °C, as shown by the linear relationship between the film thickness and number of PEALD cycles at 190 °C. (See the inset of FIG 2.17.) For temperatures >220 °C, the increased growth rate is consistent with thermal decomposition. The slight decrease at room temperature is likely related to an incomplete reaction, where the reduction of thermal energy reduces the concentration of chemisorbed DMAI molecules and/or the oxidation of the oxygen plasma. Consequently, increased exposure times increased the growth rate.

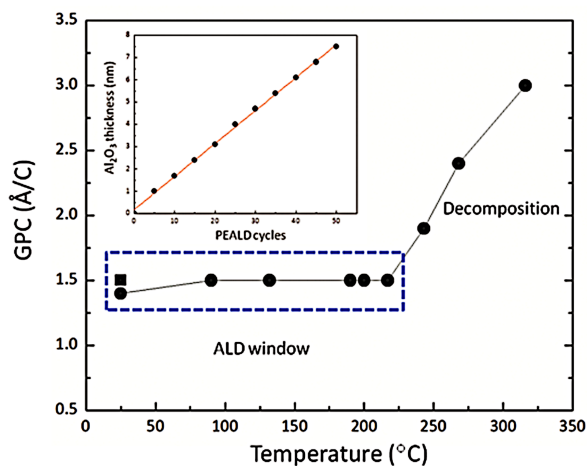


FIG 2.17 Al₂O₃ growth rate vs. substrate temperature, determining the ALD window of 25 to 220 °C. The square represents the increased growth rate caused by the longer plasma pulse time. The inset shows the film thickness vs. number of PEALD cycles for the sample at 200 °C. Reprinted from Yang *et al. J. Vac. Sci. Technol. A* **32**, 021514 (2014) [131]. Copyright 2014, American Vacuum Society.

Moreover, even though the growth rate is constant in the growth window, there are variations in the number of Al atoms deposited per cycle. (See FIG 2.17a.) More specifically, the concentration of Al atoms per cycle (3.9 ± 0.2 at.nm⁻²cycle⁻¹ compared with 5.3 ± 0.3 at.nm⁻²cycle⁻¹) is lower for lower deposition temperatures (25 °C compared to 200 °C). This discrepancy is also likely related to the incomplete chemisorption of

DMAI; however, the decreased film density ($\sim 2.7 \text{ g/cm}^3$ compared with 3.0 g/cm^3) and higher ratio of O to Al (2.1 compared with 1.6) generated a higher GPC, resulting in a constant GPC within the ALD window. At temperatures above the ALD window, the increased concentration of Al atoms deposited per cycle is consistent with thermal decomposition.

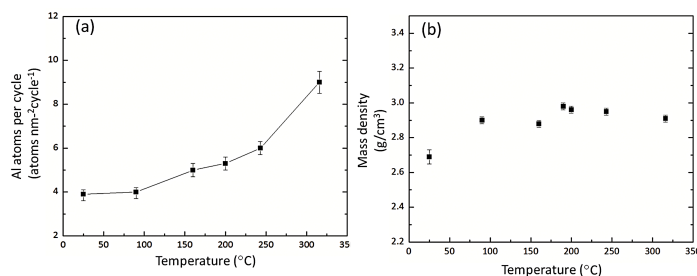


FIG 2.18 The number of Al atoms deposited per cycle as determined by RBS (a) and the film mass density as measured by XRR (b) for PEALD Al_2O_3 grown with DMAI at different temperatures. Reprinted from Yang *et al. J. Vac. Sci. Technol. A* **32**, 021514 (2014) [131]. Copyright 2014, American Vacuum Society.

4. Thin Film Composition

Film compositions and impurities were also dependent on deposition temperature; x-ray photoelectron spectroscopy (XPS) results for films deposited at 200 and 25°C are shown in FIG 2.19 and FIG 2.20, respectively.

Film Content. The stoichiometric ratio of O to Al is ~ 1.6 for annealed samples, which is slightly oxygen rich as expected for PEALD Al_2O_3 . (See FIG 2.19a and b.) However, prior to annealing, the atomic ratio is somewhat higher. Results demonstrate a stoichiometric ratio of O to Al of ~ 2.1 and 1.9 for respective 8 s and 40 s O_2 plasma exposure times for room temperature deposited Al_2O_3 . (See FIG 2.19b and FIG 2.20b.) Since the films are characterized by a single Al-O bonding state as shown FIG 2.19a and FIG 2.20a, this additional oxygen state is likely related to interstitial states as will be discussed. It is worth noting these result vary from another group's study of PEALD

Al₂O₃ using DMAI [136], which demonstrated Al₂O₃ deposited with the same materials at the same temperature was characterized by Al(OH)₃, AlO(OH), and Al(CO_x)_y bonding states. Therefore, it is likely the differences in plasma conditions did not allow for the surface chemisorption to saturate. Our work, on the other hand, utilizes the plasma more effectively to reduce impurities and increase the growth rate.

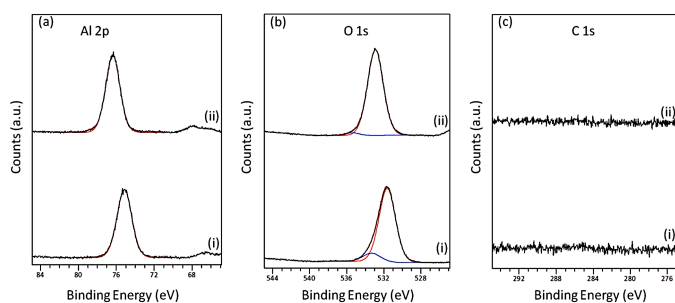


FIG 2.19 XPS spectra of Al 2p (a), O 1s (b), and C 1s (c) peaks for 10 nm Al₂O₃ thin film deposited at 200 °C. Reprinted from Yang *et al.*, *J. Vac. Sci. Technol. A* **32**, 021514 (2014) [131]. Copyright 2014, American Vacuum Society.

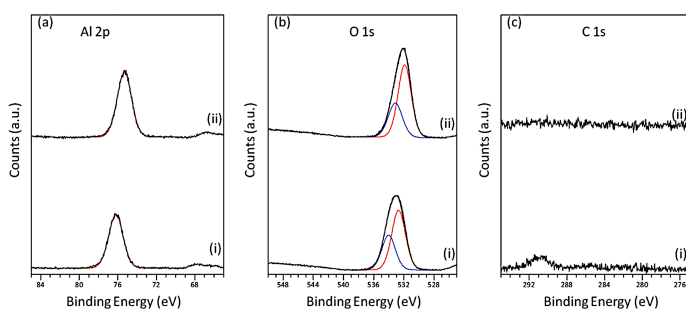


FIG 2.20 XPS spectra of Al 2p (a), O 1s (b), and C 1s (c) peaks for 10 nm Al₂O₃ thin film deposited at room temperature with (i) 8s and (ii) 40s O₂ plasma during deposition. Reprinted from Yang *et al.*, *J. Vac. Sci. Technol. A* **32**, 021514 (2014) [131]. Copyright 2014, American Vacuum Society.

Interstitial Oxygen. While the Al core level is only characterized by a single Al-O bonding state, there is evidence of multiple oxygen bonding states—see FIG 2.19b. The secondary oxygen peak is suggestive of –OH groups, which are removable with an annealing process. In addition, the lower temperature films demonstrate a larger secondary oxygen peak as shown in FIG 2.20b. This evidence suggests the -OH groups may not be readily removed at low temperatures [136]. In addition, annealing at higher temperatures results in a shift in position (~1.2 eV) of the core levels. Therefore, the removal of the oxygen interstitial must also correspond to an alteration of the interface

charge distribution. Previous work has suggested exposure to oxygen plasma likely introduces acceptor-like defects, which lead to hole accumulation in the Si substrate and the formation of an electric field across the SiO₂ layer [141,142]. Helium plasma exposure or high-temperature annealing could be used to remove the interstitials [141-143], as evidenced by the shifting of the core levels to high binding energy.

Carbon Contamination. Generally, the Al₂O₃ films are characterized by carbon contamination below the detection limit of the XPS; however, there is a slight carbon peak for Al₂O₃ deposited at room temperature, which likely corresponds to interstitial carboxyl groups in the film from the precursor ligands. (NOTE: The secondary O 1s peak associated with FIG 2.20b (ii) is slightly broader than the other spectra, further suggesting the possible presence of a carboxyl group as well as a hydroxyl.) Increasing the temperature or oxygen plasma exposure time can thus reduce the carbon contamination as shown in FIG 2.19 and FIG 2.20c.

5. Summary of Film Properties

Additional film properties are summarized in TABLE 2.2 for Al₂O₃ deposited at 25 °C and 200°C.

TABLE 2.2 Al₂O₃ thin film properties on Si wafers grown by remote PEALD and DMAI at 25 °C and 200 °C. Reprinted from Yang *et al. J. Vac. Sci. Technol. A* **32**, 021514 (2014) [131]. Copyright 2014, American Vacuum Society.

PEALD	25 °C	200 °C
Growth per cycle	1.5 Å/cycle	1.5 Å/cycle
Al atoms per cycle	3.9±0.3 at.nm ⁻² cycle ⁻¹	5.3±0.3 at.nm ⁻² cycle ⁻¹
Mass density	2.69±0.04 g/cm ³	2.96±0.02 g/cm ³
[O]/[Al] ratio	2.1±0.1	1.6±0.1
Refractive index (630 nm)	1.61±0.01	1.63±0.02
Band gap	-	6.7±0.1 eV
Electron affinity	-	2.2±0.1 eV

C. Tetrakis(ethylmethylamino)hafnium (TEMAHf)

Manpuneet Kaur established the following results for PEALD TEMAHf.

HfO₂ is a prevalent dielectric due to the high dielectric constant (~20) and reasonable band gap (5.8 eV), as previously mentioned. In ALD, tetrakis(ethylmethylamino)hafnium (TEMAHF) has been the most extensively studied precursor for HfO₂ films, as shown in Appendix B. In particular, this precursor demonstrates high-reactivity on hydroxylated surfaces, a suitable vapor pressure for ALD processes, and the weak metal-nitrogen bond generates films with low concentrations of impurities [144]. In addition, adoption of this precursor in PEALD has been shown to increase the dielectric constant (22.2) in comparison to that of thermal ALD (20.0) [145] while still achieving conformality [130].

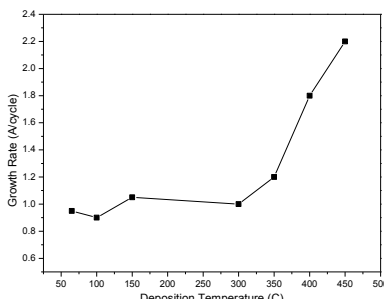
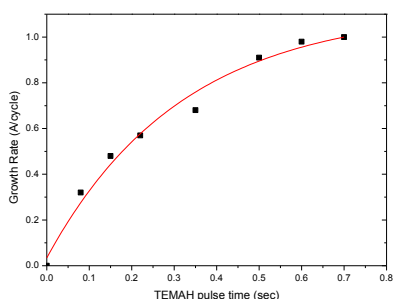


FIG 2.21 (left) Growth rate as related to the precursor pulse time.

FIG 2.22 (right) Temperature dependence of the growth rate for the TEMAHf and O₂

The Hf PEALD process in our lab has not been as extensively explored as the Al₂O₃ process at this point. However, we have optimized the gas-phase sequence as shown in FIG 2.21. In this system, the growth rate saturates at ~1.0 Å/cycle for a precursor pulse time of >0.6 s. This growth rate is comparable to results presented in literature [146].

In addition, the growth window has been established as shown in FIG 2.22, where the growth rate is approximately constant for temperatures between 150 and 300°C. It is worth noting that there is a slight decrease in the growth rate within this temperature

range, which is also similar to the results presented in literature [146]. Comparable to the Al₂O₃ films discussed, it is likely the properties of the deposited films vary with temperature—even within the growth window where the growth rate is constant. In one report by Heil *et al.*, the density of the films is shown to vary significantly as summarized in TABLE 2.3.

TABLE 2.3 Overview of the HfO₂ deposition conditions and film analysis. Summarized from S. B. S. Heil *et al.*, *J. Vac. Sci. Technol. A* **25**, 1357 (2007) [147]. Copyright 2007, American Vacuum Society.

deposition temperature	growth rate (Å/cycle)	Mass density (g/cm ³)
230°C	1.05	7.3
290°C	1.03	9.6
350°C	1.01	10.0

The large difference in density is likely related to the crystallinity of the deposited films. As summarized by Miikkulainen *et al.* [64], ALD HfO₂ has been reported in amorphous, tetragonal, monoclinic, and orthorhombic phases. In general, the crystallinity is extremely sensitive to deposition and post-deposition annealing temperatures. For example, work by Jung *et al.* [147] suggests films deposited at 200°C crystallize into the tetragonal phase after annealing while films deposited at 280°C crystallize into monoclinic phase. This group notes the tetragonal phase results in a larger EOT and reduced hysteresis in CV measurements.

Future research will focus on understanding this relationship between deposition parameters, crystallinity, and electronic properties. In particular, additional energy-enhanced methods may prove crucial in precision control of this process. In recent work, Kim *et al.* [148] have shown that a DC bias can be used to control the flux of free radicals

to the surface of the sample and increase ion bombardments. This process improved the electrical properties of the HfO_2 , including the effective oxide thickness (EOT) and the breakdown voltage, which is likely linked to the crystallinity. However, more research is necessary to better understand this relationship.

D. Tri(dimethylamino)silane (TDMAS)

The PEALD deposition of SiO_2 using TDMAS will be discussed in detail in Chapter 6.

V. Conclusion

In other words, plasma-enhanced atomic layer deposition is an extremely promising technique for novel materials in emerging applications. The conformal, high-quality growth associated with ALD is unparalleled by other deposition systems. This quality is a result of a precisely controlled chemical reaction, which enables fine-tuning of the film properties. While the chemistry-driven reactions of ALD are generally understood, PEALD introduces an additional component—a radical species. As a result, there are additional benefits, including lower impurity content, lower deposition temperatures, higher growth rates, and increased range of precursor chemistries. Moreover, the plasma component allows for additional versatility. However, despite its promise, PEALD has not been as extensively studied, and many questions remain to be answered. For example, to what extent can the radical species be altered to tune film composition, density, or other characteristics? Are there additional energy-enhanced methods capable of tuning film crystallinity such as sample biasing or ion bombardment? What innovative materials are enabled by the reactivity of PEALD? In other words, PEALD promises to be an

influential technique in the next-generation technology, but more intensive study is needed to uncover the full potential and versatility of PEALD.

VI. Acknowledgements

This research was supported by the Office of Naval Research through the DEFINE MURI program, N00014-10-1-0937. In addition, I appreciate the collaborations with Fu Tang, Chiyu Zhu, Jialing Yang, Manpuneet Kaur, and Xingye Wang, who have been instrumental in the successful operation of our PEALD system at NSL as well as the deposition processes necessary to complete the following research.

References

- [1] S. M. George, A. W. Ott, and J. W. Klaus, *J. Phys. Chem.* 100, 13121 (1996).
- [2] S. M. George, *Chem. Rev.* 110, 111 (2010).
- [3] C. H. L. Goodman and M. V. Pessa, *J. Appl. Phys.* 60, R65 (1986).
- [4] M. Leskela and M. Ritala, *J. Phys. IV* 9, Pr8/837(1999).
- [5] M. Leskela and M. Ritala, *Thin Solid Films* 409, 138 (2002).
- [6] L. Niinisto, M. Ritala, and M. Leskela, *Mater. Sci. Eng. B* 41, 23 (1996).
- [7] R. L. Puurunen, *J. Appl. Phys.* 97, 121301 (2005).
- [8] M. Ritala and M. Leskela, *Nanotechnology* 10, 19 (1999).
- [9] T. Suntola, *Mater. Sci. Rep.* 4, 261 (1989).
- [10] S. Haukka, E. L. Lakooma, and T. Suntola, *Stud. Surf. Sci. Catal.* 120A, 715 (1999).
- [11] H. B. Profijt, S. E. Potts, M. C. M. van de Sanden, and W. M. M. Kessels *J. Vac. Sci. Technol. A* 29, 050801 (2011).
- [12] T. Suntola and J. Hyvärinen, *Annu. Rev. Mater. Sci.* 15, 177 (1985).
- [13] S. M. Bedair, B. T. McDermott, Y. Ide, N. H. Karam, H. Hashemi, M. A. Tischler, M. Timmons, J. C. L. Tarn, and N. El-Masry, *J. Cryst. Growth* 93, 182 (1988).

- [14] S. P. DenBaars and P. D. Dapkus, *J. Cryst. Growth* 98, 195 (1989).
- [15] M. A. Herman, *Vacuum* 42, 61 (1991).
- [16] B. W. Gregory, and J. L. Stickney, *J. Electroanal. Chem. Interfacial Electrochem.* 300, 543 (1991).
- [17] A. Usui and H. Watanabe, *Annu. Rev. Mater. Sci.* 21, 185 (1991).
- [18] M. Ozeki, *Mater. Sci. Rep.* 8, 97 (1992).
- [19] A. Usui, *Proc. IEEE* 80, 1641 (1992).
- [20] T. Suntola, *Thin Solid Films* 216, 84 (1992).
- [21] T. Suntola, *Thin Solid Films* 225, 96 (1993).
- [22] L. Niinistö and M. Leskelä, *Thin Solid Films* 225, 130 (1993).
- [23] S. M. Bedair, *J. Vac. Sci. Technol. B* 12, 179 (1994).
- [24] S. M. Bedair, and N. A. El-Masry, *Appl. Surf. Sci.* 82/83, 7 (1994).
- [25] J. M. Heitzinger, J. M. White, and J. G. Ekerdt, *Surf. Sci.* 299, 892 (1994).
- [26] E.-L. Lakomaa, *Appl. Surf. Sci.* 75, 185 (1994).
- [27] M. A. Herman, *Thin Solid Films* 267, 1 (1995).
- [28] M. Leskelä and M. Ritala, *J. Phys. IV* 5, C5/937 (1995).
- [29] T. Suntola, *Appl. Surf. Sci.* 100/101, 391 (1996).
- [30] A. A. Malygin, A. A. Malkov, and S. D. Dubrovenskii, *Stud. Surf. Sci. Catal.* 99, 213 (1996).
- [31] M. A. Herman, *Appl. Surf. Sci.* 112, 1 (1997).
- [32] M. Ritala, *Appl. Surf. Sci.* 112, 223 (1997).
- [33] S. Haukka and T. Suntola, *Interface Sci.* 5, 119 (1997).
- [34] L. Niinistö, *Curr. Opin. Solid-State Mater. Sci.* 3, 147 (1998).
- [35] A. A. Malygin, *Compos. Interfaces* 5, 561 (1998).
- [36] L. Niinistö, *J. Therm. Anal. Calorim.* 56, 7 (1999).
- [37] K. Ikeda, J. Yanase, S. Sugahara, and M. Matsumura, *J. Korean Phys. Soc.* 39, S447 (2001).

- [38] A. C. Jones and P. R. Chalker, *J. Phys. D* 36, R80 (2003).
- [39] M. Leskelä and M. Ritala, *J. Solid-State Chem.* 171, 170 (2003).
- [40] M. Leskelä and M. Ritala, *Angew. Chem., Int. Ed.* 42, 5548 (2003).
- [41] R. M. C. de Almeida and I. J. R. Baumvol, *Surf. Sci. Rep.* 49, 1 (2003)
- [42] H. Kim, *J. Vac. Sci. Technol. B* 21, 2231 (2003).
- [43] L. Niinistö, J. Päiväsari, J. Niinistö, M. Putkonen, and M. Nieminen, *Phys. Status Solidi A* 201, 1443 (2004).
- [44] A. C. Jones, H. C. Aspinall, P. R. Chalker, R. J. Potter, K. Kukli, A. Rahtu, M. Ritala, and M. Leskelä, *J. Mater. Chem.* 14, 3101 (2004).
- [45] R. L. Puurunen, *Chem. Vap. Dep.* 11, 79 (2005).
- [46] M. Putkonen, T. Sajavaara, L. Niinistö, and J. Keinonen, *Anal., and Bioanal. Chem.* 382, 1791 (2005).
- [47] A. C. Jones, H. C. Aspinall, P. R. Chalker, R. J. Potter, T. D. Manning, Y. F. Loo, R. O'Kane, J. M. Gaskell, and L. M. Smith, *Chem. Vap. Dep.* 12, 83 (2005).
- [48] K. E. Elers, T. Blomberg, M. Peussa, B. Aitchison, S. Haukka, and S. Marcus, *Chem. Vap. Dep.* 12, 13 (2006).
- [49] H. Kim and P. C. McIntyre, *J. Korean Phys. Soc.* 48, 5 (2006).
- [50] M. Schumacher, P. K. Baumann, and T. Seidel, *Chem. Vap. Dep.* 12, 99 (2006).
- [51] C. O. Chui, H. Kim, D. Chi, P. C. McIntyre, and K. C. Saraswat, *IEEE Trans. Electron Devices* 53, 1509 (2006).
- [52] M. Knez, K. Nielsch, and L. Niinistö, *Adv. Mater.* 19, 3425 (2007).
- [53] F. T. Edelmann, *Chem. Soc. Rev.* 38, 2253 (2009).
- [54] H. Kim, H.-B.-R. Lee, and W.-J. Maeng, *Thin Solid Films* 517, 2563 (2009).
- [55] S. M. George, R. Yoon, and A. A. Dameron, *Acc. Chem. Res.* 42, 498 (2009).
- [56] E. Langereis, S. B. S. Heil, H. C. M. Knoops, W. Keuning, M. C. M. van de Sanden, and W. M. M. Kessels, *J. Phys. D: Appl. Phys.* 42, 073001 (2009).
- [57] X. Jiang and S. F. Bent, *J. Phys. Chem. C* 113, 17613 (2009).
- [58] C. Detavernier, J. Dendooven, S. P. Sree, K. F. Ludwig, and J. A. Martens, *Chem. Soc. Rev.* 40, 5242 (2011).
- [59] J. R. Bakke, K. L. Pickrahn, T. P. Brennan, and S. F. Bent, *Nanoscale* 3, 3482 (2011).
- [60] P. Poodt, D. C. Cameron, E. Dickey, S. M. George, V. Kuznetsov, G. N. Parsons, F. Roozeboom, G. Sundaram, and A. Vermeer, *J. Vac. Sci. Technol. A* 30, 010802 (2012).

- [61] F. T. Edelmann, *Chem. Soc. Rev.* 41, 7657 (2012).
- [62] G. Dingemans and W. M. M. Kessels, *J. Vac. Sci. Technol. A* 30, 040802 (2012).
- [63] X. Meng, X.-Q. Yang, and X. Sun, *Adv. Mater.* 24, 3589 (2012).
- [64] V. Miikkulainen, M. Leskelä, M. Ritala, and R. L. Puurunen, *J. Appl. Phys.* 113, 021301 (2013).
- [65] F. Zaera, *Coord. Chem. Rev.* 257, 3177 (2013).
- [66] T. J. Knisley, L. C. Kalutarage, and C. H. Winter, *Coord. Chem. Rev.* 257, 3222 (2013).
- [67] S. E. Potts and W. M. M. Kessels, *Coord. Chem. Rev.* 257, 3254 (2013).
- [68] K. B. Ramos, M. J. Saly, and Y. J. Chabal, *Coord. Chem. Rev.* 257, 3271 (2013).
- [69] T. Hatanpää, M. Ritala, and M. Leskelä, *Coord. Chem. Rev.* 257, 3297 (2013).
- [70] G. N. Parsons, S. E. Atanasov, E. C. Dandley, C. K. Devine, B. Gong, J. S. Jur, K. Lee, C. J. Oldham, Q. Peng, J. C. Spagnola, and P. S. Williams, *Coord. Chem. Rev.* 257, 3323 (2013).
- [71] G. N. Parsons, J. W. Elam, S. M. George, S. Haukka, H. Jeon, W. M. M. (Erwin).Kessels, M. Leskelä, P. Poedt, M. Ritala and S. M. Rossnagel, *J. Vac. Sci. Technol. A* 31, 050818 (2013)
- [72] R. Foest, M. Schmidt, and H. Gargouri, 68, 23 (2014).
- [73] K. Devloo-Casier, K. F. Ludwig, C. Detavernier, and J. Dendooven, *J. Vac. Sci. Technol. A* 32, 010801 (2014).
- [74] D. Longrie, D. Deduytsche, and C. Detavernier, *J. Vac. Sci. Technol. A* 32, 010802 (2014).
- [75] T. Suntola, and J. Antson, U. S. Patent No. 4,058,43015 November, 3 1977.
- [76] A. M. Shevjakov, G. N. Kuznetsova, and V. B. Aleskovskii, in Chemistry of High-Temperature Materials, Proceedings of the Second USSR Conference on High-Temperature Chemistry of Oxides, Leningrad, USSR, 26–29 November 1965 (Nauka, Leningrad, USSR, 1967), pp. 2 149–155, in Russian.
- [77] V. B. Aleskovskii, and V. E. Drozd, Chem. Technol. Ser. 195, 155 (1990).
- [78] T. Suntola, in Handbook of Thin Film Process Technology, edited by D. A. Glocker, and S. I. Shah IOP, Bristol, United Kingdom, 1995, Vol. 1, pp. B1.5:1–B1.5:17.
- [79] M. Verghese, J. W. Maes, and N. Kobayashi, Atomic layer deposition goes mainstream in 22nm logic technologies, <http://www.solid-state.com> (March 15, 2012).
- [80] International Technology Roadmap for Semiconductors, <http://www.itrs.net>, (March 15, 2012).
- [81] M. De Keijsers and C. Vamn Opdorpe, *Appl. Phys. Lett.* 58, 1187 (1991).
- [82] ASM International website, <http://www.asm.com> (March 15, 2012).

- [83] Oxford Instruments website, <http://www.oxford-instruments.com> (March 15, 2012).
- [84] Beneq website, <http://www.beneq.com> (May 31, 2011).
- [85] Cambridge NanoTech website, <http://www.cambridgenanotech.com> (March 15, 2012).
- [86] Applied Materials website, <http://www.appliedmaterials.com> (March 15, 2012).
- [87] Tokyo Electron Limited website, <http://www.tel.com> (March 15, 2012).
- [88] Picosun website, <http://www.picosun.com> (March 15, 2012).
- [89] R. L. Puurunen, *Chem. Vap. Dep.* 9, 249 (2003).
- [90] R. L. Puurunen, *Chem. Vap. Dep.* 9, 327 (2003).
- [91] G. Eres, *Appl. Phys. Lett.* 67, 1727 (1995).
- [92] H.-S. Park, J.-S. Min, J.-W. Lim, and S.-W. Kang, *Appl. Surf. Sci.* 158, 81 (2000).
- [93] M. K. Gobbert, V. Prasad, and T. S. Cale, *J. Vac. Sci. Technol. B* 20, 1031 (2002).
- [94] R. L. Puurunen, M. Lindblad, A. Root, and A. O. I. Krause, *Phys. Chem. Chem. Phys.* 3, 1093 (2001).
- [95] A. Rautiainen, M. Lindblad, L. B. Backman, and R. L. Puurunen, *Phys. Chem. Chem. Phys.* 4, 2466 (2002)
- [96] R. L. Puurunen, T. A. Zeelie, and A. O. I. Krause, *Catal. Lett.* 83, 27 (2002).
- [97] E.-L. Lakomaa, S. Haukka, and T. Suntola, *Appl. Surf. Sci.* 60/61, 742 (1992)
- [98] S. Haukka, E.-L. Lakomaa, and A. Root, *J. Phys. Chem.* 97, 5085 (1993).
- [99] S. Haukka, E.-L. Lakomaa, O. Jylhä, J. Vilhunen, and S. Hornytzkyj, *Langmuir* 9, 3497 (1993).
- [100] A. Kytökivi, E.-L. Lakomaa, and A. Root, *Langmuir* 12, 4395 (1996).
- [101] R. L. Puurunen, S. M. K. Airaksinen, and A. O. I. Krause, *J. Catal.* 213, 281 (2003).
- [102] M. Putkonen, T. Sajavaara, L.-S. Johansson, and L. Niinistö, *Chem. Vap. Deposition* 7, 44 (2001).
- [103] M. Juppo, A. Rahtu, and M. Ritala, *Chem. Mater.* 14, 281 (2002).
- [104] J. S. Becker, S. Suh, S. Wang, and R. G. Gordon, *Chem. Mater.* 15, 2969 (2003).
- [105] A. W. Ott, J. W. Klaus, J. M. Johnson, and S. M. George, *Thin Solid Films* 292, 135 (1997).
- [106] M. D. Groner, F. H. Fabreguette, J. W. Elam, and S. M. George, *Chem. Mater.* 16, 639 (2004).

- [107] A. Kytökiivi, J.-P. Jacobs, A. Hakuli, J. Meriläinen, and H. H. Brongersma, *J. Catal.* 162, 190 (1996).
- [108] A. Hakuli, A. Kytökiivi, and A. O. I. Krause, *Appl. Catal., A* 190, 219 (2000).
- [109] N. V. Dolgushev, A. A. Malkov, A. A. Malygin, S. A. Suvorov, A. V. Shchukarev, A. V. Beljaev, and V. A. Bykov, *Thin Solid Films* 293, 91 (1997).
- [110] H. Kim and S. M. Rossnagel, *J. Vac. Sci. Technol. A* 20, 802 (2002).
- [111] A. Delabie, R. L. Puurunen, B. Brijs, M. Caymax, T. Conard, B. Onsia, O. Richard, W. Vandervorst, C. Zhao, M. M. Heyns, M. Meuris, M. M. Viitanen, H. H. Brongersma, M. de Ridder, L. V. Goncharova, E. Garfunkel, T. Gustafsson, and W. Tsai, *J. Appl. Phys.* 97, 064104 (2005).
- [112] R. L. Puurunen, A. Root, P. Sarv, M. M. Viitanen, H. H. Brongersma, M. Lindblad, and A. O. I. Krause, *Chem. Mater.* 14, 720 (2002).
- [113] A. Satta, J. Schuhmacher, C. M. Whelan, W. Vandervorst, S. H. Brongersma, G. P. Beyer, K. Maex, A. Vantomme, M. M. Viitanen, H. H. Brongersma, and W. F. A. Besling, *J. Appl. Phys.* 92, 7641 (2002).
- [114] M. L. Green, M.-Y. Ho, B. Busch, G. D. Wilk, T. Sorsch, T. Conard, B. Brijs, W. Vandervorst, P. I. Räisänen, D. Muller, M. Bude, and J. Grazul, *J. Appl. Phys.* 92, 7168 (2002).
- [115] R. L. Puurunen, *J. Appl. Phys.* 95, 4777 (2004).
- [116] A. Martin Hoyas, J. Schuhmacher, D. Shamiryan, J. Waeterloos, W. Besling, J. P. Celis, and K. Maex, *J. Appl. Phys.* 95, 381 (2004).
- [117] R. L. Puurunen, W. Vandervorst, W. F. A. Besling, O. Richard, H. Bender, T. Conard, C. Zhao, A. Delabie, M. Caymax, S. De Gendt, M. Heyns, M. M. Viitanen, M. de Ridder, H. H. Brongersma, Y. Tamminga, T. Dao, T. de Win, M. Verheijen, M. Kaiser, and M. Tuominen, *J. Appl. Phys.* 96, 4878 (2004).
- [118] R. L. Puurunen, and W. Vandervorst, *J. Appl. Phys.* 96, 7686 (2004).
- [119] R. L. Puurunen, *Chem. Vap. Deposition* 10, 159 (2004).
- [120] Stanford Nanofabrication Facility, <https://snf.stanford.edu/SNF/equipment/chemical-vapor-deposition/ald> (November 17, 2014).
- [121] Cambridge Nanotech, <http://www.cambridgenanotechald.com> (November 17, 2014).
- [122] D. Hausmann, J. Becker, S. Wang, and R. G. Gordon, *Science* 298, 402 (2002).
- [123] J. W. Klaus, S. J. Farro, and S. M. George, *Thin Solid Films* 360, 145 (2000).
- [124] J. S. Park, H. S. Park, and S. W. Kang, *J. Electrochem. Soc.* 149, C28 (2002).
- [125] J. H. Lee, Y. J. Cho, Y. S. Min, D. Kim, and S. W. Rhee, *J. Vac. Sci. Technol. A* 20, 1828 (2002).

- [126] S. B. S. Heil, E. Langereis, F. Roozeboom, M. C. M. Van de Sanden, and W. M. M. Kessels, *J. Electrochem. Soc.* 153, G956 (2006).
- [127] H. B. Profijt, P. Kudlacek, M. C. M. Van de Sanden, and W. M. M. Kessels, *J. Electrochem. Soc.* 158, G88 (2011).
- [128] H. Kim, *Thin Solid Films* 519, 6639 (2011).
- [129] H. Kim and I.-K. Oh *Jpn. J. Appl. Phys.* 53, 03DA01 (2014).
- [130] M. Kariniemi, J. Niinistö, M. Vehkamäki, M. Kemell, M. Ritala, M. Leskelä, and M. Putkonen, *J. Vac. Sci. Technol. A* 30, 01A115 (2012)
- [131] J. Yang, B. S. Eller, M. Kaur, and R. J. Nemanich, *J. Vac. Sci. Technol. A* 32, 021514 (2014).
- [132] M. D. Groner, J. W. Elam, F. H. Fabreguette, and S. M. George, *Thin Solid Films* 413, 186 (2002).
- [133] J. L. van Hemmen, S. B. S. Heil, J. H. Klootwijk, F. Roozeboom, C. J. Hodson, M. C. M. van de Sanden, and W. M. M. Kessels, *J. Electrochem. Soc.* 154, G165 (2007).
- [134] E. Langereis, J. Keijmel, M. C. M. van de Sanden, and W. M. M. Kessels, *Appl. Phys. Lett.* 92, 231904 (2008).
- [135] S. E. Potts, W. Keuning, E. Langereis, G. Dingemans, M. C. M. vande Sanden, and W. M. M. Kessels, *J. Electrochem. Soc.* 157, 66 (2010)
- [136] S. E. Potts, G. Dingemans, C. Lachaud, and W. M. M. Kessels, *J. Vac. Sci. Technol. A* 30, 021505 (2012).
- [137] S. E. Potts, H. B. Profijt, R. Roelofs, and W. M. M. Kessels, *Chem. Vap. Deposition* 19 125 (2013).
- [138] W. Cho, K. Sung, K.-S. An, S. S. Lee, T.-K. Chung, and Y. Kim, *J. Vac. Sci. Technol. A* 21, 1366 (2003).
- [139] S. B. S. Heil, P. Kudlacek, E. Langereis, R. Engeln, M. C. M. van de Sanden, and W. M. M. Kessels, *Appl. Phys. Lett.* 89, 131505 (2006).
- [140] J. W. Lim, and S. J. Yun, *Electrochem. Solid-State Lett.* 7, F45 (2004).
- [141] C. C. Fulton, T. E. Cook, G. Lucovsky, and R. J. Nemanich, *J. Appl. Phys.* 96, 2665 (2004).
- [142] C. Zhu, D. J. Smith, and R. J. Nemanich, *J. Vac. Sci. Technol. B* 30, 051807 (2012).
- [143] J. Yang, B. S. Eller, C. Zhu, C. England, and R. J. Nemanich, *J. Appl. Phys.* 112, 053710 (2012).
- [144] D. H. Triyoso, R. I. Hegde, B. E. White Jr., and P. J. Tobin, *J. Appl. Phys.* 97, 124107 (2005).
- [145] P. K. Park, J.-S. Roh, B. H. Choi, and S. W. Kang, *Electrochem. Solid-State Lett.* 9, F34 (2006).
- [146] C. Richter, T. Schenik, U. Schroeder, and T. Mikolajick, *J. Vac. Sci. Technol. B* 32, 01A117 (2014).

- [147] H.-S. Jung, H. K. Kim, I.-H. Yu, S. Y. Lee, J. Lee, J. Park, J. H. Jang, S.-H. Jeon, Y. J. Chung, D.-Y. Cho, N.-I. Lee, T. J. Park, J.-H. Choi, and C. S. Hwang, *J. Electrochem. Soc.* 159, G33 (2012).
- [148] H. Kim, S. Woo, J. Lee, Y. Kim, H. Lee, I. J. Choi, Y. D. Kim, C. W. Chung, and H. Jeon, *J. Electrochem. Soc.* 158, H21 (2011).

CHAPTER 3. PHOTOELECTRON SPECTROSCOPY

Photoelectron or photoemission spectroscopy (PES) is a measurement technique used to determine the binding energy of electrons within a given material. In general, this technique is the application of the photoelectric effect as described by Albert Einstein, i.e. incident photons are used to excite—or ionize—an electron from a substrate. The kinetic energy of the photoionized electron is then determined. From energy conservation, the energy state of the electrons in the material can be determined as shown in FIG 3.1. More specifically, the kinetic energy of an electron emitted from semiconductor or dielectric as determined by Einstein's relation:

$$E_k = h\nu - E_B - \phi, \quad (1)$$

where $h\nu$ is the energy (or frequency) of the incident photon, ϕ is the work function, and E_B is the binding energy as dependent on the original electronic, vibrational, and rotational state of the electron. The photon energy can be tuned to characterize different electron profiles within the material, i.e. low-energy ultraviolet photons are used in

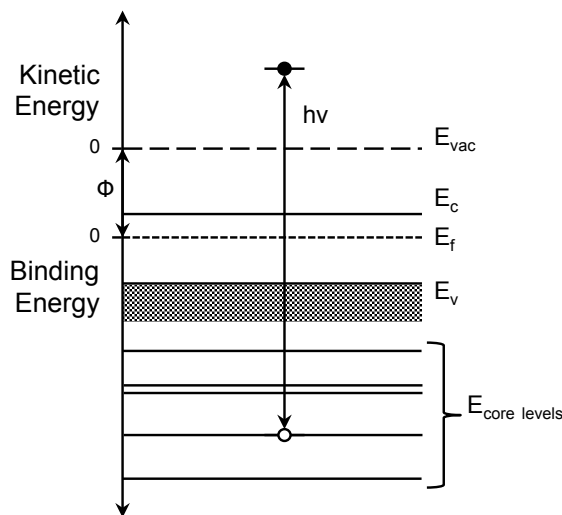


FIG 3.1 Energy diagram of a semiconductor with a photo-emitted electron of energy $h\nu$. Conservation of energy determines the binding energy, where $E_B = h\nu - \phi - E_k$.

ultraviolet photoemission spectroscopy (UPS) to probe valence band electrons, while high-energy x-rays are used in x-ray photoemission spectroscopy (XPS) to probe core level electrons. In a solid, these electrons can only escape from the first few nanometers. Consequently, this measurement technique is characterized as surface sensitive.

I. X-ray Photoelectron Spectroscopy

As mentioned, x-ray photoelectron spectroscopy is used to determine the energy levels of core electrons in a material. This technique was first developed in 1957 by Kai Siegbahn under the nomenclature of Electron Spectroscopy for Chemical Analysis (ESCA), where small chemical shifts in the core levels were detected and used to determine specific bonding states of constituent atoms. Siegbahn was later awarded the Nobel Prize in 1981.

A. X-ray Sources

In order to generate x-rays in XPS, a metallic anode is bombarded with electrons. These electrons are supplied by heating a thorium-coated iridium filament and accelerated onto a metallic anode. Consequently, core level electrons are removed from the metallic atoms. Excited metallic atoms will then return to the ground state emitting an electron characteristic of the metal. In general, there are two common metallic sources: aluminum (Al) and magnesium (Mg), where the relevant transition relates to an electron transitioning from the 2p to 1s core level, i.e. the $K\alpha$ transition. The emitted photons have an energy of 1486.6 eV for Al $K\alpha$ and 1253.6 eV for Mg $K\alpha$. In most non-monochromatic systems, both these sources are available in a two-anode x-ray source as shown in FIG 3.2a. This system design enables the user to utilize both sources for materials with overlapping core levels and Auger peaks, e.g. GaN. On the other hand, non-

monochromatic sources have a wider line width, which affects the quality and resolution of the spectrum. Adding a monochromator improves resolution. In this system design, x-rays are diffracted with a series of quartz crystals, focusing a monochromated beam on to the surface. (See FIG 3.2b). Consequently, the spot size is generally smaller. Moreover, monochromatic sources reduce the x-ray line width, satellite x-rays, and background radiation as will be discussed [1].

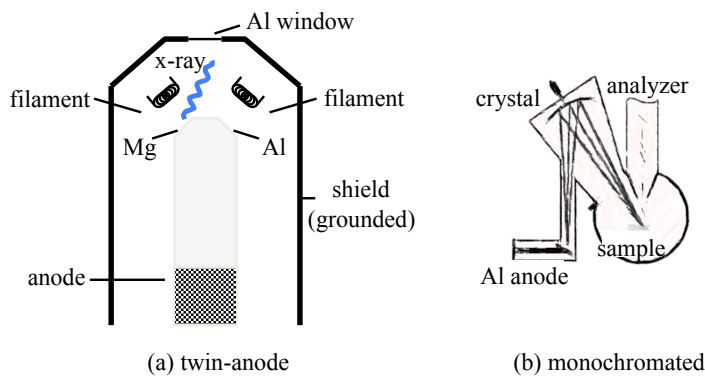


FIG 3.2 (a) Schematic of a twin anode x-ray source and (b) monochromated Al anode.

B. Analyzers

The kinetic energy of emitted electrons is then measured with an analyzer, where a schematic for the generic analyzer is shown in FIG 3.3. More specifically, a proportion of the emitted electrons are transferred through the analyzer entrance slit and focused through a series of electrostatic and magnetic lenses. Specifically, magnetic lenses focus the incoming electrons. Electrostatic forces are then used to focus the resulting electron beam, such that only specific electrons energies will arc onto the detector [1]. When measuring a desired energy spectrum, electrostatic forces retard the kinetic energy of the incoming electrons such that only electrons with the desired energy are transferred; this energy is defined as the pass energy as it refers to the energy required to pass through the

analyzer to the detector. This value influences the resolution of the spectra in conjunction with the diameter of the analyzer and type of x-ray source [3].

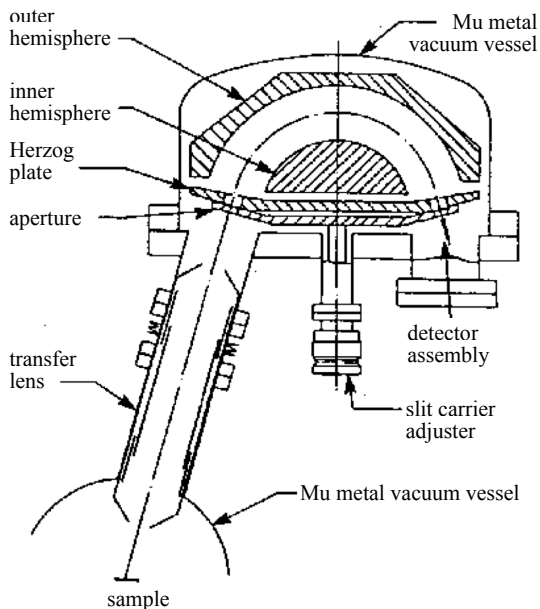


FIG 3.3 Schematic of the typical hemispherical analyzer used in XPS. Modified from R. Smart *et al.* [2]. Copyright University of Hong Kong.

C. Core Level Spectra

Electrons are confined to discrete energy values in an atom as defined by the electronic, vibrational, and rotational states in a molecule. In solids, the binding energy states are understood in terms of the valence band state and spin-orbital core levels of the constituent atoms. These energy levels can be probed by XPS.

1. Chemical Shifts and Bonding States

On the other hand, the local bonding environment of the atom may result in slight changes to the discrete energy levels. A shift of a core level—also known as a chemical shift—relates to the bonding hybridization to the nearest-neighbor atom. For example, a silicon wafer is characterized by a strong Si 2p peak at ~99 eV; however, in its oxidation

state, the Si 2p state shifts to 103.3 eV. Consequently, XPS can determine the bonding environment of a material as well as the atom concentration.

2. Peak Fittings

Identifying and analysis of the core levels and chemical state information is thus an important aspect of XPS. In general, there are several characteristics that are related to the core level spectra, which relate to the nature of the atomic bonding as shown in FIG 3.4. This information is used in the analysis of XPS spectra [3].

Background. Prior to analyzing a core level, analysis software is used to remove the background caused by secondary electrons. In general, the background is characterized by a step-down, linear, or Shirley background as demonstrated in FIG 3.4. Based on the nature of the secondary electron energy loss, Shirley backgrounds are most commonly used for reliable results. Once a background is chosen, the characteristic Gaussian-Lorentzian curve can be fit to the core levels.

Intensity. The intensity of an XPS core level is most reliably determined by integrating the area of the corresponding Gaussian-Lorentzian function; generally, XPS intensity measurements are reliable within $\pm 10\%$.

Position. The core level position is determined by fitting a Gaussian to the core level, where the center of the peak corresponds to the core level energy level within ± 0.1 eV.

Full-width half-maximum (FWHM). The peak width is determined at the half maximum, where the thickness varies with the core level and the nature of the x-ray source radiation.

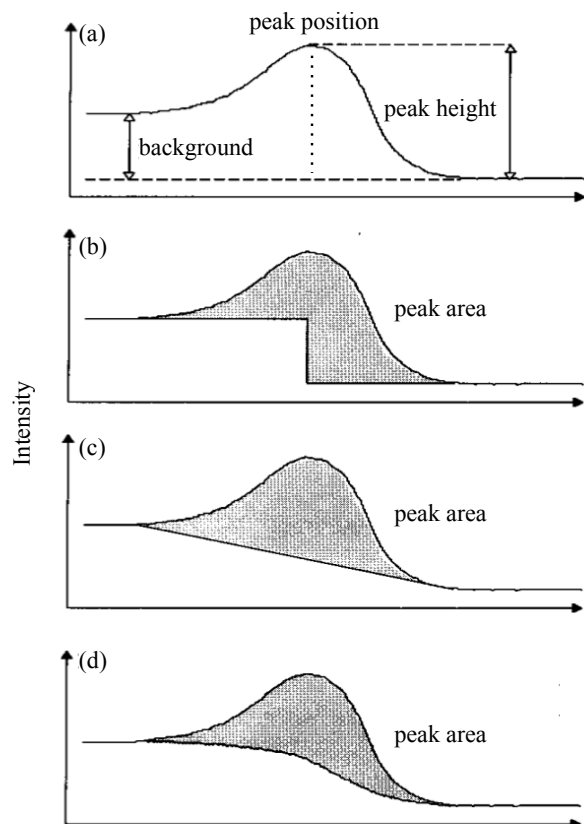


FIG 3.4 Example backgrounds for core level fittings for (a) background and core level peak fittings for (b) a step-down background fitting, (c) a linear background fitting, and (d) a Shirley background fitting. Modified from R. Smart *et al.* [2]. Copyright University of Hong Kong.

In many cases, these are overlapping peaks that must be accounted for to determine the variety of chemical shifts present in a sample. Unfortunately, this type peak fitting is not always straightforward. For most spectra, additional Gaussian-Lorentzian curves can be used to achieve a good fit without constraints. Understanding the chemistry and expectations for the chemical bonding states allows the introduction of constraints for a more reliable fit in terms of the expected core level positions, energy differences, intensities, and full-width half-maximums.

3. Example Spectra

Surface Science Spectra is a useful tool for peak fittings, as this journal published pristine examples of surface spectra for many of the ALD oxides used in this research, thus providing a foundation for good peak fittings.

Aluminum Oxide. Spectra for aluminum oxide films as deposited by thermal ALD on Ge using trimethylaluminum were collected using a magnesium source, and the O 1s, Al 2p, and Al 2s spectra; the core level results are summarized in Table 2.3 [4]:

TABLE 3.1 XPS spectral features of Al₂O₃ from Mg K_α radiation. Reprinted from Sygelloui *et al.* [4]. Copyright 2011, American Institute of Physics.

Element/ Transition	Peak Energy (eV)	Peak Width FWHM (eV)	Peak Area (eV-cts/s)	Sensitivity Factor	Concentration (at. %)
Al 2p	74.3	1.59	961	0.12	36.1
Al 2s	119.2	2.17	1204	---	---
O 1s	531.3	2.14	1138	0.57	---
O 1s (OH)	532.6	2.14	7409	0.57	63.9

Hafnium Oxide. Hafnium oxide films were deposited by thermal ALD using a guanidinate-stabilized hafnium amide precursor; XPS spectra collected using an Al monochromatic source are summarized in Table 2.4 [5]:

TABLE 3.2 XPS spectral features of HfO₂ from Al K_α monochromatic radiation. Reprinted from Milanov *et al.* [5]. Copyright 2007, American Institute of Physics.

Element/ Transition	Peak Energy (eV)	Peak Width FWHM (eV)	Peak Area (eV-cts/s)	Sensitivity Factor	Concentration (at. %)
C 1s	248.8	1.7	13481	0.296	24.4
O 1s	530.2	1.6	46189	0.711	34.8
O 1s (OH)	531.7	1.8	17083	0.711	12.9
Hf 4f _{7/2}	16.2	1.1	46515	2.221	---
Hf 4f _{5/2}	18.2	1.1	34886	2.221	---
Hf 4d _{5/2}	213.1	3.6	78458	2.516	27.9
Hf 4d _{3/2}	223.8	3.6	52305	2.516	27.9

Silicon Oxide. Core levels of silicon dioxide were studied with magnesium radiation and are summarized in Table 2.5 [6].

TABLE 3.3 XPS spectral features of SiO₂ from Mg K_α radiation. Reprinted from Chourasia *et al.* [6]. Copyright 2006, American Institute of Physics.

Element/ Transition	Peak Energy (eV)	Peak Width FWHM (eV)	Peak Area (eV-cts/s)	Sensitivity Factor	Concentration (at. %)
Si 2s	154.9	2.7	21105	---	---
Si 2p	103.9	2.1	24006	0.270	32.9
O 1s	533.2	1.9	118274	0.660	67.1
O KLL	747.2	6.3	68479	---	---

D. Characteristics and Limitations

In addition to core level and chemical state peaks, there are several additional characteristics that are characteristic in XPS spectra.

1. 'Artificial' Peaks

XPS spectra are often characterized by additional, non-core-level peaks; these peaks include auger, satellite, and ghost peaks.

Auger Peaks. Auger peaks occur from additional electron transitions in an atom. More specifically, an emitted electron leaves an excited atom behind. This atom will revert to a lower energy state, whereby an electron transitions from a higher electron orbital state into the state previously vacated by the emitted electron. This transition produces energy, which in some cases may be transferred into the kinetic energy of a second emitted electron as shown in FIG 3.5. Since the kinetic energy of the Auger electron is determined by the core level energies of an atom, the kinetic energy of the Auger electron is independent of the x-ray source used [3].

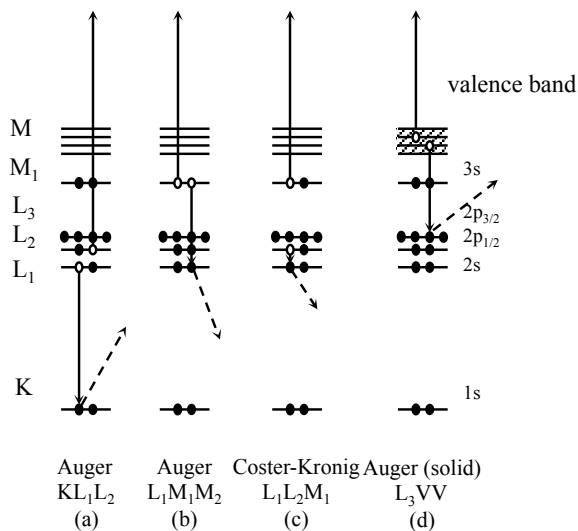


FIG 3.5 Explanation of the Auger process on the basis of atomic level schemes. A primary electron produces an initial hole in the core level and the escaping electron is indicated by a broken arrow; another electron is deexcited from a higher shell, core level in (a,b,c) and the valence band of a solid (d). The deexcited energy is then transferred to a third electron, which leaves the system as an Auger electron. Reprinted from Lüth, *Solid Surfaces, Interfaces, and Thin Films*, 5th Ed. (Springer, Heidelberg, Germany, 2010), pp. 50 [1]. Copyright 2010, Springer.

Satellite Peaks. As mentioned, Al and Mg are commonly used x-ray sources. These metals are chosen since the $K\alpha$ transition is dominant; however, additional transitions will emit x-rays with different energies. This phenomenon produces additional peaks shifted by the difference between the incident x-ray photon energies. Monochromated sources, on the other hand, eliminate these peaks [3].

Ghost Peaks. Ghost peaks appear in spectra when the x-ray source is contaminated, where contaminant atoms also produce x-rays with varied photon energies. For example, in a two-anode source, the Al source may become contaminated with Mg atoms. Consequently, the Mg atoms will also emit x-rays with an energy 233 eV lower than those of the Al source. Therefore, two peaks will appear for each core level with an energy difference of 233 eV. Similarly, oxygen or carbon contaminants on the x-ray source will produce ghost peaks [2].

2. Background and Secondary Electrons

Some emitted electrons will also undergo elastic scattering on the way to vacuum. The electrons are so-called secondary electrons and detected at lower kinetic energy. The result is a broad background that increases in intensity at lower kinetic energy as shown in FIG 3.6 [1].

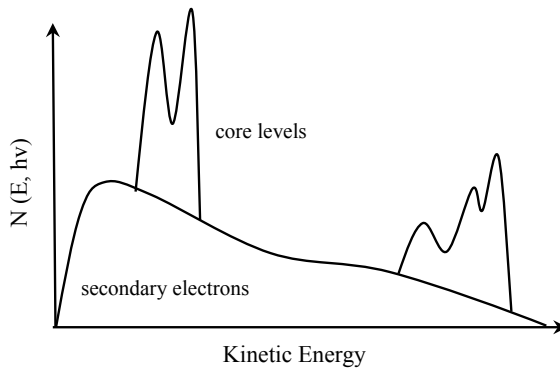


FIG 3.6 Illustration of a photoemission spectra, where the electrons that have undergone scattering processes on their way into vacuum are detected at lower energy and form a continuous background of the so-called secondary electrons. Modified from Lüth, *Solid Surfaces, Interfaces, and Thin Films*, 5th Ed. (Springer, Heidelberg, Germany, 2010), pp. 312 [1]. Copyright 2010, Springer.

Additional peaks arise due to specific energy-loss interactions:

Plasmon Peaks. In some cases, there is a distinct energy loss peak following a core level; this type of peak is associated with electron loss due to inelastic interactions with the collective oscillations of other electrons in the material [2].

Shake-up peaks. Secondary electrons may also interact with the material such to create shake-up peaks; these peaks are associated with formation of an ion in an excited state [2], where some of the photon energy excites the atom from the ground state. This loss of energy results in a secondary peak following the primary core level [3].

3. Charging

Photoelectrons, auger electrons, inelastically scattered electrons, and secondary electrons are thus all lost from a sample surface. Typically, electrons from the bulk move to the surface to compensate this electron loss; however, in some semiconducting and insulating materials, this electron replacement may not occur as readily [2]. Consequently, the core level may broaden and shift to higher binding energy, where the energy relation is given by

$$E_k = h\nu - E_B - \phi - V_{charging}. \quad (2)$$

4. X-ray damage

In addition, x-ray exposure may damage the surface of some samples; to determine the extent of this damage, several XPS spectra are completed consecutively on the same sample and compared to observe any degradation [2].

II. Ultraviolet Photoelectron Spectroscopy

Developed by David W. Turner in 1962, ultraviolet photoelectron spectroscopy (UPS) utilizes low-energy ultraviolet photons rather than high-energy x-rays. Consequently, UPS probes lower energy binding states near the valence band. Moreover, the emitted electrons have less kinetic energy as conserved from the UV photons, thus the escape depths are shorter. Consequently, UPS provides more reliable measurements of the lower-binding energy states in the valence band states. This sensitivity is useful when measuring surface properties, e.g. valence band maximum, work function, and electron affinity.

A. UV source

UPS operation requires low-energy (<41 eV), high-intensity ($>1.5 \times 10^{12}$ photons/sec) UV photons [7]. Generally, these photons are supplied by a gas discharge lamp, which uses an electric field to accelerate electrons and ionize a noble gas in a quartz capillary tube. The ionized atom will revert to the lowest energy state and emit a characteristic UV photon in the process. This emitted UV light is collimated into a beam with a small spot size (~ 1 - 3 mm). The energy of the incident photons is thus determined by the gas discharge lines of the corresponding noble gas; these energies are summarized in TABLE 3.4 for noble gas commonly used in UPS.

TABLE 3.4 Discharge lines from gas commonly used in UPS, i.e. He, Ne, and Ar. Modified from Ref [7]. Copyright 2004, Thermo Electron Corporation.

Gas	Photon Energy (eV)	Wavelength (\AA)
Ar I	11.7	1060
Ne I	16.8	738
He I	21.2	585
Ne II	26.9	461
Ar II	30.3	409
He II	40.8	304

The character of the gas discharge depends on the ionization of the noble gas atoms: neutral atom—denoted as I—have characteristically lower gas discharge lines, and singly ionized atoms—denoted by II—have characteristically higher gas discharge lines [8].

B. Precision and Limitations

As mentioned, the low-energy of the photons are advantageous for surface sensitive measurements; however, there are some cases where this surface sensitivity is a limitation. In particular, the final surface states are extremely influential, and in some

case, desired measurements may be obscured by a final surface layer, e.g. oxide termination on GaN. In addition, UPS does not often as reliable information on the low binding energy core levels as XPS, as these electrons generally experience elastic collisions resulting in broader peaks [8].

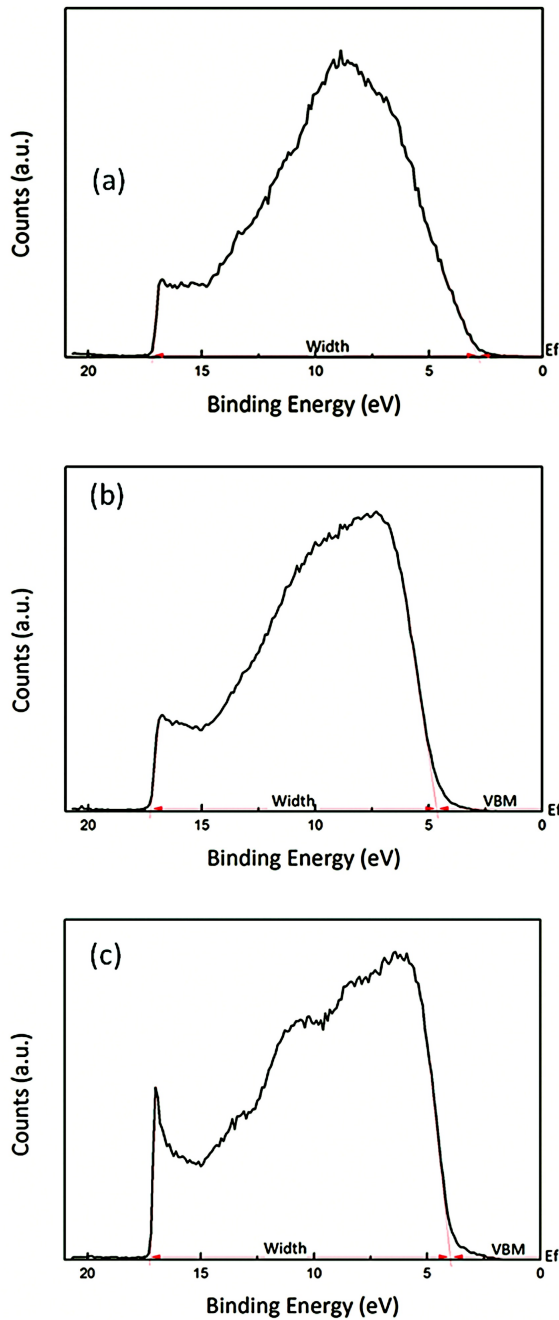


FIG 3.7 UPS spectra of (a) oxygen-terminated n-type Ga-face GaN, (b) 1 nm as-deposited Al_2O_3 on n-type, Ga-face GaN, (c) 1 nm as-deposited HfO_2 on n-type, Ga-face GaN, giving the electron affinity and VBM. The valence band maximum (VBM) is the difference between the Fermi level and the low-binding energy cutoff, and the width of the spectrum, W , is used to calculate the electron affinity of the oxide. Reprinted from Yang *et al.* [9]. Copyright 2012, American Institute of Physics.

C. Example Spectra

Spectra for a few of the materials used in this research are shown in FIG 3.7. These spectra clearly show the valence band of the corresponding semiconductor or dielectric. In particular, the valence band maximum is determined from a linear fit of the low binding energy cut-off.

III. Characterization with Photoelectron Spectroscopy

With XPS and UPS measurement techniques, extensive characterization is possible. These characterization techniques can not only determine film composition of relative chemical states and relative thickness of the constituent layers but also reveal film properties such as the electron affinity and band gap. In addition, these photoemission spectroscopy techniques enable the examination of the electronic structure, including band bending at the surface or band alignment at an interface.

A. Electron Affinity

Electron affinity is the energy required to add an electron to a material, or more specifically, the energy difference between the vacuum level and conduction band of a semiconductor. This energy difference is determined from the high- and low-energy cutoffs of a UPS spectrum:

$$E_{EA} = h\nu - W - E_g, \quad (3)$$

where $h\nu$ is the energy of the incident photon (= 21.2 eV for He), W is the width of the UPS spectrum, and E_g is the band gap energy. (See FIG 3.8.) Alternatively, this can be rewritten in terms of the ionization energy ($= E_{EA} + E_g$):

$$I = h\nu - W. \quad (4)$$

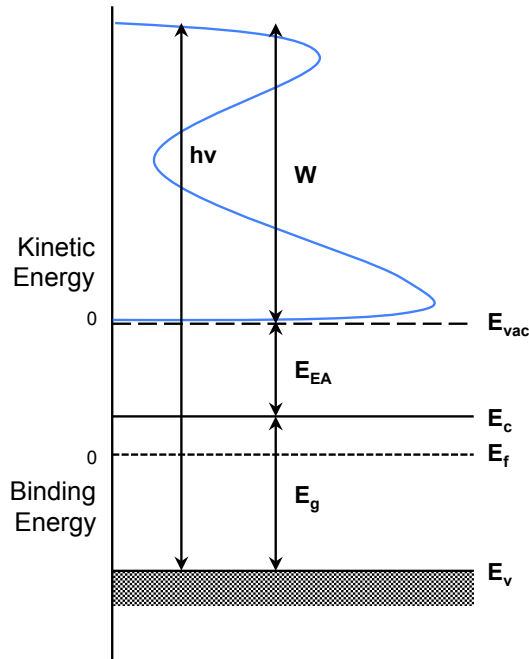


FIG 3.8 Energy distribution of a semiconductor exposed to ultraviolet light, generating a UPS spectrum. Low binding-energy (or high-kinetic energy) cutoff of the spectrum is used to determine the VBM while the high-binding energy (or low-kinetic energy) cutoff is used to determine the electron affinity or ionization energy.

B. Band Bending

Band bending (BB) of a substrate can be determined by the position of the XPS core levels and inherent material properties in a method determined Waldrop, Grant [10], and Kraut *et al.* [11]. This method gives the following relation:

$$BB = (E_{CL} - E_V)_{substrate} + E_g - E_{CL, XPS} + E_C, \quad (5)$$

where E_C is the position of the conduction band with respect to the Fermi level, E_g is the band gap the material, $E_{CL, XPS}$ is the position of the respective core level, and $(E_V - E_{CL})_{substrate}$ is the difference between the core level and the valence band maximum, which is constant for a given material. This process is demonstrated in FIG 5.5 for oxygen-terminated GaN [12]. In this example, E_C is calculated from the doping density of

GaN (-0.1 eV), and the band gap is assumed to be 3.4 eV. $(E_V - E_{CL})_{\text{GaN}}$ is assumed to be 17.8 eV as measured in other electronic-state studies [10,13,14].

It is important to note this measurement technique must account for the area of the depletion region. Generally, low doping concentrations are chosen to ensure the depletion region is significantly larger than the penetration depth of the analysis (3-10 nm), thus ensuring reliable measurements for the band bending. However, if the doping concentration is high, the width of the depletion region may approach the probing depth of the XPS. In such cases, Equation 3 must be modified to account for the quadratic

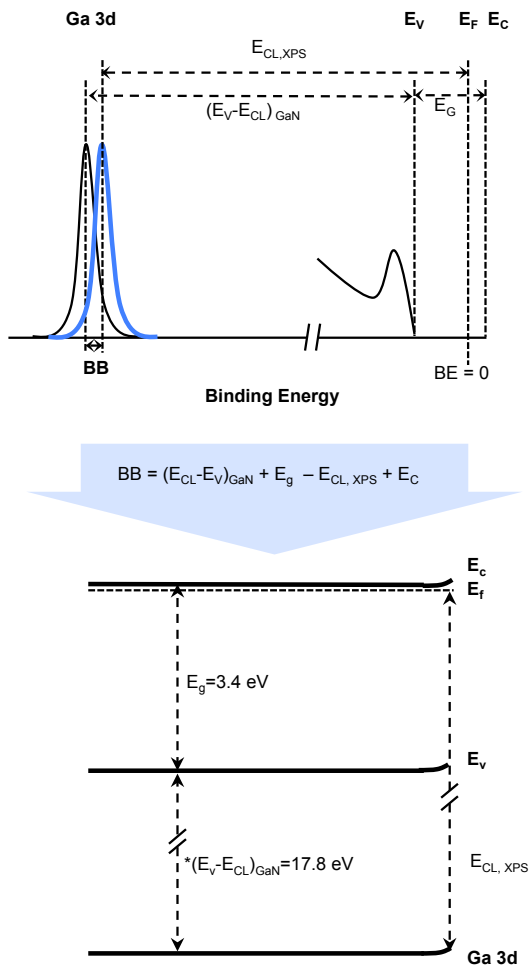


FIG 3.9. Surface band bending measurements (bottom) were determined from the position the Ga 3d core level as determined from XPS (top) by the given equation (middle). Reprinted from Eller *et al.*, *J. Electron. Mater.* **43**, 4560 (2014) [12]. Copyright 2014, Springer US.

nature of the depletion region.

An alternative method can be deduced from UPS measurements, where the low binding energy cutoff gives the VBM. Therefore,

$$BB = E_g - E_C - VBM. \quad (6)$$

However, given the surface sensitivity of this method, UPS measurements are only valid when the surface is pristine, which is not often relevant with GaN or AlGaN substrates.

C. Band Alignment

Band alignment of thin heterostructures is discernable from XPS and UPS spectra as well. More specifically, the valence band offsets (VBOs) can be determined from the difference between the corresponding core levels in the substrate and thin film:

$$\Delta E_V = (E_{CL}-E_V)_{substrate} - (E_{CL}-E_V)_{oxide} + \Delta E_{CL}, \quad (7)$$

where ΔE_{CL} is the difference between the respective core levels, and $(E_{CL}-E_V)$ is the difference between the core level and respective valence band maximum as demonstrated in FIG 3.10.

In addition, a potential drop across the dielectric can be determined from UPS and XPS measurements, where UPS gives the position of the valence band maximum with respect to the Fermi level at the surface and the XPS core level can be used to determine the position of the valence band maximum with respect to the Fermi level at the center of the film. Any difference in the two measurements corresponds to potential drop:

$$V_{drop} = 2 (VBM - E_{CL} + (E_{CL}-E_V)_{oxide}). \quad (8)$$

In other words, this technique utilizes the differing penetration depths of both photoemission spectroscopy techniques to determine the potential drop.

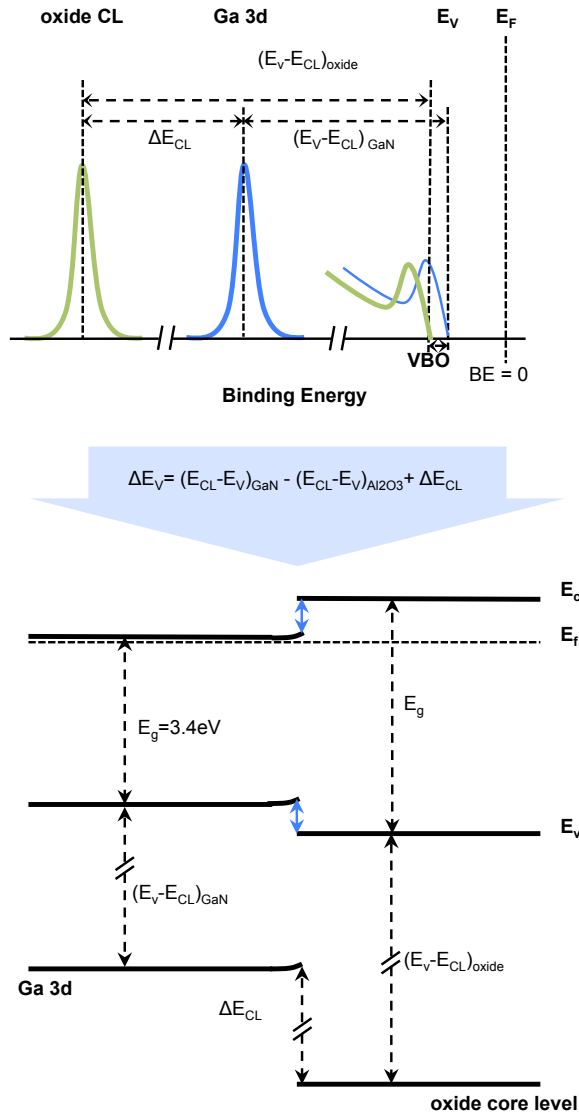


FIG 3.10 Band offsets (bottom) are determined from the difference between the Ga 3d and corresponding oxide core level as determined from the XPS (top) by the given equation (middle).

D. Film Composition

The film composition can be determined from the relative core level intensities of constituent elements. More specifically, the percent concentration of an element is given by

$$\%_{concentration} = \frac{I_i^{exp}}{S_i} / \sum_j^n \frac{I_j^{exp}}{S_j}, \quad (9)$$

where I^{exp} is the core level intensity, and S is the atomic sensitivity factor of the respective core level. This approach can determine the stoichiometry of a film, where the intensity is similarly modified by the atomic sensitivity factor for each core level.

As mentioned, chemical states of constituent elements are discernable from the XPS spectra as well, and thus the composition of constituent chemical states are characterized.

In some cases, the stoichiometry of a substrate beneath a thin film is of interest. In this case, the surface layer attenuates the intensity of the substrate, and the attenuation of different core levels is not equivalent. For example, the Ga:N ratio of GaN is often important after different surface pretreatments. In most cases, these surface pretreatments are unable to remove the native Ga-O surface layer, which attenuates the intensities of Ga and N core levels differently. In such a case, the intensity of a core level is reduced according to Beer Lambert's law:

$$I_S = I_o e^{-d/\lambda}, \quad (10)$$

where I_o is the original intensity of the core level, d is the thickness of the surface layer, and λ is the effective attenuation length of the respective core level electrons.

E. Film Thickness

As a surface sensitive technique, XPS can also determine the thickness of ultrathin film (~3-10 nm depending on the material). In this work, XPS measurements are used to determine the thickness of the metal oxide films deposited by ALD on GaN and AlGaN.

Therefore, the thickness of metal oxide thin films ($d_{metal\ oxide}$) is determined by the XPS spectra intensity of the thin film and the substrate by the following equation [15]:

$$d_{metal\ oxide} = \lambda_{metal\ oxide} \sin\theta \left[\frac{1}{\beta} \left(\frac{I_{metal}^{exp}}{I_{Ga}^{exp}} \right) + 1 \right]. \quad (11)$$

In this equation, $I_{metal}^{exp}/I_{Ga}^{exp}$ is the intensity ratio of the metal core level in the metal oxide and Ga core level from the substrate as determined from the spectra of the sample. θ is the angle between the sample surface plane and electron analyzer; this angle is 90° for our experimental setup. $\lambda_{metal\ oxide}$ is the effective attenuation length of the Ga core level electrons in the metal oxide. β is the intensity ratio of the bulk materials as determined from the maximum intensity of the respective core level, i.e. a metal core level from the metal oxide film and the Ga core level from the substrate. This value is determined from the maximum intensity of the Ga core level for a cleaned substrate and the metal core level of a thick film.

F. Band Gap

The band gap of a material can also be determined from an XPS spectrum via electron loss spectroscopy (ELS). A fraction of the emitted electrons lose energy to collective oscillations (plasmons) and single particle excitations (band-to-band transitions) [16,17]. For ALD oxides, the plasmon interactions can be determined from the O 1s spectrum where these interactions manifest in a broad and smooth spectral component at higher binding energy. Therefore, aligning the O 1s core level as the zero energy loss point and determining the onset energy of electron excitations gives the band gap [18]. This technique is demonstrated in FIG 3.11 for ALD Al_2O_3 , giving a band gap of 6.7 ± 0.1 eV

[19]. This value is comparable to other ALD Al₂O₃ measurements, which range between 6.5 and 7.0 eV [17,20-22].

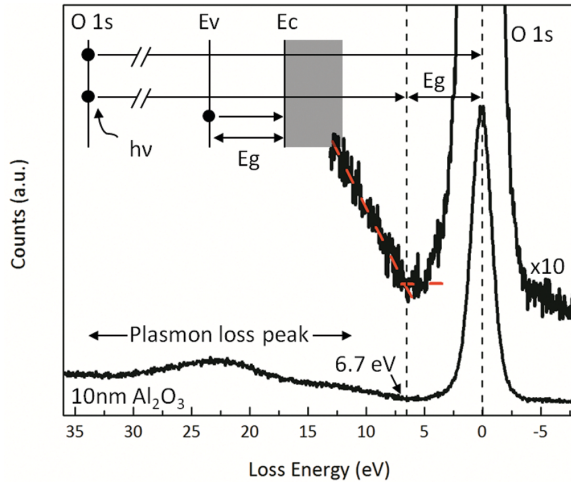


FIG 3.11 O 1s energy loss spectra from 10 nm annealed Al₂O₃ on Si as deposited at 200 °C. The zero loss energy represents the O 1s core level. Ev is the valence band maximum; Ec is the conduction band minimum; and Eg is the band gap. Reprinted from Yang *et al.* [19]. Copyright 2014, American Vacuum Society.

References

- [1] H. Lüth, *Solid Surfaces, Interfaces, and Thin Films*, 5th Ed. (Springer, Heidelberg, Germany, 2010).
- [2] R. Smart, S. McIntyre, M. Bancroft, I. Bello *et al.*, *U. Hong Kong, Dept. Phys.*
- [3] *CASAXPS help manual* (Casa Software Ltd, 2005).
- [4] L. Sygellou, V. Dianneta, N. Xanthopoulos, D. Skarlatos, S. Georga, C. Krontiras, S. Ladas, and S. Kennou, *Surf. Sci. Spec.* 18, 58 (2011).
- [5] A. Milanov, R. A. Fischer and A. Devi, *Surf. Sci. Spec.* 14, 34 (2007).
- [6] A. R. Chourasia, *Surf. Sci. Spec.* 13, 48 (2006).
- [7] “UVL Ultra-violet Source,” *Thermo Electron Corporation* Application Note: AN30058_E (2008).
- [8] L. Scudiero, *Washington State University*.
- [9] J. Yang, B. S. Eller, C. Zhu, C. England, and R. J. Nemanich, *J. Appl. Phys.* 112, 053710 (2012).
- [10] J. R. Waldrop and R. W. Grant, *Appl. Phys. Lett.* 68, 2879 (1996).
- [11] E. A. Kraut, R. W. Grant, J. R. Waldrop and S. P. Kowalczyk, *Heterojunction Band Discontinuities: Physics and Device Applications*, edited by F. Capasso and G. Margaritondo (Elsevier, New York, 1987).
- [12] B. S. Eller, J. Yang, and R. J. Nemanich, *J. Electron. Mater.* 43, 4560 (2014).

- [13] T. E. Cook, Jr., C. C. Fulton, W. J. Mecouch, R. F. Davis, G. Lucovsky and R. J. Nemanich, *J. Appl. Phys.* 94, 7155 (2003).
- [14] J. Hedman and N. Mårtensson, *Phys. Scr.* 22, 176 (1980).
- [15] D. A. Cole, J. R. Shallenberger, S. W. Novak, R. L. Moore, M. J. Edgell, S. P. Smith, C. J. Hitzman, J. F. Kirchoff, E. Principe, W. Nieveen, F. K. Huang, S. Biswas, R. J. Bleiler, and K. Jones, *J. Vac. Sci. Technol. B* 18, 440 (2000).
- [16] F. G. Bell and L. Ley, *Phys. Rev. B* 37, 8383 (1988).
- [17] H. Nohira, W. Tsai, W. Besling, E. Young, J. Petry, T. Conard, W. Vandervorst, S. De Gendt, M. Heyns, J. Maes, and M. Tuominen, *J. Non-Cryst. Solids* 303, 83 (2002).
- [18] M. Bär, M. Rusu, S. Lehmann, Th. Schedel-Niedrig, I. Lauermann, and M. C. Lux-Steiner, *Appl. Phys. Lett.* 93, 232104 (2008).
- [19] J. Yang, B. S. Eller, M. Kaur, and R. J. Nemanich, *J. Vac. Sci. Technol. A* 32, 021514 (2014).
- [20] E. Bersch, S. Rangan, R. A. Bartynski, E. Garfunkel, and E. Vescovo, *Phys. Rev. B* 78, 085114 (2008).
- [21] S. Miyazaki, *J. Vac. Sci. Technol. B* 19, 2212 (2001).
- [22] H. Y. Yu, M. F. Li, B. J. Cho, C. C. Yeo, M. S. Joo, D.-L. Kwong, J. S. Pan, C. H. Ang, J. Z. Zheng, and S. Ramanathan, *Appl. Phys. Lett.* 81, 376 (2002).

CHAPTER 4. KELVIN PROBE METHOD

Surface potential measurements are challenging. As a built-in potential, the surface potential is more complicated than measuring the difference in the Fermi level at the front and back surfaces of the material. In addition, the application of an electrical contact invariably alters the surface potential and degrades measurement quality. For this reason, surface potential measurements are conducted by non-contact methods such as with a Kelvin probe (KP), a technique developed by Lord Kelvin in 1861.

In this technique, a small tip with a known work function is brought near the surface of the sample to create a parallel plate capacitor. When the plates, i.e. the tip and sample surface, are electrically neutral, no field appears, and the materials share a vacuum level as shown in FIG 4.1a. When the KP and sample are short circuited, an electric field develops such that the Fermi levels align via charge transfer as shown in FIG 4.1b. The potential drop is referred to as the contact potential difference (CPD), i.e., $eV_{\text{CPD}} = W_1 - W_2$. Theoretically, the potential could then be determined by $Q=C_0V_{\text{CPD}}$; however, determining the stored charge, Q , is not straightforward. A DC voltage applied to the materials can help overcome this difficulty; when the voltage is equal and opposite to the V_{CPD} , the vacuum levels align, no electronic field occurs, and the capacitor will discharge

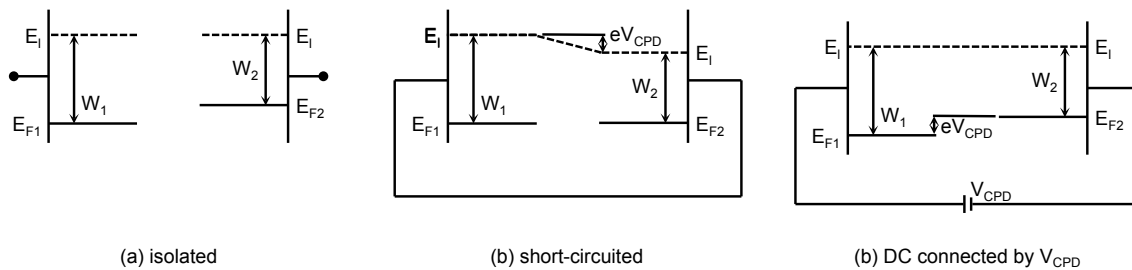


FIG 4.1 Schematic band diagram of parallel plate capacitor formed from two materials (a) in isolation, (b) short-circuited, and (c) connected by a DC bias equal and opposite to the CPD. Reprinted from L. Kronik *et al.*, *Surf. Sci. Rep.* **37**, 1 (1999) [1]. Copyright 1999, Elsevier Science B.V.

as shown in FIG 4.1c. In the Kelvin probe method, the tip of the probe is thus oscillated near the sample surface under a bias, varying the capacitance of the system. At some capacitance, the system will discharge, resulting in zero current and thus giving the CPD. In ultra high vacuum (UHV), the permittivity is known, giving an absolute value for the CPD. In addition, the surface photovoltage can be determined with KP by the change in the CPD with and without UV illumination [1].

I. Principals of Operation

As mentioned, the Kelvin probe method essentially creates a parallel plate capacitor with the surface of the sample. More specifically, the tip vibrates near the surface, creating a varying capacitance [2]:

$$C_K(t) = \epsilon_o \epsilon_r A / d(t) \quad (1)$$

where $C_K(t)$ is the Kelvin capacitance as dependent on time, ϵ_o is the permittivity of free space, ϵ_r is the relative permittivity, A is the surface area of the capacitor, i.e. the Kelvin probe tip, and $d(t)$ is the distance between the tip and sample as dependent on time. This distance is assumed to be sinusoidal as shown in FIG 4.2:

$$d(t) = d_o + d_1 \sin(\omega t), \quad (2)$$

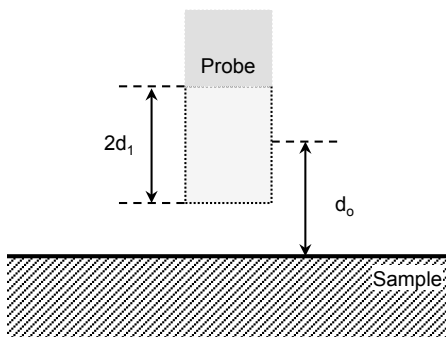


FIG 4.2 Schematic diagram of the tip-sample spacing during tip oscillation. Here d_o represents the mean spacing and d_1 the amplitude of tip motion, thus $2d_1$ represents the total tip displacement. Modified from UHVKP Technology Manual 7.3 [2].

where d_o represents the average distance between the sample and the tip, d_1 is the distance of displacement of the sinusoidal motion, and ω gives the angular frequency of the oscillation in radians/sec. Equation 11 thus becomes

$$C_K(t) = \frac{C_o}{1+e \sin(\omega t)}, \quad (3)$$

where C_o is the mean capacity and $e (= d_1/d_o)$ is the modulation index.

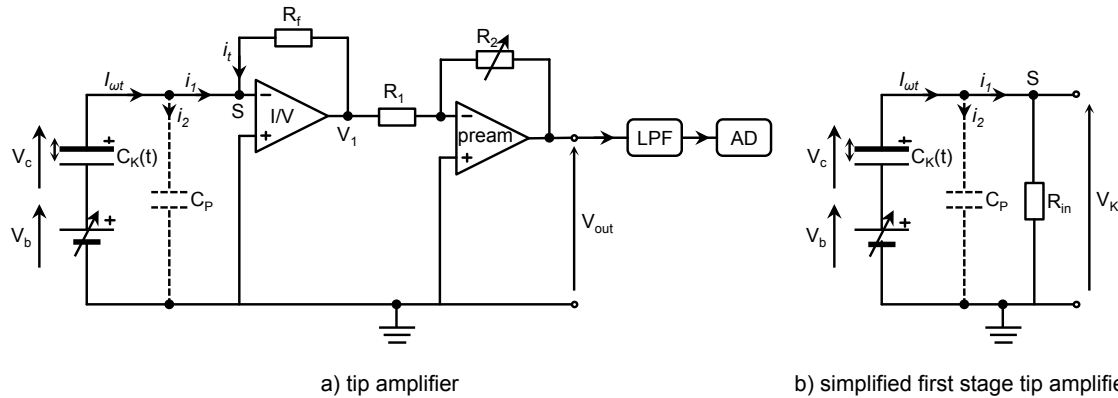


FIG 4.3 a) Circuit diagram of the tip amplifier: the specimen (bottom plate of the Kelvin capacitor C_K) is connected to earth via a computer-steered backing potential V_b . The tip signal i_{tot} is input directly to an I/V converter, having feedback resistance R_f , S denotes the first stage amplifier summing point and C_p the tip parasitic capacity. R_1 and R_2 set the voltage gain of the preamplifier stage, the output signal V_{out} passes via a low pass filter (LPF) to the analog-to-digital (AD) converter of the data acquisition system. b) Simplified diagram of the first stage amplifier where the I/V converter is represented by its input resistance R_{in} . Analysis of this circuit shows that, for low frequencies (< 1000 Hz), the signal lost to the parasitic capacitance i_2 is negligible thus $i_{tot} = i_1$. Modified from UHVKP Technology Manual 7.3 [2].

A schematic of the KP detection circuit is in FIG 4.3. In this system design, the tip amplifier is composed of two amplifiers: one high gain amplifier and another variable gain voltage amplifier. The first amplifier is current sensitive and near the surface, while the second is used to accommodate different tip sizes and variable spacing. $C_K(t)$ represents the capacitance of the vibrating Kelvin probe, C_p gives the parasitic capacity

from the surrounding circuit, and V_b is the variable backing potential. The surface charge on the probe is thus given by:

$$Q_S = (V_C + V_b) C_K. \quad (4)$$

Thus, the output current,

$$I_K(t) = dQ_S/dt = (V_C + V_b) dC_K/dt, \quad (5)$$

and the peak-to-peak output voltage,

$$V_{ptp} = (V_C + V_b) R_f G C_o \omega \sin(\omega t + j). \quad (6)$$

Here, V_C is the voltage between the tip and sample, V_b is the backing voltage used to balance or nullify the circuit, R_f is the feedback resistance of the I/V converter, $G (=R_2/R_1)$ is the gain of the pre-amplifier, C_o is the mean capacitance of the Kelvin probe, and j is the phase. (FIG 4.4 demonstrates an example of the output signal for a high modulation index, e.g. $e \ll 0.7$.) In addition, there is a linear relationship between V_{ptp} and V_b . (See FIG 4.5.) When $V_C + V_b = 0$, V_{ptp} is nullified. This process termed off-null signal detection, ensures reliable measurement regardless of parasitic capacitance in the system.

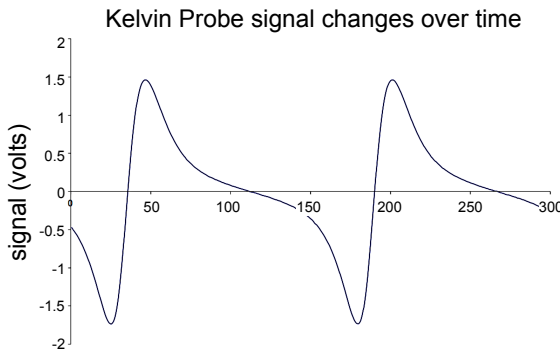


FIG 4.4 Example of a Kelvin probe signal under conditions of high modulation index. The peak-to-peak voltage, $V_{ptp} = -3.25$ V, where the peak-to-peak height is being negative if the trough appears before the peak. Modified from UHVKP Technology Manual 7.3 [2].

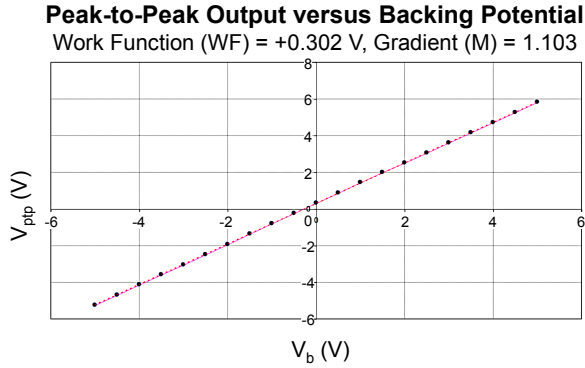


FIG 4.5 Plot of V_{ptp} versus V_b showing the linear behavior. Note that the line crosses the V_b axis at the point where the sum of the contact and backing potentials are zero. Modified from UHVKP Technology Manual 7.3 [2].

II. Surface Potentials

In general, there are several surface potential characteristics of interest that can be determined via the Kelvin probe method, including the work function, surface band bending, surface dipole, and surface photovoltage.

A. Surface Work Function

The work function (or surface potential for nonmetals) of a material refers to the minimum energy required to remove an electron from a solid to vacuum; in other words, it is the smallest energy required to remove an electron from a material. This electron is sensitive to the electrical, chemical, optical, and mechanical characteristics of the surface region. The work function is thus affected by changes to these characteristics, e.g. surface adsorbates, evaporated layers, surface charging, oxide layers, surface reconstruction, contamination. The precise work function for a given surface is thus advantageous and can be determined by the KP method, as demonstrated in FIG 4.1. More specifically, the work function (W) of a material, as determined by Kelvin probe, is given by

$$W_{sample} = W_{tip} + eV_{CPD}, \quad (7)$$

where the work function of the tip is calibrated using a gold foil.

B. Surface Band Bending

In addition, the Kelvin probe provides an alternative method to determine the surface band bending of a semiconductor. (See FIG 4.6.) Similar to work function measurements, Equation 7 can be adapted for the modified work function of the semiconductor (i.e. $W_s = eV_{CPD} + W_{tip}$). From the modified work function, band bending is deduced:

$$\begin{aligned} BB &= W_s - E_{EA} - E_c, \\ &= eV_{CPD} + W_{tip} - E_{EA} - E_c, \end{aligned} \quad (8)$$

where $E_{EA} (= E_{vac} - E_c)$ is the electron affinity of the semiconductor and E_c is the position of the conduction band with respect to the bulk Fermi level. However, this method of measurement is limited since surface conditions may alter the effective electron affinity with the introduction of a surface dipole.

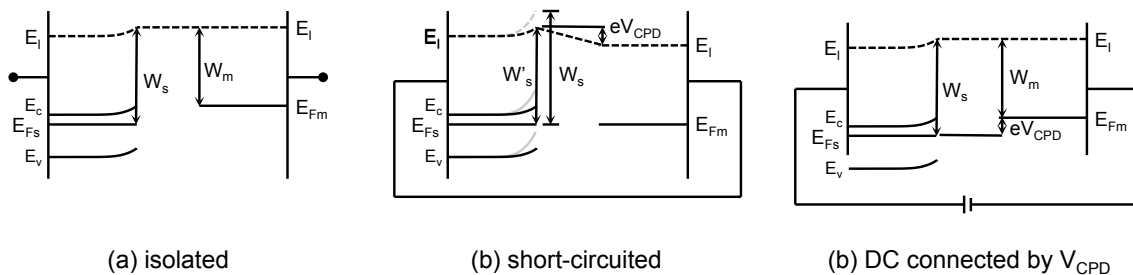


FIG 4.6 Schematic band diagram of parallel plate capacitor formed from a metal and semiconductor (a) in isolation, (b) short-circuited, and (c) connected by a DC bias equal and opposite to the CPD. Reprinted from L. Kronik *et al.*, *Surf. Sci. Rep.* **37**, 1 (1999) [1]. Copyright 1999, Elsevier Science B.V.

C. Surface Dipole

Similarly, the effective electron affinity of a material is affected by the surface conditions, e.g. surface adsorbates, evaporated layers, surface charging, oxide layers, various surface reconstructions, and contamination. The distribution of these atoms

creates an array of microscopic dipoles, which, in some cases, create a dipole at the surface of the semiconductor. This surface dipole affects surface potential measurements as shown in FIG 4.7. Here, it is apparent that the measured work function of a sample is affected by the band bending and surface dipole. For this reason, the Kelvin probe method can be used to determine the surface dipole:

$$\Delta\phi_s = BB_{XPS} + E_{EA} + E_c - (eV_{CPD} + W_{tip}). \quad (9)$$

In this case, XPS measurement is used to determine the band bending, where XPS is less surface-sensitive than Kelvin probe and thus is affected by the surface dipole.

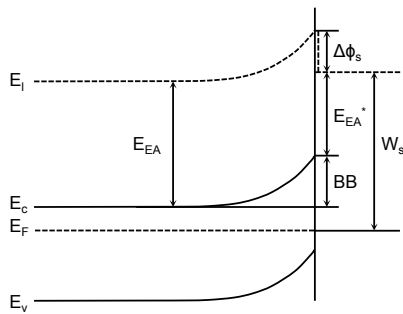


FIG 4.7 Schematic diagram of the electronic band structure at a semiconductor surface. Reprinted from L. Kronik *et al.*, *Surf. Sci. Rep.* **37**, 1 (1999) [1]. Copyright 1999, Elsevier Science B.V.

D. Surface Photovoltage

Measuring the surface potential via Kelvin probe rather than UPS offers an advantage; Kelvin probe does not induce a surface photovoltage. Surface photovoltage effects arise when a semiconductor is exposed to UV illumination. Incident UV photons generate electron-hole pairs. In the presence of a surface depletion region, the electron-hole pairs experience an electric field, which accelerates the electrons and holes in opposite directions. The accumulation of holes and electrons on opposite sides of the depletion region consequently alters the electric field. For example, in n-type materials, holes accumulate near the surface while electrons diffuse away from the surface. The result is

to create an electric field in the opposite direction of the existing field; thus, upward band bending decreases. In p-type materials, electrons accumulate near the surface while holes diffuse away from the surface; thus, downward band bending decreases. In other words, UV illumination leads to the flattening of the band bending. (See FIG 4.8.) Since the Kelvin probe can determine the surface potential with and without UV exposure, the difference in these two measurements provide the surface photovoltage (SPV).

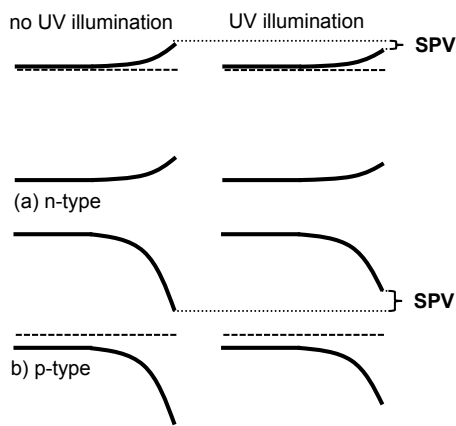


FIG 4.8 Example of surface photovoltage effects where the band bending is flattened under UV illumination. (a) In n-type material, the SPV corresponds to accumulation of photo-generated holes near the surface region while photo-generated electrons accumulate on the far side of the depletion region. Conversely, (b) in p-type material, the SPV corresponds to accumulation of photo-generated electrons near the surface region while photo-generated holes accumulate on the far side of the depletion region.

References

- [1] L. Kronik and Y. Shapira, *Surf. Sci. Rep.* 37, 1 (1999).
- [2] *UHV Kelvin Probe Manual*, Ver. 7.3 (KP Technology, Caithness, UK, 2011), pp. 26-31.

PART III: RESEARCH

CHAPTER 5. POLARIZATION EFFECTS OF GAN AND ALGAN: POLARIZATION BOUND CHARGE, BAND BENDING, AND ELECTRONIC SURFACE STATES

Abstract. GaN-based devices are currently limited by reliability issues such as gate leakage and current collapse, where the mechanisms responsible for degradation are closely related to the electronic surface state configuration. Therefore, understanding the electronic surface state configuration of GaN-based materials will help improve device performance. Since GaN has an inherent polarization, these materials are also subject to a bound polarization charge, which influences the electronic state configuration. In this study, the surface band bending of N-face GaN, Ga-face GaN, and Ga-face AlGaN was measured with x-ray photoemission spectroscopy after various cleaning steps to investigate the effects of the polarization. Despite the different surface bound charge on these materials, similar band bending was observed regardless of the magnitude or direction of the charge. Specifically, the band bending varied from -0.1 to 0.9 eV on these samples, which supported the models of a Fermi level pinning state at ~ 0.4 to 0.8 eV below the conduction band. Based on available literature, we suggest this pinning state is indirectly evident of a nitrogen vacancy or gallium-dangling bond.

As published in B. S. Eller, J. Yang, and R. J. Nemanich, J. Electron. Mater. 43, 4560 (2014).

Mitigating multi-lateral ecological and environmental concerns will define next-generation technology. In particular, improvement in power electronic technologies ensures progress towards this goal. GaN-based semiconductors thus remain promising candidates, where GaN has several advantages over competing semiconductors in power applications—e.g., Si, SiC, and GaAs—due to superlative material properties [1]. Specifically, GaN is characterized by high power per unit width, which allows for smaller devices, easier manufacturing, and higher impedance. This characteristic also facilitates system matching that may be difficult with other materials such as GaAs. Moreover, the high breakdown field of GaN supports higher operating voltages, reduced voltage conversion, decreased power requirements, and simpler cooling. Consequently, many GaN-based devices have demonstrated superior performance [2]. However, despite the success of GaN-based devices, there are three issues that require resolution before GaN technology can replace existing Si technology: (1) the development of high-quality growth methods of single-crystal epitaxial GaN, (2) the selective formation of n-type

regions, and (3) the minimization of electronic states at the gate dielectric and GaN or AlGaN interface [3]. In this article, we address the latter. More specifically, this work investigates the effects of the polarization bound charge associated with III-V nitrides on surface states in an attempt to reveal relevant pinning states. In particular, this work focuses on oxygen-terminated surfaces, which are more representative of the conditions at the device interface. Results of these oxygen-terminated surfaces show band bending is independent of the magnitude or direction of the polarization; these similarities indicate a likely pinning surface state located ~ 0.4 to 0.8 eV below the conduction band that can accommodate both positive and negative charge. Based on available literature, we suggest the relevant pinning state is likely related to the nitrogen vacancy or gallium-dangling bond.

Unlike Si, GaN and other wurtzite, III-V nitrides are characterized by a macroscopic polarization, \vec{P} . This polarization arises from the material properties of the nitrides, where \vec{P} is the sum of the spontaneous polarization inherent to the equilibrium lattice, \vec{P}_{SP} , and the piezoelectric polarization created by strain, \vec{P}_{PE} . (See FIG 5.1.) Using *ab initio* calculations and material constants, the polarization along the c-axis as induced by the piezoelectric effect is

$$\vec{P}_{PE} = 2\frac{a-a_0}{a_0}(e_{31}-\frac{C_{13}}{C_{33}}e_{33})\hat{c}, \quad (1)$$

where C_{13} and C_{33} are elastic constants, e_{31} and e_{33} are piezoelectric coefficients, and a_0 and a are lattice constants [5-13]. For relaxed GaN and AlN, the piezoelectric polarization

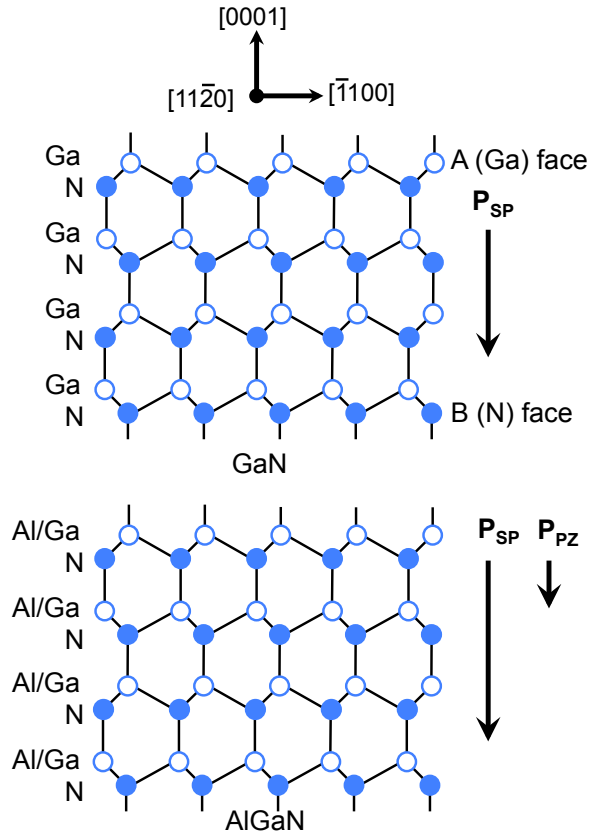


FIG 5.1 (Color online) Crystal structure, spontaneous polarization fields (\mathbf{P}_{SP}), and piezoelectric polarization fields (\mathbf{P}_{PE}) for GaN (top) and $\text{Al}_x\text{Ga}_{(1-x)}\text{N}$ (bottom). Reprinted from Yu, *et al.*, *J. Vac. Sci. Technol. B* **17**, 1742 (1999) [4]. Copyright 1999, American Vacuum Society.

is negligible [14]. (However, this component of the polarization depends on the strain of the crystal and may vary with growth method, substrate material, or temperature.)

The spontaneous polarization, on the other hand, is large for GaN and AlN; calculations using the Berry-phase approach and local density [15-17] or generalized gradient approximations [16,18] determine the spontaneous polarization is -0.029 C/m^2 and -0.081 C/m^2 for wurtzite GaN and AlN, respectively. This calculation assumes the respective (0001) Ga- and Al-face, suggesting the spontaneous polarization is directed towards the N-face. In addition, the magnitude of the polarization increases with aluminum content, as the spontaneous polarization is sensitive to structural parameters. Therefore, the longer anion-cation bond length along the (0001) axis of AlN corresponds to an increase in

magnitude along the c-axis of the wurtzite structure [4]. The polarization of $\text{Al}_x\text{Ga}_{1-x}\text{N}$ can thus be determined by linear interpolation as displayed in TABLE 5.1.

TABLE 5.1 Band gap, polarization, and corresponding polarization bound charge for GaN, AlN, and $\text{Al}_x\text{Ga}_{1-x}\text{N}$.

	GaN	AlN	$\text{Al}_x\text{Ga}_{1-x}\text{N}$
band gap (eV)	3.4	6.2	$3.4(1-x) + 6.2x$
spontaneous polarization (C/m^2)	-0.029	-0.081	$-0.029(1-x) - 0.081x$
polarization bound charge (10^{13} charges/ cm^2)	1.81	5.06	$1.81(1-x) + 5.06x$

This polarization charge gives rise to a bound surface charge,

$$\sigma_b = \vec{P} \cdot \hat{c}. \quad (2)$$

There is thus a negative bound charge of 1.81×10^{13} and 5.06×10^{13} charges/ cm^2 for the Ga- and Al-face of GaN and AlN crystals, respectively. Consequently, an equivalent positive bound polarization charge exists on the N-face of GaN and AlN. Since the internal electric field of a wide-bandgap semiconductor is zero or near zero, the system adjusts to satisfy surface conditions of near charge neutrality. Therefore, the intrinsic material properties give rise to a distribution of inherent electronic states. The nature and distribution of the compensation charge affect the internal electric field of the materials and ultimately device performance.

This phenomenon is better understood in terms of surface band bending, which is directly related to the space charge region. More specifically, compensation charge in semiconductors, can take two forms: (1) the formation of an internal space-charge layer that consists of ionized donors and defects near the surface, or (2) external charged surface or interface states. These internal and external screening mechanisms are

inversely related as shown in FIG 5.2, where the larger the compensation from the internal space-charge layer (and thus the smaller the net concentration of surface states), the larger the band bending. The band bending is thus calculated from the density of internal screening charge:

$$\Phi_s = -\frac{qN_{ss}^2}{2\epsilon\epsilon_0N_d}, \quad (3)$$

where q is the charge of an electron, ϵ is the relative permittivity, ϵ_0 is the permittivity of free space, N_d is the doping density, and N_{ss} is the net surface charge in charges/cm². Assuming a doping density of 10^{17} charges/cm³ and a net polarization charge of 1.81×10^{13} charges/cm² for GaN, this calculation suggests a surface potential of -420 V, which corresponds to 420 eV of upwards band bending and an average electric field of 200 MV/m at the surface of GaN. In equilibrium, this large internal field results in inversion or accumulation, and the band bending is thus limited to approximately the

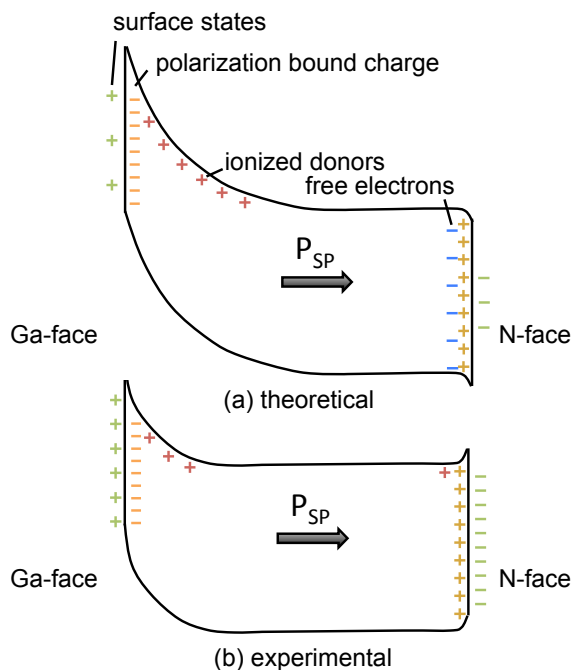


FIG 5.2 (Color online) Theoretical (a) and experimental (b) band bending schematic for Ga- and N-face GaN. Both surfaces are screened by $\sim 10^{13}$ charges/cm². (NOTE: the position of the ionized donors and electrons in the material corresponds to their physical position rather than their energy level within the band gap.) Reprinted from Eller *et al.*, *J. Vac. Sci. Technol. B* **31**, 050807 (2013) [2]. Copyright 2013, American Vacuum Society.

band gap of the material, 3.4 eV [19,20]. (See FIG 5.2a.) Therefore, ionized donors cannot be solely responsible for the compensation of the polarization bound charge.

Experimental band bending measurements indicate the band bending is well below the band gap. (See FIG 5.2b.) In fact, most experimental band bending experiments for n-type Ga-face GaN typically report measurements between 0.3 and 1.5 eV [21-23]. These measurements can then determine the concentration of charged surface states from the band bending, where

$$N_{ss} = \sqrt{-\frac{2\Phi_s \epsilon \epsilon_0 N_d}{q}}. \quad (4)$$

This equation suggests a 0.1 eV change in band bending corresponds to a 3.2×10^{11} charges/cm² change in the concentration of surface states.

I. Experiment

In this study, we thus determine the concentration of surface states from the experimentally measured band bending of several different sample surfaces, including the Ga-face of GaN and Al_{0.25}Ga_{0.75}N films as well as the Ga- and N-face of freestanding GaN. These various sample surfaces enable us to examine different surfaces associated with several polarization bound charge conditions. Freestanding wafers were ~450 μm thick, n-type, as-grown via hydride vapor phase epitaxy (HVPE) purchased from READE Advanced Materials with a Si doping density of $\sim 8 \times 10^{17}$ cm⁻³; this doping density determined the position of the Fermi level to be ~0.1 eV lower than the conduction band minimum. Additional n-type Ga-face epitaxial GaN wafers were also used. The samples were 5 ± 1 μm thick, as grown by HVPE on sapphire substrates purchased from READE

Advanced Materials. The doping density was still $\sim 10^{17} \text{ cm}^{-3}$, which established a similar Fermi level position. To investigate the effects of a larger concentration of surface bound charge, Ga-face AlGaN was also used with 25% aluminum content as purchased from NTT Advanced Technology. $\text{Al}_{0.25}\text{Ga}_{0.75}\text{N}$ samples were $\sim 50 \text{ nm}$ thick, as deposited on Si substrates with a doping density of $\sim 10^{17} \text{ cm}^{-3}$. This doping density ensured a similar Fermi level position as the other samples, $\sim 0.1 \text{ eV}$ below the conduction band.

As-received wafers were cleaned *ex situ* via sonication in acetone, methanol, and NH_4OH for 10 minutes each. Samples were then rinsed in DI water for 1 min and dried with nitrogen. After the chemical cleaning, samples were loaded into an ultra high vacuum system with base pressure of $4 \times 10^{-10} \text{ Torr}$. The inclusive UHV system allowed for *in-situ* cleaning, which reduced the oxygen coverage using NH_3 plasma and additional NH_3 gas annealing at $680 \text{ }^\circ\text{C}$ for 15 min each. The plasma was operated at 100W with a constant gas flow of 90 sccm and pressure of 60 mtorr. Characterization was subsequently conducted using *in-situ* XPS.

More specifically, XPS spectra were used to determine the stoichiometric ratios and surface band bending. These spectra were obtained at a base pressure of $8 \times 10^{-10} \text{ Torr}$. Mg $\text{K}\alpha$ ($=1253.6 \text{ eV}$) x-ray radiation was used as a radiation source, except when scanning the C 1s peak; the Ga LMM Auger lines and C 1s peak overlap, and, therefore, Al $\text{K}\alpha$ ($=1486.6 \text{ eV}$) x-rays were used. The non-monochromatic x-ray source used a 4.4 A filament current, 16 mA emission current, and 13 kV accelerating voltage. Survey scans were repeated 30-80 times with a pass energy of 20 eV. The spectra were dispersed with a Fisons Clam II hemispherical analyzer at a resolution of $\sim 1.0 \text{ eV}$. Through curve fitting

of the core level peaks, the peak positions could be resolved to ± 0.1 eV. These measurements included adjustments according to a calibration using a gold foil; typical corrections were -0.1 and -0.2 eV for respective Mg and Al radiation sources. XPS measurements were also used to determine the concentration and the atomic ratio of constituents near the surface; C 1s and O 1s spectra indicated the effectiveness of the cleaning process, while Ga 3d and N 1s spectra indicated the stoichiometric ratio of the GaN at the surface.

II. Results

The oxygen coverage was defined as the number of absorbed oxygen atoms per Ga (Al) or N atoms at the c plane surface, where one oxygen atom per surface lattice site referred to a single monolayer (ML) of coverage. This ratio was calculated by the following [24]:

$$\Theta_o = \frac{I_o}{S_o} \left(\frac{S_{Ga}}{I_{Ga}} \right) \sum_{n=0}^{\infty} \exp \left[\frac{-nd_{Ga}N}{\lambda_{Ga} \cos[\phi]} \right], \quad (5a)$$

where I_{Ga} and I_o were the integrated intensities of the respective Ga 3d and O 1s peaks, S_o and S_{Ga} were the atomic sensitivity factors for respective O 1s and Ga 3d (0.66 and 0.31)[19], λ_{Ga} was the inelastic mean free path of Ga 3d electrons with kinetic energies ~ 1200 eV (~ 24 Å) [25], ϕ was the angle between the normal direction and the analyzer (20°), and d was the distance between two Ga planes (2.6 Å). For $\text{Al}_{0.25}\text{Ga}_{0.25}\text{N}$, this calculation was modified, where one in every four Ga atoms was replaced with an Al atom, giving

$$\Theta_o = \frac{I_o}{S_o} \left/ \left[\frac{I_{Ga}}{S_{Ga} \sum_{n=0}^{\infty} \exp \left[\frac{-nd_{Ga}N}{\lambda_{Ga} \cos[\phi]} \right]} + \frac{I_{Al}}{S_{Al} \sum_{n=0}^{\infty} \exp \left[\frac{-nd_{Al}N}{\lambda_{Al} \cos[\phi]} \right]} \right] \right., \quad (5b)$$

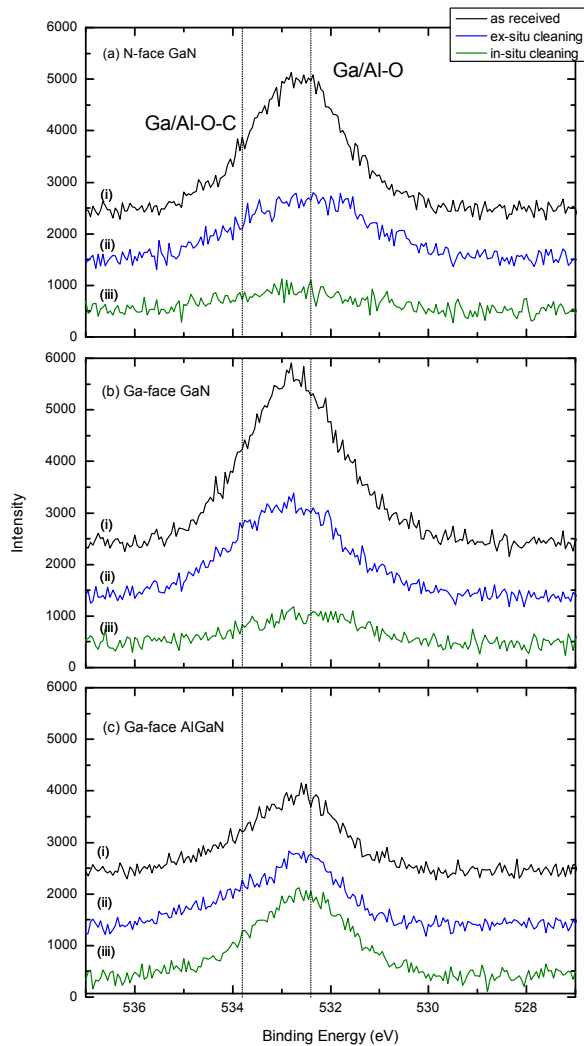


FIG 5.3 (Color online) O 1s peak for N-face GaN (a), Ga-face GaN (b), and Ga-face $\text{Al}_{0.25}\text{Ga}_{0.75}\text{N}$ (c) as received (i), after *ex-situ* cleaning (ii), and after *in-situ* cleaning (iii). Note: core levels were shifted to the corresponding flat band position, allowing direct comparison of the oxygen states.

where I_{Al} was the integrated intensity for the Al 2p peak, S_{Al} was the atomic sensitivity factor for Al 2p (0.185), λ_{Al} was the approximate average inelastic mean free path of Al 2p electrons with kinetic energies ~ 1400 eV (~ 24 Å) [26], and d_{AlGaN} was the distance between two Ga/Al planes (2.6 Å). The oxygen coverage on each sample after the different cleaning states is summarized in TABLE 5.2, and the XPS core levels are shown in FIG 5.3. In general, the AlGaN surfaces are more resistant to oxygen reduction [27-29]; this is expected given the difficulty of breaking Al-O bonds during the cleaning process. Moreover, the NH_3 cleaning reduced carbon below the XPS detection limit.

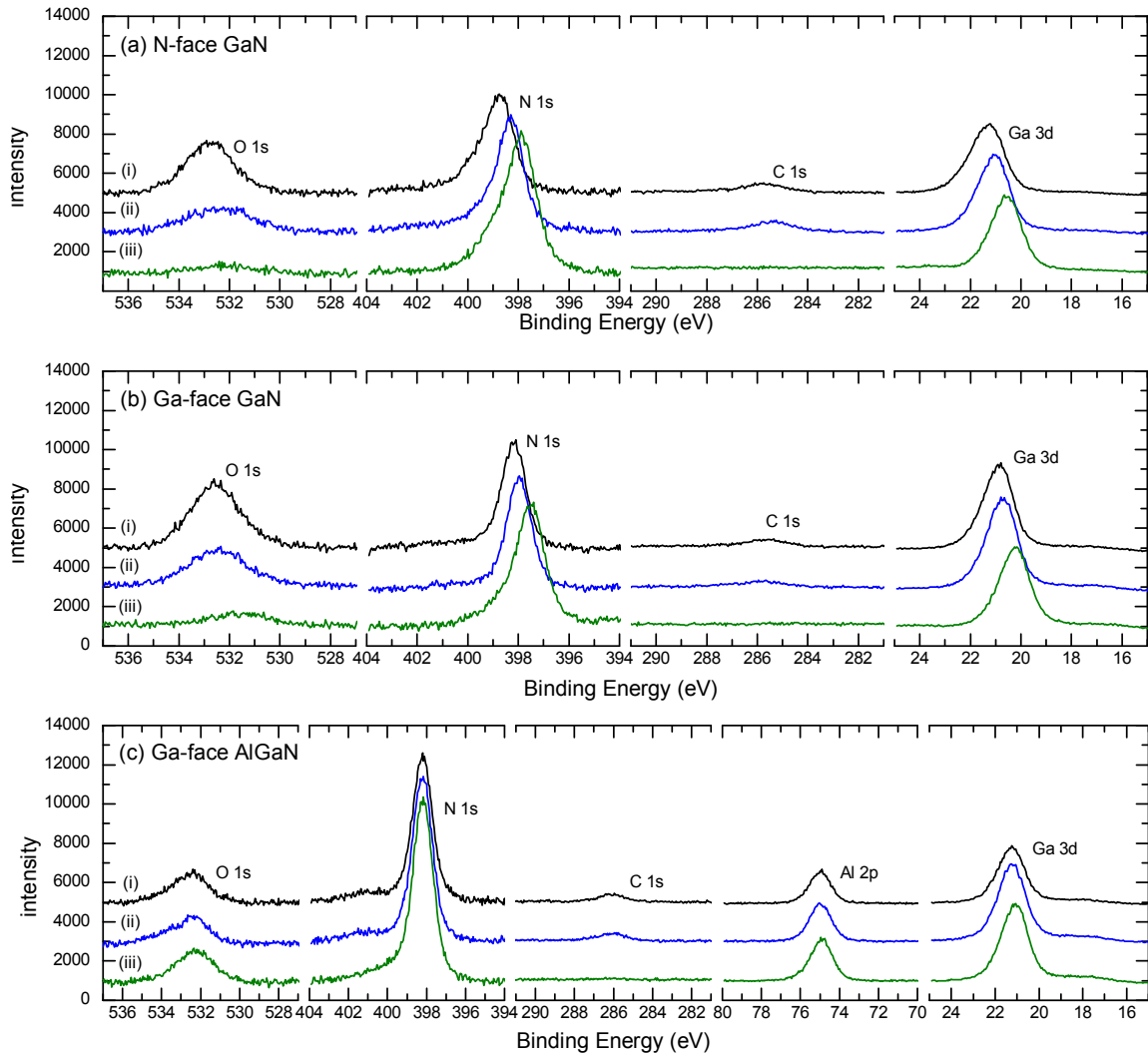


FIG 5.4 (Color online) XPS results for N-face GaN (a), Ga-face GaN (b), and Ga-face $\text{Al}_{0.25}\text{Ga}_{0.75}\text{N}$ (c) as received (i), after *ex-situ* cleaning (ii), and after *in-situ* cleaning (iii).

TABLE 5.2 Oxygen coverage (in ML) on N-face GaN, Ga-face GaN, and Ga-face $\text{Al}_{0.25}\text{Ga}_{0.75}\text{N}$ as determined after the various cleaning steps as given by XPS.

oxygen coverage	N-face GaN	Ga-face GaN	Ga-face $\text{Al}_{0.25}\text{Ga}_{0.75}\text{N}$
as received	4.5	5.1	2.6
<i>ex-situ</i> cleaning	2.6	3.1	2.2
<i>in-situ</i> cleaning	1.1	1.1	1.8

The atomic concentration ratios of the samples were also determined after the different processing steps from relative XPS intensities, as shown in FIG 5.4 and summarized in TABLE 5.3.

TABLE 5.3 Atomic ratio of N/Ga(Al) as determined from Al 2p, Ga 3d, and N 1s core level intensities, respective atomic sensitivity factors of 0.19, 0.31, and 0.42, and effective attenuation lengths as determined from the NIST database [30].

atomic ratios	N-face GaN	Ga-face GaN	Ga-face Al _{0.25} Ga _{0.75} N
as received	0.92	0.74	1.17
<i>ex-situ</i> cleaning	1.02	0.78	0.84
<i>in-situ</i> cleaning	2.03	1.42	1.28

Band bending (BB) of oxygen-terminated GaN and AlGaN was also calculated from the position of the Ga 3d core level and inherent material properties, as shown in FIG 5.5:

$$BB = (E_V - E_{CL})_{GaN} + E_g - E_{CL, XPS} + E_C, \quad (6)$$

where E_C was the position of the conduction band with respect to the Fermi level as

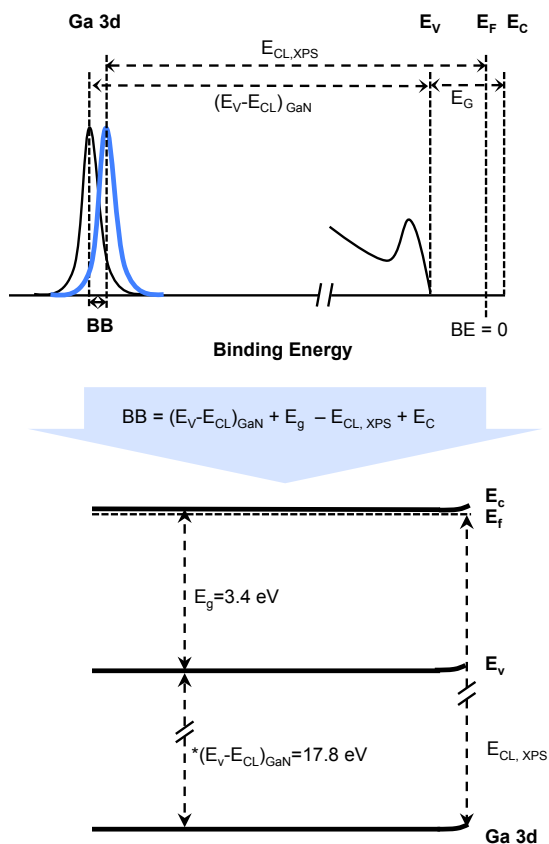


FIG 5.5 (Color online) Surface band bending measurements (bottom) were determined from the position the Ga 3d core level as determined from XPS (top) by the given equation (middle).

determined by the doping density (-0.1 eV), E_g was the band gap the material ($E_{g,GaN} = 3.4$ eV and $E_{g,AlGaN} = 4.0$ eV [31]), and $E_{CL,XPS}$ was the position of the Ga 3d core level for GaN and Al 2p core level for AlGaN. It is worth noting here that this analysis focused on the Ga 3d peak, where the core level intensity and position were less sensitive to the overlayer, thereby providing more reliable band bending measurements. Additionally, $(E_{CL}-E_V)_{GaN}$ represented the binding energy differences of the core level of Ga in GaN with respect to the VBM. According to electronic-state studies of GaN [32-34], the difference between the Ga 3d core level and the valence band maximum was 17.7-17.8 eV. In this study, 17.8 eV was assumed for $(E_{CL}-E_V)_{GaN}$. Similar electronic-state studies of $Al_{0.25}Ga_{0.75}N$ indicated 17.5 eV [35] and 71.5 eV [36] were the respective differences between the Ga 3d and Al 2p core levels and the valence band maximum, which were used to determine the band bending at the AlGaN surface. Please note that while the Ga and Al core level peaks include a component due to Ga-O and Al-O bonding, this component does not affect the peak position. The experimental band bending of each sample after various stages of cleaning is summarized in TABLE 5.4, and the corresponding external compensation charge is summarized in TABLE 5.5

TABLE 5.4 Band bending (in eV) for N-face GaN, Ga-face GaN, and Ga-face AlGaN as determined after the various cleaning steps as given by XPS.

band bending	N-face GaN	Ga-face GaN	Ga-face $Al_{0.25}Ga_{0.75}N$
as received	-0.1	0.2	0.2
<i>ex-situ</i> cleaning	0.1	0.4	0.2
<i>in-situ</i> cleaning	0.6	0.9	0.4

TABLE 5.5 Concentration of external compensation charge (10^{13} charges/cm²) on N-face GaN, Ga-face GaN, and Ga-face AlGaN as determined after the various cleaning steps as given by XPS.

net external compensation	N-face GaN	Ga-face GaN	Ga-face $Al_{0.25}Ga_{0.75}N$
as received	-1.8	+1.8	+2.6
<i>ex-situ</i> cleaning	-1.8	+1.7	+2.6
<i>in-situ</i> cleaning	-2.0	+1.5	+2.5

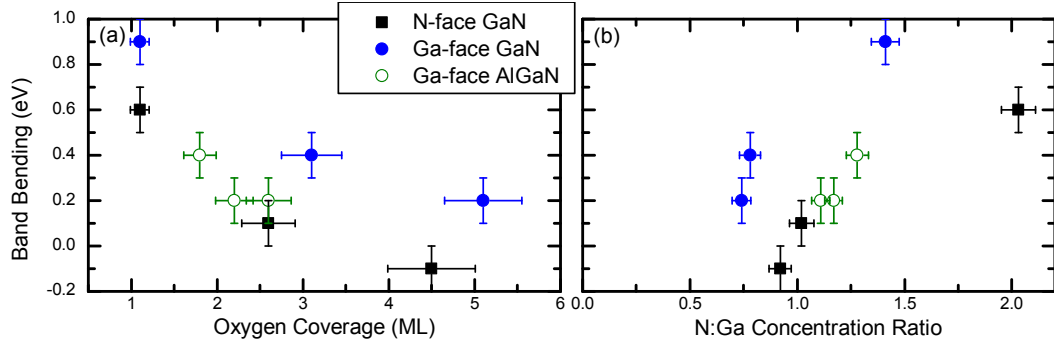


FIG 5.6 (Color online) Correlation between the surface band bending and film content, i.e. oxygen coverage (a) and relative nitrogen surface concentration (b) for N-face GaN, Ga-face GaN, and Ga-face

These results demonstrated there was a relationship between film content and band bending. In particular, it was revealed that band bending was inversely related to oxygen coverage as shown in FIG 5.6a and positively correlated to nitrogen content as shown in FIG 5.6b. In addition, while there was a small disparity in the band bending on the N- and Ga-face—which may be the result of different interface dipoles [37]—all three surfaces were characterized by similar band bending after cleaning, ranging from -0.1 to 0.9 eV. The magnitude of this band bending suggests the presence of an electronic surface state responsible for Fermi level pinning ~ 0.1 to 0.9 eV below the conduction band edge. Moreover, the similarity of the band bending regardless of the polarization bound charge suggests this pinning state can accommodate charge transfer to compensate both positive and negative charge. This pinning state is thus as modeled in FIG 5.7.

III. Discussion

In order to identify the microscopic nature of this pinning state, we have considered surface reconstructions, defect states, and adsorbates; however, direct comparison between experiment and theory is often not a straightforward means of identifying the microscopic nature of a surface.

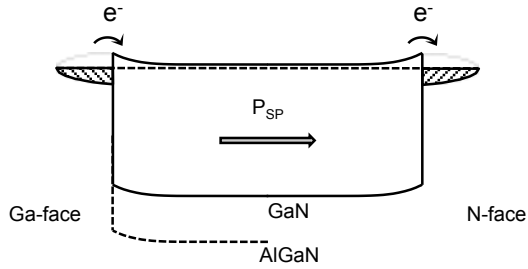


FIG 5.7 Suggested charge transfer model for pinning state on N- and Ga-face GaN and AlGaN.

To date, most related theoretical research has focused on the nature of pinning states on Ga-face GaN as dependent on surface reconstructions. For example, at the Ga-face surface, several (2×2) surface reconstructions are thought to be the most stable, including the gallium adatom, nitrogen adatom, and gallium vacancy structures [38,39]. Nevertheless, most experimental studies do not explicitly agree with these results, where (1×1), (2×2), (2×4), (5×5), and (6×4) reconstructions have all been observed [40-42]. In other words, although the existence of Fermi level pinning surface states has been well documented in GaN-based materials [43-45], a microscopic understanding of these states and their dependence on polarity is still unclear. The discrepancy between experimental and theoretical values is likely the result of two factors. First, a detailed understanding of the theoretical and experimental band structure and related density of states of experimentally relevant GaN surface reconstructions is lacking. Second, theoretical studies generally assume clean, ordered surface conditions when such surfaces rarely exist; actual GaN surfaces are commonly oxidized or metal rich [46]. Recent studies have attempted to rectify this disparity, where Himmerlich *et al.* [46] described experimental and theoretical surface studies to determine the microscopic surface conditions.

However, these perfectly ordered surface reconstructions are not sufficient to explain observed Fermi level pinning; it is thus more likely these results were caused by a defect

state. Given the magnitude of the experimentally observed band bending and the proportional relationship between the band bending and nitrogen concentrations, it has been proposed that the observed pinning state behavior is related to a nitrogen vacancy or gallium dangling bond. These states have been theoretically and experimentally determined to be located ~ 0.37 eV [47] or 0.5 to 0.7 eV [48] below the conduction band edge, which agrees with the experimental findings in this research as well. Furthermore, these defect states have been linked back to device behavior, where Hashizume and Hasegawa [47] demonstrated that passivating GaN-based samples with nitrogen improves device reliability.

While this evidence is suggestive, there are several other factors that may affect the band bending on these samples as well. In particular, we cannot overlook the effects of oxygen coverage. To date, a number of studies have investigated the effects of various *ex-situ* and *in-situ* treatments, including HF, NH_4OH , annealing, as well as N_2 and H_2 plasma [2,49-53]. These studies demonstrate the difficulty in removing native oxygen, likely GaO_2 or Ga_2O_3 [54], from GaN surfaces without damaging the surface reconstruction, as it leaves nitrogen vacancies and/or gallium dangling bonds. Consequently, the cleaning method used should passivate these states. This was the case in this experiment and may explain the reciprocal nature between the oxygen coverage and nitrogen content as shown in FIG 5.6. On the other hand, it may be possible that the oxygen coverage introduces additional charge states. For example, there is evidence that dissociation of H_2O and O_2 on GaN surfaces introduces O and OH^- groups on the surface [55,56]. Removal of this negative charge would thus describe the increase in band bending on the Ga-face as well. It is thus

unclear whether the oxygen coverage contributes to the band bending as well, especially on the N face. Moreover, the plasma used in the cleaning may also influence the band bending. While NH_3 plasma annealing has been shown to reduce oxygen effectively, the plasma may also introduce interstitial nitrogen. Therefore, an additional component of the band bending may not necessarily be attributable to surface reconstructions or point defects.

In reality, these explanations are not mutually exclusive. It is likely that nitrogen interstitials, oxygen adsorbates, and vacancies influence the observed band bending at different cleaning stages. Furthermore, additional research has provided evidence for a fixed charge at the interface [57-59], which may affect the Fermi level pinning position; however, without additional CV measurements, it is difficult to resolve the discrepancy between the electrical measurements and photoemission measurements.

IV. Conclusions

In summary, we have used XPS to determine the net concentration of surface states on N-face GaN, Ga-face GaN, and Ga-face $\text{Al}_{0.25}\text{Ga}_{0.75}\text{N}$. The results demonstrated a similar band bending regardless of the magnitude or direction of the polarization bound charge. (There is a disparity between the N- and Ga-face; however, this difference is likely the result of an interface dipole, which will be explored further.) Specifically, the band bending varies from -0.1 to 0.9 eV on these samples, which indicated that there was likely a Fermi pinning state ~ 0.4 to 0.8 eV below the conduction band minimum. We suggested the observed pinning state was related to the nitrogen related defect or gallium dangling bond, as supported by experimental and literary results—though the state was

not directly observed. This proposal is consistent with other experimental and theoretical research; however, there were likely additional mechanisms that also influence surface states. In particular, it is still unclear how oxygen adsorbates impact the electronic states configuration. Moreover, the plasma cleaning process likely introduced additional nitrogen interstitial or surface states and affected the band bending. Future research will continue to investigate the effects of polarity with more emphasis on surface bonding to better understand the microscopic nature of these states and their effects on the band bending at the surface of GaN-based materials as well as correlate CV and photoemission measurements to resolve potential inconsistencies.

V. Acknowledgements

This research was supported by the Office of Naval Research through the DEFINE MURI program, N00014-10-1-0937.

References

- [1] U. K. Mishra, P. Parikh, and Y. F. Wu, *Proc. IEEE* 90, 1022 (2002).
- [2] B. S. Eller, J. Yang, and R. J. Nemanich, *J. Vac. Sci. Technol. A* 31, 050807 (2013).
- [3] Y. Niiyama, S. Ootomo, J. Li, T. Nomura, S. Kato and T. P. Chow, *Semicond. Sci. Technol.* 25, 125006 (2010).
- [4] E. T. Yu, X. Z. Dang, P. M. Asbeck, S. S. Lau, and G. J. Sullivan, *J. Vac. Sci. Technol. B* 17, 1742 (1999).
- [5] V. A. Savastenko, and A. U. Sheleg, *Phys. Status Solidi A* 48, K135 (1978).
- [6] Y. Takagi, M. Ahart, T. Azuhata, T. Sota, K. Suzuki, and S. Nakamura, *Physica B* 219/220, 547 (1996).
- [7] A. Polian, M. Grimsditch, and I. Grezegory, *J. Appl. Phys.* 79, 3343 (1996).
- [8] R. B. Schwartz, K. Khachatryan, and E. R. Webber, *Appl. Phys. Lett.* 70, 1122 (1997).

- [9] C. Deger, E. Born, H. Angerer, O. Ambacher, M. Stutzmann, J. Hornsteiner, E. Riha, and G. Fischerauer, *Appl. Phys. Lett.* 72, 2400 (1998).
- [10] K. Tsubouchi, and N. Mikoshiba, *IEEE Trans. Sonics Ultrason.* 32, 634 (1985).
- [11] L. E. McNeil, M. Grimsditch, and R. H. French, *J. Am. Ceram. Soc.* 76, 1132 (1993).
- [12] K. Kim, W. R. L. Lambrecht, and B. Segall, *Phys. Rev. B* 53, 16310 (1996).
- [13] A. F. Wright, *J. Appl. Phys.* 82, 2833 (1997).
- [14] O. Ambacher, J. Smart, J. R. Shealy, N. G. Weimann, K. Chu, M. Murphy, W. J. Schaff, L. F. Eastman, R. Dimitrov, L. Wittmer, M. Stutzmann, W. Rieger, and J. Hilsenbeck, *J. Appl. Phys.* 85, 3222 (1999).
- [15] F. Bernardini, V. Fiorentini, and D. Vanderbilt, *Phys. Rev. B* 56, R10024 (1997).
- [16] F. Bernardini, V. Fiorentini, and D. Vanderbilt, *Phys. Rev. B* 63, 193201 (2001).
- [17] Y. Duan, J. Li, S.-S. Li, and J.-B. Xia, *J. Appl. Phys.* 103, 023705 (2008).
- [18] K. Shimada, A. Zempuku, K. Fukiwara, K. Hazu, S. F. Chichibu, M. Hata, H. Sazawa, T. Takada, and T. Sota, *J. Appl. Phys.* 110, 074114 (2011).
- [19] J. Yang, B. S. Eller, C. Zhu, C. England, and R. J. Nemanich, *J. Appl. Phys.* 112, 053710 (2012).
- [20] H. W. Jang, J.-H. Lee, and J.-L. Lee, *Appl. Phys. Lett.* 80, 3955 (2002).
- [21] M. Hong, K. A. Anselm, J. Kwo, H. M. Ng, J. N. Baillargeon, A. R. Kortan, J. P. Mannaerts, A. Y. Cho, C. M. Lee, J. I. Chyi, and T. S. Lay, *J. Vac. Sci. Technol. B* 18, 1453 (2000).
- [22] Y. Q. Wu, T. Shen, P. D. Ye, and G. D. Wilk, *Appl. Phys. Lett.* 90, 143504 (2007).
- [23] W. J. Mecouch, B. P. Wagner, Z. J. Reitmeier, R. F. Davis, C. Pandarinath, B. J. Rodriguez, and R. J. Nemanich, *J. Vac. Sci. Technol. A* 23, 72 (2005).
- [24] V. M. Bermudez, *J. Appl. Phys.* 80, 1190 (1996).
- [25] M. Krawczyk, L. Zommer, A. Jablonski, I. Grzegory, and M. Bockowski *Surf. Sci.* 566-568, 1234 (2004).
- [26] H.-H. Wu, *Ph.D. Thesis* Ohio State University, 2011.
- [27] B. Brennan, X. Qin, H. Dong, J. Kim, and R. M. Wallace, *Appl. Phys. Lett.* 101, 211604 (2012).
- [28] X. Qin, H. Dong, B. Brennan, A. Azacatl, J. Kim, and R. M. Wallace, *Appl. Phys. Lett.* 103, 221604 (2013).
- [29] X. Qin, B. Brennan, H. Dong, J. Kim, C. L. Hinkle, and R. M. Wallace, *J. Appl. Phys.* 113, 244102 (2013).
- [30] NIST *Electron Effective-Attenuation-Length Database, SRD-82, Version 1.1*; National Institute of Standards and Technology: Gaithersburg, MD, 2003.

- [31] R. R. Pela, C. Caetano, M. Marques, L. G. Ferreira, J. Furthmuller, and L. K. Teles, *Appl. Phys. Lett.* 98, 151907 (2011).
- [32] T. E. Cook, Jr., C. C. Fulton, W. J. Mecouch, R. F. Davis, G. Lucovsky, and R. J. Nemanich, *J. Appl. Phys.* 94, 7155 (2003).
- [33] J. R. Waldrop, and R. W. Grant, *Appl. Phys. Lett.* 68, 2879 (1996).
- [34] J. Hedman, and N. Mårtensson, *Phys. Scr.* 22, 176 (1980).
- [35] Y. L. Chiou, and C. T. Lee, *IEEE Trans. Electron Devices* 58, 3869 (2011).
- [36] M. H. S. Owen, M. A. Bhuiyan, Q. Zhou, Z. Zhang, J. S. Pan, and Y.-C. Yeo, *Appl. Phys. Lett.* 104, 091605 (2014).
- [37] J. Yang, B. S. Eller, and R. J. Nemanich, *J. Vac. Sci. Technol. A* 32, 021514 (2014).
- [38] J. E. Northrup, J. Neugebauer, R. M. Feenstra, and A. R. Smith, *Phys. Rev. B* 61, 9932 (2000).
- [39] D. Segev, and C. G. Van de Walle, *Surf. Sci.* 601, L15 (2007).
- [40] A. R. Smith, R. M. Feenstra, D. W. Greve, M.-S. Shin, M. Skowronski, J. Neugebauer, and J. E. Northrup, *Surf. Sci.* 423, 70 (1999).
- [41] S. W. King, C. Ronning, R. F. Davis, M. C. Benjamin, and R. J. Nemanich, *J. Appl. Phys.* 84, 2086 (1998).
- [42] S. Vézian, F. Semond, J. Massies, D. W. Bullock, Z. Ding, and P. M. Thibado, *Surf. Sci.* 541, 242 (2003).
- [43] A. R. Smith, R. M. Feenstra, D. W. Greve, M. S. Shin, M. Skowronski, J. Neugebauer, and J. E. Northrup, *J. Vac. Sci. Tech. B* 16, 2242 (1998).
- [44] C. G. Van de Walle and D. Segev, *J. Appl. Phys.* 101, 081704 (2007).
- [45] L. Ivanova, S. Borisova, H. Eisele, M. Dahne, A. Laubsch, and Ph. Eben, *Appl. Phys. Lett.* 93, 192110 (2008).
- [46] M. Himmerlich, L. Lymperakis, R. Gutt, P. Lorenz, J. Neugebauer, and S. Krischok, *Phys. Rev. B* 88, 125304 (2013).
- [47] T. Hashizume and H. Hasegawa, *Appl. Surf. Sci.* 234, 387 (2004).
- [48] D. Segev, and C. G. Van de Walle, *Europhys. Lett.* 76, 305 (2006).
- [49] S. W. King, J. P. Barnak, M. D. Bremser, K. M. Tracy, C. Ronning, R. F. Davis, and R. J. Nemanich, *J. Appl. Phys.* 84, 5248 (1998).
- [50] T. Hashizume, S. Ootomo, T. Inagaki, and H. Hasegawa, *J. Vac. Sci. Technol. B* 21, 1828 (2003).
- [51] R. D. Long, and P. C. McIntyre, *Mater.* 5, 1297 (2012).

- [52] C. L. Hu, J. Q. Li, Y. F. Zhang, X. L. Hu, N. X. Lu, and Y. Chen, *Chem. Phys. Lett.* 424, 273 (2006).
- [53] R. Meunier, A. Torres, and M. Charles, *ECS Trans.* 50, 451 (2013).
- [54] C. L. Hu, J. Q. Li, Y. F. Zhang, X. L. Hu, N. X. Lu, and Y. Chen, *Chem. Phys. Lett.* 424, 273 (2006).
- [55] J. Elsner, R. Gutierrez, B. Hourahine, R. Jones, M. Haugk, and Th. Frauenheim, *Solid State Comm.* 108, 953 (1998).
- [56] V. M. Bermudez, and J. P. Long, *Surf. Sci.* 450, 98 (2000).
- [57] M. Esposito, S. Krishnamoorthy, D. N. Nath, S. Bajaj, T.-H. Hung, and S. Rajan, *Appl. Phys. Lett.* 99, 1233503 (2011).
- [58] S. Ganguly, J. Verma, G. Li, T. Zimmermann, H. Xing, and D. Jena. *Appl. Phys. Lett.* 99, 193504 (2011).
- [59] J. Son, V. Chobpattana, B. M. McSkimming, and S. Stemmer, *Appl. Phys. Lett.* 101, 102905 (2012).

CHAPTER 6. CHARACTERIZATION OF PLASMA-ENHANCED ATOMIC LAYER DEPOSITION OF SiO₂ USING TRIS(DIMETHYLAMINO)SILANE ON GAN

Abstract. Thin silicon oxide (SiO₂) films were deposited by remote oxygen plasma-enhanced atomic layer deposition (PEALD) using tris(dimethylamino)silane (TDMAS) on GaN. The growth conditions were varied, including the precursor pulse time, nitrogen purge time, and substrate temperature to ensure self-saturating, self-limiting growth. Respective growth rates of 1.1 Å/cycle, 0.6 Å/cycle, and ~3.0 Å/cycle were determined at 30°C, 270°C, and 550°C. In addition, the growth rates were affected by a N₂/H₂ plasma pretreatment, which enhanced nucleation. At 550°C, the deposition was characterized by thermal decomposition as indicated by an increased RMS height. Elevated-temperature depositions were also characterized by the growth of a subcutaneous oxide layer at the interface. The effective valence band offsets of SiO₂/GaN interface were also determined from x-ray photoelectron spectroscopy, which decreased slightly with deposition temperature. Since band offsets are typically constant for a given interface, the difference in the measured band offsets is likely related to a potential drop across this subcutaneous oxide layer mentioned. In addition, electrical characterization suggests that the oxide layer may also reduce the electrical breakdown field of the dielectric and increase the gate leakage while simultaneously decreasing the hysteresis.

To be submitted in collaboration with Brianna S. Eller, Wenwen Li, Sarah Rupprecht, Srabanti Chowdhury, and Robert J. Nemanich (2015).

GaN shows significant promise for high-electron-mobility transistors (HEMTs) in high-power and high-frequency applications; however, despite the advantages, GaN is still limited by a relatively high leakage current, which reduces the breakdown voltage, impedes power efficiency, and increases noise. Metal-oxide- and insulator-semiconductor HEMTs (MOSHEMTs and MISHEMTs) have therefore been used to help mitigate this problem. SiO₂ is a common oxide for these devices, where the high band gap (8.9 eV) can help reduce the leakage current by ~4 orders of magnitude in addition to increasing the gate voltage that results in current collapse [1-11].

The effectiveness of the SiO₂ dielectric is linked to the deposition method. To date, high-quality SiO₂ is most commonly formed by thermal oxidation of Si substrates at temperatures >800°C in dry O₂ ambient. However, this formation method thus requires high temperatures, long processing times, and Si substrates. As a result, there is a need to

develop alternative methods for SiO₂ deposition, which are applicable on GaN with lower deposition temperatures and shorter processing times. Alternative techniques developed include PECVD, e-beam evaporation, and sputtering; however, these methods have not provided high-quality films, where the resulting films are characterized by non-stoichiometric concentrations, low breakdown fields, and high defect densities [12]. Alternatively, one of the more promising techniques for high-quality, thin-film growth is atomic layer deposition (ALD). ALD is based on sequential, self-limiting surface reactions, where the substrate is exposed to two precursors separately (i.e. a Si precursor and an oxidant) that react with the surface until saturation. After exposure to each precursor, the chamber is purged with an inert gas (e.g. N₂) to prevent CVD-like reactions between the reactants. This technique deposits uniform and conformal films with precise thickness control and often leads to improved film properties, such as a low defect density and high breakdown field [13].

However despite its potential, the ALD of SiO₂ has not been straightforward, where the reactivity of Si precursors has proven challenging. Generally, the ALD of oxides utilizes H₂O as the oxidizing reactant; however, Si precursors do not react with H₂O at lower temperatures. Some techniques have been developed to circumvent these issues using high temperatures (>300°C), long reactant exposure times [14-16], as well as catalysts such as pyridine and Al [17-19]. However, such parameters limit the versatility of the process mitigating many of the advantages associated with ALD. In addition to altering deposition parameters, research also investigated various surface reactions by varying the

reactants. The variety of Si precursors and alternative oxidation reactants is summarized in TABLE 6.1.

In particular, oxygen plasma-enhanced ALD (PEALD) is promising. In this type of ALD, the surface reaction is oxidized by plasma rather than H_2O —as is standard with traditional ALD. O_2 plasma may prove more robust in decreasing reactant exposure times and deposition temperatures, given the reactivity and versatility of the oxygen species. Consequently, PEALD allows for the use of more diverse precursors with relatively high thermal and chemical stabilities [69]. As shown in TABLE 6.1, there have been a few precursors used with oxygen PEALD, including BDEAS ($\text{SiH}_2(\text{NEt}_2)_2$), BTBAS ($\text{SiH}_2(\text{NH}^t\text{Bu})_2$), and TEOS ($\text{Si}(\text{OEt})_4$). Though PEALD growth has been achieved with BDEAS and TEOS, long reactant exposure times were still required, especially at lower temperatures [56,70]. BTBAS, on the other hand, demonstrated much better reactivity but is also toxic [58]. In this work, we have thus investigated an alternative precursor, tris(dimethylamino)silane (TDMAS), where a survey of various silicon precursors [63] revealed TDMAS displayed the highest reactivity with H_2O_2 at lower temperatures. In addition to oxidizing readily at low temperatures, TDMAS ($\text{SiH}(\text{N}(\text{CH}_3)_2)_3$) also vaporizes easily at room temperature. TDMAS may, therefore, prove an important precursor in ameliorating some of the issues with SiO_2 ALD, including the lower temperature restraints and longer reactant exposure times [61].

TABLE 6.1 Summary of ALD research with a SiO₂ growth.

Reactant A	Reactant B	References
SiCl ₄	H ₂ O	20-27
SiCl ₄	H ₂ O + cat.	17,24, 28-33
Si ₂ Cl ₆	O ₃	34
SiCl ₃ H	H ₂ O	35
SiCl ₂ H ₂	O ₃	36,37
SiH ₄	N ₂ O	38
Si(OMe) ₄	H ₂ O	39
Si(OMe) ₄	H ₂ O + cat.	40
Si(OEt) ₄	H ₂ O + cat.	41,42
Si(OEt) ₄	O ₂	43-45
Si(OEt) ₃ (CH ₂) ₃ NH ₂	H ₂ O + O ₃	46-51
Si(O ⁱ Pr) ₃ OH	AlMe ₃	52,53
SiH ₂ (N(CH ₃) ₂) ₂	O ₃	54,55
SiH ₂ (NH ⁱ Bu) ₂	O ₂	56
SiH ₂ (NEt ₂) ₂	O ₂	57
SiH ₂ (NEt ₂) ₂	O ₃	58
SiH(N(CH ₃) ₂) ₃	O ₂	9
SiH(N(CH ₃) ₂) ₃	O ₃	12,54,55,59-62
SiH(N(CH ₃) ₂) ₃	H ₂ O	63
SiH(N(CH ₃) ₂) ₃	H ₂ O ₂	63,64
Si(NCO) ₄	H ₂ O	65
Si(NCO) ₄	NEt ₃	66
MeOSi(NCO) ₃	H ₂ O ₂	67,68

In this study, we have focused on the PEALD SiO₂—deposited using TDMAS and O₂—on GaN, with particular attention to not only the deposition characteristics but also the resulting film and interface quality. The growth rates, which relates to the reactivity of the precursor, were determined as dependent on deposition conditions and temperature. *In-situ* x-ray photoelectron spectroscopy was used to determine film thicknesses, atomic concentrations, and band offsets. These measurements were supplemented with Rutherford backscattering to confirm atomic concentrations and x-ray reflectivity to confirm film thicknesses. In addition, electrical measurements, i.e. IV and CV curves, were used to determine the deposition temperature effects on film on breakdown and other electrical characteristics of the films.

I. Experiment

In this study, TDMAS was used to deposit ~ 5 nm SiO_2 on GaN in a remote plasma-enhanced ALD (PEALD) chamber as shown in FIG 6.1. Generally, this system was maintained at a background pressure of $\sim 6.0 \times 10^{-8}$ Torr. During deposition, oxygen plasma was ignited with 13.56 MHz rf-excitation applied at 200 W to a helical copper coil wrapped around a 32 mm diameter quartz tube and maintained at ~ 100 mTorr with a flow rate of 35 sccm. The bubbler temperature was maintained at 33°C , and the lines between the bubbler and the chamber were heated to $\sim 40^\circ\text{C}$ to prevent precursor condensation. These temperatures ensured the TDMAS was maintained in its liquid state with a melting point at -90°C and boiling point at 148°C . Moreover, TDMAS has a suitable vapor pressure near room temperature (~ 7.1 Torr at 25°C), where the slight increase to 33°C ensures consistency. The ALD system software controlled the pulse times of the gas phase chemicals, where the pulse time varied from 0.8 to 2.0 s for the precursor, 15 to 40 s for the N_2 purge gas, and 4 to 20 s for the O_2 plasma. The substrate temperature was also varied between 30°C and 550°C .

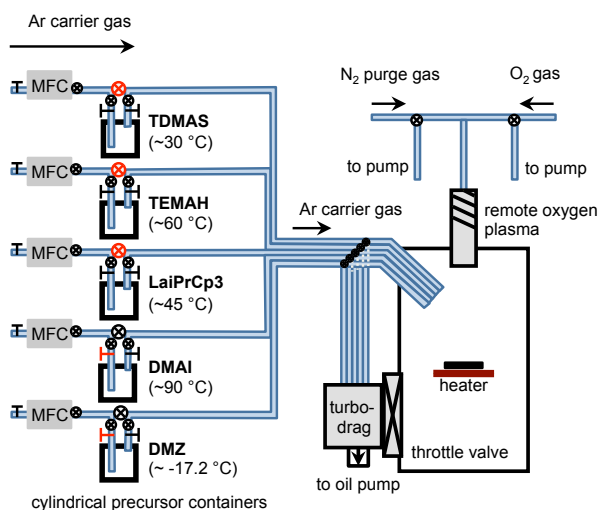


FIG 6.1 Schematic of remote oxygen-PEALD chamber.

After growth, samples were characterized by *in-situ* XPS. In this measurement, Al K α (=1486.6 eV) x-rays were used as light source, which determined the kinetic energy of the Ga 3s core level electrons as ~1325 eV and Si 2s core level electrons as ~1332 eV. This technique can be used to characterize the film composition as well as the band offsets at the interface as demonstrated in previous work [71,72]. In addition, the intensity ratio of the Si 2s peak from the ALD-deposited SiO₂, and the Ga 3s peak from the GaN substrate ($I_{Si}^{exp}/I_{Ga}^{exp}$) was used to measure the thickness of ultrathin films according to the following relation:

$$d_{SiO_2} = \ln \left[\frac{1}{\beta} \frac{I_{Si}^{exp}}{I_{Ga}^{exp}} + 1 \right] \lambda_{Si} \sin\theta, \quad (1)$$

where β is the intensity ratio of bulk GaN to bulk SiO₂, (~0.931), θ is the angle between the sample surface plane and electron analyzer (90°), and λ_{SiO_2} is the attenuation length of the Ga 3s electrons in SiO₂. Because of the proximity of the Ga 3s and Si 2s core levels, the attenuation length of the Ga 3s electrons is close to that of the Si 2s photoelectrons, which is given as 2.8 nm [73,74]. The thickness was then divided by the number of cycles to determine the growth per cycle (GPC). Rutherford backscattering (RBS), and x-ray reflectivity (XRR), were used to calibrate and confirm thickness measurements as well.

In addition, CV measurements were used to supplement the results. In this case, square centimeter sections of ~450 μ m-thick, Si-doped ($\sim 8 \times 10^{17} \text{ cm}^{-3}$), bulk GaN grown via hydride vapor phase epitaxy were used as substrates. Substrates were processed with the same *ex-situ* wet chemical treatment and then exposed to an additional N₂/H₂ remote plasma treatment at 680°C for 15 min. This additional cleaning step reduced the native

oxygen coverage to ~ 1.0 ML [72] and the carbon contamination below the detection limit of the XPS. Thick films (~ 40 nm) were then deposited using the ALD process previously described at 30°C , 270°C , and 550°C . Each sample was then processed with a post-deposition anneal in N_2 ambient at 400°C . These samples were etched using a F-based reactive ion etch and Cl-based inductively coupled plasma prior to metal deposition. E-beam Ni/Au (30/300 nm) was used for the gate electrodes, and Al/Au (30/300 nm) was used for the backside ohmic contacts. Subsequent IV and CV behavior were measured using a Keithley 4200 SCS Parametric Analyzer. The forward bias was applied to the gate electrodes to determine the electrical characteristics of the oxide. CV measurements were performed at 1 MHz with an AC modulation of 30 mV.

II. Results

The GPC as related to the timing of the gas phases is shown in FIG 6.2, where the timing sequence was modified for the precursor, oxygen plasma, and nitrogen purge for room temperature depositions. Longer reactant pulse times ensured a complete surface reaction as indicated by the saturation of the growth rate as shown in FIG 6.2a. This process demonstrated the saturated growth rate was achieved with a dosing time >1.6 s and an oxygen plasma pulse time >16 s. (See FIG 6.2b.) In addition, the nitrogen purge time ensured the removal of residual reactants, thus preventing CVD-like reactions in the chamber. These results are summarized in FIG 6.2c and show a purge time of 30 s as sufficient.

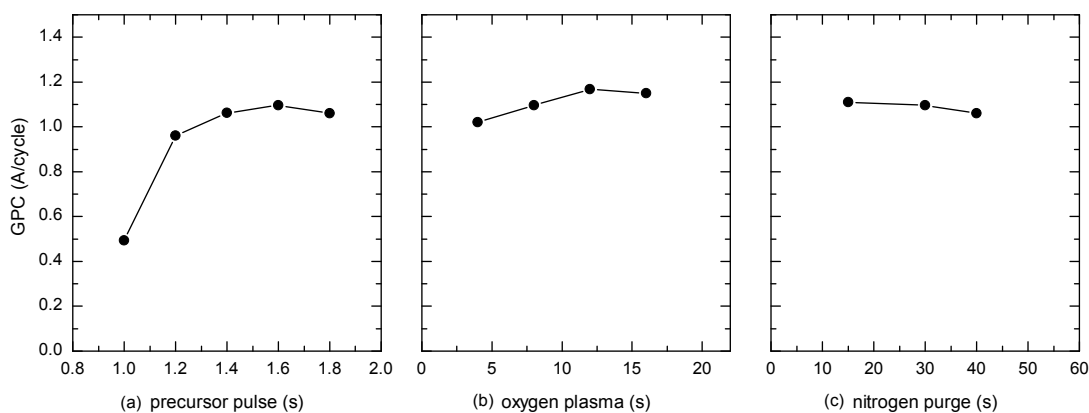


FIG 6.2 Growth per cycle (GPC) of ALD SiO₂ as a function of TDMAS (a), oxygen plasma (b), and nitrogen pulse (c) times with a constant substrate temperature of 30°C. The timing for each respective gas phase was 1.6 s, 16 s, and 30 s when not otherwise specified.

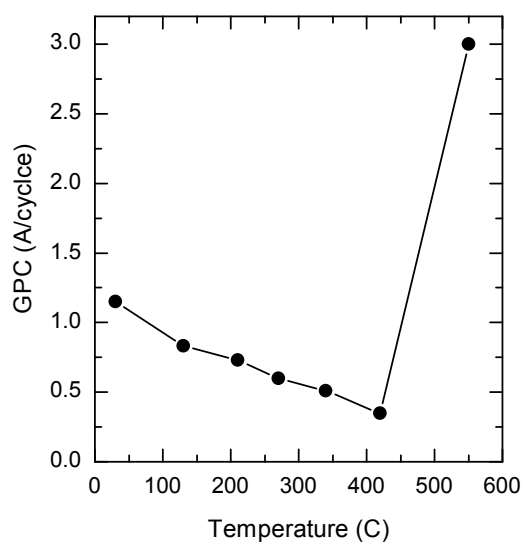


FIG 6.3 The growth per cycle (GPC) of ALD SiO₂ at substrate temperatures varying from 30 to 550°C, where the precursor dosing time was 1.6 s, oxygen plasma time was 16 s, and nitrogen purge time was 30s. Results show no apparent ALD growth window and thermal decomposition at 550°C.

The temperature dependence was also investigated under these saturation conditions. This relationship is shown in FIG 6.3, where the films were deposited using a precursor pulse time of 1.6 s, oxygen plasma time of 8 s, and nitrogen purge time of 30 s. It was demonstrated that the largest growth rate of 1.25 Å/cycle occurred at lower substrate temperatures with no well-defined growth window. Increasing temperature resulted in a

decreased growth rate for temperatures <450°C. At higher temperatures, the growth rate increased dramatically as corresponds to thermal decomposition of TDMAS and is thus not considered self-limiting ALD.

TABLE 6.2 SiO₂ content and deposition characteristics determined as by RBS and XPS. (Thickness measurements were confirmed with XRR; however, the sample deposited at 550°C did not provide reliable results, most likely due to contamination in the film.)

deposition temperature	growth rate (Å/cycle)	Si:O ratio	contamination (% concentration)
30°C	1.1	1:2	undetectable (<1%)
270°C	0.6	1:2	undetectable (<1%)
550°C	~3.0	1:2	~2% molybdenum ~2% nitrogen

Additional measurements were conducted at three different temperatures, including a low temperature at 30°C that gives the achievable highest growth rate, a middle-range temperature at 270°C that is commonly used for other TDMAS-ALD processes, and a high-temperature at 550°C that corresponds to an alternative growth mechanism. Thick SiO₂ layers were deposited on these samples such that Rutherford backscattering (RBS) and x-ray reflectivity measurements could be acquired. (See FIG 6.4.) These results, summarized in TABLE 6.2, showed temperature did not greatly affect the stoichiometry or density of the films. However, there was an increase in contamination for the thermally decomposed film, where small concentrations of nitrogen from the precursor and molybdenum from the sample holder were detected.

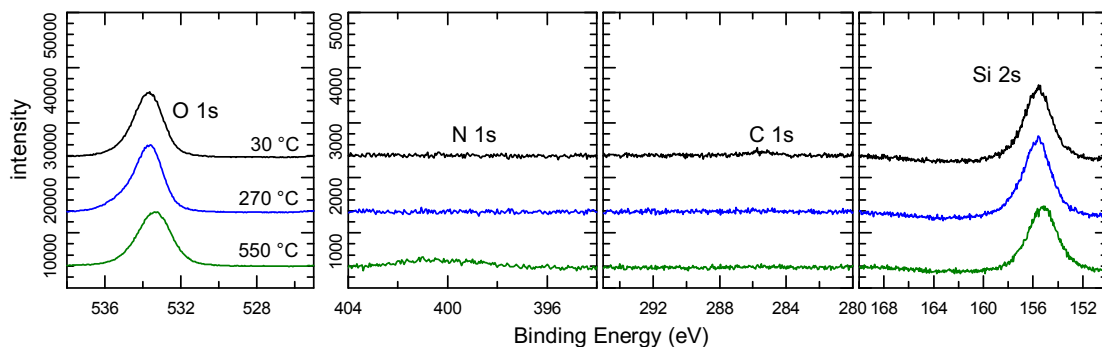


FIG 6.4 O 1s, N 1s, C 1s, and Si 2s XPS spectra of ~30 nm SiO₂ deposited at 30°C, 270°C, and 550°C.

TABLE 6.3 Interface characteristics of SiO₂ as deposited by PEALD, where an increase in temperature results in a decrease in the valence band offset (VBO) and increase in Ga-O concentration, which likely relates to the subcutaneous growth of an interfacial Ga₂O₃ layer. (In this case, the % concentration is relative to the total oxygen content in the sample as measured by XPS.)

deposition temperature	Ga-O bonding (% concentration)	Ga ₂ O ₃ thickness (nm)	VBO (eV)
30°C	11%	0.1	3.5
270°C	11%	0.4	3.3
550°C	25%	0.7	3.0

In addition, a more detailed analysis of the thin films demonstrated that increasing the deposition temperature resulted in an increase of a secondary O 1s peak as shown in FIG 6.5; however, this peak is not present for the thicker films, where the substrate is no longer detectable. Thus, this secondary peak relates to the interface and suggests the growth of a subcutaneous oxide layer as dependent on temperature. In addition, the effective valence band offsets (VBO) of the materials deposited at different temperatures varied with temperature; in particular, the respective VBO were determined to be 3.5 eV, 3.2 eV, and 3.1 eV for films deposited at 30°C, 270°C, and 550°C as shown in TABLE 6.3. (See previous work for the details of this calculation [71,72].) The discrepancy is likely related to a potential drop across the interface layer as will be discussed.

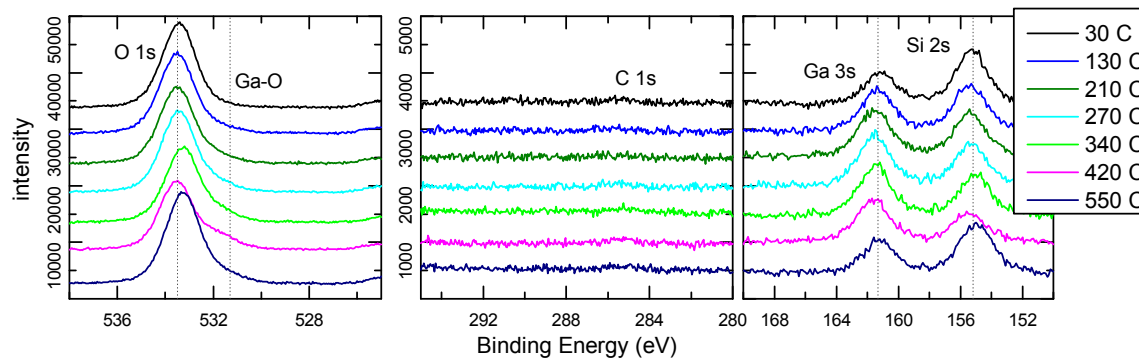


FIG 6.5 O 1s, C 1s, Si 2s, and Ga 3s core level spectra for 40 cycles of SiO₂ on GaN for various deposition temperatures. (NOTE: Given the large growth rate at 550°C, samples grown at this temperature were grown with only 20 cycles such that the substrate was still detectable.)

AFM images were also collected before and after deposition of ~30 nm film. These images are shown in FIG 6.6. After deposition, the RMS height did not increase significantly for films deposition at 30 and 270°C, suggesting deposition was uniform and conformal. However, within the thermal decomposition regimes, the RMS roughness increased significantly, suggesting that at 550°C the films lose uniformity and conformality associated with ALD.

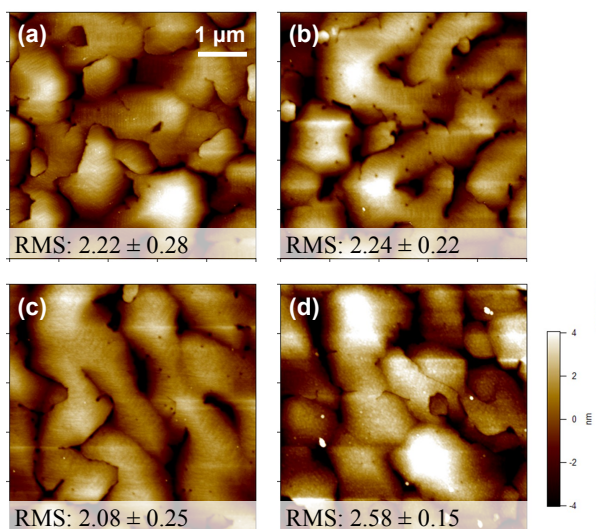


FIG 6.6 5- μm^2 AFM images of (a) wet-chemical cleaned GaN surface as well as ~30 nm SiO₂ films as deposited at (b) 30°C, (c) 270°C, and (d) 550°C. The RMS heights were averaged for three different positions on the sample. AFM images provided courtesy of Sarah Rupprecht.

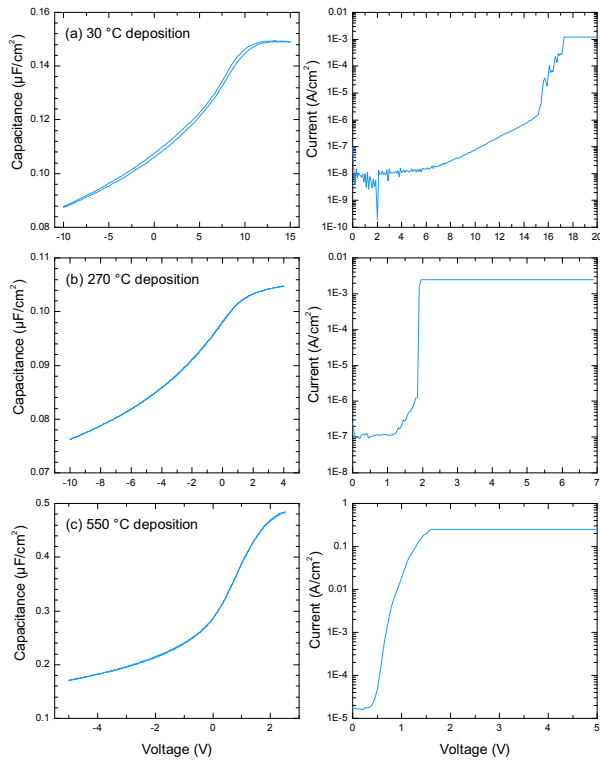


FIG 6.7 CV and IV curves for (a) 31 nm SiO₂ films deposited at 30°C, (b) 42 nm SiO₂ films deposited at 270°C, and (c) 11 nm SiO₂ films deposited at 550°C on GaN. Electrical measurements provided courtesy of Wenwen Li.

Electrical characterization of similar samples is summarized in TABLE 6.4. It is worth noting the growth rate of samples prepared in the ALD regime increased slightly, which is likely related to the surface plasma pretreatment. In addition, these samples were prepared using an Inconel sample holder to prevent molybdenum contamination at high temperatures (550°C). The resulting CV and IV curves are shown in FIG 6.7. From the typical IV curves, the breakdown voltage of ALD SiO₂ is determined to be 5.26 MV/cm, 0.42 MV/cm, and 0.64 MV/cm for films deposited at 30°C, 270°C, and 550°C, respectively. In addition, the CV curves were obtained sweeping from depletion to accumulation and then accumulation to depletion, where only RT-SiO₂/GaN was characterized by a hysteresis under non-UV conditions.

TABLE 6.4 Summary of electrical characteristics as relates to deposition temperature, including breakdown voltage in MV/cm, leakage current in A/cm², and hysteresis in V. The ALD SiO₂ dielectric layers were not the same thickness due to changes in the growth rate from the plasma pretreatment as noted.

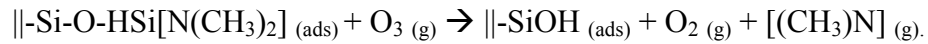
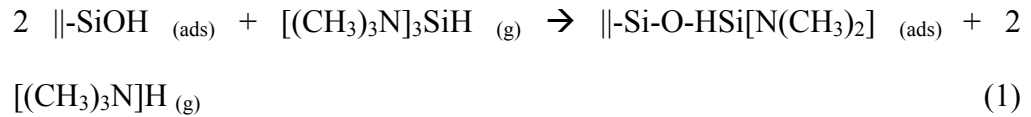
deposition temperature	growth rate (Å/cycle)	breakdown voltage (MV/cm)	leakage current (A/cm ²)	hysteresis (V)
30°C	1.2	5.26	1×10 ⁻⁸	0.4
270°C	0.8	0.42	2×10 ⁻⁷	0.0
550°C	1.1	0.64	7×10 ⁻⁵	0.0

III. Discussion

The growth of SiO₂ using ALD with TDMAS and O₂ plasma is thus obtainable at both high and low temperatures; however, the growth, electrical, and interface characteristics are affected as will be discussed.

A. Chemisorption

Kinoshita *et al.* [75] identified the specific chemisorption mechanism for TDMAS and O₃ at room temperature using *in-situ* infrared adsorption spectroscopy with multiple internal reflection geometry. The reported two-step chemisorption mechanism was as follows:



Assuming that the first half reaction is consistent, the second equation can then be adapted for O₂ plasma. Maintaining stoichiometry, the second half reaction is likely as follows in an O₂ plasma system:



A schematic representation of this reaction is shown in FIG 6.8.

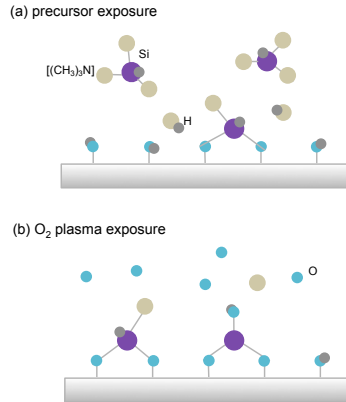


FIG 6.8 Chemisorption mechanism for TDMAS on an OH-terminated surface.

B. Growth Characteristics

The growth of SiO₂ with TDMAS satisfies the criteria of ALD growth at temperatures <450°C. Experimental results show the GPC under ALD conditions is 0.11 nm at 30°C and 0.06 nm at 270°C. The height of a traditional monolayer,

$$\overline{h^{ml}} = \left(\frac{M}{\rho N_A} \right)^{1/3} = 0.34 \text{ nm}, \quad (3)$$

and the number of Si atoms in a traditional monolayer,

$$\overline{c_{Si}^{ml}} = \left(\frac{\rho N_A}{M} \right)^{2/3} = 8.9 \text{ Si atoms nm}^{-3}. \quad (4)$$

This assumes that the density of SiO₂, ρ , is $2.65 \times 10^{-21} \text{ g nm}^{-3}$, the molar mass of SiO₂, M , is 60.08 g mol^{-1} , and N_A is Avogadro's number. The respective GPCs at 30°C and 270°C are thus ~32% and 18% of a traditional monolayer.

The decrease with temperature was surprising; given the reactivity issues commonly mentioned for Si precursors, the Si precursor was expected to be less reactive at lower temperatures. In general, a decrease of GPC with temperature generally occurs when thermal energy results in a decrease in the concentration of reactive surface sites [76-78];

however, the behavior can also be related to thermal desorption of the precursor. For other ALD processes, oxygen-plasma exposed SiO₂ does not reduce nucleation [72], therefore, the latter process seems more likely and could possibly relate to some of the other difficulties mentioned with low-temperature ALD, where low-temperature is generally considered ~200°C.

It is also worth noting that samples prepared with a N₂/H₂ plasma pretreatment were characterized by a seemingly larger growth rate: 0.12 and 0.08 nm for films deposited at 30°C and 270°C, respectively. The measured growth per cycle thus increased by 9 and 33%. However, a surface pretreatment should only affect the first few ALD cycles, where the substrate conditions are exposed to the ALD reactions. It is, therefore, likely the plasma surface pretreatment increased the nucleation at the surface. This treatment thus enhanced the growth rate for the first few ALD cycles. In addition, the growth rate at 270°C is similar to other reports at 275°C, which were determined to be 0.075 and 0.077 nm/cycle using plasma excited water vapor [74] and ozone [55], respectively.

At high temperatures (~450°C), the growth rate is significantly less consistent where the growth rate varied between 0.12-0.30 nm, which corresponds to 35-88% of an amorphous SiO₂ monolayer. Moreover, the roughness of these films increase significantly and demonstrate varied concentrations of nitrogen and molybdenum contamination—though the Mo contamination can be eliminated with the use of an alternative sample holder. The inconsistent growth characteristics in this regime are likely related to the decomposition of the precursor, which cannot be precisely controlled like a ‘true’ ALD process.

C. Interface Characteristics

The measured band offset results were unexpected, where the observed valence band offset appeared to decrease with the oxide deposition temperature; given that band offsets are determined by bonding at the interface, these values are not expected to vary for the same materials.

It is, therefore, likely the plasma exposure during ALD oxidizes GaN substrates subcutaneously. This hypothesis is further supported by the increase of the secondary oxygen peak mentioned, which likely relates to Ga-O bonding. The increase of this peak with temperature, suggests temperature assists the subcutaneous oxidation process. Consequently, the growth of a Ga_2O_3 layer affects the observed valence band offset if

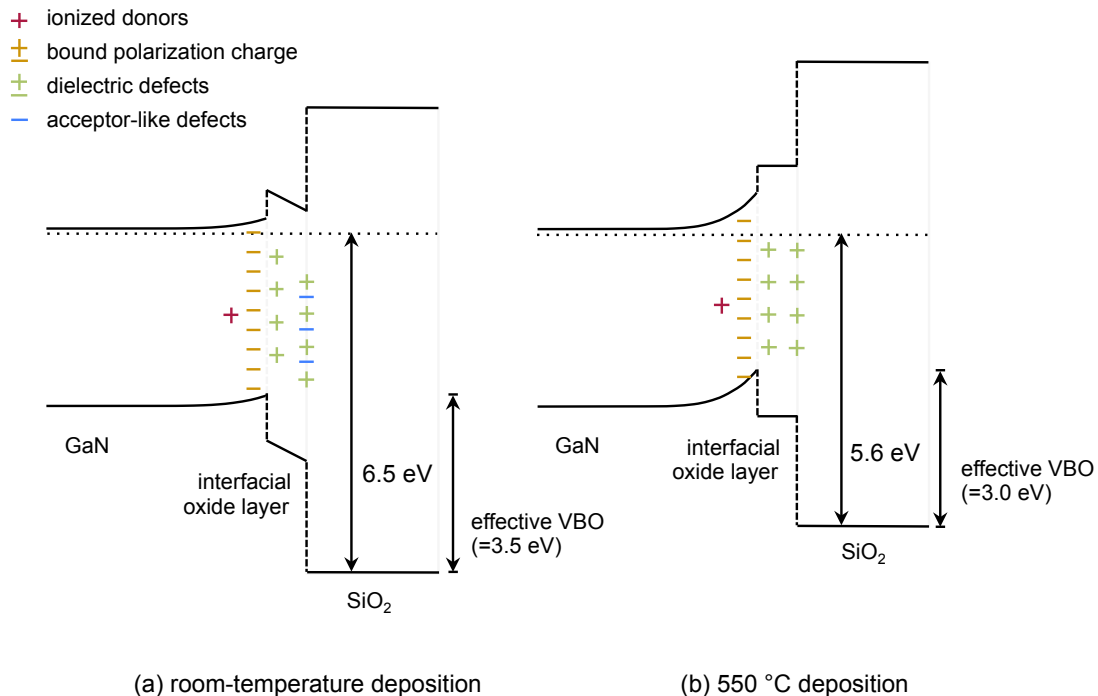


FIG 6.9 Schematic of the effective band offset measurements of SiO_2/GaN , with a subcutaneous oxide layer. The thickness of the Ga_2O_3 layer increases with temperature; however, the potential drop decreases across this layer with temperature as well. This decrease is related to the removal of acceptor-like defects that are introduced by the O_2 plasma and affected high-temperature annealing.

there is a potential drop across the interfacial layer.

Other reports suggest the VBO between SiO₂/GaN should be 3.1 eV [72,79]; therefore, the explanation given above is not complete, as it would suggest a thinner Ga₂O₃ layer would result in a more accurate measurement of the band offset. In other words, room-temperature films would be characterized by a valence band offset of 3.1 eV, rather than the high-temperature films where the oxide is thicker. However, previous work [71] has also noted that exposure to oxygen plasma during the ALD process introduces acceptor-like defects near the interface. These defects can then be removed with high-temperature annealing. It is, thus, likely the difference in the effective band offsets is more closely related to the concentration of acceptor-like defects induced rather than the thickness of the Ga₂O₃ layer. This supports the observed behavior, where high-temperature deposition removes the acceptor-like defect charge present near the Ga₂O₃, thus reducing the potential drop. As a result of the smaller electrical field in this layer, the measured band offsets for the high-temperature deposition are more representative of the expected VBO at the SiO₂/GaN interface as shown in FIG 6.9.

D. Electrical Characteristics

The electrical characteristics can also relate to the deposition temperature of the films. For example, the low breakdown of the 550°C sample is likely linked to the increased roughness related to the thermal decomposition during the deposition process, where surface roughness has been linked to lower breakdown fields [80]. High-temperature ALD using TDMAS does not therefore provide high-quality films for electrical applications.

The highest-quality oxide in terms of the breakdown voltage was obtained at room temperature, giving 5.3 MV/cm. This breakdown voltage is larger than the breakdown of SiO₂ reported for other deposition methods, where the breakdown voltage for PECVD SiO₂ is reported ~2.5-3.5 MV/cm [2,6] and e-beam SiO₂ is reported as 1.8 MV/cm [2]. On the other hand, this value is still smaller than expected for ALD SiO₂, which has been reported as 10 MV/cm [9,81]. Since breakdown voltage is characteristic of the quality of the film as well as the interface, pretreatment conditions that affect the interface have been shown to have significant effects on the breakdown voltage. Work by Takashima *et al.* [9] demonstrated that TDMAS and O₂ plasma films on GaN ranged from 6-10 MV/cm as dependent on the surface treatment conditions prior to PEALD. This suggests that the lower breakdown voltage reported here is a result of the interface quality and a higher breakdown voltage would, therefore, likely be achievable with additional optimization of the PEALD SiO₂ processes, such as a difference surface pretreatment or alternative post-deposition anneal.

The room temperature deposited films also provided the most desirable electrical behavior not only in terms of breakdown voltage but also in terms of leakage current, which was an order of magnitude lower than that of the 270°C-deposited films. While both deposition temperatures result in comparable films in terms of stoichiometry, density, film impurity concentrations, conformality, and uniformity, the main difference is linked to the growth of the subcutaneous oxide as mentioned. The comparative behavior of these films would suggest the subcutaneous oxide helps reduce the hysteresis at the expense of a lower breakdown voltage and higher gate leakage.

IV. Conclusions

Stoichiometric SiO₂ films were successfully deposited with TDMAS using remote plasma-enhanced ALD on GaN. The results suggest the optimal parameters require a precursor pulse time >1.6 s, an oxygen plasma time >16 s, and a nitrogen purge time >30 s. The growth rate was not characterized by an ALD window but showed a decrease in growth rate between 30 and 450°C; at temperatures >450°C, the growth rate increases dramatically as a result of thermal decomposition. These high-temperature films were characterized by an inconsistent growth rate, increased roughness, low breakdown field, and molybdenum and nitrogen impurities. For growth temperatures below the thermal decomposition regime, a plasma pretreatment increased the initial nucleation. These films display no carbon or other impurities within the detection limit of x-ray photoelectron spectroscopy as well as an improved breakdown field. In addition, the deposition temperature affects the interface characteristics, where higher temperatures result in subcutaneous oxide growth. In addition, the plasma in the ALD process introduces acceptor-like defects, which introduce a potential drop across this interfacial layer that is affected with annealing. Consequently, the effective band offsets appear to decrease with temperature. Moreover, it is likely that the subcutaneous oxide reduces the electrical quality of the interface in terms of breakdown voltage and leakage current. Therefore, lower temperature SiO₂ PEALD processes may provide higher quality oxides for electrical applications.

V. Acknowledgements

This research is supported by the Office of Naval Research through the DEFINE MURI program, N00014-10-1-0937 as well as the Advanced Research Projects Agency-Energy. We also appreciate the Rutherford backscattering spectrometry measurements provided by Barry Wilkens as well as the x-ray reflectivity measurements provided by Emmanuel Soignard at the Center for Solid-State Science.

References

- [1] M. Sawada, T. Sawada, Y. Yamagata, K. Imai, H. Kimura, M. Yoshino, K. Iizuka, and H. Tomozawa, *J. Cryst. Growth* 189/190, 706 (1998).
- [2] S. Arulkumaran, T. Egawa, H. Ishikawa, T. Jimbo, and M. Umeno, *Appl. Phys. Lett.* 73, 809 (1998).
- [3] B. M. Green, K. K. Chu, E. M. Chumbes, J. A. Smart, J. R. Shealy, and L. F. Eastman, *IEEE Electron. Device Lett.* 21, 268, (2000).
- [4] W. S. Tan, P. A. Houston, P. J. Parbrook, G. Hill, and R. J. Airey, *J. Phys. D: Appl. Phys.* 35, 595 (2002).
- [5] T. Hashizume, S. Ootomo, T. Inagaki, and H. Hasegawa, *J. Vac. Sci. Technol. B* 21, 1828 (2003)
- [6] C. Bae, C. Krug, G. Lucovsky, A. Chakraborty, and U. Mishra, *J. Appl. Phys.* 96, 2674 (2004).
- [7] M. Lachab, M. Sultana, H. Fatima, V. Adivarahan, Q. Fareed, and M. A. Khan, *Semicond. Sci. Technol.* 27, 125001 (2012).
- [8] C. J. Kirkpatrick, B. Lee, R. Suri, X. Yang, and V. Misra, *IEEE Electron Device Lett.* 33, 1240 (2012).
- [9] S. Takashima, Z. Li, and T. P. Chow, *Jpn. J. Appl. Phys.* 52, 08JN24 (2013).
- [10] T. Huang, X. Zhu, K. M. Wong, and K. M. Lau, *IEEE Electron Device Lett.* 33, 212 (2012).
- [11] L. Pang, Y. Lian, D.-S. Kim, J.-H. Lee, and K. Kim, *IEEE Trans. Electron Devices* 59, 2650 (2012).
- [12] L. Han and Z. Chen, *J. Solid-State Sci. Technol.* 2, N228 (2013).
- [13] R. L. Puurunen, *J. Appl. Phys.* 97, 121301 (2005).
- [14] S. M. George, O. Sneh, A. C. Dillon, M. L. Wise, A. W. Ott, L. A. Okada, and J. D. Way, *Appl. Surf. Sci.* 82, 460 (1994).
- [15] J. W. Klaus, O. W. Ott, J. M. Johnson, and S. M. George, *Appl. Phys. Lett.* 70, 1092 (1997).

- [16] J. D. Ferguson, A. W. Weimer, and S. M. George, *Appl. Surf. Sci.* 162, 280 (2000).
- [17] J. W. Klaus, O. Sneh, and S. M. George, *Science* 278, 1934 (1997).
- [18] B. A. McCool and W. J. DeSisto, *Chem. Vap. Deposition* 10, 190 (2004).
- [19] J. D. Ferguson, E. R. Smith, A. W. Weimer, and S. M. George, *J. Electrochem. Soc.* 151, G528 (2004).
- [20] S. M. George, O. Sneh, A. C. Dillon, M. L. Wise, A. W. Ott, L. A. Okada, and J. D. Way, *Appl. Surf. Sci.* 82/83, 460 (1994).
- [21] J. D. Ferguson, A. W. Weimer, and S. M. George, *Appl. Surf. Sci.* 162/163, 280 (2000).
- [22] O. Sneh, M. L. Wise, A. W. Ott, L. A. Okada, and S. M. George, *Surf. Sci.* 334, 135 (1995).
- [23] J. W. Klaus, A. W. Ott, J. M. Johnson, and S. M. George, *Appl. Phys. Lett.* 70, 1092 (1997).
- [24] J. W. Klaus, A. W. Ott, and S. M. George, *Surf. Rev. Lett.* 6, 435 (1999).
- [25] M. A. Cameron, I. P. Gartland, J. A. Smith, S. F. Diaz, and S. M. George, *Langmuir* 16, 7435 (2000).
- [26] J. D. Ferguson, A. W. Weimer, and S. M. George, *Chem. Mater.* 12, 3472 (2000).
- [27] Y. Fedorenko, J. Swerts, J. W. Maes, E. Tois, S. Haukka, C. G. Wang, G. Wilk, A. Delabie, W. Deweerdt, and S. De Gendt, *Electrochem. Solid-State Lett.* 10, H149 (2007).
- [28] J. W. Klaus and S. M. George, *Surf. Sci.* 447, 81 (2000).
- [29] B. A. McCool and W. J. DeSisto, *Ind. Eng. Chem. Res.* 43, 2478 (2004).
- [30] B. A. McCool and W. J. DeSisto, *Chem. Vap. Deposition* 10, 190 (2004).
- [31] Y. Du, X. Du, and S. M. George, *Thin Solid Films* 491, 43 (2005).
- [32] L. K. Tan, A. S. M. Chong, X. S. E. Tang, and H. Gao, *J. Phys. Chem. C* 111, 4964 (2007)
- [33] Y. Du, X. Du, and S. M. George, *J. Phys. Chem. C* 111, 219 (2007).
- [34] S. W. Lee, K. Park, B. Han, S. H. Son, S. K. Rha, C. O. Park, and W. J. Lee, *Electrochem. Solid-State Lett.* 11, G23 (2008).
- [35] S. I. Kol'tsov, *Zh. Obshch. Khim.* 71, 1616 (2001). [*Russ. J. Gen. Chem.* 71, 1531 (2001)].
- [36] J.-H. Lee, U.-J. Kim, C.-H. Han, S.-K. Rha, W.-J. Lee, and C.-O. Park, *Jpn. J. Appl. Phys., Part 2* 43, L328 (2004).
- [37] W.-J. Lee, C.-H. Han, J.-K. Park, Y.-S. Lee, and S.-K. Rha, *Jpn. J. Appl. Phys., Part 1* 49, 071504 (2010).

- [38] T. Murata, Y. Miyagawa, Y. Nishida, Y. Yamamoto, T. Yamashita, M. Matsuura, K. Asai, and H. Miyatake, *Jpn. J. Appl. Phys., Part 1* 49, 04DB11 (2010).
- [39] Z. Ma, S. Brown, J. Y. Howe, S. H. Overbury, and S. Dai, *J. Phys. Chem. C* 112, 9448 (2008).
- [40] B. Hatton, V. Kitaev, D. Perovic, G. Ozin, and J. Aizenberg, *J. Mater. Chem.* 20, 6009 (2010).
- [41] J. D. Ferguson, E. R. Smith, A. W. Weimer, and S. M. George, *J. Electrochem. Soc.* 151, G528 (2004).
- [42] Y. K. Jeong, H.-J. Kim, H. G. Kim, and B.-H. Choi, *Curr. Appl. Phys.* 9, S249 (2009).
- [43] J. W. Lim, S. J. Yun, and J. H. Lee, *Electrochem. Solid-State Lett.* 8, F25 (2005).
- [44] Y. B. Jiang, N. G. Liu, H. Gerung, J. L. Cecchi, and C. J. Brinker, *J. Am. Chem. Soc.* 128, 11018 (2006).
- [45] J. W. Lim, S. J. Yun, and J. H. Kim, *ETRI J.* 31, 675 (2009).
- [46] Y. Qin, Y. Kim, L. Zhang, S.-M. Lee, R. B. Yang, A. Pan, K. Mathwig, M. Alexe, U. Gösele, and M. Knez, *Small* 6, 910 (2010).
- [47] J. Bachmann, R. Zierold, Y. T. Chong, R. Hauert, C. Sturm, R. Schmidt-Grund, B. Rheinländer, M. Grundmann, U. Gösele, and K. Nielsch, *Angew. Chem., Int. Ed.* 47, 6177 (2008).
- [48] K. Pitzschel, J. M. M. Moreno, J. Escrig, O. Albrecht, K. Nielsch, and J. Bachmann, *ACS Nano* 3, 3463 (2009).
- [49] J. Lee, S. Farhangfar, R. Yang, R. Scholz, M. Alexe, U. Gösele, J. Lee, and K. Nielsch, *J. Mater. Chem.* 19, 7050 (2009).
- [50] D. Hiller, R. Zierold, J. Bachmann, M. Alexe, Y. Yang, J. W. Gerlach, A. Stesmans, M. Jivanescu, U. Müller, J. Vogt, H. Hilmer, P. Löper, M. Künle, F. Munnik, K. Nielsch, and M. Zacharias, *J. Appl. Phys.* 107, 064314 (2010).
- [51] O. Albrecht, R. Zierold, C. Patzig, J. Bachmann, C. Sturm, B. Rheinländer, M. Grundmann, D. Görlitz, B. Rauschenbach, and K. Nielsch, *Phys. Status Solidi B* 247, 1365 (2010).
- [52] B. B. Burton, M. P. Boleslawski, A. T. Desombre, and S. M. George, *Chem. Mater.* 20, 7031 (2008).
- [53] X. Liang, K. S. Barrett, Y.-B. Jiang, and A. W. Weimer, *ACS Appl. Mater. Interfaces* 2, 2248 (2010).
- [54] S. Kamiyama, T. Miura, and Y. Nara, *Electrochem. Solid-State Lett.* 8, F37 (2005).
- [55] S. Kamiyama, T. Miura, and Y. Nara, *Thin Solid Films* 515, 1517 (2006).
- [56] P. S. Waggoner, C. P. Tan, and H. G. Craighead, *J. Appl. Phys.* 107, 114505 (2010).
- [57] S.-J. Won, S. Suh, M. S. Huh, and H. J. Kim, *IEEE Electron Device Lett.* 31, 857 (2010).
- [58] T. Hirvikorpi, M. Vähä-Nissi, A. Harlin, J. Marles, V. Miikkulainen, and M. Karppinen, *Appl. Surf. Sci.* 257, 736 (2010).

- [59] S. Kamiyama, T. Miura, Y. Nara, and T. Arikado, *Electrochem. Solid-State Lett.* 8, G215 (2005).
- [60] Y. Kinoshita, F. Hirose, H. Miya, K. Hirahara, Y. Kimura, and M. Niwano, *Electrochem. Solid-State Lett.* 10, G80 (2007).
- [61] F. Hirose, Y. Kinoshita, S. Shibuya, Y. Narita, H. Miya, K. Hirahara, Y. Kimura, and M. Niwano, *ECS Trans.* 19, 417 (2009).
- [62] F. Hirose, Y. Kinoshita, S. Shibuya, Y. Narita, Y. Takahashi, H. Miya, K. Hirahara, Y. Kimura, and M. Niwano, *Thin Solid Films* 519, 270 (2010).
- [63] B. B. Burton, S. W. Kang, S. W. Rhee, and S. M. George, *J. Phys. Chem. C* 113, 8249 (2009).
- [64] D. M. King, X. H. Liang, B. B. Burton, M. K. Akhtar, and A. W. Weimer, *Nanotechnology* 19, 255604 (2008).
- [65] W. Gasser, Y. Uchida, and M. Matsumura, *Thin Solid Films* 250, 213 (1994).
- [66] K. Yamaguchi, S. Imai, N. Ishitobi, M. Takemoto, H. Miki, and M. Matsumura, *Appl. Surf. Sci.* 130–132, 202 (1998).
- [67] S. Morishita, Y. Uchida, and M. Matsumura, *Jpn. J. Appl. Phys., Part 1* 34, 5738 (1995).
- [68] S. Morishita, W. Gasser, K. Usami, and M. Matsumura, *J. Non-Cryst. Solids* 187, 66 (1995).
- [69] H. B. Profijt, S. E. Potts, M. C. M. van de Sanden, and W. M. M. Kessels, *J. Vac. Sci. Technol. A* 29, 050801 (2011).
- [70] S. M. George, *Chem. Rev.* 110, 111 (2010).
- [71] J. Yang, B. S. Eller, C. Zhu, C. England, and R. J. Nemanich, *J. Appl. Phys.* 112, 053710 (2012).
- [72] J. Yang, B. S. Eller, M. Kaur, and R. J. Nemanich, *J. Vac. Sci. Technol. A* 32, 021514 (2014).
- [73] D. A. Cole, J. R. Shallenberger, S. W. Novak, R. L. Moore, M. J. Edgell, S. P. Smith, C. J. Hitzman, J. F. Kirchoff, E. Principe, W. Nieveen, F. K. Huang, S. Biswas, R. J. Bleiler, and K. Jones, *J. Vac. Sci. Technol. B* 18, 440 (2000).
- [74] M. Degai, K. Kanomata, K. Momiyama, S. Kubota, K. Hirahara, and F. Hirose, *Thin Solid Films* 525, 73 (2012).
- [75] Y. Kinoshita, F. Hirose, H. Miya, K. Hirahara, Y. Kimura, and M. Niwano, *Electrochem. Solid-State Lett.* 10, G80 (2007).
- [76] R. L. Puurunen, M. Lindblad, A. Root, and A. O. I. Krause, *Phys. Chem. Chem. Phys.* 3, 1093 (2001).
- [77] A. Rautiainen, M. Lindblad, L. B. Backman, and R. L. Puurunen, *Phys. Chem. Chem. Phys.* 4, 2466 (2002).
- [78] R. L. Puurunen, T. A. Zeelie, and A. O. I. Krause, *Catal. Lett.* 83, 27 (2002).
- [79] J. Robertson and B. Falabretti, *J. Appl. Phys.* 100, 014111 (2006).

- [80] K. W. Kim, S. D. Jung, D. S. Kim, H. S. Kang, K. S. Im, J. J. Oh, J. B. Ha, J. K. Shin, and J. H. Lee, *IEEE Electron Device Lett.* 32, 1376 (2011).
- [81] S.-J. Won, S. Suh, M. S. Huh, and H. J. Kim, *IEEE Electron Device Lett.* 31, 857 (2010).

CHAPTER 7. SURFACE BAND BENDING AND INTERFACE ALIGNMENT OF PLASMA-ENHANCED ATOMIC LAYER DEPOSITED SiO_2 ON $\text{Al}_x\text{Ga}_{1-x}\text{N}$

Abstract. $\text{Al}_x\text{Ga}_{1-x}\text{N}$ is characterized by a significant spontaneous and piezoelectric polarization, which increases with aluminum content. As a result, there arises a surface bound charge that favors compensation by surface states, which influences reliability of AlGaN/GaN devices. This work, therefore, focused on the effects of the polarization charge for GaN and three different aluminum concentrations 15%, 25%, and 35%. The band bending of $\text{Al}_x\text{Ga}_{1-x}\text{N}$ surfaces was measured after a N_2/H_2 plasma pretreatment, which reduced the carbon and oxygen contamination below the detection limit of the x-ray photoelectron spectroscopy (XPS). Surface band bending was then related to surface states, where the band bending of oxygen-free surfaces scales slightly with aluminum content. In addition, the band offsets at the plasma-enhanced atomic layer deposited (PEALD) $\text{SiO}_2/\text{Al}_x\text{Ga}_{1-x}\text{N}$ interface were measured, giving 3.0 eV, 2.9 eV, 2.9 eV, and 2.8 eV for the respective 0%, 15%, 25%, and 35% aluminum content. These values are in accordance with the charge neutrality level model.

To be submitted in collaboration with Brianna S. Eller and Robert J. Nemanich (2015).

AlGaN/GaN heterostructures have demonstrated considerable promise for power and RF applications due to material properties such as a wide band gap, good thermal conductivity, and high breakdown field. Moreover, AlGaN and GaN are characterized by a spontaneous and piezoelectric polarization, where the polarization of $\text{Al}_x\text{Ga}_{1-x}\text{N}$ increases with aluminum content, x . Consequently, Ga-face AlGaN/GaN heterostructures exhibit an overall positive polarization charge at the interface, which engenders a two-dimensional electron gas (2DEG). This phenomenon enables low-resistance operation of high-electron mobility transistors (HEMTs) as well as heterostructure field-effect transistors (HFETs). However, AlGaN/GaN HEMTs and HFETs are also characterized by a relatively large leakage current and current collapse. The states responsible for these reliability issues may be related to the compensation charge, where the large polarization of these materials produces significant surface bound charge that favors compensations [1]. This work, therefore, investigates the effects of polarization and aluminum content at the GaN and AlGaN surfaces as well as at a dielectric interface.

Dielectrics have been used to mitigate these reliability issues. An ideal gate dielectric is characterized by a large band gap, which results in a conduction band offset large enough to provide an effective barrier to prevent gate leakage. In addition, an ideal gate dielectric also has a high dielectric constant to maximize device scalability [2]. Unfortunately, these characteristics are inversely related, where FIG 7.1 summarizes this trade-off for common dielectrics. Of these dielectrics, SiO₂ is characterized by the largest band gap and thus most likely to confine carriers. On the other hand, SiO₂ is a low-k dielectric and not likely to aid with device scalability. However, recent work [3-5] has investigated SiO₂ due to its potential to reduce gate leakage. Given this potential, state-of-the-art technologies have designed device structures that incorporate SiO₂ as well as high-k dielectrics—e.g. high-k HfAlO with a SiO₂ capping layer—in an attempt to obtain a dielectric passivation structure with both a high band gap and high-k dielectric constant [5-7].

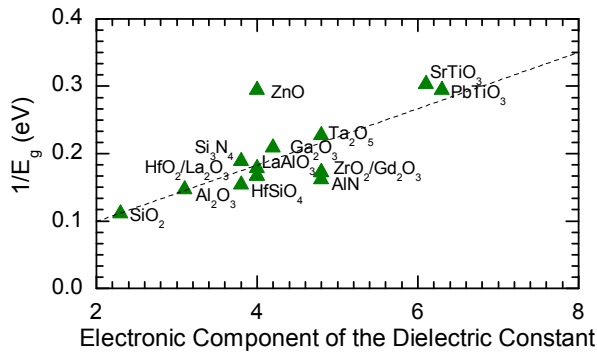


FIG 7.1 The inverse of the energy band gap with respect to the electronic component of the dielectric constant for a range of dielectrics.

In this work, we investigated the electronic state configuration of oxygen-free Al_xGa_{1-x}N, surfaces as well as plasma-enhanced atomic layer deposited (PEALD) SiO₂/Al_xGa_{1-x}N, where PEALD provides higher-quality films in comparison to many other deposition techniques in terms of stoichiometry, breakdown field, and high defect density [8,9].

Moreover, this technique deposits uniform and conformal films with precise thickness control, where the plasma often leads to improved film properties, such as fewer impurities [10]. Thin SiO₂ (~3 nm) layers were thus deposited such that x-ray photoelectron spectroscopy (XPS) could be used to characterize the electronic state configuration at the interface. This characterization was completed on plasma-cleaned Al_xGa_{1-x}N surfaces as well, thus determining the effects of the polarization and aluminum content on both surface and interface states.

I. Experiment

Ga-face, n-type Al_xGa_{1-x}N samples were purchased from NTT Advanced Technology. The samples were ~50 nm thick as-deposited on Si substrates with a Si doping density of ~10¹⁷ cm⁻³, which was used to calculate the position of the Fermi level. In addition, GaN and three different concentrations of aluminum were used to give varied band gaps and surface polarization conditions. In particular, the concentrations used were 15%, 25%, and 35%, where the resulting band gaps and Fermi levels are summarized in TABLE 7.1.

TABLE 7.1 Band gap characteristics of Al_xGa_{1-x}N as determined from aluminum content. These values were determined by linear interpolation of GaN and AlN properties [11]. The doping density determined the position of the Fermi level to be ~0.1 eV below the conduction band.

Al-content, x	E_g (eV)	Fermi level (eV below CB)
0%	3.40	0.06
15%	3.82	0.07
25%	4.10	0.08
35%	4.38	0.08

These samples were then cleaned *ex-situ* via sonication in acetone, methanol, and ammonia hydroxide for 10 min each followed by a 1 min deionized water rinse and N₂

blow dry. Samples were then transferred into an ultra-high vacuum system where plasma cleaning, ALD, and processing were all completed without breaking vacuum. The N₂/H₂ plasma cleaning process was conducted in an electron cyclotron resonance (ECR) system. This system was maintained at a background pressure of 10⁻⁹ Torr and increased to 10⁻⁵ Torr during processing. The N₂ and H₂ gasses were delivered into the chamber with respective flow rates of 20 sccm and 5 sccm giving a 4:1 ratio. The gasses were then ignited at 300 W resulting in an immersed plasma exposure. These plasma conditions were coupled with high temperatures at 680°C, which were used to reduce oxygen coverage.

Deposition of ~3 nm SiO₂ was then completed in a remote plasma-enhanced ALD (PEALD). This system was generally maintained at a background pressure of ~6.0×10⁻⁸ Torr. During deposition, oxygen plasma was ignited with 13.56 MHz rf-excitation applied at 200 W to a helical copper coil wrapped around a 32 mm diameter quartz tube and maintained at a pressure of ~100 mTorr with a flow rate of 35 sccm. The previously described PEALD process for SiO₂ using tri(dimethylamino)silane (TDMAS) [11] was adopted for this work as well, where the gas-phase cycle included 1.6 s TDMAS, 16 s O₂ plasma, and 40 s N₂ purge at room temperature. Following deposition, the SiO₂/Al_xGa_{1-x}N samples were annealed at 400°C in 60 mTorr N₂ ambient for 30 min.

Between each of the processing steps described, x-ray photoelectron spectroscopy (XPS) was used to characterize the surface and interface properties of the samples. These measurements were conducted with a background pressure of 2×10⁻⁸ Torr. X-ray photons were provided by a VG Scienta MX650 source using Al Kα radiation with incident

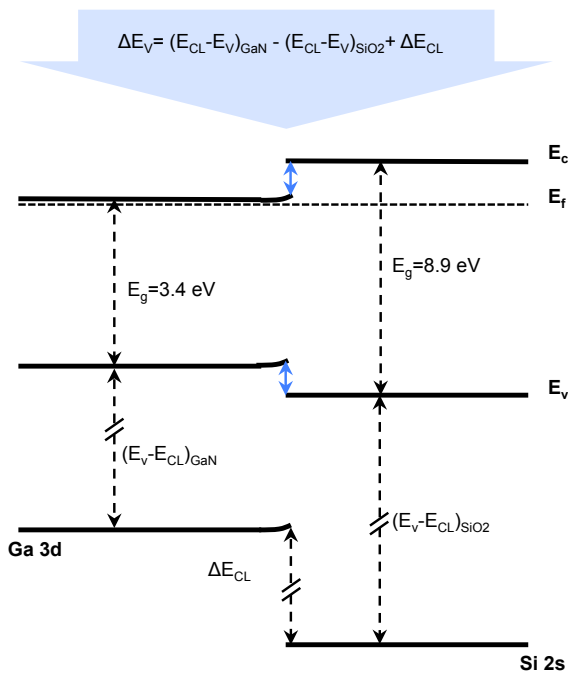
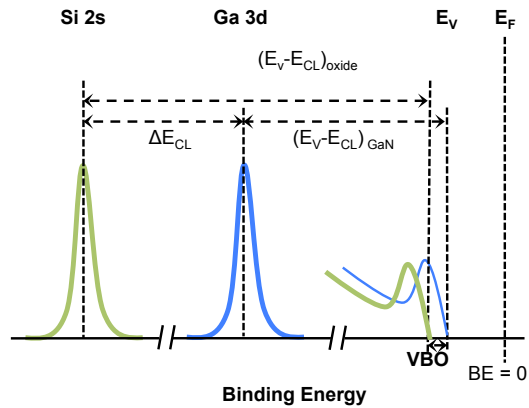


FIG 7.2 Band offsets (bottom) as determined by the difference between the XPS Ga 3d and Si 2s core levels (top) by the given equation (middle).

energy of 1486.7 eV in a narrow band of 0.2 eV; this radiation was monochromated with seven toroidal precision quartz crystals. A high-resolution VG Scienta R3000 was then used to analyze the emitted electrons with an A20 lens mode and pass energy of 100 eV.

The resulting XPS spectra were used to characterize the electronic state configuration at the $\text{Al}_x\text{Ga}_{1-x}\text{N}$, surface and $\text{SiO}_2/\text{Al}_x\text{Ga}_{1-x}\text{N}$ interface. Band bending at the surface was determined by the position of the valence band and at the interface by the position of the Ga 3d core level as described previously [1]. In addition, the valence band offsets

(VBOs) were determined from the difference between the corresponding core levels in the $\text{Al}_x\text{Ga}_{1-x}\text{N}$ substrate and SiO_2 thin film:

$$\Delta E_V = (E_{\text{Ga}3d} - E_{\text{VBM}})_{\text{Al}_x\text{Ga}_{1-x}\text{N}} - (E_{\text{Si}2s} - E_{\text{VBM}})_{\text{SiO}_2} + \Delta E_{\text{CL}}, \quad (1)$$

where $(E_{\text{Ga}3d} - E_{\text{VBM}})_{\text{Al}_x\text{Ga}_{1-x}\text{N}}$ is the difference between the Ga 3d core level and valence band maximum of $\text{Al}_x\text{Ga}_{1-x}\text{N}$, $(E_{\text{Si}2s} - E_{\text{VBM}})_{\text{SiO}_2}$ is the difference between the Si 2s core level and valence band maximum of SiO_2 , and ΔE_{CL} is the difference between the respective Si 2s and Ga 3d core levels, i.e. $E_{\text{Si}2s} - E_{\text{Ga}3d}$ as indicated in FIG 7.2. This calculation was also completed using the Ga 3s and Si 2s core levels, where the average band offsets are reported.

II. Results

The N_2/H_2 plasma cleaning process was intended to remove oxygen and carbon contamination from the surfaces of the $\text{Al}_x\text{Ga}_{1-x}\text{N}$ samples. As shown in FIG 7.3, the adopted ECR plasma process was sufficient, where there was no detectable signal from the C or O 1s levels. The Ga 3s, Al 2p, and Ga 3d core level after this cleaning process are also shown in FIG 7.4.

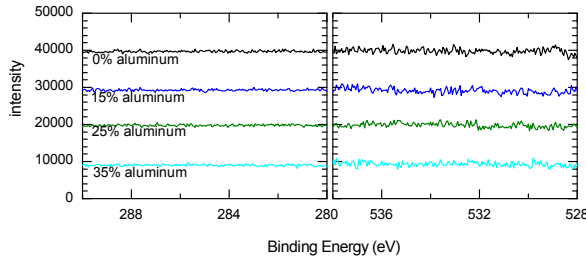


FIG 7.3 XPS spectra of residual carbon (left) and oxygen (right) contamination after 680°C N_2/H_2 plasma surface treatment. For both elements, the contamination levels were below the detection limit of the XPS.

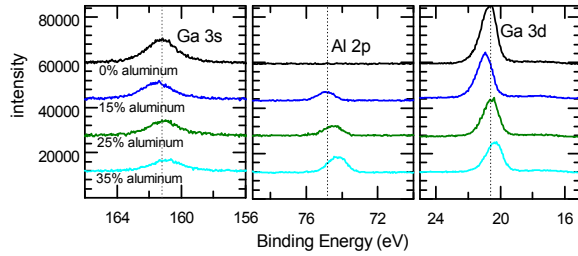


FIG 7.4 XPS spectra of Ga 3s, Al 2p, and Ga 3d core levels after 680°C N₂/H₂ plasma surface treatment. The N 1s peak is not included as it is obscured by a Ga Auger peak. The dotted lines indicate core level positions of the GaN surface.

From the oxygen-free surface, the difference between the valence band maximum and binding energy of the Ga 3d core level of clean Al_xGa_{1-x}N was determined from the XPS spectra shown in FIG 7.5. Both energy values were determined from the same spectra to ensure consistency, eliminating sample spot variances. The valence band maximum was linearly extrapolated from the low binding energy cutoff, and the core level was determined by peak fitting. The corresponding $(E_{Ga3d}-E_{VBM})_{AlxGa(1-x)N}$ are summarized in FIG 7.5, where the specific values used for the position of the Ga 3d core level and valence band maximum are summarized in TABLE 7.2. The surface band bending is also reported in TABLE 7.2, where the band bending appears to increase with aluminum content.

TABLE 7.2 Energy position of VBM and Ga 3d core level of Al_xGa_{1-x}N as dependent on aluminum content. These values determined $(E_{Ga3d}-E_{VBM})_{AlxGa(1-x)N}$ and the surface band bending. All energies are given in eV.

Al-content, <i>x</i>	E _{Ga3d}	VBM	E _{Ga3d} -E _{VBM}	BB
0%	24.3	3.2	17.4	0.1
15%	24.6	3.7	17.2	0.0
25%	24.2	3.4	17.1	0.4
35%	24.1	3.5	16.9	0.9

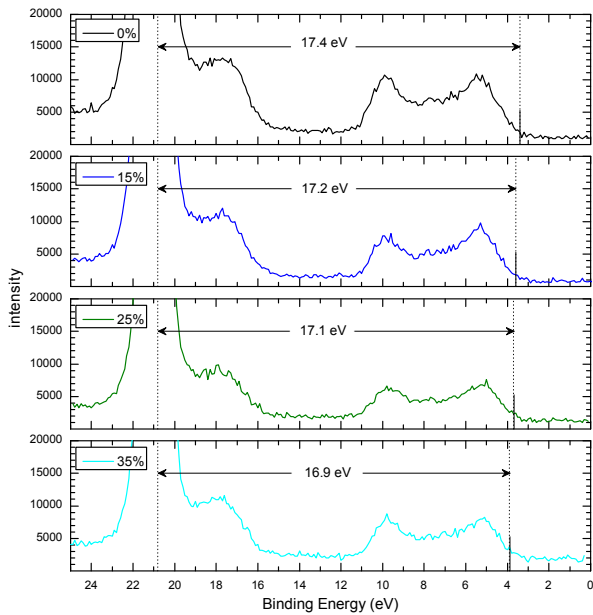


FIG 7.5 XPS spectra of Ga 3d core level to the VBM of GaN (top), $\text{Al}_{0.15}\text{Ga}_{0.85}\text{N}$ (top-middle), $\text{Al}_{0.25}\text{Ga}_{0.75}\text{N}$ (bottom-middle), and $\text{Al}_{0.35}\text{Ga}_{0.65}\text{N}$ (bottom). The position of the VBM is determined by linear extrapolation of the low-binding energy cut-off. (NOTE: the positions of the Ga 3d core level were aligned for comparison in this plot and do not, therefore, represent that experimentally determined values described for the VBM and core level positions.) In addition, the peak at ~ 17 eV is the N 2s core level.

To investigate the role of surface states, an alternative plasma clean was completed on a GaN surface. This clean included a 680°C NH_3 plasma anneal followed by a gas anneal for 15 min each, as used in a previous study [12]. This plasma surface treatment results in ~ 1 ML of oxygen coverage on the surface. The oxygen-terminated surface was characterized by a Ga 3d core level of 21.1 eV and a valence band of maximum of 4.0 eV as shown in FIG 7.6. This resulting $(E_{\text{Ga}3d} - E_{\text{VBM}})_{\text{GaN}}$ was thus 17.1 eV. In addition, the valence band edge of the oxygen-free surface is characterized by a small surface state that is not observed on the oxygen-terminated surface.

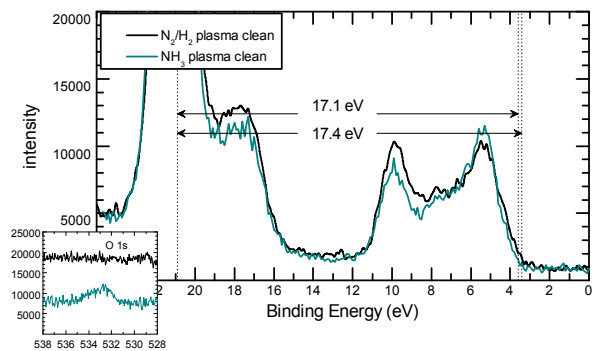


FIG 7.6 XPS spectra of Ga 3d core level to the VBM difference of GaN after different plasma treatments, resulting in different surface states. One clean results in an oxygen-free surface while the other gives ~ 1 ML of oxygen coverage as shown by the O 1s core level in the inset. (NOTE: the positions of the Ga 3d core level were aligned to account for differences in band bending.) In addition, the peak at ~ 17 eV is the N 2s core level.

To determine $(E_{Si2s}-E_{VBM})_{SiO_2}$ for bulk SiO_2 , a thick PEALD SiO_2 film (~ 10 nm) was deposited on GaN resulting in the spectra shown in FIG 7.7. In this work, the Si 2s core level is used, even though the Si 2p core level was stronger as this peak overlaps with the Ga 3p core level. In this case, the binding energy of the Si 2s core level was measured at 155.2 eV, and the valence band maximum was determined to be 6.2 eV. This gave $(E_{Si2s}-E_{VBM})_{SiO_2} = 149.0$ eV—similar to the previously reported value of 149.8 eV [12].

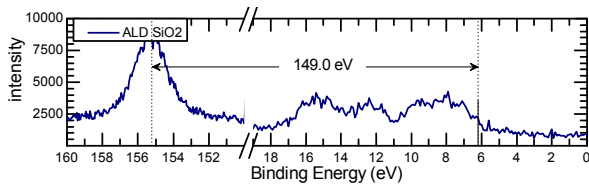


FIG 7.7 10 nm PEALD SiO_2 as deposited on GaN and annealed at $400^\circ C$ in N_2 ambient. The binding energy difference between the Si 2s core level and valence band maximum of SiO_2 was calculated as shown.

For characterization of the interface band alignment, ~ 3 nm SiO_2 was deposited and annealed on the substrates. The resulting XPS core levels for $SiO_2/Al_xGa_{1-x}N$ as-deposited and annealed on $Al_xGa_{1-x}N$ are summarized in TABLE 7.3. These values determined the binding energy differences between the Ga 3d and Si 2s core levels, i.e. $E_{Si2s}-E_{Ga3d}$, as well as the binding energy differences between the Si 2s and Ga 3s core levels, i.e. $E_{Ga3s}-E_{Si2s}$, used to determine the valence band offsets. The relevant spectra are shown in FIG 7.8 for as-deposited PEALD $SiO_2/Al_xGa_{1-x}N$ and FIG 7.9 for annealed PEALD $SiO_2/Al_xGa_{1-x}N$, where the differences in core levels, ΔE_{CL} , are indicated.

These core levels positions and valence band maximums were used to determine the respective valence band offsets (VBOs) as will be discussed.

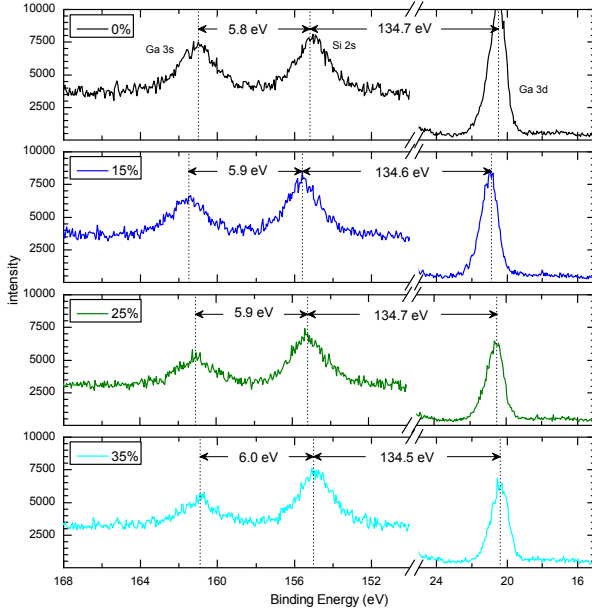


FIG 7.8 XPS spectra for the Ga 3s, Si 2s, and Ga 3d core levels of ~3 nm PEALD SiO₂ on GaN (top), Al_{0.15}Ga_{0.85}N (top-middle), Al_{0.25}Ga_{0.75}N (bottom-middle), and Al_{0.35}Ga_{0.65}N (bottom) after deposition. The peak-to-peak differences used to calculate the valence band offsets, i.e. $E_{Ga3s}-E_{Si2s}$ and $E_{Si2s}-E_{Ga3d}$, are indicated.

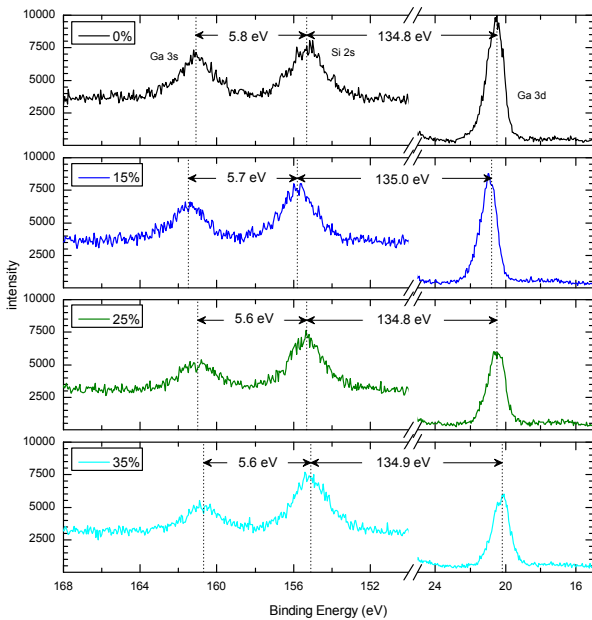


FIG 7.9 XPS spectra for the Ga 3s, Si 2s, and Ga 3d core levels of ~3 nm PEALD SiO₂ on GaN (top), Al_{0.15}Ga_{0.85}N (top-middle), Al_{0.25}Ga_{0.75}N (bottom-middle), and Al_{0.35}Ga_{0.65}N (bottom) after 400°C in N₂ ambient. The peak-to-peak differences used to calculate the valence band offsets, i.e. $E_{Ga3s}-E_{Si2s}$ and $E_{Si2s}-E_{Ga3d}$, are indicated.

TABLE 7.3 Core level results for Ga 3d, Al 2p, Ga 3s, Si 2s, and O 1s spectra of ~3 nm PEALD-deposited SiO₂ on Al_xGa_{1-x}N as dependent on aluminum content, including the peak position and full-width half-maximum (FWHM). All energies are given in eV.

Al- content t, x	SiO ₂ /Al _x Ga _{1-x} N as deposited					SiO ₂ /Al _x Ga _{1-x} N annealed														
	Ga 3d		Al 2p		O 1s	Ga 3d		Al 2p		O 1s										
	center	FWHM	center	FWHM		center	FWHM	center	FWHM											
0%	20.5	1.1	—	—	161.1	2.5	155.3	2.4	533.8	1.4	20.5	1.1	—	—	161.0	2.2	155.2	2.3	533.6	1.4
15%	20.8	1.1	75.3	1.5	161.5	2.0	159.8	2.0	534.4	1.4	20.9	1.1	75.3	1.6	161.5	2.0	155.6	2.1	534.0	1.4
25%	20.5	1.1	74.5	1.4	161.0	2.5	155.3	2.2	533.8	1.5	20.4	1.1	74.5	1.4	161.1	2.4	155.2	2.3	533.5	1.4
35%	20.2	1.2	74.2	1.4	160.7	3.1	155.1	2.5	533.6	1.5	20.4	1.2	74.4	1.3	160.9	2.7	154.9	2.3	533.2	1.4

III. Discussion

A. Ga 3d to VBM Energy Difference

According to previous electronic-state studies of GaN, the difference between the Ga 3d core level and the valence band maximum is 17.7-17.8 eV [13-15], which is the value used in all previous studies [12,16,17]. Similar electronic-state studies of $\text{Al}_{0.25}\text{Ga}_{0.75}\text{N}$ indicated 17.5 eV [18] is the respective differences between the Ga 3d core levels and the valence band maximum. In this work, the values for $(E_{\text{Ga}3d}-E_{\text{VBM}})_{\text{Al}_x\text{Ga}_{(1-x)}\text{N}}$ are ~ 0.4 eV below these expected values as summarized in TABLE 7.4.

TABLE 7.4 Summary of expected and measured energy differences between the VBM and Ga 3d core level of $\text{Al}_x\text{Ga}_{1-x}\text{N}$ as dependent on aluminum content. The measured values were ~ 0.4 eV below the expected values. All energies are given in eV.

Al-content, x	$E_{\text{Ga}3d}-E_{\text{VBM}}$	
	measured	expected
0%	17.4	17.8 [13-15]
15%	17.2	17.6
25%	17.1	17.5 [18]
35%	16.9	17.4

The energy of the valence band maximum is intricately related to surface states. The discrepancy may, thus, be related to the surface termination of the samples, which varies greatly for GaN and AlGaN surfaces. In the work presented by Waldrop and Grant [14], GaN and AlN were grown *in-situ* by molecular beam epitaxy. The resulting surface was characterized by a hexagonal 1×1 low energy electron diffraction pattern, indicating the surface was epitaxial. In the study by Cook *et al.* [13,19], the GaN surfaces were cleaned

at 860°C for 15 min in an NH₃ atmosphere after atmospheric exposure. The NH₃ gas anneal effectively produced an oxygen-free surface, and results suggested that $(E_{Ga3d} - E_{VBM})_{GaN}$ is 17.7 eV. The difference may, therefore, be related to an NH_x surface termination state introduced with plasma cleaning as shown in FIG 7.10a.

An additional cleaning process was also explored using NH₃ plasma. This clean resulted in an oxygen-terminated GaN surface with slightly less NH_x as shown in FIG 7.10b. (NOTE: The surface sensitive Ga Auger peak also suggests the NH₃ plasma and N₂/H₂ plasma treatments produce distinctly different surface termination.) The resulting $(E_{Ga3d} - E_{VBM})_{GaN}$ was determined to be 17.1 eV. This value agrees with another study presented by Martin *et al.* [20]. In this work, samples were grown *in-situ* vacuum; however, the valence band maximum was determined by aligning prominent features in the valence band rather than from the valence band edge. Consequently, though the surface would likely be characterized by a similar surface state as the previously mentioned studies, the method of calculation overlooked it. In other words, this measurement demonstrated the

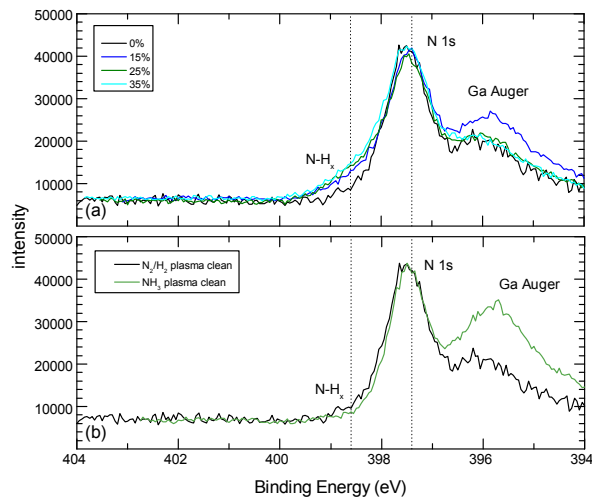


FIG 7.10 (a) N 1s core levels after 680°C N₂/H₂ plasma surface treatment as dependent on aluminum content, and (b) N 1s core levels of GaN as dependent on plasma treatment. (NOTE: These peaks were shifted to account for any differences in band bending.)

influence of surface states. These states potentially obscure the valence band edge and thus appear to shift the valence band towards lower binding energy. This ‘shift’ would consequently increase $(E_{Ga3d}-E_{VBM})_{GaN}$, and thus account for the discrepancy observed.

For the following calculations, the value measured in this work was used despite the discrepancy with previous studies.

B. Band Bending and Surface States

Previous work by Eller *et al.* [1] measured band bending of N-face GaN, Ga-face GaN, and Ga-face $Al_{0.25}Ga_{0.75}N$ after various cleaning steps, which was related to the net surface charge. Results showed band bending was virtually independent of polarization, where all three surfaces exhibited the same upward band bending. The surface states, therefore, compensated any differences in the magnitude and direction of the bound surface polarization charge, where the position of the Fermi level with respect to the conduction band was pinned. However, in this work, results show different behavior, where band bending increases with the aluminum content or polarization bound charge as shown in TABLE 7.5.

TABLE 7.5 Surface polarization conditions of $Al_xGa_{1-x}N$ as dependent on aluminum content. The polarization and polarization bound charge are determined from the concentration of aluminum, and the compensation charge is calculated from the band bending.

Al-content, x	spontaneous polarization (C/m^2)	polarization bound charge (10^{13} charges/ cm^2)	band bending (eV)	net surface compensation charge (10^{13} charges/ cm^2)
0%	-0.029	- 1.81	0.1	+ 1.78
15%	-0.037	- 2.30	0.0	+ 2.30
25%	-0.042	- 2.62	0.4	+ 2.23
35%	-0.047	- 2.95	0.9	+ 2.84

In this case, the compensation charge scales with aluminum content and thus the magnitude of the polarization bound charge—though not to the same extent are previously noted. In other words, the same pinning state thought to be associated with the N-vacancy is not specifically observed. The difference in these samples is likely correlated with oxygen-related states; previous work was oxygen-terminated and the work presented here is oxygen-free. In another study, Higashiwaki and Miao *et al.* [21-23] has shown oxidized AlGa_xN surfaces reconstruct such that oxygen-related states behave like donors. These states may explain the pinning behavior previously observed. In addition, nitrogen vacancies or Ga dangling bonds interact as donor states on the surface as well, but these states may not interact as pinning states as previously suggested. On the other hand, despite the unpinned Fermi level, these surfaces are still characterized by significant surface charge on the order of $+10^{13}$ charges/cm². It is, therefore, likely the nitrogen vacancies and/or gallium dangling bonds still interact as surface states.

In addition, surface photovoltage effects are not accounted for in these measurements. Measured band bending is, therefore, likely flatter than exhibited on the actual surface. Consequently, the net surface compensation charge may be underestimated.

C. Interface Alignment and Band Offsets

The valence band offsets relationship to aluminum content is summarized in TABLE 7.6 as determined from the Ga 3s, Si 2s, and Ga 3d core levels, which offer agreement with previous results [12]. The conduction band offsets are determined using the band gaps of Al_xGa_{1-x}N as summarized in TABLE 7.1 and of SiO₂ as 8.9 eV. These results

demonstrate the change in the band gap as a result of aluminum content largely manifests in the conduction band rather than the valence band.

TABLE 7.6 VBOs as determined from XPS Si 2s and Ga 3d core levels. The conduction band offset is determined from the known band gaps of the materials, where the band gap of SiO₂ is 8.9 eV. All energies are given in eV.

Al-content, x	SiO ₂ /Al _{x} Ga _{1-x} N as deposited		SiO ₂ /Al _{x} Ga _{1-x} N annealed	
	VBO	CBO	VBO	CBO
0%	3.2	2.3	3.0	2.5
15%	3.2	1.9	2.9	2.2
25%	3.0	1.8	2.9	1.9
35%	3.1	1.4	2.8	1.8

FIG 7.11 compares the measured band offsets after annealing with those calculated by the charge neutrality level (CNL) model, which argues the interface of two materials will align at the charge neutrality level. The CNL of SiO₂ is reported at 4.5 eV while that of GaN and AlN are reported at 2.3 and 2.8 eV above the respective valence band [24]. The CNL of Al _{x} Ga_{1- x} N is thus determined from linear interpolation: $CNL_{AlGaN}(x) = 2.8x + 2.3(1 - x)$. It is evident from this model that the difference in the band gap is largely manifested in the conduction band.

In terms of increased polarization, this behavior is unexpected. As noted by Mönch [25,26], increased polarity generally results in two effects: (1) the valence band flattens as corresponds to the higher effective hole mass and (2) the conduction bands become less direct with respect to the valence band maximum. This redistribution of the density of states pushed the charge neutrality level higher in the band gap. Consequently, the difference in the band gap manifests most significantly in the valence band. However, for GaN and AlN, both materials are direct. In addition, the hole effective masses suggest

slightly flatter bands for AlN as expected. Similarly, the electron effective mass suggests the conduction band is slightly flatter for AlN. However, this effects is more significant for the conduction band than the valence band. Thus, the higher density of states in the conduction band compensates the flattening valence band [27]. Therefore, the CNL does not move as far up in the band gap as polarization would suggest, and the difference in the band gap is largely manifested in the conduction band.

In addition, TABLE 7.6 shows a shift in the band offsets after annealing. Given that band offsets are determined by the interface bonding, this shift is likely related to a potential drop across an interfacial layer, as discussed in previous work. Though the surfaces are oxygen free prior to deposition, it is likely a very thin subcutaneous oxide layer forms during the PEALD SiO₂ process. Acceptor-like defects are also introduced during this process, generating an electric field in this layer. Subsequent annealing removes this charge and reduces the electric field across the interfacial layer.

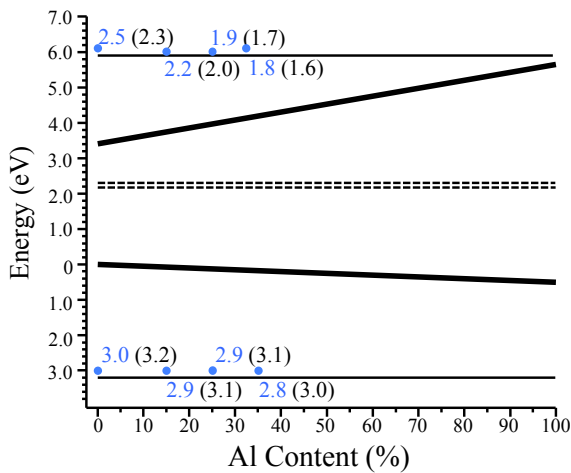


FIG 7.11 Band alignment as determined by the charge neutrality level model. The heavy lines correspond to the conduction and valence bands of Al_xGa_{1-x}N, while the thinner lines correspond to the conduction and valence bands of SiO₂. Experimental offset measurements are given for 0%, 15%, 25%, and 35% Al-content in blue followed with the theoretical results in parentheses for comparison. The theory is linearly interpolated from the CNLs given by Robertson and Falabretti [24].

IV. Conclusions

In summary, this work discussed the band bending and alignment characteristics of oxygen-free $\text{Al}_x\text{Ga}_{1-x}\text{N}$ surfaces and PEALD $\text{SiO}_2/\text{Al}_x\text{Ga}_{1-x}\text{N}$ interfaces. A 680°C , N_2/H_2 plasma surface pretreatment was able to reduce the oxygen and carbon coverage below the XPS detection limit. XPS measurement determined the respective band bending of the $\text{Al}_x\text{Ga}_{1-x}\text{N}$ surface for 0%, 15%, 25%, and 35% aluminum content. Unlike previous work, this study observed a small variation in band bending as dependent on aluminum content. This difference is related to donor-like oxygen states, which likely pin the Fermi level on an oxygen-terminated surface. In addition, the valence band offsets for PEALD $\text{SiO}_2/\text{Al}_x\text{Ga}_{1-x}\text{N}$ were determined, giving 3.0 eV, 2.9 eV, 2.9 eV, and 2.8 eV for respective concentrations of aluminum. This corresponds to conduction band offsets of 2.5 eV, 2.2 eV, 1.9 eV, and 1.8 eV. These values are in accordance with the charge neutrality level model.

V. Acknowledgements

This research is supported by the Office of Naval Research through the DEFINE MURI program, N00014-10-1-0937 as well as the Advanced Research Projects Agency-Energy.

References

- [1] B. S. Eller, J. Yang, and R. J. Nemanich, *J. Electron. Mater.* 43, 4560 (2014).
- [2] B. S. Eller, J. Yang, and R. J. Nemanich, *J. Vac. Sci. Technol. A* 31, 050807 (2012).
- [3] B. Lee, C. Kirkpatrick, Y.-H. Choi, X. Yang, A. Q. Huang, and V. Misra, *Phys. Status Solidi* 9, 868 (2012).
- [4] C. J. Kirkpatrick, B. Lee, R. Suri, X. Yang, and V. Misra, *IEEE Electron Device Lett.* 33, 1240 (2012).

- [5] N. Ramanan, B. Lee, C. Kirkpatrick, R. Suri, and V. Misra, *Semicond. Sci. Technol.* 28, 074004 (2013).
- [6] N. Ramanan, B. Lee, V. Misra, *IEEE Trans. Electron Devices* 62, 546 (2015).
- [7] F. Roccaforte, P. Fiorenza, G. Greco, R. Lo Nigro, F. Giannazzo, Al Patti, and M. Saggio, *Phys. Status Solidi A* 211, 2063 (2014).
- [8] L. Han and Z. Chen, *J. Solid-State Sci. Technol.* 2, N228 (2013).
- [9] R. L. Puurunen, *J. Appl. Phys.* 97, 121301 (2005).
- [10] G. Dingemans, C. A. A. van Helvoirt, M. C. M. van de Sanden, and W. M. M. Kessels, *ECS Transactions* 35, 191 (2011).
- [11] B. S. Eller, W. Li, S. Rupprecht, and R. J. Nemanich, to be submitted (2015).
- [12] J. Yang, B. S. Eller, and R. J. Nemanich, *J. Appl. Phys.* 116, 123702 (2014).
- [13] T. E. Cook, Jr., C. C. Fulton, W. J. Mecoouch, R. F. Davis, G. Lucovsky, and R. J. Nemanich, *J. Appl. Phys.* 94, 7155 (2003).
- [14] J. R. Waldrop, and R. W. Grant, *Appl. Phys. Lett.* 68, 2879 (1996).
- [15] J. Hedman, and N. Mårtensson, *Phys. Scr.* 22, 176 (1980).
- [16] J. Yang, B. S. Eller, C. Zhu, C. England, and R. J. Nemanich, *J. Appl. Phys.* 112, 053710 (2012).
- [17] J. Yang, B. S. Eller, M. Kaur, and R. J. Nemanich, *J. Vac. Sci. Technol. A* 32, 021514 (2014).
- [18] Y. L. Chiou, and C. T. Lee, *IEEE Trans. Electron Devices* 58, 3869 (2011).
- [19] T. E. Cook Jr., C. C. Fulton, W. J. Mecoouch, K. M. Tracy, R. F. Davis, G. Lucovsky, E. H. Hurt, and R. J. Nemanich, *J. Appl. Phys.* 93, 3995 (2003).
- [20] G. Martin, S. Strite, A. Botchkarev, A. Agarwal, A. Rockett, H. Morkoc, W. R. L. Lambrecht, and B. Segall, *Appl. Phys. Lett.* 65, 610 (1994).
- [21] M. Higashiwaki, S. Chowdhury, B. L. Swenson, and U. K. Mishra, *Appl. Phys. Lett.* 97, 222104 (2010).
- [22] M. Higashiwaki, S. Chowdhury, M.-S. Miao, B. L. Swenson, C. G. Van de Walle, and U. K. Mishra, *J. Appl. Phys.* 108, 063719 (2010).
- [23] M. S. Miao, J. R. Weber, and C. G. Van de Walle, *J. Appl. Phys.* 107, 123713 (2010).
- [24] J. Robertson and B. Falabretti, *J. Appl. Phys.* 100, 014111 (2006).
- [25] W. Mönch, *J. Appl. Phys.* 80, 5076 (1996).
- [26] J. Robertson, *J. Vac. Sci. Technol. B* 18, 1785 (2000).

[27] D. Fritsch, H. Schmidt, and M. Grundmann, *Phys. Rev. B* 67, 235205 (2003).

PART IV: CONCLUSIONS AND FUTURE WORK

CHAPTER 8. PRECISION CONTROL OF DIELECTRIC/GaN AND AlGaN INTERFACES

Precision control of interface properties will no doubt continue be of central importance for a range of applications, including electronics, optoelectronics, photochemistry, and electrochemistry.

I. Summary of Previous Work

This doctoral work focused on the surface electronic state configuration of GaN and AlGaN with particular attention to the polarization and aluminum content affects. In addition, the interface electronic states of plasma-enhanced atomic layer deposited (PEALD) dielectrics were characterized with relation to the deposition process as well as the aluminum content. In particular, there were three areas of focus including the following:

(1) Polarization effects on the surface electronic state configuration. in this paper, the surface band bending on N-face GaN, Ga-face GaN, and Ga-face AlGaN was measured with x-ray photoemission spectroscopy after various cleaning steps, indicating the distribution of compensation charge. Despite the different surface bound charge on these materials, similar band bending was observed regardless of the magnitude or direction of the charge. Evidence, thus, suggests a pinning state indirectly evident of a nitrogen vacancy or gallium-dangling bond.

(2) Film and interface characteristics of plasma-enhanced-atomic-layer-deposited-SiO₂/GaN. In this work, PEALD was used to deposit SiO₂ with tri(dimethylamino)silane on GaN. The growth, electrical, and interface properties were characterized for films deposited at different temperatures, including 30°C 270°C, and 550°C. The highest

temperature growths were characterized by thermal decomposition, where the RMS roughness increased and breakdown voltage decreased. Room-temperature deposition delivered the highest-quality oxide in terms of a breakdown voltage but also introduced a small hysteresis. In addition, the effective valence band offsets of SiO₂/GaN decreased slightly with deposition temperature, suggesting the introduction of an electrical field across an interfacial Ga₂O₃ layer during the oxygen plasma exposure during PEALD; this field was reducible with annealing. In addition, results suggest the growth of subcutaneous oxide during the deposition process, which was facilitated by high temperature.

(3) *Aluminum content effects on surface and interface electronic state configuration.* In this study, GaN and Al_xGa_{1-x}N with three different contents of aluminum—i.e. 15%, 25%, and 35%—were used to investigate the effects of the aluminum content as well as polarization bound charge on the surface and interface. The cleaning process used on the Al_xGa_{1-x}N surfaces reduced oxygen coverage and carbon contamination below the detection limit of the XPS. These oxygen-free surfaces were characterized by band bending that increased slightly with the polarization bound charge, suggesting the pinning state previously observed was likely related to oxygen states. In addition, the band offsets at the PEALD-SiO₂/Al_xGa_{1-x}N interface were measured as 3.0 eV, 2.9 eV, 2.9 eV, and 2.8 eV for 0%, 15%, 25%, and 35% aluminum content, respectively. This suggests the largest difference in that band gap manifests in the conduction band offsets, which is in agreement with the charge neutrality level model.

II. Future Potential and Development

The potential for future development of this work is extensive, largely as a result of the variability and versatility associated with the PEALD processes. However, it is likely that GaN will continue to be a promising area of research and development as well. In particular, there are three areas of proposed work focus on PEALD dielectrics on GaN and AlGaIn interfaces, including the role of Ga₂O₃ as an interfacial passivation layer, PEALD as a tool to tune the dielectric properties, and the role of the polarization charge in AlGaIn/GaN interfaces as will be discussed.

A. Ga₂O₃ as an Interface Passivation Layer

Precision control of the ALD-dielectric/GaN interface is dependent on the initial surface of GaN prior to ALD deposition. In particular, GaN surfaces are inevitably contaminated with some carbon and oxygen as part of native oxides, adsorbates, and residual species unless *in-situ* growth of GaN is possible. (As previously mentioned, Edwards *et al.* [1] suggested that air-exposed GaN consists of ~2-5 nm of contamination—about half of which is related to a native oxide.) Removal of this oxide contamination without damaging the substrate has proven difficult, e.g. high temperatures or sputtering treatments are often required to remove the oxide, which are likely to cause substrate damage as well [2]. Consequently, removal of the oxide layer may not be advantageous for devices.

On the other hand, the role of Ga₂O₃ on device performance remains unclear. To date, some studies have focused on Ga₂O₃ as a gate dielectric and passivation layer for GaN and AlGaIn MOS devices. While the band gap of Ga₂O₃ is small (4.8 eV), the dielectric

constant offers some possible advantages for device scaling (10.2-14.2). Thermal oxidation is not a viable method for Ga₂O₃ growth because high temperatures (>800°C) are required [3], which damage the GaN. Chemical methods have been employed with some success. Lee *et al.* [4] oxidized GaN with a H₃PO₄ solution and laser illumination. Results demonstrated a low D_{it} of 2.5x10¹¹ cm⁻²eV⁻¹, reasonable leakage current (6x10⁻⁷ A/cm⁻² at -20 V), and reasonable forward and reverse breakdown field (2.80 MV/cm and 5.70 MV/cm respectively). These results suggest that Ga₂O₃ may be reasonable as an interfacial passivation layer between GaN and an ALD dielectric. In particular, the lower band gap of Ga₂O₃ would likely require a large band gap dielectric—e.g. Al₂O₃—to suppress the leakage current. Moreover, it has been suggested that surface oxidation of GaN and AlN introduces donor states that favorably influence the concentration of the two-dimensional electron gas in AlGaN/GaN heterostructures [5-7].

Future work will, therefore, investigate the effects of Ga₂O₃ as an interfacial passivation layer at the dielectric/GaN interface. In particular, we will compare the effects of native Ga₂O₃ to O₂ plasma-grown and ALD-deposited Ga₂O₃ using gallium(III) acetylacetonate and oxygen plasma. Hopefully, the plasma and ALD process will provide a higher quality Ga₂O₃ layer and thus provide an effective passivation layer for other oxygen PEALD dielectric layers. In addition to the band alignment measures, this work will be augmented with electrical characterization of the interface as well.

B. Tuning Dielectric Properties

Tuning dielectric properties is possible with a PEALD process; however, to what extent this is possible for a given property in a given process requires further analysis. In

particular, incorporation of the plasma in that ALD process includes additional parameters—such as plasma power, pressure, time, and ion bombardment—that may effect film properties in addition to temperature utilized in traditional ALD. The applications for this process are countless, where ALD has applications in almost any area of nanotechnology research, with its popularity in research and industry continually growing.

1. Crystallinity

Control of interface crystallinity is typically achieved by lattice-matched substrates or elevated temperature processing. Powerful effects related to chemical interactions, molecular energy transfer, UV illumination, and molecular kinetic energy transfer are not readily available in traditional sputtering, molecular beam epitaxy, or chemical vapor deposition systems. In the last decade, there has been a revolution in interface chemistry control using atomic layer deposition (ALD). In particular, PEALD allows for more freedom in processing conditions and wider range of material properties. More specifically, the increased reactivity of the plasma enables deposition at lower substrate temperatures thereby reducing thermal damage to the substrate; permits the use of less reactive precursors thereby increasing the choice of precursors; allows for better control of stoichiometry and film composition; and accelerates growth. The results are films with improved material properties, such as film density, impurity content, and electronic properties. Furthermore, the oxygen plasma allows for more processing versatility.

Further advantages relate to the crystallinity of the deposited materials (which is specific to this RFI). It has been suggested that PEALD may reduce the temperatures required to

achieve crystallinity. In a recent review article, Miikkulainen *et al.* [2] demonstrate “the use of plasma enhancement increases the probability of depositing a crystalline film but does not guarantee it.” In addition, the article discussed the prevalence of polycrystalline ALD films consisting of columnar grains where the randomness of orientation depended on deposition temperature.

Moreover, other surface processes including molecular energy transfer, UV illumination, and molecular kinetic energy transfer can now be incorporated in ALD processes. The combination of these processes has been termed energy-enhanced ALD (EEALD). This variation of ALD is set to revolutionize thin film interfaces again with precise control of chemistry, morphology, and crystallinity.

2. Energy-Enhanced ALD

The following four processes are proposed key elements of a new strategy to employ EEALD for tunable interfaces as shown in FIG 8.2:

Remote plasma free radical formation. The most studied EEALD process is where plasma excitation is employed to increase the reactivity in one of the precursor cycles. The process creates a high concentration of radicals that interact with the surface. Oxygen plasma is the most studied process and is most often used to form a range of oxide films. Hydrogen, nitrogen, and ammonia plasma steps have also been used for metal and nitride materials. Remote plasma excitation reduces ion interactions while the increased energy provided by this method enables processes to occur at lower temperatures [8,9].

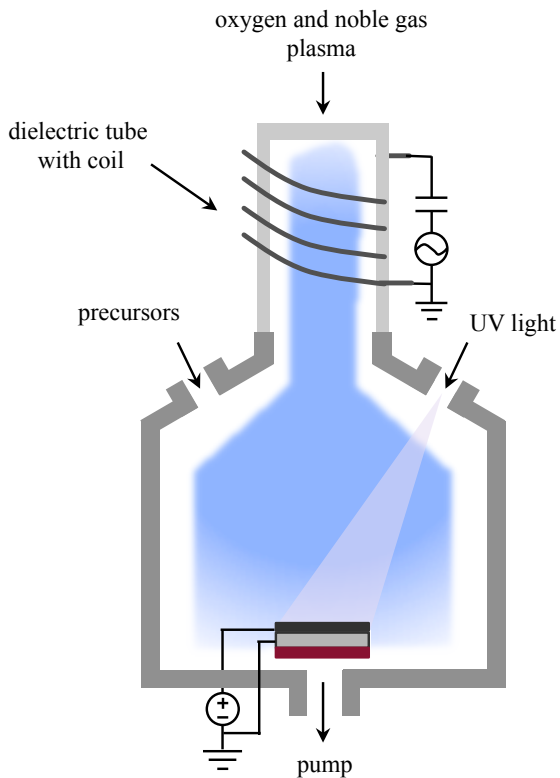


FIG 8.1 Schematic of EE-ALD chamber as modified to include plasma processing, UV illumination, and sample biasing.

Molecular energy transfer. The concept is that excited molecules can transfer a significant and controlled energy pulse to surface species. The process may involve plasma-excited noble gases (He, Ne, Ar, Kr), which can transfer eVs of energy without chemical interactions. The additional energy could enable nucleation or crystal growth at temperatures lower than achievable by MBE or other beam techniques. The implementation is through an additional plasma pulse and purge that is included in the ALD cycle.

UV illumination. UV photons can transfer eVs of energy typically to within a few nanometers of the surface. Broadband UV illumination is effective at desorbing loosely bonded species and may also contribute to improved crystallinity. Broadband illumination can be obtained from plasma-excited species (He, Ne, Ar, Kr etc.). Highly

tuned illumination from an external source can be employed to enhance surface reactivity of specific molecular structures. In each case, a separate pulse may be included in the ALD cycle.

Molecular kinetic energy transfer. Kinetic energy from ions accelerated towards the substrate can be employed to control crystallinity through forming renucleation sites. At very low substrate bias, the ions can contribute to controlling or enhancing the surface reactions [10]. The process would be implemented through a plasma step with sample bias.

EEALD growth cycle can be effectively engineered to achieve specific thin film chemistry, morphology, and crystallinity. It is notable that varying the precursor sequence in ALD can control the interface chemical composition with essentially atomic layer precision. Additional pulses can be readily incorporated into an EEALD growth cycle.

3. Implications for Dielectrics

As previously mentioned, plasma-enhanced ALD allows for more versatility and tuning of material properties. In previous work, we have demonstrated that the density of amorphous Al_2O_3 may vary not only with substrate temperature but also plasma power; however, these results require further development and only indicate the density as related to amorphous films. This variation in density likely explains the variation in band gap measurements for Al_2O_3 , which range from 6.5 to 7.0 eV [11-15]. Therefore, plasma tuning may permit tuning of the band gap of amorphous Al_2O_3 , which will ultimately help determine the carrier confinement characteristics in $\text{Al}_2\text{O}_3/\text{GaN}$ heterostructures.

Research shows that to date, crystalline Al_2O_3 has required growth conditions $>600^\circ\text{C}$ as dependent on the precursor and substrate [16], even for plasma-enhanced ALD. In this case, it is, therefore, unlikely that crystalline structures will be achieved without additional energy enhancement as provided by UV illumination and sample biasing. Kessels *et al.* [17] have shown that sample biasing effects the tensile stress in Al_2O_3 films but have not yet been able to change the crystal structure at low temperatures.

Similarly, ALD HfO_2 may also provide some insights into this process given the complex relationship between the deposition characteristics and crystalline phase. Moreover, there is evidence that crystalline HfO_2 can be achieved at lower temperatures in PEALD. For example, Kim *et al.* [18] compared HfO_2 as grown in oxygen PEALD and thermal ALD at 250°C ; the films as deposited by thermal ALD were amorphous, while those deposited by PEALD were partially crystallized. It is, therefore, likely that further development of the plasma deposition process would improve the crystallinity of the films, particularly if supported by the additional energy-enhancement methods discussed. Moreover, research has indicated that biasing in this process has led to improved electrical properties, though it stills remains unclear how this improvement is related to film properties.

Future work will continue to investigate the effects of the energy-enhanced atomic layer deposition on dielectric/GaN structures with more emphasis on the crystal structure as dependent on the deposition parameters. In particular, we will further our understanding of the role of the oxygen plasma parameters in the deposition of Al_2O_2 and HfO_2 and whether additional mechanisms of energy transfer such as molecular transfer, UV illumination, or sample biasing can induce crystalline structures at lower temperatures.

C. Dielectric/AlGa_N/Ga_N Heterostructures

AlGa_N/Ga_N heterostructures are promising as well. The different polarization of the AlGa_N and Ga_N layers results in positive polarization bound charge at the AlGa_N/Ga_N interface. Consequently, the formation of a 2D electron gas (2DEG) at the interface is favored, which effectively reduces on-resistance and power loss. This high electron mobility makes AlGa_N/Ga_N heterostructures applicable in high-frequency requirements associated with HFETs and HEMTs.

More specifically, both Ga_N and AlGa_N are characterized by a large spontaneous polarization and thus bound polarization charge of 2.2×10^{13} and 3.2×10^{13} charges/cm² at their respective surfaces. This charge must be compensated, giving rise to a large concentration of interface defects at the surface as shown in FIG 8.2. The effects of this charge are not well understood. Charge neutrality would suggest that for an undoped AlGa_N layer, a higher concentration of surface states would engender a higher 2DEG concentration; however, a large concentration of surface defects also affects the potential drop across the AlGa_N layer as well as device reliability increasing the gate leakage current and current collapse, which may be mitigated with the deposition of a dielectric layer. There is, therefore, a complex relationship between the types of surface states and device performance.

In future research, we will extend our investigation of the band alignment and bend bending of ALD dielectrics onto AlGa_N/Ga_N heterostructures. In this regard, a monochromatic x-ray source will play a crucial role; the increased resolution of the new XPS source will allow us to distinguish the Ga and N core levels in AlGa_N from those in

GaN, and we will, therefore, be able to determine the band alignment of the AlGaN/GaN heterostructure. This will allow us to continue researching the viability of the various dielectrics on AlGaN/GaN as well—including Al_2O_3 , which is also characterized by multiple core level states. Characterization of the ALD-dielectric/AlGaN/GaN heterostructure will thus focus on the band bending at the AlGaN/GaN interface as indicative of the 2DEG for various surface pretreatment, dielectric deposition, and post-deposition anneals.

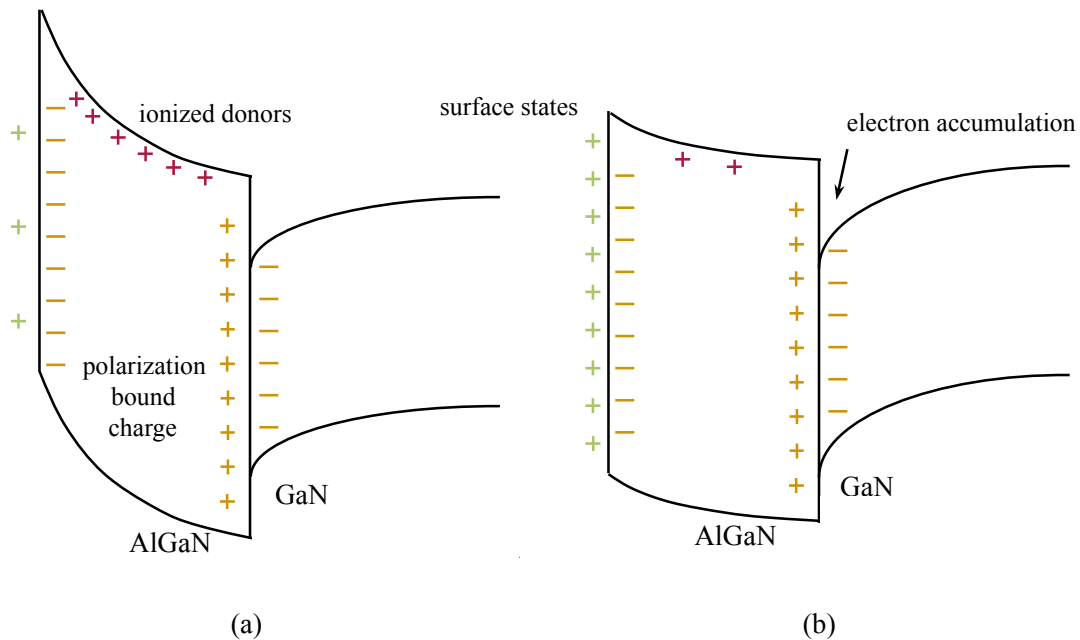


FIG 8.2 Interface charge distribution at the AlGaN/GaN heterostructure, where the changes in surface states on the AlGaN layer or dielectric/AlGaN interface will affect the charge distribution and may have possible implications on the 2DEG concentration.

References

- [1] N. V. Edwards, M. D. Bremser, T. W. Weeks, R. S. Kern, R. F. Davis, and D. E. Aspnes, *Appl. Phys. Lett.* 69, 2065 (1996).

- [2] B. S. Eller, J. Yang, and R. J. Nemanich, *J. Vac. Sci. Technol. A* 31, 050807 (2012).
- [3] S. D. Wolter, B. P. Luther, D. L. Waltmyer, C. Onneby, S. E. Mohny, and R. J. Molnar, *Appl. Phys. Lett.* 70, 2156 (1997).
- [4] C.-T. Lee, H.-W. Chen, and H.-Y. Lee, *Appl. Phys. Lett.* 82, 4304 (2003).
- [5] M. S. Miao, J. R. Weber, and C. G. Van de Walle, *J. Appl. Phys.* 107, 123713 (2010).
- [6] M. Higashiwaki, S. Chowdhury, M.-S. Miao, B. L. Swenson, C. G. Van de Walle, and U. K. Mishra, *J. Appl. Phys.* 108, 063719 (2010)
- [7] M. Higashiwaki, S. Chowdhury, B. L. Swenson, and U. K. Mishra, *Appl. Phys. Lett.* 97, 222104 (2010)
- [8] S. E. Potts and W. M. M. Kessels, *Coord. Chem. Rev.* 257, 3254 (2013).
- [9] S. E. Potts, H. B. Profijt, R. Roelofs, and W. M. M. Kessels, *Chem. Vac. Dep.* 19, 125 (2013).
- [10] H. B. Profijt, M. C. M. van de Sanden, and W. M. M. Kessels, *J. Vac. Sci. Technol. A* 31, 01A106 (2013).
- [11] E. Bersch, S. Rangan, R. A. Bartynski, E. Garfunkel, and E. Vescovo, *Phys. Rev. B* 78, 085114 (2008).
- [12] R. H. French, *J. Am. Ceram. Soc.* 73, 477 (1990).
- [13] H. Nohira, W. Tsai, W. Besling, E. Young, J. Petry, T. Conard, W. Vandervorst, S. De Gendt, M. Heyns, J. Maes, and M. Tuominen, *J. Non-Cryst. Solids* 303, 83 (2002).
- [14] S. Miyazaki, *J. Vac. Sci. Technol. B* 19, 2212 (2001).
- [15] J. Yang, B. S. Eller, M. Kaur, and R. J. Nemanich, *J. Vac. Sci. Tech. A* 32, 021514 (2014).
- [16] V. Miikkulainen, M. Leskelä, M. Ritala, and R. L. Puurunen, *J. Appl. Phys.* 113, 021301 (2013).
- [17] H. B. Profijt, M. C. M. van de Sanden, and W. M. M. Kessels, *J. Vac. Sci. Technol. A* 31, 01A106 (2013).
- [18] J. Kim, S. Kim, H. Kang, J. Choi, H. Jeon, M. Cho, K. Chung, S. Back, K. Yoo, and C. Bae, *J. Appl. Phys.* 98, 094504 (2005).

REFERENCES

- U. K. Mishra, P. Parikh, and Y. F. Wu, *Proc. IEEE* 90, 1022 (2002).
- W. Saito, Y. Takada, M. Kuraguchi, K. Tsuda, I. Omura, T. Ogura, and H. Ohashi, *IEEE Trans. Electron Devices* 50, 2528 (2003).
- Y. Niiyama, S. Ootomo, J. Li, T. Nomura, S. Kato, and T. P. Chow, *Semicond. Sci. Technol.* 25, 125006 (2010).
- S. J. Pearton, and F. Ren, *Adv. Mater.* 12, 1571 (2000).
- G. Meneghesso, G. Verzellesi, F. Danesin, F. Rampazzo, F. Zanon, A. Tazzoli, M. Meneghini, and E. Zanoni, *IEEE Trans. Device Mater. Rel.* 8, 332 (2008).
- J. A. del Alamo, and J. Joh, *Microelectron. Reliab.* 49, 1200 (2010).
- D. Marcon, J. Viaene, P. Favia, H. Bender, X. Kang, S. Lenci, S. Stoffels, and S. Decoutere, *Microelectron. Reliab.* 52, 2188 (2012).
- J. Wuerfl, E. Bahat-Treidel, F. Brunner, E. Cho, O. Hilt, P. Ivo, A. Knauer, P. Kurpas, R. Lossy, M. Schulz, S. Singwald, M. Weyers, and R. Zhytnytska, *Microelectron. Reliab.* 51, 1710 (2011).
- S. Mizuno, Y. Ohno, S. Kishimoto, K. Maezawa, and T. Mizutani, *Jpn. J. Appl. Phys. Part I* 41, 5125 (2002).
- J. C. Carrano, T. Li, P. A. Grudowski, C. J. Eiting, R. D. Dupuis, and J. C. Campbell, *Appl. Phys. Lett.* 72, 542 (1998).
- S. Oyama, T. Hashizume, and H. Hasegawa, *Appl. Surf. Sci.* 190, 322 (2002).
- H. Hasegawa, and S. Oyama, *J. Vac. Sci. Technol. B* 20, 1647 (2002).
- L. S. Yu, Q. Z. Liu, Q. J. Xing, D. J. Qiao, S. S. Lau, and J. Redwing, *J. Appl. Phys.* 84, 2099 (1998).
- C. F. Shih, K. T. Hung, C. Y. Hsiao, S. C. Shu, and W. M. Li, *J. Alloys Compd.* 480, 541 (2009).
- X. A. Cao, S. J. Pearton, G. Dang, A. P. Zhang, F. Ren, and J. M. Van Hove, *Appl. Phys. Lett.* 75, 4130 (1999).
- E. J. Miller, X. Z. Dang, and E. T. Yu, *J. Appl. Phys.* 88, 5951 (2000).
- E. J. Miller, E. T. Yu, P. Waltereit, and J. S. Speck, *Appl. Phys. Lett.* 84, 535 (2004).

- S. Karmalkar D. M. Sathaiya, and M. S. Shur, *Appl. Phys. Lett.* 82, 3976 (2003).
- B. Lambert, N. Labat, D. Carisetti, S. Karboyan, J. G. Tartarin, J. Thorpe, L. Brunel, A. Curutchet, N. Malbert, E. Latu-Romain, and M. Mermoux, *Microelectron. Reliab.* 52, 2184 (2012).
- H. Zhang, E. J. Miller, and E. T. Yu, *J. Appl. Phys.* 99, 023703 (2006).
- A. Fonserè, A. Pérez-Tomás, M. Placidi, J. Llobet, N. Baron, S. Chenot, Y. Cordier, J. C. Moreno, V. Iglesias, M. Porti, A. Bayerl, M. Lanza, and M. Nafia, *Appl. Phys. Lett.* 101, 093505 (2012).
- L.-Y. Yang, Y. Hao, X.-H. Ma, J.-C. Zhang, C.-Y. Pan, J.-G. Ma, K. Zhang, and P. Ma, *Chin. Phys. B* 20, 117302 (2011).
- Z. H. Liu, G. I. Ng, S. Arulkumaran, Y. K. T. Maung, and H. Zhou, *Appl. Phys. Lett.* 98, 163501 (2011).
- S. Sudharsanan, and S. Karmalkar, *J. Appl. Phys.* 107, 064501 (2010).
- X. A. Cao, E. B. Stokes, P. M. Sandvik, S. F. LeBoeuf, J. Kretchmer, and D. Walker, *IEEE Electron Device Lett.* 23, 535 (2002).
- E. Arslan, S. Altindal, S. Özçelik, and E. Ozbay, *J. Appl. Phys.* 105, 023705 (2009).
- D.-W. Yan, Z.-M. Zhu, J.-M. Cheng, X.-F. Gu, and H. Lu, *Chinese Phys. Lett.* 29 087204 (2012).
- D. Yan, H. Lu, D. Cao, D. Chen, R. Zhang, and Y. Zheng, *Appl. Phys. Lett.* 97, 153503 (2010).
- W. S. Tan, P. A. Houston, P. J. Parbrook, D. A. Wood, G. Hill, and C. R. Whitehouse, *Appl. Phys. Lett.* 80, 3207 (2002).
- A. Mimouni, T. Fernández, J. Rodriguez-Tellez, A. Tazon, H. Baudrand, and M. Boussuis, *Electr. Electron. Eng.* 2, 397 (2012).
- X. M. Shen, D. G. Zhao, Z. S. Liu, Z. F. Hu, H. Yang, and J. W. Liang, *Solid-State Electron.* 49, 847 (2005).
- V. Lebedev, G. Cherkashinin, G. Ecke, I. Cimalla, and O. Ambacher, *J. Appl. Phys.* 101, 033705 (2007).
- W. Xu, H. Rao, and G. Bosman, *Appl. Phys. Lett.* 100, 223504 (2012).
- S. W. Kaun, M. H. Wong, S. DasGupta, S. Choi, R. Chung, U. K. Mishra, and J. S. Speck, *Appl. Phys. Express* 4, 024101 (2011).

S. Ganguly, A. Konar, Z. Hu, H. Xing, and D. Jena, *Appl. Phys. Lett.* 101, 253519 (2012).

G. Xie, E. Xu, B. Zhang, and W. T. Ng, *Microelectron. Reliab.* 52, 964 (2012).

M. M. Bajo, C. Hodges, M. J. Uren, and M. Kubali, *Appl. Phys. Lett.* 101, 033508 (2012).

M. Baeumler, F. Gütle, V. Polyakov, M. Cäsar, M. Dammann, H. Konstanzer, W. Pletschen, W. Bronner, R. Quay, P. Waltereit, M. Mikulla, O. Ambacher, F. Bourgeois, R. Behtash, K. J. Riepe, P. J. Van de Wel, J. Klappe, and T. Rödle, *J. Electron. Mater.* 39, 756 (2010).

M. Ľapajna, S. W. Kaun, M. H. Wong, F. Gao, T. Palacios, U. K. Mishra, J. S. Speck, and M. Kuball, *Appl. Phys. Lett.* 99, 223501 (2011).

C.-Y. Hu, and T. Hashizume, *J. Appl. Phys.* 111, 084504 (2012).

P. Makaram, J. Joh, J. A. del Alamo, T. Palacios, and C. V. Thompson, *Appl. Phys. Lett.* 96, 233509 (2010).

M. R. Johnson, D. A. Cullen, L. Liu, T. S. Kang, F. Ren, C.-Y. Chang, S. J. Pearton, S. Jang, J. W. Johnson, and D. J. Smith, *J. Vac. Sci. Technol. B* 30, 062204 (2012).

H. Hasegawa, T. Inagaki, S. Ootomo, and T. Hashizume, *J. Vac. Sci. Technol. B* 21, 1844 (2003).

H. Hasegawa, and H. Ohno, *J. Vac. Sci. Technol. B* 4, 1130 (1986).

T. Hashizume, J. Kotani, and H. Hasegawa, *Appl. Phys. Lett.* 84, 4884 (2004).

K. H. Lee, P. C. Chang, S. J. Chang, and Y. K. Su, *Solid-State Electron.* 72, 38 (2012).

C. J. Kirkpatrick, B. Lee, R. Suri, X. Yang, and V. Misra, *IEEE Electron Device Lett.* 33, 1240 (2012).

L. Pang, Y. Lian, D.-S. Kim, J.-H. Lee, and K. Kim, *IEEE Trans. Electron Devices* 59, 2650 (2012).

F. Husna, M. Lachab, M. Sultana, V. Adivarahan, Q. Fareed, and M. Asif Khan, *IEEE Trans. Electron Devices* 59, 2424 (2012).

M. Lachab, M. Sultana, H. Fatima, V. Adivarahan, Q. Fareed, and M. A. Khan, *Semicond. Sci. Technol.* 27, 125001 (2012).

T. Huang, X. Zhu, K. M. Wong, and K. M. Lau, *IEEE Electron Device Lett.* 33, 212 (2012).

Y. C. Chang, W. H. Chang, Y. H. Chang, J. Kwo, Y. S. Lin, S. H. Hsu, J. M. Hong, C. C. Tsai, and M. Hong, *Microelectron. Eng.* 87, 2042 (2010).

E. Miyazaki, Y. Goda, S. Kishimoto, and T. Mizutani, *Solid-State Electron.* 62, 152 (2011).

Y. C. Chang, M. L. Huang, Y. H. Chang, Y. J. Lee, H. C. Chiu, J. Kwo, and M. Hong, *Microelectron. Eng.* 88, 1207 (2011).

Z. W. Bi, Y. Hao, Q. Feng, T. T. Jiang, Y. R. Cao, J. C. Zhang, W. Mao, L. Lu, and Y. Zhang, *Sci. Chin. Phys. Mech. Astron.* 54, 2170 (2011).

H. Hahn, A. Alam, M. Heuken, H. Kalisch, and A. Vescan, *Semicond. Sci. Technol.* 27, 062001 (2012).

T. Hashizume, S. Anantathanasarn, N. Negoro, E. Sano, H. Hasegawa, K. Kumakura, and T. Makimoto, *Jpn. J. Appl. Phys.* 43, L777 (2004).

J. J. Freedman, T. Kubo, S. L. Selvaraj, and T. Egawa, *Jpn. J. Appl. Phys.* 50, 04DF03 (2011).

H.-A. Shih, M. Kudo, M. Akabori, and T.-K. Suzuki, *Jpn. J. Appl. Phys.* 51, 02BF01 (2012).

H.-C. Chiu, C.-W. Yang, C.-H. Chen, J. S. Fu, and F.-T. Chien, *Appl. Phys. Lett.* 99, 153508 (2011).

K. D. Chabak, D. E. Walker, M. R. Johnson, A. Crespo, A. M. Dabiran, D. J. Smith, A. M. Wowchak, S. K. Tetlak, M. Kossler, J. K. Gillespie, R. C. Fitch, and M. Trejo, *IEEE Electron Device Lett.* 32, 1677 (2011).

M. Āapajna, N. Killat, U. Chowdhury, J. L. Jimenez, and M. Kuball, *Microelectron. Reliab.* 52, 29 (2012).

R. Vetury, N. Q. Zhang, S. Keller, and U. K. Mishra, *IEEE Trans. Electron Devices* 48, 560 (2001).

J. A. Bardwell, S. Haffouz, W. R. McKinnon, C. Storey, H. Tang, G. I. Sproule, D. Roth, and R. Wang, *Electrochem. Solid-State Lett.* 10, H46 (2007).

A. Koudymov, M. S. Shur, G. Simin, K. Chu, P. C. Chao, C. Lee, J. Jimenez, and A. Balistreri, *IEEE Trans. Electron Devices* 55, 712 (2008).

M. Morardi, and P. Valizadeh, *IEEE Trans. Device Mater. Rel.* 10, 287 (2010).

F. Gao, D. Chen, B. Lu, H. L. Tuller, C. V. Thompson, S. Keller, U. K. Mishra, and T. Palacios, *IEEE Electron Device Lett.* 33, 1378 (2012).

- M. Tajima, and T. Hashizume, *Jpn. J. Appl. Phys.* 50, 061001 (2011).
- G. Meneghesso, G. Verzellesi, R. Pierobon, F. Rampazzo, A. Chini, U. K. Mishra, C. Canali, and E. Zanoni, *IEEE Trans. Electron Devices* 51, 1554 (2004).
- A. M. Wells, M. J. Uren, R. S. Balmer, K. P. Hilton, T. Martin, and M. Missous, *Solid-State Electron.* 49, 279 (2005).
- J. Joh, and J. A. del Alamo, *IEEE Trans. Electron Devices* 58, 132 (2011).
- F. Berthet, Y. Guhel, H. Gualous, B. Boudart, J.-L. Trolet, M. Piccione, V. Sbrugnera, B. Grimbert, and C. Gaquière, *Solid-State Electron.* 72, 15 (2012).
- S. DasGupta L. B. Biedermann, M. Sun, R. Kaplar, M. Marinella, K. R. Zavadil, S. Atcity, and T. Palacios, *Appl. Phys. Lett.* 101, 243506 (2012).
- W. Zhang, Y. Zhang, W. Mao, X.-H. Ma, J.-C. Zhang, and Y. Hao, *IEEE Electron Device Lett.* 34, 45 (2013).
- C. Zhou, Q. Jiang, S. Huang, and K. J. Chen, *IEEE Electron Device Lett.* 33, 1132 (2012).
- M. Faqir, M. Bouya, N. Malbert, N. Labat, D. Carisetti, B. Lambert, G. Verzellesi, and F. Fantini, *Microelectron. Reliab.* 50, 1520 (2010).
- P. B. Klein, J. A. Freitas, S. C. Binari, and A. E. Wickenden, *Appl. Phys. Lett.* 75, 4016 (1999).
- P. B. Klein, S. C. Binari, K. Ikossi, A. E. Wickenden, D. D. Koleske, and R. L. Henry, *Appl. Phys. Lett.* 79, 3527 (2001).
- M. J. Uren, J. Möreke, and M Kuball, *IEEE Trans. Electron Devices* 59, 3327 (2012).
- T. B. Fehlberg, J. S. Milne, G. A. Umana-Membreno, S. Keller, U. K. Mishra, B. D. Nener, and G. Parish, *IEEE Trans. Electron Devices* 58, 2589 (2011).
- E. A. Douglas, C. Y. Chang, D. J. Cheney, B. P. Gila, C. F. Lo, L. Lu, R. Holzworth, P. Whiting, K. Jones, G. D. Via, J. Kim, S. Jang, F. Ren, and S. J. Pearton, *Microelectron. Reliab.* 51, 207 (2011).
- L. Liu, F. Ren, S. J. Pearton, R. C. Fitch, D. E. Walker, K. D. Chabak, J. K. Gillespie, M. Kossier, M. Trejo, D. Via, and A. Crespo, *J. Vac. Sci. Technol. B* 29, 060603 (2011).
- M. Esposito, V. Di Lecce, M. Bonaiuti, and A. Chini, *J. Electron. Mater.* 42, 15 (2013).
- M. Fagerlind, and N. Rorsman, *J. Appl. Phys.* 112, 014511 (2012).

B. M. Green, K. K. Chu, E. M. Chumbes, J. A. Smart, J. R. Shealy, and L. F. Eastman, *IEEE Electron Device Lett.* 21, 268 (2000).

M. F. Romero, M. M. Sanz, I. Tanarro, A. Jiménez, and E. Muñoz, *J. Phys. D: Appl. Phys.* 43, 495202 (2010).

R. C. Fitch, D. E. Walker, K. D. Chabak, J. K. Gillespie, M. Kossler, M. Trejo, A. Crespo, L. Liu, T. S. Kang, C.-F. Lo, F. Ren, D. J. Cheney, and S. J. Pearton, *J. Vac. Sci. Technol. B* 29, 061204 (2011).

T. Mizutani, Y. Ohno, M. Akita, S. Kishimoto, and K. Maezawa, *IEEE Trans. Electron Devices* 50, 2015 (2003).

M. Higashiwaki, Y. Pei, R. Chu, and U. K. Mishra, *IEEE Trans. Electron Devices* 58, 1681 (2011).

T. Hashizume, S. Ootomo, T. Inagaki, and H. Hasegawa, *J. Vac. Sci. Technol. B* 21, 1828 (2003).

T. Hashizume, S. Ootomo, and H. Hasegawa, *Appl. Phys. Lett.* 83, 2952 (2003).

J. J. Kim, G. M. Yang, K.-H. Shim, and J. W. Yang, *Jpn. J. Appl. Phys.* 50, 096501 (2011).

F. Gao, B. Lu, L. Li, S. Kuan, J. S. Speck, C. V. Thompson, and T. Palacios, *Appl. Phys. Lett.* 99, 223506 (2011).

E. T. Yu, X. Z. Dang, P. M. Asbeck, S. S. Lau, and G. J. Sullivan, *J. Vac. Sci. Technol. B* 17, 1742 (1999).

O. Ambacher, J. Smart, J. R. Shealy, N. G. Weimann, K. Chu, M. Murphy, W. J. Schaff, L. F. Eastman, R. Dimitrov, L. Wittmer, M. Stutzmann, W. Rieger, and J. Hilsenbeck, *J. Appl. Phys.* 85, 3222 (1999).

V. A. Savastenko, and A. U. Sheleg, *Phys. Status Solidi A* 48, K135 (1978).

Y. Takagi, M. Ahart, T. Azuhata, T. Sota, K. Suzuki, and S. Nakamura, *Physica B* 219/220, 547 (1996).

A. Polian, M. Grimsditch, and I. Grezegory, *J. Appl. Phys.* 79, 3343 (1996).

R. B. Schwartz, K. Khachatryan, and E. R. Webber, *Appl. Phys. Lett.* 70, 1122 (1997).

C. Deger, E. Born, H. Angerer, O. Ambacher, M. Stutzmann, J. Hornsteiner, E. Riha, and G. Fischerauer, *Appl. Phys. Lett.* 72, 2400 (1998).

K. Tsubouchi, and N. Mikoshiba, *IEEE Trans. Sonics Ultrason.* 32, 634 (1985).

L. E. McNeil, M. Grimsditch, and R. H. French, *J. Am. Ceram. Soc.* 76, 1132 (1993).

K. Kim, W. R. L. Lambrecht, and B. Segall, *Phys. Rev. B* 53, 16310 (1996).

A. F. Wright, *J. Appl. Phys.* 82, 2833 (1997).

F. Bernardini, V. Fiorentini, and D. Vanderbilt, *Phys. Rev. B* 56, R10024 (1997).

F. Bernardini, V. Fiorentini, and D. Vanderbilt, *Phys. Rev. B* 63, 193201 (2001).

Y. Duan, J. Li, S.-S. Li, and J.-B. Xia, *J. Appl. Phys.* 103, 023705 (2008).

K. Shimada, A. Zenpuku, K. Fukiwara, K. Hazu, S. F. Chichibu, M. Hata, H. Sazawa, T. Takada, and T. Sota, *J. Appl. Phys.* 110, 074114 (2011).

W. S. Yan, R. Zhang, Z. L. Xie, X. Q. Xiu, P. Han, H. Lu, P. Chen, S. L. Gu, Y. Shi, Y. D. Zheng, and Z. G. Liu, *Appl. Phys. Lett.* 94, 042106 (2009).

J. Lähnemann, O. Brandt, U. Jahn, C. Pfüller, C. Roder, P. Dogan, F. Grosse, A. Belabbes, F. Bechstedt, A. Trampert, and L. Geelhaar, *Phys. Rev. B* 86, 081302(R).(2012).

J. Yang, B. S. Eller, C. Zhu, C. England, and R. J. Nemanich, *J. Appl. Phys.* 112, 053710 (2012).

H. W. Jang, J.-H. Lee, and J.-L. Lee, *Appl. Phys. Lett.* 80, 3955 (2002).

M. Hong, K. A. Anselm, J. Kwo, H. M. Ng, J. N. Baillargeon, A. R. Kortan, J. P. Mannaerts, A. Y. Cho, C. M. Lee, J. I. Chyi, and T. S. Lay, *J. Vac. Sci. Technol. B* 18, 1453 (2000).

Y. Q. Wu, T. Shen, P. D. Ye, and G. D. Wilk, *Appl. Phys. Lett.* 90, 143504 (2007).

W. J. Mecouch, B. P. Wagner, Z. J. Reitmeier, R. F. Davis, C. Pandarinath, B. J. Rodriguez, and R. J. Nemanich, *J. Vac. Sci. Technol. A* 23, 72 (2005).

U. Karrer, O. Ambacher, and M. Stutzmann, *Appl. Phys. Lett.* 77, 2012 (2000).

P. Lorenz, T. Haensel, R. Gutt, R. J. Koch, J. A. Schaefer, and S. Krischok, *Physica Status Solidi B* 247, 1658 (2010).

V. M. Polyakov, F. S. Tautz, S. Sloboshanin, J. A. Schaefer, A. S. Usikoy, and B. Ja. Ber, *Semicond. Sci. Technol.* 13, 1396 (1998).

I. Tamm, *Physik. Zeits. Sowjetunion* 1, 733 (1932).

W. Shockley, *Phys. Rev.* 56, 317 (1939).

J. Fritsch, O. F. Sankey, K. E. Schmidt, and J. B. Page, *Phys. Rev. B* 57, 15360 (1998).

J. E. Northrop, R. Di Felice, and J. Neugebauer, *Phys. Rev. B* 55, 13878 (1997).

A. R. Smith, R. M. Feenstra, D. W. Greve, J. Neugebauer, and J. E. Northrup, *Phys. Rev. Lett.* 79, 3934 (1997).

R. H. French, *J. Am. Ceram. Soc.* 73, 477 (1990).

W. Schottky, *Phys. Z* 41, 570 (1940).

N. F. Mott, *Math. Proc. Cambridge* 34, 568 (1938).

J. Bardeen, *Phys. Rev.* 71, 717 (1947).

V. Heine, *Phys. Rev.* 138, A1689 (1965).

F. Flores, and C. Tejedor, *J. Phys. France* 38, 949 (1977).

C. Tejedor, and F. Flores, *J. Phys. C. Solid State Phys.* 11, L19 (1977).

J. Tersoff, *Phys. Rev. B* 30, 4874 (1984).

W. Mönch, *Appl. Surf. Sci.* 92, 367 (1996).

W. E. Spicer, P. W. Chye, P. R. Skeath, C. Y. Su, and I. Lindau, *J. Vac. Sci. Technol.* 16, 1422 (1979).

W. E. Spicer, I. Lindau, P. Skeath, and C. Y. Su, *J. Vac. Sci. Technol.* 17, 1019 (1980).

H. Hasegawa, and T. Sawada, *Thin Solid Films* 103, 119 (1983).

H. Hasegawa, Y. Koyama, and T. Hashizume, *Jpn. J. Appl. Phys.* 38, 2634 (1999).

J. M. Andrews, and J. C. Phillips, *Phys. Rev. Lett.* 35, 56 (1975).

L. J. Brillson, *Phys. Rev. Lett.* 40, 260 (1978).

R. L. Anderson, *Solid-State Electron.* 5, 341 (1962).

J. Tersoff, *Phys. Rev. Lett.* 52, 465 (1984).

J. Robertson, and B. Falabretti, *J. Appl. Phys.* 100, 014111 (2006).

M. Cardona, and N. E. Christensen, *Phys. Rev. B* 35, 6182 (1987).

W. Mönch, *J. Appl. Phys.* 80, 5076 (1996).

- A. Baldereschi, Phys. Rev. B 7, 5212 (1973).
- A. Franciosi, and C. G. Van de Walle, Surf. Sci. Rep. 25, 1 (1996).
- C. G. Van de Walle, and J. Neugebauer, Appl. Phys. Lett. 70, 2577 (1997).
- G. C. Van de Walle, and R. M. Martin, Phys. Rev. B 35, 8154 (1987).
- S. H. Wei, and A. Zunger, Appl. Phys. Lett. 72, 2011 (1998).
- Y-H. Li, A. Walsh, S. Chen, W.-J. Yin, J.-H. Yang, J. Li, J. L. F. Da Silva, X. G. Gong, and S. H. Wei, Appl. Phys. Lett. 94, 212109 (2009).
- T. Sawada, Y. Ito, N. Kimura, K. Imai, K. Suzuki, and S. Sakai, Appl. Surf. Sci. 190, 326 (2002).
- K. Shiojima, T. Sugahara, and S. Sakai, Appl. Phys. Lett. 74, 1936 (1999).
- K. A. Rickert, A. B. Ellis, J. K. Kim, J.-L. Lee, F. J. Himpsel, F. Dwikusuma, and T. F. Kuech, J. Appl. Phys. 92, 6671 (2002).
- J. Robertson, J. Vac. Sci. Technol. B 18, 1785 (2000).
- J. Zhang, C. Yang, S. Wu, Y. Liu, M. Zhang, H. Chen, W. Zhang, and Y. Li, Semicond. Sci. Technol. 25, 035011 (2010).
- T. Nakayama, and M. Murayama, J. Cryst. Growth 214/215, 299 (2000).
- H. S. Craft, R. Collazo, M. D. Losego, S. Mita, Z. Sitar, and J.-P. Maria, Appl. Phys. Lett. 92, 082907 (2008).
- T. S. Lay, M. Hong, J. Kwo, J. P. Mannaerts, W. H. Hung, and D. J. Huang, Solid-State Electron. 45, 1679 (2001).
- L. G. Gao, B. Xu, H. X. Guo, Y. D. Xia, J. Yin, and Z. G. Liu, Appl. Phys. Lett. 94, 252901 (2009).
- J. J. Chen, M. Hlad, A. P. Gerger, B. P. Gila, F. Ren, C. R. Abernathy, and S. J. Pearton, J. Electron. Mater. 36, 368 (2007).
- V. D. Wheeler, Ph. D. Thesis North Carolina State University, 2010.
- J.-J. Chen, B. P. Gila, M. Hlad, A. Gerger, F. Ren, C. R. Abernathy, and S. J. Pearton, Appl. Phys. Lett. 88, 142115 (2006).
- C. Liu, E. F. Chor, L. S. Tan, and Y. Dong, Appl. Phys. Lett. 88, 222113 (2006).

- H. S. Craft, Ph. D. Thesis University of North Carolina, 2010.
- S.-K. Hong, T. Hanada, H. Makino, Y. Chen, H.-J. Ko, T. Yao, A. Tanaka, H. Sasaki, and S. Sato, *Appl. Phys. Lett.* 78, 3349 (2001).
- H. F. Liu, G. X. Hu, H. Gong, K. Y. Zang, and S. J. Chua, *J. Vac. Sci. Technol. A* 26, 1462 (2008).
- Y. I. Alivov, B. Xiao, S. Akarca-Biyikli, Q. Fan, H. Morkoç, D. Johnstone, O. Lopatiuk-Tirpak, L. Chernyak, and W. Litton, *J. Phys. Condens. Matter* 20, 085201 (2008).
- B. Kramm, A. Laufer, D. Reppin, A. Kronenberger, P. Hering, A. Polity, and B. K. Meyer, *Appl. Phys. Lett.* 100, 094102 (2012).
- G. Martin, S. Strite, A. Botchkarev, A. Agarwal, A. Rockett, H. Morkoç, W. R. L. Lambrecht, and B. Segall, *Appl. Phys. Lett.* 65, 610 (1994).
- J. R. Waldrop, and R. W. Grant, *Appl. Phys. Lett.* 68, 2879 (1996).
- M. R. Coan, J. H. Woo, D. Johnson, I. R. Gatabi, and H. R. Harris, *J. Appl. Phys.* 112, 024508 (2012).
- R. Suri, Ph. D. Thesis North Carolina State University, 2010.
- M. Esposito, S. Krishnamoorthy, D. N. Nath, S. Bajaj, T. H. Hung, and S. Rajan, *Appl. Phys. Lett.* 99, 133503 (2011).
- W. Wei, Z. Qin, S. Fan, Z. Li, K. Shi, Q. Zhu, and G. Zhang, *Nanoscale Res. Lett.* 7, 562 (2012).
- T. E. Cook, C. C. Fulton, W. J. Mecouch, R. F. Davis, G. Lucovsky, and R. J. Nemanich, *J. Appl. Phys.* 94, 7155 (2003).
- C. Liu, E. F. Chor, and L. S. Tan, *Appl. Phys. Lett.* 88, 173504 (2006).
- H. S. Craft, R. Collazo, M. D. Losego, S. Mita, Z. Sitar, and J.-P. Maria, *J. Appl. Phys.* 102, 074104 (2007).
- J. J. Chen, B. P. Gila, M. Hlad, A. Gerger, F. Ren, C. R. Abernathy, and S. J. Pearton, *Appl. Phys. Lett.* 88, 042113 (2006).
- T. E. Cook, C. C. Fulton, W. J. Mecouch, R. F. Davis, G. Lucovsky, and R. J. Nemanich, *J. Appl. Phys.* 94, 3949 (2003).
- M. Kumar, B. Roul, T. N. Bhat, M. K. Rajpalke, A. T. Kalghatgi, and S. B. Krupanidhi, *Thin Solid Films* 520, 4911 (2012).

- R. Nakasaki, T. Hashizume, and H. Hasegawa, *Physica E* 7, 953 (2000).
- T. E. Cook, C. C. Fulton, W. J. Mecoouch, K. M. Tracy, R. F. Davis, E. H. Hurt, G. Lucovsky, and R. J. Nemanich, *J. Appl. Phys.* 93, 3995 (2003).
- I. Costina, and R. Franchy, *Appl. Phys. Lett.* 78, 4139 (2001).
- V. V. Afanas'ev, A. Stesmans, K. Cherkaoui, and P. K. Hurley, *Appl. Phys. Lett.* 96, 052103 (2010).
- X. Xu, X. Liu, Y. Guo, J. Wang, H. Song, S. Yang, H. Wei, Q. Zhu, and Z. Wang, *J. Appl. Phys.* 107, 104510 (2010).
- P. D. C. King, T. D. Veal, P. H. Jefferson, C. F. McConville, T. Wang, P. J. Parbrook, H. Lu, and W. J. Schaff, *Appl. Phys. Lett.* 90, 132105 (2007).
- C.-L. Wu, C.-H. Shen, and S. Gwo, *Appl. Phys. Lett.* 88, 032105 (2006).
- A. L. Yang, H. P. Song, X. L. Liu, H. Y. Wei, Y. Guo, G. L. Zheng, C. M. Jiao, S. Y. Yang, Q. S. Zhu, and Z. G. Wang, *Appl. Phys. Lett.* 94, 052101 (2009).
- T. D. Veal, P. D. C. King, S. A. Hatfield, L. R. Bailey, C. F. McConville, B. Martel, J. C. Moreno, E. Frayssinet, F. Semond, and J. Zúñiga-Pérez, *Appl. Phys. Lett.* 93, 202108 (2008).
- G. Heidelberger, Ph. D. Thesis Rheinisch–Westfälischen Technischen Hochschule Aachen, 2009.
- Y. Chiou, and C. Lee, *IEEE Trans. Electron Devices* 58, 3869 (2011).
- Y.-L. Chiou, C.-S. Lee, and C.-T. Lee, *Appl. Phys. Lett.* 97, 032107 (2010).
- N. V. Edwards, M. D. Bremser, T. W. Weeks, R. S. Kern, R. F. Davis, and D. E. Aspnes, *Appl. Phys. Lett.* 69, 2065 (1996).
- T. Hashizume, S. Ootomo, R. Nakasaki, S. Oyama, and M. Kihara, *Appl. Phys. Lett.* 76, 2880 (2000).
- F. Gonzalez-Posada, J. A. Bardwell, S. Moisa, S. Haffouz, H. Tang, A. F. Brana, and E. Munoz, *Appl. Surf. Sci.* 253, 6185 (2007).
- J. Hedman, and N. Mårtensson, *Phys. Scr.* 22, 176 (1980).
- L. L. Smith, S. W. King, R. J. Nemanich, and R. F. Davis, *J. Electron. Mater.* 25, 805 (1996).

S. W. King, J. P. Barnak, M. D. Bremser, K. M. Tracy, C. Ronning, R. F. Davis, and R. J. Nemanich, *J. Appl. Phys.* 84, 5248 (1998).

J. J. Uhlrich, L. C. Grabow, M. Mavrikakis, and T. F. Kuech, *J. Electron. Mater.* 37, 439 (2008).

S. D. Wolter, B. P. üüer, D. L. Waltmyer, C. Onneby, S. E. Mohny, and R. J. Molnar, *Appl. Phys. Lett.* 70, 2156 (1997).

K. Prabhakaran, T. G. Andersson, and K. Nozawa, *Appl. Phys. Lett.* 69, 3212 (1996).

V. M. Bermudez, *J. Appl. Phys.* 80, 1190 (1996).

P. Sivasubramani, T. J. Park, B. E. Coss, A. Lucero, J. Huang, B. Brennan, Y. Cao, D. Jena, H. Xing, R. M. Wallace, and J. Kim, *Phys. Status Solidi Rapid Res. Lett.* 6, 22 (2012).

L. Plucinski, L. Colakerol, S. Bernardis, Y. Zhang, S. Wang, C. O'Donnell, K. E. Smith, I. Friel, and T. D. Moustakas, *Surf. Sci.* 600, 116 (2006).

Y. J. Lin, C. S. Lee, and C. T. Lee, *J. Appl. Phys.* 93, 5321 (2003).

J. O. Song, S. J. Park, and T. Y. Seong, *Appl. Phys. Lett.* 80, 3129 (2002).

G. L. Martinez, M. R. Curiel, B. J. Skromme, and R. J. Molnar, *J. Electron. Mater.* 29, 325 (2000).

M. Diale, F. D. Auret, N. G. Van der Berg, R. Q. Odendaal, and W. D. Roos, *Appl. Surf. Sci.* 246, 279 (2005).

N. Nepal, N. Y. Garces, D. J. Meyer, J. K. Hite, M. A. Mastro, and C. R. Eddy, *Appl. Phys. Express* 4, 055802 (2011).

F. Machuca, Z. Liu, Y. Sun, P. Pianetta, W. E. Spicer, and R. F. W. Pease, *J. Vac. Sci. Technol. A* 20, 1784 (2002).

Z. Liu, Y. Sun, F. Machuca, P. Pianetta, W. E. Spicer, and R. F. W. Pease, *J. Vac. Sci. Technol. B* 21, 1953 (2003).

T. Hashizume, R. Nakasaki, S. Ootomo, S. Oyama, and H. Hasegawa, *Mater. Sci. Eng. B* 80, 309 (2001).

Y. Koyama, T. Hashizume, and H. Hasegawa, *Solid State Electron.* 43, 1483 (1999).

D. Li, M. Sumiya, S. Fuke, D. Yang, D. Que, Y. Suzuki, Y. Fukuda, *J. Appl. Phys.* 90, 4219 (2001).

- A. R. Smith, R. M. Feenstra, D. W. Greve, M.-S. Shin, M. Skowronski, J. Neugebauer, and J. E. Northrup, *Appl. Phys. Lett.* 72, 2114 (1998).
- Y. Jung, J. Ahn, K. H. Baik, D. Kim, S. J. Pearton, F. Ren, and J. Kim, *J. Electrochem. Soc.* 159, H117 (2012).
- K. M. Tracy, W. J. Mecouch, R. F. Davis, and R. J. Nemanich, *J. Appl. Phys.* 94, 3163 (2003).
- L. C. Grabow, J. J. Uhlrich, T. F. Kuech, and M. Mavrikakis, *Surf. Sci.* 603, 387 (2009).
- R. W. Hunt, L. Vanzetti, T. Castro, K. M. Chen, L. Sorba, P. I. Cohen, W. Gladfelter, J. M. Van Hove, J. N. Kuznia, M. Asif Khan, and A. Franciosi, *Physica B* 185, 415 (1993).
- Y.-H. Lai, C.-T. Yeh, J.-M. Hwang, H.-L. Hwang, C.-T. Chen, and W.-H. Hung, *J. Phys. Chem. B* 105, 10029 (2001).
- H. Ishikawa, S. Kobayashi, Y. Koide, S. Yamasaki, S. Nagai, J. Umezaki, M. Koike, and M. Murakami, *J. Appl. Phys.* 81, 1315 (1997).
- C. I. Wu, and A. Kahn, *J. Vac. Sci. Technol. B* 16, 2218 (1998).
- M. Asif Khan, J. N. Kuznia, D. T. Olson, and R. Kaplan, *J. Appl. Phys.* 73, 3108 (1993).
- V. M. Bermudez, R. Kaplan, M. Asif Khan, and J. N. Kuznia, *Phys. Rev. B* 48, 2436 (1993).
- V. M. Bermudez, T. M. Jung, K. Doverspike, and A. E. Wickenden, *J. Appl. Phys.* 79, 110 (1996).
- V. M. Bermudez, D. D. Koleske, and A. E. Wickenden, *Appl. Surf. Sci.* 126, 69 (1998).
- Ch. Schulz, S. Kuhr, H. Geffers, Th. Schmidt, J. I. Flege, T. Aschenbrenner, D. Hommel, and J. Falta, *J. Vac. Sci. Technol. A* 29, 011013 (2011).
- K. N. Lee, S. M. Donovan, B. Gila, M. Overberg, J. D. Mackenzie, C. R. Abernathy, and R. G. Wilson, *J. Electrochem. Soc.* 147, 3087 (2000).
- T. Hashizume, and H. Hasegawa, *Appl. Surf. Sci.* 234, 387 (2004).
- T. Inagaki, T. Hashizume, and H. Hasegawa, *Appl. Surf. Sci.* 216, 519 (2003).
- Z. Jin, T. Hashizume, and H. Hasegawa, *Appl. Surf. Sci.* 190, 361 (2002).
- D. J. Meyer, J. R. Flemish, and J. M. Redwing, *Appl. Phys. Lett.* 89, 223523 (2006).

Y. Guhel, B. Boudart, N. Vellas, C. Gaquiere, E. Delos, D. Ducatteau, Z. Bougrioua, and M. Germain, *Solid-State Electron.* 49, 1589 (2005).

S. Hoshi, T. Marui, M. Itoh, Y. Sano, and S. Seki, *IEICE Trans Electron.* E89C, 1052 (2006).

J. Kim, H. Choi, M. Ha, H. Song, C. Roh, J. Lee, J. Park,, and C. Hahn, *Jpn. J. Appl. Phys.* 49 04DF05 (2010).

A. Hierro, S. A. Ringel, M. Hansen, J. S. Speck, U. K. Mishra, and S. P. DenBaars, *Appl. Phys. Lett.* 77, 1499 (2000).

J. Neugebauer, and C. G. Van de Walle, *Phys. Rev. Lett.* 75, 4452 (1995).

S. Nakamura, N. Iwasa, M. Senoh, and T. Mukai, *Jpn. J. Appl. Phys.* 31, 1258 (1992).

M. S. Brandt, N. M. Johnson, R. J. Molnar, R. Singh, and T. D. Moustakas, *Appl. Phys. Lett.* 64, 2264 (1994).

W. Götz, N. M. Johnson, J. Walker, D. P. Bour, H. Amano, and I. Akasaki, *Appl. Phys. Lett.* 67, 2666 (1995).

S. M. George, *Chem. Rev.* 110, 111 (2010).

R. L. Puurunen, *J. Appl. Phys.* 97, 121301 (2005).

M. Milojevic, C. L. Hinkle, F. S. Aguirre-Tostado, H. C. Kim, E. M. Vogel, J. Kim, and R. M. Wallace, *Appl. Phys. Lett.* 93, 252905 (2008).

M. Milojevic, F. S. Aguirre-Tostado, C. L. Hinkle, H. C. Kim, E. M. Vogel, J. Kim, and R. M. Wallace, *Appl. Phys. Lett.* 93, 202902 (2008).

Y. Cao, X. Li, A. Li, H. Li, and D. Wu, *Appl. Surf. Sci.* 263, 497 (2012).

C. L. Hinkle, A. M. Sonnet, E. M. Vogel, S. McDonnell, G. J. Hughes, M. Milojevic, B. Lee, F. S. Aguirre-Tostado, K. J. Choi, H. C. Kim, J. Kim, and R. M. Wallace, *Appl. Phys. Lett.* 92, 071901 (2008).

X. Liu, R. Yeluri, J. Lu, and U. K. Mishra, *J. Electron. Mater.* 42, 33 (2013).

A. N. Hattori, F. Kawamura, M. Yoshimura, Y. Kitaoka, Y. Mori, K. Hattori, H. Daimon, and K. Endo, *Surf. Sci.* 604, 1247 (2010).

X. Hu, A. Koudymov, G. Simin, J. Yang, M. Asif Khan, A. Tarakji, M. S. Shur, and R. Gaska, *Appl. Phys. Lett.* 79, 2832 (2001).

- T. Mizutani, Y. Ohno, M. Akita, S. Kishimoto, and K. Maezawa, *Phys. Status Solidi A* 194, 447 (2002).
- C. Bae, C. Krug, G. Lucovsky, A. Chakraborty, and U. Mishra, *J. Appl. Phys.* 96, 2674 (2004).
- W. S. Tan, P. A. Houston, P. J. Parbrook, G. Hill, and R. J. Airey, *J. Phys. D: Appl. Phys.* 35, 595 (2002).
- H. Kim, R. M. Thompson, V. Tilak, T. R. Prunty, J. R. Shealy, and L. F. Eastman, *IEEE Electron Device Lett.* 24, 421 (2003).
- M. Sawada, T. Sawada, Y. Yamagata, K. Imai, H. Kimura, M. Yoshino, K. Iizuka, and H. Tomozawa, *J. Cryst. Growth* 189/190, 706 (1998).
- S. Arulkumaran, T. Egawa, H. Ishikawa, T. Jimbo, and M. Umeno, *Appl. Phys. Lett.* 73, 809 (1998).
- S. Arulkumaran, T. Egawa, H. Ishikawa, T. Jimbo, and Y. Sano, *Appl. Phys. Lett.* 84, 613 (2004).
- K. Balachander, S. Arulkumaran, T. Egawa, Y. Sano, and K. Baskar, *Mater. Sci. Eng. B* 119, 36 (2005).
- K. Balachander, S. Arulkumaran, Y. Sano, T. Egawa, and K. Baskar, *Phys. Status. Solidi. A* 202, R32 (2005).
- A. Zoroddu, F. Bernardini, P. Ruggerone, and V. Fiorentini, *Phys. Rev. B* 64, 045208 (2001).
- D. J. Chen, Y. Q. Tao, C. Chen, R. Zhang, Y. D. Zheng, M. J. Wang, B. Shen, Z. H. Li, G. Jiao, and T. S. Chen, *Appl. Phys. Lett.* 89, 252104 (2006).
- D. J. Chen, Y. Q. Tao, C. Chen, Z. L. Xie, Z. Y. Zhai, X. S. Wu, P. Han, R. Zhang, and Y. D. Zheng, *J. Vac. Sci. Technol. B* 25, 1896 (2007).
- T. Hashizume, E. Alekseev, D. Pavlidis, K. S. Boutros, and J. Redwing, *J. Appl. Phys.* 88, 1983 (2000).
- S. Huang, Q. Jiang, S. Yang, C. Zhou, and K. J. Chen, *IEEE Electron Device Lett.* 33, 516 (2012)
- C. J. Kao, J. K. Sheu, W. C. Lai, M. L. Lee, M. C. Chen, and G. C. Chi, *Appl. Phys. Lett.* 85, 1430 (2004).
- C. J. Kao, M. C. Chen, C. J. Tun, G. C. Chi, J. K. Sheu, W. C. Lai, M. L. Lee, F. Ren, and S. J. Pearton, *J. Appl. Phys.* 98, 064506 (2005).

D. J. Fu, Y. H. Kwon, T. W. Kang, C. J. Park, K. H. Baek, H. Y. Cho, D. H. Shin, C. H. Lee, and K. S. Chung, *Appl. Phys. Lett.* 80, 446 (2002).

C.-T. Lee, H.-W. Chen, and H.-Y. Lee, *Appl. Phys. Lett.* 82, 4304 (2003).

K. Y. Park, H. I. Cho, J. H. Lee, S. B. Bae, C. M. Jeon, J. L. Lee, D. Y. Kim, C. S. Lee, and J. H. Lee, *Phys. Status Solidi C* 0, 2351 (2003).

P. D. Ye, B. Yang, K. K. Ng, J. Bude, G. D. Wilk, S. Halder, and J. C. M. Hwang, *Appl. Phys. Lett.* 86, 063501 (2005).

Y. C. Chang, W. H. Chang, H. C. Chiu, L. T. Tung, C. H. Lee, K. H. Shiu, M. Hong, J. Kwo, J. M. Hong, and C. C. Tsai, *Appl. Phys. Lett.* 93, 053504 (2008).

Y. Yue, Y. Hao, J. Zhang, J. Ni, W. Mao, Q. Feng, and L. Liu, *IEEE Electron Device Lett.* 29, 838 (2008).

Y. C. Chang, H. C. Chiu, Y. J. Lee, M. L. Huang, K. Y. Lee, M. Hong, Y. N. Chiu, J. Kwo, and Y. H. Wang, *Appl. Phys. Lett.* 90, 232904 (2007).

W. J. Zhu, T. Tamagawa, M. Gibson, T. Furukawa, and T. P. Ma, *IEEE Electron Device Lett.* 23, 649 (2002).

E. P. Gusev, J. C. Cabral, M. Copel, C. D'Emic, and M. Gribelyuk, *Microelectron. Eng.* 69, 145 (2003).

X. H. Xu, M. Wang, Y. Hou, S. R. Zhao, H. Wang, D. Wang, and S. X. Shang, *Cryst. Res. Technol.* 37, 431 (2002).

K. Balachander, S. Arulkumar, H. Ishikawa, K. Baskar, and T. Egawa, *Phys. Status Solidi A* 202, R16 (2005).

C.-C. Hu, M.-S. Lin, T.-Y. Wu, F. Adriyanto, P.-W. Sze, C.-L. Wu, and Y.-H. Wang, *IEEE Trans. Electron Devices* 59, 121 (2012).

A. M. Herrero, B. P. Gila, C. R. Abernathy, S. J. Pearton, V. Craciun, K. Siebein, and F. Ren, *Appl. Phys. Lett.* 89, 092117 (2006).

X. Weng, W. Tian, D. G. Schlom, and E. C. Dickey, *Appl. Phys. Lett.* 96, 241901 (2010).

J. S. Jur, V. D. Wheeler, D. J. Lichtenwalner, J. P. Maria, and M. A. L. Johnson, *Appl. Phys. Lett.* 98, 042902 (2011).

X. Wang, O. I. Saadat, B. Xi, X. Lou, R. J. Molnar, T. Palacios, and R. G. Gordon, *Appl. Phys. Lett.* 101, 232109 (2012).

- R. Mehandru, B. Luo, J. Kim, F. Ren, B. P. Gila, A. H. Onstine, C. R. Abernathy, S. J. Pearton, D. Gotthold, R. Birkhahn, B. Peres, R. Fitch, J. Gillespie, T. Jenkins, J. Sewell, D. Via, and A. Crespo, *Appl. Phys. Lett.* 82, 2530 (2003).
- B. Luo, J. Kim, F. Ren, J. K. Gillespie, R. C. Fitch, J. Sewell, R. Dettmer, G. D. Via, A. Crespo, T. J. Jenkins, B. P. Gila, A. H. Onstine, K. K. Allums, C. R. Abernathy, S. J. Pearton, R. Dwivedi, T. N. Fogarty, and R. Wilkins, *Appl. Phys. Lett.* 82, 1428 (2003).
- B. Luo, J. W. Johnson, J. Kim, R. M. Mehandru, F. Ren, B. P. Gila, A. H. Onstine, C. R. Abernathy, S. J. Pearton, A. G. Baca, R. D. Briggs, R. J. Shul, C. Monier, and J. Han, *Appl. Phys. Lett.* 80, 1661 (2002).
- A. Y. Polyakov, N. B. Smirnov, B. P. Gila, M. Hlad, A. P. Gergerb, C. R. Abernathy, and S. J. Pearton, *J. Electrochem. Soc.* 154, H115 (2007).
- B. P. Gila, G. T. Thaler, A. H. Onstine, M. Hlad, A. Gerger, A. Herrero, K. K. Allums, D. Stodilka, S. Jang, B. Kang, T. Anderson, C. R. Abernathy, F. Ren, and S. J. Pearton, *Solid-State Electron.* 50, 1016 (2006).
- H. C. Chiu, C. W. Lin, C. H. Chen, C. W. Yang, C. K. Lin, J. S. Fu, L. B. Chang, R. M. Lin, and K. P. Hsueh, *J. Electrochem. Soc.* 157, H160 (2010).
- S. Yang, S. Huang, H. Chen, C. Zhou, Q. Zhou, M. Schnee, Q.-T. Zhao, J. Schubert, and K. J. Chen, *IEEE Electron Device Lett.* 33, 979 (2012).
- B. P. Gila, J. W. Johnson, R. Mehandru, B. Luo, A. H. Onstine, K. K. Allums, V. Krishnamoorthy, S. Bates, C. R. Abernathy, F. Ren, and S. J. Pearton, *Phys. Status Solidi A* 188, 239 (2001).
- A. Das, L. Chang, and R. Lin, *AIP Advances* 2, 032159 (2012).
- W. H. Chang, C. H. Lee, P. Chang, Y. C. Chang, Y. J. Lee, J. Kwo, C. C. Tsai, J. M. Hong, C.-H. Hsu, and M. Hong, *J. Cryst. Growth* 311, 2183 (2009).
- J. W. Johnson, B. Luo, F. Ren, B. P. Gila, W. Krishnamoorthy, C. R. Abernathy, S. J. Pearton, J. I. Chyi, T. E. Nee, C. M. Lee, and C. C. Chuo, *Appl. Phys. Lett.* 77, 3230 (2000).
- J. W. Johnson, B. P. Gila, B. Luo, K. P. Lee, C. R. Abernathy, S. J. Pearton, J. I. Chyi, T. E. Nee, C. M. Lee, C. C. Chuo, and F. Ren, *J. Electrochem. Soc.* 148, G303 (2001).
- M. Hong, J. Kwo, T. D. Lin, and M. L. Huang, *MRS Bull.* 34, 514 (2009).
- Y. D. Wu, T. D. Lin, T. H. Chiang, Y. C. Chang, H. C. Chiu, Y. J. Lee, M. Hong, C. A. Lin, and J. Kwo, *J. Vac. Sci. Technol. B* 28, C3H10 (2010).

F. Ren, M. Hong, S. N. G. Chu, M. A. Marcus, M. J. Schurman, A. Baca, S. J. Pearton, and C. R. Abernathy, *Appl. Phys. Lett.* 73, 3893 (1998).

C.-T. Lee, Y.-L. Chiou, and C.-S. Lee, *IEEE Electron Device Lett.* 31, 1220 (2010).

G. Vanko, M. Vallo, J. Bruncko, and T. Lalinský, *Vac.* 86, 672 (2012).

W. Wang, J. Derluyn, M. Germain, M. Leys, S. Degroote, D. Schreurs, and G. Borghs, *Jpn. J. Appl. Phys.* 45, L224 (2006).

D. Deen, D. Storm, D. Meyer, D. Scott, R. Bass, S. Binari, and T. Gougousi, *Physica Status Solidi C* 8, 2420 (2011).

C. Lin, H. Chiu, C. Lin, and J. S. Fu, *Microelectron. Reliab.* 51, 381 (2011).

H. Kim, M. Schuette, H. Jung, J. H. Song, J. Lee, W. Lu, and J. C. Mabon, *Appl. Phys. Lett.* 89, 053516 (2006).

M. Z. Peng, Y. K. Zheng, K. Wei, and X. Y. Liu, *Microelectron Eng.* 87, 2638 (2010).

H. Zhou, G. I. Ng, Z. H. Liu, and S. Arulkumaran, *Appl. Phys. Express.* 4, 104102 (2011).

K.-W. Kim, S.-D. Jung, D.-S. Kim, K.-S. Im, H.-S. Kang, J.-H. Lee, Y. Bae, D.-H. Kwon, and S. Cristoloveanu, *Microelectron. Eng.* 88, 1225 (2011).

A. P. Edwards, J. A. Mittereder, S. C. Binari, D. S. Katzer, D. F. Storm, and J. A. Roussos, *IEEE Electron Device Lett.* 26, 225 (2005).

Y.-S. Lin, Y.-W. Lain, and S. S. H. Hsu, *IEEE Electron Device Lett.* 31, 102 (2010).

S. M. George, A. W. Ott, and J. W. Klaus, *J. Phys. Chem.* 100, 13121 (1996).

S. M. George, *Chem. Rev.* 110, 111 (2010).

C. H. L. Goodman and M. V. Pessa, *J. Appl. Phys.* 60, R65 (1986).

M. Leskela and M. Ritala, *J. Phys. IV* 9, Pr8/837(1999).

M. Leskela and M. Ritala, *Thin Solid Films* 409, 138 (2002).

L. Niinisto, M. Ritala, and M. Leskela, *Mater. Sci. Eng. B* 41, 23 (1996).

R. L. Puurunen, *J. Appl. Phys.* 97, 121301 (2005).

M. Ritala and M. Leskela, *Nanotechnology* 10, 19 (1999).

- T. Suntola, *Mater. Sci. Rep.* 4, 261 (1989).
- S. Haukka, E. L. Lakooma, and T. Suntola, *Stud. Surf. Sci. Catal.* 120A, 715 (1999).
- H. B. Profijt, S. E. Potts, M. C. M. van de Sanden, and W. M. M. Kessels *J. Vac. Sci. Technol. A* 29, 050801 (2011).
- T. Suntola and J. Hyvärinen, *Annu. Rev. Mater. Sci.* 15, 177 (1985).
- S. M. Bedair, B. T. McDermott, Y. Ide, N. H. Karam, H. Hashemi, M. A. Tischler, M. Timmons, J. C. L. Tarn, and N. El-Masry, *J. Cryst. Growth* 93, 182 (1988).
- S. P. DenBaars and P. D. Dapkus, *J. Cryst. Growth* 98, 195 (1989).
- M. A. Herman, *Vacuum* 42, 61 (1991).
- B. W. Gregory, and J. L. Stickney, *J. Electroanal. Chem. Interfacial Electrochem.* 300, 543 (1991).
- A. Usui and H. Watanabe, *Annu. Rev. Mater. Sci.* 21, 185 (1991).
- M. Ozeki, *Mater. Sci. Rep.* 8, 97 (1992).
- A. Usui, *Proc. IEEE* 80, 1641 (1992).
- T. Suntola, *Thin Solid Films* 216, 84 (1992).
- T. Suntola, *Thin Solid Films* 225, 96 (1993).
- L. Niinistö and M. Leskelä, *Thin Solid Films* 225, 130 (1993).
- S. M. Bedair, *J. Vac. Sci. Technol. B* 12, 179 (1994).
- S. M. Bedair, and N. A. El-Masry, *Appl. Surf. Sci.* 82/83, 7 (1994).
- J. M. Heitzinger, J. M. White, and J. G. Ekerdt, *Surf. Sci.* 299, 892 (1994).
- E.-L. Lakomaa, *Appl. Surf. Sci.* 75, 185 (1994).
- M. A. Herman, *Thin Solid Films* 267, 1 (1995).
- M. Leskelä and M. Ritala, *J. Phys. IV* 5, C5/937 (1995).
- T. Suntola, *Appl. Surf. Sci.* 100/101, 391 (1996).
- A. A. Malygin, A. A. Malkov, and S. D. Dubrovenskii, *Stud. Surf. Sci. Catal.* 99, 213 (1996).

- M. A. Herman, *Appl. Surf. Sci.* 112, 1 (1997).
- M. Ritala, *Appl. Surf. Sci.* 112, 223 (1997).
- S. Haukka and T. Suntola, *Interface Sci.* 5, 119 (1997).
- L. Niinistö, *Curr. Opin. Solid-State Mater. Sci.* 3, 147 (1998).
- A. A. Malygin, *Compos. Interfaces* 5, 561 (1998).
- L. Niinistö, *J. Therm. Anal. Calorim.* 56, 7 (1999).
- K. Ikeda, J. Yanase, S. Sugahara, and M. Matsumura, *J. Korean Phys. Soc.* 39, S447 (2001).
- A. C. Jones and P. R. Chalker, *J. Phys. D* 36, R80 (2003).
- M. Leskelä and M. Ritala, *J. Solid-State Chem.* 171, 170 (2003).
- M. Leskelä and M. Ritala, *Angew. Chem., Int. Ed.* 42, 5548 (2003).
- R. M. C. de Almeida and I. J. R. Baumvol, *Surf. Sci. Rep.* 49, 1 (2003)
- H. Kim, *J. Vac. Sci. Technol. B* 21, 2231 (2003).
- L. Niinistö, J. Päiväsari, J. Niinistö, M. Putkonen, and M. Nieminen, *Phys. Status Solidi A* 201, 1443 (2004).
- A. C. Jones, H. C. Aspinall, P. R. Chalker, R. J. Potter, K. Kukli, A. Rahtu, M. Ritala, and M. Leskelä, *J. Mater. Chem.* 14, 3101 (2004).
- R. L. Puurunen, *Chem. Vap. Dep.* 11, 79 (2005).
- M. Putkonen, T. Sajavaara, L. Niinistö, and J. Keinonen, *Anal., and Bioanal. Chem.* 382, 1791 (2005).
- A. C. Jones, H. C. Aspinall, P. R. Chalker, R. J. Potter, T. D. Manning, Y. F. Loo, R. O'Kane, J. M. Gaskell, and L. M. Smith, *Chem. Vap. Dep.* 12, 83 (2005).
- K. E. Elers, T. Blomberg, M. Peussa, B. Aitchison, S. Haukka, and S. Marcus, *Chem. Vap. Dep.* 12, 13 (2006).
- H. Kim and P. C. McIntyre, *J. Korean Phys. Soc.* 48, 5 (2006).
- M. Schumacher, P. K. Baumann, and T. Seidel, *Chem. Vap. Dep.* 12, 99 (2006).

- C. O. Chui, H. Kim, D. Chi, P. C. McIntyre, and K. C. Saraswat, *IEEE Trans. Electron Devices* 53, 1509 (2006).
- M. Knez, K. Nielsch, and L. Niinistö, *Adv. Mater.* 19, 3425 (2007).
- F. T. Edelmann, *Chem. Soc. Rev.* 38, 2253 (2009).
- H. Kim, H.-B.-R. Lee, and W.-J. Maeng, *Thin Solid Films* 517, 2563 (2009).
- S. M. George, R. Yoon, and A. A. Dameron, *Acc. Chem. Res.* 42, 498 (2009).
- E. Langereis, S. B. S. Heil, H. C. M. Knoops, W. Keuning, M. C. M. van de Sanden, and W. M. M. Kessels, *J. Phys. D: Appl. Phys.* 42, 073001 (2009).
- X. Jiang and S. F. Bent, *J. Phys. Chem. C* 113, 17613 (2009).
- C. Detavernier, J. Dendooven, S. P. Sree, K. F. Ludwig, and J. A. Martens, *Chem. Soc. Rev.* 40, 5242 (2011).
- J. R. Bakke, K. L. Pickrahn, T. P. Brennan, and S. F. Bent, *Nanoscale* 3, 3482 (2011).
- P. Poodt, D. C. Cameron, E. Dickey, S. M. George, V. Kuznetsov, G. N. Parsons, F. Roozeboom, G. Sundaram, and A. Vermeer, *J. Vac. Sci. Technol. A* 30, 010802 (2012).
- F. T. Edelmann, *Chem. Soc. Rev.* 41, 7657 (2012).
- G. Dingemans and W. M. M. Kessels, *J. Vac. Sci. Technol. A* 30, 040802 (2012).
- X. Meng, X.-Q. Yang, and X. Sun, *Adv. Mater.* 24, 3589 (2012).
- V. Miikkulainen, M. Leskelä, M. Ritala, and R. L. Puurunen, *J. Appl. Phys.* 113, 021301 (2013).
- F. Zaera, *Coord. Chem. Rev.* 257, 3177 (2013).
- [] T. J. Knisley, L. C. Kalutarage, and C. H. Winter, *Coord. Chem. Rev.* 257, 3222 (2013).
- S. E. Potts and W. M. M. Kessels, *Coord. Chem. Rev.* 257, 3254 (2013).
- [] K. B. Ramos, M. J. Saly, and Y. J. Chabal, *Coord. Chem. Rev.* 257, 3271 (2013).
- T. Hatanpää, M. Ritala, and M. Leskelä, *Coord. Chem. Rev.* 257, 3297 (2013).
- [] G. N. Parsons, S. E. Atanasov, E. C. Dandley, C. K. Devine, B. Gong, J. S. Jur, K. Lee, C. J. Oldham, Q. Peng, J. C. Spagnola, and P. S. Williams, *Coord. Chem. Rev.* 257, 3323 (2013).

G. N. Parsons, J. W. Elam, S. M. George, S. Haukka, H. Jeon, W. M. M. (Erwin).Kessels, M. Leskelä, P. Poodt, M. Ritala and S. M. Rossnagel, *J. Vac. Sci. Technol. A* 31, 050818 (2013)

R. Foest, M. Schmidt, and H. Gargouri, 68, 23 (2014).

K. Devloo-Casier, K. F. Ludwig, C. Detavernier, and J. Dendooven, *J. Vac. Sci. Technol. A* 32, 010801 (2014).

D. Longrie, D. Deduytsche, and C. Detavernier, *J. Vac. Sci. Technol. A* 32, 010802 (2014).

T. Suntola, and J. Antson, U. S. Patent No. 4,058,430 15 November, 3 1977.

A. M. Shevjakov, G. N. Kuznetsova, and V. B. Aleskovskii, in *Chemistry of High-Temperature Materials, Proceedings of the Second USSR Conference on High-Temperature Chemistry of Oxides*, Leningrad, USSR, 26–29 November 1965 (Nauka, Leningrad, USSR, 1967), pp. 2 149–155, in Russian.

V. B. Aleskovskii, and V. E. Drozd, *Chem. Technol. Ser.* 195, 155 (1990).

T. Suntola, in *Handbook of Thin Film Process Technology*, edited by D. A. Glocker, and S. I. Shah IOP, Bristol, United Kingdom, 1995, Vol. 1, pp. B1.5:1–B1.5:17.

M. Verghese, J. W. Maes, and N. Kobayashi, Atomic layer deposition goes mainstream in 22nm logic technologies, <http://www.solid-state.com> (March 15, 2012).

International Technology Roadmap for Semiconductors, <http://www.itrs.net>, (March 15, 2012).

M. De Keijser and C. Vamn Opdorp, *Appl. Phys. Lett.* 58, 1187 (1991).

ASM International website, <http://www.asm.com> (March 15, 2012).

Oxford Instruments website, <http://www.oxford-instruments.com> (March 15, 2012).

Beneq website, <http://www.beneq.com> (May 31, 2011).

Cambridge NanoTech website, <http://www.cambridgenanotech.com> (March 15, 2012).

Applied Materials website, <http://www.appliedmaterials.com> (March 15, 2012).

Tokyo Electron Limited website, <http://www.tel.com> (March 15, 2012).

Picosun website, <http://www.picosun.com> (March 15, 2012).

R. L. Puurunen, *Chem. Vap. Dep.* 9, 249 (2003).

R. L. Puurunen, *Chem. Vap. Dep.* 9, 327 (2003).

G. Eres, *Appl. Phys. Lett.* 67, 1727 (1995).

H.-S. Park, J.-S. Min, J.-W. Lim, and S.-W. Kang, *Appl. Surf. Sci.* 158, 81 (2000).

M. K. Gobbert, V. Prasad, and T. S. Cale, *J. Vac. Sci. Technol. B* 20, 1031 (2002).

R. L. Puurunen, M. Lindblad, A. Root, and A. O. I. Krause, *Phys. Chem. Chem. Phys.* 3, 1093 (2001).

A. Rautiainen, M. Lindblad, L. B. Backman, and R. L. Puurunen, *Phys. Chem. Chem. Phys.* 4, 2466 (2002)

R. L. Puurunen, T. A. Zeelie, and A. O. I. Krause, *Catal. Lett.* 83, 27 (2002).

E.-L. Lakomaa, S. Haukka, and T. Suntola, *Appl. Surf. Sci.* 60/61, 742 (1992)

S. Haukka, E.-L. Lakomaa, and A. Root, *J. Phys. Chem.* 97, 5085 (1993).

S. Haukka, E.-L. Lakomaa, O. Jylhä, J. Vilhunen, and S. Hornytzkyj, *Langmuir* 9, 3497 (1993).

A. Kytökivi, E.-L. Lakomaa, and A. Root, *Langmuir* 12, 4395 (1996).

R. L. Puurunen, S. M. K. Airaksinen, and A. O. I. Krause, *J. Catal.* 213, 281 (2003).

M. Putkonen, T. Sajavaara, L.-S. Johansson, and L. Niinistö, *Chem. Vap. Deposition* 7, 44 (2001).

M. Juppo, A. Rahtu, and M. Ritala, *Chem. Mater.* 14, 281 (2002).

J. S. Becker, S. Suh, S. Wang, and R. G. Gordon, *Chem. Mater.* 15, 2969 (2003).

A. W. Ott, J. W. Klaus, J. M. Johnson, and S. M. George, *Thin Solid Films* 292, 135 (1997).

M. D. Groner, F. H. Fabreguette, J. W. Elam, and S. M. George, *Chem. Mater.* 16, 639 (2004).

A. Kytökivi, J.-P. Jacobs, A. Hakuli, J. Meriläinen, and H. H. Brongersma, *J. Catal.* 162, 190 (1996).

A. Hakuli, A. Kytökivi, and A. O. I. Krause, *Appl. Catal., A* 190, 219 (2000).

N. V. Dolgushev, A. A. Malkov, A. A. Malygin, S. A. Suvorov, A. V. Shchukarev, A. V. Beljaev, and V. A. Bykov, *Thin Solid Films* 293, 91 (1997).

- H. Kim and S. M. Rossnagel, *J. Vac. Sci. Technol. A* 20, 802 (2002).
- A. Delabie, R. L. Puurunen, B. Brijs, M. Caymax, T. Conard, B. Onsia, O. Richard, W. Vandervorst, C. Zhao, M. M. Heyns, M. Meuris, M. M. Viitanen, H. H. Brongersma, M. de Ridder, L. V. Goncharova, E. Garfunkel, T. Gustafsson, and W. Tsai, *J. Appl. Phys.* 97, 064104 (2005).
- R. L. Puurunen, A. Root, P. Sarv, M. M. Viitanen, H. H. Brongersma, M. Lindblad, and A. O. I. Krause, *Chem. Mater.* 14, 720 (2002)
- A. Satta, J. Schuhmacher, C. M. Whelan, W. Vandervorst, S. H. Brongersma, G. P. Beyer, K. Maex, A. Vantomme, M. M. Viitanen, H. H. Brongersma, and W. F. A. Besling, *J. Appl. Phys.* 92, 7641 (2002).
- M. L. Green, M.-Y. Ho, B. Busch, G. D. Wilk, T. Sorsch, T. Conard, B. Brijs, W. Vandervorst, P. I. Räisänen, D. Muller, M. Bude, and J. Grazul, *J. Appl. Phys.* 92, 7168 (2002).
- R. L. Puurunen, *J. Appl. Phys.* 95, 4777 (2004).
- A. Martin Hoyas, J. Schuhmacher, D. Shamiryan, J. Waeterloos, W. Besling, J. P. Celis, and K. Maex, *J. Appl. Phys.* 95, 381 (2004).
- R. L. Puurunen, W. Vandervorst, W. F. A. Besling, O. Richard, H. Bender, T. Conard, C. Zhao, A. Delabie, M. Caymax, S. De Gendt, M. Heyns, M. M. Viitanen, M. de Ridder, H. H. Brongersma, Y. Tamminga, T. Dao, T. de Win, M. Verheijen, M. Kaiser, and M. Tuominen, *J. Appl. Phys.* 96, 4878 (2004).
- R. L. Puurunen, and W. Vandervorst, *J. Appl. Phys.* 96, 7686 (2004).
- R. L. Puurunen, *Chem. Vap. Deposition* 10, 159 (2004).
- Stanford Nanofabrication Facility, <https://snf.stanford.edu/SNF/equipment/chemical-vapor-deposition/ald> (November 17, 2014).
- Cambridge Nanotech, <http://www.cambridgenanotechald.com> (November 17, 2014).
- D. Hausmann, J. Becker, S. Wang, and R. G. Gordon, *Science* 298, 402 (2002).
- J. W. Klaus, S. J. Farro, and S. M. George, *Thin Solid Films* 360, 145 (2000).
- J. S. Park, H. S. Park, and S. W. Kang, *J. Electrochem. Soc.* 149, C28 (2002).
- J. H. Lee, Y. J. Cho, Y. S. Min, D. Kim, and S. W. Rhee, *J. Vac. Sci. Technol. A* 20, 1828 (2002).

- S. B. S. Heil, E. Langereis, F. Roozeboom, M. C. M. Van de Sanden, and W. M. M. Kessels, *J. Electrochem. Soc.* 153, G956 (2006).
- H. B. Profijt, P. Kudlacek, M. C. M. Van de Sanden, and W. M. M. Kessels, *J. Electrochem. Soc.* 158, G88 (2011).
- H. Kim, *Thin Solid Films* 519, 6639 (2011).
- H. Kim and I.-K. Oh *Jpn. J. Appl. Phys.* 53, 03DA01 (2014).
- M. Kariniemi, J. Niinistö, M. Vehkamäki, M. Kemell, M. Ritala, M. Leskelä, and M. Putkonen, *J. Vac. Sci. Technol. A* 30, 01A115 (2012)
- J. Yang, B. S. Eller, M. Kaur, and R. J. Nemanich, *J. Vac. Sci. Technol. A* 32, 021514 (2014).
- M. D. Groner, J. W. Elam, F. H. Fabreguette, and S. M. George, *Thin Solid Films* 413, 186 (2002).
- J. L. van Hemmen, S. B. S. Heil, J. H. Klootwijk, F. Roozeboom, C. J. Hodson, M. C. M. van de Sanden, and W. M. M. Kessels, *J. Electrochem. Soc.* 154, G165 (2007).
- E. Langereis, J. Keijmel, M. C. M. van de Sanden, and W. M. M. Kessels, *Appl. Phys. Lett.* 92, 231904 (2008).
- S. E. Potts, W. Keuning, E. Langereis, G. Dingemans, M. C. M. vande Sanden, and W. M. M. Kessels, *J. Electrochem. Soc.* 157, 66 (2010)
- S. E. Potts, G. Dingemans, C. Lachaud, and W. M. M. Kessels, *J. Vac. Sci. Technol. A* 30, 021505 (2012).
- S. E. Potts, H. B. Profijt, R. Roelofs, and W. M. M. Kessels, *Chem. Vap. Deposition* 19, 125 (2013).
- W. Cho, K. Sung, K.-S. An, S. S. Lee, T.-K. Chung, and Y. Kim, *J. Vac. Sci. Technol. A* 21, 1366 (2003).
- S. B. S. Heil, P. Kudlacek, E. Langereis, R. Engeln, M. C. M. van de Sanden, and W. M. M. Kessels, *Appl. Phys. Lett.* 89, 131505 (2006).
- J. W. Lim, and S. J. Yun, *Electrochem. Solid-State Lett.* 7, F45 (2004).
- C. C. Fulton, T. E. Cook, G. Lucovsky, and R. J. Nemanich, *J. Appl. Phys.* 96, 2665 (2004).
- C. Zhu, D. J. Smith, and R. J. Nemanich, *J. Vac. Sci. Technol. B* 30, 051807 (2012).

- J. Yang, B. S. Eller, C. Zhu, C. England, and R. J. Nemanich, *J. Appl. Phys.* 112, 053710 (2012).
- D. H. Triyoso, R. I. Hegde, B. E. White Jr., and P. J. Tobin, *J. Appl. Phys.* 97, 124107 (2005).
- P. K. Park, J.-S. Roh, B. H. Choi, and S. W. Kang, *Electrochem. Solid-State Lett.* 9, F34 (2006).
- C. Richter, T. Schenik, U. Schroeder, and T. Mikolajick, *J. Vac. Sci. Technol. B* 32, 01A117 (2014).
- H.-S. Jung, H. K. Kim, I.-H. Yu, S. Y. Lee, J. Lee, J. Park, J. H. Jang, S.-H. Jeon, Y. J. Chung, D.-Y. Cho, N.-I. Lee, T. J. Park, J.-H. Choi, and C. S. Hwang, *J. Electrochem. Soc.* 159, G33 (2012).
- H. Kim, S. Woo, J. Lee, Y. Kim, H. Lee, I. J. Choi, Y. D. Kim, C. W. Chung, and H. Jeon, *J. Electrochem. Soc.* 158, H21 (2011).
- H. Lüth, *Solid Surfaces, Interfaces, and Thin Films*, 5th Ed. (Springer, Heidelberg, Germany, 2010).
- R. Smart, S. McIntyre, M. Bancroft, I. Bello et al., U. Hong Kong, Dept. Phys.
- CASAXPS help manual (Casa Software Ltd, 2005).
- L. Sygellou, V. Dianneta, N. Xanthopoulos, D. Skarlatos, S. Georga, C. Krontiras, S. Ladas, and S. Kennou, *Surf. Sci. Spec.* 18, 58 (2011).
- A. Milanov, R. A. Fischer and A. Devi, *Surf. Sci. Spec.* 14, 34 (2007).
- A. R. Chourasia, *Surf. Sci. Spec.* 13, 48 (2006).
- “UVL Ultra-violet Source,” Thermo Electron Corporation Application Note: AN30058_E (2008).
- L. Scudiero, Washington State University.
- J. Yang, B. S. Eller, C. Zhu, C. England, and R. J. Nemanich, *J. Appl. Phys.* 112, 053710 (2012).
- J. R. Waldrop and R. W. Grant, *Appl. Phys. Lett.* 68, 2879 (1996).
- E. A. Kraut, R. W. Grant, J. R. Waldrop and S. P. Kowalczyk, *Heterojunction Band Discontinuities: Physics and Device Applications*, edited by F. Capasso and G. Margaritondo (Elsevier, New York, 1987).

- B. S. Eller, J. Yang, and R. J. Nemanich, *J. Electron. Mater.* 43, 4560 (2014).
- T. E. Cook, Jr., C. C. Fulton, W. J. Mecouch, R. F. Davis, G. Lucovsky and R. J. Nemanich, *J. Appl. Phys.* 94, 7155 (2003).
- J. Hedman and N. Mårtensson, *Phys. Scr.* 22, 176 (1980).
- D. A. Cole, J. R. Shallenberger, S. W. Novak, R. L. Moore, M. J. Edgell, S. P. Smith, C. J. Hitzman, J. F. Kirchhoff, E. Principe, W. Nieveen, F. K. Huang, S. Biswas, R. J. Bleiler, and K. Jones, *J. Vac. Sci. Technol. B* 18, 440 (2000).
- F. G. Bell and L. Ley, *Phys. Rev. B* 37, 8383 (1988).
- H. Nohira, W. Tsai, W. Besling, E. Young, J. Petry, T. Conard, W. Vandervorst, S. De Gendt, M. Heyns, J. Maes, and M. Tuominen, *J. Non-Cryst. Solids* 303, 83 (2002).
- M. Bär, M. Rusu, S. Lehmann, Th. Schedel-Niedrig, I. Laueremann, and M. C. Lux-Steiner, *Appl. Phys. Lett.* 93, 232104 (2008).
- J. Yang, B. S. Eller, M. Kaur, and R. J. Nemanich, *J. Vac. Sci. Technol. A* 32, 021514 (2014).
- E. Bersch, S. Rangan, R. A. Bartynski, E. Garfunkel, and E. Vescovo, *Phys. Rev. B* 78, 085114 (2008).
- S. Miyazaki, *J. Vac. Sci. Technol. B* 19, 2212 (2001).
- H. Y. Yu, M. F. Li, B. J. Cho, C. C. Yeo, M. S. Joo, D.-L. Kwong, J. S. Pan, C. H. Ang, J. Z. Zheng, and S. Ramanathan, *Appl. Phys. Lett.* 81, 376 (2002).
- L. Kronik and Y. Shapira, *Surf. Sci. Rep.* 37, 1 (1999).
- UHV Kelvin Probe Manual, Ver. 7.3 (KP Technology, Caithness, UK, 2011), pp. 26-31.
- U. K. Mishra, P. Parikh, and Y. F. Wu, *Proc. IEEE* 90, 1022 (2002).
- B. S. Eller, J. Yang, and R. J. Nemanich, *J. Vac. Sci. Technol. A* 31, 050807 (2013).
- Y. Niiyama, S. Ootomo, J. Li, T. Nomura, S. Kato and T. P. Chow, *Semicond. Sci. Technol.* 25, 125006 (2010).
- E. T. Yu, X. Z. Dang, P. M. Asbeck, S. S. Lau, and G. J. Sullivan, *J. Vac. Sci. Technol. B* 17, 1742 (1999).
- V. A. Savastenko, and A. U. Sheleg, *Phys. Status Solidi A* 48, K135 (1978).

Y. Takagi, M. Ahart, T. Azuhata, T. Sota, K. Suzuki, and S. Nakamura, *Physica B* 219/220, 547 (1996).

A. Polian, M. Grimsditch, and I. Grezegory, *J. Appl. Phys.* 79, 3343 (1996).

R. B. Schwartz, K. Khachatryan, and E. R. Webber, *Appl. Phys. Lett.* 70, 1122 (1997).

C. Deger, E. Born, H. Angerer, O. Ambacher, M. Stutzmann, J. Hornsteiner, E. Riha, and G. Fischerauer, *Appl. Phys. Lett.* 72, 2400 (1998).

K. Tsubouchi, and N. Mikoshiba, *IEEE Trans. Sonics Ultrason.* 32, 634 (1985).

L. E. McNeil, M. Grimsditch, and R. H. French, *J. Am. Ceram. Soc.* 76, 1132 (1993).

K. Kim, W. R. L. Lambrecht, and B. Segall, *Phys. Rev. B* 53, 16310 (1996).

A. F. Wright, *J. Appl. Phys.* 82, 2833 (1997).

O. Ambacher, J. Smart, J. R. Shealy, N. G. Weimann, K. Chu, M. Murphy, W. J. Schaff, L. F. Eastman, R. Dimitrov, L. Wittmer, M. Stutzmann, W. Rieger, and J. Hilsenbeck, *J. Appl. Phys.* 85, 3222 (1999).

F. Bernardini, V. Fiorentini, and D. Vanderbilt, *Phys. Rev. B* 56, R10024 (1997).

F. Bernardini, V. Fiorentini, and D. Vanderbilt, *Phys. Rev. B* 63, 193201 (2001).

Y. Duan, J. Li, S.-S. Li, and J.-B. Xia, *J. Appl. Phys.* 103, 023705 (2008).

K. Shimada, A. Zenpuku, K. Fukiwara, K. Hazu, S. F. Chichibu, M. Hata, H. Sazawa, T. Takada, and T. Sota, *J. Appl. Phys.* 110, 074114 (2011).

J. Yang, B. S. Eller, C. Zhu, C. England, and R. J. Nemanich, *J. Appl. Phys.* 112, 053710 (2012).

H. W. Jang, J.-H. Lee, and J.-L. Lee, *Appl. Phys. Lett.* 80, 3955 (2002).

M. Hong, K. A. Anselm, J. Kwo, H. M. Ng, J. N. Baillargeon, A. R. Kortan, J. P. Mannaerts, A. Y. Cho, C. M. Lee, J. I. Chyi, and T. S. Lay, *J. Vac. Sci. Technol. B* 18, 1453 (2000).

Y. Q. Wu, T. Shen, P. D. Ye, and G. D. Wilk, *Appl. Phys. Lett.* 90, 143504 (2007).

W. J. Mecouch, B. P. Wagner, Z. J. Reitmeier, R. F. Davis, C. Pandarinath, B. J. Rodriguez, and R. J. Nemanich, *J. Vac. Sci. Technol. A* 23, 72 (2005).

V. M. Bermudez, *J. Appl. Phys.* 80, 1190 (1996).

M. Krawczyk, L. Zommer, A. Jablonski, I. Grzegory, and M. Bockowski Surf. Sci. 566-568, 1234 (2004).

H.-H. Wu, Ph.D. Thesis Ohio State University, 2011.

B. Brennan, X. Qin, H. Dong, J. Kim, and R. M. Wallace, Appl. Phys. Lett. 101, 211604 (2012).

X. Qin, H. Dong, B. Brennan, A. Azacatl, J. Kim, and R. M. Wallace, Appl. Phys. Lett. 103, 221604 (2013).

X. Qin, B. Brennan, H. Dong, J. Kim, C. L. Hinkle, and R. M. Wallace, J. Appl. Phys. 113, 244102 (2013).

NIST Electron Effective-Attenuation-Length Database, SRD-82, Version 1.1; National Institute of Standards and Technology: Gaithersburg, MD, 2003.

R. R. Pela, C. Caetano, M. Marques, L. G. Ferreira, J. Furthmuller, and L. K. Teles, Appl. Phys. Lett. 98, 151907 (2011).

T. E. Cook, Jr., C. C. Fulton, W. J. Mecouch, R. F. Davis, G. Lucovsky, and R. J. Nemanich, J. Appl. Phys. 94, 7155 (2003).

J. R. Waldrop, and R. W. Grant, Appl. Phys. Lett. 68, 2879 (1996).

J. Hedman, and N. Mårtensson, Phys. Scr. 22, 176 (1980).

Y. L. Chiou, and C. T. Lee, IEEE Trans. Electron Devices 58, 3869 (2011).

M. H. S. Owen, M. A. Bhuiyan, Q. Zhou, Z. Zhang, J. S. Pan, and Y.-C. Yeo, Appl. Phys. Lett. 104, 091605 (2014).

J. Yang, B. S. Eller, and R. J. Nemanich, J. Vac. Sci. Technol. A 32, 021514 (2014).

J. E. Northrup, J. Neugebauer, R. M. Feenstra, and A. R. Smith, Phys. Rev. B 61, 9932 (2000).

D. Segev, and C. G. Van de Walle, Surf. Sci. 601, L15 (2007).

[] A. R. Smith, R. M. Feenstra, D. W. Greve, M.-S. Shin, M. Skowronski, J. Neugebauer, and J. E. Northrup, Surf. Sci. 423, 70 (1999).

S. W. King, C. Ronning, R. F. Davis, M. C. Benjamin, and R. J. Nemanich, J. Appl. Phys. 84, 2086 (1998).

[] S. Vézian, F. Semond, J. Massies, D. W. Bullock, Z. Ding, and P. M. Thibado, Surf. Sci. 541, 242 (2003).

A. R. Smith, R. M. Feenstra, D. W. Greve, M. S. Shin, M. Skowronski, J. Neugebauer, and J. E. Northrup, *J. Vac. Sci. Tech. B* 16, 2242 (1998).

C. G. Van de Walle and D. Segev, *J. Appl. Phys.* 101, 081704 (2007).

L. Ivanova, S. Borisova, H. Eisele, M. Dahne, A. Laubsch, and Ph. Eben, *Appl. Phys. Lett.* 93, 192110 (2008).

M. Himmerlich, L. Lympirakis, R. Gutt, P. Lorenz, J. Neugebauer, and S. Krischok, *Phys. Rev. B* 88, 125304 (2013).

T. Hashizume and H. Hasegawa, *Appl. Surf. Sci.* 234, 387 (2004).

D. Segev, and C. G. Van de Walle, *Europhys. Lett.* 76, 305 (2006).

S. W. King, J. P. Barnak, M. D. Bremser, K. M. Tracy, C. Ronning, R. F. Davis, and R. J. Nemanich, *J. Appl. Phys.* 84, 5248 (1998).

T. Hashizume, S. Ootomo, T. Inagaki, and H. Hasegawa, *J. Vac. Sci. Technol. B* 21, 1828 (2003).

R. D. Long, and P. C. McIntyre, *Mater.* 5, 1297 (2012).

C. L. Hu, J. Q. Li, Y. F. Zhang, X. L. Hu, N. X. Lu, and Y. Chen, *Chem. Phys. Lett.* 424, 273 (2006).

R. Meunier, A. Torres, and M. Charles, *ECS Trans.* 50, 451 (2013).

C. L. Hu, J. Q. Li, Y. F. Zhang, X. L. Hu, N. X. Lu, and Y. Chen, *Chem. Phys. Lett.* 424, 273 (2006).

J. Elsner, R. Gutierrez, B. Hourahine, R. Jones, M. Haugk, and Th. Frauenheim, *Solid State Comm.* 108, 953 (1998).

V. M. Bermudez, and J. P. Long, *Surf. Sci.* 450, 98 (2000).

M. Esposito, S. Krishnamoorthy, D. N. Nath, S. Bajaj, T.-H. Hung, and S. Rajan, *Appl. Phys. Lett.* 99, 1233503 (2011).

S. Ganguly, J. Verma, G. Li, T. Zimmermann, H. Xing, and D. Jena, *Appl. Phys. Lett.* 99, 193504 (2011).

J. Son, V. Chobpattana, B. M. McSkimming, and S. Stemmer, *Appl. Phys. Lett.* 101, 102905 (2012).

M. Sawada, T. Sawada, Y. Yamagata, K. Imai, H. Kimura, M. Yoshino, K. Iizuka, and H. Tomozawa, *J. Cryst. Growth* 189/190, 706 (1998).

S. Arulkumaran, T. Egawa, H. Ishikawa, T. Jimbo, and M. Umeno, *Appl. Phys. Lett.* 73, 809 (1998).

B. M. Green, K. K. Chu, E. M. Chumbes, J. A. Smart, J. R. Shealy, and L. F. Eastman, *IEEE Electron. Device Lett.* 21, 268, (2000).

W. S. Tan, P. A. Houston, P. J. Parbrook, G. Hill, and R. J. Airey, *J. Phys. D: Appl. Phys.* 35, 595 (2002).

T. Hashizume, S. Ootomo, T. Inagaki, and H. Hasegawa, *J. Vac. Sci. Technol. B* 21, 1828 (2003)

C. Bae, C. Krug, G. Lucovsky, A. Chakraborty, and U. Mishra, *J. Appl. Phys.* 96, 2674 (2004).

M. Lachab, M. Sultana, H. Fatima, V. Adivarahan, Q. Fareed, and M. A. Khan, *Semicond. Sci. Technol.* 27, 125001 (2012).

C. J. Kirkpatrick, B. Lee, R. Suri, X. Yang, and V. Misra, *IEEE Electron Device Lett.* 33, 1240 (2012).

S. Takashima, Z. Li, and T. P. Chow, *Jpn. J. Appl. Phys.* 52, 08JN24 (2013).

T. Huang, X. Zhu, K. M. Wong, and K. M. Lau, *IEEE Electron Device Lett.* 33, 212 (2012).

L. Pang, Y. Lian, D.-S. Kim, J.-H. Lee, and K. Kim, *IEEE Trans. Electron Devices* 59, 2650 (2012).

L. Han and Z. Chen, *J. Solid-State Sci. Technol.* 2, N228 (2013).

R. L. Puurunen, *J. Appl. Phys.* 97, 121301 (2005).

S. M. George, O. Sneh, A. C. Dillon, M. L. Wise, A. W. Ott, L. A. Okada, and J. D. Way, *Appl. Surf. Sci.* 82, 460 (1994).

J. W. Klaus, O. W. Ott, J. M. Johnson, and S. M. George, *Appl. Phys. Lett.* 70, 1092 (1997).

J. D. Ferguson, A. W. Weimer, and S. M. George, *Appl. Surf. Sci.* 162, 280 (2000).

J. W. Klaus, O. Sneh, and S. M. George, *Science* 278, 1934 (1997).

B. A. McCool and W. J. DeSisto, *Chem. Vap. Deposition* 10, 190 (2004).

J. D. Ferguson, E. R. Smith, A. W. Weimer, and S. M. George, *J. Electrochem. Soc.* 151, G528 (2004).

S. M. George, O. Sneh, A. C. Dillon, M. L. Wise, A. W. Ott, L. A. Okada, and J. D. Way, *Appl. Surf. Sci.* 82/83, 460 (1994).

J. D. Ferguson, A. W. Weimer, and S. M. George, *Appl. Surf. Sci.* 162/163, 280 (2000).

O. Sneh, M. L. Wise, A. W. Ott, L. A. Okada, and S. M. George, *Surf. Sci.* 334, 135 (1995).

J. W. Klaus, A. W. Ott, J. M. Johnson, and S. M. George, *Appl. Phys. Lett.* 70, 1092 (1997).

J. W. Klaus, A. W. Ott, and S. M. George, *Surf. Rev. Lett.* 6, 435 (1999).

M. A. Cameron, I. P. Gartland, J. A. Smith, S. F. Diaz, and S. M. George, *Langmuir* 16, 7435 (2000).

J. D. Ferguson, A. W. Weimer, and S. M. George, *Chem. Mater.* 12, 3472 (2000).

Y. Fedorenko, J. Swerts, J. W. Maes, E. Tois, S. Haukka, C. G. Wang, G. Wilk, A. Delabie, W. Deweerdt, and S. De Gendt, *Electrochem. Solid-State Lett.* 10, H149 (2007).

J. W. Klaus and S. M. George, *Surf. Sci.* 447, 81 (2000).

B. A. McCool and W. J. DeSisto, *Ind. Eng. Chem. Res.* 43, 2478 (2004).

B. A. McCool and W. J. DeSisto, *Chem. Vap. Deposition* 10, 190 (2004).

Y. Du, X. Du, and S. M. George, *Thin Solid Films* 491, 43 (2005).

L. K. Tan, A. S. M. Chong, X. S. E. Tang, and H. Gao, *J. Phys. Chem. C* 111, 4964 (2007)

Y. Du, X. Du, and S. M. George, *J. Phys. Chem. C* 111, 219 (2007).

S. W. Lee, K. Park, B. Han, S. H. Son, S. K. Rha, C. O. Park, and W. J. Lee, *Electrochem. Solid-State Lett.* 11, G23 (2008).

S. I. Kol'tsov, *Zh. Obshch. Khim.* 71, 1616 (2001).[*Russ. J. Gen. Chem.* 71, 1531 (2001)].

J.-H. Lee, U.-J. Kim, C.-H. Han, S.-K. Rha, W.-J. Lee, and C.-O. Park, *Jpn. J. Appl. Phys., Part 2* 43, L328 (2004).

W.-J. Lee, C.-H. Han, J.-K. Park, Y.-S. Lee, and S.-K. Rha, *Jpn. J. Appl. Phys., Part 1* 49, 071504 (2010).

- T. Murata, Y. Miyagawa, Y. Nishida, Y. Yamamoto, T. Yamashita, M. Matsuura, K. Asai, and H. Miyatake, *Jpn. J. Appl. Phys., Part 1* 49, 04DB11 (2010).
- Z. Ma, S. Brown, J. Y. Howe, S. H. Overbury, and S. Dai, *J. Phys. Chem. C* 112, 9448 (2008).
- B. Hatton, V. Kitaev, D. Perovic, G. Ozin, and J. Aizenberg, *J. Mater. Chem.* 20, 6009 (2010).
- J. D. Ferguson, E. R. Smith, A. W. Weimer, and S. M. George, *J. Electrochem. Soc.* 151, G528 (2004).
- Y. K. Jeong, H.-J. Kim, H. G. Kim, and B.-H. Choi, *Curr. Appl. Phys.* 9, S249 (2009).
- J. W. Lim, S. J. Yun, and J. H. Lee, *Electrochem. Solid-State Lett.* 8, F25 (2005).
- Y. B. Jiang, N. G. Liu, H. Gerung, J. L. Cecchi, and C. J. Brinker, *J. Am. Chem. Soc.* 128, 11018 (2006).
- J. W. Lim, S. J. Yun, and J. H. Kim, *ETRI J.* 31, 675 (2009).
- Y. Qin, Y. Kim, L. Zhang, S.-M. Lee, R. B. Yang, A. Pan, K. Mathwig, M. Alexe, U. Gösele, and M. Knez, *Small* 6, 910 (2010).
- J. Bachmann, R. Zierold, Y. T. Chong, R. Hauert, C. Sturm, R. Schmidt-Grund, B. Rheinländer, M. Grundmann, U. Gösele, and K. Nielsch, *Angew. Chem., Int. Ed.* 47, 6177 (2008).
- K. Pitzschel, J. M. M. Moreno, J. Escrig, O. Albrecht, K. Nielsch, and J. Bachmann, *ACS Nano* 3, 3463 (2009).
- J. Lee, S. Farhangfar, R. Yang, R. Scholz, M. Alexe, U. Gösele, J. Lee, and K. Nielsch, *J. Mater. Chem.* 19, 7050 (2009).
- D. Hiller, R. Zierold, J. Bachmann, M. Alexe, Y. Yang, J. W. Gerlach, A. Stesmans, M. Jivanescu, U. Müller, J. Vogt, H. Hilmer, P. Löper, M. Künle, F. Munnik, K. Nielsch, and M. Zacharias, *J. Appl. Phys.* 107, 064314 (2010).
- O. Albrecht, R. Zierold, C. Patzig, J. Bachmann, C. Sturm, B. Rheinländer, M. Grundmann, D. Görlitz, B. Rauschenbach, and K. Nielsch, *Phys. Status Solidi B* 247, 1365 (2010).
- B. B. Burton, M. P. Boleslawski, A. T. Desombre, and S. M. George, *Chem. Mater.* 20, 7031 (2008).
- X. Liang, K. S. Barrett, Y.-B. Jiang, and A. W. Weimer, *ACS Appl. Mater. Interfaces* 2, 2248 (2010).

- S. Kamiyama, T. Miura, and Y. Nara, *Electrochem. Solid-State Lett.* 8, F37 (2005).
- S. Kamiyama, T. Miura, and Y. Nara, *Thin Solid Films* 515, 1517 (2006).
- P. S. Waggoner, C. P. Tan, and H. G. Craighead, *J. Appl. Phys.* 107, 114505 (2010).
- S.-J. Won, S. Suh, M. S. Huh, and H. J. Kim, *IEEE Electron Device Lett.* 31, 857 (2010).
- T. Hirvikorpi, M. Vähä-Nissi, A. Harlin, J. Marles, V. Miikkulainen, and M. Karppinen, *Appl. Surf. Sci.* 257, 736 (2010).
- S. Kamiyama, T. Miura, Y. Nara, and T. Arikado, *Electrochem. Solid-State Lett.* 8, G215 (2005).
- Y. Kinoshita, F. Hirose, H. Miya, K. Hirahara, Y. Kimura, and M. Niwano, *Electrochem. Solid-State Lett.* 10, G80 (2007).
- F. Hirose, Y. Kinoshita, S. Shibuya, Y. Narita, H. Miya, K. Hirahara, Y. Kimura, and M. Niwano, *ECS Trans.* 19, 417 (2009).
- F. Hirose, Y. Kinoshita, S. Shibuya, Y. Narita, Y. Takahashi, H. Miya, K. Hirahara, Y. Kimura, and M. Niwano, *Thin Solid Films* 519, 270 (2010).
- B. B. Burton, S. W. Kang, S. W. Rhee, and S. M. George, *J. Phys. Chem. C* 113, 8249 (2009).
- D. M. King, X. H. Liang, B. B. Burton, M. K. Akhtar, and A. W. Weimer, *Nanotechnology* 19, 255604 (2008).
- W. Gasser, Y. Uchida, and M. Matsumura, *Thin Solid Films* 250, 213 (1994).
- K. Yamaguchi, S. Imai, N. Ishitobi, M. Takemoto, H. Miki, and M. Matsumura, *Appl. Surf. Sci.* 130–132, 202 (1998).
- S. Morishita, Y. Uchida, and M. Matsumura, *Jpn. J. Appl. Phys., Part 1* 34, 5738 (1995).
- S. Morishita, W. Gasser, K. Usami, and M. Matsumura, *J. Non-Cryst. Solids* 187, 66 (1995).
- H. B. Profijt, S. E. Potts, M. C. M. van de Sanden, and W. M. M. Kessels, *J. Vac. Sci. Technol. A* 29, 050801 (2011).
- S. M. George, *Chem. Rev.* 110, 111 (2010).
- J. Yang, B. S. Eller, C. Zhu, C. England, and R. J. Nemanich, *J. Appl. Phys.* 112, 053710 (2012).

J. Yang, B. S. Eller, M. Kaur, and R. J. Nemanich *J. Vac. Sci. Technol. A* 32, 021514 (2014).

D. A. Cole, J. R. Shallenberger, S. W. Novak, R. L. Moore, M. J. Edgell, S. P. Smith, C. J. Hitzman, J. F. Kirchhoff, E. Principe, W. Nieveen, F. K. Huang, S. Biswas, R. J. Bleiler, and K. Jones, *J. Vac. Sci. Technol. B* 18, 440 (2000).

M. Degai, K. Kanomata, K. Momiyama, S. Kubota, K. Hirahara, and F. Hirose, *Thin Solid Films* 525, 73 (2012).

Y. Kinoshita, F. Hirose, H. Miya, K. Hirahara, Y. Kimura, and M. Niwano, *Electrochem. Solid-State Lett.* 10, G80 (2007).

R. L. Puurunen, M. Lindblad, A. Root, and A. O. I. Krause, *Phys. Chem. Chem. Phys.* 3, 1093 (2001).

A. Rautiainen, M. Lindblad, L. B. Backman, and R. L. Puurunen, *Phys. Chem. Chem. Phys.* 4, 2466 (2002)

R. L. Puurunen, T. A. Zeelie, and A. O. I. Krause, *Catal. Lett.* 83, 27 (2002).

J. Robertson and B. Falabretti, *J. Appl. Phys.* 100, 014111 (2006).

K. W. Kim, S. D. Jung, D. S. Kim, H. S. Kang, K. S. Im, J. J. Oh, J. B. Ha, J. K. Shin, and J. H. Lee, *IEEE Electron Device Lett.* 32, 1376 (2011).

S.-J. Won, S. Suh, M. S. Huh, and H. J. Kim, *IEEE Electron Device Lett.* 31, 857 (2010).

B. S. Eller, J. Yang, and R. J. Nemanich, *J. Electron. Mater.* 43, 4560 (2014).

B. S. Eller, J. Yang, and R. J. Nemanich, *J. Vac. Sci. Technol. A* 31, 050807 (2012).

B. Lee, C. Kirkpatrick, Y.-H. Choi, X. Yang, A. Q. Huang, and V. Misra, *Phys. Status Solidi* 9, 868 (2012).

C. J. Kirkpatrick, B. Lee, R. Suri, X. Yang, and V. Misra, *IEEE Electron Device Lett.* 33, 1240 (2012).

N. Ramanan, B. Lee, C. Kirkpatrick, R. Suri, and V. Misra, *Semicond. Sci. Technol.* 28, 074004 (2013).

N. Ramanan, B. Lee, V. Misra, *IEEE Trans. Electron Devices* 62, 546 (2015).

F. Roccaforte, P. Fiorenza, G. Greco, R. Lo Nigro, F. Giannazzo, Al Patti, and M. Saggio, *Phys. Status Solidi A* 211, 2063 (2014).

L. Han and Z. Chen, *J. Solid-State Sci. Technol.* 2, N228 (2013).

R. L. Puurunen, *J. Appl. Phys.* 97, 121301 (2005).

G. Dingemans, C. A. A. van Helvoirt, M. C. M. van de Sanden, and W. M. M. Kessels, *ECS Transactions* 35, 191 (2011).

B. S. Eller, W. Li, S. Rupprecht, and R. J. Nemanich, to be submitted (2015).

J. Yang, B. S. Eller, and R. J. Nemanich, *J. Appl. Phys.* 116, 123702 (2014).

T. E. Cook, Jr., C. C. Fulton, W. J. Mecouch, R. F. Davis, G. Lucovsky, and R. J. Nemanich, *J. Appl. Phys.* 94, 7155 (2003).

J. R. Waldrop, and R. W. Grant, *Appl. Phys. Lett.* 68, 2879 (1996).

J. Hedman, and N. Mårtensson, *Phys. Scr.* 22, 176 (1980).

J. Yang, B. S. Eller, C. Zhu, C. England, and R. J. Nemanich, *J. Appl. Phys.* 112, 053710 (2012).

J. Yang, B. S. Eller, M. Kaur, and R. J. Nemanich, *J. Vac. Sci. Technol. A* 32, 021514 (2014).

Y. L. Chiou, and C. T. Lee, *IEEE Trans. Electron Devices* 58, 3869 (2011).

T. E. Cook Jr., C. C. Fulton, W. J. Mecouch, K. M. Tracy, R. F. Davis, G. Lucovsky, E. H. Hurt, and R. J. Nemanich, *J. Appl. Phys.* 93, 3995 (2003).

G. Martin, S. Strite, A. Botchkarev, A. Agarwal, A. Rockett, H. Morkoc, W. R. L. Lambrecht, and B. Segall, *Appl. Phys. Lett.* 65, 610 (1994).

M. Higashiwaki, S. Chowdhury, B. L. Swenson, and U. K. Mishra, *Appl. Phys. Lett.* 97, 222104 (2010).

M. Higashiwaki, S. Chowdhury, M.-S. Miao, B. L. Swenson, C. G. Van de Walle, and U. K. Mishra, *J. Appl. Phys.* 108, 063719 (2010)

M. S. Miao, J. R. Weber, and C. G. Van de Walle, *J. Appl. Phys.* 107, 123713 (2010).

J. Robertson and B. Falabretti, *J. Appl. Phys.* 100, 014111 (2006)

W. Mönch, *J. Appl. Phys.* 80, 5076 (1996).

J. Robertson, *J. Vac. Sci. Technol. B* 18, 1785 (2000).

D. Fritsch, H. Schmidt, and M. Grundmann, *Phys. Rev. B* 67, 235205 (2003).

N. V. Edwards, M. D. Bremser, T. W. Weeks, R. S. Kern, R. F. Davis, and D. E. Aspnes, *Appl. Phys. Lett.* 69, 2065 (1996).

B. S. Eller, J. Yang, and R. J. Nemanich, *J. Vac. Sci. Technol. A* 31, 050807 (2012).

S. D. Wolter, B. P. Luther, D. L. Waltmyer, C. Onneby, S. E. Mohny, and R. J. Molnar, *Appl. Phys. Lett.* 70, 2156 (1997).

C.-T. Lee, H.-W. Chen, and H.-Y. Lee, *Appl. Phys. Lett.* 82, 4304 (2003).

M. S. Miao, J. R. Weber, and C. G. Van de Walle, *J. Appl. Phys.* 107, 123713 (2010).

M. Higashiwaki, S. Chowdhury, M.-S. Miao, B. L. Swenson, C. G. Van de Walle, and U. K. Mishra, *J. Appl. Phys.* 108, 063719 (2010)

M. Higashiwaki, S. Chowdhury, B. L. Swenson, and U. K. Mishra, *Appl. Phys. Lett.* 97, 222104 (2010)

S. E. Potts and W. M. M. Kessels, *Coord. Chem. Rev.* 257, 3254 (2013).

S. E. Potts, H. B. Profijt, R. Roelofs, and W. M. M. Kessels, *Chem. Vap. Dep.* 19, 125 (2013).

H. B. Profijt, M. C. M. van de Sanden, and W. M. M. Kessels, *J. Vac. Sci. Technol. A* 31, 01A106 (2013).

E. Bersch, S. Rangan, R. A. Bartynski, E. Garfunkel, and E. Vescovo, *Phys. Rev. B* 78, 085114 (2008).

R. H. French, *J. Am. Ceram. Soc.* 73, 477 (1990).

H. Nohira, W. Tsai, W. Besling, E. Young, J. Petry, T. Conard, W. Vandervorst, S. De Gendt, M. Heyns, J. Maes, and M. Tuominen, *J. Non-Cryst. Solids* 303, 83 (2002).

S. Miyazaki, *J. Vac. Sci. Technol. B* 19, 2212 (2001).

J. Yang, B. S. Eller, M. Kaur, and R. J. Nemanich, *J. Vac. Sci. Tech. A* 32, 021514 (2014).

V. Miikkulainen, M. Leskelä, M. Ritala, and R. L. Puurunen, *J. Appl. Phys.* 113, 021301 (2013).

H. B. Profijt, M. C. M. van de Sanden, and W. M. M. Kessels, *J. Vac. Sci. Technol. A* 31, 01A106 (2013).

J. Kim, S. Kim, H. Kang, J. Choi, H. Jeon, M. Cho, K. Chung, S. Back, K. Yoo, and C. Bae, *J. Appl. Phys.* 98, 094504 (2005).

H. B. Profijt, S. E. Potts, M. C. M. van de Sanden, and W. M. M Kessels, *J. Vac. Sci. Technol. A* 29, 050801 (2011).

Web of Knowledge, <http://apps.isiknowledge.com> (May 31, 2014).

A. Niskanen, T. Hatanpaa, K. Arstila, M. Leskela, and M. Ritala, *Chem. Vap. Dep.* 13, 408 (2007).

M. Kariniemi, J. Niinistö, T. Hatanpää, M. Kemell, T. Sajavaara, M. Ritala, and M. Leskelä, *Chem. Mater.* 23, 2901 (2011).

M. Kariniemi, J. Niinistö, M. Vehkamäki, M. Kemell, M. Ritala, M. Leskelä, and M. Putkonen, *J. Vac. Sci. Technol. A* 30, 01A115 (2012).

C. W. Jeong, B. I. Lee, and S. K. Joo, *Mater. Sci. Eng. C* 16, 59 (2001).

C. W. Jeong, J. S. Lee, and S. K. Joo, *Jpn. J. Appl. Phys., Part 1* 40, 285 (2001).

J.-H. Park, D.-S. Han, Y.-J. Kang, S.-R. Shin, and J.-W. Park, *J. Vac. Sci. Technol. A* 32, 01A131 (2014).

B. H. Kim, W. S. Jeon, S. H. Jung, and B. T. Ahn, *Electrochem. Solid-State Lett.* 8, G294 (2005).

J. Koo, S. Kim, S. Jeon, H. Jeon, Y. Kim, and Y. Won, *J. Korean Phys. Soc.* 48, 131 (2006).

S. E. Pott, G. Dingemans, C. Lachaud, and W. M. M. Kessels, *J. Vac. Sci. Technol. A* 30, 021505 (2012).

A. Ali, H. S. Madan, A. P. Kirk, D. A. Zhao, D. A. Mourey, M. K. Hudait, R. M. Wallace, T. N. Jackson, B. R. Bennett, J. B. Boos, and S. Datta, *Appl. Phys. Lett.* 97, 143502 (2010).

P. Poodt, B. Kniknie, A. Branca, H. Winands, and F. Roozeboom, *Phys. Status Solidi RRL* 5, 165 (2011).

Y. H. Kim, J. Moon, C. H. Chung, S. J. Yun, D. J. Park, J. W. Lim, Y. H. Song, and J. H. Lee, *IEEE Electron Dev. Lett.* 27, 896 (2006).

D. J. Park, J. W. Lim, and B. O. Park, *Solid-State Electron.* 54, 323 (2010).

Y. H. Kim, C. Y. Sohn, J. W. Lim, S. J. Yun, C. S. Hwang, C. H. Chung, Y. W. Ko, and J. H. Lee, *IEEE Electron. Dev. Lett.* 25, 550 (2004).

J. Moon, Y. H. Kim, D. J. Park, C. H. Chung, S. Y. Kang, and J. H. Lee, *Solid-State Electron.* 54, 1326 (2010).

- S. Lee, and H. Jeon, *Electron. Mater. Lett.* 3, 17 (2007).
- M. T. Seman, D. N. Richards, P. Rowlette, and C. A. Wolden, *Chem. Vap. Dep.* 14, 296 (2008).
- J. W. Lim, and S. J. Yun, *Jpn. J. Appl. Phys., Part 2* 42, L663 (2003).
- S. W. Choi, C. M. Jang, D. Y. Kim, J. S. Ha, H. S. Park, W. Koh, and C. S. Lee, *J. Korean Phys. Soc.* 42, 975 (2003).
- J. W. Lim, and S. J. Yun, *Electrochem. Solid-State Lett.* 7, F45 (2004).
- P. K. Park, and S. W. Kang, *Appl. Phys. Lett.* 89, 192905 (2006).
- P. K. Park, E. S. Cha, and S. W. Kang, *Appl. Phys. Lett.* 90, 232906 (2007).
- J. W. Lim, J. B. Koo, S. J. Yun, and H. T. Kim, *Electrochem. Solid-State Lett.* 10, J136 (2007).
- K. Y. Park, H. I. Cho, H. C. Choi, Y. H. Bae, C. S. Lee, J. L. Lee, and J. H. Lee, *Jpn. J. Appl. Phys., Part 2* 43, L1433 (2004).
- S. M. Yoon, S. H. K. Park, C. W. Byun, S. H. Yang, and C. S. Hwang, *J. Electrochem. Soc.* 157, H727 (2010).
- S. J. Yun, Y. W. Ko, and J. W. Lim, *Appl. Phys. Lett.* 85, 4896 (2004).
- W. S. Kim, D. Y. Moon, B. W. Kang, J. W. Park, and J. G. Park, *J. Korean Phys. Soc.* 55, 55 (2009).
- A. Niskanen, K. Arstila, M. Ritala, and M. Leskela, *J. Electrochem. Soc.* 152, F90 (2005).
- M. Caymax, G. Brammertz, A. Delabie, S. Sioncke, D. Lin, M. Scarrozza, G. Pourtois, W. E. Wang, M. Meuris, and M. Heyns, *Microelectron. Eng.* 86, 1529 (2009).
- J. Dendooven, D. Deduytsche, J. Musschoot, R. L. Vanmeirhaeghe, and C. Detavernier, *J. Electrochem. Soc.* 157, G111 (2010).
- G. Dingemans, N. M. Terlinden, D. Pierreux, H. B. Profijt, M. C. M. van de Sanden, and W. M. M Kessels, *Electrochem. Solid-State Lett.* 14, H1 (2010).
- G. Dingemans, R. Seguin, P. Engelhart, M. C. M. van de Sanden, and W. M. M Kessels, *Phys. Status Solidi (RRL)* 4, 10 (2010).
- J. J. H. Gielis, P. M. Gevers, I. M. P. Aarts, M. C. M. van de Sanden, and W. M. M Kessels, *J. Vac. Sci. Technol. A* 26, 1519 (2008).

S. B. S. Heil, P. Kudlacek, E. Langereis, R. Engeln, M. C. M. van de Sanden, and W. M. M Kessels, *Appl. Phys. Lett.* 89, 131505 (2006).

S. B. S. Heil, J. L. van Hemmen, M. C. M. van de Sanden, and W. M. M Kessels, *J. Appl. Phys.* 103, 103302 (2008).

B. Hoex, S. B. S. Heil, E. Langereis, M. C. M. van de Sanden, and W. M. M Kessels, *Appl. Phys. Lett.* 89, 042112 (2006).

B. Hoex, J. Schmidt, R. Bock, P. P. Altermatt, M. C. M. van de Sanden, and W. M. M Kessels, *Appl. Phys. Lett.* 91, 112107 (2007).

B. Hoex, J. Schmidt, P. Pohl, M. C. M. van de Sanden, and W. M. M Kessels, *J. Appl. Phys.* 104, 044903 (2008).

D. Hoogeland, K. B. Jinesh, F. Roozeboom, W. F. A. Besling, M. C. M. van de Sanden, and W. M. M Kessels, *J. Appl. Phys.* 106, 114107 (2009).

H. Kim, S. Woo, J. Lee, H. Lee, and H. Jeon, *J. Phys. D* 43, 505301(2010).

Y. Kim, S. Woo, H. Kim, J. Lee, H. Kim, H. Lee, and H. Jeon, *J. Mater. Res.* 25, 1898 (2010).

E. Langereis, M. Creatore, S. B. S. Heil, M. C. M. van de Sanden, and W. M. M Kessels, *Appl. Phys. Lett.* 89, 081915 (2006).

E. Langereis, J. Keijmel, M. C. M. van de Sanden, and W. M. M Kessels, *Appl. Phys. Lett.* 92, 231904 (2008).

S. E. Potts, W. Keuning, E. Langereis, G. Dingemans, M. C. M. van de Sanden, and W. M. M Kessels, *J. Electrochem. Soc.* 157, P66 (2010).

V. R. Rai, V. Vandalon, and S. Agarwal, *Langmuir* 26, 13732 (2010).

S. Sioncke, A. Delabie, G. Brammertz, T. Conard, A. Franquet, M. Caymax, A. Urbanczyk, M. Heyns, M. Meuris, J. L. van Hemmen, W. Keuning, and W. M. M Kessels, *J. Electrochem. Soc.* 156, H255 (2009).

N. M. Terlinden, G. Dingemans, M. C. M. van de Sanden, and W. M. M Kessels, *Appl. Phys. Lett.* 96, 112101 (2010).

J. L. van Hemmen, S. B. S. Heil, J. H. Klootwijk, F. Roozeboom, C. J. Hodson, M. C. M. van de Sanden, and W. M. M Kessels, *J. Electrochem. Soc.* 154, G165 (2007).

H. S. Yun, and K. H. Kim, *J. Korean Phys. Soc.* 54, 707 (2009).

T. O. Kaariainen, and D. C. Cameron, *Plasma Processes Polym.* 6, S237 (2009).

- K. Lambert, J. Dendooven, C. Detavernier, and Z. Hens, *Chem. Mater.* 23, 126 (2011).
- K. B. Jinesh, J. L. van Hemmen, M. C. M. van de Sanden, F. Roozeboom, J. H. Klootwijk, W. F. A. Besling, and W. M. M Kessels, *J. Electrochem. Soc.* 158, G21 (2011).
- S. E. Potts, L. Schmalz, M. Fenker, B. Diaz, J. Swiatowska, V. Maurice, A. Seyeux, P. Marcus, G. Radnoczi, L. Toth, and W. M. M Kessels, *J. Electrochem. Soc.* 158, C132 (2011).
- P. Poodt, B. Kniknie, A. Branca, H. Winands, and F. Roozeboom, *Phys. Status Solidi (RRL)* 5, 165 (2011).
- O. M. Nayfeh, T. Marr, and M. Dubey, *IEEE Electron. Dev. Lett.* 32, 473 (2011).
- R. Driad, F. Benkhelifa, L. Kirste, M. Mikulla, and O. Ambacher, *J. Electrochem. Soc.* 158, H1279 (2011).
- S. E. Potts, L. Schmalz, M. Fenker, B. Díaz, J. Światowska, V. Maurice, A. Seyeux, P. Marcus, G. Radnóczy, L. Tóth, and W. M. M. Kessels, *J. Electrochem. Soc.* 158, C132 (2011).
- K. Lambert, J. Dendooven, C. Detavernier, and Z. Hens, *Chem. Mater.* 23, 126 (2011).
- R. Driad, F. Benkhelifa, L. Kirste, M. Mikulla, and O. Ambacher, *J. Electrochem. Soc.* 158, H1279 (2011).
- G. Dingemans, N. M. Terlinden, D. Pierreux, H. B. Profijt, M. C. M. van de Sanden, and W. M. M. Kessels, *Electrochem. Solid-State Lett.* 14, H1 (2011).
- K.-H. Kim, H.-J. Kim, P. Jang, C. Jung, and K. Seomoon, *Electron. Mater. Lett.* 7, 171 (2011).
- D. Longruea, D. Deduytschea, J. Haemersa, K. Driesenb, and C. Detaverniera, *Surf. Coat. Technol.* 213, 183 (2012).
- R. Fu, and J. Pattison, *Opt. Eng.* 51, 104003 (2012).
- J. Musschoot, J. Dendooven, D. Deduytsche, J. Haemers, G. Buyle, and C. Detavernier, *Surf. Coat. Technol.* 206, 4511 (2012).
- C.-H. Wu, K.-M. Chang, S.-H. Huang, I.-C. Deng, C.-J. Wu, W.-H. Chiang, and C.-C. Chang, *IEEE Electron Dev. Lett.* 33, 552 (2012).
- Y. Kawamura, M. Tani, N. Hattori, N. Miyatake, M. Horita, Y. Ishikawa, and Y. Uraoka, *Jpn. J. Appl. Phys.* 51, 02BF04 (2012).

C. Peroz, S. Dhuey, M. Cornet, M. Vogler, D. Olynick, and S Cabrini, *Nanotechnology* 23, 015305 (2012).

V. R. Rai, V. Vandalon, and S. Agarwal, *Langmuir* 28, 350 (2012).

A. Foroughi-Abariz, and K. C. Cadien, *J. Electrochem. Soc.* 159, D59 (2012).

W. Keuning, P. van de Weijer, H. Lifka, W. M. M. Kessels, and M. Creatore, *J. Vac. Sci. Technol. A* 30, 01A131 (2012).

L. Wenwen, L. Xingcun, C. Qiang, and W. Zhengduo, *Plasma Sci. Technol.* 14, 12 (2012).

B. Hoex, M. C. M. van de Sanden, J. Schmidt, R. Brendel, and W. M. M. Kessels, *Phys. Status Solidi RRL* 6, 4 (2012).

S.-F. Ding, Q. Xie, F. Chen, H.-Sh. Lu, S.-R. Deng, D. Deduytsche, C. Detavernier, and X.-P. Qu, *Solid-State Lett.* 1, P54 (2012).

S. Yang, Z. Tang, K.-Y. Wong, Y.-S. Lin, C. Liu, Y. Lu, S. Huang, and K. J. Chen, *IEEE Electron Dev. Lett.* 34, 1497 (2013).

M. Blaho, D. Gregušová, M. Jurkovič, Š. Haščík, J. Fedor, P. Kordoš, K. Fröhlich, F. Brunner, M. Cho, O. Hilt, J. Würfl, and J. Kuzmík, *Microelectron. Eng.* 112, 204 (2013).

J. Haeberle, K. Henkel, H. Gargouri, F. Naumann, B. Gruska, M. Arens, M. Tallarida, and D. Schmeißer, *Beilstein J. Nanotechnol.* 4, 732 (2013).

H. Jung, H. Choi, H. Jeon, S. Lee, and H. Jeon, *J. Appl. Phys.* 114, 173511 (2013).

S. Ozaki, T. Ohki, M. Kanamura, N. Okamoto, and T. Kikkawa, *Jap. J. Appl. Phys.* 52, 11NG04 (2013).

B. Hoex, M. Bosman, N. Nandakumar, and W. M. M. Kessels, *Physica Status Solidi RRL* 7, 937 (2013).

J. Zuidema, X. Ruan, and T. S. Fisher, *Optics Express* 21, 22053 (2013).

X. Zhang, and A. Cuevas, *Physica Status Solidi RRL* 7, 619 (2013).

E. Härkönen, S. E. Potts, W. M. M. Kessels, B. Díaz, A. Seyeux, J. Światowska, V. Maurice, P. Marcus, G. Radnóczy, L. Tóth, M. Kariniemi, J. Niinistö, and M. Ritala, *Thin Solid Films* 534, 384 (2013).

J. G. Lee, H. G. Kim, and S. S. Kim, *Thin Solid Films* 534, 515 (2013).

- A. C. Kozen, M. A. Schroeder, K. D. Osborn, C. J. Lobb, and G. W. Rubloff, *Appl. Phys. Lett.* 102, 173501 (2013).
- W. Liang, K. J. Weber, D. Suh, S. P. Phang, J. Yu, A. K. McAuley, and B. R. Legg, *IEEE J. Photovoltaics* 3, 678 (2013).
- W. Yoon, A. R. Smith, E. E. Foos, J. E. Boercker, W. B. Heuer, and J. G. Tischler, *IEEE Trans. Nanotechnol.* 12, 146 (2013).
- R. Edy, X. Huang, Y. Guo, J. Zhang, and J. Shi, *Nanoscale Res. Lett.* 8, 79 (2013).
- A. K. Roy, D. Deduytsche, and C. Detavernier, *J. Vac. Sci. Technol. A* 31, 01A147 (2013).
- A. Richter, J. Benick, and M. Hermle, *IEEE J. Photovoltaics* 3, 236 (2013).
- H. B. Profijt, M. C. M. van de Sanden, and W. M. M. Kessels, *J. Vac. Sci. Technol. A* 31, 01A106 (2013).
- S. Y. Song, *J. Korean Inst. Electrical Electron. Mater. Engineers* 26, 754 (2013).
- X. Yuqing, S. Lijun, C. Qiang, Y. Lizhen, W. Zhengduo, and L. Zhongwei, *Plasma Sci. Technol.* 15, 52 (2013).
- T. Bülow, H. Gargouri, M. Siebert, R. Rudolph, H.-H. Johannes, and W. Kowalsky, *Nanoscale Res. Lett.* 9, 223 (2014).
- A. M. Mahajana, A. G. Khairnara, and B. J. Thibeault, *Semiconductors* 48, 497 (2014).
- S. Lee, H. Choi, S. Shin, J. Park, G. Ham, H. Jung, and H. Jeon, *Curr. Appl. Phys.* 14, 552 (2014).
- A. Perrotta, E. R. J. van Beekum, G. Aresta, A. Jagia, W. Keuning, R. M. C. M. van de Sanden, E. W. M. M. Kessels, and M. Creatore, *Microporous, and Mesoporous Mater.* 188, 163 (2014).
- Y.-C. Lee, T.-T. Kao, J. J. Merola, and S.-C. Shen, *IEEE Trans. Electron Dev.* 61, 493 (2014).
- D. Wei, T. Hossain, D. P. Briggs, and J. H. Edgar, *J. Solid-State Sci. Technol.* 3, N127 (2014).
- K. Henkel, H. Gargouri, B. Gruska, M. Arens, M. Tallarida, and D. Schmeißer, *J. Vac. Sci. Technol. A* 32, 01A107 (2014).
- Y. J. Lee, and S. W. Kang, *Thin Solid Films* 446, 227 (2004).

- Y. J. Lee, *J. Cryst. Growth* 266, 568 (2004).
- C. Ozgit-Akgun, E. Goldenberg, A. K. Okyay, and N. Biyikli, *J. Mater. Chem. C* 2, 2123 (2014).
- K. H. Kim, N. W. Kwak, and S. H. Lee, *Electron. Mater. Lett.* 5, 83 (2009).
- S. Huang; Q. Jiang, S. Yang, C. Zhou, and K. J. Chen, *IEEE Electron. Dev. Lett.* 33, 516 (2012).
- C. Liu, S. Liu, S. Huang, and K. J. Chen, *IEEE Electron Dev. Lett.* 34, 1106 (2013).
- K. J. Chen, and S. Huang, *Semicond. Sci. Technol.* 28, 074015 (2013).
- J. Zhang, Q. Zhang, H. Yang, H. Wu, J. Zhou, and L. Hu, *Appl. Surf. Sci.* 315, 110 (2014).
- A. Haider, C. Ozgit-Akgun, F. Kayaci, A. K. Okyay, T. Uyar, and N. Biyikli, *APL Mat.* 2, 096109 (2014).
- K. J. Voon, K. M. Bothe, P. Motamedi, K. C. Cadien, and D. W. Barlage, *J. Phys. D: Appl. Phys.* 47, 345104 (2014).
- M. Bosund, P. Mattila, A. Aierken, T. Hakkarainen, H. Koskenvaara, M. Sopanen, V. M. Airaksinen, and H. Lipsanen, *Appl. Surf. Sci.* 256, 7434 (2010).
- M. Bosund, T. Sajavaara, M. Laitinen, T. Huhtio, M. Putkonen, V. M. Airaksinen, and H. Lipsanen, *Appl. Surf. Sci.* 257, 7827 (2011).
- M. Alevli, C. Ozgit, I. Donmez, and N. Biyikli, *J. Cryst. Growth* 335, 51 (2011).
- N. Biyikli, G. Ozgit, and I. Donmez, *Nanosci. Nanotechnol. Lett.* 4, 1008 (2012).
- M. Alevli, C. Ozgit, I. Donmez, and N. Biyikli, *Physica Status Solidi A* 209, 266 (2012).
- R. Meunier, A. Torres, E. Morvan, M. Charles, P. Gaud, and F. Morancho, *Microelectron. Eng.* 109, 378 (2013).
- X. Li, W. Lei, Q. Zhao, and Q. Chen, *Surf. Coat. Technol.* 228, S55 (2013).
- D. Suh, and W. S. Liang, *Thin Solid Films* 539, 309 (2013).
- E. R. Cleveland, L. B. Ruppalt, B. R. Bennett, and S. M. Prokes, *Appl. Surf. Sci.* 277, 167 (2013).
- R. E. Sah, R. Driad, F. Bernhardt, L. Kirste, C.-C. Leancu, H. Czap, F. Benkhelifa, M. Mikulla, and O. Ambacher, *J. Vac. Sci. Technol. A* 31, 041502 (2013).

- W. Lei, and Q. Chen, *J. Vac. Sci. Technol. A* 31, 01A114 (2013).
- P. Mattila, M. Bosund, H. Jussila, A. Aierken, J. Riikonen, T. Huhtio, H. Lipsanen, and M. Sopenan, *Appl. Surf. Sci.* 314, 570 (2014).
- T.-E. Hsieh, E. Y. Chang, Y.-Z. Song, Y.-C. Lin, H.-C. Wang, S.-C. Liu, S. Salahuddin, and C. C. Hu, *IEEE Electron Dev. Lett.* 35, 732 (2014).
- J. W. Lim, and S. J. Yun, *Electrochem. Solid-State Lett.* 7, H33 (2004).
- J. W. Lim, S. J. Yun, and J. H. Lee, *Electrochem. Solid-State Lett.* 9, F8 (2006).
- J. W. Lim, S. J. Yun, and J. H. Lee, *Electrochem. Solid-State Lett.* 8, F25 (2005).
- J. W. Lim, S. J. Yun, and H. T. Kim, *J. Electrochem. Soc.* 154, G239 (2007).
- J. W. Lim, S. J. Yun, and H. T. Kim, *Jpn. J. Appl. Phys.* 47, 6934 (2008).
- J. W. Lim, S. J. Yun, and S. H. Lee, *J. Korean Phys. Soc.* 56, 96 (2010).
- G. J. Choi, S. K. Kim, S. J. Won, H. J. Kim, and C. S. Hwang, *J. Electrochem. Soc.* 156, G138 (2009).
- W.-H. Kim, I.-K. Oh, M.-K. Kim, W. J. Maeng, C.-W. Lee, G. Lee, C. Lansalot-Matras, W. Noh, D. Thompson, D. Chu, and H. Kim, *J. Mater. Chem. C* 2, 5805 (2014).
- W.-H. Kim, M.-K. Kim, W. J. Maeng, J. Gatineau, V. Pallem, C. Dussarrat, A. Noori, D. Thompson, S. Chu, and H. Kim, *J. Electrochem. Soc.* 158, G169 (2011).
- W.-H. Kim, W. J. Maeng, M.-K. Kim, J. Gatineau, and H. Kim, *J. Electrochem. Soc.* 158, G217 (2011).
- K. Kim, K. Lee, S. Han, W. Jeong, and H. Jeon, *J. Electrochem. Soc.* 154, H177 (2007).
- K. Kim, K. Lee, S. Han, T. Park, Y. Lee, J. Kim, S. Yeom, and H. Jeon, *Jpn. J. Appl. Phys., Part 2* 46, L173 (2007).
- K. Lee, K. Kim, T. Park, H. Jeon, Y. Lee, J. Kim, and S. Yeom, *J. Electrochem. Soc.* 154, H899 (2007).
- K. Lee, K. Kim, H. Jeon, Y. Lee, J. Kim, and S. Yeom, *J. Korean Phys. Soc.* 50, 1141 (2007).
- J. M. Kim, H. B. R. Lee, C. Lansalot, C. Dussarrat, J. Gatineau, and H. Kim, *Jpn. J. Appl. Phys.* 49, 05FA10 (2010).

J. Yoon, H.-B.-R. Lee, D. Kim, T. Cheon, S.-H. Kim, and H. Kim, *J. Electrochem. Soc.* 158, H1179 (2011).

H. B. R. Lee, and H. Kim, *Electrochem. Solid-State Lett.* 9, G323 (2006).

H. B. R. Lee, J. Y. Son, and H. Kim, *Appl. Phys. Lett.* 90, 213509 (2007).

H.-B.-R. Lee, Y. J. Park, S. Baik, and H. Kim, *Chem. Vap. Dep.* 18, 41 (2012).

H. Shimizu, K. Sakoda, T. Momose, M. Koshi, and Y. Shimogaki, *J. Vac. Sci. Technol. A* 30, 01A144 (2012).

H. B. R. Lee, J. Kim, H. Kim, W. H. Kim, J. W. Lee, and I. Hwang, *J. Korean Phys. Soc.* 56, 104 (2010).

H. Kim, *Microelectron. Eng.* 106, 69 (2013).

R. P. Chaukulkar, N. F. W. Thissen, V. R. Rai, and S. Agarwal, *J. Vac. Sci. Technol. A* 32, 01A108 (2014).

J. Park, H.-B.-R. Lee, D. Kim, J. Yoon, C. Lansalot, J. Gatineau, H. Chevrel, and H. Kim, *J. Energy Chem.* 22, 403 (2013).

M. E. Donders, H. C. M. Knoops, M. C. M. van de Sanden, W. M. M. Kessels, and P. H. L. Notten, *J. Electrochem. Soc.* 158, G92 (2011).

M. E. Donders, H. C. M. Knoops, W. M. M. Kessels, and P. H. L. Notten, *J. Power Sources* 203, 72 (2012).

H. B. R. Lee, G. H. Gu, J. Y. Son, C. G. Park, and H. Kim, *Small* 4, 2247 (2008).

H. B. R. Lee, and H. Kim, *J. Cryst. Growth* 312, 2215 (2010).

L. Wu, and E. Eisenbraun, *J. Vac. Sci. Technol. B* 25, 2581 (2007).

L. Wu, and E. Eisenbraun, *Electrochem. Solid-State Lett.* 11, H107 (2008).

L. Wu, and E. Eisenbraun, *J. Electrochem. Soc.* 156, H734 (2009).

A. Niskanen, A. Rahtu, T. Sajavaara, K. Arstila, M. Ritala, and M. Leskela, *J. Electrochem. Soc.* 152, G25 (2005).

D. J. Hagen, J. Connolly, R. Nagle, I. M. Povey, S. Rushworth, P. Carolan, P. Ma, and M. E. Pemble, *Surf. Coat. Technol.* 230, 3 (2013).

B. K. Lee, S. H. Kim, B. K. Park, S. S. Lee, J.-H. Hwang, T.-M. Chung, Y. K. Lee, C. G. Kim, and K.-S. An, *J. Nanosci. Nanotechnol.* 11, 5887 (2011).

D. Y. Moon, D. S. Han, S. Y. Shin, J. W. Park, B. M. Kim, and J. H. Kim, *Thin Solid Films* 519, 3636 (2011).

D. Y. Moon, W. S. Kim, T. S. Kim, B. W. Kang, J. W. Park, S. J. Yeom, and J. H. Kim, *J. Korean Phys. Soc.* 54, 1330 (2009).

J. P. Coyle, G. Dey, E. R. Sirianni, M. L. Kemell, G. P. A. Yap, M. Ritala, M. Leskelä, S. D. Elliott, and S. T. Barry, *Chem. Mater.* 25, 1132 (2013).

C. Jezewski, W. A. Lanford, C. J. Wiegand, J. P. Singh, P. I. Wang, J. J. Senkevich, and T. M. Lu, *J. Electrochem. Soc.* 152, C60 (2005).

T. T. Van, and J. P. Chang, *Appl. Surf. Sci.* 246, 250 (2005).

M. de Keijser, and C. van Opdorp, *Appl. Phys. Lett.* 58, 1187 (1991).

S. Bolat, C. Ozgit-Akgun, B. Tekcan, N. Biyikli, and A. K. Okyay, *Appl. Phys. Lett.* 104, 243505 (2014).

I. Donmez, C. Ozgit-Akgun, and N. Biyikli, *J. Vac. Sci. Technol. A* 31, 01A110 (2013).

T. Nam, C. W. Lee, H. J. Kim, and H. Kim, *Appl. Surf. Sci.* 295, 260 (2014).

G. X. Liu, F. K. Shan, W. J. Lee, G. H. Lee, I. S. Kim, and B. C. Shin, *Integr. Ferroelectr.* 85, 155 (2006).

G. X. Liu, F. K. Shan, W. J. Lee, B. C. Shin, S. C. Kim, H. S. Kim, and C. R. Cho, *Integr. Ferroelectr.* 94, 11 (2007).

N. J. Seong, S. G. Yoon, and W. J. Lee, *Appl. Phys. Lett.* 87, 082909 (2005).

N. J. Seong, E. T. Kim, and S. G. Yoon, *Integr. Ferroelectr.* 74, 181(2005).

F. K. Shan, G. X. Liu, W. J. Lee, G. H. Lee, I. S. Kim, and B. C. Shin, *J. Appl. Phys.* 98, 023504 (2005).

F. K. Shan, G. X. Liu, W. J. Lee, G. H. Lee, I. S. Kim, and B. C. Shin, *Integr. Ferroelectr.* 80, 197 (2006).

Y.-L. Lee, T.-H. Huang, C.-L. Ho, and M.-C. Wu, *J. Solid-State Sci. Technol.* 2, Q182 (2013).

Y.-L. Lee, C.-C. Huang, C.-L. Ho, and M.-C. Wu, *IEEE Electron Dev. Lett.* 34, 1406 (2013).

C.-C. Huang, C.-L. Ho, S.-F. Chen, Y.-F. Chang, and M.-C. Wu, *J. Solid-State Sci. Technol.* 3, P159 (2014).

- B. J. Choi, S. Choi, T. Eom, S. W. Ryu, D. Y. Cho, J. Heo, H. J. Kim, C. S. Hwang, Y. J. Kim, and S. K. Hong, *Chem. Mater.* 21, 2386 (2009).
- J. Lee, S. Choi, C. Lee, Y. Kang, and D. Kim, *Appl. Surf. Sci.* 253, 3969 (2007).
- G. X. Liu, F. K. Shan, J. J. Park, W. J. Lee, G. H. Lee, I. S. Kim, B. C. Shin, and S. G. Yoon, *J. Electroceram.* 17, 145 (2006).
- S. A. Vitale, P. W. Wyatt, and C. J. Hodson, *J. Vac. Sci. Technol. A* 30, 01A130 (2012).
- Z. Fang, P. A. Williams, R. Odedra, H. Jeon, and R. J. Potter, *J. Cryst. Growth* 338, 111 (2012).
- S. Consiglio, W. X. Zeng, N. Berliner, and E. T. Eisenbraun, *J. Electrochem. Soc.* 155, H196 (2008).
- W. J. Maeng, G. H. Gu, C. G. Park, K. Lee, T. Lee, and H. Kim, *J. Electrochem. Soc.* 156, G109 (2009).
- E. J. Kim, and D. H. Kim, *Electrochem. Solid-State Lett.* 9, C123 (2006).
- W. Jeong, Y. Ko, S. Bang, S. Lee, and H. Jeon, *J. Korean Phys. Soc.* 56, 905 (2010).
- Y. Lee, S. Kim, J. Koo, I. Kim, J. Choi, H. Jeon, and Y. Won, *J. Electrochem. Soc.* 153, G353 (2006).
- J. Choi, S. Kim, J. Kim, H. Kang, H. Jeon, and C. Bae, *J. Vac. Sci. Technol. A* 24, 900 (2006).
- S. Choi, J. Koo, H. Jeon, and Y. Kim, *J. Korean Phys. Soc.* 44, 35 (2004).
- H. Hong, S. Kim, S. Woo, H. Kim, H. Kim, W. Jeong, S. Jeon, S. Bang, S. Lfe, and H. Jeon, *J. Korean Phys. Soc.* 52, 1114 (2008).
- H. Kang, S. Kim, J. Choi, J. Kim, H. Jeon, and C. Bae, *Electrochem. Solid-State Lett.* 9, G211 (2006).
- I. Kim, S. Kuk, S. Kim, J. Kim, H. Jeon, M. H. Cho, and K. B. Chung, *Appl. Phys. Lett.* 90, 222101 (2007).
- J. Kim, S. Kim, H. Kang, J. Choi, H. Jeon, M. Cho, K. Chung, S. Back, K. Yoo, and C. Bae, *J. Appl. Phys.* 98, 094504 (2005).
- J. Kim, S. Kim, H. Jeon, M. H. Cho, K. B. Chung, and C. Bae, *Appl. Phys. Lett.* 87, 053108 (2005).

- S. Kim, J. Kim, J. Choi, H. S. Kang, H. Jeon, and C. Bae, *J. Vac. Sci. Technol. B* 24, 1088 (2006).
- S. Kim, J. Kim, J. Choi, H. Kang, H. Jeon, W. Cho, K. S. An, T. M. Chung, Y. Kim, and C. Bae, *Electrochem. Solid-State Lett.* 9, G200 (2006).
- S. Kim, S. Woo, H. Kim, W. Jeong, T. Park, H. Kim, S. B. Kim, and H. Jeon, *J. Vac. Sci. Technol. B* 25, 1922 (2007).
- S. Kim, S. Woo, H. Hong, H. Kim, H. Jeon, and C. Bae, *J. Electrochem. Soc.* 154, H97 (2007).
- S. Kim, S. Woo, H. Kim, I. Kim, K. Lee, W. Jeong, T. Park, and H. Jeon, *J. Korean Phys. Soc.* 52, 1103 (2008).
- Y. Won, S. Park, J. Koo, S. Kim, J. Kim, and H. Jeon, *Appl. Phys. Lett.* 87, 262901 (2005).
- S. Woo, H. Hong, S. Kim, H. Kim, J. Kim, H. Jeon, C. Bae, T. Okada, K. Sawada, and M. Ishida, *Jpn. J. Appl. Phys.* 47, 6196 (2008).
- Y. C. Byun, C. H. An, J. Y. Choi, C. Y. Kim, M. H. Cho, and H. Kim, *J. Electrochem. Soc.* 158, G141 (2011).
- P. K. Park, J. S. Roh, B. H. Choi, and S. W. Kang, *Electrochem. Solid-State Lett.* 9, F34 (2006).
- S. B. S. Heil, J. L. van Hemmen, C. J. Hodson, N. Singh, J. H. Klootwijk, F. Roozeboom, M. C. M. van de Sanden, and W. M. M Kessels, *J. Vac. Sci. Technol. A* 25, 1357 (2007).
- J. Joo, and S. M. Rossnagel, *J. Korean Phys. Soc.* 54, 1048 (2009).
- H. Kim, S. Woo, J. Lee, Y. Kim, H. Lee, I. J. Choi, Y. D. Kim, C. W. Chung, and H. Jeon, *J. Electrochem. Soc.* 158, H21 (2011).
- W. S. Kim, S. K. Park, D. Y. Moon, T. S. Kim, B. W. Kang, J. K. Seo, H. D. Kim, and J. W. Park, *J. Korean Phys. Soc.* 53, 3334 (2008).
- A. K. Rumaiz, J. C. Woicik, C. Weiland, Q. Xie, D. P. Siddons, G. H. Jaffari, and C. Detavernier, *Appl. Phys. Lett.* 101, 222110 (2012).
- H.-S. Jung, H. K. Kim, I.-H. Yu, S. Y. Lee, J. Lee, J. Park, J. H. Jang, S.-H. Jeon, Y. J. Chung, D.-Y. Cho, N.-I. Lee, T. J. Park, J.-H. Choi, and C. S. Hwang, *J. Electrochem. Soc.* 159, G33 (2012).
- C. Richter, T. Schenk, U. Schroeder, and T. Mikolajick, *J. Vac. Sci. Technol. A* 32, 01A117 (2014).

M. Modreanu, S. Monaghan, I. M. Povey, K. Cherkaoui, P. K. Hurley, and M. Androulidaki, *Microelectron. Eng.* 88, 1499 (2011).

W. J. Maeng, and H. Kim, *Appl. Phys. Lett.* 91, 092901 (2007).

W. J. Maeng, and H. Kim, *J. Electrochem. Soc.* 155, H267 (2008).

W. J. Maeng, J. Y. Son, and H. Kim, *J. Electrochem. Soc.* 156, G33 (2009).

W. J. Maeng, W. H. Kim, J. H. Koo, S. J. Lim, C. S. Lee, T. Lee, and H. Kim, *Appl. Phys. Lett.* 96, 082905 (2010).

B. D. Briggs, S. M. Bishop, K. D. Leedy, and N. C. Cady, *Thin Solid Films* 562, 519 (2014).

H. Jeon, and Y. Won, *Appl. Phys. Lett.* 93, 124104 (2008).

S. X. Lao, R. M. Martin, and J. P. Chang, *J. Vac. Sci. Technol. A* 23, 488 (2005).

H. Kim, S. Kim, S. Woo, H. Y. Chung, H. Kim, J. Park, and H. Jeon, *J. Electrochem. Soc.* 155, G299 (2008).

W. J. Maeng, and H. Kim, *J. Appl. Phys.* 104, 064111 (2008).

J. R. Liu, R. M. Martin, and J. P. Chang, *J. Vac. Sci. Technol. A* 26, 1251 (2008).

D. K. Joo, J. S. Park, and S. W. Kang, *Electrochem. Solid-State Lett.* 12, H77 (2009).

S. W. Kim, S. H. Kwon, S. J. Jeong, J. S. Park, and S. W. Kang, *Electrochem. Solid-State Lett.* 11, H303 (2008).

B. H. Choi, J. H. Lee, H. N. Lee, and H. K. Lee, *J. Nanosci. Nanotechnol.* 11, 7416 (2011).

S. I. Songa, J. H. Leea, B. H. Choia, H. K. Leeb, D. C. Shinc, and J. W. Leed, *Surf. Coat. Technol.* 211, 14 (2012).

M. R. Kim, J. H. Lee, and B. H. Choi, *Microelectron. Eng.* 98, 400 (2012).

B. Y. Kim, M. G. Ko, E. J. Lee, M. S. Hong, Y. J. Jeon, and J. W. Park, *J. Korean Phys. Soc.* 49, 1303 (2006).

E. J. Lee, M. G. Ko, B. Y. Kim, S. K. Park, H. D. Kim, and J. W. Park, *J. Korean Phys. Soc.* 49, 1243 (2006).

H. Kim, S. Woo, J. Lee, H. Kim, Y. Kim, H. Lee, and H. Jeon, *J. Electrochem. Soc.* 157, H479 (2010).

- W. H. Kim, W. J. Maeng, K. J. Moon, J. M. Myoung, and H. Kim, *Thin Solid Films* 519, 362 (2010).
- L. Chen, W. Yang, Y. Li, Q.-Q. Sun, P. Zhou, H.-L. Lu, S.-J. Ding, and D. W. Zhang, *J. Vac. Sci. Technol. A* 30, 01A148 (2012).
- W. S. Kim, S. K. Park, D. Y. Moon, B. W. Kang, H. D. Kim, and J. W. Park, *Thin Solid Films* 517, 3900 (2009).
- F. Tang, C. Zhu, D. J. Smith, and R. J. Nemanich, *J. Vac. Sci. Technol. A* 30, 01A147 (2012).
- M. E. Donders, W. M. Arnoldbik, H. C. M. Knoop, W. M. M. Kessels, and P. H. L. Notten, *J. Electrochem. Soc.* 160, A3066 (2013).
- J.-G. Song, J. Park, J. Yoon, K. Kim, Y. Jang, K. Kim, and H. Kim, *J. Alloys Comp.* 588, 716 (2014).
- J.-G. Song, J. Park, J. Yoon, H. Woo, K. Ko, T. Lee, S.-H. Hwang, J.-M. Myoung, K. Kim, Y. Jang, K. Kim, and H. Kim, *J. Luminescence* 145, 307 (2014).
- J. Hinz, A. J. Bauer, and L. Frey, *Semicond. Sci. Technol.* 25, 045009 (2010).
- J. Hinz, A. J. Bauer, T. Thiede, R. A. Fischer, and L. Frey, *Semicond. Sci. Technol.* 25, 075009 (2010).
- M. Ziegler, L. Fritsch, J. Day, S. Linzen, S. Anders, J. Toussaint, and H.-G. Meyer, *Supercond. Sci. Technol.* 26, 025008 (2013).
- H. B. R. Lee, S. H. Bang, W. H. Kim, G. H. Gu, Y. K. Lee, T. M. Chung, C. G. Kim, C. G. Park, and H. Kim, *Jpn. J. Appl. Phys.* 49, 05FA11 (2010).
- K. M. Lee, C. Y. Kim, C. K. Choi, S. W. Yun, J. B. Ha, J. H. Lee, and J. Y. Lee, *J. Korean Phys. Soc.* 55, 1153 (2009).
- G. Yuan, H. Shimizu, T. Momose, and Y. Shimogaki, *Microelectron. Eng.* 120, 230 (2014).
- G. Yuan, H. Shimizu, T. Momose, and Y. Shimogaki, *J. Vac. Sci. Technol. A* 32, 01A104 (2014).
- J. H. Lee, I. N. Lund, E. T. Eisenbraun, and R. E. Geer, *Nanotechnology* 22, 085603 (2011).
- S. J. Song, S. Woon Lee, G. H. Kim, J. Y. Seok, K. J. Yoon, J. H. Yoon, C. S. Hwang, J. Gatineau, and C. Ko, *Chem. Mater.* 24, 4675 (2012).

- N. E. Lay, G. A. T. Eyck, D. J. Duquette, and T. M. Lu, *Electrochem. Solid-State Lett.* 10, D13 (2007).
- G. A. Ten Eyck, J. J. Senkevich, F. Tang, D. L. Liu, S. Pimanpang, T. Karaback, G. C. Wang, T. M. Lu, C. Jezewski, and W. A. Lanford, *Chem. Vap. Dep.* 11, 60 (2005).
- M. J. Weber, A. J. M. Mackus, M. A. Verheijen, V. Longo, A. A. Bol, and W. M. M. Kessels, *J. Phys. Chem. C* 118, 8702 (2014).
- G. A. Ten Eyck, S. Pimanpang, J. S. Juneja, H. Bakhru, T. M. Lu, and G. C. Wang, *Chem. Vap. Dep.* 13, 307 (2007).
- B.-H. Liu, H. J. Huang, S.-H. Huang, and C.-N. Hsiao, *Thin Solid Films* 566, 93 (2014).
- L. Baker, A. S. Cavanagh, J. Yin, S. M. George, A. Kongkanand, and F. T. Wagner, *Appl. Phys. Lett.* 101, 111601 (2012).
- D. Longrie, K. Devloo-Casier, D. Deduytsche, S. Van den Berghe, K. Driesen, and C. Detavernier, *J. Solid State Sci. Technol.* 1, Q123 (2012).
- H. C. M. Knoop, A. J. M. Mackus, M. E. Donders, M. C. M. van de Sanden, P. H. L. Notten, and W. M. M. Kessels, *Electrochem. Solid-State Lett.* 12, G34 (2009).
- O. Bethge, G. Pozzovivo, C. Henkel, S. Abermann, and E. Bertagnolli, *J. Micromech. Microeng.* 22, 085013 (2012).
- A. J. M. Mackus, D. Garcia-Alonso, H. C. M. Knoop, A. A. Bol, and W. M. M. Kessels, *Chem. Mater.* 25, 1769 (2013).
- I. J. M. Erkens, M. A. Verheijen, H. C. M. Knoop, T. F. Landaluce, F. Roozeboom, and W. M. M. Kessels, *Chem. Vap. Dep.* 20, 258 (2014).
- N. Leick, R. O. F. Verkuijlen, E. Langereis, S. Rushworth, F. Roozeboom, M. C. M. van de Sanden, and W. M. M. Kessels, *J. Vac. Sci. Technol. A* 29, 021016 (2011).
- D. Greenslit, T. Chakraborty, and E. Eisenbraun, *J. Vac. Sci. Technol. B* 27, 631 (2009).
- S. Kumar, D. Greenslit, T. Chakraborty, and E. T. Eisenbraun, *J. Vac. Sci. Technol. A* 27, 572 (2009).
- S. W. Kim, S. H. Kwon, S. J. Jeong, and S. W. Kang, *J. Electrochem. Soc.* 155, H885 (2008).
- S. H. Kwon, O. K. Kwon, J. S. Min, and S. W. Kang, *J. Electrochem. Soc.* 153, G578 (2006).

S. J. Jeong, D. I. Kim, S. O. Kim, T. H. Han, J. D. Kwon, J. S. Park, and S. H. Kwon, *J. Nanosci. Nanotechnol.* 11, 671 (2011).

C. C. Chang, and F. M. Pan, *J. Electrochem. Soc.* 158, G97 (2011).

M. G. Ko, W. S. Kim, S. K. Park, H. D. Kim, and J. W. Park, *J. Korean Phys. Soc.* 53, 2123 (2008).

O. K. Kwon, S. H. Kwon, H. S. Park, and S. W. Kang, *J. Electrochem. Soc.* 151, C753 (2004).

W.-S. Kwack, H.-J. Choia, W.-C. Choi, H.-R. Oh, S.-Y. Shin, K. I Moon, J.-Y. Kwak, Y.-K. Jeong, and S.-H. Kwon, *J. Ceramic Process. Res.* 13, 338 (2012).

T. Park, D. Choi, H. Choi, and H. Jeon, *Physica Status Solidi A* 209, 302 (2012).

O. K. Kwon, S. H. Kwon, H. S. Park, and S. W. Kang, *Electrochem. Solid-State Lett.* 7, C46 (2004).

S. H. Kwon, O. K. Kwon, J. H. Kim, H. R. Oh, K. H. Kim, and S. W. Kang, *J. Electrochem. Soc.* 155, H296 (2008).

S. S. Yim, M. S. Lee, K. S. Kim, and K. B. Kim, *Appl. Phys. Lett.* 89, 093115 (2006).

S. S. Yim, D. J. Lee, K. S. Kim, M. S. Lee, S. H. Kim, and K. B. Kim, *Electrochem. Solid-State Lett.* 11, K89 (2008).

J. Musschoot, Q. Xie, D. Deduytsche, K. De Keyser, D. Longrie, J. Haemers, S. van den Berghe, R. L. van Meirhaeghe, J. D'Haen, and C. Detavernier, *Microelectron. Eng.* 87, 1879 (2010).

B. H. Choi, Y. H. Lim, J. H. Lee, Y. B. Kim, H. N. Lee, and H. K. Lee, *Microelectron. Eng.* 87, 1391 (2010).

S. J. Park, W. H. Kim, H. B. R. Lee, W. J. Maeng, and H. Kim, *Microelectron. Eng.* 85, 39 (2008).

Q. Xie, Y. L. Jiang, J. Musschoot, D. Deduytsche, C. Detavernier, R. L. Van Meirhaeghe, S. van den Berghe, G. P. Ru, B. Z. Li, and X. P. Qu, *Thin Solid Films* 517, 4689 (2009).

K.-Y. Mun, T. E. Hong, T. Cheon, Y. Jang, B.-Y. Lim, S. Kim, and S.-H. Kim, *Thin Solid Films* 562, 118 (2014).

T. K. Eom, S. H. Kim, K. S. Park, S. Kim, and H. Kim, *Electrochem. Solid-State Lett.* 14, D10 (2011).

W. Sari, T. K. Eom, S. H. Kim, and H. Kim, *J. Electrochem. Soc.* 158, D42 (2011).

- J. Swerts, Y.-K. Siew, E. V. Besien, Y. Barbarin, K. Opsomer, J. Bömmels, Z. Tőkei, and S. Van Elshocht, *Microelectron. Eng.* 120, 235 (2014).
- M. Degai, K. Kanomata, K. Momiyama, S. Kubota, K. Hirahara, and F. Hirose, *Thin Solid Films* 525, 73 (2012).
- M. Putkonen, M. Bosund, O. M. E. Ylivaara, R. L. Puurunen, L. Kilpi, H. Ronkainen, S. Sintonen, S. Ali, H. Lipsanen, X. Liu, E. Haimi, S.-P. Hannula, T. Sajavaara, I. Buchanan, E. Karwacki, and M. Vähä-Nissi, *Thin Solid Films* 558, 93 (2014).
- S. J. Won, S. Suh, M. S. Huh, and H. J. Kim, *IEEE Electron. Dev. Lett.* 31, 857 (2010).
- G. Dingemans, C. A. A. van Helvoirt, D. Pierreux, W. Keuning, and W. M. M. Kessels, *J. Electrochem. Soc.* 159, H277 (2012).
- J. S. Choi, B. S. Yang, S.-J. Won, J. R. Kim, S. Suh, H. K. Park, J. Heo, and H. J. Kim, *Solid-State Lett.* 2, P114 (2013).
- T. Usui, C. A. Donnelly, M. Logar, R. Sinclair, J. Schoonman, and F. B. Prinz, *Acta Materialia* 61, 7660 (2013).
- A. Kobayashi, N. Tsuji, A. Fukazawa, and N. Kobayashi, "Temperature dependence of GPC with PE-ALD SiO₂," in *Book of Abstracts, 10th International Conference on Atomic Layer Deposition*, Seoul, Korea, 20 June 2010.
- T. Murata, Y. Miyagawa, Y. Nishida, Y. Yamamoto, T. Yamashita, M. Matsuura, K. Asai, and H. Miyatake, *Jpn. J. Appl. Phys.* 49, 04DB11 (2010).
- A. Cacciato, L. Breuil, H. Dekker, M. Zahid, G. S. Kar, J. L. Everaert, G. Schoofs, X. Shi, G. van den Bosch, M. Jurczak, I. Debusschere, J. van Houdt, A. Cockburn, L. Date, L. Q. Xa, M. Le, and W. Lee, *Electrochem. Solid-State Lett.* 14, H271 (2011).
- J. W. Lim, S. J. Yun, and J. H. Lee, *ETRI J.* 27, 118 (2005).
- Y. B. Jiang, N. G. Liu, H. Gerung, J. L. Cecchi, and C. J. Brinker, *J. Am. Chem. Soc.* 128, 11018 (2006).
- P. Morin, G. Raymond, D. Benoit, P. Maury, and R. Beneyton, *Appl. Surf. Sci.* 260, 69 (2012).
- B. K. Leea, E. Jung, S. H. Kim, D. C. Moon, S. S. Lee, B. K. Park, J. H. Hwang, T.-M. Chung, C. G. Kim, and K.-S. An, *Mater. Res. Bull.* 47, 3052 (2012).
- G. Choi, L. Satyanarayana, and J. Park, *Appl. Surf. Sci.* 252, 7878 (2006).
- D. H. Kim, W. S. Kim, S. B. Lee, and S. H. Hong, *Sens. Actuators B* 147, 653 (2010).

- W. Lee, K. Hong, Y. Park, N. H. Kim, Y. Choi, and J. Park, *Electron. Lett.* 41, 475 (2005).
- W. Lee, Y. Choi, K. Hong, N. H. Kim, Y. Park, and J. Park, *J. Korean Phys. Soc.* 46, 756 (2005).
- D. H. Kim, J. H. Kwon, M. Kim, and S. H. Hong, *J. Cryst. Growth* 322, 33 (2011).
- K. Black, M. Werner, R. Rowlands-Jones, P. R. Chalker, and M. J. Rosseinsky, *Chem. Mater.* 23, 2518 (2011).
- E. Langereis, R. Roijmans, F. Roozeboom, M. C. M. van de Sanden, and W. M. M. Kessels, *J. Electrochem. Soc.* 158, G34 (2011).
- J. H. Ahn, J. Y. Kim, and S. W. Kang, *Appl. Phys. Lett.* 91, 062910 (2007).
- J. H. Ahn, S. W. Kang, J. Y. Kim, J. H. Kim, and J. S. Roh, *J. Electrochem. Soc.* 155, G185 (2008).
- J. H. Ahn, J. Y. Kim, J. H. Kim, J. S. Roh, and S. W. Kang, *Electrochem. Solid-State Lett.* 12, G5 (2009).
- J. H. Lee, Y. J. Cho, Y. S. Min, D. Kim, and S. W. Rhee, *J. Vac. Sci. Technol. A* 20, 1828 (2002).
- W. J. Lee, I. K. You, S. O. Ryu, B. G. Yu, K. I. Cho, S. G. Yoon, and C. S. Lee, *Jpn. J. Appl. Phys., Part 1* 40, 6941 (2001).
- W. C. Shin, S. O. Ryu, I. K. You, B. G. Yu, W. J. Lee, K. J. Choi, and S. G. Yoon, *J. Electrochem. Soc.* 151, C292 (2004).
- W. J. Lee, W. C. Shin, B. G. Chae, S. O. Ryu, I. K. You, S. M. Cho, B. G. Yu, and B. C. Shin, *Integr. Ferroelectr.* 46, 275 (2002).
- V. Longo, M. A. Verheijen, F. Roozeboom, and W. M. M. Kessels, *J. Solid-State Sci. Technol.* 2, N120 (2013).
- V. Longo, N. Leick, F. Roozeboom, and W. M. M. Kessels, *J. Solid-State Sci. Technol.* 2, N15 (2013).
- N. Aslam, V. Longo, C. Rodenbücher, F. Roozeboom, W. M. M. Kessels, K. Szot, R. Waser, and S. Hoffmann-Eifert, *J. Appl. Phys.* 116, 064503 (2014).
- N. Aslam, V. Longo, W. Keuning, F. Roozeboom, W. M. M. Kessels, R. Waser, and S. Hoffmann-Eifert, *Physica Status Solidi A* 211, 389 (2014).

W. C. Shin, S. O. Ryu, I. K. You, S. M. Yoon, S. M. Cho, N. Y. Lee, K. D. Kim, B. G. Yu, W. J. Lee, K. J. Choi, and S. G. Yoon, *Electrochem. Solid-State Lett.* 7, F31 (2004).

H. Kim, C. Cabral, C. Lavoie, and S. M. Rosnagel, *J. Vac. Sci. Technol. B* 20, 1321 (2002).

H. Kim, and S. M. Rosnagel, *Thin Solid Films* 441, 311 (2003).

S. M. Rosnagel, A. Sherman, and F. Turner, *J. Vac. Sci. Technol. B* 18, 2016 (2000).

W. J. Maeng, S. J. Park, and H. Kim, *J. Vac. Sci. Technol. B* 24, 2276 (2006).

W. J. Maeng, and H. Kim, *Electrochem. Solid-State Lett.* 9, G191 (2006).

W. J. Maeng, J. W. Lee, J. M. Myoung, and H. Kim, *Jpn. J. Appl. Phys., Part 1* 46, 3224 (2007).

A. Niskanen, U. Kreissig, M. Leskela, and M. Ritala, *Chem. Mater.* 19, 2316 (2007).

D. F. Gu, J. Li, S. K. Dey, H. De Waard, and S. Marcus, *J. Vac. Sci. Technol. B* 24, 2230 (2006).

T.-H. Kim, T.-K. Eom, S.-H. Kim, D.-H. Kang, H. Kim, S. Yu, and J. M. Lim, *Electrochem. Solid-State Lett.* 14, D89 (2011).

T. E. Hong, T.-H. Kim, J.-H. Jung, S.-H. Kim, and H. Kim, *J. Am. Cer. Soc.* 97, 127 (2014).

C. Hossbach, S. Teichert, J. Thomas, L. Wilde, H. Wojcik, D. Schmidt, B. Adolphi, M. Bertram, U. Muhle, M. Albert, S. Menzel, B. Hintze, and J. W. Bartha, *J. Electrochem. Soc.* 156, H852 (2009).

M. K. Song, and S. W. Rhee, *Chem. Vap. Dep.* 14, 334 (2008).

F. Piallat, V. Beugin, R. Gassilloud, P. Michallon, L. Dussault, B. Pelissier, T. Asikainen, J. W. Maes, F. Martin, P. Morin, and C. Vallée, *Microelectron. Eng.* 107, 156 (2013).

M. K. Song, and S. W. Rhee, *J. Electrochem. Soc.* 155, H823 (2008).

G. H. Cho, and S. W. Rhee, *Electrochem. Solid-State Lett.* 13, H426 (2010).

T. J. Park, J. H. Kim, J. H. Jang, K. D. Na, C. S. Hwang, J. H. Kim, G. M. Kim, J. H. Choi, K. J. Choi, and J. H. Jeong, *Appl. Phys. Lett.* 91, 252106 (2007).

Q. Xie, D. Deduytsche, J. Musschoot, R. L. van Meirhaeghe, C. Detavernier, S. F. Ding, and X. P. Qu, *Microelectron. Eng.* 88, 646 (2011).

- H. Kim, A. J. Kellock, and S. M. Rossnagel, *J. Appl. Phys.* 92, 7080 (2002).
- H. Kim, C. Lavoie, M. Copel, V. Narayanan, D. G. Park, and S. M. Rossnagel, *J. Appl. Phys.* 95, 5848 (2004).
- C. C. Chang, F. M. Pan, and C. W. Chen, *J. Electrochem. Soc.* 157, G62 (2010).
- H. S. Chung, J. D. Kwon, and S. W. Kang, *J. Electrochem. Soc.* 153, C751 (2006).
- H. C. M. Knoop, L. Baggetto, E. Langereis, M. C. M. van de Sanden, J. H. Klootwijk, F. Roozeboom, R. A. H. Niessen, P. H. L. Notten, and W. M. M. Kessels, *J. Electrochem. Soc.* 155, G287 (2008).
- E. Langereis, H. C. M. Knoop, A. J. M. Mackus, F. Roozeboom, M. C. M. van de Sanden, and W. M. M. Kessels, *J. Appl. Phys.* 102, 083517 (2007).
- A. Furuya, H. Tsuda, and S. Ogawa, *J. Vac. Sci. Technol. B* 23, 979 (2005).
- Q. Xie, J. Musschoot, C. Detavernier, D. Deduytsche, R. L. van Meirhaeghe, S. van den Berghe, Y. L. Jiang, G. P. Ru, B. Z. Li, and X. P. Qu, *Microelectron. Eng.* 85, 2059 (2008).
- H. C. M. Knoop, E. Langereis, M. C. M. van de Sanden, and W. M. M. Kessels, *J. Vac. Sci. Technol. A* 30, 01A101 (2012).
- H. Kim, C. Detavernier, O. van der Straten, S. M. Rossnagel, A. J. Kellock, and D. G. Park, *J. Appl. Phys.* 98, 014308 (2005).
- J. S. Park, M. J. Lee, C. S. Lee, and S. W. Kang, *Electrochem. Solid-State Lett.* 4, C17 (2001).
- J. S. Park, H. S. Park, and S. W. Kang, *J. Electrochem. Soc.* 149, C28 (2002).
- J. Y. Kim, K. W. Lee, H. O. Park, Y. D. Kim, H. Jeon, and Y. Kim, *J. Korean Phys. Soc.* 45, 1069 (2004).
- D. K. Kim, B. H. Kim, H. G. Woo, D. H. Kim, and H. K. Shin, *J. Nanosci. Nanotechnol.* 6, 3392 (2006).
- R. Sreenivasan, T. Sugawara, K. C. Saraswat, and P. C. McIntyre, *Appl. Phys. Lett.* 90, 102101 (2007).
- S.-G. Park, H.-G. Woo, C. Sunwoo, and D.-H. Kim, *J. Nanosci. Nanotechnol.* 13, 40976 (2013).
- H. Kim, and S. M. Rossnagel, *J. Vac. Sci. Technol. A* 20, 802 (2002).

K. E. Elers, J. Winkler, K. Weeks, and S. Marcus, *J. Electrochem. Soc.* 152, G589 (2005).

J. D. Kwon, and J. S. Park, *J. Korean Phys. Soc.* 57, 806 (2010).

J. S. Park, S. W. Kang, and H. Kim, *J. Vac. Sci. Technol. B* 24, 1327 (2006).

S. B. S. Heil, E. Langereis, A. Kemmeren, F. Roozeboom, M. C. M. van de Sanden, and W. M. M Kessels, *J. Vac. Sci. Technol. A* 23, L5 (2005).

S. B. S. Heil, E. Langereis, F. Roozeboom, M. C. M. van de Sanden, and W. M. M Kessels, *J. Electrochem. Soc.* 153, G956 (2006).

E. Langereis, S. B. S. Heil, M. C. M. van de Sanden, and W. M. M Kessels, *J. Appl. Phys.* 100, 023534 (2006).

M. Saadaoui, H. van Zeijl, W. H. A. Wien, H. T. M. Pham, C. Kwakernaak, H. C. M. Knoop, W. M. M. Kessels, M. C. M. van de Sanden, F. C. Voogt, F. Roozeboom, and P. M. Sarro, *IEEE Trans. Components Packaging Manufacturing Technol.* 1, 1728, (2011).

Y. Y. Chen, L. Goux, J. Swerts, M. Toeller, C. Adelman, J. Kittl, M. Jurczak, G. Groeseneken, and D. J. Wouters, *IEEE Electron. Dev. Lett.* 33, 483 (2012).

F. Greer, D. Fraser, J. W. Coburn, and D. B. Graves, *J. Vac. Sci. Technol. A* 21, 96 (2003).

D. H. Kim, Y. J. Kima, J. H. Park, and J. H. Kim, *Mater. Sci. Eng. C* 24, 289 (2004).

J. Y. Kim, S. Seo, D. Y. Kim, H. Jeon, and Y. Kim, *J. Vac. Sci. Technol. A* 22, 8 (2004).

J. Y. Kim, D. Y. Kim, H. O. Park, and H. T. Jeon, *J. Electrochem. Soc.* 152, G29 (2005).

P. Caubet, T. Blomberg, R. Benaboud, C. Wyon, E. Blanquet, J. P. Gonchond, M. Juhel, P. Bouvet, M. Gros-Jean, J. Michailos, C. Richard, and B. Iteprat, *J. Electrochem. Soc.* 155, H625 (2008).

N. Samal, H. Du, R. Luberoff, K. Chetry, R. Bubber, A. Hayes, and A. Devasahayam, *J. Vac. Sci. Technol. A* 31, 01A137 (2013).

J. Y. Kim, Y. Kim, and H. Jeon, *Jpn. J. Appl. Phys., Part 2* 42, L414 (2003).

M. Burke, A. Blake, I. M. Povey, M. Schmidt, N. Petkov, P. Carolan, and A. J. Quinn, *J. Vac. Sci. Technol. A* 32, 031506 (2014).

J. Y. Kim, D. Y. Kim, H. O. Park, and H. Jeon, *J. Korean Phys. Soc.* 45, 1639 (2004).

S. C. Heo, and C. Choi, *Microelectron. Eng.* 94, 11 (2012).

- D. Longrie, D. Deduytsche, J. Haemers, P. F. Smet, K. Driesen, and C. Detavernier, *Appl. Mater. Interfaces* 6, 7316 (2014).
- L. Assaud, K. Pitzschel, M. Hanbücken, and L. Santinacci, *J. Solid-State Sci. Technol.* 3, P253 (2014).
- N. G. Kubala, P. C. Rowlette, and C. A. Wolden, *J. Phys. Chem. C* 113, 16307 (2009).
- [227] N. G. Kubala, and C. A. Wolden, *Thin Solid Films* 518, 6733 (2010).
- T. H. Y. Tran, W. G. Haije, V. Longo, W. M. M. Kessels, and J. Schoonman, *J. Membrane Sci.* 378, 438 (2011).
- C. Zhao, M. N. Hedhili, J. Li, Q. Wang, Y. Yang, L. Chen, and L. Li, *Thin Solid Films* 542, 38 (2013).
- A. Sarkar, S. E. Potts, S. A. Rushworth, F. Roozeboom, M. C. M. van de Sanden, and W. M. M. Kessels, *Trans.* 33, 385 (2010).
- H. B. Profijt, M. C. M. van de Sanden, and W. M. M. Kessels, *Electrochem. Solid-State Lett.* 15, G1 (2012).
- V.-S. Dang¹, H. Parala, J. H. Kim, K. Xu, N. B. Srinivasan, E. Edengeiser, M. Havenith, A. D. Wieck, T. de los Arcos, R. A. Fischer, and A. Devi, *Physica Status Solidi A* 211, 416 (2014).
- K. Kanomata, P. Pansila, B. Ahmmad, S. Kubota, K. Hirahara, and F. Hirose, *Appl. Surf. Sci.* 308, 328 (2014).
- G. X. Liu, F. K. Shan, W. J. Lee, and B. C. Shin, *J. Korean Phys. Soc.* 50, 1827 (2007).
- J. J. Park, W. J. Lee, G. H. Lee, I. S. Kim, B. C. Shin, and S. G. Yoon, *Integr. Ferroelectr.* 68, 129 (2004).
- B. W. Kang, W. S. Kim, C. M. Hwang, D. Y. Moon, J. J. Kim, J. G. Park, and J. W. Park, *Jpn. J. Appl. Phys.* 49, 08JG05 (2010).
- C. S. Lee, J. Kim, J. Y. Son, W. Choi, and H. Kim, *Appl. Catal. B* 91, 628 (2009).
- C. S. Lee, J. Kim, G. H. Gu, D. H. Jo, C. G. Park, W. Choi, and H. Kim, *Thin Solid Films* 518, 4757 (2010).
- Q. Xie, J. Musschoot, D. Deduytsche, R. L. van Meirhaeghe, C. Detavernier, S. van den Berghe, Y. L. Jiang, G. P. Ru, B. Z. Li, and X. P. Qu, *J. Electrochem. Soc.* 155, H688 (2008).
- J. H. Kim, W. J. Lee, and S. G. Yoon, *Integr. Ferroelectr.* 68, 63 (2004).

- W. S. Kim, M. G. Ko, T. S. Kim, S. K. Park, Y. K. Moon, S. H. Lee, J. G. Park, and J. W. Park, *J. Nanosci. Nanotechnol.* 8, 4726 (2008).
- Y. K. Moon, S. H. Kim, D. Y. Moon, W. S. Kim, and J. W. Park, *J. Korean Phys. Soc.* 51, 1732 (2007).
- T. O. Kääriäinen, S. Lehti, M.-L. Kääriäinen, and D. C. Cameron, *Surf. Coat. Tech.* 205, S475 (2011).
- D. Wei, T. Hossain, N. Y. Garces, N. Nepal, H. M. Meyer III, M. J. Kirkham, C. R. Eddy Jr., and J. H. Edgar, *J. Solid-State Sci. Technol.* 2, N110 (2013).
- H. Y. Jeong, Y. I. Kim, J. Y. Lee, and S. Y. Choi, *Nanotechnology* 21, 115203 (2010).
- S. J. Won, S. Suh, S. W. Lee, G. J. Choi, C. S. Hwang, and H. J. Kim, *Electrochem. Solid-State Lett.* 13, G13 (2010).
- V. R. Rai, and S. Agarwal, *J. Phys. Chem. C* 113, 12962 (2009).
- A. Niskanen, K. Arstila, M. Leskela, and M. Ritala, *Chem. Vap. Dep.* 13, 152 (2007).
- H. Y. Jeong, J. Y. Lee, M. K. Ryu, and S. Y. Choi, *Phys. Status Solidi (RRL)* 4, 28 (2010).
- S. Kim, S. L. Brown, S. M. Rossnagel, J. Bruley, M. Copel, M. J. P. Hopstaken, V. Narayanan, and M. M. Frank, *J. Appl. Phys.* 107, 054102 (2010).
- J. W. Park, D. Lee, H. Kwon, S. Yoo, and J. Huh, *IEEE Electron. Dev. Lett.* 30, 739 (2009).
- J. W. Park, D. Y. Lee, H. Kwon, and S. Yoo, *IEEE Electron. Dev. Lett.* 30, 362 (2009).
- V. R. Rai, and S. Agarwal, *J. Vac. Sci. Technol. A* 30, 01A158 (2012).
- D. Theirich, R. Müller, K. Zilberberg, S. Trost, A. Behrendt, and T. Riedl, *Chem. Vap. Dep.* 19, 167 (2013).
- R. P. Chaukulkar, and S. Agarwal, *J. Vac. Sci. Technol. A* 31, 031509 (2013).
- W. S. Yang, and S. W. Kang, *Thin Solid Films* 500, 231 (2006).
- Y. J. Lee, and S. W. Kang, *Appl. Phys. Lett.* 86, 071919 (2005).
- Y. J. Lee, and S. W. Kang, *Electrochem. Solid-State Lett.* 6, C70 (2003).
- J. S. Park, and S. W. Kang, *Electrochem. Solid-State Lett.* 7, C87 (2004).

- J. W. Lim, S. J. Yun, and J. H. Kim, *ETRI J.* 31, 675 (2009).
- J. Musschoot, D. Deduytsche, H. Poelman, J. Haemers, R. L. Van Meirhaeghe, S. van den Berghe, and C. Detavernier, *J. Electrochem. Soc.* 156, 122 (2009).
- D. H. Kim, Y. J. Kim, Y. S. Song, B. T. Lee, J. H. Kim, S. Suh, and R. Gordon, *J. Electrochem. Soc.* 150, C740 (2003).
- Y. T. Kim, and J. H. Park, *Phys. Status Solidi A* 202, R164 (2005).
- H. S. Sim, S. I. Kim, H. Jeon, and Y. T. Kim, *Jpn. J. Appl. Phys., Part 1* 42, 6359 (2003).
- Y.-H. Hwang, W.-J. Cho, and Y. Kim, *Jap. J. Appl. Phys.* 52, 10MC07 (2013).
- T. T. Van, and J. P. Chang, *Surf. Sci.* 596, 1 (2005).
- J. Hoang, T. T. Van, M. Sawkar-Mathur, B. Hoex, M. C. M. van de Sanden, W. M. M. Kessels, R. Ostroumov, K. L. Wang, J. R. Bargar, and J. P. Chang, *J. Appl. Phys.* 101, 123116 (2007).
- T. T. Van, and J. P. Chang, *Appl. Phys. Lett.* 87, 011907 (2005).
- T. T. Van, J. R. Bargar, and J. P. Chang, *J. Appl. Phys.* 100, 023115 (2006).
- T. T. Van, J. Hoang, R. Ostroumov, K. L. Wang, J. R. Bargar, J. Lu, H. O. Blom, and J. P. Chang, *J. Appl. Phys.* 100, 073512 (2006).
- H.-W. Huang, W.-C. Chang, S.-J. Lin, and Y.-L. Chue, *J. Appl. Phys.* 112, 124102 (2012).
- D. A. Mourey, D. L. A. Zhao, and T. N. Jackson, *IEEE Electron Dev. Lett.* 31, 326 (2010).
- D. A. Mourey, D. A. L. Zhao, J. Sun, and T. N. Jackson, *IEEE Trans. Electron Devices* 57, 530 (2010).
- D. L. Zhao, D. A. Mourey, and T. N. Jackson, *IEEE Electron Dev. Lett.* 31, 323 (2010).
- S. H. K. Park, C. S. Hwang, H. S. Kwack, J. H. Lee, and H. Y. Chu, *Electrochem. Solid-State Lett.* 9, G299 (2006).
- C. R. Kim, C. M. Shin, J. Y. Lee, J. H. Heo, T. M. Lee, J. H. Park, H. Ryu, C. S. Son, and J. H. Chang, *Curr. Appl. Phys.* 10, S294 (2010).
- S. J. Lim, J. M. Kim, D. Kim, C. Lee, J. S. Park, and H. Kim, *Electrochem. Solid-State Lett.* 13, H151 (2010).

- D. Kim, H. Kang, J. M. Kim, and H. Kim, *Appl. Surf. Sci.* 257, 3776 (2011).
- S. M. Sultan, O. D. Clark, T. B. Masaud, Q. Fang, R. Gunn, M. M. A. Hakim, K. Sun, P. Ashburn, and H. M. H. Chong, *Microelectron. Eng.* 97, 162 (2012).
- M. A. Thomas, and J. B. Cui, *ACS Appl. Mater. Interfaces* 4, 3122 (2012).
- S. M Sultan, K. Sun, O. D. Clark, T. B, Masaud, Q. Fang, R. Gunn, J. Partridge, M. W. Allen, P. Ashburn, and H. M. H. Chong, *IEEE Electron Dev. Lett.* 33, 203 (2012).
- V. S. Kale, R. R. Prabhakar, S. S. Pramana, M. Rao, C.-H. Sow, K. B. Jinesh, and S. G. Mhaisalkarab, *Physical Chem. Chemical Phys.* 14, 4614 (2012).
- J. Zhang, H. Yang, Q.-L. Zhanga, S. Dong, and J. K. Luo, *Appl. Surf. Sci.* 282, 390 (2013).
- J. H. Heo, H. Ryua, and W.-J. Lee, *J. In. Eng. Chem.* 19, 1638 (2013).
- Y. Kawamura, M. Horita, Y. Ishikawa, and Y. Uraoka, *J. Display Technol.* 9, 694 (2013).
- P. C. Rowlette, C. G. Allen, O. B. Bromley, and C. A. Wolden, *J. Vac. Sci. Technol. A* 27, 761 (2009).
- P. C. Rowlette, C. G. Allen, O. B. Bromley, A. E. Dubetz, and C. A. Wolden, *Chem. Vap. Dep.* 15, 15 (2009).
- J. Y. Kim, S. H. Kim, H. Seo, J. H. Kim, and H. Jeon, *Electrochem. Solid-State Lett.* 8, G82 (2005).
- Y. Kim, J. Koo, J. W. Han, S. Choi, H. Jeon, and C. G. Park, *J. Appl. Phys.* 92, 5443 (2002).
- S. J. Yun, J. W. Lim, and J. H. Lee, *Electrochem. Solid-State Lett.* 7, F81 (2004).
- S. J. Yun, J. B. Koo, J. W. Lim, and S. H. Kim, *Electrochem. Solid-State Lett.* 10, H90 (2007).
- S. J. Yun, J. W. Lim, and J. H. Lee, *Electrochem. Solid-State Lett.* 8, F47 (2005).
- Y. Tak, and K. Yong, *Surf. Rev. Lett.* 12, 215 (2005).
- J. Koo, Y. Kim, and H. Jeon, *Jpn. J. Appl. Phys., Part 1* 41, 3043 (2002).
- S. Cho, K. Lee, P. Song, H. Jeon, and Y. Kim, *Jpn. J. Appl. Phys., Part 1* 46, 4085 (2007).

S. E. Potts, C. J. Carmalt, C. S. Blackman, F. Abou-Chahine, N. Leick, W. M. M. Kessels, H. O. Davies, and P. N. Heys, *Inorg. Chim. Acta* 363, 1077 (2010).

APPENDIX A. NOTATION USED FOR PRECURSOR LIGANDS

acac	–	acetylacetonate
apo	–	2-amino-pent-2-en-4-onate
Ay	–	allyl
B	–	bromide
Cl	–	chloride
chd	–	η^4 -cyclohexa-1,3-diene
cod	–	1,4-cyclooctadiene
Cp	–	η^5 -cyclopentadienyl
Cp*	–	η^5 -pentamethylcyclopentadienyl
Cp ^{Et}	–	η^5 -ethylcyclopentadienyl
Cp ^{iPr}	–	η^5 -isopropylcyclopentadienyl
Cp ^{Me}	–	η^5 -methylcyclopentadienyl
Cp(SiMe ₃)	–	trimethylsilylcyclopentadienyl
dedt	–	diethyldithiocarbamate
dmae	–	dimethylaminoethoxy
dmamb	–	1-dimethylamino-2-methyl-2-butanolate
dmambo	–	1-dimethylamino-2-methyl-2-butoxy
dme	–	dimethoxyethane
dmg	–	dimethylglyoximate
dmoe	–	dimethyloxyethoxy
Et	–	ethyl
F	–	fluoride
fod	–	6,6,7,7,8,8,8-heptafluoro-2,2-dimethyl-3,5-octanedionate
H	–	hydride
hfac	–	1,1,1,5,5,5-hexafluoroacetylacetonate
I	–	iodide
^t Bu	–	isobutyl
ipmb	–	η^6 -1-isopropyl-4-methylbenzene
ⁱ Pr	–	isopropyl
ⁱ PrAMD	–	N,N'-diisopropylacetamidinate
Me	–	methyl
methd	–	1-(2-methoxyethoxy)-2,2,6,6-tetramethyl-3,5-heptanedionate
mmp	–	1-methoxy-2-methyl-2-propoxy
mp	–	3-methyl-3-pentoxyl
ⁿ Bu	–	<i>n</i> -butyl
NEt ₂	–	diethylamido
NEtMe	–	ethylmethylamido
NMe ₂	–	dimethylamido
Np	–	neopentyl
N(SiMe ₃) ₂	–	bis(trimethylsilyl)amido
N ^t Bu	–	<i>tert</i> -butylmido
O	–	oxo
OAc	–	acetoxy
od	–	octane-2,4-dionate
OEt	–	ethoxy
O ⁱ Bu	–	isobutoxy
O ⁱ Pr	–	isopropoxy
OMe	–	methoxy
O ^t Bu	–	<i>tert</i> -butoxy
phen	–	1,10-phenanthroline
ph	–	phenyl
^t Bu	–	tertiary butyl
^t BuAMD	–	N,N'-ditertbutylacetamidinate
thd	–	2,2,6,6-tetramethyl-3,5-heptanedionate
^t Pn	–	tertiarypentyl
vtmos	–	vinyltrimethoxysilane

APPENDIX B. ADDITIONAL PEALD RESEARCH

Summary of materials deposited with PEALD. The precursor, plasma, and reactor type are specified, where re = radical enhanced, r = remote, and d = direct. The table was copied from reference Profijt *et al.* [1], and then added to for publications between May 31, 2011 and Nov 12, 2014 using Web of Science [2]. For a more complete description of the notation used for the precursors, please refer to Appendices 2A and B.

Material	Precursor	Plasma	Reactor	Reference
Ag	Ag(O ₂ C ^t Bu)(PEt ₃)	H ₂	r, re	3-5
	Ag(O ₂ C ^t Bu)(P ⁿ Et ₃)	H ₂	re	3
Al	AlH ₃ (NEtMe ₂)	H ₂	d	6,7
	AlMe ₃	H ₃	—	8
Al ₂ O ₃	AlH ₃ (MeNC ₄ H ₄)	O ₂	d	9
	AlMe ₂ (O ⁱ Pr)	O ₂	r, —	10,11
	AlMe ₃	CO ₂	—	12
		He/O ₂	—	13
		N ₂ /O ₂	d, —	14-17,22
		N ₂ O	d	18
		O ₂	d, r, re, —	5,10-101
AlN	AlCl ₃	NH ₃ /H ₂	d	102,103
	AlMe ₃	H ₂	r	104
		H ₂ /N ₂	r	56,104-111
		NH ₃	d, r	32,64,104,112-124
AlO _x N _y	AlMe ₃	O ₂ /N ₂	d	20,28,125
AlSi _x O _y	AlMe ₃ and Si(OEt) ₄	O ₂	—	126
		O ₂ /N ₂	d	127
AlTi _x O _y	AlMe ₃ and Ti(O ⁱ Pr) ₄	N ₂ O	d	131
		O ₂	d	128-131
		O ₂	—	132
B ₂ O ₃	BMe ₃	O ₂	—	132
CeO ₂	Ce(iPrCp) ₃	O ₂	d	133,134
Co	Co ₂ (CO) ₈	H ₂	r	135
		H ₂ /N ₂	r	136
		H ₂	r	137,138
	CoCp(CO) ₂	H ₂ /N ₂	r	136
		NH ₃	r	141,146
		NH ₃	d	139
		H ₂ /N ₂	—	140
	Co(Cp)(ⁱ PrAMD)	NH ₃	r, —	141-144,146
		NH ₃	d	145,146
	Cu(hfac) ₂	H ₂ /Ar	r	147
	Co(MeCp) ₂	H ₂	d	148
		NH ₃	d	148
	Co ₃ O ₄	CoCp ₂	O ₂	r
CoSi ₂	CoCp ₂	NH ₃ and SiH ₄	d	151,152
Cu	Cu(acac) ₂	H ₂	d, re	153-157
	Cu(dmamb) ₂	H ₂	—	158
	Cu(dmambo) ₂	H ₂	—	8,159
	Cu(dmap) ₂	H ₂	d	157
	Cu((hfac)(vtmos)	H ₂	—	160
	Cu[N(SiMe ₃) ₂] ₂	H ₂	r	161

Material	Precursor	Plasma	Reactor	Reference
	Cu(thd) ₂	H ₂	r	162
Er ₂ O ₃	Er(thd) ₃	O ₂	re	163
GaAs	GaMe ₃ and AsH ₄	H ₂	re	164
GaN	GaMe ₃	H ₂	r	104
		H ₂ /N ₂	r, —	104,165
		NH ₃	r, —	104,115
Ga ₂ O ₃	GaMe ₃	O ₂	r, —	166,167
	[Ga(Me) ₂ NH ₂] ₃	O ₂	d	168-173
GaZn _x O _y	GaEt ₃ and ZnEt ₂	O ₂	—	174-176
GeSb _x Te _y	Ge ⁱ Bu ₄ , Sb ⁱ Pr ₃ , and Te ⁱ Pr ₂	H ₂	d	177
	Ge(NMe ₂) ₄ , Sb(NMe ₂) ₄ , and Te ⁱ Pr ₂	H ₂	d	178
GaTi _x O _y	[Ga(Me) ₂ NH ₂] ₃ and Ti(NMe ₂) ₄	O ₂	d	168,170,171,179
Gd ₂ O ₃	Gd(ⁱ PrCp) ₃	O ₂	—	180
GdN	Gd(MeCp) ₃	N ₂	r	181
HfN	Hf(NMe ₂) ₄	H ₂	d	182-184
		H ₂ /N ₂	d	184
		N ₂	d, r	184,185
HfO ₂	Hf(NEt ₂) ₄	N ₂ O	d, —	186,194
		O ₂	d, r, —	187-201
	Hf(NEtMe) ₄	O ₂	d, r, re	5,23,24,202-209
		O ₂ /Ar	—	210
	Hf(NMe ₂) ₄	N ₂ /O ₂	r	211
		O ₂	d, r, —	183,212-215
	Hf(mp) ₄	O ₂	r	195
	Hf(OH) ₃ NH ₂	O ₂	—	216
	Hf(O ⁱ Bu) ₄	O ₂	re	217
HfAl _x O _y	Al(Me) ₃ and Hf(NEtMe) ₄	O ₂	d	23,24
HfO _x N _y	Hf(NEt ₂) ₄	N ₂ /O ₂	r	218
	Hf(NMe ₂) ₄	N ₂ /O ₂	r	211,212,219
HfSi _x O _y	Hf(NEtMe) ₄ and Si(NMe ₂) ₃ H	O ₂	r	218
	Hf(O ⁱ Bu) ₄ and Si(OEt) ₄	O ₂	re	220
Ir	Ir(Cp ^{Et})(COD)	NH ₃	d, —	221-223
		H ₂	—	224,225
La ₂ O ₃	La(Cp ^{Et}) ₃	O ₂	re	226,227
	La(Cp ^{iPr}) ₃	O ₂	r, re	43,206,228,229
	La(thd) ₃	O ₂	d	230
LaHf _x O _y	La(Cp ^{iPr}) and Hf(NEtMe) ₄	O ₂	re	206,231,232
LiCoO ₂	LiO ⁱ Bu and CoCp ₂	O ₂	r	233
MgO	MgCp ₂	O ₂	—	234,235
NbN	Nb(N ⁱ Bu)(NEtMe) ₃	H ₂	r	236-238
		H ₂ /N ₂	r	236,237
		NH ₃	r	236,237
Ni	Ni(dmamb) ₂	H ₂	d, —	239,240
		NH ₃	d	146,239
	NiCp ₂	NH ₃	d, r	146,241,242
	Ni(Cp ^{Et}) ₂	H ₂	—	243
NiO	Ni(MeCp) ₂	O ₂	—	244

Material	Precursor	Plasma	Reactor	Reference	
NiSi ₂	Ni(dmamb) ₂	NH ₃ /SiH ₄	d	151	
Pd	Pd(hfac) ₂	H ₂	r	245-247	
		H ₂ /N ₂	r	248	
		O ₂	r	247	
Pt	Pt(Cp ^{Me})Me ₃	Ar/O ₂	r	249	
		H ₂	d	250	
		N ₂	r	251	
		NH ₃	r	251	
		O ₂	r	251-253	
		O ₂ /H ₂	—	254	
		O ₂	r	252,255	
PtO ₂	Pt(Cp ^{Me})Me ₃	O ₂	r	252,255	
Ru	Ru(Cp(CO) ₂)Et	O ₂	r	256	
	Ru(Cp ^{Et})(NC ₄ H ₄)	NH ₃	d, —	257,258	
	Ru(Cp ^{Et}) ₂	H ₂ /N ₂	d, —	259-262	
		NH ₃	d, r, —	263-266	
	Ru(Cp) ₂	NH ₃	—	273	
	Ru(ipmb)(chd)	H ₂ /N ₂	—	275	
		NH ₃	d	276,277	
RuTiN	PyCpRu and Ti(NMe ₂) ₄	H ₂ /N ₂	d	278	
SiO ₂	SiH(NMe ₂) ₃	H ₂ O	r	279	
		O ₂	r	5,280	
		O ₂	d, r	132,281,282	
		SiH ₂ (NEt ₂) ₂	O ₂	—	283
		SiH ₂ (NH ^t Bu) ₂	O ₂	r	280,284
		SiH ₃ NH ₂	O ₂	d	285
		SiH ₄	N ₂ O	—	286
		[SiMe ₂ O-] ₄	O ₂	—	287
		Si(NMe ₂) ₄ and Si(NMe ₂) ₃ Cl (mix)	O ₂ /N ₂	d	288
		Si(OEt) ₄	O ₂	r	289
	SiN _x	SiH(N ⁱ PrH) ₃	NH ₃	d	276
		SiH ₂ Cl ₂	NH ₃	—	290
	SnO ₂	Sn(dmamp) ₂	O ₂	—	291
Sn(O ₂ CMe) ₂ (^t Bu) ₂		O ₂	—	292-296	
SrHfO ₃	Sr(ⁱ Pr ₃ Cp) ₂ and (MeCp) ₂ Hf(OMe)Me	O ₂	—	297	
SrO	Sr(C ₅ H ₂ ⁱ Pr ₃) ₂ (dme)	O ₂	r	298	
	Sr(C ₁₁ H ₁₉ O ₂) ₂	O ₂	—	299-301	
	Sr(thd) ₂	O ₂	d	302	
SrTaO ₆	Sr[Ta(OEt) ₅ (OCH ₂ CH ₂ NMe ₂) ₂]	O ₂	d	303	
	Sr[Ta(OEt) ₅ (OCH ₂ CH ₂ OMe) ₂]	O ₂	d	304,305	
SrTiO ₃	Sr(C ₅ H ₂ ⁱ Pr ₃) ₂ and Ti(Cp*)(OMe) ₃	O ₂	r	298	
	Sr(ⁱ Pr ₃ Cp) ₂ dme and CpMe ₅ Ti(OMe) ₃	O ₂	—	306-309	
	Sr(thd) ₂ and Ti(O ⁱ Pr) ₄	O ₂	d	299-301	
	SrB ₂ Ta ₂ O ₃	Sr[Ta(OEt) ₅ (dmoe) ₂ and BiPh ₃	O ₂	d	310
Ta	TaCl ₅	H ₂	r	311-313	
TaO _x	Ta(NMe ₂) ₅	O ₂	r	46,314-316	

Material	Precursor	Plasma	Reactor	Reference
		O ₂ /N ₂	r	316
	Ta(OEt) ₅	O ₂	r, re, —	5,317,318
TaC _x	Ta[CH ₂ C(CH ₃) ₃] ₃ Cl ₂	H ₂	d, —	319,320
TaC _x N _y	Ta(N ^t Bu)(NEt ₂) ₃	H ₂	d	321,322
		H ₂ /Ar	—	323
		NH ₃	d	324
		CH ₄ /H ₂	d	325
	Ta(N ^t Pn)(NMe ₂) ₃	H ₂	d	326
	Ta(NMe ₂) ₅	H ₂	r	327
TaN _x	TaCl ₅	H ₂ /N ₂	r, —	328-330
	TaF ₅	H ₂ /N ₂	d	331
	Ta(NMe ₂) ₅	H ₂	r, —	170,332-334
		N ₂	r	335,336
		H ₂ /N ₂	r	333,337
		NH ₃	r, —	274,333,337
	Ta(N ^t Bu)(NEt ₂) ₃	H ₂	d, r	338-340
		NH ₃	—	258
	Ta(N ^t Bu)(NEtMe) ₃	H ₂	—	341
	Ta(N ^t Pr)(NEtMe) ₃	H ₂ /N ₂	r	342
	Ta(N ^t Pn)(NMe ₂) ₃	H ₂	—	259
Ta(Si)N	Ta(N ^t Bu)(NEt ₂) ₃ and SiEt ₃	H ₂	—	343
Ti	TiCl ₄	H ₂	r	313,344
TiN _x	TiCl ₄	H ₂ /N ₂	d, r	21,41,203,332,345-352
		H ₂ , D ₂	re	353
	Ti(NMe ₂) ₄	H ₂	d, r	354-358
		N ₂	d, r, —	261,354-356,359
		H ₂ /N ₂	r, —	260,355,360
		NH ₃	r	271,356,361-364
TiO ₂	TiCl ₄	O ₂	r	365,366
	Ti(Cp ^{Me})(O ⁱ Pr) ₃	O ₂	r	46
	Ti(Cp ^{Me})(OMe) ₃	O ₂	r	46,92,367,368
	Ti(Cp ^{Me})(NMe ₂) ₃	O ₂	r	369,370
	Ti(NMe ₂) ₃ (guan)	O ₂	d	371
	Ti(NMe ₂) ₄	H ₂ O	r	378,372
		O ₂	d, r, —	179,207,214,315,373-383
	Ti(O ⁱ Pr) ₄	H ₂ O	r	378
		N ₂ O	d	131,385
		O ₂	d, r, re, —	5,46,125,131,204,221, 378,384-394
		O ₂ /N ₂	d, —	125,395
TiO _x N _y	AlMe ₃	O ₂ /N ₂	d	125
TiAl _x N _y	TiCl ₄ and AlCl ₃	Ar/H ₂ /N ₂ and Ar/NH ₃ /H ₂	d	396
	Ti(NMe ₂) ₃ and AlMe ₃	H ₂ and NH ₃	d	397
TiSi _x N _y	TiCl ₄ and SiH ₄	H ₂ /N ₂	d	398
TiSi _x O _y	Ti(O ⁱ Pr) ₄ and Si(OEt) ₄	O ₂	d	399
V _x O _y	VO(O ⁱ Pr) ₃	O ₂	r	400
WC _y	W(N ^t Bu) ₂ (NMe ₂) ₂	H ₂ /N ₂	d	401
WN _x	WF ₆	NH ₃	d, r	402-404
WC _x N _y	W(Cp ^{Et})(CO) ₂ (NO)	H ₂	d	257

Material	Precursor	Plasma	Reactor	Reference
	WF ₆	N ₂ /NH ₃ and CH ₄	d	402
Y ₂ O ₃	Y(thd) ₃	O ₂	re	163,405
Y ₂ O ₃ :Er	Y(thd) ₃ and Er(thd) ₃	O ₂	re	405-409
ZnO	ZnEt ₂	H ₂ O	d	410
		N ₂ O	d	411-413
		O ₂	d, r, —	27,68,90,167,414-424
	ZnMe ₂	O ₂	d	425,426
ZrO ₂	Zr(NEt ₂) ₄	O ₂	r, —	427,428
	Zr(NEtMe) ₄	O ₂	d	97,429,430
		O ₂ /N ₂	d	395,429-431
	Zr(O ^t Bu) ₄	H ₂	—	432
		O ₂	re, —	217,428,433
ZrN	Zr(NEt ₂) ₄	N ₂	r	434
	ZrCp ₂ (NMe ₂) ₂	H ₂ /N ₂ ,	r	435
		N ₂	r	435
		NH ₃	r	435
		O ₂	r	435
	ZrCp ₂ (η ² -MeNCH ₂ CH ₂ NMe)	H ₂ /N ₂ ,	r	435
		N ₂	r	435
		NH ₃	r	435
		O ₂	r	435

References

- [1] H. B. Profijt, S. E. Potts, M. C. M. van de Sanden, and W. M. M. Kessels, *J. Vac. Sci. Technol. A* 29, 050801 (2011).
- [2] Web of Knowledge, <http://apps.isiknowledge.com> (May 31, 2014).
- [3] A. Niskanen, T. Hatanpää, K. Arstila, M. Leskela, and M. Ritala, *Chem. Vap. Dep.* 13, 408 (2007).
- [4] M. Kariniemi, J. Niinistö, T. Hatanpää, M. Kemell, T. Sajavaara, M. Ritala, and M. Leskelä, *Chem. Mater.* 23, 2901 (2011).
- [5] M. Kariniemi, J. Niinistö, M. Vehkamäki, M. Kemell, M. Ritala, M. Leskelä, and M. Putkonen, *J. Vac. Sci. Technol. A* 30, 01A115 (2012).
- [6] C. W. Jeong, B. I. Lee, and S. K. Joo, *Mater. Sci. Eng. C* 16, 59 (2001).
- [7] C. W. Jeong, J. S. Lee, and S. K. Joo, *Jpn. J. Appl. Phys., Part 1* 40, 285 (2001).
- [8] J.-H. Park, D.-S. Han, Y.-J. Kang, S.-R. Shin, and J.-W. Park, *J. Vac. Sci. Technol. A* 32, 01A131 (2014).
- [9] B. H. Kim, W. S. Jeon, S. H. Jung, and B. T. Ahn, *Electrochem. Solid-State Lett.* 8, G294 (2005).

- [10] J. Koo, S. Kim, S. Jeon, H. Jeon, Y. Kim, and Y. Won, *J. Korean Phys. Soc.* 48, 131 (2006).
- [11] S. E. Pott, G. Dingemans, C. Lachaud, and W. M. M. Kessels, *J. Vac. Sci. Technol. A* 30, 021505 (2012).
- [12] A. Ali, H. S. Madan, A. P. Kirk, D. A. Zhao, D. A. Mourey, M. K. Hudait, R. M. Wallace, T. N. Jackson, B. R. Bennett, J. B. Boos, and S. Datta, *Appl. Phys. Lett.* 97, 143502 (2010).
- [13] P. Poodt, B. Kniknie, A. Branca, H. Winands, and F. Roozeboom, *Phys. Status Solidi RRL* 5, 165 (2011).
- [14] Y. H. Kim, J. Moon, C. H. Chung, S. J. Yun, D. J. Park, J. W. Lim, Y. H. Song, and J. H. Lee, *IEEE Electron Dev. Lett.* 27, 896 (2006).
- [15] D. J. Park, J. W. Lim, and B. O. Park, *Solid-State Electron.* 54, 323 (2010).
- [16] Y. H. Kim, C. Y. Sohn, J. W. Lim, S. J. Yun, C. S. Hwang, C. H. Chung, Y. W. Ko, and J. H. Lee, *IEEE Electron. Dev. Lett.* 25, 550 (2004).
- [17] J. Moon, Y. H. Kim, D. J. Park, C. H. Chung, S. Y. Kang, and J. H. Lee, *Solid-State Electron.* 54, 1326 (2010).
- [18] S. Lee, and H. Jeon, *Electron. Mater. Lett.* 3, 17 (2007).
- [19] M. T. Seman, D. N. Richards, P. Rowlette, and C. A. Wolden, *Chem. Vap. Dep.* 14, 296 (2008).
- [20] J. W. Lim, and S. J. Yun, *Jpn. J. Appl. Phys., Part 2* 42, L663 (2003).
- [21] S. W. Choi, C. M. Jang, D. Y. Kim, J. S. Ha, H. S. Park, W. Koh, and C. S. Lee, *J. Korean Phys. Soc.* 42, 975 (2003).
- [22] J. W. Lim, and S. J. Yun, *Electrochem. Solid-State Lett.* 7, F45 (2004).
- [23] P. K. Park, and S. W. Kang, *Appl. Phys. Lett.* 89, 192905 (2006).
- [24] P. K. Park E. S. Cha, and S. W. Kang, *Appl. Phys. Lett.* 90, 232906 (2007).
- [25] J. W. Lim, J. B. Koo, S. J. Yun, and H. T. Kim, *Electrochem. Solid-State Lett.* 10, J136 (2007).
- [26] K. Y. Park, H. I. Cho, H. C. Choi, Y. H. Bae, C. S. Lee, J. L. Lee, and J. H. Lee, *Jpn. J. Appl. Phys., Part 2* 43, L1433 (2004).
- [27] S. M. Yoon, S. H. K. Park, C. W. Byun, S. H. Yang, and C. S. Hwang, *J. Electrochem. Soc.* 157, H727 (2010).
- [28] S. J. Yun, Y. W. Ko, and J. W. Lim, *Appl. Phys. Lett.* 85, 4896 (2004).
- [29] W. S. Kim, D. Y. Moon, B. W. Kang, J. W. Park, and J. G. Park, *J. Korean Phys. Soc.* 55, 55 (2009).
- [30] A. Niskanen, K. Arstila, M. Ritala, and M. Leskela, *J. Electrochem. Soc.* 152, F90 (2005).
- [31] M. Caymax, G. Brammertz, A. Delabie, S. Sioncke, D. Lin, M. Scarrozza, G. Pourtois, W. E. Wang, M. Meuris, and M. Heyns, *Microelectron. Eng.* 86, 1529 (2009).

- [32] J. Dendooven, D. Deduytsche, J. Musschoot, R. L. Vanmeirhaeghe, and C. Detavernier, *J. Electrochem. Soc.* 157, G111 (2010).
- [33] G. Dingemans, N. M. Terlinden, D. Pierreux, H. B. Profijt, M. C. M. van de Sanden, and W. M. M Kessels, *Electrochem. Solid-State Lett.* 14, H1 (2010).
- [34] G. Dingemans, R. Seguin, P. Engelhart, M. C. M. van de Sanden, and W. M. M Kessels, *Phys. Status Solidi (RRL)* 4, 10 (2010).
- [35] J. J. H. Gielis, P. M. Gevers, I. M. P. Aarts, M. C. M. van de Sanden, and W. M. M Kessels, *J. Vac. Sci. Technol. A* 26, 1519 (2008).
- [36] S. B. S. Heil, P. Kudlacek, E. Langereis, R. Engeln, M. C. M. van de Sanden, and W. M. M Kessels, *Appl. Phys. Lett.* 89, 131505 (2006).
- [37] S. B. S. Heil, J. L. van Hemmen, M. C. M. van de Sanden, and W. M. M Kessels, *J. Appl. Phys.* 103, 103302 (2008).
- [38] B. Hoex, S. B. S. Heil, E. Langereis, M. C. M. van de Sanden, and W. M. M Kessels, *Appl. Phys. Lett.* 89, 042112 (2006).
- [39] B. Hoex, J. Schmidt, R. Bock, P. P. Altermatt, M. C. M. van de Sanden, and W. M. M Kessels, *Appl. Phys. Lett.* 91, 112107 (2007).
- [40] B. Hoex, J. Schmidt, P. Pohl, M. C. M. van de Sanden, and W. M. M Kessels, *J. Appl. Phys.* 104, 044903 (2008).
- [41] D. Hoogeland, K. B. Jinesh, F. Roozeboom, W. F. A. Besling, M. C. M. van de Sanden, and W. M. M Kessels, *J. Appl. Phys.* 106, 114107 (2009).
- [42] H. Kim, S. Woo, J. Lee, H. Lee, and H. Jeon, *J. Phys. D* 43, 505301(2010).
- [43] Y. Kim, S. Woo, H. Kim, J. Lee, H. Kim, H. Lee, and H. Jeon, *J. Mater. Res.* 25, 1898 (2010).
- [44] E. Langereis, M. Creatore, S. B. S. Heil, M. C. M. van de Sanden, and W. M. M Kessels, *Appl. Phys. Lett.* 89, 081915 (2006).
- [45] E. Langereis, J. Keijmel, M. C. M. van de Sanden, and W. M. M Kessels, *Appl. Phys. Lett.* 92, 231904 (2008).
- [46] S. E. Potts, W. Keuning, E. Langereis, G. Dingemans, M. C. M. van de Sanden, and W. M. M Kessels, *J. Electrochem. Soc.* 157, P66 (2010).
- [47] V. R. Rai, V. Vandalon, and S. Agarwal, *Langmuir* 26, 13732 (2010).
- [48] S. Sioncke, A. Delabie, G. Brammertz, T. Conard, A. Franquet, M. Caymax, A. Urbanzyk, M. Heyns, M. Meuris, J. L. van Hemmen, W. Keuning, and W. M. M Kessels, *J. Electrochem. Soc.* 156, H255 (2009).
- [49] N. M. Terlinden, G. Dingemans, M. C. M. van de Sanden, and W. M. M Kessels, *Appl. Phys. Lett.* 96, 112101 (2010).

- [50] J. L. van Hemmen, S. B. S. Heil, J. H. Klootwijk, F. Roozeboom, C. J. Hodson, M. C. M. van de Sanden, and W. M. M. Kessels, *J. Electrochem. Soc.* 154, G165 (2007).
- [51] H. S. Yun, and K. H. Kim, *J. Korean Phys. Soc.* 54, 707 (2009).
- [52] T. O. Kaariainen, and D. C. Cameron, *Plasma Processes Polym.* 6, S237 (2009).
- [53] K. Lambert, J. Dendooven, C. Detavernier, and Z. Hens, *Chem. Mater.* 23, 126 (2011).
- [54] K. B. Jinesh, J. L. van Hemmen, M. C. M. van de Sanden, F. Roozeboom, J. H. Klootwijk, W. F. A. Besling, and W. M. M. Kessels, *J. Electrochem. Soc.* 158, G21 (2011).
- [55] S. E. Potts, L. Schmalz, M. Fenker, B. Diaz, J. Swiatowska, V. Maurice, A. Seyeux, P. Marcus, G. Radnoczi, L. Toth, and W. M. M. Kessels, *J. Electrochem. Soc.* 158, C132 (2011).
- [56] P. Poodt, B. Kniknie, A. Branca, H. Winands, and F. Roozeboom, *Phys. Status Solidi (RRL)* 5, 165 (2011).
- [57] O. M. Nayfeh, T. Marr, and M. Dubey, *IEEE Electron. Dev. Lett.* 32, 473 (2011).
- [58] R. Driad, F. Benkhelifa, L. Kirste, M. Mikulla, and O. Ambacher, *J. Electrochem. Soc.* 158, H1279 (2011).
- [59] S. E. Potts, L. Schmalz, M. Fenker, B. Díaz, J. Światowska, V. Maurice, A. Seyeux, P. Marcus, G. Radnóczy, L. Tóth, and W. M. M. Kessels, *J. Electrochem. Soc.* 158, C132 (2011).
- [60] K. Lambert, J. Dendooven, C. Detavernier, and Z. Hens, *Chem. Mater.* 23, 126 (2011).
- [61] R. Driad, F. Benkhelifa, L. Kirste, M. Mikulla, and O. Ambacher, *J. Electrochem. Soc.* 158, H1279 (2011).
- [62] G. Dingemans, N. M. Terlinden, D. Pierreux, H. B. Profijt, M. C. M. van de Sanden, and W. M. M. Kessels, *Electrochem. Solid-State Lett.* 14, H1 (2011).
- [63] K.-H. Kim, H.-J. Kim, P. Jang, C. Jung, and K. Seomoon, *Electron. Mater. Lett.* 7, 171 (2011).
- [64] D. Longrlea, D. Deduytschea, J. Haemersa, K. Driesenb, and C. Detaverniera, *Surf. Coat. Technol.* 213, 183 (2012).
- [65] R. Fu, and J. Pattison, *Opt. Eng.* 51, 104003 (2012).
- [66] J. Musschoot, J. Dendooven, D. Deduytsche, J. Haemers, G. Buyle, and C. Detavernier, *Surf. Coat. Technol.* 206, 4511 (2012).
- [67] C.-H. Wu, K.-M. Chang, S.-H. Huang, I.-C. Deng, C.-J. Wu, W.-H. Chiang, and C.-C. Chang, *IEEE Electron Dev. Lett.* 33, 552 (2012).
- [68] Y. Kawamura, M. Tani, N. Hattori, N. Miyatake, M. Horita, Y. Ishikawa, and Y. Uraoka, *Jpn. J. Appl. Phys.* 51, 02BF04 (2012).
- [69] C. Peroz, S. Dhuey, M. Cornet, M. Vogler, D. Olynick, and S. Cabrini, *Nanotechnology* 23, 015305 (2012).

- [70] V. R. Rai, V. Vandalon, and S. Agarwal, *Langmuir* 28, 350 (2012).
- [71] A. Foroughi-Abariz, and K. C. Cadien, *J. Electrochem. Soc.* 159, D59 (2012).
- [72] W. Keuning, P. van de Weijer, H. Lifka, W. M. M. Kessels, and M. Creatore, *J. Vac. Sci. Technol. A* 30, 01A131 (2012).
- [73] L. Wenwen, L. Xingcun, C. Qiang, and W. Zhengduo, *Plasma Sci. Technol.* 14, 12 (2012).
- [74] B. Hoex, M. C. M. van de Sanden, J. Schmidt, R. Brendel, and W. M. M. Kessels, *Phys. Status Solidi RRL* 6, 4 (2012).
- [75] S.-F. Ding, Q. Xie, F. Chen, H.-Sh. Lu, S.-R. Deng, D. Deduytsche, C. Detavernier, and X.-P. Qu, *Solid-State Lett.* 1, P54 (2012).
- [76] S. Yang, Z. Tang, K.-Y. Wong, Y.-S. Lin, C. Liu, Y. Lu, S. Huang, and K. J. Chen, *IEEE Electron Dev. Lett.* 34, 1497 (2013).
- [77] M. Blaho, D. Gregušová, M. Jurkovič, Š. Haščík, J. Fedor, P. Kordoš, K. Fröhlich, F. Brunner, M. Cho, O. Hilt, J. Würfl, and J. Kuzmík, *Microelectron. Eng.* 112, 204 (2013).
- [78] J. Haeberle, K. Henkel, H. Gargouri, F. Naumann, B. Gruska, M. Arens, M. Tallarida, and D. Schmeißer, *Beilstein J. Nanotechnol.* 4, 732 (2013).
- [79] H. Jung, H. Choi, H. Jeon, S. Lee, and H. Jeon, *J. Appl. Phys.* 114, 173511 (2013).
- [80] S. Ozaki, T. Ohki, M. Kanamura, N. Okamoto, and T. Kikkawa, *Jap. J. Appl. Phys.* 52, 11NG04 (2013).
- [81] B. Hoex, M. Bosman, N. Nandakumar, and W. M. M. Kessels, *Physica Status Solidi RRL* 7, 937 (2013).
- [82] J. Zuidema, X. Ruan, and T. S. Fisher, *Optics Express* 21, 22053 (2013).
- [83] X. Zhang, and A. Cuevas, *Physica Status Solidi RRL* 7, 619 (2013).
- [84] E. Härkönen, S. E. Potts, W. M. M. Kessels, B. Díaz, A. Seyeux, J. Światowska, V. Maurice, P. Marcus, G. Radnóczy, L. Tóth, M. Kariniemi, J. Niinistö, and M. Ritala, *Thin Solid Films* 534, 384 (2013).
- [85] J. G. Lee, H. G. Kim, and S. S. Kim, *Thin Solid Films* 534, 515 (2013).
- [86] A. C. Kozen, M. A. Schroeder, K. D. Osborn, C. J. Lobb, and G. W. Rubloff, *Appl. Phys. Lett.* 102, 173501 (2013).
- [87] W. Liang, K. J. Weber, D. Suh, S. P. Phang, J. Yu, A. K. McAuley, and B. R. Legg, *IEEE J. Photovoltaics* 3, 678 (2013).
- [88] W. Yoon, A. R. Smith, E. E. Foos, J. E. Boercker, W. B. Heuer, and J. G. Tischler, *IEEE Trans. Nanotechnol.* 12, 146 (2013).
- [89] R. Edy, X. Huang, Y. Guo, J. Zhang, and J. Shi, *Nanoscale Res. Lett.* 8, 79 (2013).

- [90] A. K. Roy, D. Deduytsche, and C. Detavernier, *J. Vac. Sci. Technol. A* 31, 01A147 (2013).
- [91] A. Richter, J. Benick, and M. Hermle, *IEEE J. Photovoltaics* 3, 236 (2013).
- [92] H. B. Profijt, M. C. M. van de Sanden, and W. M. M. Kessels, *J. Vac. Sci. Technol. A* 31, 01A106 (2013).
- [93] S. Y. Song, *J. Korean Inst. Electrical Electron. Mater. Engineers* 26, 754 (2013).
- [94] X. Yuqing, S. Lijun, C. Qiang, Y. Lizhen, W. Zhengduo, and L. Zhongwei, *Plasma Sci. Technol.* 15, 52 (2013).
- [95] T. Bülow, H. Gargouri, M. Siebert, R. Rudolph, H.-H. Johannes, and W. Kowalsky, *Nanoscale Res. Lett.* 9, 223 (2014).
- [96] A. M. Mahajana, A. G. Khairnara, and B. J. Thibeault, *Semiconductors* 48, 497 (2014).
- [97] S. Lee, H. Choi, S. Shin, J. Park, G. Ham, H. Jung, and H. Jeon, *Curr. Appl. Phys.* 14, 552 (2014).
- [98] A. Perrotta, E. R. J. van Beekum, G. Aresta, A. Jagia, W. Keuning, R. M. C. M. van de Sanden, E. W. M. M. Kessels, and M. Creatore, *Microporous, and Mesoporous Mater.* 188, 163 (2014).
- [99] Y.-C. Lee, T.-T. Kao, J. J. Merola, and S.-C. Shen, *IEEE Trans. Electron Dev.* 61, 493 (2014).
- [100] D. Wei, T. Hossain, D. P. Briggs, and J. H. Edgar, *J. Solid-State Sci. Technol.* 3, N127 (2014).
- [101] K. Henkel, H. Gargouri, B. Gruska, M. Arens, M. Tallarida, and D. Schmeißer, *J. Vac. Sci. Technol. A* 32, 01A107 (2014).
- [102] Y. J. Lee, and S. W. Kang, *Thin Solid Films* 446, 227 (2004).
- [103] Y. J. Lee, *J. Cryst. Growth* 266, 568 (2004).
- [104] C. Ozgit-Akgun, E. Goldenberg, A. K. Okyay, and N. Biyikli, *J. Mater. Chem. C* 2, 2123 (2014).
- [105] K. H. Kim, N. W. Kwak, and S. H. Lee, *Electron. Mater. Lett.* 5, 83 (2009).
- [106] S. Huang; Q. Jiang, S. Yang, C. Zhou, and K. J. Chen, *IEEE Electron. Dev. Lett.* 33, 516 (2012).
- [107] C. Liu, S. Liu, S. Huang, and K. J. Chen, *IEEE Electron Dev. Lett.* 34, 1106 (2013).
- [108] K. J. Chen, and S. Huang, *Semicond. Sci. Technol.* 28, 074015 (2013).
- [109] J. Zhang, Q. Zhang, H. Yang, H. Wu, J. Zhou, and L. Hu, *Appl. Surf. Sci.* 315, 110 (2014).
- [110] A. Haider, C. Ozgit-Akgun, F. Kayaci, A. K. Okyay, T. Uyar, and N. Biyikli, *APL Mat.* 2, 096109 (2014).
- [111] K. J. Voon, K. M. Bothe, P. Motamedi, K. C. Cadien, and D. W. Barlage, *J. Phys. D: Appl. Phys.* 47, 345104 (2014).

- [112] M. Bosund, P. Mattila, A. Aierken, T. Hakkarainen, H. Koskenvaara, M. Sopenan, V. M. Airaksinen, and H. Lipsanen, *Appl. Surf. Sci.* 256, 7434 (2010).
- [113] M. Bosund, T. Sajavaara, M. Laitinen, T. Huhtio, M. Putkonen, V. M. Airaksinen, and H. Lipsanen, *Appl. Surf. Sci.* 257, 7827 (2011).
- [114] M. Alevli, C. Ozgit, I. Donmez, and N. Biyikli, *J. Cryst. Growth* 335, 51 (2011).
- [115] N. Biyikli, G. Ozgit, and I. Donmez, *Nanosci. Nanotechnol. Lett.* 4, 1008 (2012).
- [116] M. Alevli, C. Ozgit, I. Donmez, and N. Biyikli, *Physica Status Solidi A* 209, 266 (2012).
- [117] R. Meunier, A. Torres, E. Morvan, M. Charles, P. Gaud, and F. Morancho, *Microelectron. Eng.* 109, 378 (2013).
- [118] X. Li, W. Lei, Q. Zhao, and Q. Chen, *Surf. Coat. Technol.* 228, S55 (2013).
- [119] D. Suh, and W. S. Liang, *Thin Solid Films* 539, 309 (2013).
- [120] E. R. Cleveland, L. B. Ruppalt, B. R. Bennett, and S. M. Prokes, *Appl. Surf. Sci.* 277, 167 (2013).
- [121] R. E. Sah, R. Driad, F. Bernhardt, L. Kirste, C.-C. Leancu, H. Czap, F. Benkhelifa, M. Mikulla, and O. Ambacher, *J. Vac. Sci. Technol. A* 31, 041502 (2013).
- [122] W. Lei, and Q. Chen, *J. Vac. Sci. Technol. A* 31, 01A114 (2013).
- [123] P. Mattila, M. Bosund, H. Jussila, A. Aierken, J. Riikonen, T. Huhtio, H. Lipsanen, and M. Sopenan, *Appl. Surf. Sci.* 314, 570 (2014).
- [124] T.-E. Hsieh, E. Y. Chang, Y.-Z. Song, Y.-C. Lin, H.-C. Wang, S.-C. Liu, S. Salahuddin, and C. C. Hu, *IEEE Electron Dev. Lett.* 35, 732 (2014).
- [125] J. W. Lim, and S. J. Yun, *Electrochem. Solid-State Lett.* 7, H33 (2004).
- [126] J. W. Lim, S. J. Yun, and J. H. Lee, *Electrochem. Solid-State Lett.* 9, F8 (2006).
- [127] J. W. Lim, S. J. Yun, and J. H. Lee, *Electrochem. Solid-State Lett.* 8, F25 (2005).
- [128] J. W. Lim, S. J. Yun, and H. T. Kim, *J. Electrochem. Soc.* 154, G239 (2007).
- [129] J. W. Lim, S. J. Yun, and H. T. Kim, *Jpn. J. Appl. Phys.* 47, 6934 (2008).
- [130] J. W. Lim, S. J. Yun, and S. H. Lee, *J. Korean Phys. Soc.* 56, 96 (2010).
- [131] G. J. Choi, S. K. Kim, S. J. Won, H. J. Kim, and C. S. Hwang, *J. Electrochem. Soc.* 156, G138 (2009).
- [132] W.-H. Kim, I.-K. Oh, M.-K. Kim, W. J. Maeng, C.-W. Lee, G. Lee, C. Lansalot-Matras, W. Noh, D. Thompson, D. Chu, and H. Kim, *J. Mater. Chem. C* 2, 5805 (2014).

- [133] W.-H. Kim, M.-K. Kim, W. J. Maeng, J. Gatineau, V. Pallem, C. Dussarrat, A. Noori, D. Thompson, S. Chu, and H. Kim, *J. Electrochem. Soc.* 158, G169 (2011).
- [134] W.-H. Kim, W. J. Maeng, M.-K. Kim, J. Gatineau, and H. Kim, *J. Electrochem. Soc.* 158, G217 (2011).
- [135] K. Kim, K. Lee, S. Han, W. Jeong, and H. Jeon, *J. Electrochem. Soc.* 154, H177 (2007).
- [136] K. Kim, K. Lee, S. Han, T. Park, Y. Lee, J. Kim, S. Yeom, and H. Jeon, *Jpn. J. Appl. Phys., Part 2* 46, L173 (2007).
- [137] K. Lee, K. Kim, T. Park, H. Jeon, Y. Lee, J. Kim, and S. Yeom, *J. Electrochem. Soc.* 154, H899 (2007).
- [138] K. Lee, K. Kim, H. Jeon, Y. Lee, J. Kim, and S. Yeom, *J. Korean Phys. Soc.* 50, 1141 (2007).
- [139] J. M. Kim, H. B. R. Lee, C. Lansalot, C. Dussarrat, J. Gatineau, and H. Kim, *Jpn. J. Appl. Phys.* 49, 05FA10 (2010).
- [140] J. Yoon, H.-B.-R. Lee, D. Kim, T. Cheon, S.-H. Kim, and H. Kim, *J. Electrochem. Soc.* 158, H1179 (2011).
- [141] H. B. R. Lee, and H. Kim, *Electrochem. Solid-State Lett.* 9, G323 (2006).
- [142] H. B. R. Lee, J. Y. Son, and H. Kim, *Appl. Phys. Lett.* 90, 213509 (2007).
- [143] H.-B.-R. Lee, Y. J. Park, S. Baik, and H. Kim, *Chem. Vap. Dep.* 18, 41 (2012).
- [144] H. Shimizu, K. Sakoda, T. Momose, M. Koshi, and Y. Shimogaki, *J. Vac. Sci. Technol. A* 30, 01A144 (2012).
- [145] H. B. R. Lee, J. Kim, H. Kim, W. H. Kim, J. W. Lee, and I. Hwang, *J. Korean Phys. Soc.* 56, 104 (2010).
- [146] H. Kim, *Microelectron. Eng.* 106, 69 (2013).
- [147] R. P. Chaukulkar, N. F. W. Thissen, V. R. Rai, and S. Agarwal, *J. Vac. Sci. Technol. A* 32, 01A108 (2014).
- [148] J. Park, H.-B.-R. Lee, D. Kim, J. Yoon, C. Lansalot, J. Gatineau, H. Chevrel, and H. Kim, *J. Energy Chem.* 22, 403 (2013).
- [149] M. E. Donders, H. C. M. Knoops, M. C. M. van de Sanden, W. M. M. Kessels, and P. H. L. Notten, *J. Electrochem. Soc.* 158, G92 (2011).
- [150] M. E. Donders, H. C. M. Knoops, W. M. M. Kessels, and P. H. L. Notten, *J. Power Sources* 203, 72 (2012).
- [151] H. B. R. Lee, G. H. Gu, J. Y. Son, C. G. Park, and H. Kim, *Small* 4, 2247 (2008).
- [152] H. B. R. Lee, and H. Kim, *J. Cryst. Growth* 312, 2215 (2010).
- [153] L. Wu, and E. Eisenbraun, *J. Vac. Sci. Technol. B* 25, 2581 (2007).
- [154] L. Wu, and E. Eisenbraun, *Electrochem. Solid-State Lett.* 11, H107 (2008).

- [155] L. Wu, and E. Eisenbraun, *J. Electrochem. Soc.* 156, H734 (2009).
- [156] A. Niskanen, A. Rahtu, T. Sajavaara, K. Arstila, M. Ritala, and M. Leskela, *J. Electrochem. Soc.* 152, G25 (2005).
- [157] D. J. Hagen, J. Connolly, R. Nagle, I. M. Povey, S. Rushworth, P. Carolan, P. Ma, and M. E. Pemble, *Surf. Coat. Technol.* 230, 3 (2013).
- [158] B. K. Lee, S. H. Kim, B. K. Park, S. S. Lee, J.-H. Hwang, T.-M. Chung, Y. K. Lee, C. G. Kim, and K.-S. An, *J. Nanosci. Nanotechnol.* 11, 5887 (2011).
- [159] D. Y. Moon, D. S. Han, S. Y. Shin, J. W. Park, B. M. Kim, and J. H. Kim, *Thin Solid Films* 519, 3636 (2011).
- [160] D. Y. Moon, W. S. Kim, T. S. Kim, B. W. Kang, J. W. Park, S. J. Yeom, and J. H. Kim, *J. Korean Phys. Soc.* 54, 1330 (2009).
- [161] J. P. Coyle, G. Dey, E. R. Sirianni, M. L. Kemell, G. P. A. Yap, M. Ritala, M. Leskelä, S. D. Elliott, and S. T. Barry, *Chem. Mater.* 25, 1132 (2013).
- [162] C. Jezewski, W. A. Lanford, C. J. Wiegand, J. P. Singh, P. I. Wang, J. J. Senkevich, and T. M. Lu, *J. Electrochem. Soc.* 152, C60 (2005).
- [163] T. T. Van, and J. P. Chang, *Appl. Surf. Sci.* 246, 250 (2005).
- [164] M. de Keijser, and C. van Opdorp, *Appl. Phys. Lett.* 58, 1187 (1991).
- [165] S. Bolat, C. Ozgit-Akgun, B. Tekcan, N. Biyikli, and A. K. Okyay, *Appl. Phys. Lett.* 104, 243505 (2014).
- [166] I. Donmez, C. Ozgit-Akgun, and N. Biyikli, *J. Vac. Sci. Technol. A* 31, 01A110 (2013).
- [167] T. Nam, C. W. Lee, H. J. Kim, and H. Kim, *Appl. Surf. Sci.* 295, 260 (2014).
- [168] G. X. Liu, F. K. Shan, W. J. Lee, G. H. Lee, I. S. Kim, and B. C. Shin, *Integr. Ferroelectr.* 85, 155 (2006).
- [169] G. X. Liu, F. K. Shan, W. J. Lee, B. C. Shin, S. C. Kim, H. S. Kim, and C. R. Cho, *Integr. Ferroelectr.* 94, 11 (2007).
- [170] N. J. Seong, S. G. Yoon, and W. J. Lee, *Appl. Phys. Lett.* 87, 082909 (2005).
- [171] N. J. Seong, E. T. Kim, and S. G. Yoon, *Integr. Ferroelectr.* 74, 181(2005).
- [172] F. K. Shan, G. X. Liu, W. J. Lee, G. H. Lee, I. S. Kim, and B. C. Shin, *J. Appl. Phys.* 98, 023504 (2005).
- [173] F. K. Shan, G. X. Liu, W. J. Lee, G. H. Lee, I. S. Kim, and B. C. Shin, *Integr. Ferroelectr.* 80, 197 (2006).
- [174] Y.-L. Lee, T.-H. Huang, C.-L. Ho, and M.-C. Wu, *J. Solid-State Sci. Technol.* 2, Q182 (2013).
- [175] Y.-L. Lee, C.-C. Huang, C.-L. Ho, and M.-C. Wu, *IEEE Electron Dev. Lett.* 34, 1406 (2013).

- [176] C.-C. Huang, C.-L. Ho, S.-F. Chen, Y.-F. Chang, and M.-C. Wu, *J. Solid-State Sci. Technol.* 3, P159 (2014).
- [177] B. J. Choi, S. Choi, T. Eom, S. W. Ryu, D. Y. Cho, J. Heo, H. J. Kim, C. S. Hwang, Y. J. Kim, and S. K. Hong, *Chem. Mater.* 21, 2386 (2009).
- [178] J. Lee, S. Choi, C. Lee, Y. Kang, and D. Kim, *Appl. Surf. Sci.* 253, 3969 (2007).
- [179] G. X. Liu, F. K. Shan, J. J. Park, W. J. Lee, G. H. Lee, I. S. Kim, B. C. Shin, and S. G. Yoon, *J. Electroceram.* 17, 145 (2006).
- [180] S. A. Vitale, P. W. Wyatt, and C. J. Hodson, *J. Vac. Sci. Technol. A* 30, 01A130 (2012).
- [181] Z. Fang, P. A. Williams, R. Odedra, H. Jeon, and R. J. Potter, *J. Cryst. Growth* 338, 111 (2012).
- [182] S. Consiglio, W. X. Zeng, N. Berliner, and E. T. Eisenbraun, *J. Electrochem. Soc.* 155, H196 (2008).
- [183] W. J. Maeng, G. H. Gu, C. G. Park, K. Lee, T. Lee, and H. Kim, *J. Electrochem. Soc.* 156, G109 (2009).
- [184] E. J. Kim, and D. H. Kim, *Electrochem. Solid-State Lett.* 9, C123 (2006).
- [185] W. Jeong, Y. Ko, S. Bang, S. Lee, and H. Jeon, *J. Korean Phys. Soc.* 56, 905 (2010).
- [186] Y. Lee, S. Kim, J. Koo, I. Kim, J. Choi, H. Jeon, and Y. Won, *J. Electrochem. Soc.* 153, G353 (2006).
- [187] J. Choi, S. Kim, J. Kim, H. Kang, H. Jeon, and C. Bae, *J. Vac. Sci. Technol. A* 24, 900 (2006).
- [188] S. Choi, J. Koo, H. Jeon, and Y. Kim, *J. Korean Phys. Soc.* 44, 35 (2004).
- [189] H. Hong, S. Kim, S. Woo, H. Kim, H. Kim, W. Jeong, S. Jeon, S. Bang, S. Lfe, and H. Jeon, *J. Korean Phys. Soc.* 52, 1114 (2008).
- [190] H. Kang, S. Kim, J. Choi, J. Kim, H. Jeon, and C. Bae, *Electrochem. Solid-State Lett.* 9, G211 (2006).
- [191] I. Kim, S. Kuk, S. Kim, J. Kim, H. Jeon, M. H. Cho, and K. B. Chung, *Appl. Phys. Lett.* 90, 222101 (2007).
- [192] J. Kim, S. Kim, H. Kang, J. Choi, H. Jeon, M. Cho, K. Chung, S. Back, K. Yoo, and C. Bae, *J. Appl. Phys.* 98, 094504 (2005).
- [193] J. Kim, S. Kim, H. Jeon, M. H. Cho, K. B. Chung, and C. Bae, *Appl. Phys. Lett.* 87, 053108 (2005).
- [194] S. Kim, J. Kim, J. Choi, H. S. Kang, H. Jeon, and C. Bae, *J. Vac. Sci. Technol. B* 24, 1088 (2006).
- [195] S. Kim, J. Kim, J. Choi, H. Kang, H. Jeon, W. Cho, K. S. An, T. M. Chung, Y. Kim, and C. Bae, *Electrochem. Solid-State Lett.* 9, G200 (2006).
- [196] S. Kim, S. Woo, H. Kim, W. Jeong, T. Park, H. Kim, S. B. Kim, and H. Jeon, *J. Vac. Sci. Technol. B* 25, 1922 (2007).
- [197] S. Kim, S. Woo, H. Hong, H. Kim, H. Jeon, and C. Bae, *J. Electrochem. Soc.* 154, H97 (2007).

- [198] S. Kim, S. Woo, H. Kim, I. Kim, K. Lee, W. Jeong, T. Park, and H. Jeon, *J. Korean Phys. Soc.* 52, 1103 (2008).
- [199] Y. Won, S. Park, J. Koo, S. Kim, J. Kim, and H. Jeon, *Appl. Phys. Lett.* 87, 262901 (2005).
- [200] S. Woo, H. Hong, S. Kim, H. Kim, J. Kim, H. Jeon, C. Bae, T. Okada, K. Sawada, and M. Ishida, *Jpn. J. Appl. Phys.* 47, 6196 (2008).
- [201] Y. C. Byun, C. H. An, J. Y. Choi, C. Y. Kim, M. H. Cho, and H. Kim, *J. Electrochem. Soc.* 158, G141 (2011).
- [202] P. K. Park, J. S. Roh, B. H. Choi, and S. W. Kang, *Electrochem. Solid-State Lett.* 9, F34 (2006).
- [203] S. B. S. Heil, J. L. van Hemmen, C. J. Hodson, N. Singh, J. H. Klootwijk, F. Roozeboom, M. C. M. van de Sanden, and W. M. M. Kessels, *J. Vac. Sci. Technol. A* 25, 1357 (2007).
- [204] J. Joo, and S. M. Rossnagel, *J. Korean Phys. Soc.* 54, 1048 (2009).
- [205] H. Kim, S. Woo, J. Lee, Y. Kim, H. Lee, I. J. Choi, Y. D. Kim, C. W. Chung, and H. Jeon, *J. Electrochem. Soc.* 158, H21 (2011).
- [206] W. S. Kim, S. K. Park, D. Y. Moon, T. S. Kim, B. W. Kang, J. K. Seo, H. D. Kim, and J. W. Park, *J. Korean Phys. Soc.* 53, 3334 (2008).
- [207] A. K. Rumaiz, J. C. Woicik, C. Weiland, Q. Xie, D. P. Siddons, G. H. Jaffari, and C. Detavernier, *Appl. Phys. Lett.* 101, 222110 (2012).
- [208] H.-S. Jung, H. K. Kim, I.-H. Yu, S. Y. Lee, J. Lee, J. Park, J. H. Jang, S.-H. Jeon, Y. J. Chung, D.-Y. Cho, N.-I. Lee, T. J. Park, J.-H. Choi, and C. S. Hwang, *J. Electrochem. Soc.* 159, G33 (2012).
- [209] C. Richter, T. Schenk, U. Schroeder, and T. Mikolajick, *J. Vac. Sci. Technol. A* 32, 01A117 (2014).
- [210] M. Modreanu, S. Monaghan, I. M. Povey, K. Cherkaoui, P. K. Hurley, and M. Androulidaki, *Microelectron. Eng.* 88, 1499 (2011).
- [211] W. J. Maeng, and H. Kim, *Appl. Phys. Lett.* 91, 092901 (2007).
- [212] W. J. Maeng, and H. Kim, *J. Electrochem. Soc.* 155, H267 (2008).
- [213] W. J. Maeng, J. Y. Son, and H. Kim, *J. Electrochem. Soc.* 156, G33 (2009).
- [214] W. J. Maeng, W. H. Kim, J. H. Koo, S. J. Lim, C. S. Lee, T. Lee, and H. Kim, *Appl. Phys. Lett.* 96, 082905 (2010).
- [215] B. D. Briggs, S. M. Bishop, K. D. Leedy, and N. C. Cady, *Thin Solid Films* 562, 519 (2014).
- [216] H. Jeon, and Y. Won, *Appl. Phys. Lett.* 93, 124104 (2008).
- [217] S. X. Lao, R. M. Martin, and J. P. Chang, *J. Vac. Sci. Technol. A* 23, 488 (2005).
- [218] H. Kim, S. Kim, S. Woo, H. Y. Chung, H. Kim, J. Park, and H. Jeon, *J. Electrochem. Soc.* 155, G299 (2008).

- [219] W. J. Maeng, and H. Kim, *J. Appl. Phys.* 104, 064111 (2008).
- [220] J. R. Liu, R. M. Martin, and J. P. Chang, *J. Vac. Sci. Technol. A* 26, 1251 (2008).
- [221] D. K. Joo, J. S. Park, and S. W. Kang, *Electrochem. Solid-State Lett.* 12, H77 (2009).
- [222] S. W. Kim, S. H. Kwon, S. J. Jeong, J. S. Park, and S. W. Kang, *Electrochem. Solid-State Lett.* 11, H303 (2008).
- [223] B. H. Choi, J. H. Lee, H. N. Lee, and H. K. Lee, *J. Nanosci. Nanotechnol.* 11, 7416 (2011).
- [224] S. I. Songa, J. H. Leea, B. H. Choia, H. K. Leeb, D. C. Shinc, and J. W. Leed, *Surf. Coat. Technol.* 211, 14 (2012).
- [225] M. R. Kim, J. H. Lee, and B. H. Choi, *Microelectron. Eng.* 98, 400 (2012).
- [226] B. Y. Kim, M. G. Ko, E. J. Lee, M. S. Hong, Y. J. Jeon, and J. W. Park, *J. Korean Phys. Soc.* 49, 1303 (2006).
- [227] E. J. Lee, M. G. Ko, B. Y. Kim, S. K. Park, H. D. Kim, and J. W. Park, *J. Korean Phys. Soc.* 49, 1243 (2006).
- [228] H. Kim, S. Woo, J. Lee, H. Kim, Y. Kim, H. Lee, and H. Jeon, *J. Electrochem. Soc.* 157, H479 (2010).
- [229] W. H. Kim, W. J. Maeng, K. J. Moon, J. M. Myoung, and H. Kim, *Thin Solid Films* 519, 362 (2010).
- [230] L. Chen, W. Yang, Y. Li, Q.-Q. Sun, P. Zhou, H.-L. Lu, S.-J. Ding, and D. W. Zhang, *J. Vac. Sci. Technol. A* 30, 01A148 (2012).
- [231] W. S. Kim, S. K. Park, D. Y. Moon, B. W. Kang, H. D. Kim, and J. W. Park, *Thin Solid Films* 517, 3900 (2009).
- [232] F. Tang, C. Zhu, D. J. Smith, and R. J. Nemanich, *J. Vac. Sci. Technol. A* 30, 01A147 (2012).
- [233] M. E. Donders, W. M. Arnoldbik, H. C. M. Knoop, W. M. M. Kessels, and P. H. L. Notten, *J. Electrochem. Soc.* 160, A3066 (2013).
- [234] J.-G. Song, J. Park, J. Yoon, K. Kim, Y. Jang, K. Kim, and H. Kim, *J. Alloys Comp.* 588, 716 (2014).
- [235] J.-G. Song, J. Park, J. Yoon, H. Woo, K. Ko, T. Lee, S.-H. Hwang, J.-M. Myoung, K. Kim, Y. Jang, K. Kim, and H. Kim, *J. Luminescence* 145, 307 (2014).
- [236] J. Hinz, A. J. Bauer, and L. Frey, *Semicond. Sci. Technol.* 25, 045009 (2010).
- [237] J. Hinz, A. J. Bauer, T. Thiede, R. A. Fischer, and L. Frey, *Semicond. Sci. Technol.* 25, 075009 (2010).
- [238] M. Ziegler, L. Fritsch, J. Day, S. Linzen, S. Anders, J. Toussaint, and H.-G. Meyer, *Supercond. Sci. Technol.* 26, 025008 (2013).
- [239] H. B. R. Lee, S. H. Bang, W. H. Kim, G. H. Gu, Y. K. Lee, T. M. Chung, C. G. Kim, C. G. Park, and H. Kim, *Jpn. J. Appl. Phys.* 49, 05FA11 (2010).

- [240] K. M. Lee, C. Y. Kim, C. K. Choi, S. W. Yun, J. B. Ha, J. H. Lee, and J. Y. Lee, *J. Korean Phys. Soc.* 55, 1153 (2009).
- [241] G. Yuan, H. Shimizu, T. Momose, and Y. Shimogaki, *Microelectron. Eng.* 120, 230 (2014).
- [242] G. Yuan, H. Shimizu, T. Momose, and Y. Shimogaki, *J. Vac. Sci. Technol. A* 32, 01A104 (2014).
- [243] J. H. Lee, I. N. Lund, E. T. Eisenbraun, and R. E. Geer, *Nanotechnology* 22, 085603 (2011).
- [244] S. J. Song, S. Woon Lee, G. H. Kim, J. Y. Seok, K. J. Yoon, J. H. Yoon, C. S. Hwang, J. Gatineau, and C. Ko, *Chem. Mater.* 24, 4675 (2012).
- [245] N. E. Lay, G. A. T. Eyck, D. J. Duquette, and T. M. Lu, *Electrochem. Solid-State Lett.* 10, D13 (2007).
- [246] G. A. Ten Eyck, J. J. Senkevich, F. Tang, D. L. Liu, S. Pimanpang, T. Karaback, G. C. Wang, T. M. Lu, C. Jezewski, and W. A. Lanford, *Chem. Vap. Dep.* 11, 60 (2005).
- [247] M. J. Weber, A. J. M. Mackus, M. A. Verheijen, V. Longo, A. A. Bol, and W. M. M. Kessels, *J. Phys. Chem. C* 118, 8702 (2014).
- [248] G. A. Ten Eyck, S. Pimanpang, J. S. Juneja, H. Bakhr, T. M. Lu, and G. C. Wang, *Chem. Vap. Dep.* 13, 307 (2007).
- [249] B.-H. Liu, H. J. Huang, S.-H. Huang, and C.-N. Hsiao, *Thin Solid Films* 566, 93 (2014).
- [250] L. Baker, A. S. Cavanagh, J. Yin, S. M. George, A. Kongkanand, and F. T. Wagner, *Appl. Phys. Lett.* 101, 111601 (2012).
- [251] D. Longrie, K. Devloo-Casier, D. Deduytsche, S. Van den Berghe, K. Driesen, and C. Detavernier, *J. Solid State Sci. Technol.* 1, Q123 (2012).
- [252] H. C. M. Knoop, A. J. M. Mackus, M. E. Donders, M. C. M. van de Sanden, P. H. L. Notten, and W. M. M. Kessels, *Electrochem. Solid-State Lett.* 12, G34 (2009).
- [253] O. Bethge, G. Pozzovivo, C. Henkel, S. Abermann, and E. Bertagnolli, *J. Micromech. Microeng.* 22, 085013 (2012).
- [254] A. J. M. Mackus, D. Garcia-Alonso, H. C. M. Knoop, A. A. Bol, and W. M. M. Kessels, *Chem. Mater.* 25, 1769 (2013).
- [255] I. J. M. Erkens, M. A. Verheijen, H. C. M. Knoop, T. F. Landaluce, F. Roozeboom, and W. M. M. Kessels, *Chem. Vap. Dep.* 20, 258 (2014).
- [256] N. Leick, R. O. F. Verkuijlen, E. Langereis, S. Rushworth, F. Roozeboom, M. C. M. van de Sanden, and W. M. M. Kessels, *J. Vac. Sci. Technol. A* 29, 021016 (2011).
- [257] D. Greenslit, T. Chakraborty, and E. Eisenbraun, *J. Vac. Sci. Technol. B* 27, 631 (2009).
- [258] S. Kumar, D. Greenslit, T. Chakraborty, and E. T. Eisenbraun, *J. Vac. Sci. Technol. A* 27, 572 (2009).

- [259] S. W. Kim, S. H. Kwon, S. J. Jeong, and S. W. Kang, *J. Electrochem. Soc.* 155, H885 (2008).
- [260] S. H. Kwon, O. K. Kwon, J. S. Min, and S. W. Kang, *J. Electrochem. Soc.* 153, G578 (2006).
- [261] S. J. Jeong, D. I. Kim, S. O. Kim, T. H. Han, J. D. Kwon, J. S. Park, and S. H. Kwon, *J. Nanosci. Nanotechnol.* 11, 671 (2011).
- [262] C. C. Chang, and F. M. Pan, *J. Electrochem. Soc.* 158, G97 (2011).
- [263] M. G. Ko, W. S. Kim, S. K. Park, H. D. Kim, and J. W. Park, *J. Korean Phys. Soc.* 53, 2123 (2008).
- [264] O. K. Kwon, S. H. Kwon, H. S. Park, and S. W. Kang, *J. Electrochem. Soc.* 151, C753 (2004).
- [265] W.-S. Kwack, H.-J. Choia, W.-C. Choi, H.-R. Oh, S.-Y. Shin, K. I Moon, J.-Y. Kwak, Y.-K. Jeong, and S.-H. Kwon, *J. Ceramic Process. Res.* 13, 338 (2012).
- [266] T. Park, D. Choi, H. Choi, and H. Jeon, *Physica Status Solidi A* 209, 302 (2012).
- [267] O. K. Kwon, S. H. Kwon, H. S. Park, and S. W. Kang, *Electrochem. Solid-State Lett.* 7, C46 (2004).
- [268] S. H. Kwon, O. K. Kwon, J. H. Kim, H. R. Oh, K. H. Kim, and S. W. Kang, *J. Electrochem. Soc.* 155, H296 (2008).
- [269] S. S. Yim, M. S. Lee, K. S. Kim, and K. B. Kim, *Appl. Phys. Lett.* 89, 093115 (2006).
- [270] S. S. Yim, D. J. Lee, K. S. Kim, M. S. Lee, S. H. Kim, and K. B. Kim, *Electrochem. Solid-State Lett.* 11, K89 (2008).
- [271] J. Musschoot, Q. Xie, D. Deduytsche, K. De Keyser, D. Longrie, J. Haemers, S. van den Berghe, R. L. van Meirhaeghe, J. D'Haen, and C. Detavernier, *Microelectron. Eng.* 87, 1879 (2010).
- [272] B. H. Choi, Y. H. Lim, J. H. Lee, Y. B. Kim, H. N. Lee, and H. K. Lee, *Microelectron. Eng.* 87, 1391 (2010).
- [273] S. J. Park, W. H. Kim, H. B. R. Lee, W. J. Maeng, and H. Kim, *Microelectron. Eng.* 85, 39 (2008).
- [274] Q. Xie, Y. L. Jiang, J. Musschoot, D. Deduytsche, C. Detavernier, R. L. Van Meirhaeghe, S. van den Berghe, G. P. Ru, B. Z. Li, and X. P. Qu, *Thin Solid Films* 517, 4689 (2009).
- [275] K.-Y. Mun, T. E. Hong, T. Cheon, Y. Jang, B.-Y. Lim, S. Kim, and S.-H. Kim, *Thin Solid Films* 562, 118 (2014).
- [276] T. K. Eom, S. H. Kim, K. S. Park, S. Kim, and H. Kim, *Electrochem. Solid-State Lett.* 14, D10 (2011).
- [277] W. Sari, T. K. Eom, S. H. Kim, and H. Kim, *J. Electrochem. Soc.* 158, D42 (2011).
- [278] J. Swerts, Y.-K. Siew, E. V. Besien, Y. Barbarin, K. Opsomer, J. Bömmels, Z. Tőkei, and S. Van Elshocht, *Microelectron. Eng.* 120, 235 (2014).
- [279] M. Degai, K. Kanomata, K. Momiyama, S. Kubota, K. Hirahara, and F. Hirose, *Thin Solid Films* 525, 73 (2012).

- [280] M. Putkonen, M. Bosund, O. M. E. Ylivaara, R. L. Puurunen, L. Kilpi, H. Ronkainen, S. Sintonen, S. Ali, H. Lipsanen, X. Liu, E. Haimi, S.-P. Hannula, T. Sajavaara, I. Buchanan, E. Karwacki, and M. Vähä-Nissi, *Thin Solid Films* 558, 93 (2014).
- [281] S. J. Won, S. Suh, M. S. Huh, and H. J. Kim, *IEEE Electron. Dev. Lett.* 31, 857 (2010).
- [282] G. Dingemans, C. A. A. van Helvoirt, D. Pierreux, W. Keuning, and W. M. M. Kessels, *J. Electrochem. Soc.* 159, H277 (2012).
- [283] J. S. Choi, B. S. Yang, S.-J. Won, J. R. Kim, S. Suh, H. K. Park, J. Heo, and H. J. Kim, *Solid-State Lett.* 2, P114 (2013).
- [284] T. Usui, C. A. Donnelly, M. Logar, R. Sinclair, J. Schoonman, and F. B. Prinz, *Acta Materialia* 61, 7660 (2013).
- [285] A. Kobayashi, N. Tsuji, A. Fukazawa, and N. Kobayashi, "Temperature dependence of GPC with PE-ALD SiO₂," in Book of Abstracts, 10th International Conference on Atomic Layer Deposition, Seoul, Korea, 20 June 2010.
- [286] T. Murata, Y. Miyagawa, Y. Nishida, Y. Yamamoto, T. Yamashita, M. Matsuura, K. Asai, and H. Miyatake, *Jpn. J. Appl. Phys.* 49, 04DB11 (2010).
- [287] A. Cacciato, L. Breuil, H. Dekker, M. Zahid, G. S. Kar, J. L. Everaert, G. Schoofs, X. Shi, G. van den Bosch, M. Jurczak, I. Debusschere, J. van Houdt, A. Cockburn, L. Date, L. Q. Xa, M. Le, and W. Lee, *Electrochem. Solid-State Lett.* 14, H271 (2011).
- [288] J. W. Lim, S. J. Yun, and J. H. Lee, *ETRI J.* 27, 118 (2005).
- [289] Y. B. Jiang, N. G. Liu, H. Gerung, J. L. Cecchi, and C. J. Brinker, *J. Am. Chem. Soc.* 128, 11018 (2006).
- [290] P. Morin, G. Raymond, D. Benoit, P. Maury, and R. Beneyton, *Appl. Surf. Sci.* 260, 69 (2012).
- [291] B. K. Leea, E. Jung, S. H. Kim, D. C. Moon, S. S. Lee, B. K. Park, J. H. Hwang, T.-M. Chung, C. G. Kim, and K.-S. An, *Mater. Res. Bull.* 47, 3052 (2012).
- [292] G. Choi, L. Satyanarayana, and J. Park, *Appl. Surf. Sci.* 252, 7878 (2006).
- [293] D. H. Kim, W. S. Kim, S. B. Lee, and S. H. Hong, *Sens. Actuators B* 147, 653 (2010).
- [294] W. Lee, K. Hong, Y. Park, N. H. Kim, Y. Choi, and J. Park, *Electron. Lett.* 41, 475 (2005).
- [295] W. Lee, Y. Choi, K. Hong, N. H. Kim, Y. Park, and J. Park, *J. Korean Phys. Soc.* 46, 756 (2005).
- [296] D. H. Kim, J. H. Kwon, M. Kim, and S. H. Hong, *J. Cryst. Growth* 322, 33 (2011).
- [297] K. Black, M. Werner, R. Rowlands-Jones, P. R. Chalker, and M. J. Rosseinsky, *Chem. Mater.* 23, 2518 (2011).
- [298] E. Langereis, R. Roijmans, F. Roozeboom, M. C. M. van de Sanden, and W. M. M Kessels, *J. Electrochem. Soc.* 158, G34 (2011).

- [299] J. H. Ahn, J. Y. Kim, and S. W. Kang, *Appl. Phys. Lett.* 91, 062910 (2007).
- [300] J. H. Ahn, S. W. Kang, J. Y. Kim, J. H. Kim, and J. S. Roh, *J. Electrochem. Soc.* 155, G185 (2008).
- [301] J. H. Ahn, J. Y. Kim, J. H. Kim, J. S. Roh, and S. W. Kang, *Electrochem. Solid-State Lett.* 12, G5 (2009).
- [302] J. H. Lee, Y. J. Cho, Y. S. Min, D. Kim, and S. W. Rhee, *J. Vac. Sci. Technol. A* 20, 1828 (2002).
- [303] W. J. Lee, I. K. You, S. O. Ryu, B. G. Yu, K. I. Cho, S. G. Yoon, and C. S. Lee, *Jpn. J. Appl. Phys., Part 1* 40, 6941 (2001).
- [304] W. C. Shin, S. O. Ryu, I. K. You, B. G. Yu, W. J. Lee, K. J. Choi, and S. G. Yoon, *J. Electrochem. Soc.* 151, C292 (2004).
- [305] W. J. Lee, W. C. Shin, B. G. Chae, S. O. Ryu, I. K. You, S. M. Cho, B. G. Yu, and B. C. Shin, *Integr. Ferroelectr.* 46, 275 (2002).
- [306] V. Longo, M. A. Verheijen, F. Roozeboom, and W. M. M. Kessels, *J. Solid-State Sci. Technol.* 2, N120 (2013).
- [307] V. Longo, N. Leick, F. Roozeboom, and W. M. M. Kessels, *J. Solid-State Sci. Technol.* 2, N15 (2013).
- [308] N. Aslam, V. Longo, C. Rodenbücher, F. Roozeboom, W. M. M. Kessels, K. Szot, R. Waser, and S. Hoffmann-Eifert, *J. Appl. Phys.* 116, 064503 (2014).
- [309] N. Aslam, V. Longo, W. Keuning, F. Roozeboom, W. M. M. Kessels, R. Waser, and S. Hoffmann-Eifert, *Physica Status Solidi A* 211, 389 (2014).
- [310] W. C. Shin, S. O. Ryu, I. K. You, S. M. Yoon, S. M. Cho, N. Y. Lee, K. D. Kim, B. G. Yu, W. J. Lee, K. J. Choi, and S. G. Yoon, *Electrochem. Solid-State Lett.* 7, F31 (2004).
- [311] H. Kim, C. Cabral, C. Lavoie, and S. M. Rossnagel, *J. Vac. Sci. Technol. B* 20, 1321 (2002).
- [312] H. Kim, and S. M. Rossnagel, *Thin Solid Films* 441, 311 (2003).
- [313] S. M. Rossnagel, A. Sherman, and F. Turner, *J. Vac. Sci. Technol. B* 18, 2016 (2000).
- [314] W. J. Maeng, S. J. Park, and H. Kim, *J. Vac. Sci. Technol. B* 24, 2276 (2006).
- [315] W. J. Maeng, and H. Kim, *Electrochem. Solid-State Lett.* 9, G191 (2006).
- [316] W. J. Maeng, J. W. Lee, J. M. Myoung, and H. Kim, *Jpn. J. Appl. Phys., Part 1* 46, 3224 (2007).
- [317] A. Niskanen, U. Kreissig, M. Leskela, and M. Ritala, *Chem. Mater.* 19, 2316 (2007).
- [318] D. F. Gu, J. Li, S. K. Dey, H. De Waard, and S. Marcus, *J. Vac. Sci. Technol. B* 24, 2230 (2006).
- [319] T.-H. Kim, T.-K. Eom, S.-H. Kim, D.-H. Kang, H. Kim, S. Yu, and J. M. Lim, *Electrochem. Solid-State Lett.* 14, D89 (2011).

- [320] T. E. Hong, T.-H. Kim, J.-H. Jung, S.-H. Kim, and H. Kim, *J. Am. Cer. Soc.* 97, 127 (2014).
- [321] C. Hossbach, S. Teichert, J. Thomas, L. Wilde, H. Wojcik, D. Schmidt, B. Adolphi, M. Bertram, U. Muhle, M. Albert, S. Menzel, B. Hintze, and J. W. Bartha, *J. Electrochem. Soc.* 156, H852 (2009).
- [322] M. K. Song, and S. W. Rhee, *Chem. Vap. Dep.* 14, 334 (2008).
- [323] F. Pierrat, V. Beugin, R. Gassilloud, P. Michallon, L. Dussault, B. Pelissier, T. Asikainen, J. W. Maes, F. Martin, P. Morin, and C. Vallée, *Microelectron. Eng.* 107, 156 (2013).
- [324] M. K. Song, and S. W. Rhee, *J. Electrochem. Soc.* 155, H823 (2008).
- [325] G. H. Cho, and S. W. Rhee, *Electrochem. Solid-State Lett.* 13, H426 (2010).
- [326] T. J. Park, J. H. Kim, J. H. Jang, K. D. Na, C. S. Hwang, J. H. Kim, G. M. Kim, J. H. Choi, K. J. Choi, and J. H. Jeong, *Appl. Phys. Lett.* 91, 252106 (2007).
- [327] Q. Xie, D. Deduytsche, J. Musschoot, R. L. van Meirhaeghe, C. Detavernier, S. F. Ding, and X. P. Qu, *Microelectron. Eng.* 88, 646 (2011).
- [328] H. Kim, A. J. Kellock, and S. M. Rosnagel, *J. Appl. Phys.* 92, 7080 (2002).
- [329] H. Kim, C. Lavoie, M. Copel, V. Narayanan, D. G. Park, and S. M. Rosnagel, *J. Appl. Phys.* 95, 5848 (2004).
- [330] C. C. Chang, F. M. Pan, and C. W. Chen, *J. Electrochem. Soc.* 157, G62 (2010).
- [331] H. S. Chung, J. D. Kwon, and S. W. Kang, *J. Electrochem. Soc.* 153, C751 (2006).
- [332] H. C. M. Knoops, L. Baggetto, E. Langereis, M. C. M. van de Sanden, J. H. Klootwijk, F. Roozeboom, R. A. H. Niessen, P. H. L. Notten, and W. M. M. Kessels, *J. Electrochem. Soc.* 155, G287 (2008).
- [333] E. Langereis, H. C. M. Knoops, A. J. M. Mackus, F. Roozeboom, M. C. M. van de Sanden, and W. M. M. Kessels, *J. Appl. Phys.* 102, 083517 (2007).
- [334] A. Furuya, H. Tsuda, and S. Ogawa, *J. Vac. Sci. Technol. B* 23, 979 (2005).
- [335] Q. Xie, J. Musschoot, C. Detavernier, D. Deduytsche, R. L. van Meirhaeghe, S. van den Berghe, Y. L. Jiang, G. P. Ru, B. Z. Li, and X. P. Qu, *Microelectron. Eng.* 85, 2059 (2008).
- [336] H. C. M. Knoops, E. Langereis, M. C. M. van de Sanden, and W. M. M. Kessels, *J. Vac. Sci. Technol. A* 30, 01A101 (2012).
- [337] H. Kim, C. Detavernier, O. van der Straten, S. M. Rosnagel, A. J. Kellock, and D. G. Park, *J. Appl. Phys.* 98, 014308 (2005).
- [338] J. S. Park, M. J. Lee, C. S. Lee, and S. W. Kang, *Electrochem. Solid-State Lett.* 4, C17 (2001).
- [339] J. S. Park, H. S. Park, and S. W. Kang, *J. Electrochem. Soc.* 149, C28 (2002).

- [340] J. Y. Kim, K. W. Lee, H. O. Park, Y. D. Kim, H. Jeon, and Y. Kim, *J. Korean Phys. Soc.* 45, 1069 (2004).
- [341] D. K. Kim, B. H. Kim, H. G. Woo, D. H. Kim, and H. K. Shin, *J. Nanosci. Nanotechnol.* 6, 3392 (2006).
- [342] R. Sreenivasan, T. Sugawara, K. C. Saraswat, and P. C. McIntyre, *Appl. Phys. Lett.* 90, 102101 (2007).
- [343] S.-G. Park, H.-G. Woo, C. Sunwoo, and D.-H. Kim, *J. Nanosci. Nanotechnol.* 13, 40976 (2013).
- [344] H. Kim, and S. M. Rossnagel, *J. Vac. Sci. Technol. A* 20, 802 (2002).
- [345] K. E. Elers, J. Winkler, K. Weeks, and S. Marcus, *J. Electrochem. Soc.* 152, G589 (2005).
- [346] J. D. Kwon, and J. S. Park, *J. Korean Phys. Soc.* 57, 806 (2010).
- [347] J. S. Park, S. W. Kang, and H. Kim, *J. Vac. Sci. Technol. B* 24, 1327 (2006).
- [348] S. B. S. Heil, E. Langereis, A. Kemmeren, F. Roozeboom, M. C. M. van de Sanden, and W. M. M Kessels, *J. Vac. Sci. Technol. A* 23, L5 (2005).
- [349] S. B. S. Heil, E. Langereis, F. Roozeboom, M. C. M. van de Sanden, and W. M. M Kessels, *J. Electrochem. Soc.* 153, G956 (2006).
- [350] E. Langereis, S. B. S. Heil, M. C. M. van de Sanden, and W. M. M Kessels, *J. Appl. Phys.* 100, 023534 (2006).
- [351] M. Saadaoui, H. van Zeijl, W. H. A. Wien, H. T. M. Pham, C. Kwakernaak, H. C. M. Knoop, W. M. M. Kessels, M. C. M. van de Sanden, F. C. Voogt, F. Roozeboom, and P. M. Sarro, *IEEE Trans. Components Packaging Manufacturing Technol.* 1, 1728, (2011).
- [352] Y. Y. Chen, L. Goux, J. Swerts, M. Toeller, C. Adelman, J. Kittl, M. Jurczak, G. Groeseneken, and D. J. Wouters, *IEEE Electron. Dev. Lett.* 33, 483 (2012).
- [353] F. Greer, D. Fraser, J. W. Coburn, and D. B. Graves, *J. Vac. Sci. Technol. A* 21, 96 (2003).
- [354] D. H. Kim, Y. J. Kima, J. H. Park, and J. H. Kim, *Mater. Sci. Eng. C* 24, 289 (2004).
- [355] J. Y. Kim, S. Seo, D. Y. Kim, H. Jeon, and Y. Kim, *J. Vac. Sci. Technol. A* 22, 8 (2004).
- [356] J. Y. Kim, D. Y. Kim, H. O. Park, and H. T. Jeon, *J. Electrochem. Soc.* 152, G29 (2005).
- [357] P. Caubet, T. Blomberg, R. Benaboud, C. Wyon, E. Blanquet, J. P. Gonchond, M. Juhel, P. Bouvet, M. Gros-Jean, J. Michailos, C. Richard, and B. Iteprat, *J. Electrochem. Soc.* 155, H625 (2008).
- [358] N. Samal, H. Du, R. Luberooff, K. Chetry, R. Bubber, A. Hayes, and A. Devasahayam, *J. Vac. Sci. Technol. A* 31, 01A137 (2013).
- [359] J. Y. Kim, Y. Kim, and H. Jeon, *Jpn. J. Appl. Phys., Part 2* 42, L414 (2003).
- [360] M. Burke, A. Blake, I. M. Povey, M. Schmidt, N. Petkov, P. Carolan, and A. J. Quinn, *J. Vac. Sci. Technol. A* 32, 031506 (2014).

- [361] J. Y. Kim, D. Y. Kim, H. O. Park, and H. Jeon, *J. Korean Phys. Soc.* 45, 1639 (2004).
- [362] S. C. Heo, and C. Choi, *Microelectron. Eng.* 94, 11 (2012).
- [363] D. Longrie, D. Deduytsche, J. Haemers, P. F. Smet, K. Driesen, and C. Detavernier, *Appl. Mater. Interfaces* 6, 7316 (2014).
- [364] L. Assaud, K. Pitzschel, M. Hanbücken, and L. Santinacci, *J. Solid-State Sci. Technol.* 3, P253 (2014).
- [365] N. G. Kubala, P. C. Rowlette, and C. A. Wolden, *J. Phys. Chem. C* 113, 16307 (2009).
- [227] N. G. Kubala, and C. A. Wolden, *Thin Solid Films* 518, 6733 (2010).
- [367] T. H. Y. Tran, W. G. Haije, V. Longo, W. M. M. Kessels, and J. Schoonman, *J. Membrane Sci.* 378, 438 (2011).
- [368] C. Zhao, M. N. Hedhili, J. Li, Q. Wang, Y. Yang, L. Chen, and L. Li, *Thin Solid Films* 542, 38 (2013).
- [369] A. Sarkar, S. E. Potts, S. A. Rushworth, F. Roozeboom, M. C. M. van de Sanden, and W. M. M. Kessels, *Trans.* 33, 385 (2010).
- [370] H. B. Profijt, M. C. M. van de Sanden, and W. M. M. Kessels, *Electrochem. Solid-State Lett.* 15, G1 (2012).
- [371] V.-S. Dangl, H. Parala, J. H. Kim, K. Xu, N. B. Srinivasan, E. Edengeiser, M. Havenith, A. D. Wieck, T. de los Arcos, R. A. Fischer, and A. Devi, *Physica Status Solidi A* 211, 416 (2014).
- [372] K. Kanomata, P. Pansila, B. Ahmmad, S. Kubota, K. Hirahara, and F. Hirose, *Appl. Surf. Sci.* 308, 328 (2014).
- [373] G. X. Liu, F. K. Shan, W. J. Lee, and B. C. Shin, *J. Korean Phys. Soc.* 50, 1827 (2007).
- [374] J. J. Park, W. J. Lee, G. H. Lee, I. S. Kim, B. C. Shin, and S. G. Yoon, *Integr. Ferroelectr.* 68, 129 (2004).
- [375] B. W. Kang, W. S. Kim, C. M. Hwang, D. Y. Moon, J. J. Kim, J. G. Park, and J. W. Park, *Jpn. J. Appl. Phys.* 49, 08JG05 (2010).
- [376] C. S. Lee, J. Kim, J. Y. Son, W. Choi, and H. Kim, *Appl. Catal. B* 91, 628 (2009).
- [377] C. S. Lee, J. Kim, G. H. Gu, D. H. Jo, C. G. Park, W. Choi, and H. Kim, *Thin Solid Films* 518, 4757 (2010).
- [378] Q. Xie, J. Musschoot, D. Deduytsche, R. L. van Meirhaeghe, C. Detavernier, S. van den Berghe, Y. L. Jiang, G. P. Ru, B. Z. Li, and X. P. Qu, *J. Electrochem. Soc.* 155, H688 (2008).
- [379] J. H. Kim, W. J. Lee, and S. G. Yoon, *Integr. Ferroelectr.* 68, 63 (2004).
- [380] W. S. Kim, M. G. Ko, T. S. Kim, S. K. Park, Y. K. Moon, S. H. Lee, J. G. Park, and J. W. Park, *J. Nanosci. Nanotechnol.* 8, 4726 (2008).
- [381] Y. K. Moon, S. H. Kim, D. Y. Moon, W. S. Kim, and J. W. Park, *J. Korean Phys. Soc.* 51, 1732 (2007).
- [382] T. O. Kääriäinen, S. Lehti, M.-L. Kääriäinen, and D. C. Cameron, *Surf. Coat. Tech.* 205, S475 (2011).

- [383] D. Wei, T. Hossain, N. Y. Garces, N. Nepal, H. M. Meyer III, M. J. Kirkham, C. R. Eddy Jr., and J. H. Edgar, *J. Solid-State Sci. Technol.* 2, N110 (2013).
- [384] H. Y. Jeong, Y. I. Kim, J. Y. Lee, and S. Y. Choi, *Nanotechnology* 21, 115203 (2010).
- [385] S. J. Won, S. Suh, S. W. Lee, G. J. Choi, C. S. Hwang, and H. J. Kim, *Electrochem. Solid-State Lett.* 13, G13 (2010).
- [386] V. R. Rai, and S. Agarwal, *J. Phys. Chem. C* 113, 12962 (2009).
- [387] A. Niskanen, K. Arstila, M. Leskela, and M. Ritala, *Chem. Vap. Dep.* 13, 152 (2007).
- [388] H. Y. Jeong, J. Y. Lee, M. K. Ryu, and S. Y. Choi, *Phys. Status Solidi (RRL)* 4, 28 (2010).
- [389] S. Kim, S. L. Brown, S. M. Rossnagel, J. Bruley, M. Copel, M. J. P. Hopstaken, V. Narayanan, and M. M. Frank, *J. Appl. Phys.* 107, 054102 (2010).
- [390] J. W. Park, D. Lee, H. Kwon, S. Yoo, and J. Huh, *IEEE Electron. Dev. Lett.* 30, 739 (2009).
- [391] J. W. Park, D. Y. Lee, H. Kwon, and S. Yoo, *IEEE Electron. Dev. Lett.* 30, 362 (2009).
- [392] V. R. Rai, and S. Agarwal, *J. Vac. Sci. Technol. A* 30, 01A158 (2012).
- [393] D. Theirich, R. Müller, K. Zilberberg, S. Trost, A. Behrendt, and T. Riedl, *Chem. Vap. Dep.* 19, 167 (2013).
- [394] R. P. Chaukulkar, and S. Agarwal, *J. Vac. Sci. Technol. A* 31, 031509 (2013).
- [395] W. S. Yang, and S. W. Kang, *Thin Solid Films* 500, 231 (2006).
- [396] Y. J. Lee, and S. W. Kang, *Appl. Phys. Lett.* 86, 071919 (2005).
- [397] Y. J. Lee, and S. W. Kang, *Electrochem. Solid-State Lett.* 6, C70 (2003).
- [398] J. S. Park, and S. W. Kang, *Electrochem. Solid-State Lett.* 7, C87 (2004).
- [399] J. W. Lim, S. J. Yun, and J. H. Kim, *ETRI J.* 31, 675 (2009).
- [400] J. Musschoot, D. Deduytsche, H. Poelman, J. Haemers, R. L. Van Meirhaeghe, S. van den Berghe, and C. Detavernier, *J. Electrochem. Soc.* 156, 122 (2009).
- [401] D. H. Kim, Y. J. Kim, Y. S. Song, B. T. Lee, J. H. Kim, S. Suh, and R. Gordon, *J. Electrochem. Soc.* 150, C740 (2003).
- [402] Y. T. Kim, and J. H. Park, *Phys. Status Solidi A* 202, R164 (2005).
- [403] H. S. Sim, S. I. Kim, H. Jeon, and Y. T. Kim, *Jpn. J. Appl. Phys., Part 1* 42, 6359 (2003).
- [404] Y.-H. Hwang, W.-J. Cho, and Y. Kim, *Jap. J. Appl. Phys.* 52, 10MC07 (2013).

- [405] T. T. Van, and J. P. Chang, *Surf. Sci.* 596, 1 (2005).
- [406] J. Hoang, T. T. Van, M. Sawkar-Mathur, B. Hoex, M. C. M. van de Sanden, W. M. M Kessels, R. Ostroumov, K. L. Wang, J. R. Bargar, and J. P. Chang, *J. Appl. Phys.* 101, 123116 (2007).
- [407] T. T. Van, and J. P. Chang, *Appl. Phys. Lett.* 87, 011907 (2005).
- [408] T. T. Van, J. R. Bargar, and J. P. Chang, *J. Appl. Phys.* 100, 023115 (2006).
- [409] T. T. Van, J. Hoang, R. Ostroumov, K. L. Wang, J. R. Bargar, J. Lu, H. O. Blom, and J. P. Chang, *J. Appl. Phys.* 100, 073512 (2006).
- [410] H.-W. Huang, W.-C. Chang, S.-J. Lin, and Y.-L. Chue, *J. Appl. Phys.* 112, 124102 (2012).
- [411] D. A. Mourey, D. L. A. Zhao, and T. N. Jackson, *IEEE Electron Dev. Lett.* 31, 326 (2010).
- [412] D. A. Mourey, D. A. L. Zhao, J. Sun, and T. N. Jackson, *IEEE Trans. Electron Devices* 57, 530 (2010).
- [413] D. L. Zhao, D. A. Mourey, and T. N. Jackson, *IEEE Electron Dev. Lett.* 31, 323 (2010).
- [414] S. H. K. Park, C. S. Hwang, H. S. Kwack, J. H. Lee, and H. Y. Chu, *Electrochem. Solid-State Lett.* 9, G299 (2006).
- [415] C. R. Kim, C. M. Shin, J. Y. Lee, J. H. Heo, T. M. Lee, J. H. Park, H. Ryu, C. S. Son, and J. H. Chang, *Curr. Appl. Phys.* 10, S294 (2010).
- [416] S. J. Lim, J. M. Kim, D. Kim, C. Lee, J. S. Park, and H. Kim, *Electrochem. Solid-State Lett.* 13, H151 (2010).
- [417] D. Kim, H. Kang, J. M. Kim, and H. Kim, *Appl. Surf. Sci.* 257, 3776 (2011).
- [418] S. M. Sultan, O. D. Clark, T. B. Masaud, Q. Fang, R. Gunn, M. M. A. Hakim, K. Sun, P. Ashburn, and H. M. H. Chong, *Microelectron. Eng.* 97, 162 (2012).
- [419] M. A. Thomas, and J. B. Cui, *ACS Appl. Mater. Interfaces* 4, 3122 (2012).
- [420] S. M Sultan, K. Sun, O. D. Clark, T. B. Masaud, Q. Fang, R. Gunn, J. Partridge, M. W. Allen, P. Ashburn, and H. M. H. Chong, *IEEE Electron Dev. Lett.* 33, 203 (2012).
- [421] V. S. Kale, R. R. Prabhakar, S. S. Pramana, M. Rao, C.-H. Sow, K. B. Jinesh, and S. G. Mhaisalkarab, *Physical Chem. Chemical Phys.* 14, 4614 (2012).
- [422] J. Zhang, H. Yang, Q.-L. Zhanga, S. Dong, and J. K. Luo, *Appl. Surf. Sci.* 282, 390 (2013).
- [423] J. H. Heo, H. Ryua, and W.-J. Lee, *J. In. Eng. Chem.* 19, 1638 (2013).
- [424] Y. Kawamura, M. Horita, Y. Ishikawa, and Y. Uraoka, *J. Display Technol.* 9, 694 (2013).
- [425] P. C. Rowlette, C. G. Allen, O. B. Bromley, and C. A. Wolden, *J. Vac. Sci. Technol. A* 27, 761 (2009).

- [426] P. C. Rowlette, C. G. Allen, O. B. Bromley, A. E. Dubetz, and C. A. Wolden, *Chem. Vap. Dep.* 15, 15 (2009).
- [427] J. Y. Kim, S. H. Kim, H. Seo, J. H. Kim, and H. Jeon, *Electrochem. Solid-State Lett.* 8, G82 (2005).
- [428] Y. Kim, J. Koo, J. W. Han, S. Choi, H. Jeon, and C. G. Park, *J. Appl. Phys.* 92, 5443 (2002).
- [429] S. J. Yun, J. W. Lim, and J. H. Lee, *Electrochem. Solid-State Lett.* 7, F81 (2004).
- [430] S. J. Yun, J. B. Koo, J. W. Lim, and S. H. Kim, *Electrochem. Solid-State Lett.* 10, H90 (2007).
- [431] S. J. Yun, J. W. Lim, and J. H. Lee, *Electrochem. Solid-State Lett.* 8, F47 (2005).
- [432] Y. Tak, and K. Yong, *Surf. Rev. Lett.* 12, 215 (2005).
- [433] J. Koo, Y. Kim, and H. Jeon, *Jpn. J. Appl. Phys., Part 1* 41, 3043 (2002).
- [434] S. Cho, K. Lee, P. Song, H. Jeon, and Y. Kim, *Jpn. J. Appl. Phys., Part 1* 46, 4085 (2007).
- [435] S. E. Potts, C. J. Carmalt, C. S. Blackman, F. Abou-Chahine, N. Leick, W. M. M. Kessels, H. O. Davies, and P. N. Heys, *Inorg. Chim. Acta* 363, 1077 (2010).